U.PORTO

FEUP FACULDADE DE ENGENHARIA
UNIVERSIDADE DO PORTO

Analysis of Composite Laminated Plates using High-Order Shear Deformation Theories: a Meshless Approach.

Solid Mechanics and Composite Materials Applications.

by
Daniel do Espírito Santo Rodrigues

Thesis submitted to
Faculdade de Engenharia da Universidade do Porto
as a requirement to obtain the MSc degree in Mechanical Engineering.

under the supervision of
Professor Jorge Américo Oliveira Pinto Belinha
and
Professor Aurélio Araújo
Professor Renato Natal Jorge

Porto, July 2016

"I have no idea what I am doing but incompetence has never prevented me from plunging in with enthusiasm."

Woody Allen

Agradecimentos

Ao Professor Jorge Belinha, um obrigado pela oportunidade. Não me refiro apenas à oportunidade única de poder trabalhar sob orientação de alguém possuidor de tão vasto conhecimento e que sempre demonstrou um empenho e uma dedicação ímpares pelos seus alunos, mas sobretudo pela persistência em oferecer-me essa oportunidade. Ainda tenho vivas memórias da minha estupefação quando recebi um e-mail com uma proposta do Professor Jorge Belinha para fazer parte do seu grupo de investigação. Foi para mim um orgulho, e continuará sempre a sê-lo.

Ao Professor Renato Natal Jorge obrigado por me incutir uma paixão que julgava impossível pelos métodos numéricos e por reconhecer em mim capacidades suficientes para pertencer ao seu grupo de investigação. À Professora Lúcia Dinis, agradeço simpatia, a disponibilidade e sobretudo por me ter introduzido ao vasto universo das placas.

Um agradecimento especial também ao Professor António Torres Marques, ao Professor Paulo Tavares de Castro e ao Professor José Dias Rodrigues pelo entusiasmo com que lecionam as suas aulas e pelo imenso conhecimento que todos os dias partilham e fazem gerar.

À Isa, à Mariana e à Tania obrigado por estarem comigo há tantos anos e nunca se terem sentido tentadas a dizer um adeus definitivo. Obrigado pela amizade, pela companhia, pelo apoio, pelos risos compulsivos, pelas memórias. Sem vocês nada disto teria sido possível.

Um obrigado muito sentido aos meus companheiros da Magazine.HD, em especial ao Rui e à Catarina, por acreditarem não só nas minhas capacidades em termos de expressão escrita, mas sobretudo por reconhecerem nos meus pensamentos e ideias uma relevância que nunca antes tinha sentido. A cada dia que foi passando ao longo destes últimos cinco anos de percurso académico, foi naquele canto online plantado que reconheci que a Engenharia tinha no Cinema um rival à altura e que pretendo irremediavelmente viver em comunhão com ambos durante muitos anos.

À minha família, em especial à minha madrinha e às minhas avós, obrigado por se transformarem sempre naquilo que eu mais precisava: ora alguém que me acordasse do sono pesado, ora alguém que cozinhasse aquela

sobremesa predileta, ou simplesmente alguém com uma palavra de força e de ânimo nos momentos mais sensíveis.

Aos meus pais, mesmo que nem tudo tenha corrido como idealizado, obrigado por acreditarem sempre que aquele miúdo franzino de olhos fixados no seu Gameboy iria ser alguém. Obrigado pelos inúmeros incentivos e pelo orgulho reiterado.

Funding

The author truly acknowledge the funding provided by Ministério da Educação e Ciência – Fundação para a Ciência e a Tecnologia (Portugal), by project funding UID/EMS/50022/2013 - Advanced materials for noise reduction: modeling, optimization and experimental validation (funding provided by the inter-institutional projects from LAETA and INEGI).

The author truly acknowledge the work conditions provided by the Department of Mechanical Engineering from FEUP and INEGI.

Analysis of Composite Laminated Plates using High-Order Shear Deformation Theories: a Meshless Approach.

Solid Mechanics and Composite Materials Applications.

by

Daniel do Espírito Santo Rodrigues

Thesis submitted in fulfilment of the degree of Master of Science in Mechanical Engineering in the Faculdade de Engenharia da Universidade do Porto under the supervision of:

Professor **Jorge Américo Oliveira Pinto Belinha**
Professor of Faculdade de Engenharia da Universidade do Porto

and

Professor **Aurélio Araújo**
Associated Professor of Instituto Superior Técnico

Professor **Renato Natal Jorge**
Associated Professor of Faculdade de Engenharia da Universidade do Porto

Abstract

Composite structures are commonly analysed using the Finite Element Method (FEM). However, new accurate and efficient discrete numerical techniques have appeared recently - the meshless methods. Thus, this work uses two meshless methods to perform an elasto-static analysis of composite laminated plates. Meshless methods only require an unstructured nodal distribution to discretize the problem domain. In order to numerically integrate the integro-differential equation from the Galerkin weak formulation, a background integration mesh is constructed. Then, the nodal connectivity is enforced using the influence-domain concept and the shape functions are obtained. In this work, the deformation field of the solid domain is ruled by several equivalent single layer theories, assuming different transverse high-order shear deformation theories. In the end, several composite laminates are analysed and the meshless solutions are compared with the solution from other numerical techniques available in the literature.

Analysis of Composite Laminated Plates using High-Order Shear Deformation Theories: a Meshless Approach.

Solid Mechanics and Composite Materials Applications.

por

Daniel do Espírito Santo Rodrigues

Tese apresentada à Faculdade de Engenharia da Universidade do Porto, para a obtenção do grau de Mestre em Engenharia Mecânica, sob a orientação de:

Professor **Jorge Américo Oliveira Pinto Belinha**
Professor da Faculdade de Engenharia da Universidade do Porto

e

Professor **Aurélio Araújo**
Professor Associado do Instituto Superior Técnico

Professor **Renato Natal Jorge**
Professor Associado da Faculdade de Engenharia da Universidade do Porto

Sumário

Estruturas compósitas são geralmente analisadas utilizando o Método dos Elementos Finitos (MEF). No entanto, novas técnicas de discretização numéricas, precisas e eficientes, têm aparecido recentemente - os métodos sem malha. Por conseguinte, este trabalho utiliza dois métodos sem malha para realizar análises elasto-estáticas de placas compósitas laminadas. Os métodos sem malha só exigem uma distribuição nodal não estruturada para discretizar o domínio do problema. A fim de integrar numericamente a equação integro-diferencial a partir da forma fraca de Galerkin, uma malha de integração é construída. Em seguida, a conectividade nodal é imposta utilizando o conceito de domínio de influência e as funções de forma são obtidas. O campo de deformação do domínio sólido é governado por modelos de placa de camada equivalente, assumindo diferentes teorias de deformação de corte de alta ordem. No final, vários compósitos laminados são analisados e as soluções obtidas pelos métodos sem malha são comparadas com a solução de outras técnicas numéricas disponíveis na literatura.

Table of Contents

List of Figures

List of Tables

Chapter 1

1 Introduction

The finite element method (FEM) is a numerical method widely used in continuum mechanics in order to handle the engineering design phases: modulation, simulation and analysis. Despite this numerical method has been the most accepted by the scientific community in recent years, there are other methods recently developed capable to meet the design needs of an engineer and, in some cases, with considerable advantages concerning a better reproduction of the studied phenomenon. The phenomenon studied in this work is the structural behaviour of composite laminated plates that are a key system in modern aircraft structures. Two alternative numerical methods will be presented and applied, by means of MATLAB® algorithms, to the structural analysis of composite laminated plates from the point of view of some High-Order Shear Deformation Theories (HSDT) studied.

1.1 Meshless Methods

The Finite Element Method (FEM) saw the first efforts to use continuous functions over triangular domains with the work of Courant in 1943, that used an assemblage of triangular elements and the principle of minimum potential energy to study the St. Venant torsion problem [1]. But only in 1959 Greenstadt presented a discretization approach, where "*he imagined the solution domain to be divided into a set of contiguous subdomains."* [1] Since then, and with the development of more efficient ways to solve complex structural analysis problems (i.e. computer software, FEM commercial packages), the FEM has been used as a fundamental tool for design engineers.

Thus, the concept of the Finite Element Method is the discretization of the analysed problem into smaller parts called elements [2]. It's the association of these elements that forms a mesh where the nodal connectivity can be found. But, as Noronha et al. [2] written about, "*due to being mesh-reliant, the FEM has some limitations*". In problems where there are large deformations, it's hard to assure the mesh connectivity without highly distorting it, which leads to inaccurate results. Re-meshing can be a solution to this problem, but the

time consumption and the high computational costs could be dissuasive factors. Also, for 3D problems and for problems such as time-dependent and crack propagation problems (that also requires frequent re-meshing), the cost of creating good quality meshes can be high [3].

To solve some of the aforementioned problems, meshless methods were created only some years after the FEM (in 1977 with the introduction of the Smooth Particle Hydrodynamics Method (SPH) [4]), but they were only extended to solid mechanics in 1990, although the first global weak form based meshless method was only presented in 1994 (the Element Free Galerkin Method (EFGM) [2], [5]).

By opposition to the traditional Finite Element Method, in the meshless methods the concept of mesh or element is inexistent. In these methods, the nodes can be arbitrary distributed and the field functions are approximated within an influence domain rather than an element [6]. The 'influence-domain' is an area or volume (depending if the studied phenomenon is a 2D or a 3D problem) that can be concentric with an interesting point (an integration point if it is used the Gauss-Legendre Integration Method) or an 'influence-cell' that is constructed in the problem domain resulting in a node dependent integration background mesh [7]. As a consequence, meshless methods could be divided in two categories, depending on how the numerical integration is done: the 'truly' meshless methods and 'not truly' meshless methods. The truly meshless methods use integrations meshes that are constructed in the problem domain considering the nodal discretization and the other ones use a background integration mesh (with Gauss-Legendre integration points) to perform the numerical integration, which eliminates the mesh-free characteristic of these methods [8]. Also in opposition to the FEM (which has a no-overlap rule between elements), in the meshless methods the nodal connectivity is imposed by the overlap of the 'influence-domains' [6].

In the following subchapters the author presents the general procedure for meshless methods, with particular incidence on the two meshless techniques that were implemented in MATLAB® algorithms for the analysis of laminated composite plates using High-Order Shear Deformation Theories.

1.1.1 On the General Meshless Procedure

As almost all kind of numerical methods, it is possible to define and classify a meshless method by three fundamental modules: the field

approximation (or interpolation) function, the used formulation and the integration. [9]

The most relevant approximation (or interpolation) functions. are the Taylor approximation, the moving least-square approximation, the reproducing kernel approximation, the hp-cloud approximation function, the polynomial interpolation, the parametric interpolation, the radial interpolation and the Sibson interpolation [9]. These functions needs to verify the compact support property, which requires a domain of applicability and outside this domain the function assumes zero values. Additionally, another very attractive and useful numerical property is desirable: the delta Kronecker property. Field functions possessing the delta Kronecker property simplify numerically the imposition of the essential and natural boundary conditions.

The two meshless methods analysed in the present work use radial interpolation functions, possessing the compact support and the delta Kronecker properties. In the FEM, the mentioned domain is the 'element' and in the meshless methods this domain is the above-mentioned 'influence-domain'. [9] The 'influence-domain' is determined for each node (or interest point) within the nodal mesh and its shape and size vary with the considered node. Also, the 'influence-domain' is determined with different procedures depending on the meshless method considered.

In terms of formulation, the meshless methods can be classified, as the FEM, in two categories: the strong and weak form formulations. The first one establishes the governing partial differential equations along with the essential and natural boundary conditions and the solution is exact. The second one is a lower order problem that uses a variational principle to minimize the residual weight of the differential equations ruling the phenomenon. [9] "*The residual is obtained by substituting the exact solution by an approximated function affected by a test function*." [9] There are distinct weak form numerical methods and that depends on the test function that is used. Weak forms are very important because the strong form may have solutions that cannot be established. This outcomes that the preferable way of solving such differential equations is by a weak form formulation. The meshless methods presented in this work use the Galerkin weak form.

The last fundamental module of a numerical method is the integration scheme. As already mentioned in the subchapter 1.1. that can be made using a background mesh that covers the problem domain and it is composed by integration points (with correspondent weight), but this solution is nodal

independent, which does not meet the designation of 'meshless method' [9]. Other meshless methods, such as the one developed by Belinha et. al [6], uses a Voronoï Diagram concept to determine 'influence-cells' and the integration scheme is based on these cells. This work uses two meshless methods with nodal dependent and nodal independent integration schemes.

1.1.2 Relevant Meshless Methods

Besides the SPH and the EFGM referred in 1.1., many different meshless methods have been created in the past years, mostly using approximation functions since it produces more smooth solutions, the implementation of the influence-domain concept is easier and the background integration scheme is nodal independent [9].

Other very popular approximant meshless methods are: the Meshless Local Petrov-Galerkin Method (MLPG) [10], the Reproducing Kernel Particle Method (RKPM) [11], The Finite Point Method (FPM) [12] or the Radial Basis Function Method (RBFM) [13], [14] . The RBFM uses the strong form formulation and the radial basis functions, respecting a Euclidean norm, for the approximation of the variable fields (which can be done in the entire domain or in small domains).

Despite they have been successfully applied, the mentioned methods use approximations shape functions and, because of this, an issue can be found: the lack of delta Kronecker property, $\varphi_i(\boldsymbol{x}_j) \neq \delta_{ij}$ on the approximation functions, which make the imposition of essential and natural boundary conditions difficult. [2]

Recent developments solved this problem by creating several interpolation meshless methods such as the Point Interpolation Method (PIM) [15], the Point Assembly Method [16] or the Radial Point Interpolation Method (RPIM) [17] that is used in this work. The RPIM uses radial basis functions (RBF) that were added to the construction of the interpolation function in order to stabilize the method. The RBF used in these early works were the Gaussian and the multiquadric RBF. [6] More recently, the development of the concept of natural neighbours (the Voronoï Diagram concept) combined with RPIM resulted in the creation of the Natural Neighbour Radial Point Interpolation Method (NNRPIM) [6], that is also used for the structural analysis of laminated composite plates in following chapters.

1.1.3 Radial Point Interpolation Method

The RPIM emerged as a development of PIM, that only uses polynomial basis functions and, because of that, "*some singularities could occur, as for example, the perfect alignment of the nodes would produce singular solutions in the shape function construction process"* [2] The RPIM was proposed in 2002 and suggests a combination of the polynomial basis functions used in PIM with Radial Basis Functions (RBF) to construct the shape functions. With this combination, the method is stabilized.

The RPIM uses the 'influence-domain' concept and the nodal connectivity is established by the overlap of each 'influence-domain' (generating sparse and banded stiffness matrices, more adequate to complex geometry problems, by opposition to the 'global domain' concept [9]). Additionally, as written in 1.1.2., its shape functions possess the delta Kronecker property, which means that they pass through every single node. Thus, the shape functions in RPIM are interpolation shape functions, which solves the issue of the essential and natural boundary imposition.[2]

Regarding the integration scheme, the RPIM uses a background integration mesh that is nodal independent.

1.1.4 The Natural Neighbour Radial Point Interpolation Method

The Natural Neighbour Radial Point Interpolation Method (NNRPIM) is a recent developed meshless method which combines the Radial Point Interpolators (RPI) with the Natural Neighbours geometric concept.

The main difference between the NNRPIM and the RPIM concerns the imposition of the nodal connectivity. In the NNRPIM, the concept of 'influence-domain' used in the RPIM is substituted by the 'influence-cell' concept [6]. In order to obtain the 'influence-cells' the NNRPIM uses geometrical and mathematical constructions such as the Voronoï diagrams and the Delaunay tessellation [6]. "*Because of the way the nodal connectivity is enforced, both the displacement and the stress fields obtained are generally smoother and more accurate when compared to the results obtained with other methods."* [2]

For shape functions used in the Galerkin weak form, the NNRPIM makes use of the same interpolation functions as RPIM, therefore, it possess the delta Kronecker property.

The Delaunay triangles, which are the dual of the Voronoï cells, are applied to create a node-depending background mesh used in the numerical integration of the NNRPIM, which makes this method a 'truly' meshless method. [6]

Although the NNRPIM is a recent developed meshless method, it was used in many fields of applications such as the static analysis of isotropic and orthotropic plates [7], the 3D shell-like approach for laminated plates and shells [18], [19], nonlinearity problems [20], crack opening path prediction [21], bone tissue remodelling applications [9], and many others. This work aims to apply for the first time this method to the analysis of laminated composite plates considering High-Order Shear Deformation Theories.

1.2 Laminated Composite Materials

Laminated composite materials have been used in the past fifty years and established as one of the most important materials for scientific and engineering purposes, such as aircraft, aerospace, automotive industry, vessels, biomedical industry, agriculture, infrastructures, sports, etc. Because of their adaptability and high specific strength, they have also been studied not only in terms of material selection but also in terms of simulation of its structural behaviour.

The composite laminated plates studied in this work are made up of orthotropic lamina (composed of fibres bounded by a polymeric matrix) which are adhered together with different orientations of its fibres – it's this particular aspect that can vary the specific strength of a laminate when compared with a similar one that as the same material, the same thickness and the same number of plies, but with different orientations of these plies.

In these structures often used in situations where it is required high-performance and the damage tolerance is intended to be low, the failure mechanisms (such as delamination, micro-buckling of fibres, cross cracking, etc) are dependent of the normal and transverse shear stresses that the laminate is subjected. Consequently, it is easy to understand the importance of accurately predicting the stress tensor in each point of the laminate.

1.3 High-Order Shear Deformation Plate Theories

Pagano and Hatfield [22] were the first ones to analyse the static behaviour of this kind of plates, resulting in the publication of their exact solutions using the three-dimensional (3D) elasticity method [23]. However, the 3D solution is not practicable tool "*to deal with complex geometries and arbitrary boundary conditions*". [23]

Hence, some 2D models were developed as an easier alternative. These models could be divided in three classes: the equivalent single layer (ESL) theories, the layer-wise (LW) theories (which consider independent degrees of freedom for each layer resulting in accurate results but also computationally expensive) [24] and the zigzag (ZZ) theories [25] ("*wherein the displacements approximation is given by the superposition of a smeared kinematics, describing the kinematic behaviour on the whole laminate, and a local refinement, acting on the scale of the layer thickness*" [25]).

The ESL theories were considered in this work. The simplest ESL known is the Kirchhoff-Love plate theory or the classical plate theory (CLPT) which considers that the plane section perpendicular to the mid-plane of the plate before deformation remains plane, rigid, and perpendicular to the deformed mid-plane after deformation. By neglecting the shear strain, CLPT can only be used for the structural analysis of thin plates (for thick plates, this theory underestimates deflection). [23]

The Reissner-Mindlin plate theory, or the first-order shear deformation theory (FSDT), developed some of the limitation of the CLPT. According to the assumptions of Mindlin, a plane section will still be plane after deformation, nevertheless, it won't be normal to mid-plane after deformation. As written by Nguyen et al. [23], "*this assumption causes the constant transverse shear stress through the plate's thickness which violates the traction boundary conditions on the top and bottom surface of plates*". Thus, FSDT needs a shear correction factor to satisfy the traction on the top and bottom surface plates. The accuracy of the FSDT highly depends on this correction factor which is difficult to define for a general problem. Furthermore, FSDT meets a shear locking phenomenon when the ratio between the length of the plate and the thickness becomes higher.

The disadvantages of CLPT and FSDT were at the origin of the development of high-order shear deformation theories (HSDTs), which possess transverse shear functions capable to describe the nonlinear

parabolic variation of transverse shear stresses through thickness of plate [23].

In literature, it can be found many of these HSDTs with different types of transverse shear functions such as polynomial [26]–[28], trigonometric [29], exponential [30], [31], hyperbolic [32], or the combination of trigonometric and exponential functions [33].

Although the HSDTs are a major breakthrough in the analysis of laminated composite plates, in fact, there still exists some errors when comparing the solutions of the HSDTs and the 3D solutions. The numerical differences come from the discontinuity at interface of two adjacent layers - due to the fact that the material properties are different for each layer - in the case of the transverse shear stresses being computed by constitutive equations (which is the circumstance of the algorithms developed in this work). This problem can be contoured by computing the transverse shear stresses based on equilibrium equations representing the realistic distribution of transverse shear stresses of laminated composite plates [23].

Some of these HSDTs were selected, analysed and implemented in two algorithms written in MATLAB® for the two meshless methods considered: the RPIM and the NNRPIM. Various laminated composite plates were studied with different plate theories and different numerical methods.

1.4 Thesis Objectives

The main objective of this thesis is to combine, for the first time, the static analysis of laminated composite plates using high-order shear deformation theories with two recently developed meshless methods.

Such combination will be performed through the creation of two algorithms in MATLAB® to accommodate the two meshless methods in analysis.

Before the implementation of the algorithm takes place, the objectives are:

i. Define a state-of-art concerning the theory of thin/thick plates;
ii. Understand the principles of the meshless methods in study;
iii. Develop, manually, the displacement and strain field, and the essential matrixes for each considered theories taking into account the formulation of the meshless methods.

The MATLAB® algorithm must be able to:

i. Calculate displacements and stresses for interest points of the plate (and along the thickness);
ii. 3D Plot displacements, rotations, stresses, moments, transverse shear and membrane forces;
iii. Analyse several kinds of laminated composite plates (symmetric cross-ply, antisymmetric cross-ply and angle-ply laminates) with all the chosen HSDTs, with different geometries and material properties, several kinds of boundary conditions and different types of loads.

Finally, with the algorithm concluded, these are the following objectives:

i. Perform static analysis of laminated composite plates with different combinations of:

a. Meshless method (RPIM and NNRPIM);
b. HSDT;
c. Laminate;
d. Geometry properties;
e. Load;
f. Boundary conditions;

ii. Draw further comparisons between the results obtained with RPIM and NNRPIM and the published results for the exact solutions and FEM solutions, when available;
iii. Understand what are the HSDTs whose results best approximates the results of the 3D Elasticity;
iv. Compare the behaviour of different laminates when subjected to similar conditions.

1.5 Thesis Arrangement

This thesis is divided in six chapters: Introduction, Meshless Methods, Soldid Mechanics Fundamentals, Plates Theory, Numerical Results and Conclusions.

In the first chapter, **Introduction**, it is introduced the thesis purposed. A general overview on the meshless method is presented, highlighting the RPIM and the NNRPIM. It also contains a brief state-of-the-art regarding laminated composite plates and plates theory.

In the second chapter, **Meshless Methods**, the two methods are described and their formulation is presented.

In the third chapter, **Solid Mechanics Fundamentals**, the mechanical fundamentals are developed. The weak form formulation is presented and the discrete system equations is obtained.

In the fourth chapter, **Plates Theory**, a state-of-the-art concerning the theory of the plates is presented (in particular the classical plate theory and the first-order shear deformation plate theory). Then, for each equivalent single layer selected, the displacement and strain field is determined and fundamental matrixes are obtained for the algorithm implementation.

In the fifth chapter, **Numerical Results**, are presented and discussed the results obtained for several kinds of laminates, theories and meshless methods, using the algorithms developed.

In the sixth chapter, **Conclusions**, the main conclusions of this work are drawn. This chapter also features some recommendations for future work.

Chapter 2

2 Meshless Methods

In this chapter the Radial Point Interpolation Method (RPIM) and the Natural Neighbour Radial Point Interpolation Method (NNRPIM) are presented. The chapter starts with an introduction to the generic procedure of a meshless method. Then, the RPIM and the NNRPIM are introduced along with the concepts of influence-domain and nodal connectivity as well as the integration scheme and the interpolations functions that are used in both methods. In the case of the NNRPIM, it is introduced the notion of influence-cell and the way that these influence-cells are constructed through Voronoï diagrams.

2.1 Generic Procedure of a Meshless Method

Most of the meshless methods, such as the RPIM and the NNRPIM follow a standard procedure. After the description of the problem (with the essential and natural boundary conditions), the problem domain is discretized in a nodal mesh (figure 1). The nodal discretization can be regular or irregular, with the last one having, in general, a lower accuracy. However, in some problems where the locations of the stress concentration are predictable (crack propagation, holes, clamped boundaries, etc), it is necessary to have a higher nodal density in those locations, which will lead to better results. Thus, it is essential to choose a correct nodal density of the mesh and the best nodal distribution possible that do not conduct to a significant increase of the computational cost, since these discretization parameters influence the method performance. An unbalanced distribution of the nodes could lead to less accurate results. [6]

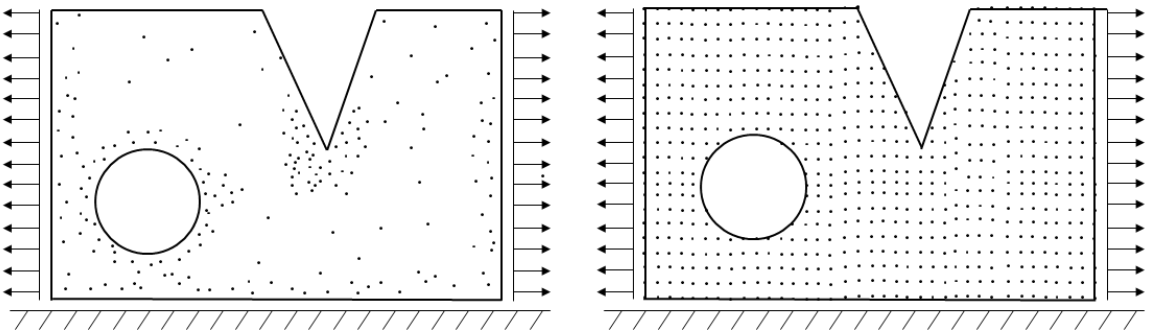

(a) (b)

figure 1 – Nodal discretization example. (a) Irregular mesh. (b) Regular mesh.

After the nodal discretization a background integration mesh is constructed. The integration mesh can be nodal dependent (NNRPIM) or nodal independent (RPIM), and can have *"the size of the problem domain or even a larger one, without affecting too much the final results*" [6]. A nodal independent integration mesh, in general, uses Gauss points, as in the FEM, fitted to the problem domain (figure 2(a)) or not (eliminating the Gauss points that are outside the problem domain – figure 2(b)). Another way to integrate the weak form equations is using the nodal integration by means of the concept of natural neighbours and the Voronoï diagrams. Here, the nodal mesh will also be the integration mesh, figure 2(c). The NNRPIM uses an improved version of this last mentioned technique.

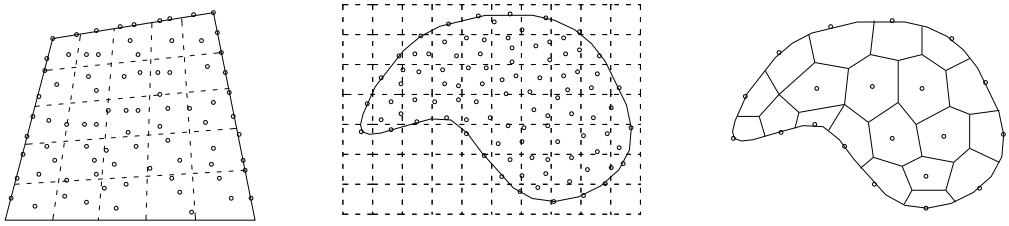

(a) (b) (c)

figure 2 – (a) Fitted Gaussian integration mesh. (b) General Gaussian integration mesh. (c) Voronoï diagram for nodal integration. [6]

After the definition of the integration mesh, the nodal connectivity can be imposed. While in the FEM this nodal connectivity is done with the interaction of the finite elements with the neighbour elements (there is a no-overlap rule between elements) and also at the element level (where the nodes belonging to the same element interact with each other), in most of the meshless methods the nodal connectivity is imposed by the overlap of influence domains. Thus, for each interest point x_I of the problem domain, are generated concentric areas (for 2D problems) or volumes (for 3D

problems) and the nodes inside these areas or volumes belong to the 'influence-domain' of point x_I [6]. In the NNRPIM, the areas or volumes defined are Voronoï cells that are geometric constructions based on the nodal distribution. In most of the meshless methods, the interest points are the integration points from the background integration mesh. However, there are other methods which consider the nodes as interest points and use the nodal integration scheme.

The next step is to obtain the field variables, using approximation or interpolation functions (the two meshless methods considered in this work use the same interpolation functions).

Consider the displacement field $\boldsymbol{u}$ which components $\boldsymbol{u}(\boldsymbol{x}_I) = (u, v, w)$ are obtained at an interest point $\boldsymbol{x}_I$ within the problem domain and were interpolated using the nodal displacement of the nodes inside the 'influence-domain' (or 'influence-cell') of the correspondent interest point, $\boldsymbol{x}_I$. Thus, the following equation can the defined,

$$\boldsymbol{u}(\boldsymbol{x}_I) = \sum_{j=1}^{n} \varphi_j(\boldsymbol{x}_I)\,\boldsymbol{u}_j \tag{1}$$

where n is the number of nodes inside the 'influence-domain' of the interest point $\boldsymbol{x}_I$, $\boldsymbol{u}_j$ is a vector of the displacement components of each node within the 'influence-domain' – each of these nodes is given by j – and $\varphi_j(\boldsymbol{x}_I)$ is the approximation or interpolation function of the node j obtained using only the n nodes inside the 'influence-domain' and calculated at the interest point $\boldsymbol{x}_I$. [6].

As already mentioned, both RPIM and NNRPIM use interpolation functions based on the combination of multiquadric (MQ) radial basis functions (RBF) with polynomial basis functions.

After the determination of the interpolation functions, the system of equations can be established and then arranged in a local nodal matrix and assembled into a global system of matrix equations. To obtain the displacement field, it can be used, for instance, the Gauss elimination method. [6]

2.2 Radial Point Interpolation Method Formulation

2.2.1 Influence-Domains and Nodal Connectivity

In the RPIM, the nodal connectivity between each node is achieved with the overlap of the 'influence-domains', created following the nodal discretization and the definition of the background integration mesh. In the 2D problems analysed in this work, the 'influence-domains' for each interest point can be concentric areas with the interest point (such as circles – figure 3(a) – or rectangles with a predefined size) or, on the other hand, a certain number of nodes that are closer to that point, as shown in figure 3(b).

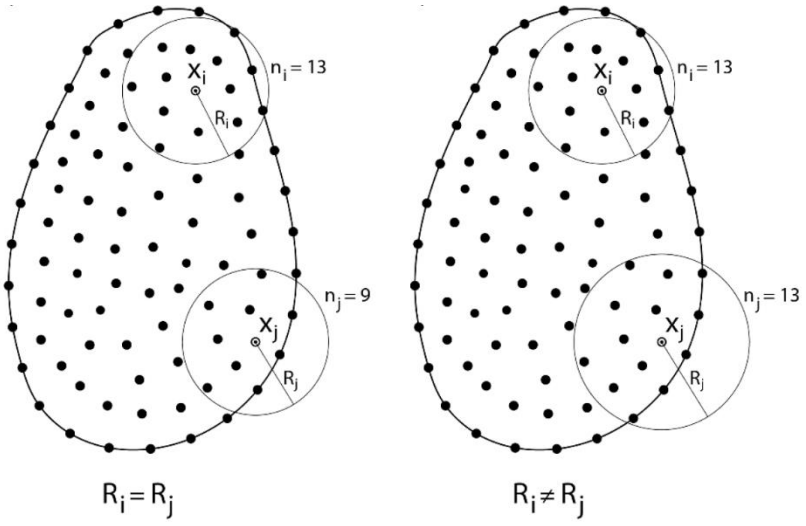

figure 3 – (a) Fixed size 'influence-domain'. (b) Variable size 'influence-domain'.

The shape and size of an 'influence-domain' may vary depending on the position of the interest points, the nodal distribution and the nodal density. For example, for a variable size 'influence-domain', it may occur that an 'influence-domain' with the same shape has a different number of nodes within it if the nodal distribution is irregular. On the opposite side, for a fixed size 'influence-domain', it is common that the shape of each domain is different. The recommendations of the literature [9] lead to the necessity of 'influence-domains' with the same number of nodes inside (for 2D problems, it is recommended between 9 and 16 nodes per 'influence-domain' [17]), which allows the construction of shape functions with the same degree of complexity.

2.2.2 Numerical Integration

In the RPIM, the differential equations of the Galerkin weak form are integrated using the Gauss-Legendre quadrature. Thus, a background integration mesh is created. Because this work is related to the analysis of square plates, the background integration mesh is composed by quadrilateral cells (isoparametric quadrilateral shape) and in each cell are placed the integration points – figure 4 - with the locations and weights presented in the table 1.

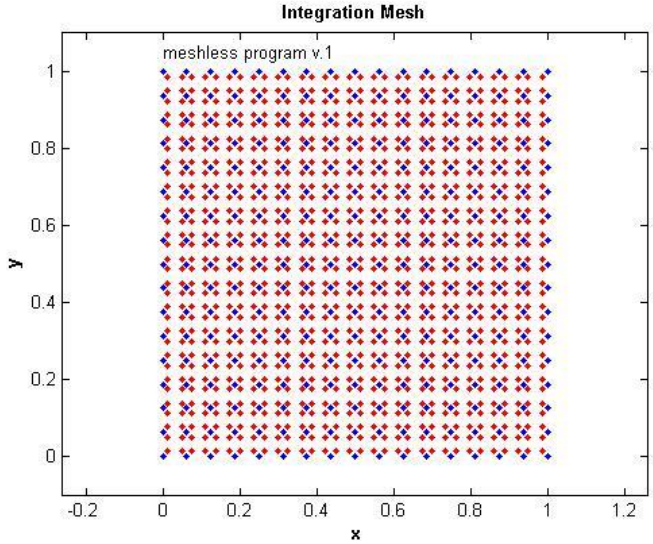

figure 4 – Square plate discretized with 17x17 nodes (blue nodes) and with a background integration mesh with 2x2 Gauss points (red points) in each cell.

The Gauss-Legendre integration scheme follows the equation (2).

$$I = \int_{-1}^{1}\int_{-1}^{1} f(\xi,\eta)\, d\xi\, d\eta = \sum_{i=1}^{n\xi}\sum_{j=1}^{n\eta} f(\xi_i,\eta_i)\cdot w_i \cdot w_j \qquad (2)$$

being $f(\xi,\eta)$ the integrand function depending on the natural coordinates, $f(\xi_i,\eta_i)$ the value of the function in the integration point and w_i and w_j the weights of the integration point.

table 1 – Integration points and correspondent weights for quadrilateral isoparametric cells (integration with one, four and nine Guass-Legendre integration points).

Gauss-Legendre Points	ξ	η	Weight, $w_I = w_i \cdot w_j$	
I	0	0	4	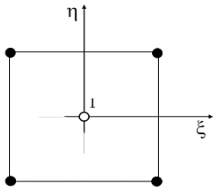
I	$-\frac{1}{\sqrt{3}}$	$-\frac{1}{\sqrt{3}}$	1	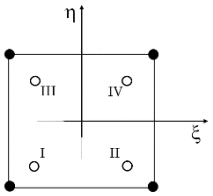
II	$+\frac{1}{\sqrt{3}}$	$-\frac{1}{\sqrt{3}}$	1	
III	$-\frac{1}{\sqrt{3}}$	$+\frac{1}{\sqrt{3}}$	1	
IV	$+\frac{1}{\sqrt{3}}$	$+\frac{1}{\sqrt{3}}$	1	
I	$-\sqrt{3/5}$	$-\sqrt{3/5}$	$\frac{25}{81}$	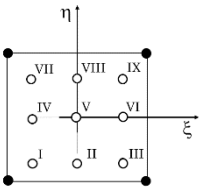
II	0	$-\sqrt{3/5}$	$\frac{40}{81}$	
III	$+\sqrt{3/5}$	$-\sqrt{3/5}$	$\frac{25}{81}$	
IV	$-\sqrt{3/5}$	0	$\frac{40}{81}$	
V	0	0	$\frac{64}{81}$	
VI	$+\sqrt{3/5}$	0	$\frac{40}{81}$	
VII	$-\sqrt{3/5}$	$+\sqrt{3/5}$	$\frac{25}{81}$	
VIII	0	$+\sqrt{3/5}$	$\frac{40}{81}$	
IX	$+\sqrt{3/5}$	$+\sqrt{3/5}$	$\frac{25}{81}$	

With the distribution of the integration points concluded, the general integral (2) can be calculated.

In the algorithm developed, the coordinates of the integrations point were transformed to the global coordinate system using the equations (3) and (4).

$$x = \sum_{i=1}^{m} N_i(\xi, \eta) \cdot x_i \tag{3}$$

$$y = \sum_{i=1}^{m} N_i(\xi, \eta) \cdot y_i \tag{4}$$

where $N_i(\xi,\eta)$ is the isoparametric shape function, m is the number of nodes defining the cell, and (x_i, y_i) the Cartesian coordinates of the node i. For quadrilaterals,

$$N_1(\xi,\eta) = \frac{1}{4}(1-\xi)\cdot(1-\eta) \tag{5}$$

$$N_2(\xi,\eta) = \frac{1}{4}(1-\xi)\cdot(1+\eta) \tag{6}$$

$$N_3(\xi,\eta) = \frac{1}{4}(1+\xi)\cdot(1+\eta) \tag{7}$$

$$N_4(\xi,\eta) = \frac{1}{4}(1+\xi)\cdot(1-\eta) \tag{8}$$

Thus, the integration weight is obtained by multiplying the isoparametric weight of the integration point with the determinant of the Jacobian matrix:

$$\boldsymbol{J} = \begin{bmatrix} \dfrac{\partial x}{\partial \xi} & \dfrac{\partial x}{\partial \eta} \\ \dfrac{\partial y}{\partial \xi} & \dfrac{\partial y}{\partial \eta} \end{bmatrix} \tag{9}$$

Hence, the differential equation integration can be performed in the integration point $\boldsymbol{x}_I$,

$$I = \int_A f(\boldsymbol{x}_I)\, dA = \int_{-1}^{1}\int_{-1}^{1} f(\boldsymbol{x}_I)\cdot \det(\boldsymbol{J})\, d\xi\, d\eta = \sum_{i=1}^{m}\sum_{j=1}^{n} f(\boldsymbol{x}_I)\cdot w_i \cdot w_j \cdot \det(\boldsymbol{J}) \tag{10}$$

where $m = n$, as seen in table 1 - for quadrilateral cells it is used [1x1], [2x2], [3x3], etc integration schemes.

2.2.1 Interpolation Functions

Both RPIM and NNRPIM use the same interpolation functions. Therefore, the formulation presented in this subchapter is also applicable to the NNRPIM and it will not be repeated in a next subchapter.

Consider a function $\boldsymbol{u}(\boldsymbol{x})$ defined in the domain Ω, which is discretized by a set of N nodes. In the RPIM, the function $\boldsymbol{u}(\boldsymbol{x})$ passes through all nodes using a radial basis function (RBF). Assuming that only the nodes within the

'influence-domain' of the interest point x_I affect the value of the function $\boldsymbol{u}(\boldsymbol{x}_I)$, the equation (11) can be established:

$$\boldsymbol{u}(\boldsymbol{x}_I)=\sum_{i=1}^{n}R_i(\boldsymbol{x}_I)a_i(\boldsymbol{x}_I)+\sum_{j=1}^{m}p_j(\boldsymbol{x}_I)b_j(\boldsymbol{x}_I)=\boldsymbol{R}^{\mathrm{T}}(\boldsymbol{x}_I)\,\boldsymbol{a}(\boldsymbol{x}_I)+\boldsymbol{p}^{\mathrm{T}}(\boldsymbol{x}_I)\,\boldsymbol{b}(\boldsymbol{x}_I) \quad (11)$$

where n is the number of nodes within the influence-domain of x_I, $R_i(\boldsymbol{x}_I)$ is the RBF, $a_i(\boldsymbol{x}_I)$ and $b_j(\boldsymbol{x}_I)$ are non-constant coefficients of $R_i(\boldsymbol{x}_I)$ and $p_j(\boldsymbol{x}_I)$, the polynomial basis, respectively, with m being the basis monomial number. The vectors presented in the equation (11) are as follows,

$$\boldsymbol{R}(\boldsymbol{x}_I)=\left\{R_1(\boldsymbol{x}_I),\ R_2(\boldsymbol{x}_I),\ \ldots\ R_n(\boldsymbol{x}_I)\right\}^{\mathrm{T}} \quad (12)$$

$$\boldsymbol{p}(\boldsymbol{x}_I)=\left\{p_1(\boldsymbol{x}_I),\ p_2(\boldsymbol{x}_I),\ \ldots\ p_m(\boldsymbol{x}_I)\right\}^{\mathrm{T}} \quad (13)$$

$$\boldsymbol{a}(\boldsymbol{x}_I)=\left\{a_1(\boldsymbol{x}_I),\ a_2(\boldsymbol{x}_I),\ \ldots\ a_n(\boldsymbol{x}_I)\right\}^{\mathrm{T}} \quad (14)$$

$$\boldsymbol{b}(\boldsymbol{x}_I)=\left\{b_1(\boldsymbol{x}_I),\ b_2(\boldsymbol{x}_I),\ \ldots\ b_m(\boldsymbol{x}_I)\right\}^{\mathrm{T}} \quad (15)$$

The equation (11) can be rewritten,

$$\boldsymbol{u}(\boldsymbol{x}_I)=\left\{\boldsymbol{R}^{\mathrm{T}}(\boldsymbol{x}_I)\quad \boldsymbol{p}^{\mathrm{T}}(\boldsymbol{x}_I)\right\}\cdot\begin{Bmatrix}\boldsymbol{a}\\ \boldsymbol{b}\end{Bmatrix} \quad (16)$$

The purpose of adding the polynomial basis functions is to ensure consistency of RPI functions because "*adding to the RBF a linear polynomial ensures the reproducing of the linear field (C^1 consistency) and consequently help the RPI passing the standard patch test.*" [6] The monomial number should be $m<n$ in order to obtain a more stable function. Nevertheless, Belinha et al. [7] evidenced that the RPI does not need a polynomial basis function to pass the standard patch test. This conclusion leads to the reduction of the computational cost, resulting in shape functions only reliant on of the RBFs.

In 2D problems, the RBFs are dependent of the vector r_{Ii}, the Euclidian distance between the interest point x_I and a node x_i belonging to the 'influence-domain' of x_I, and have the following general form,

$$R(r_{Ii}) = \left(r_{Ii}^{\,2} + c^2\right)^p \tag{17}$$

$$r_{Ii} = \sqrt{(x_I - x_i)^2 + (y_I - y_i)^2} \tag{18}$$

where equation (17) represents the multiquadric (MQ) RBFs proposed initially by Hardy [34]. c and p are shape parameters that should be $c = 0.0001$ and $p = 0.9999$ in order to maximize the method's performance [7].

The polynomial basis functions, when used, have the following sequence of terms,

$$\boldsymbol{p}^{\mathrm{T}}(\boldsymbol{x}_I) = \left\{1, x, y, x^2, xy, y^2, \ldots\right\} \tag{19}$$

which depends on the chosen monomial number m. For the 2D analysis, there are the polynomial basis functions (20),

$$\begin{aligned}
&\textit{Null basis } (m=0): && \boldsymbol{p}^{\mathrm{T}}(\boldsymbol{x}) = \{0\} \;;\; \mathrm{m} = 0 \\
&\textit{Constant basis } (m=1): && \boldsymbol{p}^{\mathrm{T}}(\boldsymbol{x}) = \{1\} \;;\; \mathrm{m} = 1 \\
&\textit{Linear basis } (m=3): && \boldsymbol{p}^{\mathrm{T}}(\boldsymbol{x}) = \{1 \quad x \quad y\} \;;\; \mathrm{m} = 3 \\
&\textit{Quadratic basis } (m=6): && \boldsymbol{p}^{\mathrm{T}}(\boldsymbol{x}) = \{1 \quad x \quad y \quad x^2 \quad xy \quad y^2\} \;;\; \mathrm{m} = 6
\end{aligned} \tag{20}$$

being the *null base* the absence of polynomial basis aforementioned. In this case, the equation (11) becomes simpler, once the polynomial terms disappear. On the order hand, if is chosen a polynomial basis with $m > 0$, it has to satisfy an extra requirement – a penalty to impose that the shape functions passes through the nodes – in order to obtain a unique solution:

$$\sum_{i=1}^{n} p_j(\boldsymbol{x}_i)\, a_i(\boldsymbol{x}_i) = 0 \Leftrightarrow \boldsymbol{p}^{\mathrm{T}}(\boldsymbol{x}_i)\, \boldsymbol{a}(\boldsymbol{x}_i) = 0 \quad , \quad \mathrm{j} = \{1, 2, \ldots, \mathrm{m}\} \tag{21}$$

Combining the equation ((16) with equation (21)

$$\begin{Bmatrix} \boldsymbol{u}_s \\ \boldsymbol{0} \end{Bmatrix} = \begin{bmatrix} \boldsymbol{R} & \boldsymbol{p} \\ \boldsymbol{p}^{\mathrm{T}} & \boldsymbol{0} \end{bmatrix} \begin{Bmatrix} \boldsymbol{a} \\ \boldsymbol{b} \end{Bmatrix} = \boldsymbol{G} \begin{Bmatrix} \boldsymbol{a} \\ \boldsymbol{b} \end{Bmatrix} \tag{22}$$

where $\boldsymbol{u}_s$ is given by,

$$\boldsymbol{u}_s = \{u_1, u_2, ..., u_n\}^{\mathrm{T}} \tag{23}$$

the matrix $\boldsymbol{R}$ $[n \times n]$ contains the RBFs of all interest points calculated by the equation (17),

$$\boldsymbol{R} = \begin{bmatrix} R(r_{11}) & R(r_{12}) & \dots & R(r_{1n}) \\ \mathrm{R}(r_{21}) & R(r_{22}) & \dots & R(r_{2n}) \\ \vdots & \vdots & \ddots & \vdots \\ R(r_{n1}) & R(r_{n2}) & \cdots & R(r_{nn}) \end{bmatrix} \tag{24}$$

and the matrix $\boldsymbol{p}$ $[n \times m]$ of the polynomial basis is given by,

$$\boldsymbol{p} = \begin{bmatrix} \mathrm{p}_1(\boldsymbol{x}_1) & \mathrm{p}_2(\boldsymbol{x}_1) & \dots & \mathrm{p}_m(\boldsymbol{x}_1) \\ \mathrm{p}_1(\boldsymbol{x}_2) & \mathrm{p}_2(\boldsymbol{x}_2) & \dots & \mathrm{p}_m(\boldsymbol{x}_2) \\ \vdots & \vdots & \ddots & \vdots \\ \mathrm{p}_1(\boldsymbol{x}_n) & \mathrm{p}_2(\boldsymbol{x}_n) & \cdots & \mathrm{p}_m(\boldsymbol{x}_n) \end{bmatrix} \tag{25}$$

For a constant polynomial basis, $\boldsymbol{p}$ is a column vector with n components. If the polynomial basis does not exist, in the equation (22), becomes $\boldsymbol{R} = \boldsymbol{G}$. The matrix $\boldsymbol{G}$ is a symmetric because the distance between the interest points and the nodes that belong to its 'influence-domain' is directional independent.

Solving equation (22),

$$\begin{Bmatrix} \boldsymbol{a} \\ \boldsymbol{b} \end{Bmatrix} = \boldsymbol{G}^{-1} \begin{Bmatrix} \boldsymbol{u}_s \\ \boldsymbol{0} \end{Bmatrix} \tag{26}$$

Finally, substituting (26) in (16),

$$\boldsymbol{u}(\boldsymbol{x}_I) = \left\{ \boldsymbol{R}^{\mathrm{T}}(\boldsymbol{x}_I), \boldsymbol{p}^{\mathrm{T}}(\boldsymbol{x}_I) \right\} \boldsymbol{G}^{-1} \begin{Bmatrix} \boldsymbol{u}_{\mathrm{s}} \\ 0 \end{Bmatrix} = \boldsymbol{\varphi}(\boldsymbol{x}_{\mathrm{I}}) \boldsymbol{u}_s \tag{27}$$

where $\boldsymbol{\varphi}(\boldsymbol{x}_{\mathrm{I}})$ is the interpolation function on interest point $\boldsymbol{x}_{\mathrm{I}}$,

$$\boldsymbol{\varphi}(\boldsymbol{x}_{\mathrm{I}}) = \left\{ \boldsymbol{R}^{\mathrm{T}}(\boldsymbol{x}_I), \boldsymbol{p}^{\mathrm{T}}(\boldsymbol{x}_I) \right\} \boldsymbol{G}^{-1} = \{ \varphi_1(\boldsymbol{x}_I), \varphi_2(\boldsymbol{x}_I), ..., \varphi_n(\boldsymbol{x}_I) \} \tag{28}$$

The Galerkin weak form, as will be seen in Chapter 4, depends on the partial derivative of $\boldsymbol{\varphi}(\boldsymbol{x}_{\mathrm{I}})$. Thus, the partial derivative of $\boldsymbol{\varphi}(\boldsymbol{x}_{\mathrm{I}})$ in order to a variable ξ is defined as, [6]

$$\boldsymbol{\varphi}_{,\xi}(\boldsymbol{x}_I) = \left\{ \boldsymbol{R}^{\mathrm{T}}_{,\xi}(\boldsymbol{x}_I),\, \boldsymbol{p}^{\mathrm{T}}_{,\xi}(\boldsymbol{x}_I) \right\} \boldsymbol{G}^{-1} \tag{29}$$

being the derivative of the MQ-RBFs in order to the same variable ξ,

$$\boldsymbol{R}_{,\xi}(r_{ij}) = 2p\left(r_{ij}^2 + c^2\right)^{p-1}\left(\xi_j - \xi_i\right) \tag{30}$$

As already mentioned, the RPI functions are interpolation functions so they possess the delta Kronecker property stated on equation (31).

$$\varphi_i(\boldsymbol{x}_j) = \delta_{ij} = \begin{cases} 1 & (i = j) \\ 0 & (i \neq j) \end{cases} \quad i, j = 1, \ldots, n \tag{31}$$

which means they pass through all nodes of the 'influence-domain' (or 'influence-cell' in the case o NNRPIM), making the imposition of the essential and natural boundary conditions easier.

These shape functions also satisfy the partition of unity property,

$$\sum_{i=1}^{n} \varphi_i(\boldsymbol{x}_i) = 1 \tag{32}$$

if the constant polynomial basis is included in the equation (16), and they possess also reproducing properties,

$$\sum_{i=1}^{n} \varphi_i(\boldsymbol{x}_i) x_i = \boldsymbol{x} \tag{33}$$

if the first order monomial is included in the polynomial basis.

2.3 Natural Neighbour Radial Point Interpolation Method

2.3.1 Voronoï Diagram Concept and Natural Neighbours

As stated in the introductory chapter, the main difference between RPIM and NNRPIM relies on the concepts of 'influence-domain' and 'influence-cell' containing the natural neighbours. While in the RPIM, the nodal connectivity is imposed by the overlap of 'influence-domains', in the NNRPIM is used the natural neighbour concept. The 'influence-cells' are determinate based on the geometric and spatial relations between Voronoï cells, obtained from the Voronoï diagram [2].

The Voronoï diagram is a mathematical tool that allows the determination of the natural neighbours for each node that discretizes the problem domain. The concept can be applied to a D-dimensional space, but the formulation shown below is an example for a two dimensional space, $\Omega \in \mathbb{R}^2$. Considering a set $\boldsymbol{N}$ of N distinct nodes,

$$\boldsymbol{N} = \{n_1, n_2, ..., n_N\} \in \mathbb{R}^2 \tag{34}$$

As shown in figure 5(d), the Voronoï diagram of $\boldsymbol{N}$ is a set of sub-regions V_I, closed and convex, each sub-region V_I associated to the node I, n_I, in a way that any point in the interior of the V_I is closer to n_I than any other node n_J, where $n_J \in N \wedge J \neq I$. Thus, V_I is the geometric place where all points are closer to n_I than to any other node and is called 'Voronoï cell'. Mathematically,

$$V_I = \left\{ \boldsymbol{x} \in \mathbb{R}^2 : \mathrm{E}_n(\boldsymbol{x}, \boldsymbol{x}_I) < \mathrm{E}_n(\boldsymbol{x}, \boldsymbol{x}_J) \ \forall J \neq I \right\} \tag{35}$$

being $\mathrm{E}_n(\boldsymbol{x}, \boldsymbol{x}_I)$, the Euclidian distance between an interest point and a node I, with coordinates defined by $\boldsymbol{x}$ and $\boldsymbol{x}_I$, and $\mathrm{E}_n(\boldsymbol{x}, \boldsymbol{x}_J)$ the same distance but regarding a node outside $J \neq I$.

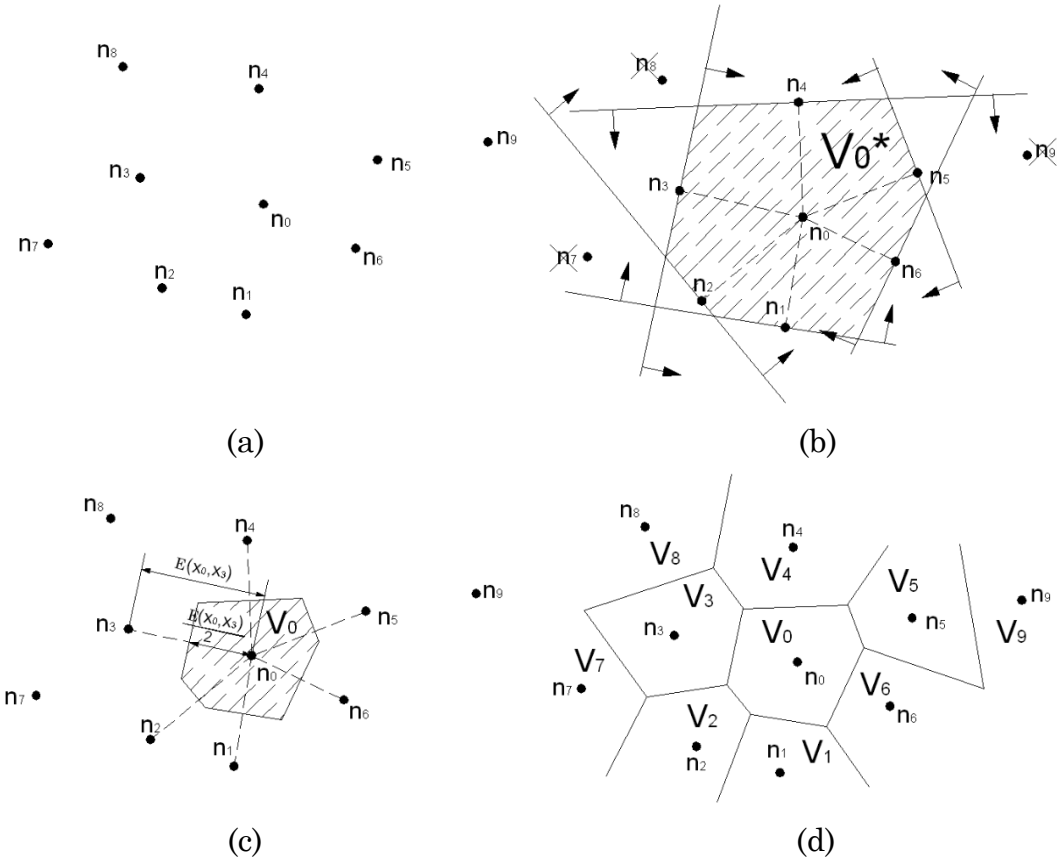

figure 5 – (a) Initial nodal set of potential neighbour nodes. (b) Construction of the cell containing only neighbour nodes. (c) Voronoï cell. (d) Voronoï diagram. [6]

In figure 5, the construction of the sub-region V_I is represented. It starts with the nodal set of potential neighbour nodes – figure 5(a). Then, are drawn the straight dashed lines that connect the node n_I and the potential neighbour nodes n_J – figure 5(b). In the same figure are indicated the neighbour nodes which are obtained by the intersection of domains whose limits are defined by the lines that intersects the nodes J and are normal to the dashed lines. The nodes located outside the cell constructed in figure 5(b), V_0^*, are discarded. The final Voronoï cell obtained, V_0, is determined as figure 5(c) indicates. The cell V_0 is the homothetic form of V_0^* and the distance between the node n_0 and the boundary of the cell V_0 is half of the Euclidian distance between n_0 and the neighbour node in question.

2.3.2 Influence-Cells and Nodal Connectivity

The size or shape variation of 'influence-domains' in RPIM affects the performance of the meshless method. Consequently, in the NNRPIM the nodal connectivity is imposed by the overlapping of the 'influence-cells' - formed by n nodes that contributes to the interpolation of the interest point x_I - obtained from the Voronoï cells.

There are two types of 'influence-cells', depending on the level of the nodal connectivity:

i. ***First degree influence-cells***: are composed by the first natural neighbours of a certain interest point;

ii. ***Second degree influence-cell***: are composed by the first natural neighbours of a certain interest point and the first neighbours of all the nodes that belong to the first degree influence-cell.

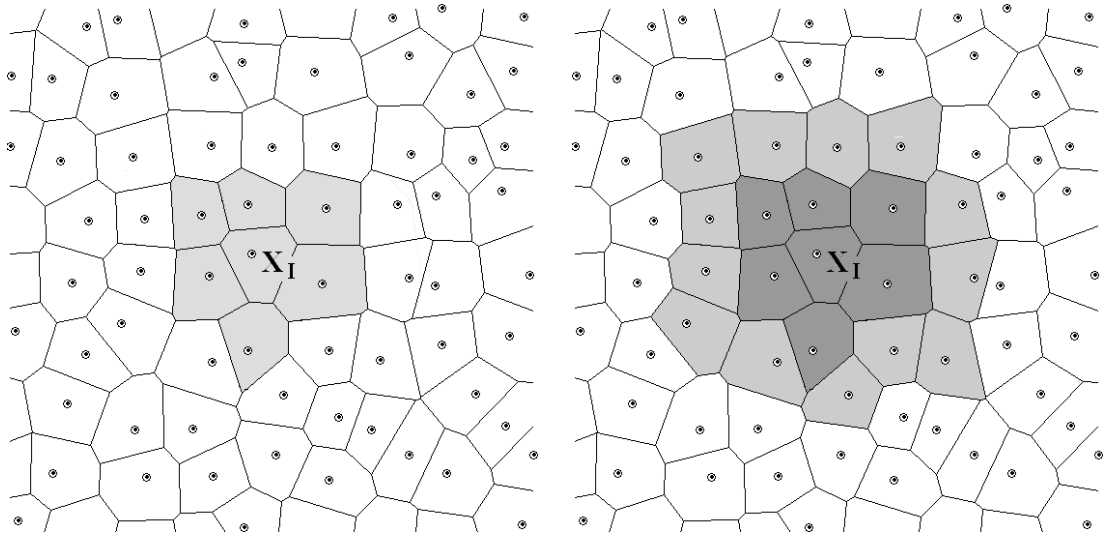

figure 6 – (a) First degree influence-cell. (b) Second degree influence-cell. [6]

As it can be seen in figure 6, the second degree influence-cell has a larger area and a higher nodal connectivity.

In a brief review, initially, in the NNRPIM, after the domain discretization in a regular or an irregular nodal mesh, the Voronoï cells of each node are constructed. These cells work as a background mesh for integration purpose. Then, the integration points are placed within the influence-cells of each node, as will be seen in section 2.3.3, and, after this, is determined the influence-cell for each one of these integration points.

2.3.3 Numerical Integration

The numerical integration in the NNRPIM is performed using another geometric construction, the Delaunay triangulation. This tool is the geometrical dual of the Voronoï diagram and it is constructed by connecting the nodes of each Voronoï cell with the nodes whose Voronoï cells have common boundaries with the first one, as shown in figure 7.

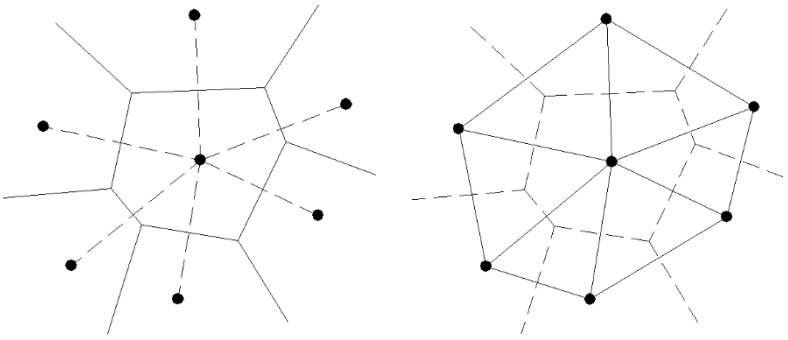

(a) (b)

figure 7 – (a) Initial Voronoi diagram. (b) Delaunay triangulation. [6]

Figure 7(b) evidences that *a "Delaunay edge exists between two nodes in the plane if and only if their Voronoï cells share a common edge*" .

Belinha et al. [6] proposed an integration scheme based on the Voronoï diagram and the Delaunay triangulation. The 2D integration scheme is explained below.

As seen in figure 8, using these two geometric constructions, small areas (quadrilaterals of triangles, depending if the nodal mesh is regular or irregular) are created. These areas have as vertices the intersection points of the neighbour edges of V_I, the mid points of the Delaunay edges, M_{Ii}, and the interest point itself, n_I. Therefore, the Voronoï cells are divided in n quadrilateral sub-cell, S_{Ii}, being n the number of neighbour nodes of the node n_I i.e. the nodes within the 'influence-cell' of n_I. Additionally, the sum of the areas occupied by each region has to be equal to the area of the correspondent Voronoï cell.

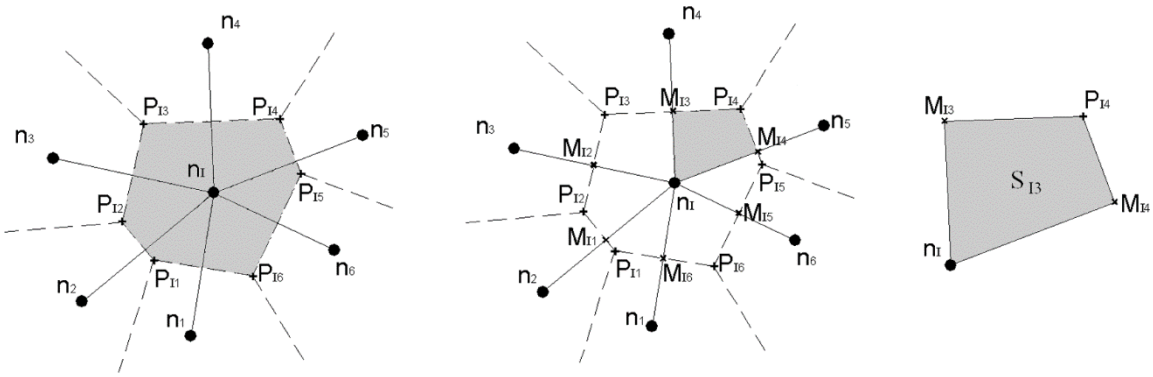

(a) (b) (c)

figure 8 – (a) Voronoï cell and the respective P_{Ii} intersection points. (b) Middle points M_{Ii}. (c) Quadrilateral $\overline{M_{I3}P_{I4}M_{I4}n_I}$. [6]

For a regular mesh, figure 9, the middle points M_{Ii} are coincident with the edge intersection points P_{Ii}. Then, as already mentioned, this leads to the construction of triangles instead of quadrilaterals, as is the case of the irregular mesh.

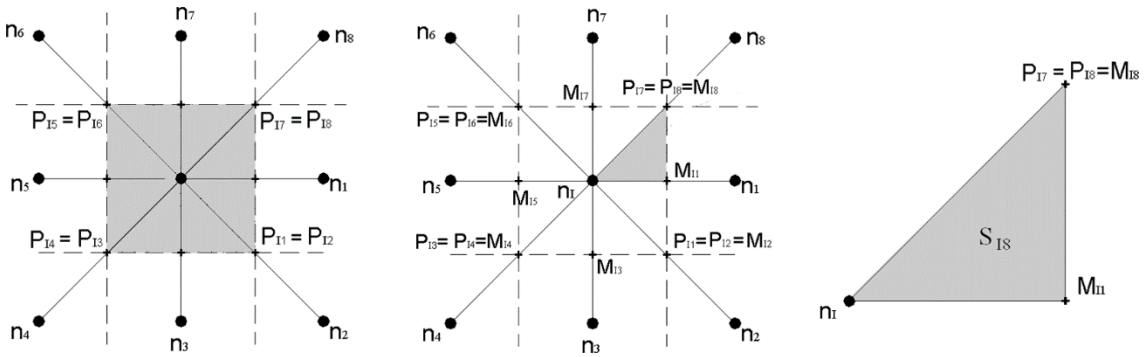

(a) (b) (c)

figure 9 – (a) Voronoï cell and the respective P_{Ii} intersection points. (b) Middle points M_{Ii}. (c) Triangle $\overline{M_{I8}M_{I1}n_I}$. [6]

Based on the Gauss-Legendre numerical integration, the next step is to insert an integration point in the geometric centroid of each sub-cell. This is a '*Order 0*' integration scheme and consists in calculating the Cartesian coordinates of each integration point, figure 10, and perform the integration using the area of the sub-cell as the weight of each integration point, which is equivalent with the 1x1 integration point Gauss-Legendre scheme for triangle and quadrilateral shapes.

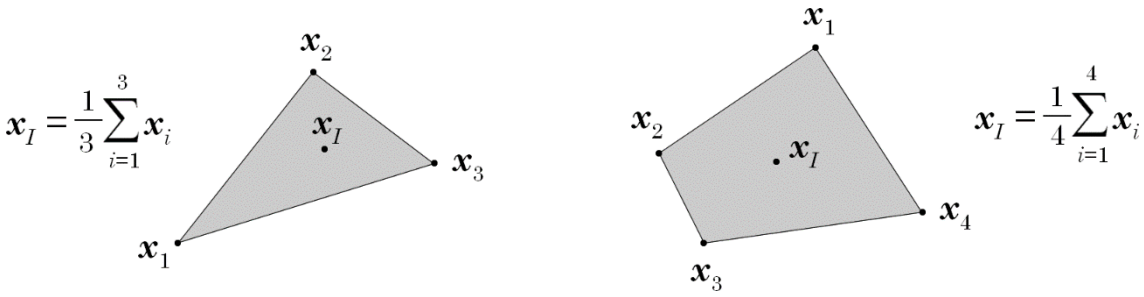

(a) (b)

figure 10 – (a) Triangular shape and (b) Quadrilateral shape and the respective integration points x_I. [6]

The area of the triangle shape sub-cell is defined by,

$$A_I^{\triangle} = \frac{1}{2}\left|\det\begin{bmatrix} x_2 - x_1 & y_2 - y_1 \\ x_3 - x_1 & y_3 - y_1 \end{bmatrix}\right| \tag{36}$$

and for the quadrilateral shape the area is,

$$A_I^{\square} = \frac{1}{2}\left|\det\begin{bmatrix} x_2 - x_1 & y_2 - y_1 \\ x_3 - x_1 & y_3 - y_1 \end{bmatrix} + \det\begin{bmatrix} x_4 - x_1 & y_4 - y_1 \\ x_3 - x_1 & y_3 - y_1 \end{bmatrix}\right| \tag{37}$$

There are other integration schemes that divide each sub-cell into smaller quadrilateral sub-cells to add more integration points to the original sub-cells. Yet, adding more integration points increases the computational cost and, at the same time, does not increase significantly the accuracy of the solution.

Chapter 3

3 Solid Mechanics Fundamentals

In this chapter are presented the solid mechanical fundamentals behind the numerical applications, namely, the weak form formulation mentioned in Chapter 2 that is used in both meshless methods already presented. Thereafter, is established the discrete equation system based on the principle of virtual work, with the shape functions presented in Chapter 2 being used as trial functions.

3.1 General Concepts of Strain Field, Stress Tensor and Equilibrium Equations

For a 3D problem, the Cauchy tensor of the stresses can be defined as,

$$\boldsymbol{\Lambda} = \begin{bmatrix} \sigma_{xx} & \sigma_{xy} & \sigma_{xz} \\ \sigma_{yx} & \sigma_{yy} & \sigma_{yz} \\ \sigma_{zx} & \sigma_{zy} & \sigma_{zz} \end{bmatrix} \tag{38}$$

or as the Voigt notation,

$$\boldsymbol{\sigma} = \left\{ \sigma_{xx} \quad \sigma_{yy} \quad \sigma_{zz} \quad \sigma_{xy} \quad \sigma_{yz} \quad \sigma_{zx} \right\}^{\mathrm{T}} \tag{39}$$

The stress tensor is obtained by multiplying the constitutive matrix, $\mathbf{c}$, (which has the material properties – equation (41)) by the strain tensor that is given by,

$$\boldsymbol{\varepsilon} = \left\{ \varepsilon_{xx} \quad \varepsilon_{yy} \quad \varepsilon_{zz} \quad \gamma_{xy} \quad \gamma_{yz} \quad \gamma_{zx} \right\}^{\mathrm{T}} \tag{40}$$

$$\boldsymbol{\sigma} = \mathbf{c} \cdot \boldsymbol{\varepsilon} \tag{41}$$

where the components of the strain tensor can be calculated form the displacement field that is composed by the displacements along the three directions of the Cartesian coordinate system (i.e. u, v and w, the displacements along the axis x, y and z, respectively),

$$\varepsilon_{xx} = \frac{\partial u}{\partial x} \;\; ; \;\; \varepsilon_{yy} = \frac{\partial v}{\partial y} \;\; ; \;\; \varepsilon_{zz} = \frac{\partial w}{\partial z}$$
$$\gamma_{xy} = \frac{\partial v}{\partial x} + \frac{\partial u}{\partial y} \;\; ; \;\; \gamma_{xz} = \frac{\partial w}{\partial x} + \frac{\partial u}{\partial z} \;\; ; \;\; \gamma_{yz} = \frac{\partial w}{\partial y} + \frac{\partial v}{\partial z} \tag{42}$$

For the same general 3D problem, equilibrium equations can be recognised for an infinitesimal element,

$$\begin{cases} \dfrac{\partial \sigma_{xx}}{\partial x} + \dfrac{\partial \tau_{xy}}{\partial y} + \dfrac{\partial \tau_{xz}}{\partial z} + F_x = 0 \\ \dfrac{\partial \tau_{xy}}{\partial x} + \dfrac{\partial \sigma_{yy}}{\partial y} + \dfrac{\partial \tau_{yz}}{\partial z} + F_y = 0 \\ \dfrac{\partial \tau_{xz}}{\partial x} + \dfrac{\partial \tau_{yz}}{\partial y} + \dfrac{\partial \sigma_{zz}}{\partial z} + F_z = 0 \end{cases} \tag{43}$$

where F_x, F_y and F_z are the body forces applied on the infinitesimal volume along the directions of the Cartesian axis.

3.2 Strong Form and Weak Form Formulations

The differential equations that govern the behaviour of an arbitrary problem in solid mechanics must obey to the equilibrium equations (43) or other kind of equilibrium equations that are the result of simplifications of the equations (43), depending on the problem under study. This is the strong form formulation in solid mechanics which means that the differential equations must be satisfied at every single mathematical point of the domain. Solving these equations, in particular when the problem domain has an intricate shape and the boundary conditions are complex, is difficult.

The weak form formulation is often used to fulfil the insufficiencies in the field of computational mechanics of the strong form. Instead of solving differential equations, the weak form "*produces a set of discretized system of equations in integral form*" [2]. The weak form is established in every integration point which means that the accuracy of the solution depends on the number of nodes that discretises the problem domain. Additionally, the implementation of the boundary conditions is much easier than with the strong form formulation, since they can be applied directly in an arbitrary node.

3.2.1 Galerkin Weak Form

The RPIM and the NNRPIM use the Galerkin weak form formulation to obtain approximated solutions to the strong form formulation. The Galerkin weak form uses an energy principle – the Hamilton's principle.

The Hamilton's principle allows the derivation of the partial differential equations and it states that the "*of all admissible displacement configurations satisfying the compatibility conditions, the essential boundary conditions and the initial and final time conditions, the real solution correspondent configuration is the one which minimizes the Lagrangian functional* L*"* [6],

$$L = T - U + W_f \tag{44}$$

where T the kinetic energy, U is the strain energy and W_f is the work produced by the external forces. The Lagrangian function contains all physical information about the problem and the forces acting on it.

Knowing equation (44) and the idea behind the Hamilton's principle, the equation (45) can be written,

$$\int_{t1}^{t2} \left[\delta T - \delta U + \delta W_f \right] \mathrm{d}t = 0 \tag{45}$$

or substituting (44) in (45),

$$\delta \int_{t1}^{t2} L \, \mathrm{d}t = 0 \tag{46}$$

Considering a solid with a domain Ω and an external boundary Γ, represented in figure figure 11, it is possible to define the surface on which the external forces $\bar{\boldsymbol{t}}$ are applied (natural boundary) and the surface Γ_u where the displacements are constrained (essential boundary).

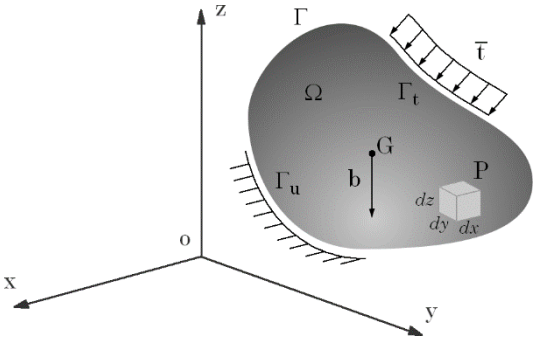

figure 11 – Continuous solid subject to volume forces and external forces. [6]

Now, the energy terms in equation (44) can be defined,

$$T = \tfrac{1}{2}\int_{\Omega} \rho\, \dot{\boldsymbol{u}}^{\mathrm{T}} \dot{\boldsymbol{u}}\, \mathrm{d}\Omega \tag{47}$$

$$U = \tfrac{1}{2}\int_{\Omega} \boldsymbol{\varepsilon}^{\mathrm{T}}\, \boldsymbol{\sigma}\, \mathrm{d}\Omega \tag{48}$$

$$W_f = \int_{\Omega} \boldsymbol{u}^{\mathrm{T}} \boldsymbol{b}\, \mathrm{d}\Omega + \int_{\Gamma_t} \boldsymbol{u}^{\mathrm{T}} \bar{\boldsymbol{t}}\, \mathrm{d}\Gamma \tag{49}$$

where the solid volume is defined by Ω and $\dot{\boldsymbol{u}}$ is the velocity, the solid mass density is defined by ρ, being $\boldsymbol{\varepsilon}$ the strain vector, $\boldsymbol{\sigma}$ the stress, $\boldsymbol{u}$ the displacement, $\boldsymbol{b}$ the body forces and Γ_t the traction boundary where the external forces $\bar{\boldsymbol{t}}$ are applied.

Substituting equations (47), (48) and (49) in equation (44), the Lagrangian functional L can be rewritten as,

$$L = \tfrac{1}{2}\int_{\Omega} \rho\, \dot{\boldsymbol{u}}^{\mathrm{T}} \dot{\boldsymbol{u}}\, \mathrm{d}\Omega - \tfrac{1}{2}\int_{\Omega} \boldsymbol{\varepsilon}^{\mathrm{T}}\, \boldsymbol{\sigma}\, \mathrm{d}\Omega + \int_{\Omega} \boldsymbol{u}^{\mathrm{T}} \boldsymbol{b}\, \mathrm{d}\Omega + \int_{\Gamma_t} \boldsymbol{u}^{\mathrm{T}} \bar{\boldsymbol{t}}\, \mathrm{d}\Gamma \tag{50}$$

and applying the Hamilton's principle,

$$\delta \int_{t_1}^{t_2} \left[\tfrac{1}{2}\int_{\Omega} \rho\, \dot{\boldsymbol{u}}^{\mathrm{T}} \dot{\boldsymbol{u}}\, \mathrm{d}\Omega - \tfrac{1}{2}\int_{\Omega} \boldsymbol{\varepsilon}^{\mathrm{T}}\, \boldsymbol{\sigma}\, \mathrm{d}\Omega + \int_{\Omega} \boldsymbol{u}^{\mathrm{T}} \boldsymbol{b}\, \mathrm{d}\Omega + \int_{\Gamma_t} \boldsymbol{u}^{\mathrm{T}} \bar{\boldsymbol{t}}\, \mathrm{d}\Gamma \right] \mathrm{d}t = 0 \tag{51}$$

Since this work only concerns to static problems, the first term of the integral (51) can be discarded. Moving now the variation operator δ inside the integrals,

$$\int_{t_1}^{t_2} \left[-\tfrac{1}{2}\int_{\Omega} \delta\left(\boldsymbol{\varepsilon}^{\mathrm{T}}\, \boldsymbol{\sigma}\right) \mathrm{d}\Omega + \int_{\Omega} \delta \boldsymbol{u}^{\mathrm{T}} \boldsymbol{b}\, \mathrm{d}\Omega + \int_{\Gamma_t} \delta \boldsymbol{u}^{\mathrm{T}} \bar{\boldsymbol{t}}\, \mathrm{d}\Gamma \right] \mathrm{d}t = 0 \tag{52}$$

The integrand in the first term on equation (52) can be written as follows,

$$\delta\left(\boldsymbol{\varepsilon}^{\mathrm{T}}\,\boldsymbol{\sigma}\right)=\delta\boldsymbol{\varepsilon}^{\mathrm{T}}\,\boldsymbol{\sigma}+\boldsymbol{\varepsilon}^{\mathrm{T}}\,\delta\boldsymbol{\sigma} \tag{53}$$

The terms in equation (53) are scalar, so they can be transposed without affecting the result,

$$\boldsymbol{\varepsilon}^{\mathrm{T}}\,\delta\boldsymbol{\sigma}=\left(\,\boldsymbol{\varepsilon}^{\mathrm{T}}\,\delta\boldsymbol{\sigma}\,\right)^{\mathrm{T}}=\delta\boldsymbol{\sigma}^{\mathrm{T}}\,\boldsymbol{\varepsilon} \tag{54}$$

Using equation (41) and considering that $\boldsymbol{c}^{\mathrm{T}}=\boldsymbol{c}$ (the constitutive matrix is symmetric),

$$\delta\boldsymbol{\sigma}^{\mathrm{T}}\,\boldsymbol{\varepsilon}=\delta\left(\boldsymbol{c}\,\boldsymbol{\varepsilon}\right)^{\mathrm{T}}\,\boldsymbol{\varepsilon}=\delta\,\boldsymbol{\varepsilon}^{\mathrm{T}}\,\boldsymbol{c}^{\mathrm{T}}\,\boldsymbol{\varepsilon}=\delta\,\boldsymbol{\varepsilon}^{\mathrm{T}}\,\boldsymbol{c}\,\boldsymbol{\varepsilon}=\delta\boldsymbol{\varepsilon}^{\mathrm{T}}\,\boldsymbol{\sigma} \tag{55}$$

and substituting (55) in equation (53),

$$\delta\left(\boldsymbol{\varepsilon}^{\mathrm{T}}\,\boldsymbol{\sigma}\right)=2\delta\boldsymbol{\varepsilon}^{\mathrm{T}}\,\boldsymbol{\sigma} \tag{56}$$

Replacing de second term of equation (56) in full (52),

$$\int_{t_1}^{t_2}\left[-\int_{\Omega}\delta\boldsymbol{\varepsilon}^{\mathrm{T}}\boldsymbol{\sigma}\,\mathrm{d}\Omega+\int_{\Omega}\delta\boldsymbol{u}^{\mathrm{T}}\boldsymbol{b}\,\mathrm{d}\Omega+\int_{\Gamma_{\mathrm{t}}}\delta\boldsymbol{u}^{\mathrm{T}}\overline{\boldsymbol{t}}\,\mathrm{d}\Gamma\right]\mathrm{d}t=0 \tag{57}$$

For the equation (57) be satisfied for all possible $\boldsymbol{u}$ for any initial and final time, t_1 and t_2, the integrand must be null which leads to the 'Galerkin weak form' equation,

$$-\int_{\Omega}\delta\boldsymbol{\varepsilon}^{\mathrm{T}}\boldsymbol{\sigma}\,\mathrm{d}\Omega+\int_{\Omega}\delta\boldsymbol{u}^{\mathrm{T}}\boldsymbol{b}\,\mathrm{d}\Omega+\int_{\Gamma_{\mathrm{t}}}\delta\boldsymbol{u}^{\mathrm{T}}\overline{\boldsymbol{t}}\,\mathrm{d}\Gamma=0 \tag{58}$$

Considering the stress-strain relation enunciated by equation (41) and rewriting equations (42) as a multiplication of a differential operator, $\boldsymbol{L}$, by the generalized displacements, $\boldsymbol{u}$, i.e. $\boldsymbol{\varepsilon}=\boldsymbol{L}\,\boldsymbol{u}$, equation (58) can be written in terms of displacement,

$$\int_{\Omega}\delta\left(\boldsymbol{L}\,\boldsymbol{u}\right)^{\mathrm{T}}\boldsymbol{c}\left(\boldsymbol{L}\,\boldsymbol{u}\right)\mathrm{d}\Omega-\int_{\Omega}\delta\boldsymbol{u}^{\mathrm{T}}\boldsymbol{b}\,\mathrm{d}\Omega-\int_{\Gamma_{\mathrm{t}}}\delta\boldsymbol{u}^{\mathrm{T}}\overline{\boldsymbol{t}}\,\mathrm{d}\Gamma=0 \tag{59}$$

3.3 Discrete System of Equations

For a solid in equilibrium, the principle of virtual work states that the total virtual work done by the body internal stresses and the applied external forces on a system in static equilibrium is zero for a set of infinitesimal virtual displacements from equilibrium. The discrete system of equations in meshless methods is obtained based on this principle.

Considering again equation (1),

$$\boldsymbol{u}(\boldsymbol{x}_{\mathrm{I}}) = \sum_{j=1}^{n} \varphi_j(\boldsymbol{x}_{\mathrm{I}})\, \boldsymbol{u}_j \tag{60}$$

Then, by the principle of the virtual work, virtual displacements of nodes within the 'influence-domain' or 'influence-cell' of an interest point $\boldsymbol{x}_{\mathrm{I}}$ cause a virtual displacement in the integration point itself, and it can be interpolated considering the interpolation functions already presented in Chapter 2,

$$\delta\boldsymbol{u}(\boldsymbol{x}_{\mathrm{I}}) = \sum_{j=1}^{n} \varphi_j(\boldsymbol{x}_{\mathrm{I}})\, \delta\boldsymbol{u}_j \tag{61}$$

which can be combined with equations (59) and (60),

$$\begin{aligned} \int_{\Omega} \left(\sum_{j=1}^{n} \varphi_j(\boldsymbol{x}_{\mathrm{I}})\, \delta\boldsymbol{u}_j \right)^{\mathrm{T}} \boldsymbol{L}^{\mathrm{T}} \boldsymbol{c}\, \boldsymbol{L} \left(\sum_{j=1}^{n} \varphi_j(\boldsymbol{x}_{\mathrm{I}})\, \boldsymbol{u}_j \right) \mathrm{d}\Omega - \int_{\Omega} \left(\sum_{j=1}^{n} \varphi_j(\boldsymbol{x}_{\mathrm{I}})\, \delta\boldsymbol{u}_j \right)^{\mathrm{T}} \boldsymbol{b}\, \mathrm{d}\Omega - \\ - \int_{\Gamma_{\mathrm{t}}} \left(\sum_{j=1}^{n} \varphi_j(\boldsymbol{x}_{\mathrm{I}})\, \delta\boldsymbol{u}_j \right)^{\mathrm{T}} \bar{\boldsymbol{t}}\, \mathrm{d}\Gamma = 0 \end{aligned} \tag{62}$$

The equation above can be rewritten as a matrix equation, eliminating the summations. So, defining a general matrix of the interpolations functions for a 3D problem as,

$$\boldsymbol{\varphi}(\boldsymbol{x}) = \begin{bmatrix} \varphi_1(x) & 0 & 0 & \varphi_2(x) & 0 & 0 & \ldots & \varphi_{\mathrm{n}}(x) & 0 & 0 \\ 0 & \varphi_1(x) & 0 & 0 & \varphi_2(x) & 0 & \ldots & 0 & \varphi_{\mathrm{n}}(x) & 0 \\ 0 & 0 & \varphi_1(x) & 0 & 0 & \varphi_2(x) & \ldots & 0 & 0 & \varphi_{\mathrm{n}}(x) \end{bmatrix} \tag{63}$$

which has 3 rows (because it is considered, as an example, a 3D problem with only three degrees of freedom) and 3n columns, being n the number of nodes that belong to the 'influence-domain' or 'influence-cell' of the interest point x_I. Defining also a general differential operator $\boldsymbol{L}$ for a 3D problem with $\boldsymbol{\varepsilon} = \boldsymbol{L}\boldsymbol{u}$ and $\boldsymbol{u} = \{u(x,y,z), v(x,y,z), w(x,y,z)\}^T$,

$$\boldsymbol{L} = \begin{bmatrix} \frac{\partial}{\partial x} & 0 & 0 \\ 0 & \frac{\partial}{\partial y} & 0 \\ 0 & 0 & \frac{\partial}{\partial z} \\ \frac{\partial}{\partial y} & \frac{\partial}{\partial x} & 0 \\ 0 & \frac{\partial}{\partial z} & \frac{\partial}{\partial y} \\ \frac{\partial}{\partial z} & 0 & \frac{\partial}{\partial x} \end{bmatrix} \tag{64}$$

the equation (62) takes the form of,

$$\delta\boldsymbol{u} \cdot \int_\Omega \left[\left(\boldsymbol{\varphi}(\boldsymbol{x}_I)\right)^T \boldsymbol{L}^T \right] \cdot \boldsymbol{c} \cdot \left[\boldsymbol{L}\,\boldsymbol{\varphi}(\boldsymbol{x}_I) \right] d\Omega \cdot \boldsymbol{u} - \delta\boldsymbol{u} \cdot \int_\Omega \boldsymbol{\varphi}(\boldsymbol{x}_I)^T \boldsymbol{b}\, d\Omega - \delta\boldsymbol{u} \cdot \int_{\Gamma_t} \boldsymbol{\varphi}(\boldsymbol{x}_I)^T \bar{\boldsymbol{t}}\, d\Gamma = 0 \tag{65}$$

where $\boldsymbol{u}$ is the vector of the nodal displacements of the nodes inside the 'influence-domain/cell', and is given by,

$$\boldsymbol{u} = \{u_1, v_1, w_1, u_2, v_2, w_2, \ \ldots\ u_n, v_n, w_n\}^T \tag{66}$$

A deformability matrix, $\boldsymbol{B}(\boldsymbol{x}_I)$ can now be defined as the multiplication of the matrixes $\boldsymbol{L}$ and $\boldsymbol{\varphi}(\boldsymbol{x}_I)$,

$$\boldsymbol{B}(\boldsymbol{x}_I)=\boldsymbol{L}\cdot\boldsymbol{\varphi}(\boldsymbol{x}_I)=\begin{bmatrix} \dfrac{\partial\varphi_i(\boldsymbol{x}_I)}{\partial x} & 0 & 0 & \dfrac{\partial\varphi_i(\boldsymbol{x}_I)}{\partial y} & 0 & \dfrac{\partial\varphi_i(\boldsymbol{x}_I)}{\partial z} \\ 0 & \dfrac{\partial\varphi_i(\boldsymbol{x}_I)}{\partial y} & 0 & \dfrac{\partial\varphi_i(\boldsymbol{x}_I)}{\partial x} & \dfrac{\partial\varphi_i(\boldsymbol{x}_I)}{\partial z} & 0 \\ 0 & 0 & \dfrac{\partial\varphi_i(\boldsymbol{x}_I)}{\partial z} & 0 & \dfrac{\partial\varphi_i(\boldsymbol{x}_I)}{\partial y} & \dfrac{\partial\varphi_i(\boldsymbol{x}_I)}{\partial x} \end{bmatrix}_i^T \tag{67}$$

being $i=\{1,2,...n\}$ the order of the node within the 'influence-domain' (or 'influence-cell') of $\boldsymbol{x}_I$.

Finally rearranging the equation (65) and replacing $\boldsymbol{L}\cdot\boldsymbol{\varphi}(\boldsymbol{x}_I)$ by $\boldsymbol{B}(\boldsymbol{x}_I)$,

$$\delta\boldsymbol{u}\cdot\left[\int_\Omega \boldsymbol{B}(\boldsymbol{x}_I)^T\boldsymbol{c}\,\boldsymbol{B}(\boldsymbol{x}_I)\,d\Omega\cdot\boldsymbol{u}-\int_\Omega\boldsymbol{\varphi}(\boldsymbol{x}_I)\cdot\boldsymbol{b}\,d\Omega-\int_{\Gamma_t}\boldsymbol{\varphi}(\boldsymbol{x}_I)\cdot\bar{\boldsymbol{t}}\,d\Gamma\right]=0 \tag{68}$$

which results in the linear equation (69),

$$\int_\Omega \boldsymbol{B}(\boldsymbol{x}_I)^T\boldsymbol{c}\,\boldsymbol{B}(\boldsymbol{x}_I)\,d\Omega\cdot\boldsymbol{u}-\int_\Omega\boldsymbol{\varphi}(\boldsymbol{x}_I)\cdot\boldsymbol{b}\,d\Omega-\int_{\Gamma_t}\boldsymbol{\varphi}(\boldsymbol{x}_I)\cdot\bar{\boldsymbol{t}}\,d\Gamma=0 \tag{69}$$

that represents the local static equilibrium of the 'influence-domain/cell' of the interest point $\boldsymbol{x}_I$, being the integral in the first term the stiffness matrix, $\boldsymbol{K}$, $\boldsymbol{u}$ the nodal displacement vector and the sum of the other two terms the global force vector, $\boldsymbol{F}$,

$$\boldsymbol{K}\cdot\boldsymbol{u}=\boldsymbol{F} \tag{70}$$

By assembling all the local stiffness matrixes and force vectors considering the nodal connectivity imposed by the overlap of the 'influence-domains/cells', a global discrete system of equations similar to (70) can be found. The strain state at the interest point $\boldsymbol{x}_I$ can easily be calculated form the solution of equation (70),

$$\boldsymbol{\varepsilon}(\boldsymbol{x}_I)=\boldsymbol{B}(\boldsymbol{x}_I)\cdot\boldsymbol{u} \tag{71}$$

being the stress state obtained from equation (41).

As final remarks, it can be concluded that, knowing the body and external forces applied to a solid and the boundary conditions, the meshless method, in terms of computation, follows these main steps:

i. Discretization of the problem domain into a nodal mesh;

ii. Creation of an integration mesh: in the RPIM it is created a nodal independent background mesh and in the NNRPIM, using the Voronoï diagram and the Delaunay triangulation, is created a nodal dependent integration mesh;

iii. Definition of the 'influence-domains' or 'influence-cells' for each integration points, whose overlap ensures the nodal connectivity;

iv. Determination of the interpolation functions considering the nodes within the 'influence-domain/cell' of each integration point;

v. Determination of the deformability matrixes in every single interest point, x_I, followed by the calculus of local stiffness matrixes using the Gaussian integration scheme presented in Chapter 2, being the integrand function $\boldsymbol{B}(\boldsymbol{x}_I)^T \boldsymbol{c}(\boldsymbol{x}_I)\, \boldsymbol{B}(\boldsymbol{x}_I)$;

vi. Construction of the global stiffness matrix considering the nodal connectivity already imposed;

vii. Determination of the global force vector, which is obtained by the overlap of the local force vectors calculated in each 'influence-domain/cell':

viii. Imposition of the essential boundaries which be directly applied in the stiffness, $\boldsymbol{K}$, matrix, since the interpolation functions possesses the delta Kronecker property;

ix. Solving the system of equations (68) and finally determine the displacements.

Chapter 4

4 Plates Theory

In this Chapter, are stated a background about the theories for plates and the purpose of the existence of high-order shear deformation theories (HSDTs). Then, the first two theories created are presented: the Classical Plate Theory (CLPT) by Krichhoff-Love and the First-Order Shear Deformation Theory (FSDT) by Reissner-Mindlin. Afterwards, the HSDTs selected to be implemented are described. For each HSDT, are defined the displacement and strain fields and deducted all the fundamental matrixes required for the meshless formulation and the corresponding implementation.

4.1 Background

Plates are very important structural elements in engineering since they are major load carrying parts, being predominantly flexure requested (which often causes significant compression forces and shear loading). They are very useful in the fields of aeronautics, land and naval engineering, especially when made by laminated composites, essentially because of their high specific modulus and strength in fibres direction, although they have a very weak interfacial strength. Because of this disadvantage, interlaminar delamination may occur, being this the most frequent failure mode. As a consequence, it is necessary to evaluate the interlaminar stresses and create efficient computational models that can predict the behaviour of this structural element and be able to archive a safe design.

There are various theories that claim to describe the static behaviour of such plates, many of them are based on displacement approximations and simplifying a 3D problem into a 2D one, which leads to the consideration of a plate as a bidimensional solid. [35]. The first one was proposed by Gustav Kirchhoff and it is an extension of the Euler-Bernoulli beam theory. It was suggested in the middle of the 19th century and then developed by Augustus-Love in 1888 and, because of that, is now known as the Kirchhoff-Love plate theory or the Classical Plate Theory (CLPT). Kirchhoff enunciated that, when

a plate is subjected to a bending load, (1) straight lines perpendicular to the mid-surface before deformation remain straight after deformation, (2) straight lines normal to the mid-surface remain normal to the mid-surface after deformation, (3) the plate does not experience elongation along the thickness. The assumptions of Kirchhoff lead to the exclusion of the shear effects, which constitutes an incongruity of the theory. Since the CLPT neglects the shear stresses, its application is not indicated to laminated composite plates, being suitable only for thin plates (it underestimates deflection and overestimates natural frequencies and buckling load for thick plates).

Almost 100 years later, Mindlin [36] developed the First-Order Shear Deformation Theory (FSDT), which considers shear effects. The assumptions of Mindlin are extensions of the Kirchhoff ones but with a main difference: straight lines perpendicular to the mid-surface before deformation remain straight but not necessarily normal to the mid-surface after deformation. A few years after Mindlin, Reissner developed a plate theory also including shear effects. Both are similar, and they are often referred as the Reissner-Mindlin plate theory. In the Reissner-Mindlin plate theory, the displacement field is obtained considering that the in-plane displacements are linearly distributed through the plate thickness, which leads to the transverse shear stresses being constant across the plate thickness, so the condition that on the plate faces the shear stresses are zero is not satisfied. Thus, are needed shear correction factors comparable to those needed for the Timoshenko beam theory. These shear correction factors are difficult to accurately evaluate for a general case when the FSDT is applied to composite laminated plates.[35]

Approximately in 1980, Higher-Order Shear Deformation Theories (HSDTs) were proposed to respond to some insufficiencies of the CLPT and the FSDT when applied to thick/thin laminated composite plates (figure 12 shows the differences between CLPT, FSDT and HSDTs). These theories intend to properly approximate the nonlinear distribution of transverse shear strains along the plate thickness, which is a major step forward to actually determine the stress state in each point of the laminate and, in particular, between layers.

Many higher order shear deformation theories have been developed in the last 30 years, being the one of J. N. Reddy [26] the most popular. Reddy considers a cubic variation of the in-plane displacement along the thickness of the plate, resulting in a parabolic variation of the shear stresses. In 2007, Guangyu Shi [27] presented a new shear deformation theory for plates, which

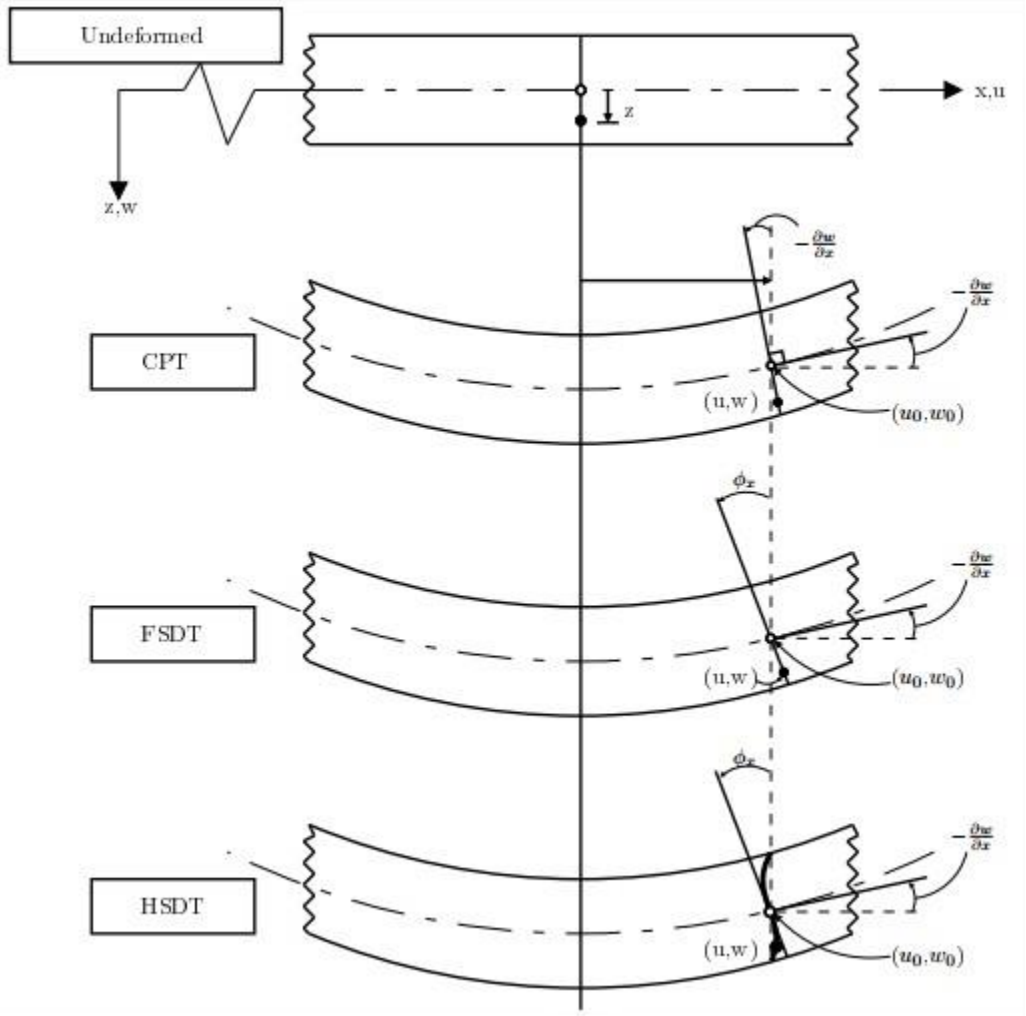

figure 12 – Undeformed and deformed section of an edge of a plate in different plate theories. [35]

similar to Reddy's in the sense that both are Third-Order Shear Deformation Theories (TSDTs). But the Ambartsumian [28] theory was the first proposed HSDT and it was used firstly in the analysis of anisotropic plates and shallow shells. This is also a TSDT and was later adapted for composite materials.

Although the first three HSDT presented in the last paragraphs are TSDTs, there are many others that predicts the variation of the in-plane displacements along the thickness with different nonlinear functions, such as exponential HSDTs by Karama [30] and Aydogdu [31], trigonometric HSDTs by Touratier [29] and Grover [37], combinations of trigonometric and exponential HSDT by Mantari [33], hyperbolic HSDT by Soldatos [32], Five-Order Shear Deformation Theory by Nguyen-Xuan [38], etc.

Though the higher-order theories "*can represent the kinematics better, may not involve shear correction factors and can yield more accurate interlaminar stress distributions, they contain higher-order stress resultants*

that are difficult to interpret physically and require considerably more computational effort". [35] This means that these theories are meant to be used only when necessary.

4.2 Classical Plate Theory

4.2.1 Kirchhoff Assumptions

Consider the plate represented in figure 13, with thickness h, associted to the Cartesian axis and carring a bending load q,

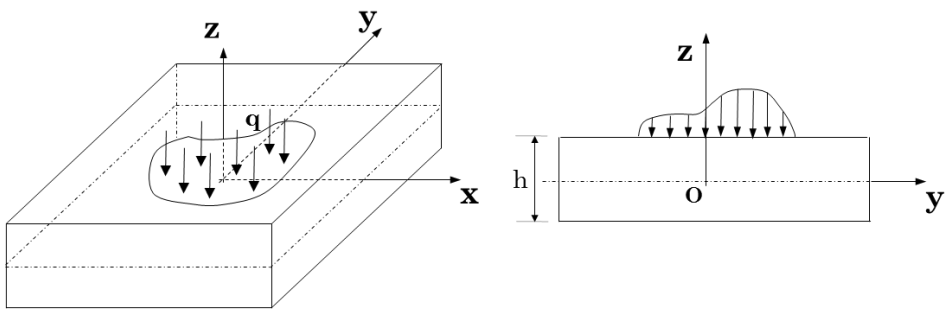

figure 13 – General plate subjected to a bending load.

Consider also the mid-surface represented with dash-dot that divides the plate by its thickness and contains the origin of the coordinated axis.

The Kirchhoff assumptions or hypotheses considered by the Classical Plate Theory were detailed by Eduard Ventsel and Theodor Krauthammer as [39]:

i. The material of the plate is elastic, homogeneous, and isotropic;
ii. The plate is initially flat;
iii. The deflection (the normal component of the displacement vector, w) of the mid-surface is small compared with the thickness of the plate. The slope of the deflected surface is therefore very small and the square of the slope is a negligible quantity in comparison with unity;
iv. The straight lines, initially normal to the mid-surface before bending, remain straight and normal to it during the deformation, and the length of such elements is not altered. This means that the vertical shear strains, γ_{xz} and γ_{yz} are negligible and the normal strain, ε_{zz} may also be omitted. This assumption is referred to as the "hypothesis of straight normals";

v. The stress normal to the mid-surface, σ_{zz}, is small compared with the other stress components and may be neglected in the stress–strain relations;

vi. Since the displacements of a plate are small, it is assumed that the mid-surface remains unstrained after bending (i.e. $\varepsilon_{xx} = \varepsilon_{yy} = \gamma_{xy} = 0$ at $z = 0$).

4.2.2 Kinematic Relations

Considering the assumptions of Kirchhoff, the displacement field can be defined, observing also figure 12,

$$\begin{cases} u(x,y,z) = -z \cdot \phi_x = -z \cdot \dfrac{\partial w(x,y)}{\partial x} \\ v(x,y,z) = -z \cdot \phi_y = -z \cdot \dfrac{\partial w(x,y)}{\partial y} \\ w(x,y,z) = w(x,y) \end{cases} \tag{72}$$

where the displacements u and v of a point located at a distance z from the mid-surface are dependent of rotations $\dfrac{\partial w(x,y)}{\partial x}$ and $\dfrac{\partial w(x,y)}{\partial z}$ relative to the axis Ox and Oy, respectively, and the distance z itself.

In view of the fourth assumption of Kirchhoff, a simple strain field can be obtained from the displacement field,

$$\begin{cases} \varepsilon_{xx} = \dfrac{\partial u}{\partial x} = -z \cdot \dfrac{\partial^2 w(x,y)}{\partial x^2} \\ \varepsilon_{yy} = \dfrac{\partial v}{\partial y} = -z \cdot \dfrac{\partial^2 w(x,y)}{\partial y^2} \\ \gamma_{xy} = \dfrac{\partial v}{\partial x} + \dfrac{\partial u}{\partial y} = -2z \cdot \dfrac{\partial^2 w(x,y)}{\partial x \partial y} \end{cases} \tag{73}$$

4.2.3 Constitutive Equations

The nonzero bending strains of equation (72) produce bending stresses σ_{xx}, σ_{yy} and τ_{xy}. For an isotropic and homogeneous plate in plane stress state

(because CLPT is applied to thin plates), the constitutive relations can be written considering the generalized Hooke's law,

$$\begin{Bmatrix} \sigma_{xx} \\ \sigma_{yy} \\ \tau_{xy} \end{Bmatrix} = \begin{bmatrix} \frac{E}{1-\nu^2} & \frac{\nu E}{1-\nu^2} & 0 \\ \frac{\nu E}{1-\nu^2} & \frac{E}{1-\nu^2} & 0 \\ 0 & 0 & G \end{bmatrix} \cdot \begin{Bmatrix} \varepsilon_{xx} \\ \varepsilon_{yy} \\ \gamma_{xy} \end{Bmatrix} \tag{74}$$

where E is the Young modulus, ν the Poisson coefficient and $G = \frac{E}{2(1+\nu)}$ the shear modulus.

4.3 First-Order Shear Deformation Theory (Reisser-Mindlin Plate Theory)

The First-Order Shear Deformation Theory (FSDT) was the first plate theory included in the algorithms of the RPIM and the NNRPIM whose procedures were already presented in Chapter 2. Although it isn't a high-order shear deformation theory, the FSDT served as a control of the first results obtained by the two algorithms developed, since many solutions of different kinds of composite laminated plates computed with this theory can be found in literature [26].

In the following subchapters, the FSDT is presented using the Mindlin assumptions. Then, the kinematic relations are established, as well as the constitutive equations written for each layer of a general laminate. Finally, from the strain field, the deformability matrixes are deducted and specifically organized for an easier implementation of the algorithms, and the constitutive matrixes are homogenised for the construction of the global stiffness matrix.

4.3.1 Mindlin Assumptions

The Reissner-Mindlin plate theory [36] emerges because of the existence of plates that cannot be considered as thin because the effects of transverse shear stresses can be significant. For this type of plates, the hypotheses of

Kirchhoff considered valid for thin plates are no longer admissible. In case of small transverse displacements (when compared to the thickness of the plate), it is possible to modify the simplified assumptions of Kirchhoff in order to include the possibility of the plate to be thick.

Considering the same plate and coordinate system of figure 12, the assumptions of Reissner-Mindlin that are considered valid for thick and moderately thick plates (used for the purpose of representing the displacement field and stresses in plates subjected to normal actions to the mid-surface) are:

i. For small deformations, the mid-surface is plane and undeformed (i.e. $\varepsilon_{xx} = \varepsilon_{yy} = \gamma_{xy} = 0$ at $z = 0$);

ii. The straight lines, initially normal to the mid-surface before bending, remain straight but not necessarily normal to it during the deformation;

iii. The stress normal to the mid-surface, σ_{zz}, is small compared with the other stress components and may be neglected in the stress–strain relations (and $\varepsilon_{zz} = 0$).

4.3.2 Kinematic Relations

Considering again the schematic representation of the deformed plate with the FSDT in figure 12, and the hypothesis (ii) set out in 4.3.1., the displacement field can be determined,

$$\begin{cases} u(x,y,z) = u_0(x,y) - z \cdot \phi_x \\ v(x,y,z) = v_0(x,y) - z \cdot \phi_y \\ w(x,y,z) = w_0(x,y) \end{cases} \tag{75}$$

where ϕ_x and ϕ_y are the plane's rotations of plate in relation to the axis Ox and Oy, respectively. Note that these rotations, by considering that straight lines (initially normal to the plate) do not remain necessarily normal to it during deformation, are now independent of the transverse displacement, $w(x,y)$.

By derivation of the displacement field, the strain tensor can be found,

$$\begin{cases} \varepsilon_{xx} = \dfrac{\partial u}{\partial x} = \dfrac{\partial u_0}{\partial x} - z \cdot \dfrac{\partial \phi_x}{\partial x} \\ \varepsilon_{yy} = \dfrac{\partial v}{\partial y} = \dfrac{\partial v_0}{\partial x} - z \cdot \dfrac{\partial \phi_y}{\partial y} \\ \gamma_{xy} = \dfrac{\partial v}{\partial x} + \dfrac{\partial u}{\partial y} = \dfrac{\partial v_0}{\partial x} + \dfrac{\partial u_0}{\partial y} - z \cdot \left(\dfrac{\partial \phi_x}{\partial y} + \dfrac{\partial \phi_y}{\partial x} \right) \\ \gamma_{yz} = \dfrac{\partial v}{\partial z} + \dfrac{\partial w}{\partial y} = -\phi_y + \dfrac{\partial w}{\partial y} \\ \gamma_{xz} = \dfrac{\partial u}{\partial z} + \dfrac{\partial w}{\partial x} = -\phi_x + \dfrac{\partial w}{\partial x} \\ \varepsilon_{zz} = 0 \end{cases} \tag{76}$$

The degrees of freedom (DOFs) considered for the FSDT and the other theories to be introduced in a next subchapter will be $u_0, v_0, w, \phi_x, \phi_y$ (three displacements and two rotations).

4.3.3 Constitutive Equations and Stress Resultants

Consider the following composite laminated plate with n layers, each one with an orientation θ of its plies, and represented in the same coordinate system introduced before,

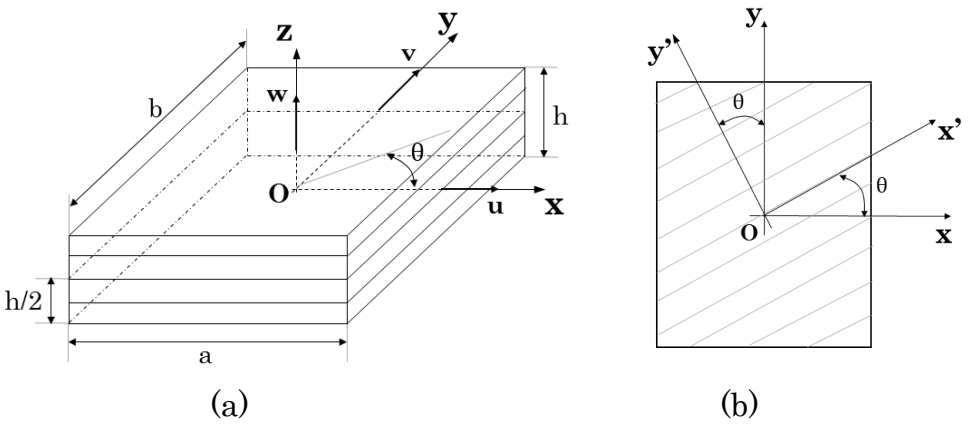

figure 14 – (a) Composite laminated plate with n layers, each one with an orientation θ of its fibres; (b) View from the top of the local axis, $Ox'y'$.

For each layer, it is possible to define a local constitutive matrix, $\boldsymbol{c}^i$ regarding the local coordinated system $Ox'y'$,

$$\boldsymbol{c}^{i} = \begin{bmatrix} \frac{1}{E_1} & \frac{-\nu_{21}}{E_2} & 0 & 0 & 0 \\ \frac{-\nu_{12}}{E_1} & \frac{1}{E_2} & 0 & 0 & 0 \\ 0 & 0 & \frac{1}{G_{12}} & 0 & 0 \\ 0 & 0 & 0 & \frac{1}{k_{sh}G_{23}} & 0 \\ 0 & 0 & 0 & 0 & \frac{1}{k_{sh}G_{31}} \end{bmatrix}^{-1} \tag{77}$$

where E_1 is the Young modulus along the fibres direction, E_2 is the Young modulus along the normal of the fibres direction, υ_{ij} is the Poisson ratio which characterizes the deformation rate in direction j when a force is applied in direction i, G_{ij} is the shear modulus which characterizes the variation angle between directions i and j, being 3 the direction along the thickness of the lamina. Due to symmetry, it can also be concluded that,

$$E_i \upsilon_{ji} = E_j \upsilon_{ij} \tag{78}$$

The constant k_{sh} in equation (77) is the shear correction factor which was considered to be $5/6$. In the FSDT, shear correction factors are introduced to correct for the discrepancy between the actual transverse shear-force distributions and those computed using the kinematics relations of FSDT. [40].

The constitutive matrix $\boldsymbol{c}^{i}$ can be transferred to the global coordinate system, applying the transformation of coordinates equation, resulting in the transformed constitutive matrix, $\boldsymbol{c}_k$,

$$\boldsymbol{c}_k = \boldsymbol{T}^{T} \boldsymbol{c}^{i} \boldsymbol{T} \tag{79}$$

$$\boldsymbol{T} = \begin{bmatrix} \cos^2\theta & \sin^2\theta & -\sin(2\theta) & 0 & 0 \\ \sin^2\theta & \cos^2\theta & \sin(2\theta) & 0 & 0 \\ \sin\theta\cdot\cos\theta & -\sin\theta\cdot\cos\theta & \cos^2\theta-\sin^2\theta & 0 & 0 \\ 0 & 0 & 0 & \cos\theta & -\sin\theta \\ 0 & 0 & 0 & \sin\theta & \cos\theta \end{bmatrix} \tag{80}$$

Thus, each lamina has its constitutive matrix. The stress tensor can now be calculated using equation (41).

For bending plates, especially in the case of composite laminated plates, it is convenient to define stresses in terms of equivalent forces acting at the mid-surface. Thus, considering infinitesimal increments of laminas with dz thickness, the stress resultants can be calculated taking into account the layer distribution represented in figure 15.

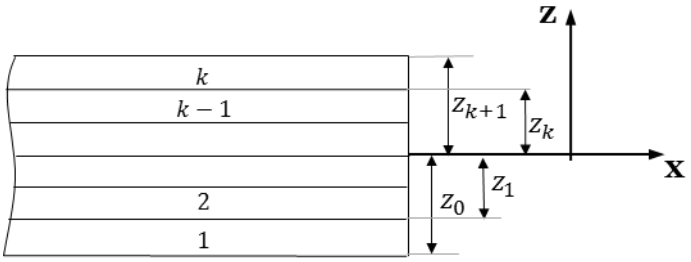

figure 15 – Composite laminate layer distribution.

$$M_{xx} = \sum_{i=1}^{k} \int_{z_{i-1}}^{z_i} z \cdot \sigma_{xx}\, dz \quad ; \quad N_{xx} = \sum_{i=1}^{k} \int_{z_{i-1}}^{z_i} \sigma_{xx}\, dz$$

$$M_{yy} = \sum_{i=1}^{k} \int_{z_{i-1}}^{z_i} z \cdot \sigma_{yy}\, dz \quad ; \quad N_{yy} = \sum_{i=1}^{k} \int_{z_{i-1}}^{z_i} \sigma_{yy}\, dz \tag{81}$$

$$M_{xy} = \sum_{i=1}^{k} \int_{z_{i-1}}^{z_i} z \cdot \tau_{xy}\, dz \quad ; \quad N_{xy} = \sum_{i=1}^{k} \int_{z_{i-1}}^{z_i} \tau_{xy}\, dz$$

$$V_x = \sum_{i=1}^{k} \int_{z_{i-1}}^{z_i} \tau_{xz}\, dz \tag{82}$$

$$V_y = \sum_{i=1}^{k} \int_{z_{i-1}}^{z_i} \tau_{yz}\, dz$$

being M_{xx} and M_{yy} the bending moments, M_{xy} the yaw moment, N_{xx}, N_{yy} and N_{xy} the membrane or in-plane forces (which are zero for symmetric laminated plates) and finally V_x and V_y the shear forces. k is the number of layers of the considered laminated plate. These stress resultants are easily calculated in a computational algorithm after the determination of the stresses.

4.3.4 Deformability Matrixes

To establish the deformability matrix for the FSDT that will be used in determination of the stiffness matrix, firstly it is necessary to define the differential operator $\boldsymbol{L}$ based on the equations (76), so that $\boldsymbol{\varepsilon} = \boldsymbol{L} \cdot \boldsymbol{u}$, being $\boldsymbol{u} = \left\{ u_0, v_0, w, \phi_x, \phi_y \right\}^{\mathrm{T}}$,

$$\boldsymbol{L} = \begin{bmatrix} \partial/\partial x & 0 & 0 & -z \cdot \partial/\partial x & 0 \\ 0 & \partial/\partial y & 0 & 0 & -z \cdot \partial/\partial y \\ \partial/\partial y & \partial/\partial x & 0 & -z \cdot \partial/\partial y & -z \cdot \partial/\partial x \\ 0 & 0 & \partial/\partial y & 0 & -1 \\ 0 & 0 & \partial/\partial x & -1 & 0 \end{bmatrix} \tag{83}$$

The deformability matrix comes, as defined in Chapter 3, as,

$$\boldsymbol{B}(\boldsymbol{x}_I) = \boldsymbol{L} \cdot \boldsymbol{\varphi}(\boldsymbol{x}_I) \tag{84}$$

being now $\boldsymbol{\varphi}(\boldsymbol{x}_I)$ a $[5 \times 5n]$ matrix, since there are five DOFs. n is the number of nodes inside the 'influence-domain/cell',

$$\boldsymbol{\varphi}_i(\boldsymbol{x}_I) = \begin{bmatrix} \varphi_i(\boldsymbol{x}_I) & 0 & 0 & 0 & 0 \\ 0 & \varphi_i(\boldsymbol{x}_I) & 0 & 0 & 0 \\ 0 & 0 & \varphi_i(\boldsymbol{x}_I) & 0 & 0 \\ 0 & 0 & 0 & \varphi_i(\boldsymbol{x}_I) & 0 \\ 0 & 0 & 0 & 0 & \varphi_i(\boldsymbol{x}_I) \end{bmatrix}_i \quad i = \left\{ 1, 2, \ldots n \right\} \tag{85}$$

Combining equations (83), (84) and (85),

$$\boldsymbol{B}_i(\boldsymbol{x}_I) = \begin{bmatrix} \dfrac{\partial \varphi_i(\boldsymbol{x}_I)}{\partial x} & 0 & 0 & -z \cdot \dfrac{\partial \varphi_i(\boldsymbol{x}_I)}{\partial x} & 0 \\ 0 & \dfrac{\partial \varphi_i(\boldsymbol{x}_I)}{\partial y} & 0 & 0 & -z \cdot \dfrac{\partial \varphi_i(\boldsymbol{x}_I)}{\partial y} \\ \dfrac{\partial \varphi_i(\boldsymbol{x}_I)}{\partial y} & \dfrac{\partial \varphi_i(\boldsymbol{x}_I)}{\partial x} & 0 & -z \cdot \dfrac{\partial \varphi_i(\boldsymbol{x}_I)}{\partial y} & -z \cdot \dfrac{\partial \varphi_i(\boldsymbol{x}_I)}{\partial x} \\ 0 & 0 & \dfrac{\partial \varphi_i(\boldsymbol{x}_I)}{\partial y} & 0 & -\varphi_i(\boldsymbol{x}_I) \\ 0 & 0 & \dfrac{\partial \varphi_i(\boldsymbol{x}_I)}{\partial x} & -\varphi_i(\boldsymbol{x}_I) & 0 \end{bmatrix}_i \quad i = \left\{ 1, 2, \ldots n \right\} \tag{86}$$

that can be divided into two distinct matrixes such that $\boldsymbol{B}(\boldsymbol{x}_I) = \boldsymbol{B}_0(\boldsymbol{x}_I) + z \cdot \boldsymbol{B}_1(\boldsymbol{x}_I)$,

$$\boldsymbol{B}^i{}_0(\boldsymbol{x}_I) = \begin{bmatrix} \frac{\partial \varphi_i(\boldsymbol{x}_I)}{\partial x} & 0 & 0 & 0 & 0 \\ 0 & \frac{\partial \varphi_i(\boldsymbol{x}_I)}{\partial y} & 0 & 0 & 0 \\ \frac{\partial \varphi_i(\boldsymbol{x}_I)}{\partial y} & \frac{\partial \varphi_i(\boldsymbol{x}_I)}{\partial x} & 0 & 0 & 0 \\ 0 & 0 & \frac{\partial \varphi_i(\boldsymbol{x}_I)}{\partial y} & 0 & -\varphi_i(\boldsymbol{x}_I) \\ 0 & 0 & \frac{\partial \varphi_i(\boldsymbol{x}_I)}{\partial x} & -\varphi_i(\boldsymbol{x}_I) & 0 \end{bmatrix}_i \quad i = \{1, 2, \ldots n\} \tag{87}$$

$$\boldsymbol{B}_1(\boldsymbol{x}_I) = \begin{bmatrix} 0 & 0 & 0 & -\frac{\partial \varphi_i(\boldsymbol{x}_I)}{\partial x} & 0 \\ 0 & 0 & 0 & 0 & -\frac{\partial \varphi_i(\boldsymbol{x}_I)}{\partial y} \\ 0 & 0 & 0 & -\frac{\partial \varphi_i(\boldsymbol{x}_I)}{\partial y} & -\frac{\partial \varphi_i(\boldsymbol{x}_I)}{\partial x} \\ 0 & 0 & 0 & 0 & 0 \\ 0 & 0 & 0 & 0 & 0 \end{bmatrix}_i \quad i = \{1, 2, \ldots n\} \tag{88}$$

4.3.5 Homogenised Constitutive Matrixes and Construction of the Global Stiffness Matrix

Being defined the matrixes of section 4.3.4, the stiffness matrix can finally be calculated using the Gauss-Legendre integration scheme introduced in Chapter 2 and considering the discrete system of equations deducted in Chapter 3,

$$\begin{aligned} \boldsymbol{K} &= \int_{\Omega} \boldsymbol{B}^{\mathrm{T}} \boldsymbol{c}\, \boldsymbol{B}\ \mathrm{d}\Omega = \sum_{I=1}^{nQ} \omega_I \left(\sum_{i=1}^{k} \int_{z_{i-1}}^{z_i} \boldsymbol{B}^{\mathrm{T}}(\boldsymbol{x}_I)\, \boldsymbol{c}_k\, \boldsymbol{B}(\boldsymbol{x}_I) \mathrm{d}z \right) = \\ &= \sum_{I=1}^{nQ} \omega_I \left(\sum_{i=1}^{k} \int_{z_{i-1}}^{z_i} \left(\boldsymbol{B}_0^T(\boldsymbol{x}_I) \cdot \boldsymbol{c}_k \cdot \boldsymbol{B}_0(\boldsymbol{x}_I) + \boldsymbol{B}_0^T(\boldsymbol{x}_I) \cdot \boldsymbol{c}_k \cdot z \cdot \boldsymbol{B}_1(\boldsymbol{x}_I) + \boldsymbol{B}_1^T(\boldsymbol{x}_I) \cdot \boldsymbol{c}_k \cdot z \cdot \boldsymbol{B}_0(\boldsymbol{x}_I) + \boldsymbol{B}_1^T(\boldsymbol{x}_I) \cdot \boldsymbol{c}_k \cdot \boldsymbol{B}_1(\boldsymbol{x}_I) \cdot z^2 \right) \mathrm{d}z \right) \end{aligned} \tag{89}$$

From equation (89), it becomes clear that the matrixes $\boldsymbol{B}_0$ and $\boldsymbol{B}_1$ do not depend on the laminate, so their combinations of multiplications can be put outside of the integral. Considering, for example, the second term of the integrand in equation (89), it can be defined a matrix $\boldsymbol{K}_{01}$,

$$\boldsymbol{K}_{01} = \sum_{I=1}^{nQ} \omega_I \left(\sum_{i=1}^{k} \int_{z_{i-1}}^{z_i} \left(\boldsymbol{B}_0^T(\boldsymbol{x}_I) \cdot \boldsymbol{c}_k \cdot z \cdot \boldsymbol{B}_1(\boldsymbol{x}_I) \right) \mathrm{d}z \right) = \sum_{I=1}^{nQ} \omega_I \cdot \boldsymbol{B}_0^T(\boldsymbol{x}_I) \cdot \boldsymbol{c}_2 \cdot \boldsymbol{B}_1(\boldsymbol{x}_I) = \boldsymbol{K}_{10} \tag{90}$$

where the matrix $\boldsymbol{c}_2$ is a homogenised constitutive matrix that can separately be determined without increasing the computational cost of the algorithms when they go through all integration points $\boldsymbol{x}_I$ (if this operation was not taken, the integral in equation (89) would always be determined for each integration point),

$$\boldsymbol{c}_2 = \sum_{i=1}^{k} \int_{z_{i-1}}^{z_i} \left(\boldsymbol{c}_k \cdot z \right) \mathrm{d}z = \sum_{i=1}^{k} \left(\frac{z_i^{\,2}}{2} - \frac{z_{i-1}^{\,2}}{2} \right) \cdot \boldsymbol{c}_k \tag{91}$$

Proceeding the same way for the other three terms of the integrand in equation (89), other two homogenised constitutive matrixes can be found,

$$\boldsymbol{c}_1 = \sum_{i=1}^{k} \int_{z_{i-1}}^{z_i} \boldsymbol{c}_k \, \mathrm{d}z = \sum_{i=1}^{k} \left(z_i - z_{i-1} \right) \cdot \boldsymbol{c}_k \tag{92}$$

$$\boldsymbol{c}_3 = \sum_{i=1}^{k} \int_{z_{i-1}}^{z_i} \left(\boldsymbol{c}_k \cdot z^2 \right) \mathrm{d}z = \sum_{i=1}^{k} \left(\frac{z_i^{\,3}}{3} - \frac{z_{i-1}^{\,3}}{3} \right) \cdot \boldsymbol{c}_k \tag{93}$$

which are used to calculate $\boldsymbol{K}_{00}$ and $\boldsymbol{K}_{11}$,

$$\boldsymbol{K}_{00} = \sum_{I=1}^{nQ} \omega_I \left(\sum_{i=1}^{k} \int_{z_{i-1}}^{z_i} \left(\boldsymbol{B}_0^T(\boldsymbol{x}_I) \cdot \boldsymbol{c}_k \cdot \boldsymbol{B}_0(\boldsymbol{x}_I) \right) \mathrm{d}z \right) = \sum_{I=1}^{nQ} \omega_I \cdot \boldsymbol{B}_0^T(\boldsymbol{x}_I) \cdot \boldsymbol{c}_1 \cdot \boldsymbol{B}_0(\boldsymbol{x}_I) \tag{94}$$

$$\boldsymbol{K}_{11} = \sum_{I=1}^{nQ} \omega_I \left(\sum_{i=1}^{k} \int_{z_{i-1}}^{z_i} \left(\boldsymbol{B}_1^T(\boldsymbol{x}_I) \cdot \boldsymbol{c}_k \cdot \boldsymbol{B}_1(\boldsymbol{x}_I) \cdot z^2 \right) \mathrm{d}z \right) = \sum_{I=1}^{nQ} \omega_I \cdot \boldsymbol{B}_1^T(\boldsymbol{x}_I) \cdot \boldsymbol{c}_3 \cdot \boldsymbol{B}_1(\boldsymbol{x}_I) \tag{95}$$

and the stiffness matrix for the 'influence-domain' or 'influence-cell' of the interest point $\boldsymbol{x}_I$ can finally be determined,

$$\boldsymbol{K} = \boldsymbol{K}_{00} + \boldsymbol{K}_{01} + \boldsymbol{K}_{10} + \boldsymbol{K}_{11} \tag{96}$$

Notice that the homogenised constitutive matrixes depend on the constitutive matrix of each lamina previously transformed to the global coordinate system, $\boldsymbol{C}_k$, and depend also on the layer position $\left(\frac{z_i^{\,j}}{j} - \frac{z_{i-1}^{\,j}}{j} \right)$. This is valid for plate theories that consider the variation of the in-plane displacements as polynomial functions, so this strategy will also be applied in the section 4.4.1. that regards Third-Order Shear Deformation Theories.

4.4 High-Order Shear Deformation Theories

Unlike the FSDT, the HSDTs state nonlinear variations of the in-plane displacements through the plate thickness, which results in non-constant shear stresses along the thickness and so the condition of zero shear stresses on the bottom and top faces of the laminated plate is fulfilled.

Of all the theories set out in 4.1., and many other theories developed in the literature, seven different HSDTs were selected (the seven theories with more accessible exact results for comparison purposes that could be found in the literature) for the analysis of composite laminated plates.

The generalized displacement field for a HSDT can be given by,

$$\begin{cases} u(x,y,z) = u_0(x,y) - z \cdot \dfrac{\partial w(x,y)}{\partial x} + f(z) \cdot \left[\phi_x(x,y) + \dfrac{\partial w(x,y)}{\partial x} \right] \\ v(x,y,z) = v_0(x,y) - z \cdot \dfrac{\partial w(x,y)}{\partial y} + f(z) \cdot \left[\phi_y(x,y) + \dfrac{\partial w(x,y)}{\partial y} \right] \\ w(x,y,z) = w_0(x,y) \end{cases} \tag{97}$$

where $f(z)$ is the function that describes the variation of the in-plane displacements along the thickness. Notice that for the FSDT $f(z) = z$ and for the CLPT $f(z) = 0$. Once again, are considered five DOFs: $u_0, v_0, w_0, \phi_x, \phi_y$.

The seven selected HSDTs are presented in table 2 and figure 16.

table 2 – HSDTs to implement in the algorithms of the RPIM and NNRPIM for static analysis of composite laminated plates.

HSDT	$f(z)$
Third-Order Shear Deformation Theory (TSDT) – Levinson [41], Murthy [42] and Reddy [26]	$z\left(1-\frac{4z^2}{3h^2}\right)$
Kaczkowski [43], Panc [44], Reissner [45] and Shi [27]	$\frac{5z}{4}\left(1-\frac{4z^2}{3h^2}\right)$
Ambartsumian [28]	$\frac{z}{2}\left(\frac{h^2}{4}-\frac{z^2}{3}\right)$
Aydogdu [31]	$z\alpha^{\frac{2\left(\frac{z}{h}\right)^2}{\ln(\alpha)}}$, $\alpha=3$
Karama [30]	$ze^{-2\left(\frac{z}{h}\right)^2}$
Touratier [29]	$\frac{h}{\pi}\sin\left(\frac{\pi z}{h}\right)$
Mantari [33]	$\frac{h}{\pi}\left[\sin\left(\frac{\pi z}{h}\right)\cdot e^{\frac{1}{2}\cos\left(\frac{\pi z}{h}\right)}+\frac{\pi z}{2h}\right]$

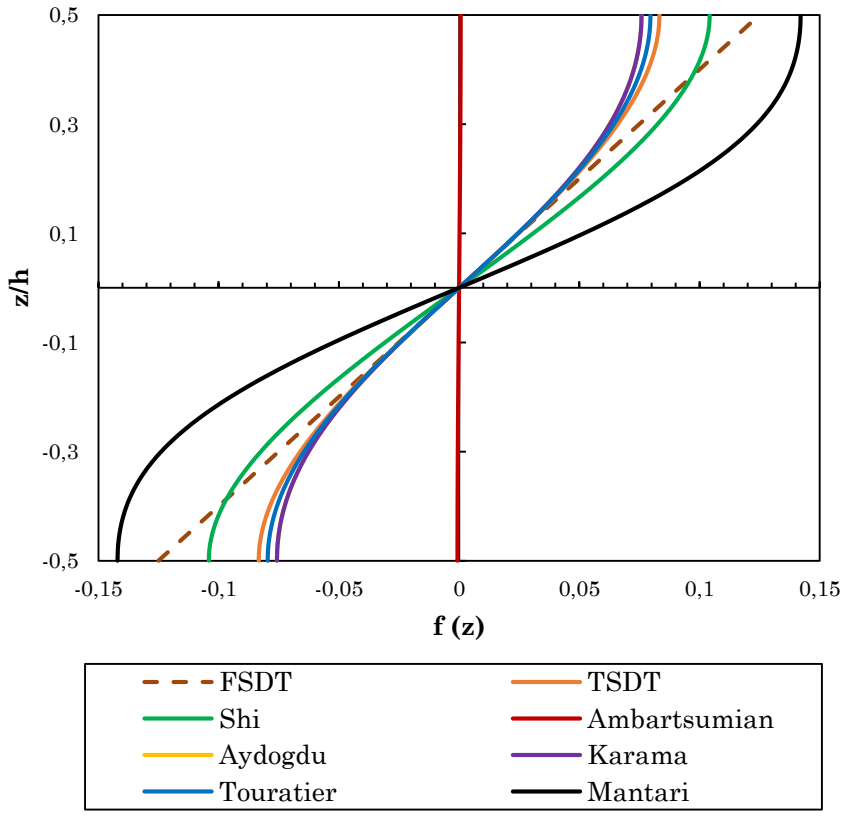

figure 16 – Distribution of the function $f(z)$ for different HSDTs and also for the FSDT as a function of the normalized thickness z/h.

4.4.1 Third-Order Shear Deformation Theories (Reddy, Shi and Ambatsumian Plate Theories)

The first three theories presented in table 2 define the variation of the in-plane displacements along the thickness as polynomial functions, more specifically as cubic functions. Thus, the implementation of the Reddy, Shi and Ambartsumian theories followed the same procedure, being included also in the same algorithm routines.

From table 2 , it is possible to write the $f(z)$ functions of these TSDTs in a standard form,

$$\begin{aligned}
&\text{Reddy}: f(z) = z\left(1-\frac{4z^2}{3h^2}\right) = z-\frac{4z^3}{3h^2} = k_1 z + k_2 z^3 \\
&\text{Shi}: f(z) = \frac{5}{4}z\left(1-\frac{4z^2}{3h^2}\right) = \frac{5}{4}z-\frac{5z^3}{3h^2} = k_1 z + k_2 z^3 \\
&\text{Ambartsumian}: f(z) = \frac{z}{2}\left(\frac{h^2}{4}-\frac{z^2}{3}\right) = \frac{h^2}{8}z-\frac{z^3}{6} = k_1 z + k_2 z^3
\end{aligned} \tag{98}$$

In computational terms, it is possible treat the above mentioned HSDTs as a single theory and simply change the constants k_1 and k_2 - table 3.

table 3 – Constants k_1 and k_2 for three TSDTs.

HSDT	k_1	k_2
Third-Order Shear Deformation Theory (TSDT) – Reddy [26]	1	$-\frac{4}{3h^2}$
Shi [27]	$\frac{5}{4}$	$-\frac{5}{3h^2}$
Ambartsumian [28]	$\frac{h^2}{8}$	$-\frac{1}{6}$

Because they have parabolic functions as derivatives, these TSDTs satisfy the boundary conditions on top and bottom surfaces of the plate (condition of zero shear stresses).

The main difference between these three cubic theories may be found on the expansions of its terms,

$$\begin{aligned}
&\text{Reddy}: f(z) = z\left(1-\frac{4z^2}{3h^2}\right) = z - 1.333\frac{z^3}{h^2} \\
&\text{Shi}: f(z) = \frac{5}{4}z\left(1-\frac{4z^2}{3h^2}\right) = 1.25z - 1.667\frac{z^3}{h^2} \\
&\text{Ambartsumian}: f(z) = \frac{z}{2}\left(\frac{h^2}{4}-\frac{z^2}{3}\right) = 0.125h^2 z - 0.333z^3
\end{aligned} \tag{99}$$

From equation (99) it can be said that, in theory, Shi formulation seems very similar to Reddy's model because the coefficients of the terms obtained are identical. On the other hand, due to have a lower third order term, Ambartsumian's theory is that for which are expected less satisfactory results. Also, as it can be seen in figure 16, the distribution of $f(z)$ as function of z/h is almost vertical and equal to zero for the Ambartsumian plate model, which is also the case of the CLPT (where $f(z)=0$). This makes the Ambatsumian plate theory an improved theory of the CLPT that takes into account the effects of shear deformation (notice also that this TSDT theory was proposed in 1960 [28]).

Kinematic Relations

From equations (97) and introducing $f(z) = k_1 z + k_2 z^3$, the displacement field for these TSDTs can be found,

$$\begin{cases}
u(x,y,z) = u_0(x,y) - z\cdot\dfrac{\partial w(x,y)}{\partial x} + \left(k_1 z + k_2 z^3\right)\cdot\left[\phi_x(x,y) + \dfrac{\partial w(x,y)}{\partial x}\right] \\
v(x,y,z) = v_0(x,y) - z\cdot\dfrac{\partial w(x,y)}{\partial y} + \left(k_1 z + k_2 z^3\right)\cdot\left[\phi_y(x,y) + \dfrac{\partial w(x,y)}{\partial y}\right] \\
w(x,y,z) = w_0(x,y)
\end{cases} \tag{100}$$

$$= \begin{cases}
u(x,y,z) = u_0(x,y) + \left(k_1 z + k_2 z^3 - z\right)\cdot\dfrac{\partial w(x,y)}{\partial x} + \left(k_1 z + k_2 z^3\right)\cdot\phi_x(x,y) \\
v(x,y,z) = v_0(x,y) + \left(k_1 z + k_2 z^3 - z\right)\cdot\dfrac{\partial w(x,y)}{\partial y} + \left(k_1 z + k_2 z^3\right)\cdot\phi_y(x,y) \\
w(x,y,z) = w_0(x,y)
\end{cases}$$

By derivation of the displacement field, the strain field is determined,

$$\begin{cases} \varepsilon_{xx} = \dfrac{\partial u}{\partial x} = \dfrac{\partial u_0}{\partial x} + \left(k_1 z + k_2 z^3\right) \cdot \dfrac{\partial \phi_x}{\partial x} + \left(k_1 z + k_2 z^3 - z\right) \cdot \dfrac{\partial^2 w}{\partial x^2} \\ \varepsilon_{yy} = \dfrac{\partial v}{\partial y} = \dfrac{\partial v_0}{\partial x} + \left(k_1 z + k_2 z^3\right) \cdot \dfrac{\partial \phi_y}{\partial y} + \left(k_1 z + k_2 z^3 - z\right) \cdot \dfrac{\partial^2 w}{\partial y^2} \\ \gamma_{xy} = \dfrac{\partial v}{\partial x} + \dfrac{\partial u}{\partial y} = \dfrac{\partial v_0}{\partial x} + \dfrac{\partial u_0}{\partial y} + \left(k_1 z + k_2 z^3\right) \cdot \left(\dfrac{\partial \phi_x}{\partial y} + \dfrac{\partial \phi_y}{\partial x} \right) + 2\left(k_1 z + k_2 z^3 - z\right) \dfrac{\partial^2 w}{\partial x \partial y} \\ \gamma_{yz} = \dfrac{\partial v}{\partial z} + \dfrac{\partial w}{\partial y} = \dfrac{\partial w}{\partial y} + \left(k_1 + 3k_2 z^2\right) \phi_y + \left(k_1 + 3k_2 z^2 - 1\right) \dfrac{\partial w}{\partial y} = \left(k_1 + 3k_2 z^2\right) \phi_y + \left(k_1 + 3k_2 z^2\right) \dfrac{\partial w}{\partial y} \\ \gamma_{xz} = \dfrac{\partial u}{\partial z} + \dfrac{\partial w}{\partial x} = \dfrac{\partial w}{\partial x} + \left(k_1 + 3k_2 z^2\right) \phi_x + \left(k_1 + 3k_2 z^2 - 1\right) \dfrac{\partial w}{\partial x} = \left(k_1 + 3k_2 z^2\right) \phi_x + \left(k_1 + 3k_2 z^2\right) \dfrac{\partial w}{\partial x} \\ \varepsilon_{zz} = 0 \end{cases} \tag{101}$$

Deformability Matrixes

The first step to construct the deformability matrixes is to establish the differential operator $\boldsymbol{L}$,

$$\boldsymbol{L} = \begin{bmatrix} \dfrac{\partial}{\partial x} & 0 & \left(k_1 z + k_2 z^3 - z\right) \dfrac{\partial^2}{\partial x^2} & \left(k_1 z + k_2 z^3\right) \dfrac{\partial}{\partial x} & 0 \\ 0 & \dfrac{\partial}{\partial y} & \left(k_1 z + k_2 z^3 - z\right) \dfrac{\partial^2}{\partial y^2} & 0 & \left(k_1 z + k_2 z^3\right) \dfrac{\partial}{\partial y} \\ \dfrac{\partial}{\partial y} & \dfrac{\partial}{\partial x} & 2\left(k_1 z + k_2 z^3 - z\right) \dfrac{\partial^2}{\partial x \partial y} & \left(k_1 z + k_2 z^3\right) \dfrac{\partial}{\partial y} & \left(k_1 z + k_2 z^3\right) \dfrac{\partial}{\partial x} \\ 0 & 0 & \left(k_1 + 3k_2 z^2\right) \dfrac{\partial}{\partial y} & 0 & \left(k_1 + 3k_2 z^2\right) \\ 0 & 0 & \left(k_1 + 3k_2 z^2\right) \dfrac{\partial}{\partial x} & \left(k_1 + 3k_2 z^2\right) & 0 \end{bmatrix} \tag{102}$$

As it was done in 4.3.4., the strategy now is to divide the deformability matrix $\boldsymbol{B}(\boldsymbol{x}_I) = \boldsymbol{L} \cdot \boldsymbol{\varphi}(\boldsymbol{x}_I)$ into sub-matrixes such that,

$$\boldsymbol{B}(\boldsymbol{x}_I) = \boldsymbol{B}_{0M}(\boldsymbol{x}_I) + \boldsymbol{B}_{0S}(\boldsymbol{x}_I) + k_1 z \cdot \boldsymbol{B}_1(\boldsymbol{x}_I) + 3k_2 z^2 \cdot \boldsymbol{B}_2(\boldsymbol{x}_I) + k_2 z^3 \boldsymbol{B}_3(\boldsymbol{x}_I) + (k_1 z - z) \cdot \boldsymbol{B}_4(\boldsymbol{x}_I) \tag{103}$$

where,

$$\boldsymbol{B}^{i}{}_{0M}(\boldsymbol{x}_I) = \begin{bmatrix} \dfrac{\partial \varphi_i(\boldsymbol{x}_I)}{\partial x} & 0 & 0 & 0 & 0 \\ 0 & \dfrac{\partial \varphi_i(\boldsymbol{x}_I)}{\partial y} & 0 & 0 & 0 \\ \dfrac{\partial \varphi_i(\boldsymbol{x}_I)}{\partial y} & \dfrac{\partial \varphi_i(\boldsymbol{x}_I)}{\partial x} & 0 & 0 & 0 \\ 0 & 0 & 0 & 0 & 0 \\ 0 & 0 & 0 & 0 & 0 \end{bmatrix}_i \quad i = \{1, 2, \ldots n\} \tag{104}$$

$$\boldsymbol{B}^{i}{}_{0S}(\boldsymbol{x}_I) = \begin{bmatrix} 0 & 0 & 0 & 0 & 0 \\ 0 & 0 & 0 & 0 & 0 \\ 0 & 0 & 0 & 0 & 0 \\ 0 & 0 & k_1 \cdot \dfrac{\partial \varphi_i(\boldsymbol{x}_I)}{\partial y} & 0 & k_1 \cdot \varphi_i(\boldsymbol{x}_I) \\ 0 & 0 & k_1 \cdot \dfrac{\partial \varphi_i(\boldsymbol{x}_I)}{\partial x} & k_1 \cdot \varphi_i(\boldsymbol{x}_I) & 0 \end{bmatrix}_i \quad i = \{1, 2, \ldots n\} \tag{105}$$

$$k_1 z \cdot \boldsymbol{B}^{i}{}_{1}(\boldsymbol{x}_I) = k_1 z \cdot \begin{bmatrix} 0 & 0 & 0 & \dfrac{\partial \varphi_i(\boldsymbol{x}_I)}{\partial x} & 0 \\ 0 & 0 & 0 & 0 & \dfrac{\partial \varphi_i(\boldsymbol{x}_I)}{\partial y} \\ 0 & 0 & 0 & \dfrac{\partial \varphi_i(\boldsymbol{x}_I)}{\partial y} & \dfrac{\partial \varphi_i(\boldsymbol{x}_I)}{\partial x} \\ 0 & 0 & 0 & 0 & 0 \\ 0 & 0 & 0 & 0 & 0 \end{bmatrix}_i \quad i = \{1, 2, \ldots n\} \tag{106}$$

$$3k_2 z^2 \cdot \boldsymbol{B}^{i}{}_{2}(\boldsymbol{x}_I) = 3k_2 z^2 \cdot \begin{bmatrix} 0 & 0 & 0 & 0 & 0 \\ 0 & 0 & 0 & 0 & 0 \\ 0 & 0 & 0 & 0 & 0 \\ 0 & 0 & \dfrac{\partial \varphi_i(\boldsymbol{x}_I)}{\partial y} & 0 & \varphi_i(\boldsymbol{x}_I) \\ 0 & 0 & \dfrac{\partial \varphi_i(\boldsymbol{x}_I)}{\partial x} & \varphi_i(\boldsymbol{x}_I) & 0 \end{bmatrix}_i \quad i = \{1, 2, \ldots n\} \tag{107}$$

$$k_2 z^3 \cdot \boldsymbol{B}^i{}_3(\boldsymbol{x}_I) = k_2 z^3 \cdot \begin{bmatrix} 0 & 0 & \dfrac{\partial^2 \varphi_i(\boldsymbol{x}_I)}{\partial x^2} & \dfrac{\partial \varphi_i(\boldsymbol{x}_I)}{\partial x} & 0 \\ 0 & 0 & \dfrac{\partial^2 \varphi_i(\boldsymbol{x}_I)}{\partial y^2} & 0 & \dfrac{\partial \varphi_i(\boldsymbol{x}_I)}{\partial y} \\ 0 & 0 & 2\dfrac{\partial^2 \varphi_i(\boldsymbol{x}_I)}{\partial x \partial y} & \dfrac{\partial \varphi_i(\boldsymbol{x}_I)}{\partial y} & \dfrac{\partial \varphi_i(\boldsymbol{x}_I)}{\partial x} \\ 0 & 0 & 0 & 0 & 0 \\ 0 & 0 & 0 & 0 & 0 \end{bmatrix}_i \quad i = \{1, 2, \ldots n\} \tag{108}$$

$$(k_1 z - z) \cdot \boldsymbol{B}^i{}_4(\boldsymbol{x}_I) = (k_1 z - z) \cdot \begin{bmatrix} 0 & 0 & \dfrac{\partial^2 \varphi_i(\boldsymbol{x}_I)}{\partial x^2} & 0 & 0 \\ 0 & 0 & \dfrac{\partial^2 \varphi_i(\boldsymbol{x}_I)}{\partial y^2} & 0 & 0 \\ 0 & 0 & 2\dfrac{\partial^2 \varphi_i(\boldsymbol{x}_I)}{\partial x \partial y} & 0 & 0 \\ 0 & 0 & 0 & 0 & 0 \\ 0 & 0 & 0 & 0 & 0 \end{bmatrix}_i \quad i = \{1, 2, \ldots n\} \tag{109}$$

and,

$$\boldsymbol{B}_0(\boldsymbol{x}_I) = \boldsymbol{B}_{0M}(\boldsymbol{x}_I) + \boldsymbol{B}_{0S}(\boldsymbol{x}_I) \tag{110}$$

Homogenised Constitutive Matrixes and Construction of the Global Stiffness Matrix

The local stiffness matrix $\boldsymbol{K}$ is determined considering the combination of the equations (103) and (110) and calculated as a sum of sub-matrixes $\boldsymbol{K}_{ij}$ with $i, j = \{0,1,2,3,4\}$,

$$\boldsymbol{K} = \int_{\Omega} \boldsymbol{B}^{\mathrm{T}} \boldsymbol{c}\, \boldsymbol{B}\, \mathrm{d}\Omega = \sum_{I=1}^{nQ} \omega_I \left(\sum_{i=1}^{k} \int_{z_{i-1}}^{z_i} \boldsymbol{B}^{\mathrm{T}}(\boldsymbol{x}_I)\, \boldsymbol{c}_k\, \boldsymbol{B}(\boldsymbol{x}_I) \mathrm{d}z \right) \tag{111}$$

$$\boldsymbol{K} = \sum_{i=0}^{4} \sum_{j=0}^{4} \boldsymbol{K}_{ij} \tag{112}$$

where $\boldsymbol{c}_k$ can be found in equation (77), doing $k_{sh} = 1$ since the HSDTs do not need shear correction factors. The sub-matrixes $\boldsymbol{K}_{ij}$ and the correspondent homogenised constitutive matrixes are,

$$\begin{cases} \boldsymbol{K}_{00} = \sum_{I=1}^{nQ} \omega_I \left(\sum_{i=1}^{k} \int_{z_{i-1}}^{z_i} \left(\boldsymbol{B}_0^T(\boldsymbol{x}_I) \cdot \boldsymbol{c}_k \cdot \boldsymbol{B}_0(\boldsymbol{x}_I) \right) \mathrm{d}z \right) = \sum_{I=1}^{nQ} \omega_I \cdot \boldsymbol{B}_0^T(\boldsymbol{x}_I) \cdot \boldsymbol{c}_1 \cdot \boldsymbol{B}_0(\boldsymbol{x}_I) \\ \boldsymbol{c}_1 = \sum_{i=1}^{k} \int_{z_{i-1}}^{z_i} \boldsymbol{c}_k \, \mathrm{d}z = \sum_{i=1}^{k} \left(z_i - z_{i-1} \right) \cdot \boldsymbol{c}_k \end{cases} \tag{113}$$

$$\begin{cases} \boldsymbol{K}_{01} = \sum_{I=1}^{nQ} \omega_I \left(\sum_{i=1}^{k} \int_{z_{i-1}}^{z_i} \left(\boldsymbol{B}_0^T(\boldsymbol{x}_I) \cdot \boldsymbol{c}_k \cdot k_1 z \cdot \boldsymbol{B}_1(\boldsymbol{x}_I) \right) \mathrm{d}z \right) = \sum_{I=1}^{nQ} \omega_I \cdot \boldsymbol{B}_0^T(\boldsymbol{x}_I) \cdot \boldsymbol{c}_2 \cdot \boldsymbol{B}_1(\boldsymbol{x}_I) = \boldsymbol{K}_{10} \\ \boldsymbol{c}_2 = \sum_{i=1}^{k} \int_{z_{i-1}}^{z_i} \left(\boldsymbol{c}_k \cdot k_1 z \right) \mathrm{d}z = k_1 \cdot \sum_{i=1}^{k} \left(\frac{z_i^2}{2} - \frac{z_{i-1}^2}{2} \right) \cdot \boldsymbol{c}_k \end{cases} \tag{114}$$

$$\begin{cases} \boldsymbol{K}_{02} = \sum_{I=1}^{nQ} \omega_I \left(\sum_{i=1}^{k} \int_{z_{i-1}}^{z_i} \left(\boldsymbol{B}_0^T(\boldsymbol{x}_I) \cdot \boldsymbol{c}_k \cdot 3k_2 z^2 \cdot \boldsymbol{B}_2(\boldsymbol{x}_I) \right) \mathrm{d}z \right) = \sum_{I=1}^{nQ} \omega_I \cdot \boldsymbol{B}_0^T(\boldsymbol{x}_I) \cdot \boldsymbol{c}_3 \cdot \boldsymbol{B}_2(\boldsymbol{x}_I) = \boldsymbol{K}_{20} \\ \boldsymbol{c}_3 = \sum_{i=1}^{k} \int_{z_{i-1}}^{z_i} \left(\boldsymbol{c}_k \cdot 3k_2 z^2 \right) \mathrm{d}z = 3k_2 \cdot \sum_{i=1}^{k} \left(\frac{z_i^3}{3} - \frac{z_{i-1}^3}{3} \right) \cdot \boldsymbol{c}_k \end{cases} \tag{115}$$

$$\begin{cases} \boldsymbol{K}_{03} = \sum_{I=1}^{nQ} \omega_I \left(\sum_{i=1}^{k} \int_{z_{i-1}}^{z_i} \left(\boldsymbol{B}_0^T(\boldsymbol{x}_I) \cdot \boldsymbol{c}_k \cdot k_2 z^3 \cdot \boldsymbol{B}_3(\boldsymbol{x}_I) \right) \mathrm{d}z \right) = \sum_{I=1}^{nQ} \omega_I \cdot \boldsymbol{B}_0^T(\boldsymbol{x}_I) \cdot \boldsymbol{c}_4 \cdot \boldsymbol{B}_3(\boldsymbol{x}_I) = \boldsymbol{K}_{30} \\ \boldsymbol{c}_4 = \sum_{i=1}^{k} \int_{z_{i-1}}^{z_i} \left(\boldsymbol{c}_k \cdot k_2 z^3 \right) \mathrm{d}z = k_2 \cdot \sum_{i=1}^{k} \left(\frac{z_i^4}{4} - \frac{z_{i-1}^4}{4} \right) \cdot \boldsymbol{c}_k \end{cases} \tag{116}$$

$$\begin{cases} \boldsymbol{K}_{04} = \sum_{I=1}^{nQ} \omega_I \left(\sum_{i=1}^{k} \int_{z_{i-1}}^{z_i} \left(\boldsymbol{B}_0^T(\boldsymbol{x}_I) \cdot \boldsymbol{c}_k \cdot (k_1 z - z) \cdot \boldsymbol{B}_4(\boldsymbol{x}_I) \right) \mathrm{d}z \right) = \sum_{I=1}^{nQ} \omega_I \cdot \boldsymbol{B}_0^T(\boldsymbol{x}_I) \cdot \boldsymbol{c}_5 \cdot \boldsymbol{B}_4(\boldsymbol{x}_I) = \boldsymbol{K}_{40} \\ \boldsymbol{c}_5 = \sum_{i=1}^{k} \int_{z_{i-1}}^{z_i} \left[\boldsymbol{c}_k \cdot (k_1 z - z) \right] \mathrm{d}z = (k_1 - 1) \cdot \sum_{i=1}^{k} \left(\frac{z_i^2}{2} - \frac{z_{i-1}^2}{2} \right) \cdot \boldsymbol{c}_k \end{cases} \tag{117}$$

$$\begin{cases} \boldsymbol{K}_{11} = \sum_{I=1}^{nQ} \omega_I \left(\sum_{i=1}^{k} \int_{z_{i-1}}^{z_i} \left(\boldsymbol{B}_1^T(\boldsymbol{x}_I) \cdot \boldsymbol{c}_k \cdot \left(k_1 z\right)^2 \cdot \boldsymbol{B}_1(\boldsymbol{x}_I) \right) \mathrm{d}z \right) = \sum_{I=1}^{nQ} \omega_I \cdot \boldsymbol{B}_1^T(\boldsymbol{x}_I) \cdot \boldsymbol{c}_6 \cdot \boldsymbol{B}_1(\boldsymbol{x}_I) \\ \boldsymbol{c}_6 = \sum_{i=1}^{k} \int_{z_{i-1}}^{z_i} \left[\boldsymbol{c}_k \cdot \left(k_1 z\right)^2 \right] \mathrm{d}z = k_1^{\,2} \cdot \sum_{i=1}^{k} \left(\frac{z_i^{\,3}}{3} - \frac{z_{i-1}^{\,3}}{3} \right) \cdot \boldsymbol{c}_k \end{cases} \tag{118}$$

$$\begin{cases} \boldsymbol{K}_{12} = \sum_{I=1}^{nQ} \omega_I \left(\sum_{i=1}^{k} \int_{z_{i-1}}^{z_i} \left(\boldsymbol{B}_1^T(\boldsymbol{x}_I) \cdot \boldsymbol{c}_k \cdot (k_1 z) \cdot (3k_2 z^2) \cdot \boldsymbol{B}_2(\boldsymbol{x}_I) \right) \mathrm{d}z \right) = \sum_{I=1}^{nQ} \omega_I \cdot \boldsymbol{B}_1^T(\boldsymbol{x}_I) \cdot \boldsymbol{c}_7 \cdot \boldsymbol{B}_2(\boldsymbol{x}_I) = \boldsymbol{K}_{21} \\ \boldsymbol{c}_7 = \sum_{i=1}^{k} \int_{z_{i-1}}^{z_i} \left[\boldsymbol{c}_k \cdot (k_1 z) \cdot (3k_2 z^2) \right] \mathrm{d}z = 3k_1 k_2 \cdot \sum_{i=1}^{k} \left(\frac{z_i^{\,4}}{4} - \frac{z_{i-1}^{\,4}}{4} \right) \cdot \boldsymbol{c}_k \end{cases} \tag{119}$$

$$\begin{cases} \boldsymbol{K}_{13} = \sum_{I=1}^{nQ} \omega_I \left(\sum_{i=1}^{k} \int_{z_{i-1}}^{z_i} \left(\boldsymbol{B}_1^T(\boldsymbol{x}_I) \cdot \boldsymbol{c}_k \cdot (k_1 z) \cdot (k_2 z^3) \cdot \boldsymbol{B}_3(\boldsymbol{x}_I) \right) \mathrm{d}z \right) = \sum_{I=1}^{nQ} \omega_I \cdot \boldsymbol{B}_1^T(\boldsymbol{x}_I) \cdot \boldsymbol{c}_8 \cdot \boldsymbol{B}_3(\boldsymbol{x}_I) = \boldsymbol{K}_{31} \\ \boldsymbol{c}_8 = \sum_{i=1}^{k} \int_{z_{i-1}}^{z_i} \left[\boldsymbol{c}_k \cdot (k_1 z) \cdot (k_2 z^3) \right] \mathrm{d}z = k_1 k_2 \cdot \sum_{i=1}^{k} \left(\frac{z_i^{\,5}}{5} - \frac{z_{i-1}^{\,5}}{5} \right) \cdot \boldsymbol{c}_k \end{cases} \tag{120}$$

$$\begin{cases} \boldsymbol{K}_{14} = \sum_{I=1}^{nQ} \omega_I \left(\sum_{i=1}^{k} \int_{z_{i-1}}^{z_i} \left(\boldsymbol{B}_1^T(\boldsymbol{x}_I) \cdot \boldsymbol{c}_k \cdot k_1 z \cdot (k_1 z - z) \cdot \boldsymbol{B}_4(\boldsymbol{x}_I) \right) \mathrm{d}z \right) = \sum_{I=1}^{nQ} \omega_I \cdot \boldsymbol{B}_1^T(\boldsymbol{x}_I) \cdot \boldsymbol{c}_9 \cdot \boldsymbol{B}_4(\boldsymbol{x}_I) = \boldsymbol{K}_{41} \\ \boldsymbol{c}_9 = \sum_{i=1}^{k} \int_{z_{i-1}}^{z_i} \left[\boldsymbol{c}_k \cdot k_1 z \cdot (k_1 z - z) \right] \mathrm{d}z = k_1 (k_1 - 1) \cdot \sum_{i=1}^{k} \left(\frac{z_i^{\,3}}{3} - \frac{z_{i-1}^{\,3}}{3} \right) \cdot \boldsymbol{c}_k \end{cases} \tag{121}$$

$$\begin{cases} \boldsymbol{K}_{22} = \sum_{I=1}^{nQ} \omega_I \left(\sum_{i=1}^{k} \int_{z_{i-1}}^{z_i} \left(\boldsymbol{B}_2^T(\boldsymbol{x}_I) \cdot \boldsymbol{c}_k \cdot \left(3k_2 z^2\right)^2 \cdot \boldsymbol{B}_2(\boldsymbol{x}_I) \right) \mathrm{d}z \right) = \sum_{I=1}^{nQ} \omega_I \cdot \boldsymbol{B}_2^T(\boldsymbol{x}_I) \cdot \boldsymbol{c}_{10} \cdot \boldsymbol{B}_2(\boldsymbol{x}_I) \\ \boldsymbol{c}_{10} = \sum_{i=1}^{k} \int_{z_{i-1}}^{z_i} \left[\boldsymbol{c}_k \cdot \left(3k_2 z^2\right)^2 \right] \mathrm{d}z = 9k_2^{\,2} \cdot \sum_{i=1}^{k} \left(\frac{z_i^{\,5}}{5} - \frac{z_{i-1}^{\,5}}{5} \right) \cdot \boldsymbol{c}_k \end{cases} \tag{122}$$

$$\begin{cases} \boldsymbol{K}_{23} = \sum_{I=1}^{nQ} \omega_I \left(\sum_{i=1}^{k} \int_{z_{i-1}}^{z_i} \left(\boldsymbol{B}_2^T(x_I) \cdot \boldsymbol{c}_k \cdot \left(3k_2 z^2 \cdot k_2 z^3 \right) \cdot \boldsymbol{B}_3(x_I) \right) \mathrm{d}z \right) = \sum_{I=1}^{nQ} \omega_I \cdot \boldsymbol{B}_2^T(x_I) \cdot \boldsymbol{c}_{11} \cdot \boldsymbol{B}_3(x_I) = \boldsymbol{K}_{32} \\ \boldsymbol{c}_{11} = \sum_{i=1}^{k} \int_{z_{i-1}}^{z_i} \left[\boldsymbol{c}_k \cdot \left(3k_2 z^2 \cdot k_2 z^3 \right) \right] \mathrm{d}z = 3k_1^2 \cdot \sum_{i=1}^{k} \left(\frac{z_i^6}{6} - \frac{z_{i-1}^6}{6} \right) \cdot \boldsymbol{c}_k \end{cases} \tag{123}$$

$$\begin{cases} \boldsymbol{K}_{24} = \sum_{I=1}^{nQ} \omega_I \left(\sum_{i=1}^{k} \int_{z_{i-1}}^{z_i} \left(\boldsymbol{B}_2^T(x_I) \cdot \boldsymbol{c}_k \cdot \left[3k_2 z^2 \cdot (k_1 z - z) \right] \cdot \boldsymbol{B}_4(x_I) \right) \mathrm{d}z \right) = \sum_{I=1}^{nQ} \omega_I \cdot \boldsymbol{B}_2^T(x_I) \cdot \boldsymbol{c}_{12} \cdot \boldsymbol{B}_4(x_I) = \boldsymbol{K}_{42} \\ \boldsymbol{c}_{12} = \sum_{i=1}^{k} \int_{z_{i-1}}^{z_i} \left[\boldsymbol{c}_k \cdot 3k_2 z^2 \cdot (k_1 z - z) \right] \mathrm{d}z = 3k_2(k_1 - 1) \cdot \sum_{i=1}^{k} \left(\frac{z_i^6}{6} - \frac{z_{i-1}^6}{6} \right) \cdot \boldsymbol{c}_k \end{cases} \tag{124}$$

$$\begin{cases} \boldsymbol{K}_{33} = \sum_{I=1}^{nQ} \omega_I \left(\sum_{i=1}^{k} \int_{z_{i-1}}^{z_i} \left(\boldsymbol{B}_3^T(x_I) \cdot \boldsymbol{c}_k \cdot \left(k_2 z^3 \right)^2 \cdot \boldsymbol{B}_3(x_I) \right) \mathrm{d}z \right) = \sum_{I=1}^{nQ} \omega_I \cdot \boldsymbol{B}_3^T(x_I) \cdot \boldsymbol{c}_{12} \cdot \boldsymbol{B}_3(x_I) \\ \boldsymbol{c}_{13} = \sum_{i=1}^{k} \int_{z_{i-1}}^{z_i} \left[\boldsymbol{c}_k \cdot \left(k_2 z^3 \right)^2 \right] \mathrm{d}z = k_2^2 \cdot \sum_{i=1}^{k} \left(\frac{z_i^7}{7} - \frac{z_{i-1}^7}{7} \right) \cdot \boldsymbol{c}_k \end{cases} \tag{125}$$

$$\begin{cases} \boldsymbol{K}_{34} = \sum_{I=1}^{nQ} \omega_I \left(\sum_{i=1}^{k} \int_{z_{i-1}}^{z_i} \left(\boldsymbol{B}_3^T(x_I) \cdot \boldsymbol{c}_k \cdot \left[k_2 z^3 \cdot (k_1 z - z) \right] \cdot \boldsymbol{B}_4(x_I) \right) \mathrm{d}z \right) = \sum_{I=1}^{nQ} \omega_I \cdot \boldsymbol{B}_3^T(x_I) \cdot \boldsymbol{c}_{14} \cdot \boldsymbol{B}_4(x_I) = \boldsymbol{K}_{43} \\ \boldsymbol{c}_{14} = \sum_{i=1}^{k} \int_{z_{i-1}}^{z_i} \left[\boldsymbol{c}_k \cdot k_2 z^3 \cdot (k_1 z - z) \right] \mathrm{d}z = k_2(k_1 - 1) \cdot \sum_{i=1}^{k} \left(\frac{z_i^5}{5} - \frac{z_{i-1}^5}{5} \right) \cdot \boldsymbol{c}_k \end{cases} \tag{126}$$

$$\begin{cases} \boldsymbol{K}_{44} = \sum_{I=1}^{nQ} \omega_I \left(\sum_{i=1}^{k} \int_{z_{i-1}}^{z_i} \left(\boldsymbol{B}_4^T(x_I) \cdot \boldsymbol{c}_k \cdot \left[(k_1 z - z) \cdot (k_1 z - z) \right] \cdot \boldsymbol{B}_4(x_I) \right) \mathrm{d}z \right) = \sum_{I=1}^{nQ} \omega_I \cdot \boldsymbol{B}_4^T(x_I) \cdot \boldsymbol{c}_{15} \cdot \boldsymbol{B}_4(x_I) \\ \boldsymbol{c}_{15} = \sum_{i=1}^{k} \int_{z_{i-1}}^{z_i} \left[\boldsymbol{c}_k \cdot (k_1 z - z) \cdot (k_1 z - z) \right] \mathrm{d}z = (k_1 - 1)(k_1 - 1) \cdot \sum_{i=1}^{k} \left(\frac{z_i^3}{3} - \frac{z_{i-1}^3}{3} \right) \cdot \boldsymbol{c}_k \end{cases} \tag{127}$$

4.4.2 Karama and Aydodgu Plate Theories

Karama and Aydogdu models are called Exponential Shear Deformation Theories (ESDTs) since the variation of the in-plane displacements along the thickness of the plate is described by an exponential function. Both models

appeared in 2008 and are equivalent since it is possible to obtain the Karama model through Aydogdu one just by changing the value of transverse shear stress parameter, α:

$$\begin{aligned} &\text{Aydogdu}: f(z) = z\alpha^{\frac{-2\left(\frac{z}{h}\right)^2}{\ln(\alpha)}} \\ &\text{Karama}: f(z) = ze^{\frac{-2\left(\frac{z}{h}\right)^2}{\ln(e)}} = ze^{-2\left(\frac{z}{h}\right)^2} \end{aligned} \tag{128}$$

If $\alpha = e$, the Aydogdu model is driven to Karama model. Aydogdu studied [31] the optimal value for this parameter and found that $\alpha = 3$ and $\alpha = 0.38$ values gives good performance when he compared his results for different laminates with 3D solutions of Pagano and Hatfield [22]. He concluded by using $\alpha = 3$ as the transverse shear stress parameter, which makes his solutions extremely close to the ones of the Karama Model (since $\alpha = 3$ is very similar to $\alpha = e$).

This foreword allows to study both HSDTs as a single one, as has been done with TSDTs in 4.4.1., simply by changing the α parameter because the two models are exactly identical from viewpoint of mathematical equivalence.

If one takes a look on the expansions [30], [46] of the transverse shear stress function proposed by Karama considering only the odd powers as,

$$\text{Karama}: f(z) = ze^{-2\left(\frac{z}{h}\right)^2} = z - 2\frac{z^3}{h^2} + 2\frac{z^5}{h^4} - 1.333\frac{z^7}{h^6} + 0.667\frac{z^9}{h^8} + \ldots \tag{129}$$

It can be concluded that the Karama model is considerably stronger than the TSDTs, because it considers terms with higher order than the third. The expansion of equation (129) suggests also that all available functions $f(z)$ that can be found in literature can be explicitly approximated in form of a unified polynomial form (as noted and studied by Nguyen et al. [23]).

Kinematic Relations

In view of the conclusions of the last paragraph, the displacement field for the Aydogdu and Karama HSDTs come as,

$$\begin{cases} u(x,y,z) = u_0(x,y) - z\cdot\dfrac{\partial w(x,y)}{\partial x} + z\alpha^{\frac{-2\left(\frac{z}{h}\right)^2}{\ln(\alpha)}}\cdot\left[\phi_x(x,y) + \dfrac{\partial w(x,y)}{\partial x}\right] \\ v(x,y,z) = v_0(x,y) - z\cdot\dfrac{\partial w(x,y)}{\partial y} + z\alpha^{\frac{-2\left(\frac{z}{h}\right)^2}{\ln(\alpha)}}\cdot\left[\phi_y(x,y) + \dfrac{\partial w(x,y)}{\partial y}\right] \\ w(x,y,z) = w_0(x,y) \end{cases} \tag{130}$$

$$= \begin{cases} u(x,y,z) = u_0(x,y) - z\cdot\dfrac{\partial w(x,y)}{\partial x} + z\alpha^{az^2}\cdot\left[\phi_x(x,y) + \dfrac{\partial w(x,y)}{\partial x}\right] \\ v(x,y,z) = v_0(x,y) - z\cdot\dfrac{\partial w(x,y)}{\partial y} + z\alpha^{az^2}\cdot\left[\phi_y(x,y) + \dfrac{\partial w(x,y)}{\partial y}\right] \\ w(x,y,z) = w_0(x,y) \end{cases}$$

where $a = -\dfrac{2}{\ln(\alpha)\cdot h^2}$.

And the strain field is given by,

$$\begin{cases} \varepsilon_{xx} = \dfrac{\partial u}{\partial x} = \dfrac{\partial u_0}{\partial x} + \left(z\alpha^{az^2}\right)\cdot\dfrac{\partial \phi_x}{\partial x} + \left(z\alpha^{az^2} - z\right)\cdot\dfrac{\partial^2 w}{\partial x^2} \\ \varepsilon_{yy} = \dfrac{\partial v}{\partial y} = \dfrac{\partial v_0}{\partial x} + \left(z\alpha^{az^2}\right)\cdot\dfrac{\partial \phi_y}{\partial y} + \left(z\alpha^{az^2} - z\right)\cdot\dfrac{\partial^2 w}{\partial y^2} \\ \gamma_{xy} = \dfrac{\partial v}{\partial x} + \dfrac{\partial u}{\partial y} = \dfrac{\partial v_0}{\partial x} + \dfrac{\partial u_0}{\partial y} + \left(z\alpha^{az^2}\right)\cdot\left(\dfrac{\partial \phi_x}{\partial y} + \dfrac{\partial \phi_y}{\partial x}\right) + 2\left(z\alpha^{az^2} - z\right)\dfrac{\partial^2 w}{\partial x\,\partial y} \\ \gamma_{yz} = \dfrac{\partial v}{\partial z} + \dfrac{\partial w}{\partial y} = \left[\alpha^{az^2} + 2a\cdot\alpha^{az^2}\cdot z^2\cdot\ln(\alpha)\right]\cdot\left(\dfrac{\partial w}{\partial y} + \phi_y\right) \\ \gamma_{xz} = \dfrac{\partial u}{\partial z} + \dfrac{\partial w}{\partial x} = \left[\alpha^{az^2} + 2a\cdot\alpha^{az^2}\cdot z^2\cdot\ln(\alpha)\right]\cdot\left(\dfrac{\partial w}{\partial x} + \phi_x\right) \\ \varepsilon_{zz} = 0 \end{cases} \tag{131}$$

Deformability Matrixes

The differential operator $\boldsymbol{L}$ is, yet again, obtained from the strain field,

$$\boldsymbol{L}=\begin{bmatrix} \dfrac{\partial}{\partial x} & 0 & \left(z\alpha^{\alpha z^2}-z\right)\dfrac{\partial^2}{\partial x^2} & z\alpha^{\alpha z^2}\cdot\dfrac{\partial}{\partial x} & 0 \\ 0 & \dfrac{\partial}{\partial y} & \left(z\alpha^{\alpha z^2}-z\right)\dfrac{\partial^2}{\partial y^2} & 0 & z\alpha^{\alpha z^2}\cdot\dfrac{\partial}{\partial y} \\ \dfrac{\partial}{\partial y} & \dfrac{\partial}{\partial x} & 2\left(z\alpha^{\alpha z^2}-z\right)\dfrac{\partial^2}{\partial x\partial y} & z\alpha^{\alpha z^2}\cdot\dfrac{\partial}{\partial y} & z\alpha^{\alpha z^2}\cdot\dfrac{\partial}{\partial x} \\ 0 & 0 & \left(\alpha^{\alpha z^2}+2a\cdot\alpha^{\alpha z^2}\cdot z^2\cdot\ln(\alpha)\right)\dfrac{\partial}{\partial y} & 0 & \alpha^{\alpha z^2}+2a\cdot\alpha^{\alpha z^2}\cdot z^2\cdot\ln(\alpha) \\ 0 & 0 & \left(\alpha^{\alpha z^2}+2a\cdot\alpha^{\alpha z^2}\cdot z^2\cdot\ln(\alpha)\right)\dfrac{\partial}{\partial x} & \alpha^{\alpha z^2}+2a\cdot\alpha^{\alpha z^2}\cdot z^2\cdot\ln(\alpha) & 0 \end{bmatrix} \tag{132}$$

Following the same procedure adopted before, the deformability matrix, $\boldsymbol{B}(\boldsymbol{x}_I)$, can be expressed as a sum of the terms mentioned in equation (131),

$$\boldsymbol{B}(\boldsymbol{x}_I)=\boldsymbol{B}_0(\boldsymbol{x}_I)+\alpha^{\alpha z^2}\cdot\boldsymbol{B}_1(\boldsymbol{x}_I)+z\alpha^{\alpha z^2}\cdot\boldsymbol{B}_2(\boldsymbol{x}_I)+(-z)\cdot\boldsymbol{B}_3(\boldsymbol{x}_I)+2a\cdot\alpha^{\alpha z^2}\cdot z^2\cdot\ln(\alpha)\cdot\boldsymbol{B}_4(\boldsymbol{x}_I) \tag{133}$$

where the terms of the sum are given by,

$$\boldsymbol{B}^{i}{}_0(\boldsymbol{x}_I)=\begin{bmatrix} \dfrac{\partial\varphi_i(\boldsymbol{x}_I)}{\partial x} & 0 & 0 & 0 & 0 \\ 0 & \dfrac{\partial\varphi_i(\boldsymbol{x}_I)}{\partial y} & 0 & 0 & 0 \\ \dfrac{\partial\varphi_i(\boldsymbol{x}_I)}{\partial y} & \dfrac{\partial\varphi_i(\boldsymbol{x}_I)}{\partial x} & 0 & 0 & 0 \\ 0 & 0 & 0 & 0 & 0 \\ 0 & 0 & 0 & 0 & 0 \end{bmatrix}_i \qquad i=\{1,\,2,\,\ldots\,n\} \tag{134}$$

$$\boldsymbol{B}^{i}_1(\boldsymbol{x}_I)=\alpha^{\,a\,z^2}\cdot\begin{bmatrix} 0 & 0 & 0 & 0 & 0 \\ 0 & 0 & 0 & 0 & 0 \\ 0 & 0 & 0 & 0 & 0 \\ 0 & 0 & \dfrac{\partial\varphi_i(\boldsymbol{x}_I)}{\partial y} & 0 & \varphi_i(\boldsymbol{x}_I) \\ 0 & 0 & \dfrac{\partial\varphi_i(\boldsymbol{x}_I)}{\partial x} & \varphi_i(\boldsymbol{x}_I) & 0 \end{bmatrix}_i \qquad i=\{1,\,2,\,\ldots\,n\} \tag{135}$$

$$z\alpha^{az^2}\cdot \boldsymbol{B}^{i}{}_{2}(\boldsymbol{x}_I) = z\,\alpha^{a\,z^2}\cdot \begin{bmatrix} 0 & 0 & \dfrac{\partial^2\varphi_i(\boldsymbol{x}_I)}{\partial x^2} & \dfrac{\partial\varphi_i(\boldsymbol{x}_I)}{\partial x} & 0 \\ 0 & 0 & \dfrac{\partial^2\varphi_i(\boldsymbol{x}_I)}{\partial y^2} & 0 & \dfrac{\partial\varphi_i(\boldsymbol{x}_I)}{\partial y} \\ 0 & 0 & 2\dfrac{\partial^2\varphi_i(\boldsymbol{x}_I)}{\partial x\partial y} & \dfrac{\partial\varphi_i(\boldsymbol{x}_I)}{\partial y} & \dfrac{\partial\varphi_i(\boldsymbol{x}_I)}{\partial x} \\ 0 & 0 & 0 & 0 & 0 \\ 0 & 0 & 0 & 0 & 0 \end{bmatrix}_i \qquad i=\{1,\,2,\,\ldots\,n\} \tag{136}$$

$$(-z)\cdot \boldsymbol{B}^{i}{}_{3}(\boldsymbol{x}_I) = (-z)\cdot \begin{bmatrix} 0 & 0 & \dfrac{\partial^2\varphi_i(\boldsymbol{x}_I)}{\partial x^2} & 0 & 0 \\ 0 & 0 & \dfrac{\partial^2\varphi_i(\boldsymbol{x}_I)}{\partial y^2} & 0 & 0 \\ 0 & 0 & 2\dfrac{\partial^2\varphi_i(\boldsymbol{x}_I)}{\partial x\partial y} & 0 & 0 \\ 0 & 0 & 0 & 0 & 0 \\ 0 & 0 & 0 & 0 & 0 \end{bmatrix}_i \qquad i=\{1,\,2,\,\ldots\,n\} \tag{137}$$

$$2\,a\cdot\alpha^{az^2}\cdot z^2\cdot\ln(\alpha)\cdot \boldsymbol{B}^{i}{}_{4}(\boldsymbol{x}_I) = 2a\cdot\alpha^{az^2}\cdot z^2\cdot\ln(\alpha)\cdot \begin{bmatrix} 0 & 0 & 0 & 0 & 0 \\ 0 & 0 & 0 & 0 & 0 \\ 0 & 0 & 0 & 0 & 0 \\ 0 & 0 & \dfrac{\partial\varphi_i(\boldsymbol{x}_I)}{\partial y} & 0 & \varphi_i(\boldsymbol{x}_I) \\ 0 & 0 & \dfrac{\partial\varphi_i(\boldsymbol{x}_I)}{\partial x} & \varphi_i(\boldsymbol{x}_I) & 0 \end{bmatrix}_i \qquad i=\{1,\,2,\,\ldots\,n\} \tag{138}$$

Homogenised Constitutive Matrixes and Construction of the Global Stiffness Matrix

Unlike equation (103), where the terms are combinations of constants and powers, equation (133) describes the deformability matrix in the interest point $\boldsymbol{x}_I$ as a sum of terms with more complexity, which makes the determination of the integrals of the homogenised constitutive matrixes more difficult. Because of that, some of those matrixes are presented in the integral form, which is the simplest form to introduce them in the algorithm.

Considering again the equations (111) and (112), the stiffness matrix for the 'influence-domain' (or cell) of the interest point $\boldsymbol{x}_I$ can be calculated, using the homogenised constitutive matrixes and the deformability matrixes already defined,

$$\begin{cases} \boldsymbol{K}_{00} = \sum_{I=1}^{nQ} \omega_I \left(\sum_{i=1}^{k} \int_{z_{i-1}}^{z_i} \left(\boldsymbol{B}_0^T(\boldsymbol{x}_I) \cdot \boldsymbol{c}_k \cdot \boldsymbol{B}_0(\boldsymbol{x}_I) \right) \mathrm{d}z \right) = \sum_{I=1}^{nQ} \omega_I \cdot \boldsymbol{B}_0^T(\boldsymbol{x}_I) \cdot \boldsymbol{c}_1 \cdot \boldsymbol{B}_0(\boldsymbol{x}_I) \\ \boldsymbol{c}_1 = \sum_{i=1}^{k} \int_{z_{i-1}}^{z_i} \boldsymbol{c}_k \, \mathrm{d}z = \sum_{i=1}^{k} \left(z_i - z_{i-1} \right) \cdot \boldsymbol{c}_k \end{cases} \tag{139}$$

$$\begin{cases} \boldsymbol{K}_{01} = \sum_{I=1}^{nQ} \omega_I \left(\sum_{i=1}^{k} \int_{z_{i-1}}^{z_i} \left(\boldsymbol{B}_0^T(\boldsymbol{x}_I) \cdot \boldsymbol{c}_k \cdot \alpha^{az^2} \cdot \boldsymbol{B}_1(\boldsymbol{x}_I) \right) \mathrm{d}z \right) = \sum_{I=1}^{nQ} \omega_I \cdot \boldsymbol{B}_0^T(\boldsymbol{x}_I) \cdot \boldsymbol{c}_2 \cdot \boldsymbol{B}_1(\boldsymbol{x}_I) = \boldsymbol{K}_{10} \\ \boldsymbol{c}_2 = \sum_{i=1}^{k} \int_{z_{i-1}}^{z_i} \left(\boldsymbol{c}_k \cdot \alpha^{az^2} \right) \mathrm{d}z \end{cases} \tag{140}$$

$$\begin{cases} \boldsymbol{K}_{02} = \sum_{I=1}^{nQ} \omega_I \left(\sum_{i=1}^{k} \int_{z_{i-1}}^{z_i} \left(\boldsymbol{B}_0^T(\boldsymbol{x}_I) \cdot \boldsymbol{c}_k \cdot z\alpha^{az^2} \cdot \boldsymbol{B}_2(\boldsymbol{x}_I) \right) \mathrm{d}z \right) = \sum_{I=1}^{nQ} \omega_I \cdot \boldsymbol{B}_0^T(\boldsymbol{x}_I) \cdot \boldsymbol{c}_3 \cdot \boldsymbol{B}_2(\boldsymbol{x}_I) = \boldsymbol{K}_{20} \\ \boldsymbol{c}_3 = \sum_{i=1}^{k} \int_{z_{i-1}}^{z_i} \left(\boldsymbol{c}_k \cdot z\alpha^{az^2} \right) \mathrm{d}z = \frac{1}{2a \cdot \ln(\alpha)} \cdot \sum_{i=1}^{k} \left(\alpha^{az_i^2} - \alpha^{az_{i-1}^2} \right) \cdot \boldsymbol{c}_k \end{cases} \tag{141}$$

$$\begin{cases} \boldsymbol{K}_{03} = \sum_{I=1}^{nQ} \omega_I \left(\sum_{i=1}^{k} \int_{z_{i-1}}^{z_i} \left(\boldsymbol{B}_0^T(\boldsymbol{x}_I) \cdot \boldsymbol{c}_k \cdot (-z) \cdot \boldsymbol{B}_3(\boldsymbol{x}_I) \right) \mathrm{d}z \right) = \sum_{I=1}^{nQ} \omega_I \cdot \boldsymbol{B}_0^T(\boldsymbol{x}_I) \cdot \boldsymbol{c}_4 \cdot \boldsymbol{B}_3(\boldsymbol{x}_I) = \boldsymbol{K}_{30} \\ \boldsymbol{c}_4 = \sum_{i=1}^{k} \int_{z_{i-1}}^{z_i} \left[\boldsymbol{c}_k \cdot (-z) \right] \mathrm{d}z = \sum_{i=1}^{k} \left(\frac{z_{i-1}^2}{2} - \frac{z_i^2}{2} \right) \cdot \boldsymbol{c}_k \end{cases} \tag{142}$$

$$\begin{cases} \boldsymbol{K}_{04} = \sum_{I=1}^{nQ} \omega_I \left(\sum_{i=1}^{k} \int_{z_{i-1}}^{z_i} \left(\boldsymbol{B}_0^T(\boldsymbol{x}_I) \cdot \boldsymbol{c}_k \cdot \left[2a \cdot \alpha^{az^2} \cdot z^2 \cdot \ln(\alpha) \right] \cdot \boldsymbol{B}_4(\boldsymbol{x}_I) \right) \mathrm{d}z \right) = \sum_{I=1}^{nQ} \omega_I \cdot \boldsymbol{B}_0^T(\boldsymbol{x}_I) \cdot \boldsymbol{c}_5 \cdot \boldsymbol{B}_4(\boldsymbol{x}_I) = \boldsymbol{K}_{40} \\ \boldsymbol{c}_5 = \sum_{i=1}^{k} \int_{z_{i-1}}^{z_i} \left[\boldsymbol{c}_k \cdot 2a \cdot \alpha^{az^2} \cdot z^2 \cdot \ln(\alpha) \right] \mathrm{d}z \end{cases} \tag{143}$$

$$\begin{cases} \boldsymbol{K}_{11} = \sum_{I=1}^{nQ} \omega_I \left(\sum_{i=1}^{k} \int_{z_{i-1}}^{z_i} \left(\boldsymbol{B}_1^T(\boldsymbol{x}_I) \cdot \boldsymbol{c}_k \cdot \left(\alpha^{a z^2} \cdot \alpha^{a z^2} \right) \cdot \boldsymbol{B}_1(\boldsymbol{x}_I) \right) \mathrm{d}z \right) = \sum_{I=1}^{nQ} \omega_I \cdot \boldsymbol{B}_1^T(\boldsymbol{x}_I) \cdot \boldsymbol{c}_6 \cdot \boldsymbol{B}_1(\boldsymbol{x}_I) \\ \boldsymbol{c}_6 = \sum_{i=1}^{k} \int_{z_{i-1}}^{z_i} \left[\boldsymbol{c}_k \cdot \left(\alpha^{2 a z^2} \right) \right] \mathrm{d}z \end{cases} \tag{144}$$

$$\begin{cases} \boldsymbol{K}_{12} = \sum_{I=1}^{nQ} \omega_I \left(\sum_{i=1}^{k} \int_{z_{i-1}}^{z_i} \left(\boldsymbol{B}_1^T(\boldsymbol{x}_I) \cdot \boldsymbol{c}_k \cdot \left(z\alpha^{a z^2} \cdot \alpha^{a z^2} \right) \cdot \boldsymbol{B}_2(\boldsymbol{x}_I) \right) \mathrm{d}z \right) = \sum_{I=1}^{nQ} \omega_I \cdot \boldsymbol{B}_1^T(\boldsymbol{x}_I) \cdot \boldsymbol{c}_7 \cdot \boldsymbol{B}_2(\boldsymbol{x}_I) = \boldsymbol{K}_{21} \\ \boldsymbol{c}_7 = \sum_{i=1}^{k} \int_{z_{i-1}}^{z_i} \left[\boldsymbol{c}_k \cdot \left(z\alpha^{2a z^2} \right) \right] \mathrm{d}z = \frac{1}{4a \cdot \ln(\alpha)} \cdot \sum_{i=1}^{k} \left(\alpha^{2a z_i^2} - \alpha^{2a z_{i-1}^2} \right) \cdot \boldsymbol{c}_k \end{cases} \tag{145}$$

$$\begin{cases} \boldsymbol{K}_{13} = \sum_{I=1}^{nQ} \omega_I \left(\sum_{i=1}^{k} \int_{z_{i-1}}^{z_i} \left(\boldsymbol{B}_1^T(\boldsymbol{x}_I) \cdot \boldsymbol{c}_k \cdot (-z) \cdot (\alpha^{a z^2}) \cdot \boldsymbol{B}_3(\boldsymbol{x}_I) \right) \mathrm{d}z \right) = \sum_{I=1}^{nQ} \omega_I \cdot \boldsymbol{B}_1^T(\boldsymbol{x}_I) \cdot \boldsymbol{c}_8 \cdot \boldsymbol{B}_3(\boldsymbol{x}_I) = \boldsymbol{K}_{31} \\ \boldsymbol{c}_8 = -\boldsymbol{c}_3 \end{cases} \tag{146}$$

$$\begin{cases} \boldsymbol{K}_{14} = \sum_{I=1}^{nQ} \omega_I \left(\sum_{i=1}^{k} \int_{z_{i-1}}^{z_i} \left(\boldsymbol{B}_1^T(\boldsymbol{x}_I) \cdot \boldsymbol{c}_k \cdot \alpha^{a z^2} \cdot \left[2a \cdot \alpha^{a z^2} \cdot z^2 \cdot \ln(\alpha) \right] \cdot \boldsymbol{B}_4(\boldsymbol{x}_I) \right) \mathrm{d}z \right) = \sum_{I=1}^{nQ} \omega_I \cdot \boldsymbol{B}_1^T(\boldsymbol{x}_I) \cdot \boldsymbol{c}_9 \cdot \boldsymbol{B}_4(\boldsymbol{x}_I) = \boldsymbol{K}_{41} \\ \boldsymbol{c}_9 = \sum_{i=1}^{k} \int_{z_{i-1}}^{z_i} \left(\boldsymbol{c}_k \cdot \left[2a \cdot \alpha^{2a z^2} \cdot z^2 \cdot \ln(\alpha) \right] \right) \mathrm{d}z \end{cases} \tag{147}$$

$$\begin{cases} \boldsymbol{K}_{22} = \sum_{I=1}^{nQ} \omega_I \left(\sum_{i=1}^{k} \int_{z_{i-1}}^{z_i} \left(\boldsymbol{B}_2^T(\boldsymbol{x}_I) \cdot \boldsymbol{c}_k \cdot \left(z\alpha^{a z^2} \right)^2 \cdot \boldsymbol{B}_2(\boldsymbol{x}_I) \right) \mathrm{d}z \right) = \sum_{I=1}^{nQ} \omega_I \cdot \boldsymbol{B}_2^T(\boldsymbol{x}_I) \cdot \boldsymbol{c}_{10} \cdot \boldsymbol{B}_2(\boldsymbol{x}_I) \\ \boldsymbol{c}_{10} = \sum_{i=1}^{k} \int_{z_{i-1}}^{z_i} \left[\boldsymbol{c}_k \cdot \left(z\alpha^{a z^2} \right)^2 \right] \mathrm{d}z \end{cases} \tag{148}$$

$$\begin{cases} \boldsymbol{K}_{23} = \sum_{I=1}^{nQ} \omega_I \left(\sum_{i=1}^{k} \int_{z_{i-1}}^{z_i} \left(\boldsymbol{B}_2^T(\boldsymbol{x}_I) \cdot \boldsymbol{c}_k \cdot \left[z\alpha^{a z^2} \cdot (-z) \right] \cdot \boldsymbol{B}_3(\boldsymbol{x}_I) \right) \mathrm{d}z \right) = \sum_{I=1}^{nQ} \omega_I \cdot \boldsymbol{B}_2^T(\boldsymbol{x}_I) \cdot \boldsymbol{c}_{11} \cdot \boldsymbol{B}_3(\boldsymbol{x}_I) = \boldsymbol{K}_{32} \\ \boldsymbol{c}_{11} = \sum_{i=1}^{k} \int_{z_{i-1}}^{z_i} \left[\boldsymbol{c}_k \cdot \left(z\alpha^{a z^2} \cdot (-z) \right) \right] \mathrm{d}z = -\frac{\boldsymbol{c}_5}{2a \cdot \ln(\alpha)} \end{cases} \tag{149}$$

$$\begin{cases} \boldsymbol{K}_{24} = \sum_{I=1}^{nQ} \omega_I \left(\sum_{i=1}^{k} \int_{z_{i-1}}^{z_i} \left(\boldsymbol{B}_2^T(\boldsymbol{x}_I) \cdot \boldsymbol{c}_k \cdot \left[2a \cdot \alpha^{a z^2} \cdot z^2 \cdot \ln(\alpha) \cdot \left(z\alpha^{a z^2} \right) \right] \cdot \boldsymbol{B}_4(\boldsymbol{x}_I) \right) \mathrm{d}z \right) = \\ \quad = \sum_{I=1}^{nQ} \omega_I \cdot \boldsymbol{B}_2^T(\boldsymbol{x}_I) \cdot \boldsymbol{c}_{12} \cdot \boldsymbol{B}_4(\boldsymbol{x}_I) = \boldsymbol{K}_{42} \\ \boldsymbol{c}_{12} = \sum_{i=1}^{k} \int_{z_{i-1}}^{z_i} \left[\boldsymbol{c}_k \cdot 2a \cdot \alpha^{a z^2} \cdot z^2 \cdot \ln(\alpha) \cdot \left(z\alpha^{a z^2} \right) \right] \mathrm{d}z = \\ \quad = \frac{1}{2a \cdot \ln(\alpha)} \cdot \sum_{i=1}^{k} \left[\alpha^{2a z_i^2} \cdot \left(a \cdot \ln(\alpha) \cdot z_i^2 - 1/2 \right) - \alpha^{2a z_{i-1}^2} \cdot \left(a \cdot \ln(\alpha) \cdot z_{i-1}^2 - 1/2 \right) \right] \cdot \boldsymbol{c}_k \end{cases} \tag{150}$$

$$\begin{cases} \boldsymbol{K}_{33} = \sum_{I=1}^{nQ} \omega_I \left(\sum_{i=1}^{k} \int_{z_{i-1}}^{z_i} \left(\boldsymbol{B}_3^T(\boldsymbol{x}_I) \cdot \boldsymbol{c}_k \cdot (-z)^2 \cdot \boldsymbol{B}_3(\boldsymbol{x}_I) \right) \mathrm{d}z \right) = \sum_{I=1}^{nQ} \omega_I \cdot \boldsymbol{B}_3^T(\boldsymbol{x}_I) \cdot \boldsymbol{c}_{12} \cdot \boldsymbol{B}_3(\boldsymbol{x}_I) \\ \boldsymbol{c}_{13} = \sum_{i=1}^{k} \int_{z_{i-1}}^{z_i} \left[\boldsymbol{c}_k \cdot (-z)^2 \right] \mathrm{d}z = \sum_{i=1}^{k} \left(\frac{z_i^3}{3} - \frac{z_{i-1}^3}{3} \right) \cdot \boldsymbol{c}_k \end{cases} \tag{151}$$

$$\begin{cases} \boldsymbol{K}_{34} = \sum_{I=1}^{nQ} \omega_I \left(\sum_{i=1}^{k} \int_{z_{i-1}}^{z_i} \left(\boldsymbol{B}_3^T(\boldsymbol{x}_I) \cdot \boldsymbol{c}_k \cdot \left[(-z) \cdot 2a \cdot \alpha^{a z^2} \cdot z^2 \cdot \ln(\alpha) \right] \cdot \boldsymbol{B}_4(\boldsymbol{x}_I) \right) \mathrm{d}z \right) = \\ \quad = \sum_{I=1}^{nQ} \omega_I \cdot \boldsymbol{B}_3^T(\boldsymbol{x}_I) \cdot \boldsymbol{c}_{14} \cdot \boldsymbol{B}_4(\boldsymbol{x}_I) = \boldsymbol{K}_{43} \\ \boldsymbol{c}_{14} = \sum_{i=1}^{k} \int_{z_{i-1}}^{z_i} \left[\boldsymbol{c}_k \cdot (-z) \cdot 2a \cdot \alpha^{a z^2} \cdot z^2 \cdot \ln(\alpha) \right] \mathrm{d}z = \\ \quad = \frac{2}{a \cdot \ln(\alpha)} \cdot \sum_{i=1}^{k} \left[\alpha^{a z_{i-1}^2} \cdot \left(\frac{a \cdot \ln(\alpha) \cdot z_{i-1}^2 - 1}{2} \right) - \alpha^{a z_i^2} \cdot \left(\frac{a \cdot \ln(\alpha) \cdot z_i^2 - 1}{2} \right) \right] \cdot \boldsymbol{c}_k \end{cases} \tag{152}$$

$$\begin{cases} \boldsymbol{K}_{44} = \sum_{I=1}^{nQ} \omega_I \left(\sum_{i=1}^{k} \int_{z_{i-1}}^{z_i} \left(\boldsymbol{B}_4^T(x_I) \cdot \boldsymbol{c}_k \cdot \left[2a \cdot \alpha^{a z^2} \cdot z^2 \cdot \ln(\alpha) \right]^2 \cdot \boldsymbol{B}_4(x_I) \right) \mathrm{d}z \right) = \sum_{I=1}^{nQ} \omega_I \cdot \boldsymbol{B}_4^T(x_I) \cdot \boldsymbol{c}_{15} \cdot \boldsymbol{B}_4(x_I) \\ \boldsymbol{c}_{15} = \sum_{i=1}^{k} \int_{z_{i-1}}^{z_i} \left[\boldsymbol{c}_k \cdot \left(2a \cdot \alpha^{a z^2} \cdot z^2 \cdot \ln(\alpha) \right)^2 \right] \mathrm{d}z \end{cases} \quad (153)$$

4.4.3 Touratier Plate Theory

The Touratier model predicts the variation of the in-plane displacements along the thickness of the plate as trigonometric function (it is a Trigonometric Shear Deformation Theory).

Similarly to ESDTs, the Touratier theory can also be approximated as a polynomial function,

$$\text{Touratier}: f(z) = \frac{h}{\pi} \sin\left(\frac{\pi z}{h} \right) = z - 1.645 \frac{z^3}{h^2} + 0.812 \frac{z^5}{h^4} - 0.191 \frac{z^7}{h^6} + 0.0261 \frac{z^9}{h^8} + \ldots \quad (154)$$

It becomes clear that, by comparison to Karama's theory - equation (129) - , in Touratier model the coefficients of successive terms are decreasing more rapidly. This makes the Karama model (2009 [30]) stronger than the one by Touratier (that was proposed in 1991 [29]).

Kinematic Relations

In equations (155) and (156), the displacement and strain field, respectively, are determined,

$$\begin{cases} u(x,y,z) = u_0(x,y) - z\cdot\dfrac{\partial w(x,y)}{\partial x} + \left[\dfrac{h}{\pi}\sin\left(\dfrac{\pi z}{h}\right)\right]\cdot\left[\phi_x(x,y) + \dfrac{\partial w(x,y)}{\partial x}\right] \\ v(x,y,z) = v_0(x,y) - z\cdot\dfrac{\partial w(x,y)}{\partial y} + \left[\dfrac{h}{\pi}\sin\left(\dfrac{\pi z}{h}\right)\right]\cdot\left[\phi_y(x,y) + \dfrac{\partial w(x,y)}{\partial y}\right] \\ w(x,y,z) = w_0(x,y) \end{cases} \tag{155}$$

$$= \begin{cases} u(x,y,z) = u_0(x,y) + \left(\dfrac{h}{\pi}\sin\left(\dfrac{\pi z}{h}\right) - z\right)\cdot\dfrac{\partial w(x,y)}{\partial x} + \left[\dfrac{h}{\pi}\sin\left(\dfrac{\pi z}{h}\right)\right]\cdot\phi_x(x,y) \\ v(x,y,z) = v_0(x,y) + \left(\dfrac{h}{\pi}\sin\left(\dfrac{\pi z}{h}\right) - z\right)\cdot\dfrac{\partial w(x,y)}{\partial y} + \left[\dfrac{h}{\pi}\sin\left(\dfrac{\pi z}{h}\right)\right]\cdot\phi_y(x,y) \\ w(x,y,z) = w_0(x,y) \end{cases}$$

$$\begin{cases} \varepsilon_{xx} = \dfrac{\partial u}{\partial x} = \dfrac{\partial u_0}{\partial x} + \left[\dfrac{h}{\pi}\sin\left(\dfrac{\pi z}{h}\right)\right]\cdot\dfrac{\partial \phi_x}{\partial x} + \left[\dfrac{h}{\pi}\sin\left(\dfrac{\pi z}{h}\right) - z\right]\cdot\dfrac{\partial^2 w}{\partial x^2} \\ \varepsilon_{yy} = \dfrac{\partial v}{\partial y} = \dfrac{\partial v_0}{\partial x} + \left[\dfrac{h}{\pi}\sin\left(\dfrac{\pi z}{h}\right)\right]\cdot\dfrac{\partial \phi_y}{\partial y} + \left[\dfrac{h}{\pi}\sin\left(\dfrac{\pi z}{h}\right) - z\right]\cdot\dfrac{\partial^2 w}{\partial y^2} \\ \gamma_{xy} = \dfrac{\partial v}{\partial x} + \dfrac{\partial u}{\partial y} = \dfrac{\partial v_0}{\partial x} + \dfrac{\partial u_0}{\partial y} + \left[\dfrac{h}{\pi}\sin\left(\dfrac{\pi z}{h}\right)\right]\cdot\left(\dfrac{\partial \phi_x}{\partial y} + \dfrac{\partial \phi_y}{\partial x}\right) + 2\left[\dfrac{h}{\pi}\sin\left(\dfrac{\pi z}{h}\right) - z\right]\dfrac{\partial^2 w}{\partial x\partial y} \\ \gamma_{yz} = \dfrac{\partial v}{\partial z} + \dfrac{\partial w}{\partial y} = \dfrac{\partial w}{\partial y} + \cos\left(\dfrac{\pi z}{h}\right)\phi_y + \left[\cos\left(\dfrac{\pi z}{h}\right) - 1\right]\dfrac{\partial w}{\partial y} = \cos\left(\dfrac{\pi z}{h}\right)\cdot\left(\phi_y + \dfrac{\partial w}{\partial y}\right) \\ \gamma_{xz} = \dfrac{\partial u}{\partial z} + \dfrac{\partial w}{\partial x} = \dfrac{\partial w}{\partial x} + \cos\left(\dfrac{\pi z}{h}\right)\phi_x + \left[\cos\left(\dfrac{\pi z}{h}\right) - 1\right]\dfrac{\partial w}{\partial x} = \cos\left(\dfrac{\pi z}{h}\right)\cdot\left(\phi_x + \dfrac{\partial w}{\partial x}\right) \\ \varepsilon_{zz} = 0 \end{cases} \tag{156}$$

Deformability Matrixes

From equation (156), the differential operator $\boldsymbol{L}$ is defined,

$$\boldsymbol{L}=\begin{bmatrix} \dfrac{\partial}{\partial x} & 0 & \left[\dfrac{h}{\pi}\sin\left(\dfrac{\pi z}{h}\right)-z\right]\dfrac{\partial^2}{\partial x^2} & \dfrac{h}{\pi}\sin\left(\dfrac{\pi z}{h}\right)\dfrac{\partial}{\partial x} & 0 \\ 0 & \dfrac{\partial}{\partial y} & \left[\dfrac{h}{\pi}\sin\left(\dfrac{\pi z}{h}\right)-z\right]\dfrac{\partial^2}{\partial y^2} & 0 & \dfrac{h}{\pi}\sin\left(\dfrac{\pi z}{h}\right)\dfrac{\partial}{\partial y} \\ \dfrac{\partial}{\partial y} & \dfrac{\partial}{\partial x} & 2\left[\dfrac{h}{\pi}\sin\left(\dfrac{\pi z}{h}\right)-z\right]\dfrac{\partial^2}{\partial x\partial y} & \dfrac{h}{\pi}\sin\left(\dfrac{\pi z}{h}\right)\dfrac{\partial}{\partial y} & \dfrac{h}{\pi}\sin\left(\dfrac{\pi z}{h}\right)\dfrac{\partial}{\partial x} \\ 0 & 0 & \cos\left(\dfrac{\pi z}{h}\right)\dfrac{\partial}{\partial y} & 0 & \cos\left(\dfrac{\pi z}{h}\right) \\ 0 & 0 & \cos\left(\dfrac{\pi z}{h}\right)\dfrac{\partial}{\partial x} & \cos\left(\dfrac{\pi z}{h}\right) & 0 \end{bmatrix} \tag{157}$$

and the deformability matrix,

$$\boldsymbol{B}(\boldsymbol{x}_I)=\boldsymbol{B}_0(\boldsymbol{x}_I)+\cos\left(\frac{\pi z}{h}\right)\cdot\boldsymbol{B}_1(\boldsymbol{x}_I)+\frac{h}{\pi}\sin\left(\frac{\pi z}{h}\right)\cdot\boldsymbol{B}_2(\boldsymbol{x}_I)+(-z)\boldsymbol{B}_3(\boldsymbol{x}_I) \tag{158}$$

where,

$$\boldsymbol{B}^i{}_0(\boldsymbol{x}_I)=\begin{bmatrix} \dfrac{\partial\varphi_i(\boldsymbol{x}_I)}{\partial x} & 0 & 0 & 0 & 0 \\ 0 & \dfrac{\partial\varphi_i(\boldsymbol{x}_I)}{\partial y} & 0 & 0 & 0 \\ \dfrac{\partial\varphi_i(\boldsymbol{x}_I)}{\partial y} & \dfrac{\partial\varphi_i(\boldsymbol{x}_I)}{\partial x} & 0 & 0 & 0 \\ 0 & 0 & 0 & 0 & 0 \\ 0 & 0 & 0 & 0 & 0 \end{bmatrix}_i \quad i=\{1,\,2,\,\ldots\,n\} \tag{159}$$

$$\cos\left(\frac{\pi z}{h}\right)\cdot\boldsymbol{B}^i{}_1(\boldsymbol{x}_I)=\cos\left(\frac{\pi z}{h}\right)\cdot\begin{bmatrix} 0 & 0 & 0 & 0 & 0 \\ 0 & 0 & 0 & 0 & 0 \\ 0 & 0 & 0 & 0 & 0 \\ 0 & 0 & \dfrac{\partial\varphi_i(\boldsymbol{x}_I)}{\partial y} & 0 & \varphi_i(\boldsymbol{x}_I) \\ 0 & 0 & \dfrac{\partial\varphi_i(\boldsymbol{x}_I)}{\partial x} & \varphi_i(\boldsymbol{x}_I) & 0 \end{bmatrix}_i \quad i=\{1,\,2,\,\ldots\,n\} \tag{160}$$

$$\frac{h}{\pi}\sin\left(\frac{\pi z}{h}\right)\cdot \boldsymbol{B}^{i}{}_{2}(\boldsymbol{x}_I) = \frac{h}{\pi}\sin\left(\frac{\pi z}{h}\right)\cdot \begin{bmatrix} 0 & 0 & \dfrac{\partial^2 \varphi_i(\boldsymbol{x}_I)}{\partial x^2} & \dfrac{\partial \varphi_i(\boldsymbol{x}_I)}{\partial x} & 0 \\ 0 & 0 & \dfrac{\partial^2 \varphi_i(\boldsymbol{x}_I)}{\partial y^2} & 0 & \dfrac{\partial \varphi_i(\boldsymbol{x}_I)}{\partial y} \\ 0 & 0 & 2\dfrac{\partial^2 \varphi_i(\boldsymbol{x}_I)}{\partial x \partial y} & \dfrac{\partial \varphi_i(\boldsymbol{x}_I)}{\partial y} & \dfrac{\partial \varphi_i(\boldsymbol{x}_I)}{\partial x} \\ 0 & 0 & 0 & 0 & 0 \\ 0 & 0 & 0 & 0 & 0 \end{bmatrix}_i \quad i = \{1, 2, \ldots n\} \tag{161}$$

$$(-z)\cdot \boldsymbol{B}^{i}{}_{3}(\boldsymbol{x}_I) = (-z)\cdot \begin{bmatrix} 0 & 0 & \dfrac{\partial^2 \varphi_i(\boldsymbol{x}_I)}{\partial x^2} & 0 & 0 \\ 0 & 0 & \dfrac{\partial^2 \varphi_i(\boldsymbol{x}_I)}{\partial y^2} & 0 & 0 \\ 0 & 0 & 2\dfrac{\partial^2 \varphi_i(\boldsymbol{x}_I)}{\partial x \partial y} & 0 & 0 \\ 0 & 0 & 0 & 0 & 0 \\ 0 & 0 & 0 & 0 & 0 \end{bmatrix}_i \quad i = \{1, 2, \ldots n\} \tag{162}$$

Homogenised Constitutive Matrixes and Construction of the Global Stiffness Matrix

Following the same procedure adopted before and noticing that, in this case,

$$\boldsymbol{K} = \sum_{i=0}^{3}\sum_{j=0}^{3} \boldsymbol{K}_{ij} \tag{163}$$

the stiffness sub-matrixes and the homogeneised constitutive matrixes are calculate,

$$\begin{cases} \boldsymbol{K}_{00} = \sum_{I=1}^{nQ} \omega_I \left(\sum_{i=1}^{k} \int_{z_{i-1}}^{z_i} \left(\boldsymbol{B}_0^T(\boldsymbol{x}_I)\cdot \boldsymbol{c}_k \cdot \boldsymbol{B}_0(\boldsymbol{x}_I) \right) \mathrm{d}z \right) = \sum_{I=1}^{nQ} \omega_I \cdot \boldsymbol{B}_0^T(\boldsymbol{x}_I)\cdot \boldsymbol{c}_1 \cdot \boldsymbol{B}_0(\boldsymbol{x}_I) \\ \boldsymbol{c}_1 = \sum_{i=1}^{k} \int_{z_{i-1}}^{z_i} \boldsymbol{c}_k \, \mathrm{d}z = \sum_{i=1}^{k} \left(z_i - z_{i-1} \right)\cdot \boldsymbol{c}_k \end{cases} \tag{164}$$

$$\begin{cases} \boldsymbol{K}_{01} = \sum_{I=1}^{nQ} \omega_I \left(\sum_{i=1}^{k} \int_{z_{i-1}}^{z_i} \left(\boldsymbol{B}_0^T(\boldsymbol{x}_I) \cdot \boldsymbol{c}_k \cdot \cos\left(\frac{\pi z}{h}\right) \cdot \boldsymbol{B}_1(\boldsymbol{x}_I) \right) \mathrm{d}z \right) = \sum_{I=1}^{nQ} \omega_I \cdot \boldsymbol{B}_0^T(\boldsymbol{x}_I) \cdot \boldsymbol{c}_2 \cdot \boldsymbol{B}_1(\boldsymbol{x}_I) = \boldsymbol{K}_{10} \\ \boldsymbol{c}_2 = \sum_{i=1}^{k} \int_{z_{i-1}}^{z_i} \left[\boldsymbol{c}_k \cdot \cos\left(\frac{\pi z}{h}\right) \right] \mathrm{d}z = -\frac{h}{\pi} \cdot \sum_{i=1}^{k} \left[\sin\left(\frac{\pi z_{i-1}}{h}\right) - \sin\left(\frac{\pi z_i}{h}\right) \right] \cdot \boldsymbol{c}_k \end{cases} \tag{165}$$

$$\begin{cases} \boldsymbol{K}_{02} = \sum_{I=1}^{nQ} \omega_I \left(\sum_{i=1}^{k} \int_{z_{i-1}}^{z_i} \left(\boldsymbol{B}_0^T(\boldsymbol{x}_I) \cdot \boldsymbol{c}_k \cdot \frac{h}{\pi} \sin\left(\frac{\pi z}{h}\right) \cdot \boldsymbol{B}_2(\boldsymbol{x}_I) \right) \mathrm{d}z \right) = \sum_{I=1}^{nQ} \omega_I \cdot \boldsymbol{B}_0^T(\boldsymbol{x}_I) \cdot \boldsymbol{c}_3 \cdot \boldsymbol{B}_2(\boldsymbol{x}_I) = \boldsymbol{K}_{20} \\ \boldsymbol{c}_3 = \sum_{i=1}^{k} \int_{z_{i-1}}^{z_i} \left[\boldsymbol{c}_k \cdot \frac{h}{\pi} \sin\left(\frac{\pi z}{h}\right) \right] \mathrm{d}z = \left(\frac{h}{\pi}\right)^2 \cdot \sum_{i=1}^{k} \left[\cos\left(\frac{\pi z_{i-1}}{h}\right) - \cos\left(\frac{\pi z_i}{h}\right) \right] \cdot \boldsymbol{c}_k \end{cases} \tag{166}$$

$$\begin{cases} \boldsymbol{K}_{03} = \sum_{I=1}^{nQ} \omega_I \left(\sum_{i=1}^{k} \int_{z_{i-1}}^{z_i} \left(\boldsymbol{B}_0^T(\boldsymbol{x}_I) \cdot \boldsymbol{c}_k \cdot (-z) \cdot \boldsymbol{B}_3(\boldsymbol{x}_I) \right) \mathrm{d}z \right) = \sum_{I=1}^{nQ} \omega_I \cdot \boldsymbol{B}_0^T(\boldsymbol{x}_I) \cdot \boldsymbol{c}_4 \cdot \boldsymbol{B}_3(\boldsymbol{x}_I) = \boldsymbol{K}_{30} \\ \boldsymbol{c}_4 = \sum_{i=1}^{k} \int_{z_{i-1}}^{z_i} \left[\boldsymbol{c}_k \cdot (-z) \right] \mathrm{d}z = \sum_{i=1}^{k} \left(\frac{z_{i-1}^2}{2} - \frac{z_i^2}{2} \right) \cdot \boldsymbol{c}_k \end{cases} \tag{167}$$

$$\begin{cases} \boldsymbol{K}_{11} = \sum_{I=1}^{nQ} \omega_I \left(\sum_{i=1}^{k} \int_{z_{i-1}}^{z_i} \left(\boldsymbol{B}_1^T(\boldsymbol{x}_I) \cdot \boldsymbol{c}_k \cdot \cos^2\left(\frac{\pi z}{h}\right) \cdot \boldsymbol{B}_1(\boldsymbol{x}_I) \right) \mathrm{d}z \right) = \sum_{I=1}^{nQ} \omega_I \cdot \boldsymbol{B}_1^T(\boldsymbol{x}_I) \cdot \boldsymbol{c}_5 \cdot \boldsymbol{B}_1(\boldsymbol{x}_I) \\ \boldsymbol{c}_5 = \sum_{i=1}^{k} \int_{z_{i-1}}^{z_i} \left[\boldsymbol{c}_k \cdot \cos^2\left(\frac{\pi z}{h}\right) \right] \mathrm{d}z = \sum_{i=1}^{k} \left[\frac{z_i}{2} - \frac{z_{i-1}}{2} - \frac{h}{4\pi} \left(\sin\left(\frac{2\pi \cdot z_{i-1}}{h}\right) - \sin\left(\frac{2\pi \cdot z_i}{h}\right) \right) \right] \cdot \boldsymbol{c}_k \end{cases} \tag{168}$$

$$\begin{cases} \boldsymbol{K}_{12} = \sum_{I=1}^{nQ} \omega_I \left(\sum_{i=1}^{k} \int_{z_{i-1}}^{z_i} \left(\boldsymbol{B}_1^T(\boldsymbol{x}_I) \cdot \boldsymbol{c}_k \cdot \cos\left(\frac{\pi z}{h}\right) \cdot \frac{h}{\pi} \sin\left(\frac{\pi z}{h}\right) \cdot \boldsymbol{B}_2(\boldsymbol{x}_I) \right) \mathrm{d}z \right) = \sum_{I=1}^{nQ} \omega_I \cdot \boldsymbol{B}_1^T(\boldsymbol{x}_I) \cdot \boldsymbol{c}_6 \cdot \boldsymbol{B}_2(\boldsymbol{x}_I) = \boldsymbol{K}_{21} \\ \boldsymbol{c}_6 = \sum_{i=1}^{k} \int_{z_{i-1}}^{z_i} \left[\boldsymbol{c}_k \cdot \cos\left(\frac{\pi z}{h}\right) \cdot \frac{h}{\pi} \sin\left(\frac{\pi z}{h}\right) \right] \mathrm{d}z = \frac{h^2}{2\pi^2} \cdot \sum_{i=1}^{k} \left[\cos^2\left(\frac{\pi z_{i-1}}{h}\right) - \cos^2\left(\frac{\pi z_i}{h}\right) \right] \cdot \boldsymbol{c}_k \end{cases} \tag{169}$$

$$\begin{cases} \boldsymbol{K}_{13} = \sum_{I=1}^{nQ} \omega_I \left(\sum_{i=1}^{k} \int_{z_{i-1}}^{z_i} \left(\boldsymbol{B}_1^T(\boldsymbol{x}_I) \cdot \boldsymbol{c}_k \cdot (-z) \cdot \cos\left(\frac{\pi z}{h}\right) \cdot \boldsymbol{B}_3(\boldsymbol{x}_I) \right) \mathrm{d}z \right) = \sum_{I=1}^{nQ} \omega_I \cdot \boldsymbol{B}_1^T(\boldsymbol{x}_I) \cdot \boldsymbol{c}_7 \cdot \boldsymbol{B}_3(\boldsymbol{x}_I) = \boldsymbol{K}_{31} \\ \boldsymbol{c}_7 = \sum_{i=1}^{k} \int_{z_{i-1}}^{z_i} \left[\boldsymbol{c}_k \cdot (-z) \cdot \cos\left(\frac{\pi z}{h}\right) \right] \mathrm{d}z = \\ \quad = \frac{h}{\pi^2} \sum_{i=1}^{k} \left[\left(h \sin\left(\frac{\pi z_{i-1}}{h}\right) - \pi z_{i-1} \cos\left(\frac{\pi z_{i-1}}{h}\right) \right) - \left(h \sin\left(\frac{\pi z_i}{h}\right) - \pi z_i \cos\left(\frac{\pi z_i}{h}\right) \right) \right] \cdot \boldsymbol{c}_k \end{cases} \tag{170}$$

$$\begin{cases} \boldsymbol{K}_{22} = \sum_{I=1}^{nQ} \omega_I \left(\sum_{i=1}^{k} \int_{z_{i-1}}^{z_i} \left(\boldsymbol{B}_2^T(\boldsymbol{x}_I) \cdot \boldsymbol{c}_k \cdot \left[\frac{h}{\pi} \sin\left(\frac{\pi z}{h}\right) \right]^2 \cdot \boldsymbol{B}_2(\boldsymbol{x}_I) \right) \mathrm{d}z \right) = \sum_{I=1}^{nQ} \omega_I \cdot \boldsymbol{B}_2^T(\boldsymbol{x}_I) \cdot \boldsymbol{c}_8 \cdot \boldsymbol{B}_2(\boldsymbol{x}_I) \\ \boldsymbol{c}_8 = \sum_{i=1}^{k} \int_{z_{i-1}}^{z_i} \left[\boldsymbol{c}_k \cdot \left[\frac{h}{\pi} \sin\left(\frac{\pi z}{h}\right) \right]^2 \right] \mathrm{d}z = -\frac{h^2}{4\pi^3} \cdot \sum_{i=1}^{k} \left[2\pi \left(z_{i-1} - z_i \right) - h \sin\left(\frac{\pi z_{i-1}}{h}\right) + h \sin\left(\frac{\pi z_i}{h}\right) \right] \cdot \boldsymbol{c}_k \end{cases} \tag{171}$$

$$\begin{cases} \boldsymbol{K}_{23} = \sum_{I=1}^{nQ} \omega_I \left(\sum_{i=1}^{k} \int_{z_{i-1}}^{z_i} \left(\boldsymbol{B}_2^T(\boldsymbol{x}_I) \cdot \boldsymbol{c}_k \cdot \left[-z \cdot \frac{h}{\pi} \sin\left(\frac{\pi z}{h}\right) \right] \cdot \boldsymbol{B}_3(\boldsymbol{x}_I) \right) \mathrm{d}z \right) = \sum_{I=1}^{nQ} \omega_I \cdot \boldsymbol{B}_2^T(\boldsymbol{x}_I) \cdot \boldsymbol{c}_9 \cdot \boldsymbol{B}_3(\boldsymbol{x}_I) = \boldsymbol{K}_{32} \\ \boldsymbol{c}_{10} = \sum_{i=1}^{k} \int_{z_{i-1}}^{z_i} \left[\boldsymbol{c}_k \cdot (-z) \cdot \frac{h}{\pi} \sin\left(\frac{\pi z}{h}\right) \right] \mathrm{d}z = \\ \quad = \frac{h^2}{\pi^3} \sum_{i=1}^{k} \left[h \sin\left(\frac{\pi z_{i-1}}{h}\right) - \pi z_{i-1} \cos\left(\frac{\pi z_{i-1}}{h}\right) - h \sin\left(\frac{\pi z_i}{h}\right) + \pi z_i \cos\left(\frac{\pi z_i}{h}\right) \right] \cdot \boldsymbol{c}_k \end{cases} \tag{172}$$

$$\begin{cases} \boldsymbol{K}_{33} = \sum_{I=1}^{nQ} \omega_I \left(\sum_{i=1}^{k} \int_{z_{i-1}}^{z_i} \left(\boldsymbol{B}_3^T(\boldsymbol{x}_I) \cdot \boldsymbol{c}_k \cdot (-z)^2 \cdot \boldsymbol{B}_3(\boldsymbol{x}_I) \right) \mathrm{d}z \right) = \sum_{I=1}^{nQ} \omega_I \cdot \boldsymbol{B}_3^T(\boldsymbol{x}_I) \cdot \boldsymbol{c}_{11} \cdot \boldsymbol{B}_3(\boldsymbol{x}_I) \\ \boldsymbol{c}_{11} = \sum_{i=1}^{k} \int_{z_{i-1}}^{z_i} \left[\boldsymbol{c}_k \cdot (-z)^2 \right] \mathrm{d}z = \sum_{i=1}^{k} \left(\frac{z_i^3}{3} - \frac{z_{i-1}^3}{3} \right) \cdot \boldsymbol{c}_k \end{cases} \tag{173}$$

4.4.4 Mantari Theory

Karama et al. [30], [47] mentioned the advantage of modelling the shape strain function as exponential function rather than sine function., which is used in Touratier model. Exponential function has all even and odd powers in its expansion unlike the sine function, which has only the odd components. Thus, an exponential function is much richer than a sine function, as Karama

pointed. However, as Mantari [33] stated in 2012 (three year after Karama), "*a combination of trigonometric and exponential shape functions seems to produce a model which represents a better and perhaps a simpler model than the one proposed by Karama et al.*"

So, Mantari proposed a series of different functions $f(z)$ that are combinations of exponential and trigonometric functions, being the following HSDT the one that was selected to be implemented in the algorithms,

$$\text{Mantari}: f(z) = \frac{h}{\pi}\left(\sin\left(\frac{\pi z}{h}\right) e^{m\cdot\cos\left(\frac{\pi z}{h}\right)} + \frac{\pi z}{h} m \right) \quad , \quad m \geq 0 \tag{174}$$

where m is a parameter that was optimized by Mantari so that his theory approached best the 3D Elasticity solutions. When $m = 0$, Touratier theory can be reproduced as a special case. Mantari proved that for $m = 0.5$ the errors between 3D and 2D solutions are lowered in the majority of calculations than other existing theories. So the final form of the function $f(z)$ is,

$$\text{Mantari}: f(z) = \frac{h}{\pi}\left(\sin\left(\frac{\pi z}{h}\right) e^{\frac{1}{2}\cdot\cos\left(\frac{\pi z}{h}\right)} + \frac{\pi z}{2h} \right) \tag{175}$$

Kinematic Relations

For simplification purposes the following variables are defined,

$$c = \frac{h}{\pi} \tag{176}$$

$$a = c\cdot\frac{\pi}{2h} = \frac{1}{2} \tag{177}$$

$$f_1(z) = \frac{h}{\pi}\sin\left(\frac{\pi z}{h}\right) e^{\frac{1}{2}\cdot\cos\left(\frac{\pi z}{h}\right)} = c\cdot\sin\left(\frac{\pi z}{h}\right) e^{a\cdot\cos\left(\frac{\pi z}{h}\right)} \tag{178}$$

and the derivative of $f(z)$,

$$
\begin{aligned}
f'(z) &= \frac{h}{\pi}\frac{\pi}{2h} + \frac{h}{\pi}\frac{\pi}{h}\cdot e^{\frac{1}{2}\cdot\cos\left(\frac{\pi z}{h}\right)}\cdot\left(\cos\left(\frac{\pi z}{h}\right) - \frac{\sin^2\left(\frac{\pi z}{h}\right)}{2}\right) \\
&= \frac{1}{2} + e^{\frac{1}{2}\cdot\cos\left(\frac{\pi z}{h}\right)}\cdot\left(\cos\left(\frac{\pi z}{h}\right) - \frac{\sin^2\left(\frac{\pi z}{h}\right)}{2}\right) = a + f_2(z)
\end{aligned}
\tag{179}
$$

The displacement field is given by equations (180) and the correspondent strain field can be found in the equations (181),

$$
\begin{cases}
u(x,y,z) = u_0(x,y) - z\cdot\dfrac{\partial w(x,y)}{\partial x} + \left[az + f_1(z)\right]\cdot\left[\phi_x(x,y) + \dfrac{\partial w(x,y)}{\partial x}\right] \\
v(x,y,z) = v_0(x,y) - z\cdot\dfrac{\partial w(x,y)}{\partial y} + \left[az + f_1(z)\right]\cdot\left[\phi_y(x,y) + \dfrac{\partial w(x,y)}{\partial y}\right] \\
w(x,y,z) = w_0(x,y)
\end{cases}
\tag{180}
$$

$$
\begin{cases}
\varepsilon_{xx} = \dfrac{\partial u}{\partial x} = \dfrac{\partial u_0}{\partial x} + \left[az + f_1(z)\right]\cdot\dfrac{\partial \phi_x}{\partial x} + \left[az + f_1(z) - z\right]\cdot\dfrac{\partial^2 w}{\partial x^2} \\
\varepsilon_{yy} = \dfrac{\partial v}{\partial y} = \dfrac{\partial v_0}{\partial x} + \left[az + f_1(z)\right]\cdot\dfrac{\partial \phi_y}{\partial y} + \left[az + f_1(z) - z\right]\cdot\dfrac{\partial^2 w}{\partial y^2} \\
\gamma_{xy} = \dfrac{\partial v}{\partial x} + \dfrac{\partial u}{\partial y} = \dfrac{\partial v_0}{\partial x} + \dfrac{\partial u_0}{\partial y} + \left[az + f_1(z)\right]\cdot\left(\dfrac{\partial \phi_x}{\partial y} + \dfrac{\partial \phi_y}{\partial x}\right) + 2\left[az + f_1(z) - z\right]\dfrac{\partial^2 w}{\partial x\,\partial y} \\
\gamma_{yz} = \dfrac{\partial v}{\partial z} + \dfrac{\partial w}{\partial y} = \dfrac{\partial w}{\partial y} + \left[a + f_2(z)\right]\phi_y + \left[a + f_2(z) - 1\right]\dfrac{\partial w}{\partial y} \\
\gamma_{xz} = \dfrac{\partial u}{\partial z} + \dfrac{\partial w}{\partial x} = \dfrac{\partial w}{\partial x} + \left[a + f_2(z)\right]\phi_x + \left[a + f_2(z) - 1\right]\dfrac{\partial w}{\partial x} \\
\varepsilon_{zz} = 0
\end{cases}
\tag{181}
$$

Deformability Matrixes

The differential operator $\boldsymbol{L}$ comes as,

$$\boldsymbol{L}=\begin{bmatrix} \dfrac{\partial}{\partial x} & 0 & \left[az+f_1(z)-z\right]\dfrac{\partial^2}{\partial x^2} & \left[az+f_1(z)\right]\dfrac{\partial}{\partial x} & 0 \\ 0 & \dfrac{\partial}{\partial y} & \left[az+f_1(z)-z\right]\dfrac{\partial^2}{\partial y^2} & 0 & \left[az+f_1(z)\right]\dfrac{\partial}{\partial y} \\ \dfrac{\partial}{\partial y} & \dfrac{\partial}{\partial x} & 2\left[az+f_1(z)-z\right]\dfrac{\partial^2}{\partial x\,\partial y} & \left[az+f_1(z)\right]\dfrac{\partial}{\partial y} & \left[az+f_1(z)\right]\dfrac{\partial}{\partial x} \\ 0 & 0 & \left[a+f_2(z)\right]\dfrac{\partial}{\partial y} & 0 & \left[a+f_2(z)\right] \\ 0 & 0 & \left[a+f_2(z)\right]\dfrac{\partial}{\partial x} & \left[a+f_2(z)\right] & 0 \end{bmatrix} \tag{182}$$

Again, the deformability matrix is calculated using equation (183)

$$\boldsymbol{B}(x_I)=\boldsymbol{B}_{0M}(x_I)+\boldsymbol{B}_{0S}(x_I)+az\cdot\boldsymbol{B}_1(x_I)+f_2(z)\cdot\boldsymbol{B}_2(x_I)+f_1(z)\boldsymbol{B}_3(x_I)+(az-z)\cdot\boldsymbol{B}_4(x_I) \tag{183}$$

where the sub-matrixes $\boldsymbol{B}_{0M}(x_I)$, $\boldsymbol{B}_{0S}(x_I)$, $\boldsymbol{B}_1(x_I)$, $\boldsymbol{B}_2(x_I)$, $\boldsymbol{B}_3(x_I)$ and $\boldsymbol{B}_4(x_I)$ are exactly the same matrixes defined by equations (104)-(109), only with the exception of $\boldsymbol{B}_{0S}(x_I)$ where k_1 is replaced by a. It is also assumed that $\boldsymbol{B}_0(x_I)=\boldsymbol{B}_{0M}(x_I)+\boldsymbol{B}_{0S}(x_I)$.

Homogenised Constitutive Matrixes and Construction of the Global Stiffness Matrix

The homogenised constitutive matrixes were determined the same way as before, with the particularity that some of that are similar to those obtained in 4.4.1. for the TSDTs.

Due to the complexity of the functions $f_1(z)$ and $f_2(z)$, explicit integrals could not be found for the homogenised constitutive matrixes in equations (191), (193), (194) and (196). In those cases, the mentioned functions were approximated by Taylor series in the algorithm (by approximation of the sine, cosine and exponential factors).

$$\begin{cases} \boldsymbol{K}_{00}=\displaystyle\sum_{I=1}^{nQ}\omega_I\left(\sum_{i=1}^{k}\int_{z_{i-1}}^{z_i}\left(\boldsymbol{B}_0^T(x_I)\cdot\boldsymbol{c}_k\cdot\boldsymbol{B}_0(x_I)\right)\mathrm{d}z\right)=\sum_{I=1}^{nQ}\omega_I\cdot\boldsymbol{B}_0^T(x_I)\cdot\boldsymbol{c}_1\cdot\boldsymbol{B}_0(x_I) \\ \boldsymbol{c}_1=\displaystyle\sum_{i=1}^{k}\int_{z_{i-1}}^{z_i}\boldsymbol{c}_k\,\mathrm{d}z=\sum_{i=1}^{k}\left(z_i-z_{i-1}\right)\cdot\boldsymbol{c}_k \end{cases} \tag{184}$$

$$\begin{cases} \boldsymbol{K}_{01} = \sum_{I=1}^{nQ} \omega_I \left(\sum_{i=1}^{k} \int_{z_{i-1}}^{z_i} \left(\boldsymbol{B}_0^T(\boldsymbol{x}_I) \cdot \boldsymbol{c}_k \cdot a\, z \cdot \boldsymbol{B}_1(\boldsymbol{x}_I) \right) \mathrm{d}\, z \right) = \sum_{I=1}^{nQ} \omega_I \cdot \boldsymbol{B}_0^T(\boldsymbol{x}_I) \cdot \boldsymbol{c}_2 \cdot \boldsymbol{B}_1(\boldsymbol{x}_I) = \boldsymbol{K}_{10} \\ \boldsymbol{c}_2 = \sum_{i=1}^{k} \int_{z_{i-1}}^{z_i} \left(\boldsymbol{c}_k \cdot a\, z \right) \mathrm{d}\, z = a \cdot \sum_{i=1}^{k} \left(\frac{z_i^{\,2}}{2} - \frac{z_{i-1}^{\,2}}{2} \right) \cdot \boldsymbol{c}_k \end{cases} \tag{185}$$

$$\begin{cases} \boldsymbol{K}_{02} = \sum_{I=1}^{nQ} \omega_I \left(\sum_{i=1}^{k} \int_{z_{i-1}}^{z_i} \left(\boldsymbol{B}_0^T(\boldsymbol{x}_I) \cdot \boldsymbol{c}_k \cdot f_2(z) \cdot \boldsymbol{B}_2(\boldsymbol{x}_I) \right) \mathrm{d}\, z \right) = \sum_{I=1}^{nQ} \omega_I \cdot \boldsymbol{B}_0^T(\boldsymbol{x}_I) \cdot \boldsymbol{c}_3 \cdot \boldsymbol{B}_2(\boldsymbol{x}_I) = \boldsymbol{K}_{20} \\ \boldsymbol{c}_3 = \sum_{i=1}^{k} \int_{z_{i-1}}^{z_i} \boldsymbol{c}_k \cdot f_2(z)\ \mathrm{d}\, z = \frac{h}{\pi} \cdot \sum_{i=1}^{k} \left[\sin\left(\frac{\pi z_i}{h} \right) e^{\frac{1}{2} \cdot \cos\left(\frac{\pi z_i}{h} \right)} - \sin\left(\frac{\pi z_{i-1}}{h} \right) e^{\frac{1}{2} \cdot \cos\left(\frac{\pi z_{i-1}}{h} \right)} \right] \cdot \boldsymbol{c}_k \end{cases} \tag{186}$$

$$\begin{cases} \boldsymbol{K}_{03} = \sum_{I=1}^{nQ} \omega_I \left(\sum_{i=1}^{k} \int_{z_{i-1}}^{z_i} \left(\boldsymbol{B}_0^T(\boldsymbol{x}_I) \cdot \boldsymbol{c}_k \cdot f_1(z) \cdot \boldsymbol{B}_3(\boldsymbol{x}_I) \right) \mathrm{d}z \right) = \sum_{I=1}^{nQ} \omega_I \cdot \boldsymbol{B}_0^T(\boldsymbol{x}_I) \cdot \boldsymbol{c}_4 \cdot \boldsymbol{B}_3(\boldsymbol{x}_I) = \boldsymbol{K}_{30} \\ \boldsymbol{c}_4 = \sum_{i=1}^{k} \int_{z_{i-1}}^{z_i} \boldsymbol{c}_k \cdot f_1(z)\ \mathrm{d}z = \frac{2h^2}{\pi^2} \cdot \sum_{i=1}^{k} \left[e^{\frac{1}{2} \cdot \cos\left(\frac{\pi z_{i-1}}{h} \right)} - e^{\frac{1}{2} \cdot \cos\left(\frac{\pi z_i}{h} \right)} \right] \cdot \boldsymbol{c}_k \end{cases} \tag{187}$$

$$\begin{cases} \boldsymbol{K}_{04} = \sum_{I=1}^{nQ} \omega_I \left(\sum_{i=1}^{k} \int_{z_{i-1}}^{z_i} \left(\boldsymbol{B}_0^T(\boldsymbol{x}_I) \cdot \boldsymbol{c}_k \cdot (a\, z - z) \cdot \boldsymbol{B}_4(\boldsymbol{x}_I) \right) \mathrm{d}\, z \right) = \sum_{I=1}^{nQ} \omega_I \cdot \boldsymbol{B}_0^T(\boldsymbol{x}_I) \cdot \boldsymbol{c}_5 \cdot \boldsymbol{B}_4(\boldsymbol{x}_I) = \boldsymbol{K}_{40} \\ \boldsymbol{c}_5 = \sum_{i=1}^{k} \int_{z_{i-1}}^{z_i} \left[\boldsymbol{c}_k \cdot (a\, z - z) \right] \mathrm{d}\, z = (a-1) \cdot \sum_{i=1}^{k} \left(\frac{z_i^{\,2}}{2} - \frac{z_{i-1}^{\,2}}{2} \right) \cdot \boldsymbol{c}_k \end{cases} \tag{188}$$

$$\begin{cases} \boldsymbol{K}_{11} = \sum_{I=1}^{nQ} \omega_I \left(\sum_{i=1}^{k} \int_{z_{i-1}}^{z_i} \left(\boldsymbol{B}_1^T(\boldsymbol{x}_I) \cdot \boldsymbol{c}_k \cdot (az)^2 \cdot \boldsymbol{B}_1(\boldsymbol{x}_I) \right) \mathrm{d}\, z \right) = \sum_{I=1}^{nQ} \omega_I \cdot \boldsymbol{B}_1^T(\boldsymbol{x}_I) \cdot \boldsymbol{c}_6 \cdot \boldsymbol{B}_1(\boldsymbol{x}_I) \\ \boldsymbol{c}_6 = \sum_{i=1}^{k} \int_{z_{i-1}}^{z_i} \left[\boldsymbol{c}_k \cdot (a\, z)^2 \right] \mathrm{d}\, z = a^2 \cdot \sum_{i=1}^{k} \left(\frac{z_i^{\,3}}{3} - \frac{z_{i-1}^{\,3}}{3} \right) \cdot \boldsymbol{c}_k \end{cases} \tag{189}$$

$$\begin{cases} \boldsymbol{K}_{12} = \sum_{I=1}^{nQ} \omega_I \left(\sum_{i=1}^{k} \int_{z_{i-1}}^{z_i} \left(\boldsymbol{B}_1^T(x_I) \cdot \boldsymbol{c}_k \cdot a\, z \cdot f_2(z) \cdot \boldsymbol{B}_2(x_I) \right) \mathrm{d}\, z \right) = \sum_{I=1}^{nQ} \omega_I \cdot \boldsymbol{B}_1^T(x_I) \cdot \boldsymbol{c}_7 \cdot \boldsymbol{B}_2(x_I) = \boldsymbol{K}_{21} \\ \boldsymbol{c}_7 = \sum_{i=1}^{k} \int_{z_{i-1}}^{z_i} \left[\boldsymbol{c}_k \cdot a\, z \cdot f_2(z) \right] \mathrm{d}\, z \\ \quad = a \frac{h}{\pi^2} \cdot \sum_{i=1}^{k} \left[e^{\frac{1}{2} \cdot \cos\left(\frac{\pi z_i}{h}\right)} \cdot \left(2h + z_i \cdot \sin\left(\frac{\pi z_i}{h} \right) \right) - e^{\frac{1}{2} \cdot \cos\left(\frac{\pi z_{i-1}}{h}\right)} \cdot \left(2h + z_{i-1} \cdot \sin\left(\frac{\pi z_{i-1}}{h} \right) \right) \right] \cdot \boldsymbol{c}_k \end{cases} \tag{190}$$

$$\begin{cases} \boldsymbol{K}_{13} = \sum_{I=1}^{nQ} \omega_I \left(\sum_{i=1}^{k} \int_{z_{i-1}}^{z_i} \left(\boldsymbol{B}_1^T(x_I) \cdot \boldsymbol{c}_k \cdot a\, z \cdot f_1(z) \cdot \boldsymbol{B}_3(x_I) \right) \mathrm{d}\, z \right) = \sum_{I=1}^{nQ} \omega_I \cdot \boldsymbol{B}_1^T(x_I) \cdot \boldsymbol{c}_8 \cdot \boldsymbol{B}_3(x_I) = \boldsymbol{K}_{31} \\ \boldsymbol{c}_8 = \sum_{i=1}^{k} \int_{z_{i-1}}^{z_i} \left[\boldsymbol{c}_k \cdot a\, z \cdot f_1(z) \right] \mathrm{d}\, z \end{cases} \tag{191}$$

$$\begin{cases} \boldsymbol{K}_{14} = \sum_{I=1}^{nQ} \omega_I \left(\sum_{i=1}^{k} \int_{z_{i-1}}^{z_i} \left(\boldsymbol{B}_1^T(x_I) \cdot \boldsymbol{c}_k \cdot a\, z \cdot (a\, z - z) \cdot \boldsymbol{B}_4(x_I) \right) \mathrm{d}\, z \right) = \sum_{I=1}^{nQ} \omega_I \cdot \boldsymbol{B}_1^T(x_I) \cdot \boldsymbol{c}_9 \cdot \boldsymbol{B}_4(x_I) = \boldsymbol{K}_{41} \\ \boldsymbol{c}_9 = \sum_{i=1}^{k} \int_{z_{i-1}}^{z_i} \left[\boldsymbol{c}_k \cdot az \cdot (a\, z - z) \right] \mathrm{d}\, z = a(a-1) \cdot \sum_{i=1}^{k} \left(\frac{z_i^{\,3}}{3} - \frac{z_{i-1}^{\,3}}{3} \right) \cdot \boldsymbol{c}_k \end{cases} \tag{192}$$

$$\begin{cases} \boldsymbol{K}_{22} = \sum_{I=1}^{nQ} \omega_I \left(\sum_{i=1}^{k} \int_{z_{i-1}}^{z_i} \left(\boldsymbol{B}_2^T(x_I) \cdot \boldsymbol{c}_k \cdot \left[f_2(z) \right]^2 \cdot \boldsymbol{B}_2(x_I) \right) \mathrm{d}\, z \right) = \sum_{I=1}^{nQ} \omega_I \cdot \boldsymbol{B}_2^T(x_I) \cdot \boldsymbol{c}_{10} \cdot \boldsymbol{B}_2(x_I) \\ \boldsymbol{c}_{10} = \sum_{i=1}^{k} \int_{z_{i-1}}^{z_i} \left[\boldsymbol{c}_k \cdot \left[f_2(z) \right]^2 \right] \mathrm{d}\, z \end{cases} \tag{193}$$

$$\begin{cases} \boldsymbol{K}_{23} = \sum_{I=1}^{nQ} \omega_I \left(\sum_{i=1}^{k} \int_{z_{i-1}}^{z_i} \left(\boldsymbol{B}_2^T(x_I) \cdot \boldsymbol{c}_k \cdot f_1(z) \cdot f_2(z) \cdot \boldsymbol{B}_3(x_I) \right) \mathrm{d}\, z \right) = \sum_{I=1}^{nQ} \omega_I \cdot \boldsymbol{B}_2^T(x_I) \cdot \boldsymbol{c}_{11} \cdot \boldsymbol{B}_3(x_I) = \boldsymbol{K}_{32} \\ \boldsymbol{c}_{11} = \sum_{i=1}^{k} \int_{z_{i-1}}^{z_i} \left[\boldsymbol{c}_k \cdot f_1(z) \cdot f_2(z) \right] \mathrm{d}\, z \end{cases} \tag{194}$$

$$\begin{cases} \boldsymbol{K}_{24} = \sum_{I=1}^{nQ} \omega_I \left(\sum_{i=1}^{k} \int_{z_{i-1}}^{z_i} \left(\boldsymbol{B}_2^T(\boldsymbol{x}_I) \cdot \boldsymbol{c}_k \cdot \left[f_2(z) \cdot (a\,z - z) \right] \cdot \boldsymbol{B}_4(\boldsymbol{x}_I) \right) \mathrm{d}\,z \right) = \sum_{I=1}^{nQ} \omega_I \cdot \boldsymbol{B}_2^T(\boldsymbol{x}_I) \cdot \boldsymbol{c}_{12} \cdot \boldsymbol{B}_4(\boldsymbol{x}_I) = \boldsymbol{K}_{42} \\ \boldsymbol{c}_{12} = \sum_{i=1}^{k} \int_{z_{i-1}}^{z_i} \left[\boldsymbol{c}_k \cdot f_2(z) \cdot (a\,z - z) \right] \mathrm{d}\,z = \boldsymbol{c}_7 \cdot \frac{a-1}{a} \end{cases} \tag{195}$$

$$\begin{cases} \boldsymbol{K}_{33} = \sum_{I=1}^{nQ} \omega_I \left(\sum_{i=1}^{k} \int_{z_{i-1}}^{z_i} \left(\boldsymbol{B}_3^T(\boldsymbol{x}_I) \cdot \boldsymbol{c}_k \cdot \left[f_1(z) \right]^2 \cdot \boldsymbol{B}_3(\boldsymbol{x}_I) \right) \mathrm{d}\,z \right) = \sum_{I=1}^{nQ} \omega_I \cdot \boldsymbol{B}_3^T(\boldsymbol{x}_I) \cdot \boldsymbol{c}_{12} \cdot \boldsymbol{B}_3(\boldsymbol{x}_I) \\ \boldsymbol{c}_{13} = \sum_{i=1}^{k} \int_{z_{i-1}}^{z_i} \left[\boldsymbol{c}_k \cdot \left[f_1(z) \right]^2 \right] \mathrm{d}\,z \end{cases} \tag{196}$$

$$\begin{cases} \boldsymbol{K}_{34} = \sum_{I=1}^{nQ} \omega_I \left(\sum_{i=1}^{k} \int_{z_{i-1}}^{z_i} \left(\boldsymbol{B}_3^T(\boldsymbol{x}_I) \cdot \boldsymbol{c}_k \cdot \left[f_1(z) \cdot (az - z) \right] \cdot \boldsymbol{B}_4(\boldsymbol{x}_I) \right) \mathrm{d}\,z \right) = \sum_{I=1}^{nQ} \omega_I \cdot \boldsymbol{B}_3^T(\boldsymbol{x}_I) \cdot \boldsymbol{c}_{14} \cdot \boldsymbol{B}_4(\boldsymbol{x}_I) = \boldsymbol{K}_{43} \\ \boldsymbol{c}_{14} = \sum_{i=1}^{k} \int_{z_{i-1}}^{z_i} \left[\boldsymbol{c}_k \cdot f_1(z) \cdot (az - z) \right] \mathrm{d}\,z = \boldsymbol{c}_8 \cdot \frac{a-1}{a} \end{cases} \tag{197}$$

$$\begin{cases} \boldsymbol{K}_{44} = \sum_{I=1}^{nQ} \omega_I \left(\sum_{i=1}^{k} \int_{z_{i-1}}^{z_i} \left(\boldsymbol{B}_4^T(\boldsymbol{x}_I) \cdot \boldsymbol{c}_k \cdot \left[(az - z) \cdot (az - z) \right] \cdot \boldsymbol{B}_4(\boldsymbol{x}_I) \right) \mathrm{d}\,z \right) = \sum_{I=1}^{nQ} \omega_I \cdot \boldsymbol{B}_4^T(\boldsymbol{x}_I) \cdot \boldsymbol{c}_{15} \cdot \boldsymbol{B}_4(\boldsymbol{x}_I) \\ \boldsymbol{c}_{15} = \sum_{i=1}^{k} \int_{z_{i-1}}^{z_i} \left[\boldsymbol{c}_k \cdot (az - z) \cdot (az - z) \right] \mathrm{d}\,z = (a-1)(a-1) \cdot \sum_{i=1}^{k} \left(\frac{z_i^3}{3} - \frac{z_{i-1}^3}{3} \right) \cdot \boldsymbol{c}_k \end{cases} \tag{198}$$

Chapter 5

5 Numerical Examples

After the introduction of the formulations of the RPIM and the NNRPIM, in Chapter 2, and the deduction of the fundamental matrixes for all plate theories selected to be introduced in the algorithms, in this Chapter are presented the obtained results (for symmetric cross-ply laminates and for antisymmetric cross-ply and angle ply laminates). Firstly, the convergence studies are presented. Then, the solutions for the nondimensionalized displacements and stresses are obtained for different laminates (varying its geometry and the load applied). Nondimensionalized maximum stresses along the thickness for various laminates are also calculated and represented in graphs for comparison purposes. The study of the relation between the normalized transverse displacement and the lamination angle for antisymmetric angle-ply laminates is also performed. Over the subchapters, several comparisons are made, specially between the results obtained and the solutions of the literature, between the solutions of the two meshless methods and also between all the HSDTs.

5.1 Orthotropic Plates and Symmetric Cross-Ply Laminates

5.1.1 Introduction to the Problem Analysis

Bending analysis was performed in orthotropic plates and symmetric cross-ply laminates with stacking sequences indicated in table 4. Considering the same coordinate system of the figure 14(a), the principle directions (longitudinal and transverse directions) of a lamina can be defined,

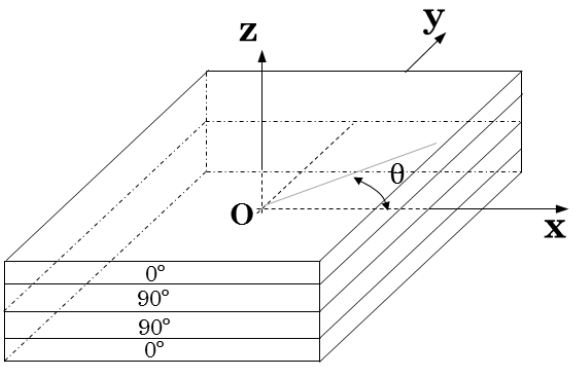

figure 17 – Symmetric cross-ply laminate (0/90/90/0) and the Cartesian coordinate system.

where, for the first layer with 0°, the Ox axis is defined as the longitudinal direction (the direction of the fibres), being the Oy axis its transverse direction. The layers were numbered from bottom to the top of the plate, being $k=1$ the bottom layer and $k=n$ the top layer (n is the total number of layers of a laminate).

The results obtained from the RPIM and the NNRPIM for the different HSDTs were compared, when available, with those proposed by the literature. Comparison studies were also performed between laminates, geometries and HSDTs, not only from the maximum values of the central transverse displacements and stresses, but also based on graphs of stress distributions for each laminate studied.

The material used in all static analysis for symmetric cross-ply laminates is indicated in table 4,

table 4 – Mechanical properties of the material used for all the static analysis of symmetric cross-ply laminates.

E_1	E_2	ν_{12}	$G_{12}=G_{13}$	G_{23}
25 GPa	1 GPa	0.25	0.5 E_2	0.2 E_2

being E_1 the Young modulus for the longitudinal direction (the direction of the fibres for each layer), E_2 the Young modulus along the transverse direction, ν_{12} the Poisson coefficient and G_{12}, G_{13} and G_{23} the shear modulus.

5.1.2 Considerations on the Generic Geometry

The laminates analysed in this work have the general geometry reproduced in figure 18,

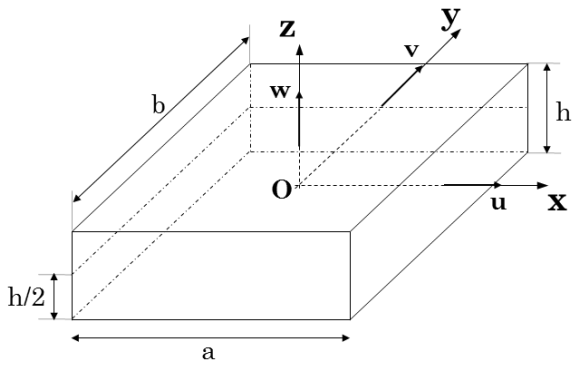

figure 18 – General geometry of the laminated plates analysed.

where a and b are the dimensions of the plate in the directions of the axis Ox and Oy, respectively, and h is the total thickness.

In each analysis for symmetric cross-ply laminates, the boundary conditions of the plates were simply supported (this conditions were directly imposed in the global stiffness matrix) and the loads applied in the top face of the plate are represented in figure 19,

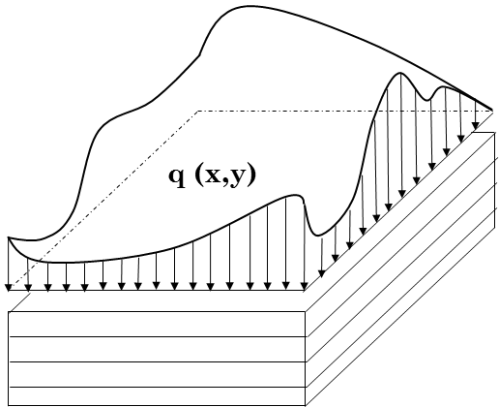

figure 19 – General load q(x,y).

Uniformly distributed loads (UDL) and sinusoidal distributed transverse loads (UDL) were used for the static analysis. In those cases, the function $q(x,y)$ is equal to, respectively,

$$\begin{aligned} q(x,y) &= q_0 \\ q(x,y) &= q_0 \sin\left(\frac{\pi x}{a}\right)\sin\left(\frac{\pi y}{b}\right) \end{aligned} \tag{199}$$

For each laminate, maximum nondimensionalized transverse displacements and stresses were obtained considering the equations (200),

$$\overline{w} = w(A,z)\cdot\frac{E_2 h^3}{q_0\cdot a^4} \qquad \overline{\sigma_{xx}} = \sigma_{xx}(A,z)\cdot\frac{h^2}{q_0\cdot a^2} \qquad \overline{\sigma_{yy}} = \sigma_{yy}(A,z)\cdot\frac{h^2}{q_0\cdot a^2}$$
$$\overline{\tau_{xy}} = \tau_{xy}(B,z)\cdot\frac{h}{q_0\cdot a} \qquad \overline{\tau_{yz}} = \tau_{yz}(C,z)\cdot\frac{h}{q_0\cdot a} \qquad \overline{\tau_{xz}} = \tau_{xz}(D,z)\cdot\frac{h}{q_0\cdot a} \tag{200}$$

where q_0 is the nominal load. The maximum dimensionalized transverse displacements and stresses were calculated in specific points of the laminate. The letters A, B, C and D denotes a point in the plane Oxy (figure 20) and the z coordinate is indicated in table 5.

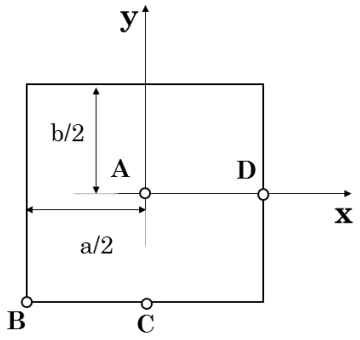

figure 20 – Locations in the plane *Oxy* of the points A, B, C and D.

table 5 – z coordinate where the nondimensionalized transverse displacement and stresses are computed.

	w	σ_{xx}	σ_{yy}	τ_{xy}	τ_{yz}	τ_{xz}
Orthotropic Plate	0	h/2	h/2	-h/2	0	0
(0/90/0)	0	h/2 (k=3)	h/6 (k=2)	-h/2	0 (k=2)	0 (k=2)
(0/90/90/0)	0	h/2 (k=4)	h/4 (k=3)	-h/2	0 (k=3)	0 (k=3)
(0/90/0/90/0)	0	h/2 (k=5)	h/3 (k=4)	-h/2	2h/24 (k = 4)	0 (k = 3)
(0/90/90/0/90/90/0)	0	h/2 (k=7)	5h/14 (k=6)	-h/2	h/14 (k = 5)	0 (k = 4)

All the layers of the cross-ply laminates referred in table 5 have the same thickness. The exception is the cross-ply laminate (0/90/0/90/0) with five layers where $h_1 = h_3 = h_5 = h/6$ and $h_2 = h_4 = h/4$.

5.1.3 Convergence Studies

Before the solutions for different laminates and geometries have been found, some convergence studies have taken place in order to select the discretization of the regular nodal mesh that was used both in the RPIM and the NNRPIM. For the two algorithms developed, the following parameters were used,

table 6 – RPIM and NNRPIM parameters.

		RPIM	**NNRPIM**
Type of mesh		Regular	Regular
Kind of nodal connectivity imposition		Fixed radial 'influence – domain'	First-degree 'influence-cell' (V1) or Second-degree influence-cell' (V2)'
Shape parameters	**c**	0.0001	0.0001
	p	0.9999	0.9999
Polynomial basis		Null	Null
Integration points		Four per quadrilateral	One per sub-cell

The nondimensionalized transverse displacements were obtained for nodal meshes with an increasing number of nodes discretizing the problem domain. For each convergence step n , the number of nodes is given by $(2+1)^n \times (2+1)^n$. The limitation of the computer processor that was used for these analyses was about 18000 DOFs, which made impossible to determined central transverse displacements for a nodal mesh with $(64+1)\times(64+1)$ nodes.

In the figures 21-23 are represented the convergence studies for different combinations of simply supported laminated/orthotropic square plates, geometries and loads, as well as for different meshless methods (RPIM, NNRPIM with first-degree 'influence-cells' – V1 – and NNRPIM with second-degree 'influence-cells' – V2),

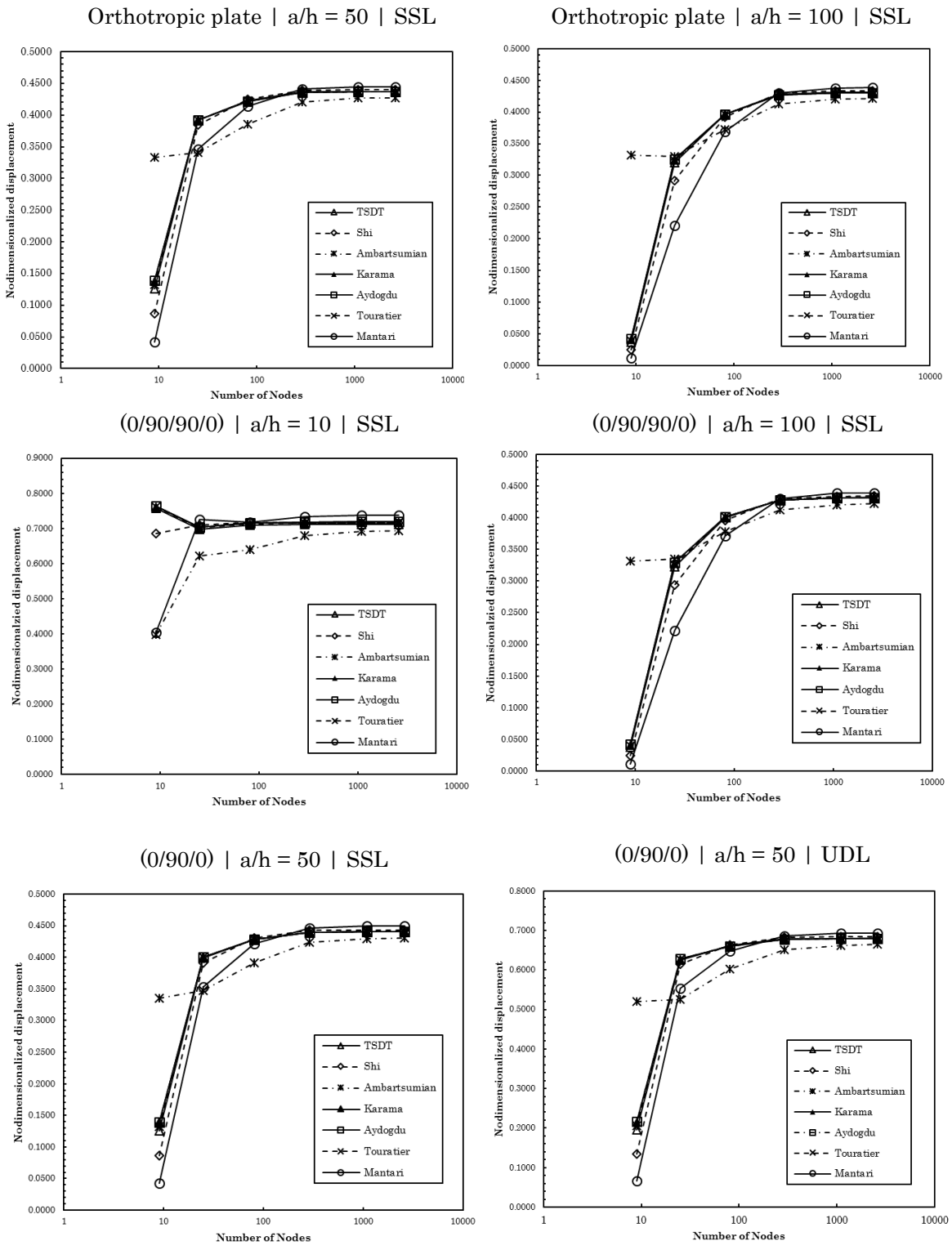

figure 21 – Convergence studies for the RPIM with different types of plates, geometries and loads. TSDT is the third-order shear deformation theory of Reddy.

Orthotropic plate | a/h = 50 | SSL

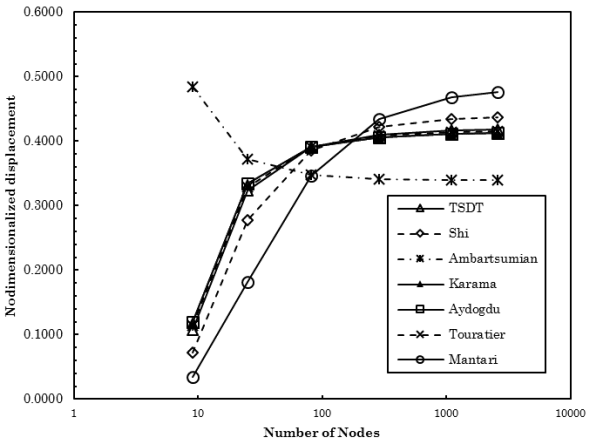

Orthotropic plate | a/h = 100 | SSL

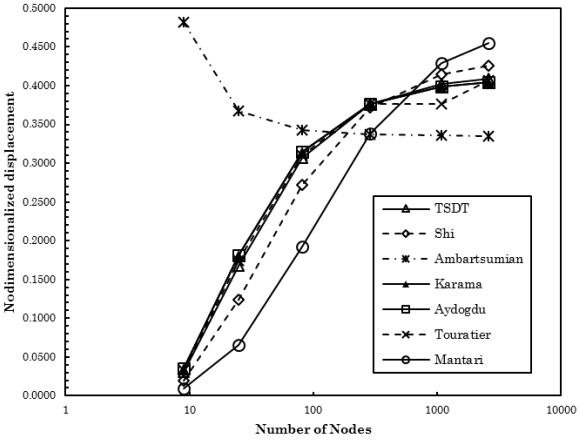

(0/90/90/0) | a/h = 10 | SSL

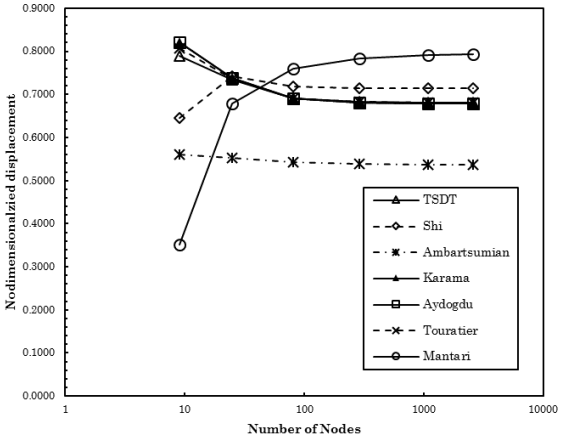

(0/90/90/0) | a/h = 100 | SSL

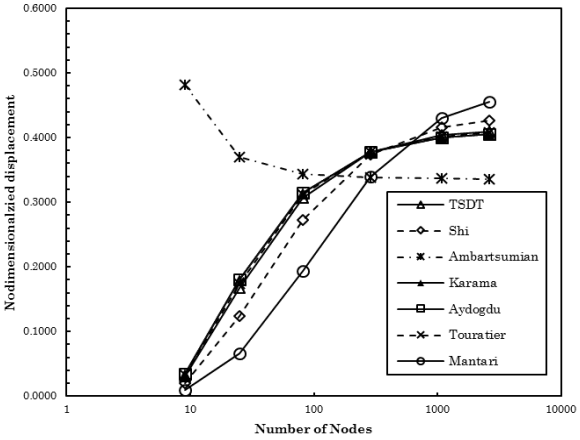

(0/90/0) | a/h = 50 | SSL

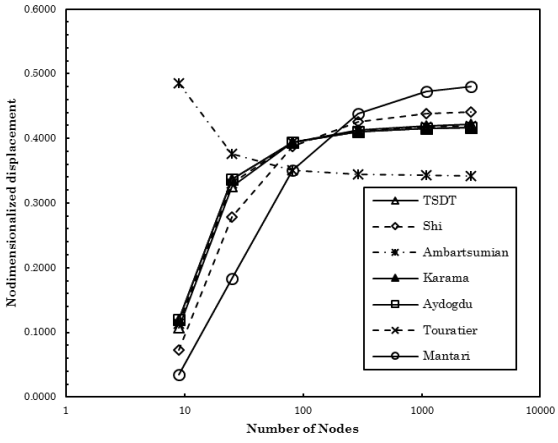

(0/90/0) | a/h = 50 | UDL

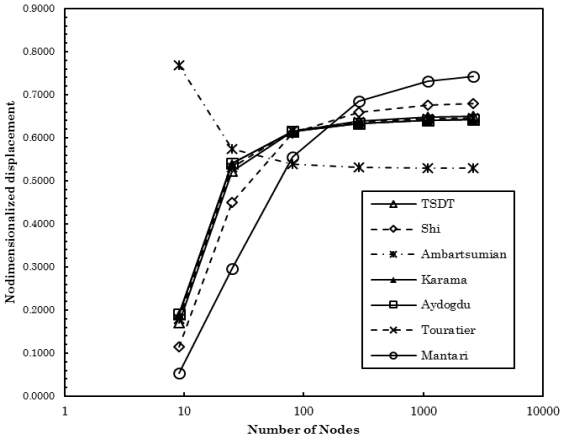

figure 22 – Convergence studies for the NNRPIM (V1) with different types of plates, geometries and loads. TSDT is the third-order shear deformation theory of Reddy.

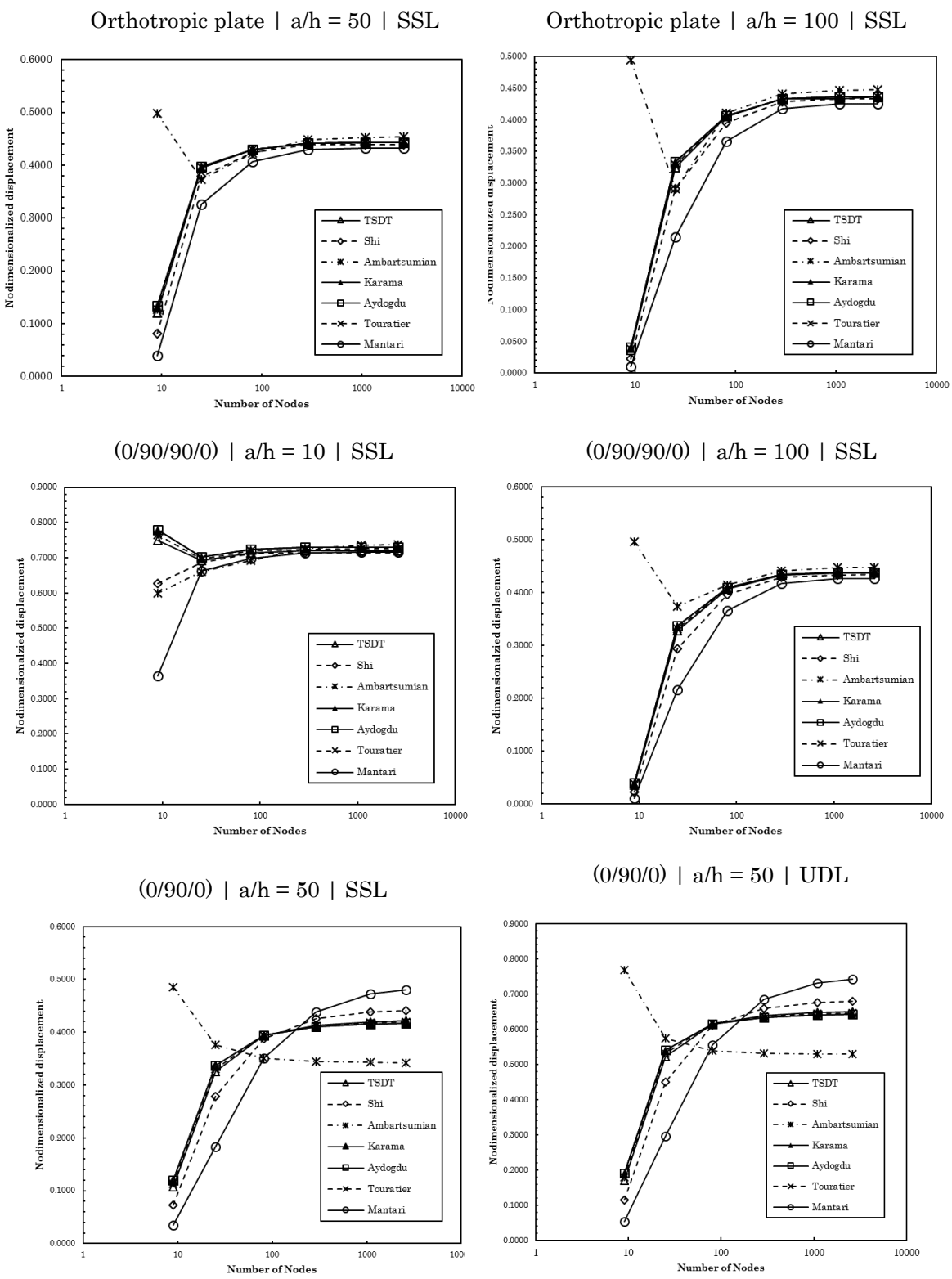

figure 23 – Convergence studies for the NNRPIM (V2) with different types of plates, geometries and loads. TSDT is the third-order shear deformation theory of Reddy.

From the eighteen convergence studies presented, it becomes clear that the convergence rate is different from HSDT to HSDT, and also varies depending on the laminate, its characteristics and the numerical method used.

For example, in figure 21, where are represented the convergence studies for the RPIM, it can be seen that for the laminate (0/90/90/0), a thicker plate converges faster than a thin plate. It can also be concluded that the fact that the plate is subjected to a uniformly distributed load or sinusoidal load does not affect the significantly the convergence rate.

The Ambartsumian theory has a dissimilar way to converge when compared to the other theories. Instead of beginning with small displacements for the first step of convergence, it begins with a value near the final converged central transverse displacement. This fact may be related to another fact that the Ambartsumian theory is, as shown in Chapter 4, more like CLPT than with the remaining high-order theories.

In terms of comparison of the three numerical methods used (since for the NNRPIM were used two concepts of 'influence-cell' – first and second order), it is clear that the NNRPIM V1 has more difficulty to converge and, in some cases (such as the laminate (0/90/90/90) and the orthotropic plate with a/h=100) the method cannot converge even for the maximum number of nodes possible. It can also be concluded that the RPIM and the NNRPIM V2 have similar behaviours when convergence takes place.

Despite the differences between methods and, particularly, between thicknesses, a 33×33 nodal mesh (i.e,, a total of 1089 nodes – figure 24) allows to reach satisfactory solutions. This was the discretization that was used in all the static analysis in the subchapter 5.1..

Another perspective of the convergence studies here presented is included in section 5.1.6.

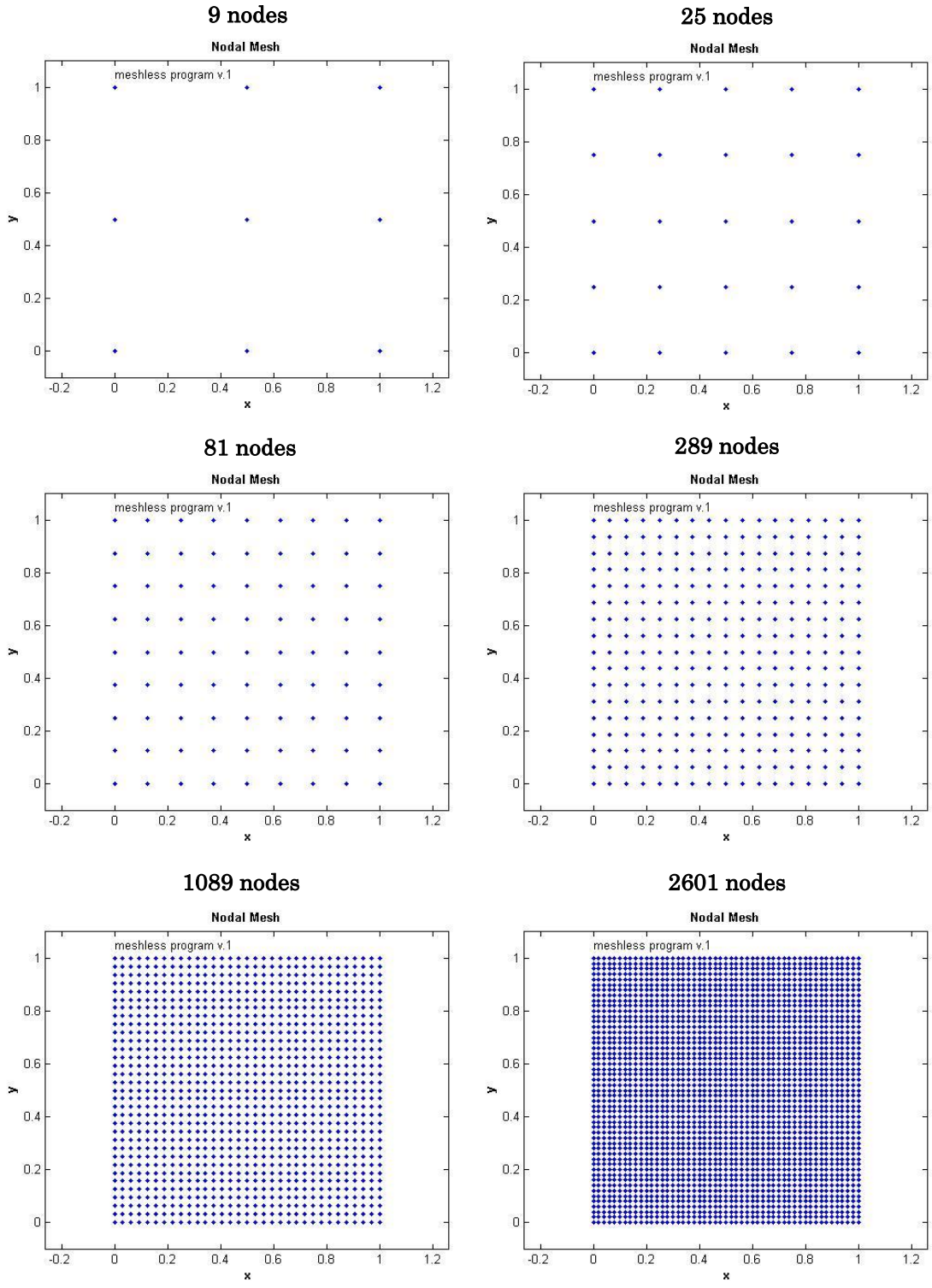

figure 24 – Nodal meshes used to calculate the central transverse displacements represented in figures 19-22.

5.1.4 Solutions of Nondimensionalized Transverse Displacements and Stresses for Various Laminates

Once found the nodal mesh to be used in all analyses, solutions were obtained for different laminates, thicknesses and types of loads, using the three numerical methods (RPIM, NNRPIM V1 and NNRPIM V2) and the eight equivalent single layer theories (first-order – FSDT –, third-order by Reddy – TSDT –, Shi, Ambartsumian, Karama, Aydogdu, Touratier and Mantari theories).

The solutions calculated by the two algorithms developed were then compared to the exact solutions, when available, proposed by the authors of the homonymous theories. This comparison study is stated in tables 11-52 of the Appendix A were can be found the maximum nondimensionalized displacements and stresses for orthotropic plates and symmetric cross-ply laminates – (0/90/0), (0/90/90/0), (0/90/0/90) and (0/90/90/0/90/90/0) configurations – with increasing thicknesses and two types of load. However, there are only exact solutions proposed by the authors of the different HSDTs for the laminates (0/90/0) and (0/90/90/0), simply supported and subjected to sinusoidal transverse loads. The exact solutions present in the tables of the Appendix A related to these laminates were consulted in references [31] for the Aydogdu's solutions, in [33] for Mantari and Karama's solutions, in [26] and [48] for Reddy's exact and finite element method (FEM – computed with quadrilateral Lagrange elements) solutions of the TSDT and FSDT, in [49] for Shi's solutions and finally in [29] for Touratier's solutions. Ambartsumian solutions could not be found for composite laminated plates. The 3D Elasticity solutions of Pagano and Hatfield mentioned in the referred tables were consulted in "*Mechanics of laminated composite plates and shells: theory and analysis*" [26] by J.N. Reddy. For the other types of plates (orthotropic, (0/90/0/90/0) and (0/90/90/0/90/90/0)), although there are not many published results, the obtained solutions were compared, whenever possible, with the exact solutions of Reddy for the FSDT and TSDT (which allowed to control the results and realized if the algorithms were working properly).

Thus, a line in each table of the Appendix A corresponds to a single static analysis in the MATLAB® program, which means that the data files of the algorithms had to be updated whenever it was desired to do the analysis with another HSDT. For the already mentioned cases where it was possible to compare the results with the proposed solutions by the authors of the homonymous theories, it can be seen that on the right side of each table are calculated the absolute values of the relative errors regarding the respective exact solution (with grey the errors $>10\%$ but $<20\%$ and with a darker grey

the errors $>20\%$). The absolute error presented in the tables is obtained with: $\varepsilon_{absolute}=100\times\left|\xi_{present}-\xi_{exact}\right|/\left|\xi_{exact}\right|$. For example, in the case of the laminate (0/90/90/0), those errors presented in tables 29-32 of Appendix A are synthetized in figures 25-30. In these figures, it is presented the total error obtained with: $\varepsilon_{total}=100\times\left(\xi_{present}-\xi_{exact}\right)/\left(\xi_{exact}\right)$, which permits a better graphical comparison than the absolute error of the tables.

As seen in figure 25, the errors for the nondimensionalized transverse displacements and normal stresses computed with the RPIM are quite small for different ratios a/h. In fact, the percentage errors for central transverse displacements is inferior to 3% and for the normal stresses the errors are inferior to 6%. Roughly the same goes with the normalized in-plane shear stress (figure 26) which has errors inferior to 4% for thinner plates. The crux of the matter is in the normalized shear transverse stresses that are intended to be well calculated by the algorithm in order to accurately predict the maximum stress state in a laminate. By observation of figure 26, the results obtained are satisfactory for all the theories except Shi's TSDT since the errors vary between 20 and 25%. It was not found the origin of such errors, in particularly because this theory is integrated in the same routines of the algorithm that Reddy and Ambartsumian's theories are. Thus, a plausible explanation could not be found, but it was observed that this kind of errors for Shi's theory were repeated for the laminate (0/90/0) – this can be seen in the tables 19-24 of the Appendix A – which may mean that the errors are not related to a specific laminate.

After performing the analysis with the RPIM, the same data was introduced in the NNRPIM to extract the results using first and second-degree 'influence-cells' (configurations V1 and V2, respectively). The computational cost of the NNRPIM V2 is much higher than NNRPIM V1 but the results obtained are considerably different. For example, for the normalized central transverse displacements and normal stresses, the errors using the NNRPIM V1 can be more than three times higher when compared with the solutions obtained from the NNRPIM V2. In fact, the NNRPIM V2 can archive very low errors for these parameters, even lower than RPIM. As regards shear transverse stresses (figure 28), the NNRPIM V1 allows to obtain similar results to RPIM. In the case of the NNRPIM V2 (figure 30), the latter situation changes drastically because of the shear locking phenomenon that occurs for ratios of a/h higher than 20. The reduced integration could solve this problem.

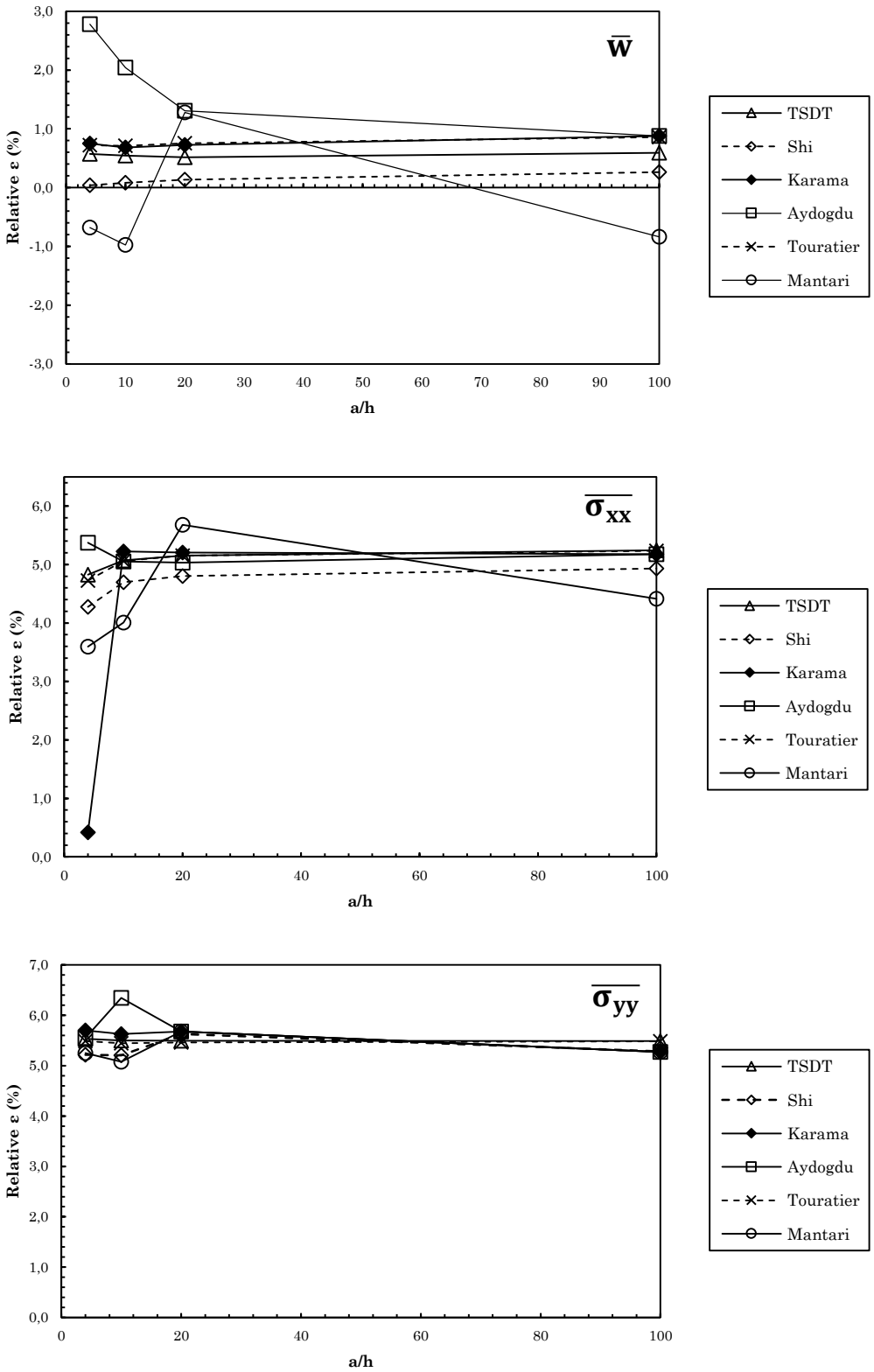

figure 25 – Relative ε(%) regarding the respective exact solution for the maximum normalized transverse displacements and normal stresses for a simply supported (0/90/90/0) laminate subjected to a sinusoidal load (SSL) using the RPIM.

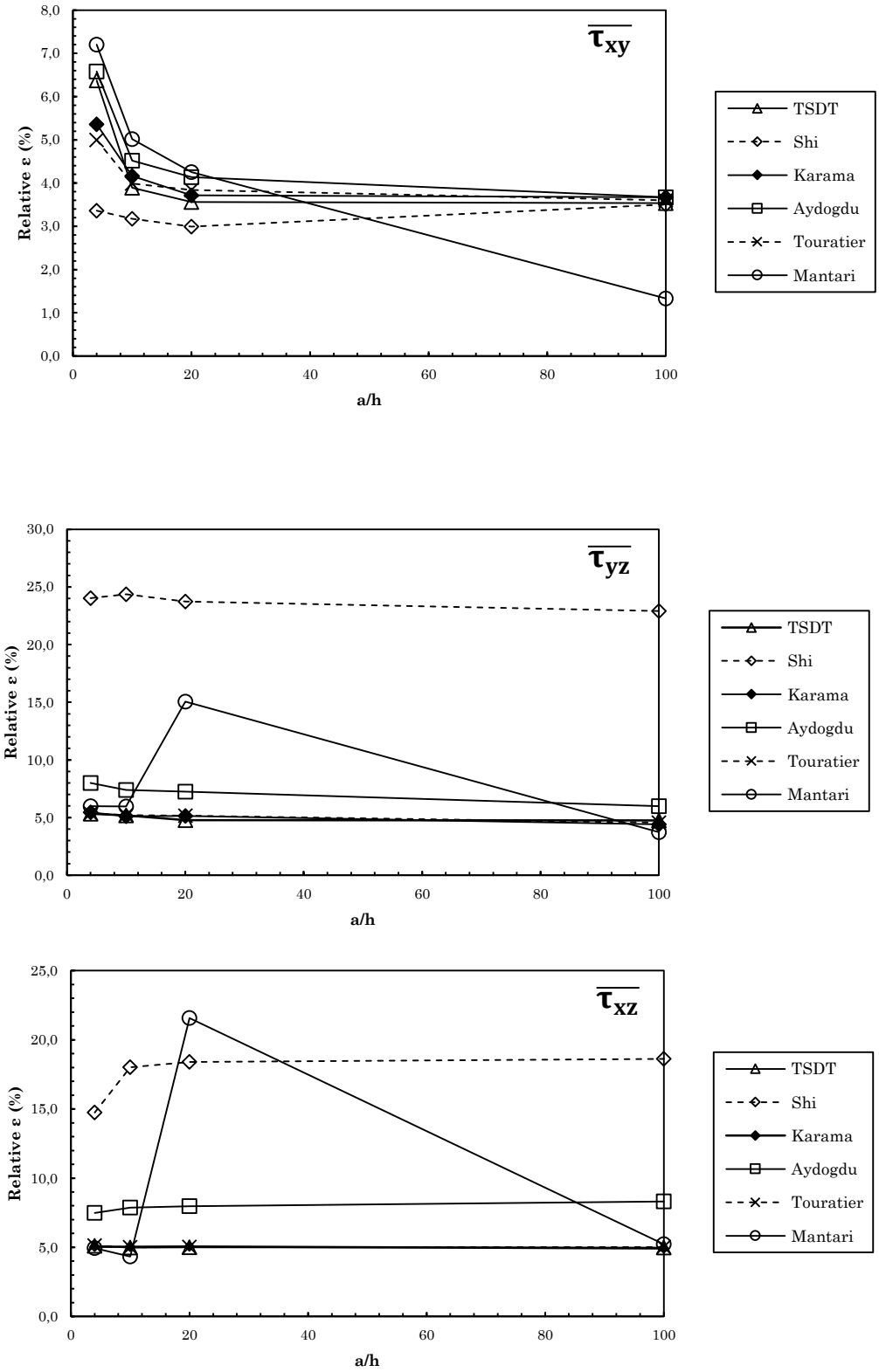

figure 26 – Relative errors ε(%) regarding the respective exact solution for the maximum normalized in-plane and transverse shear stresses for a simply supported (0/90/90/0) laminate subjected to a sinusoidal load (SSL) using the RPIM.

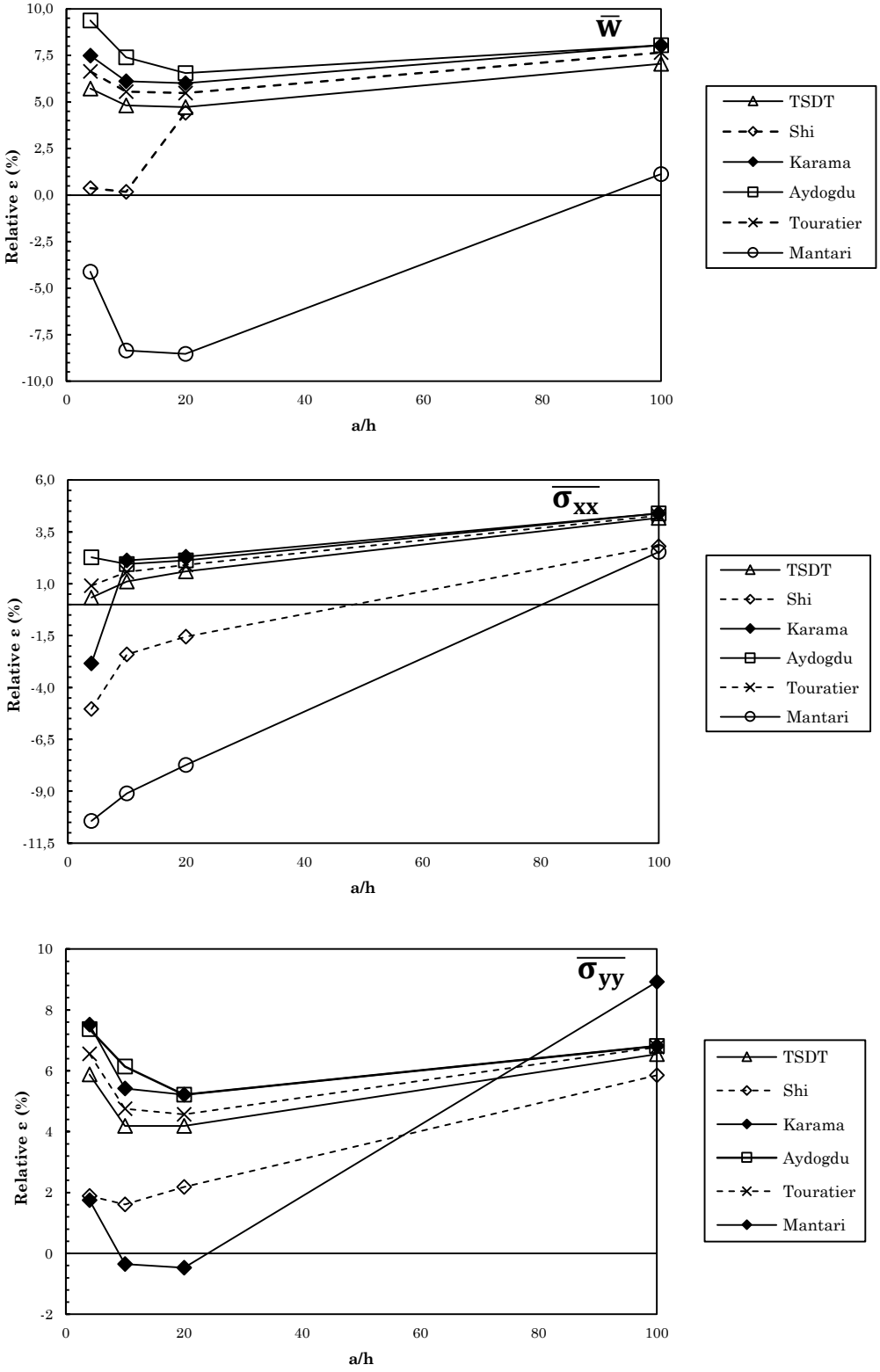

figure 27 – Relative errors ε(%) regarding the respective exact solution for the maximum normalized transverse displacements and normal stresses for a simply supported (0/90/90/0) laminate subjected to a sinusoidal load (SSL) using the NNRPIM V1.

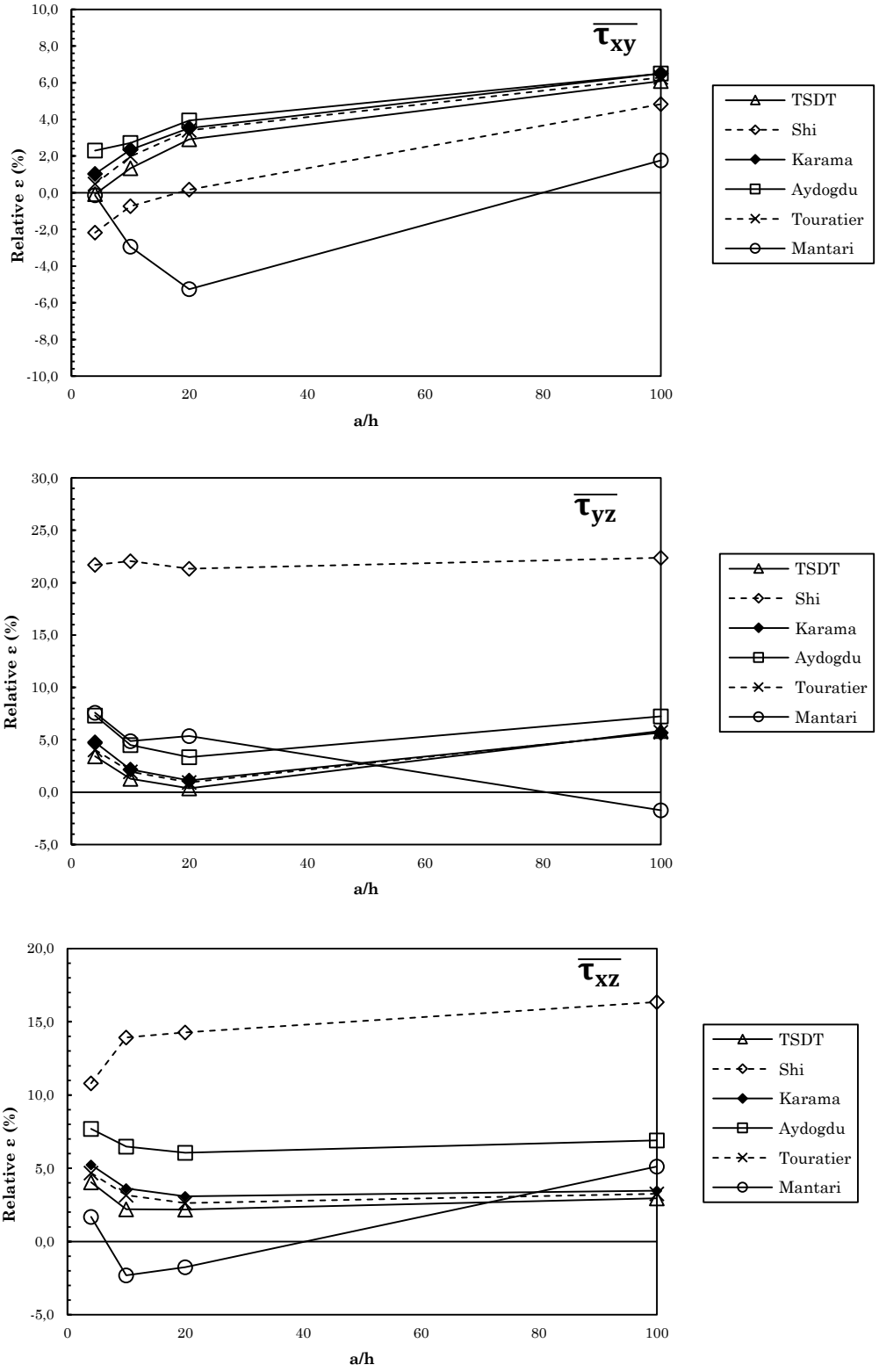

figure 28 – Relative errors ε(%) regarding the respective exact solution for the maximum in-plane and shear stresses for a simply supported (0/90/90/0) laminate subjected to a sinusoidal load (SSL) using the NNRPIM V1.

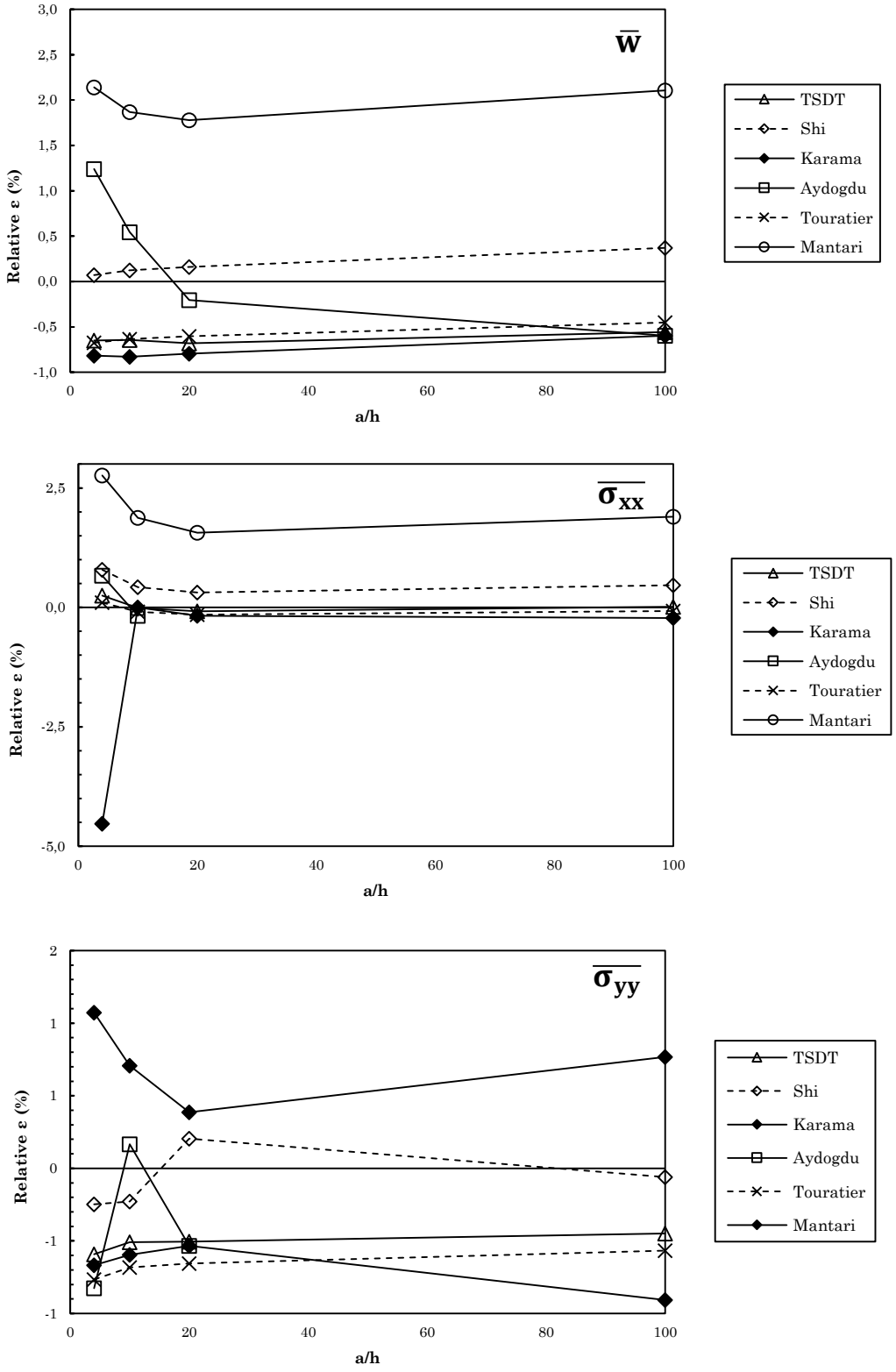

figure 29 – Relative errors ε(%) regarding the respective exact solution for the maximum normalized transverse displacements and normal stresses for a simply supported (0/90/90/0) laminate subjected to a sinusoidal load (SSL) using the NNRPIM V2.

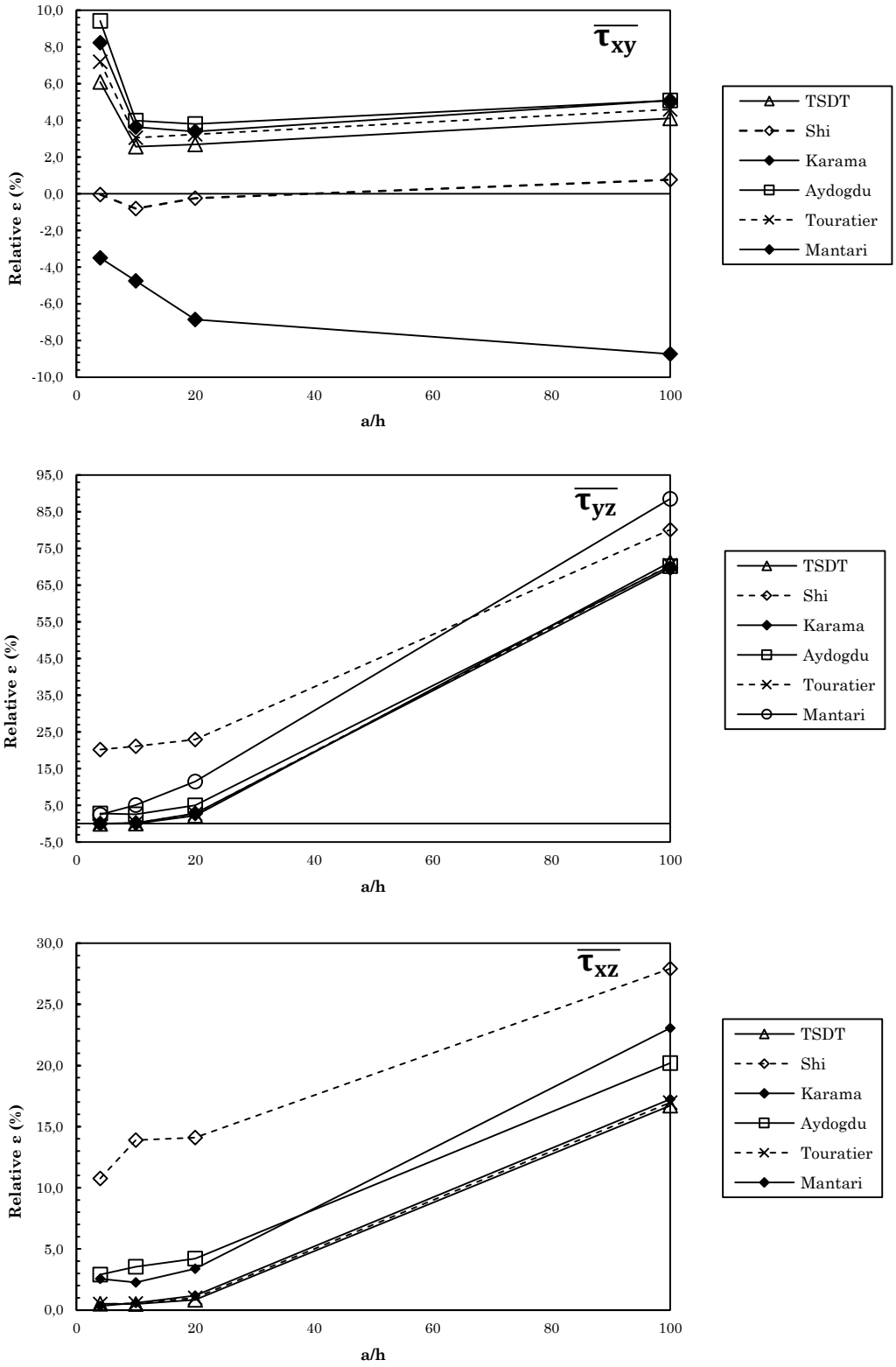

figure 30 – Relative errors ε(%) regarding the respective exact solution for the maximum in-plane and shear stresses for a simply supported (0/90/90/0) laminate subjected to a sinusoidal load (SSL) using the NNRPIM V2.

Now, by observation of the table 29 of the Appendix A (where a/h=4 so the shear locking did not yet occur for the NNRPIM V2), it becomes clear that, although the exact solutions for the transverse shear stresses of the Shi's theory best approximates the results of the 3D Elasticity, it is the Mantari's theory that has closer results to the 3D Elasticity in these shear stresses computed with meshless methods. This fact supports the idea of Mantari (which was referred in section 4.4.4.) that the errors between the 3D Elasticity and the 2D solutions of Mantari are lowered in the majority of calculations than other existing high-order shear deformation theories. This happens not only in transverse shear stresses but also in the other components of the stresses and in the normalized transverse displacements. As concerns to the errors regarding the exact respective solution, curiously, it is Shi's theory computed with the RPIM and the NNRPIM V2 that shows the lower errors, except for the aforementioned case of the transverse shear stresses, when the error can be as high as 25%.

The observations and conclusions here presented for the composite laminated plate (0/90/90/0) are extensible to the laminate (0/90/0), as it can be seen in the tables of the Appendix A, taking into account the percentage errors also calculated. In this Appendix, are also exposed many results for orthotropic plates and other symmetric cross-ply laminates.

5.1.5 Nondimensionalized Maximum Stresses Along the Thickness for Various Laminates

In addition to determining the maximum normalized stresses and transverse displacements, were also obtained graphs of the nondimensionalized normal and transverse shear stresses along the thickness of each laminate and for ratios of a/h=4, 10 and 100. This type of graphs allowed to compare more efficiently the behaviour of each HSDT and also have a broad view of the stress state installed in each laminate when subjected to the same essential and natural boundary conditions.

As it was done in the section 5.1.4, the symmetric laminate with cross-ply layers (0/90/90/0) with a ratio of a/h=4 was selected as an example for comparison purposes between meshless methods and HSDTs. In the Appendix B are exposed the obtained graphs for the other laminates – (0/90/0), (0/900/90/0), (0/90/90/0/90/90/0) as well as the laminate (0/90/90/0) with ratios of a/h equal to 10 and 100.

Figures 31-34 represent the variation of the nondimensionalized normal stresses across the thickness of the simply supported laminate subjected to a sinusoidal load, computed with the RPIM, the NNRPIM V1 and the NNRPIM V2, using the HSDTs and also the FSDT. The distributions of these stresses were also represented using the exact solutions of the FSDT and the TSDT [26]. It becomes clear that the results obtained from the RPIM and the NNRPIM V2 are almost indistinguishable and extremely close to the exact solutions (when comparing the FSDT and the TSDT solutions computed with the meshless methods and the respective exact solutions). However, in the NNRPIM V1 there is a greater dispersion of lines and the distribution of the stresses by Ambartsumian's theory seems to be underestimated.

When analysing the detail indicated in figure 32 – which corresponds to the distribution of the normal stress $\overline{\sigma_{yy}}$ in the layer $k=4$ – for an increasing ratio of a/h, the figure 35 is obtained. In figure 35(a), it can be seen that the lines for the FSDT (exact and RPIM) are parallel and close together. The same happens for the HSDTs, where the lines for the HSDTs have a smoother distribution and are parallel to the line of 'TSDT – Exact'. Decreasing the thickness, the composite laminated plate becomes a thin plate, so all the lines tends to be straight and closer to the CLPT solution (figure 35 (c)).

In the case of the transverse shear stresses – which concentrates the purpose of using HSDTs –, represented in figures 33 and 34, the difference between the results obtained from different HSDTs is more clear. Once again, the results found from the RPIM and the NNRPIM V2 are very similar and the NNRPIM V1 seems not only to underestimate the solutions computed with the Ambartsumian theory, but also overestimates the solutions for Mantari's theory. By analysing these figures, it can be concluded that the most recent exponential or combinations of exponential theories (Mantari, Karama and Aydogdu) predict higher shear stresses than the older theories (Reddy, Ambartsumian and Touratier), with the Shi's theory proving to be very close to the Reddy's theory in terms of these transverse shear stresses. As expected, the FSDT predicts constant transverse shear stresses along the thickness of each layer.

RPIM

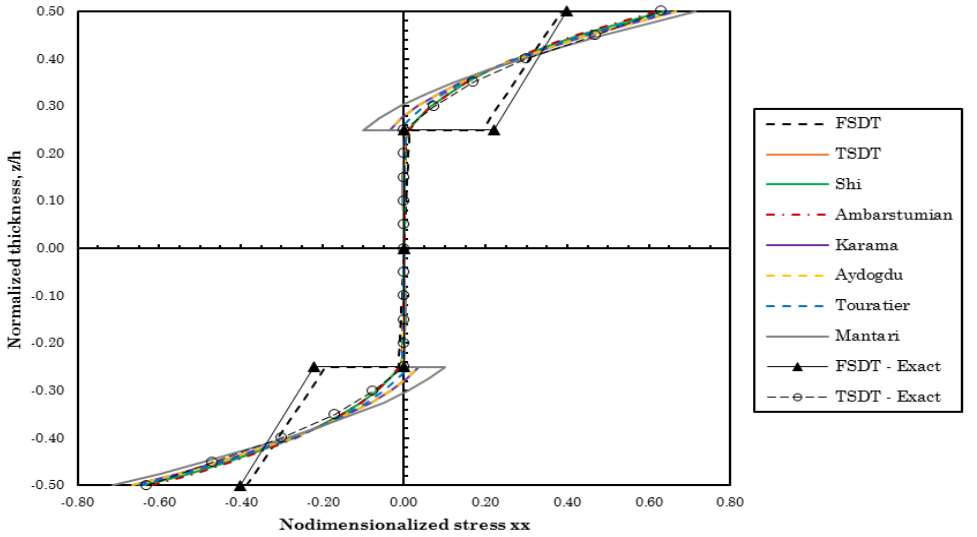

NNRPIM V1

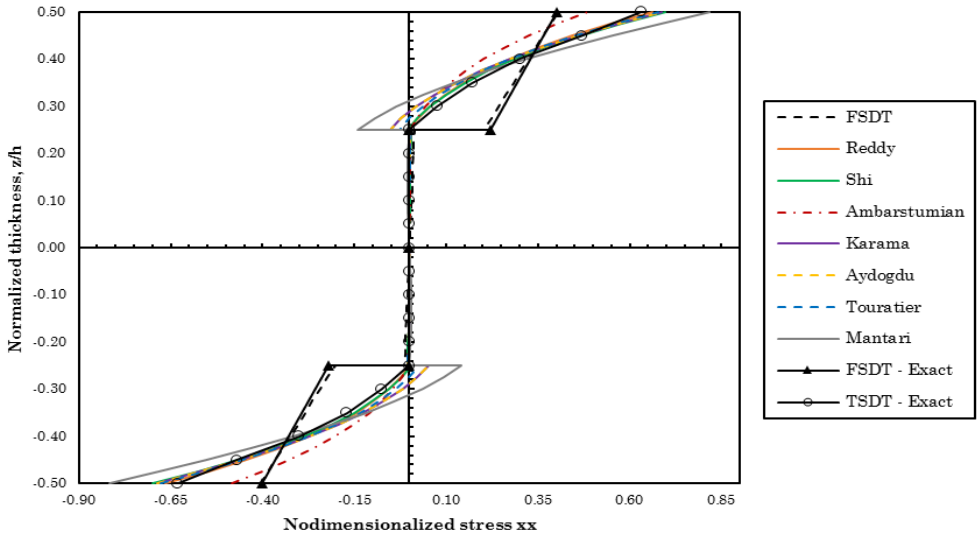

NNRPIM V2

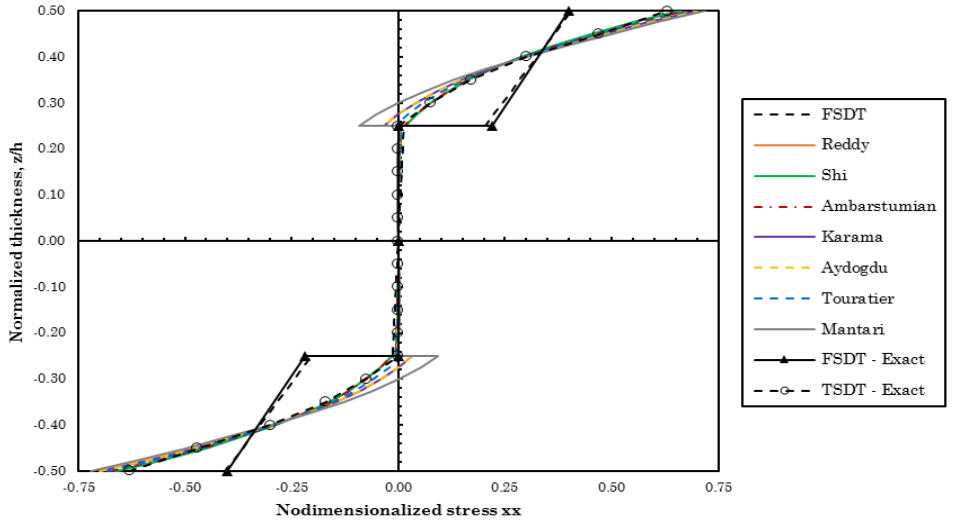

figure 31 – Nondimensionalized stresses σ_{xx} computed with the three numerical methods for a simply supported symmetric square laminate with cross-ply layers (0/90/90/0) subjected to a sinusoidal load (SSL), a/h=4.

RPIM

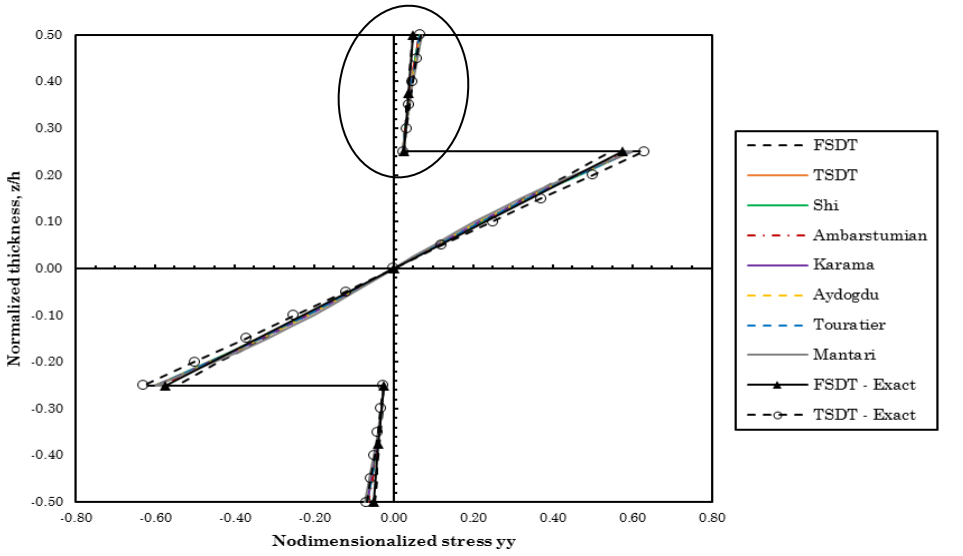

NNRPIM V1

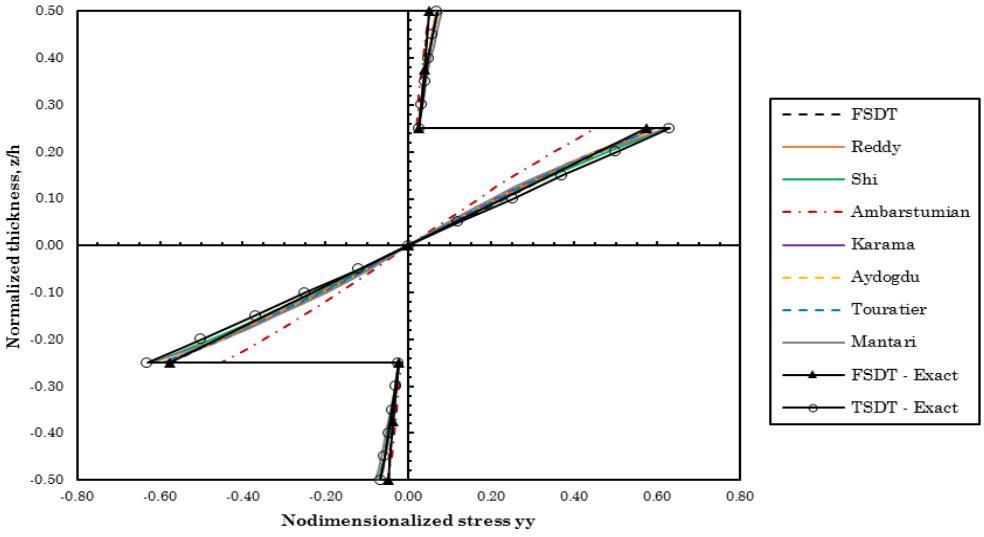

NNRPIM V2

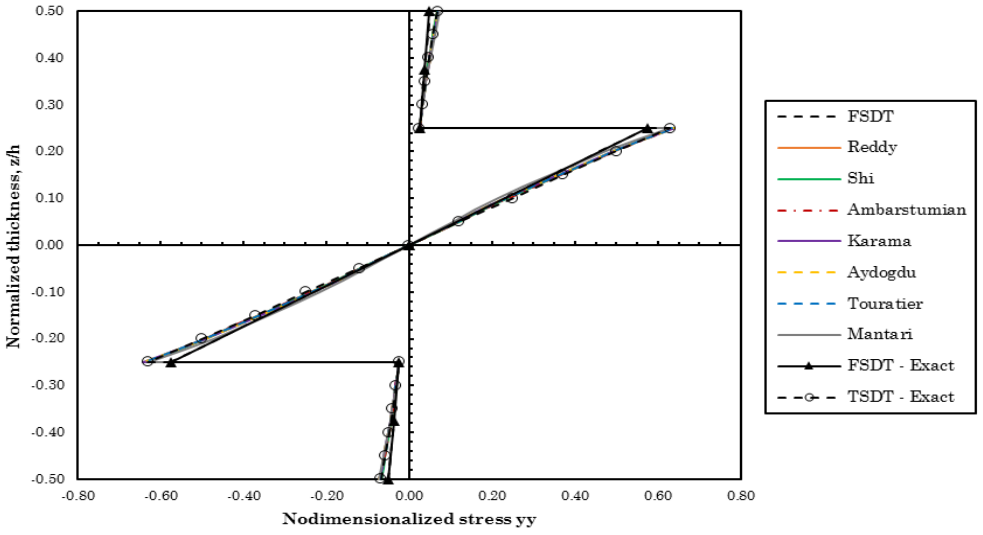

figure 32 – Nondimensionalized stresses σ_{yy} computed with the three numerical methods for a simply supported symmetric square laminate with cross-ply layers (0/90/90/0) subjected to a sinusoidal load (SSL), a/h=4.

RPIM

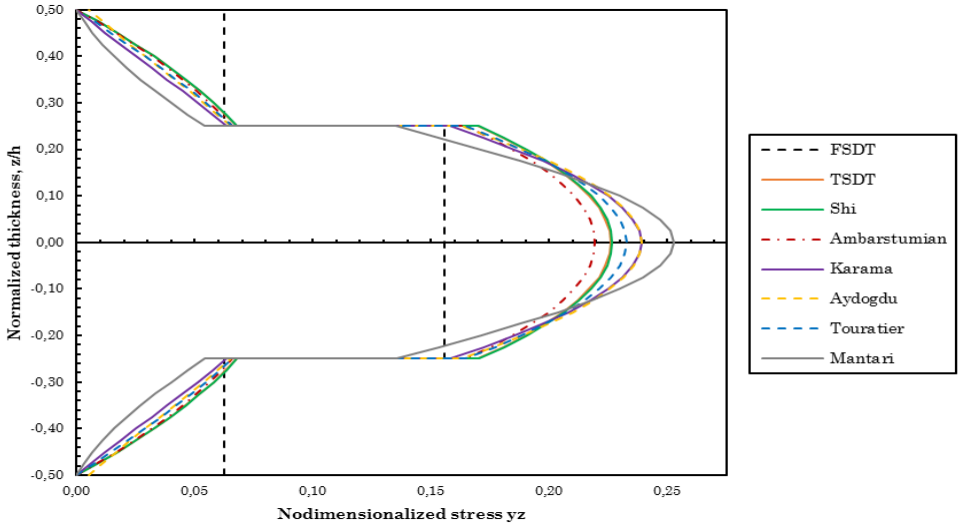

NNRPIM V1

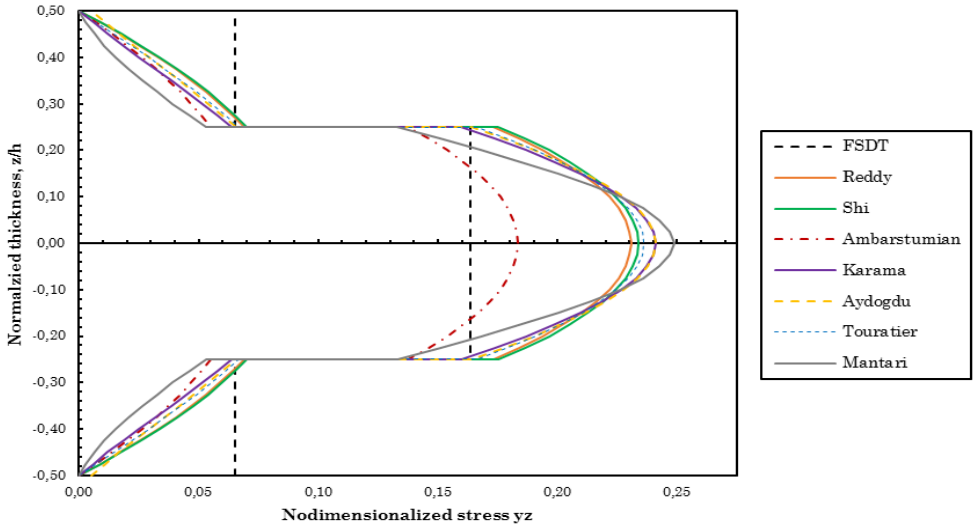

NNRPIM V2

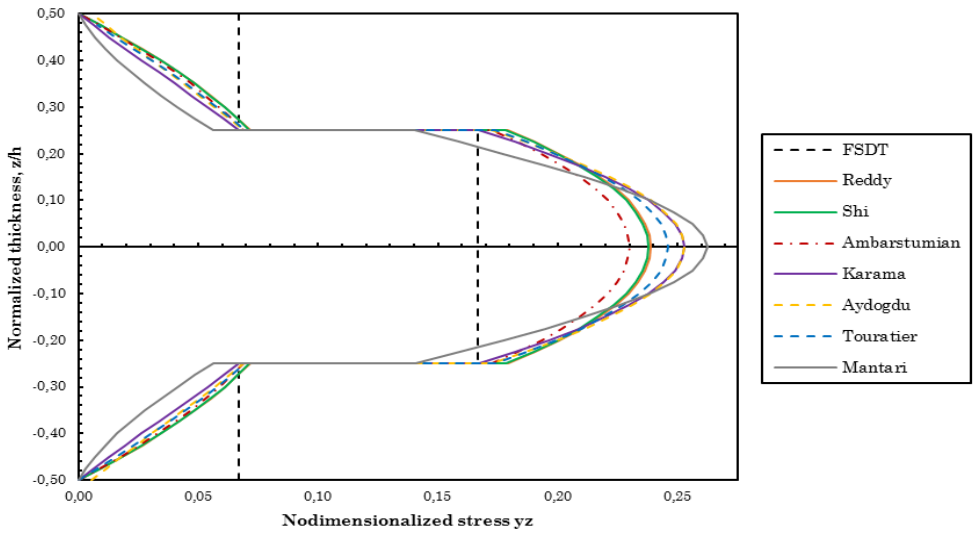

figure 33 – Nondimensionalized stresses τ_{yz} computed with the three numerical methods for a simply supported symmetric square laminate with cross-ply layers (0/90/90/0) subjected to a sinusoidal load (SSL), a/h=4.

RPIM

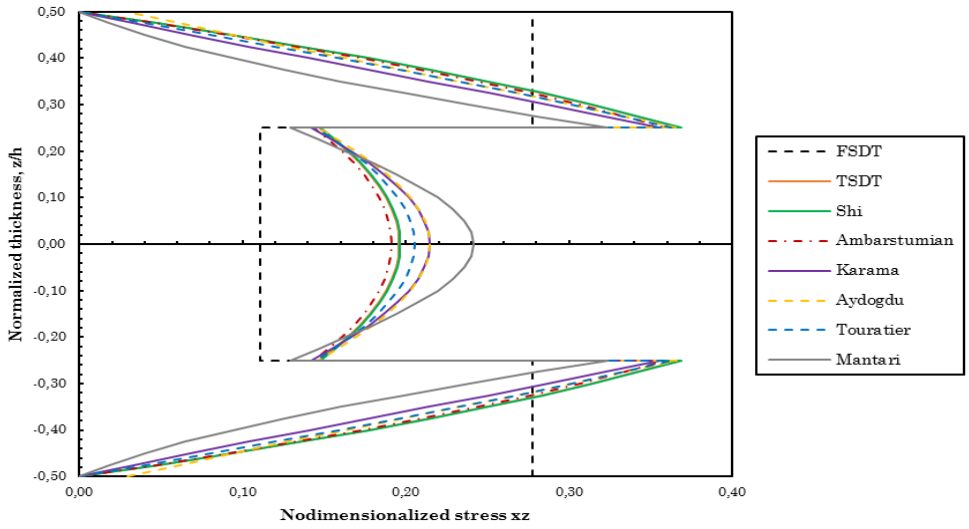

NNRPIM V1

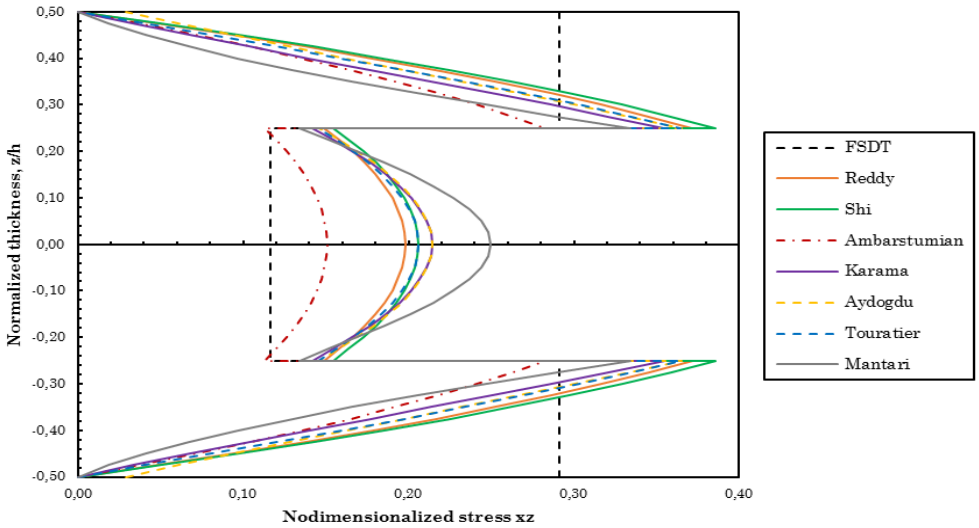

NNRPIM V2

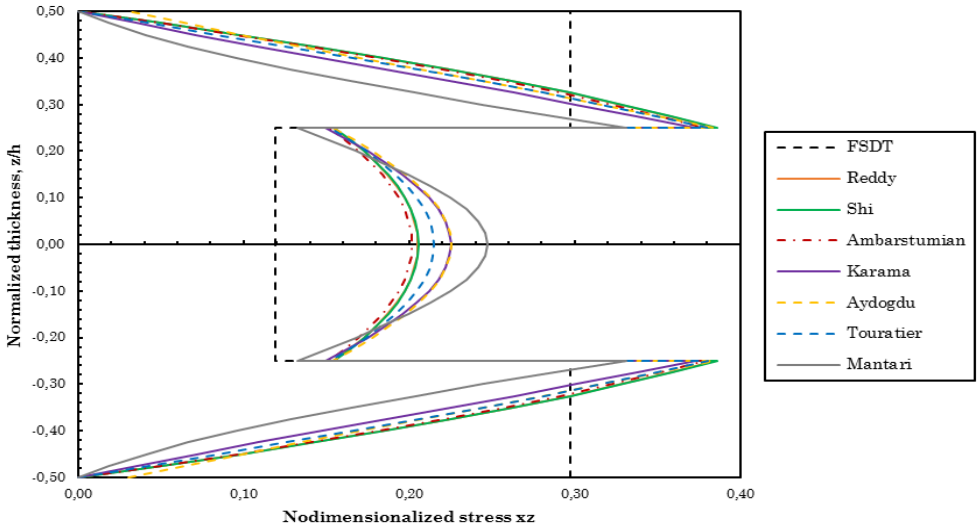

figure 34 – Nondimensionalized stresses τ_{xz} computed with the three numerical methods for a simply supported symmetric square laminate with cross-ply layers (0/90/90/0) subjected to a sinusoidal load (SSL), a/h=4.

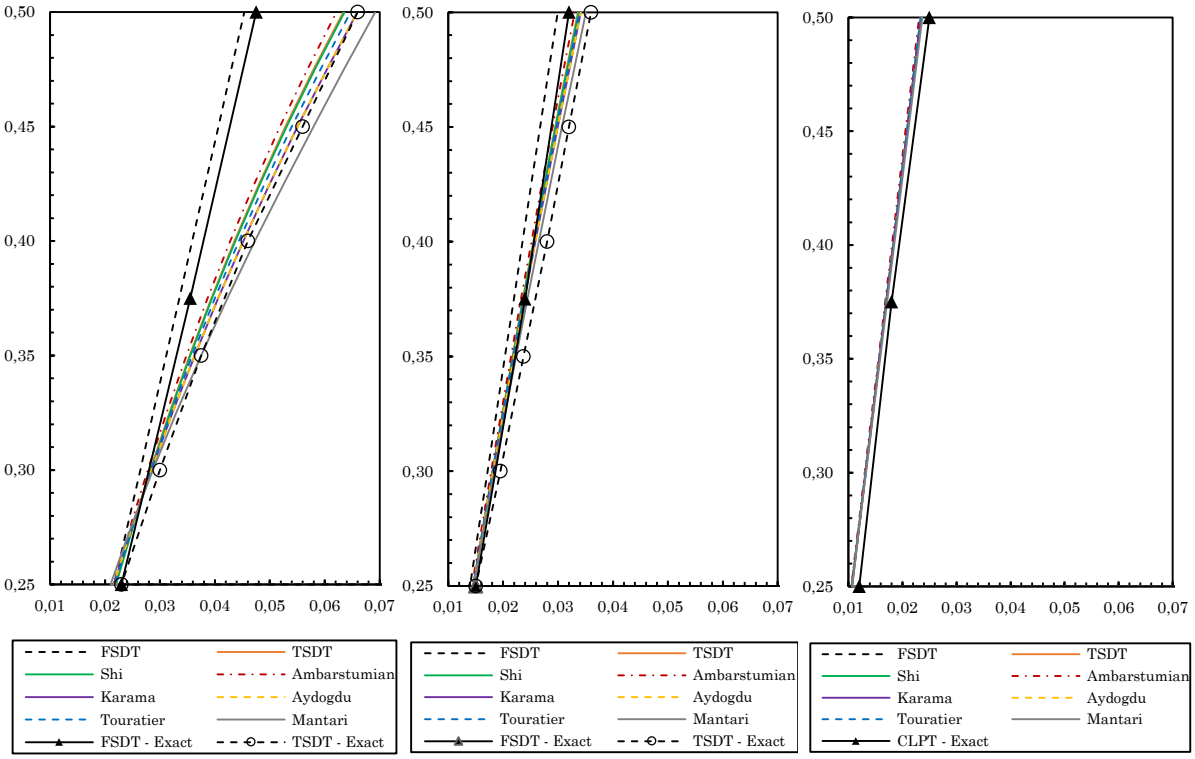

(a) (b) (c)

figure 35 – Details for the nondimensionalized normal stresses σ_{yy} computed with the RPIM for a simply supported symmetric square laminate with cross-ply layers (0/90/90/0) subjected to a sinusoidal load (SSL). (a) a/h=4, (b) a/h=10 and (c) a/h=100.

As stated in the introductory chapter (1.3.), the equivalent single layer theories give a sufficiently accurate description of the global laminate response but while the strains are continuous across the plate thickness, the corresponding stresses have jumps at the layer interfaces due to the fact that the material properties are different for each layer. This problem can be contoured using zig-zag or layerwise theories. In the case of the layerwise theories, they may provide a better representation of interlaminar stresses (continuous transverse stresses at layer interfaces) and moderate to severe cross-sectional warping, thus they allow to analyse the local behaviour of laminated structures when needed but they can be computationally expensive. [33], [50]. Post-processing approaches based on equilibrium equations can also solve this problem. For the laminate (0/90/0) with a/h=4 (figures 60 and 67 of Appendix B), despite all the solutions obtained for the transverse shear stresses were calculated from constitutive equations, they are compared with the 3D Elasticity solutions [26] that have continuous transverse shear stresses at layer in interfaces. Once again, it is, Mantari's theory that it closer to the solutions of Pagano and Hatfield.

Observing now the figures 68 and 69 of the Appendix B that represent the transverse shear stresses for the same laminate (0/90/0) but with a/h=100, the shear locking phenomenon is once again found for the NNRPIM V2. Thus, while the NNRPIM V2 gives accurately results for thick and moderately thick plates, the numerical method shows problems to compute the transverse shear stresses for thin plates.

With the analysis of figures 31-34, 58-61, 78-81 and 90-93 which represent the transverse shear stresses of all the simply supported square symmetric cross-ply laminates subjected to SSL but with a/h=4, it can be said that adding a 90^{o} layer to the laminate (0/90/0) – in other words, comparing this laminate with the (0/90/90/0) – helps to decrease the maximum shear stress $\overline{\tau_{xz}}$ and the normal stress $\overline{\sigma_{xx}}$, while the stresses referred to the axis Oy remain almost the same. Adding now a 0^{o} layer in the middle of the laminate (0/90/90/0), the transverse shear stresses can be reduced, but on the other hand there is an increase in the normal stresses. Finally, by comparing the latter laminate with the one with the stacking sequence (0/90/90/0/90/90/0), were not found noteworthy improvements in bending analysis by adding two more layers with 90^{o} orientations.

5.1.6 Computation Time Study

As mentioned in section 5.1.3., the convergence studies were performed in another perspective in order to understand the computational cost of each numerical method.

For the simply supported square symmetric cross-ply laminate (0/90/0) subjected to a sinusoidal load and with a ratio between its length and thickness of 50, nondimensionalized transverse displacements were calculated for nodal meshes with an increasing number of nodes. The computation time for each analysis was noted and the graphs of the figure 36 were obtained, grouped by HSDT. The data that provided the presentation of such graphs is presented in Appendix C.

Mantari's theory takes slightly more time to compute because of the introduction of an auxiliary function to calculate the integrals introduced in Chapter 4 by means of Taylor series. But the total computational time of each analysis is not greatly influenced by the type of HSDT. If it is considered the total computational time of each numerical method (from tables 76 and 77 in Appendix C), it can be concluded that the NNRPIM V1 is the less time consuming, followed by the RPIM. The NNRPIM V2, because of the necessity

of finding second-degree natural neighbours, needs more time to complete the analysis. However, by observation of figure 36, generally the NNRPIM V2 can obtain higher transverse displacements for the same computational time. The only exception is the Mantari theory which is overestimated by the NNRPIM V1.

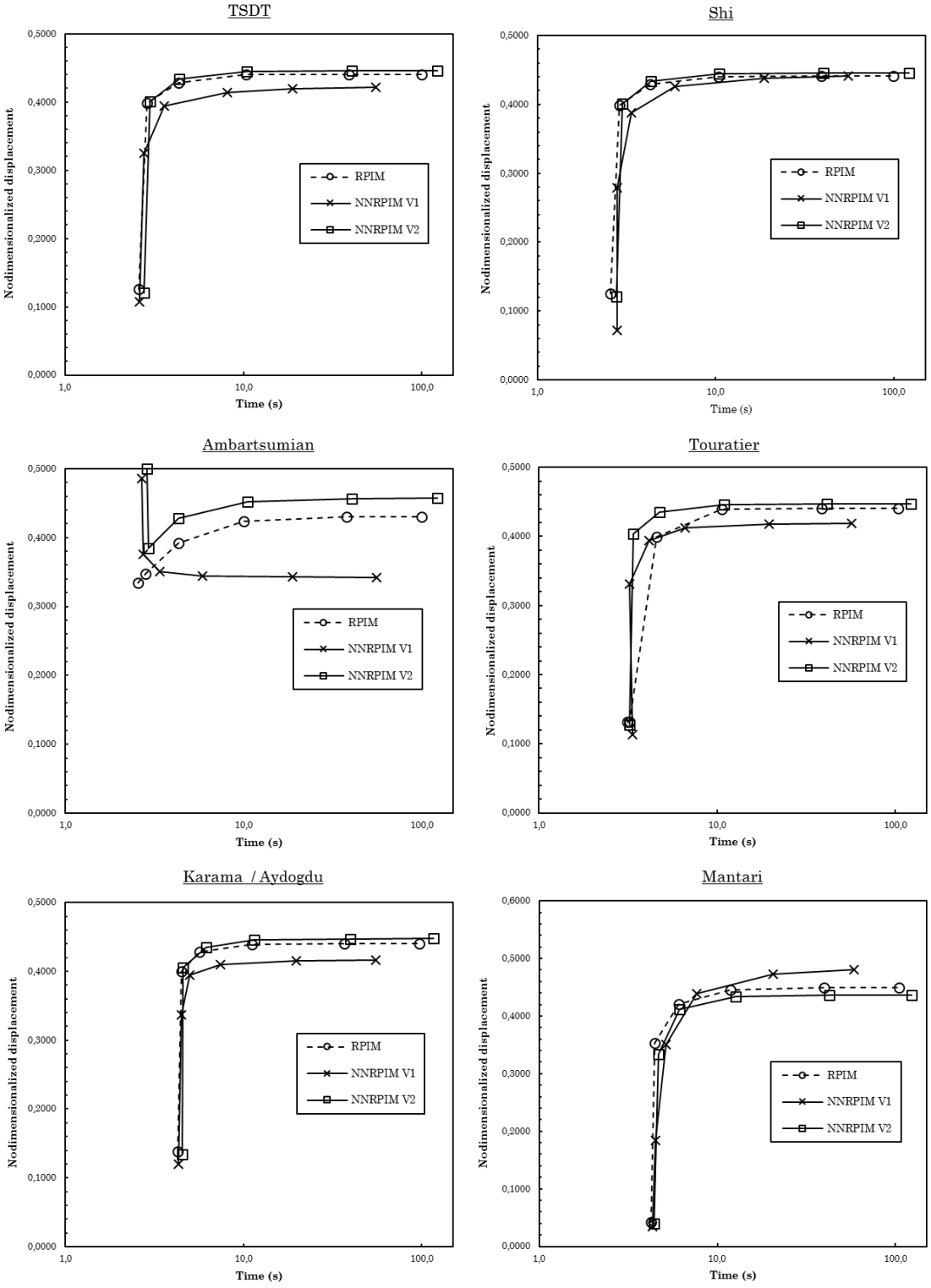

figure 36 – Computation time study for the seven HSDTs computed with the three numerical methods.

5.1.7 Final Remarks

In this Chapter, bending analyses of composite laminated plates with symmetric cross-ply layers were performed with two meshless methods, being one of them, the NNRPIM, investigated with two concepts of natural neighbours.

While the NNRPIM V2 is the numerical method that allows to obtain lower results when comparing the solutions of the meshless method with the exact solutions, it also has shear locking for thin plates. The NNRPIM V1 has the lower computational time but the solutions are not as accurate as the NNRPIM V2 or the RPIM. Thus, for thick symmetric cross-ply laminates, the NNRPIM V2 stands as the best option studied, while for thin laminates, it is better to use the RPIM.

By comparison of the different HSDT, Mantari's theory shown the best results when comparing the results obtained for the transverse shear stresses with analytical solutions.

5.2 Antisymmetric Cross-Ply Laminates

5.2.1 Introduction to the Problem Analysis

Bending analysis was performed in antisymmetric cross-ply laminates with stacking sequences that are multiple of that shown in figure 37.

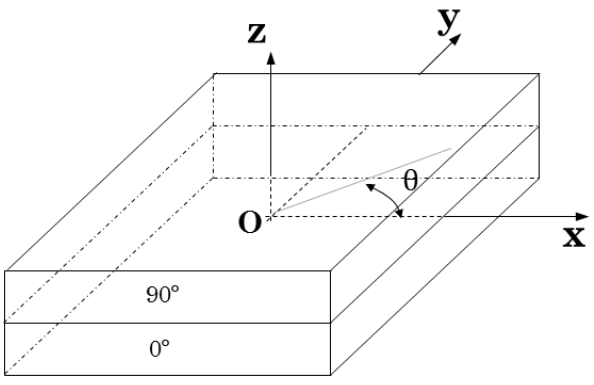

figure 37 – Antisymmetric cross-ply laminate (0/90) and the Cartesian coordinate system.

The results obtained from the RPIM and the NNRPIM for the different HSDTs and using different boundary conditions were compared with the

solutions of J.N. Reddy for the FSDT and the TSDT, due to the lack of analytical results for the respective HSDTs.

The material used in all static analysis for symmetric cross-ply laminates was the same one considered for the symmetric cross-ply laminates.

5.2.2 Considerations on the Generic Geometry

Although the generic geometry was already presented in section 5.1.2., some topics need to be considered such as the notation used for the applied boundary conditions and the z coordinates were the stresses were computed.

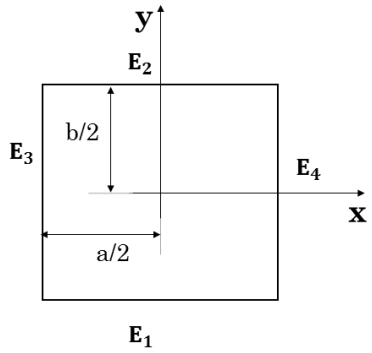

figure 38 – Nomenclature assigned to the edges of the plate

table 7 – Considered boundary conditions: S = Simply supported; C = Clamped; F = Free.

	E_1	E_2	E_3	E_4
Case 1	S	S	S	S
Case 2	S	S	S	C
Case 3	S	C	S	C
Case 4	S	F	S	F
Case 5	S	F	S	S
Case 6	S	F	S	C

Figure 38 and table 7 describe the nomenclature adopted to differentiate six types of tested boundary conditions.

Defining a general antisymmetric cross-ply laminate with 2n layers, with the stacking sequence $(0/90)_n$, the nondimensionalized transverse displacements and stresses can be obtained in the following z coordinates,

table 8 – z coordinate where the nondimensionalized transverse displacement and stresses are computed.

	w	σ_{xx}	σ_{yy}	τ_{xy}	τ_{yz}	τ_{xz}
$(0/90)_n$	0	h/2 (k=n)	h/2 (k=n)	-h/2 (k=1)	0 (k=2)	0 (k=1)

being the coordinates x and y equal to those already presented for the case of the symmetric cross-ply laminates.

5.2.3 Convergence Studies

Although it was not expected significant changes in comparison to the convergence studies performed for symmetric cross-ply laminates, two convergence studies were done for two different antisymmetric cross-ply laminates. Using the same parameters for the meshless methods (table 6), were studied simply supported square plates subjected to sinusoidal loads (figures 39-41).

Despite all the theories have shown good performance for symmetrical laminates, in the case of the antisymmetric laminates this did not happen. Exponential theories of Karama and Aydogdu produced completely different results for the preliminary convergence studies in comparison with other HSDTs, and were therefore excluded from analysis in this subchapter dedicated to antisymmetric laminates.

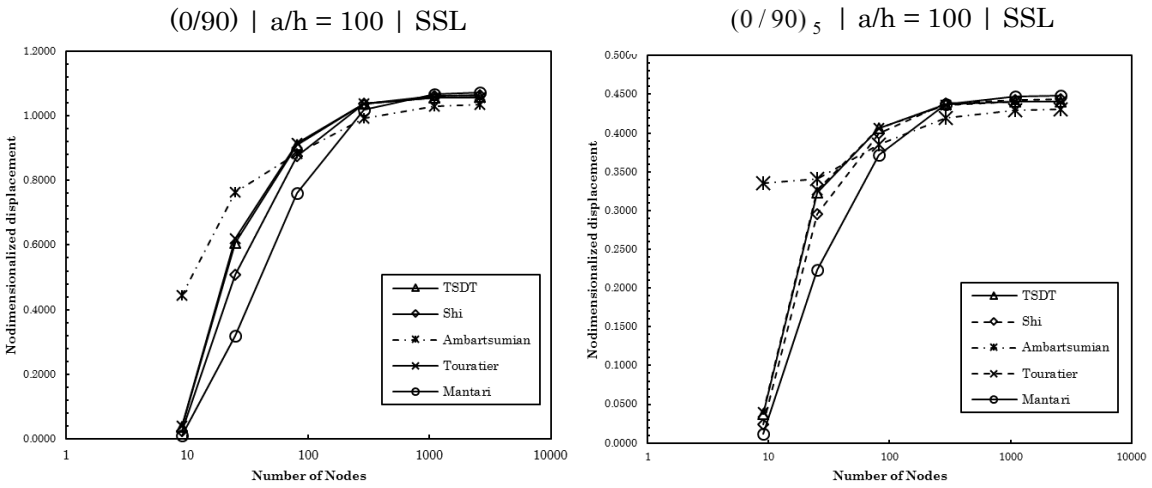

figure 39 – Convergence studies for the RPIM with two antisymmetric cross-ply laminates.

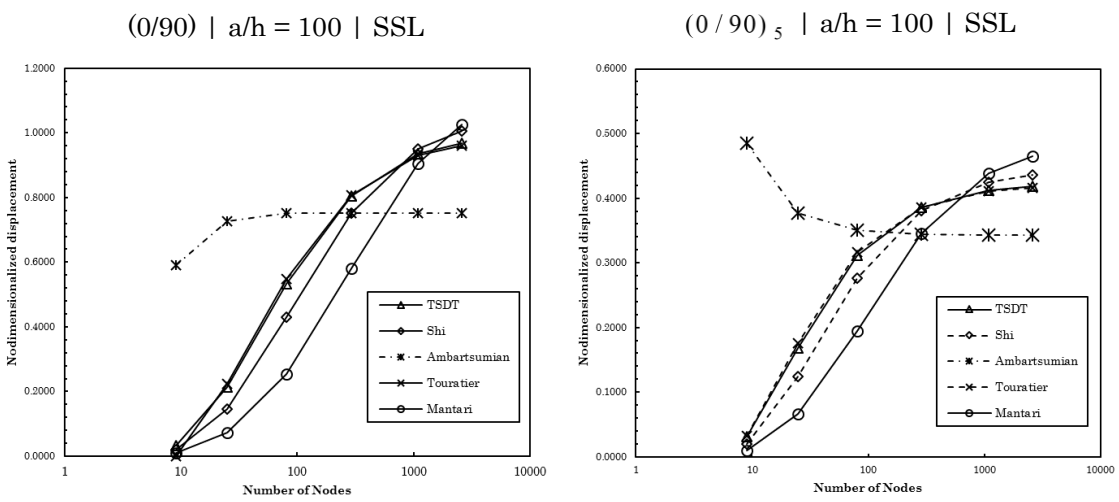

figure 40 – Convergence studies for the NNRPIM V1 with two antisymmetric cross-ply laminates.

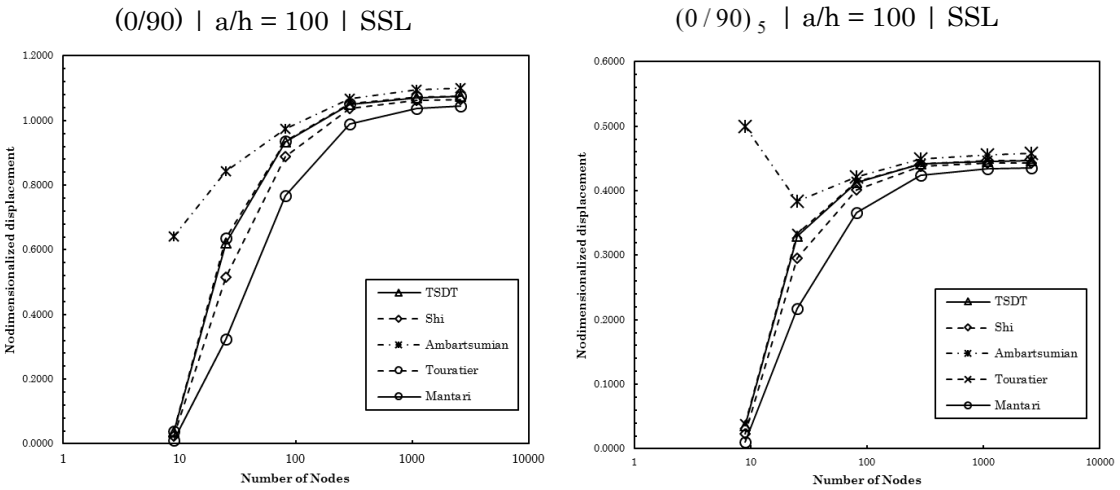

figure 41 – Convergence studies for the NNRPIM V2 with two antisymmetric cross-ply laminates.

Yet again, for the NNRPIM V1, a mesh with 2601 nodes is not sufficient for the convergence takes place. It is also observed that for this numerical method, the lines of convergence for the different HSDTs are farther apart than in the RPIM and the NNRPIM V2.

By observing figures 39 and 41, the convergence rate for the RPIM and the NNRPIM V2 is almost the same, and a laminate with more layers (that can be observed at the right side of each of these figures) converge faster than a laminate with only two layers.

Despite the pointed situation for the NNRPIM V1, a nodal mesh with 1089 nodes was once again selected.

5.2.4 Solutions of Nondimensionalized Transverse Displacements and Stresses for Various Laminates

Solutions were obtained for the nondimensionalized transverse displacements and stresses considering six types of boundary conditions and sinusoidal distributed loads. Those results are presented in tables 53-64 of the Appendix A, where are also presented the exact and FEM (computed with quadrilateral elements of Lagrange) solutions for the FSDT and TSDT [26]. Analytical solutions for the HSDTs applied to antisymmetric cross-ply laminates could not be found in literature. Tables 65-67 contain the results of the normalized transverse displacements and stresses for simply supported antisymmetric cross-ply laminates subjected to uniformly distributed loads.

Since a comparative study similar to the one performed for the symmetric cross-ply laminates in section 5.1.4. was not possible (due to the lack of analytical solutions for HSDTs), the results presented in Appendix A for Case 1 and a/h=10, were organized in the bar graphs of the figures 42-44 for comparison purposes. These graphs show the solutions for the normalized central transverse displacements, normal stresses and transverse shear stress (notice that in this case $\overline{\sigma_{xx}} = \overline{\sigma_{yy}}$ and $\overline{\tau_{xz}} = \overline{\tau_{yz}}$) computed with the RPIM, the NNRPIM V1 and the NNRPIM V2 for all the HSDTs (except Karama and Aydogdu's theories), as well as the exact results for the TSDT and the FEM solutions for the same theory (with the exception of the transverse shear stress because J.N. Reddy did not publish those results). Notice that the scales of the axes of ordinates are equal for the three numerical methods, which makes the comparison easier and, to show the variability of the results, the same scale does not begin with zero.

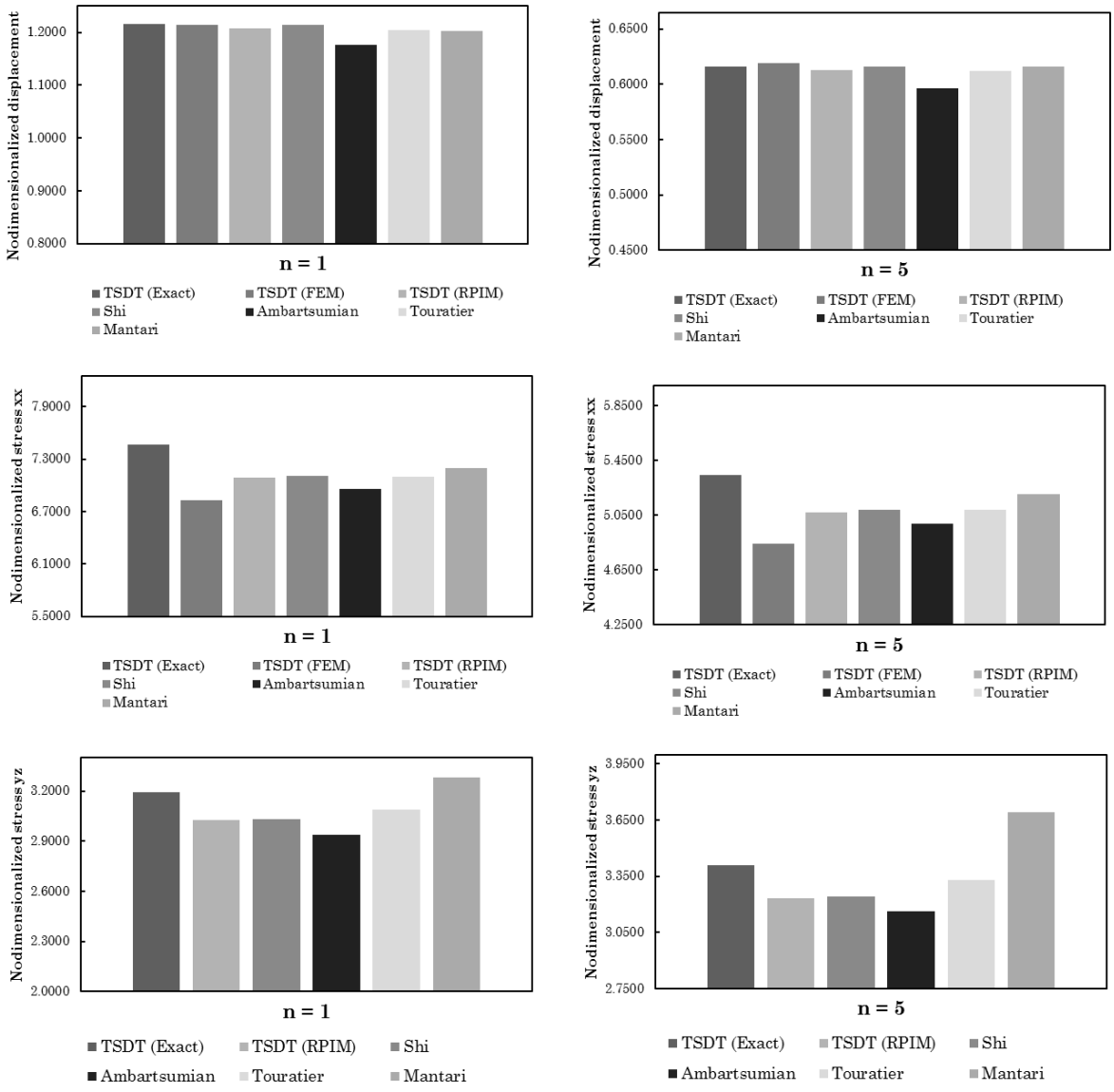

figure 42 – Maximum normalized transverse displacements and stresses for two antisymmetric cross-ply square laminates - $(0/90)_n$ with n=1 and n=5 - subjected to a sinusoidal load (SSL), with the boundary conditions of the Case 1, a/h=10. Solutions for the HSDTs computed with the RPIM.

For the RPIM, the central displacements obtained from the TSDT are furthest from the analytical result than the solution obtained by the FEM. However, in the case of the normal stresses, the inverse situation is verified. As expected, the solutions computed with Shi's theory are very close to J.N. Reddy's TSDT for the two antisymmetric cross-ply laminates. As it will be shown in section 5.2.5., Ambartsumian and Mantari's theories are those that show major differences between them, since Mantari predicts the higher stresses and Ambartsumian is situated at the opposite side.

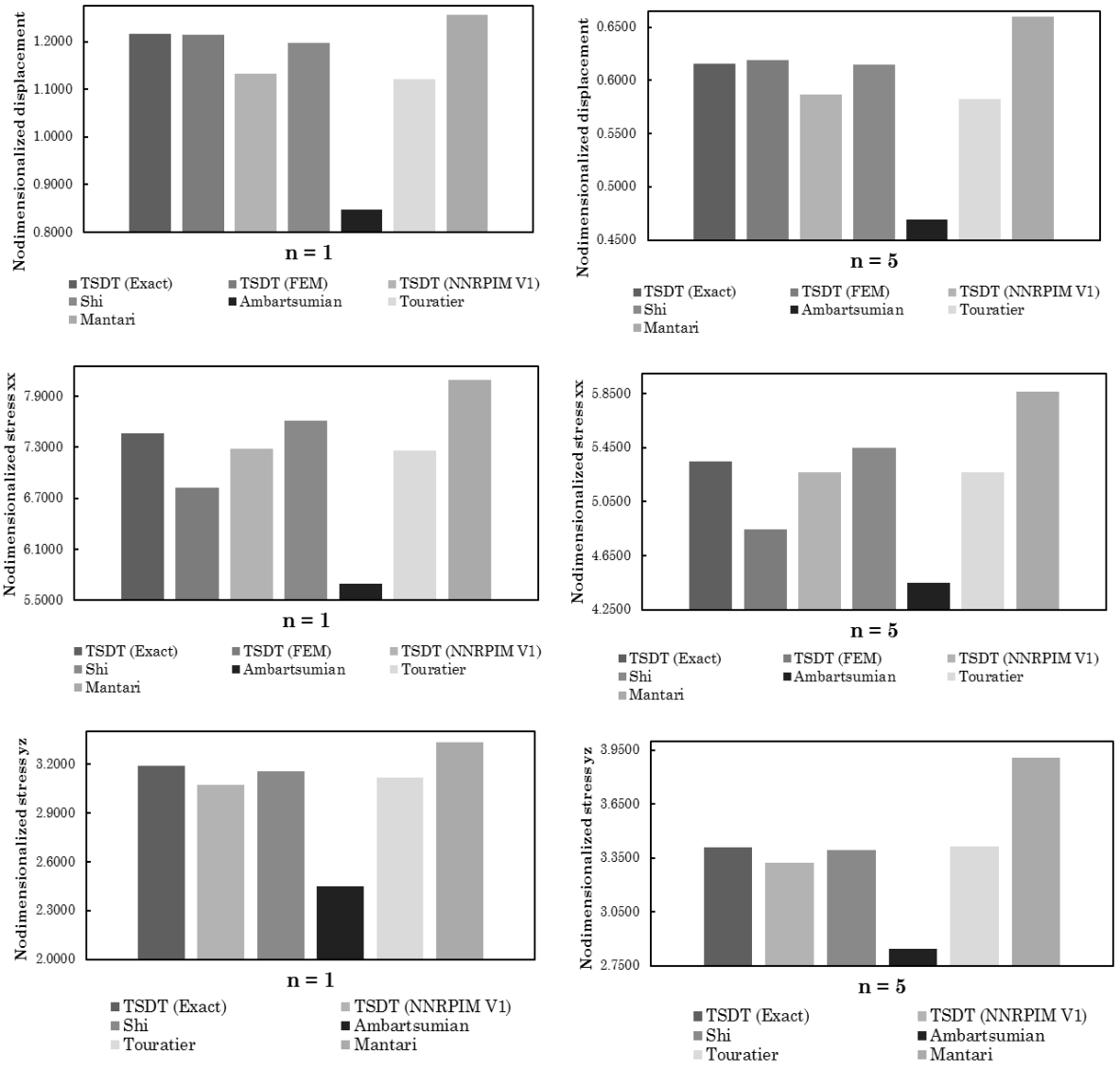

figure 43 – Maximum normalized transverse displacements and stresses for two antisymmetric cross-ply square laminates -$(0/90)_n$ with n=1 and n=5 - subjected to a sinusoidal load (SSL), with the boundary conditions of the Case 1, a/h=10. Solutions for the HSDTs computed with the NNRPIM V1.

Comparing the behaviour of the two antisymmetric cross-ply laminates, it is clear that the shear stresses are increased when passing from the laminate with two layers to the laminate with ten layers, but the transverse displacements and normal stresses are greatly reduced.

Observing figure 43, an evidence stated before is confirmed: the NNRPIM V1 underestimates the solutions form Ambartsumian's theory and overestimates the ones form Mantari's theory. Additionally, Shi's TSDT and Reddy's TSDT have now bars with different heights, which does not seem correct considering the analyses made earlier.

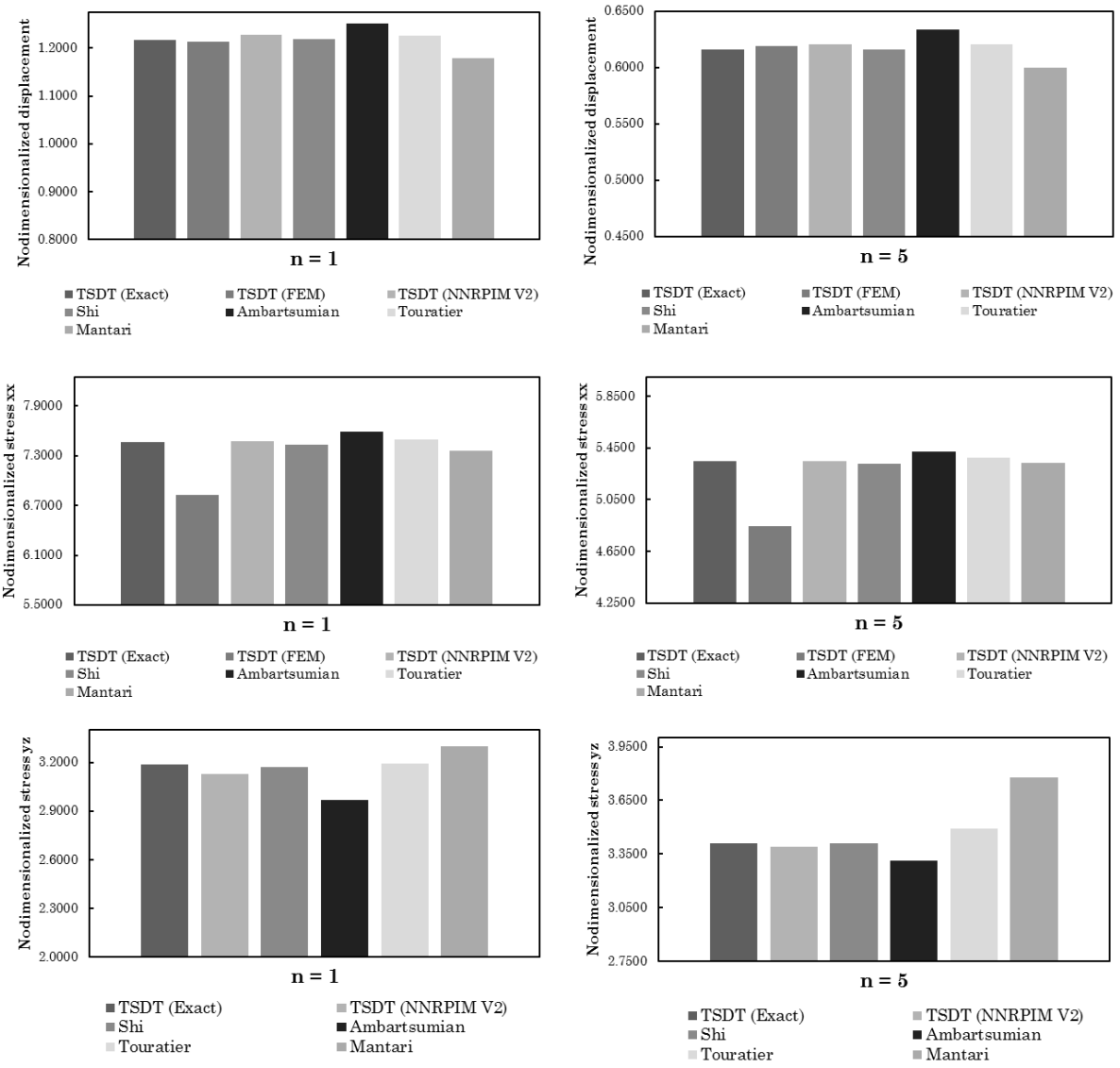

figure 44 – Maximum normalized transverse displacements and stresses for two antisymmetric cross-ply square laminates - $(0/90)_n$ with n=1 and n=5 - subjected to a sinusoidal load (SSL), with the boundary conditions of the Case 1, a/h=10. Solutions for the HSDTs computed with the NNRPIM V2.

As shown in figure 44, the NNRPIM V2 achieves more similar results to the RPIM and, in the cases of the stresses, the bars related to the 'TSDT (NNRPIM V2)' are even more closer to the bar related to 'TSDT – Exact'. However, in the case of the central displacements, there is an uncommon behaviour since the solution obtained from Ambartsumian's theory is higher than the same solution obtained from the Mantari theory.

5.2.5 Study of the Influence of the Boundary Conditions

For the other cases mentioned in table 7 and whose results are exposed in the tables of Appendix A, the normalized transverse displacements calculated from the RPIM, the NNRPIM V1, the NNPRIM V2 and the FEM computed with the TSDT were selected and compared with the exact solutions of Reddy. The results for the absolute values of the relative errors (%) are as follows,

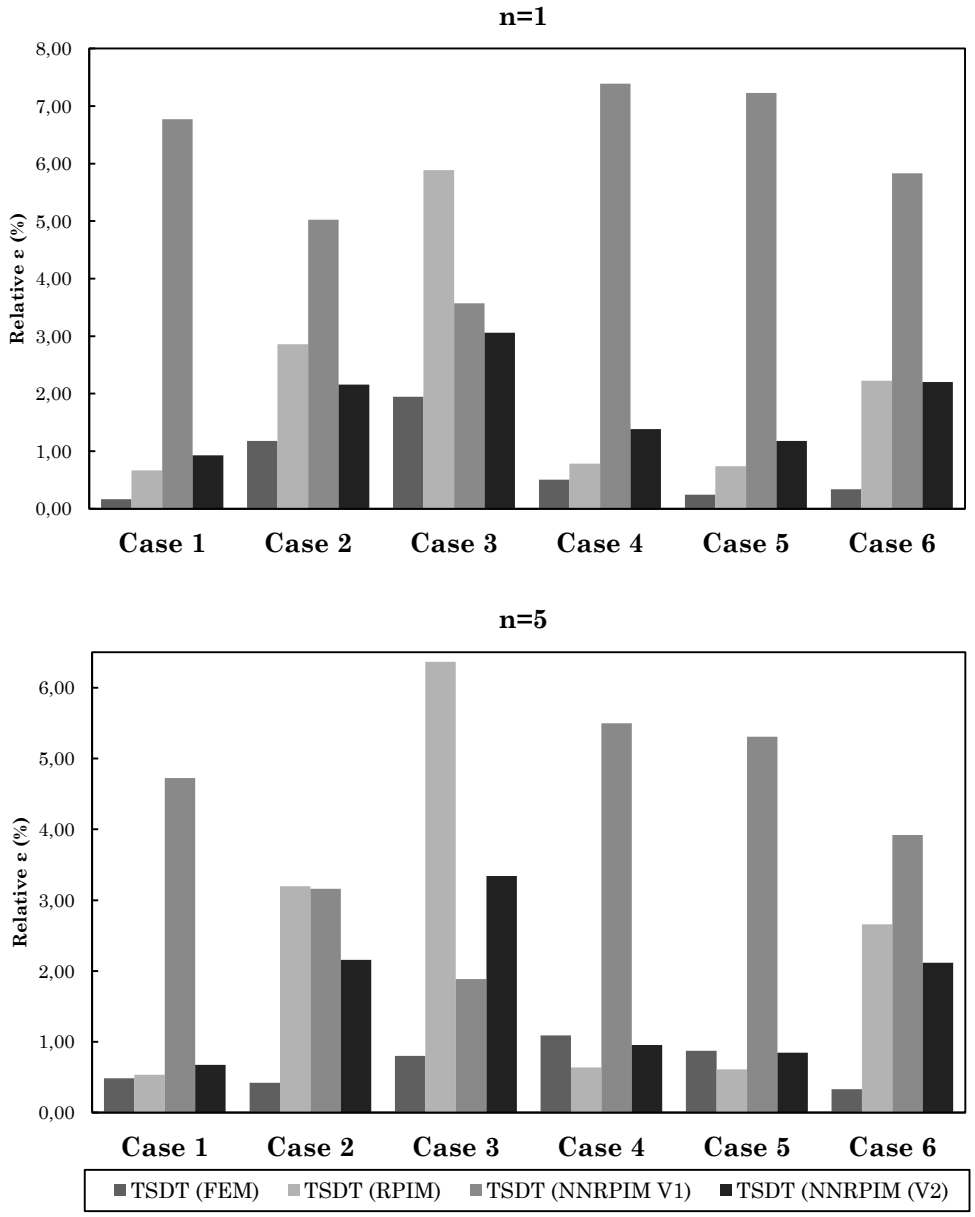

figure 45 – Relative errors (%) regarding the exact solution of the maximum normalized transverse displacements for two antisymmetric cross-ply square laminates - $(0/90)_n$ with n=1 and n=5 - subjected to a sinusoidal load (SSL), a/h=10.

Despite the errors stated in figure 45 were in all cases inferior to 8%, there still are some singularities that need a further analysis. Firstly, as already pointed, the FEM solutions for displacements are closer to the exact solution

than any other solution obtained from meshless methods. Secondly, figure 45 reinforces the conclusion that NNRPIM V1 generates higher errors. It can also be concluded that for a ten layer antisymmetric cross-ply laminate the errors are reduced, except in the case of the RPIM. But the major conclusion to be drawn from figure is that the errors are much higher when at least one of the edges of the plate is clamped - Cases 2, 3 and 6. . In those cases, the NNRPIM V2 shows better performance in comparison to the RPIM since its errors are roughly half of RPIM's errors. Although, for example in Case 6, the percent error still is substantial, it has been significantly reduced by changing the form of imposition of boundary conditions in the algorithm. Initially, for clamped boundaries, only the boundary nodes had their central displacements constrained, which leaded to much higher errors than those presented in this work. As recommended in the literature [9], the clamped condition was reinforced by the addition of nodes beyond the problem domain - as shown in the figure 46 - and impose the boundary conditions on these nodes and on the nodes of the clamped border.

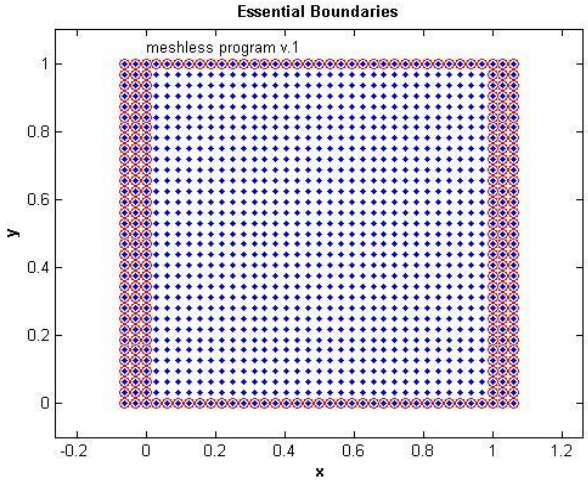

(a)

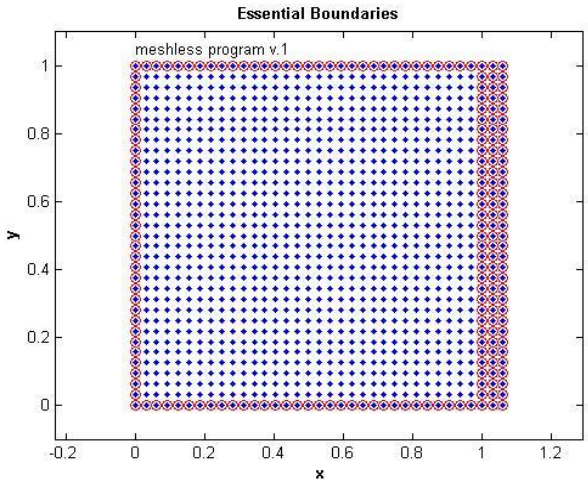

(b)

figure 46 – Imposition of the essential boundary conditions for (a) two clamped edges of the plate; (b) only the right edge of the plate is clamped.

5.2.6 Nondimensionalized Maximum Stresses Along the Thickness for Various Laminates

For two composite laminated plates with antisymmetric cross-ply layers with stacking sequences $(0/90)$ and $(0/90)_4$ – which is equal to (0/90/0/90/0/90/0/90) – the normal and shear transverse stresses along the thickness were computed and represented in graphs. For a ratio of the side length and the thickness equal to 4, 10 and 100, the normal stress $\overline{\sigma_{yy}}$ and the shear stress $\overline{\tau_{xz}}$ were determined as a function of the normalized thickness z/h. Due to the fact that the laminates in analysis are simply supported antisymmetric cross-ply laminates subjected to sinusoidal loads, it is not necessary to represent the normal stress $\overline{\sigma_{xx}}$ and the shear stress $\overline{\tau_{yz}}$ because they follow the same distribution as the other mentioned stresses.

When a/h=4, the figures 47-50 shows the obtained results (for the ratios of a/h=10 and 100, the results are presented in Appendix C). These graphs allow to compare the behaviour of the two laminates, since the comparisons between HSDTs and meshless methods were already taken.

Firstly, by the analysis of graphs related to the normal stresses, it is confirmed that the stress distribution is not symmetric, so the membrane forces of the equations (81) will not be zero. Then, from the observation of the distribution of normal stresses of the two laminates, the laminate with eight layers is more balanced and has a lower maximum nondimensionalized normal stress. As regards the shear stresses, despite the maximum values are almost the same, the laminate with eight layers shows a better consistency since in this case there is not an abrupt differential between the shear stress above and below the mid-surface of the plate.

RPIM

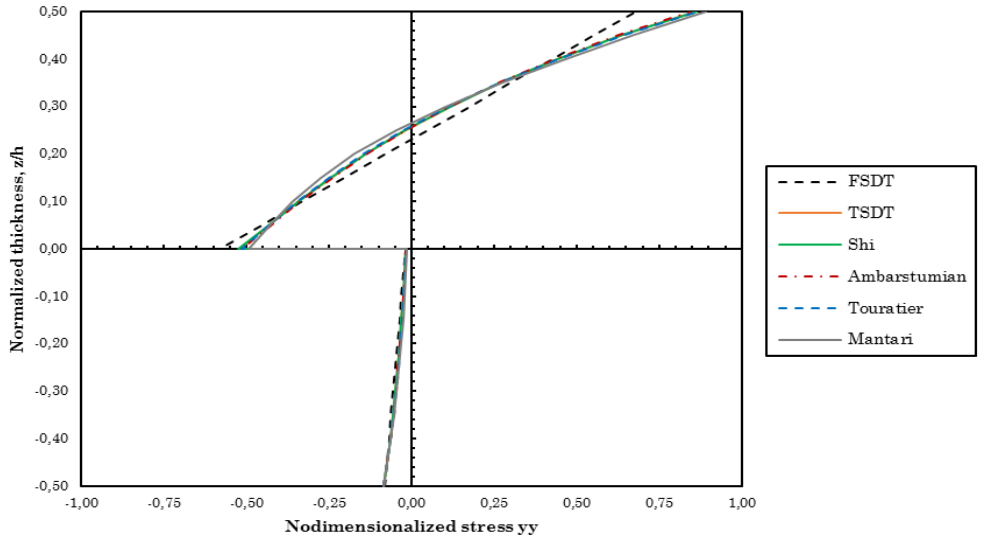

NNRPIM V1

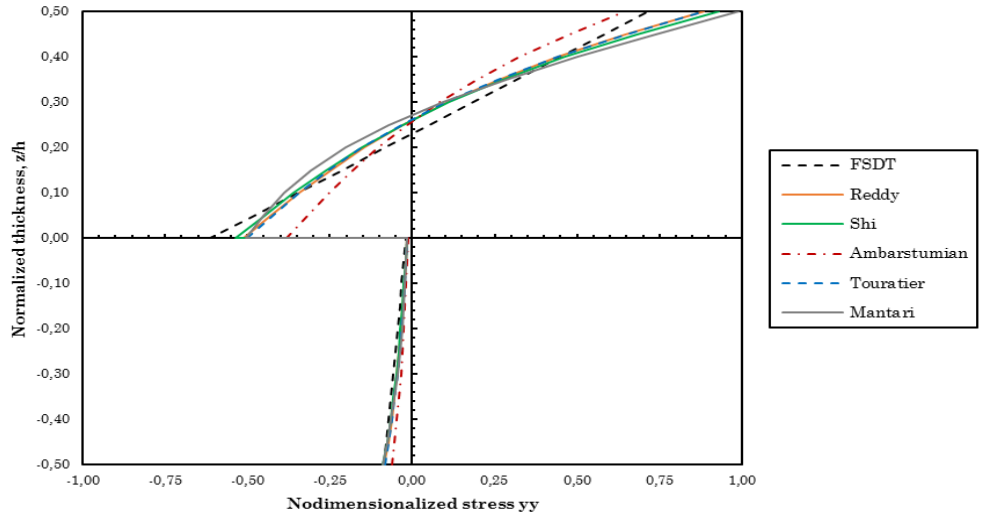

NNRPIM V2

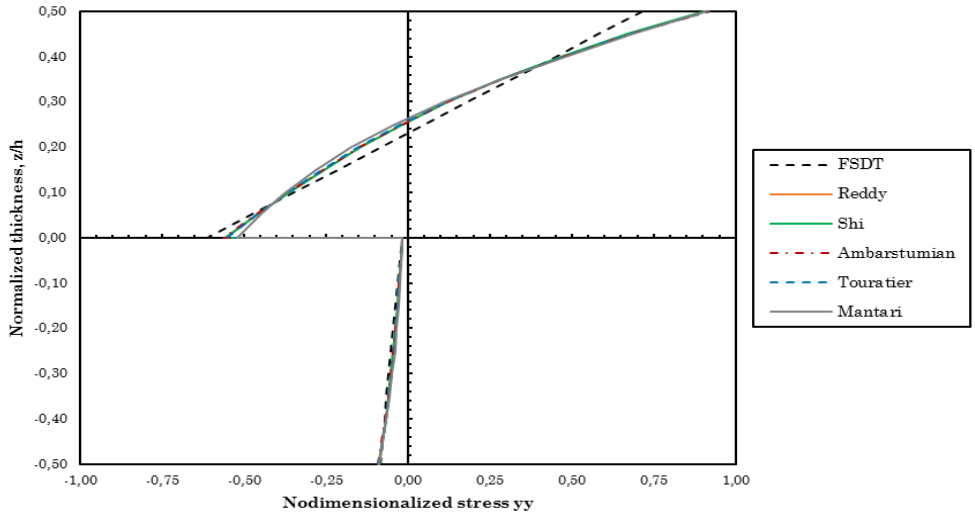

figure 47 – Nondimensionalized stresses σ_{yy} computed with the three numerical methods for a simply supported antisymmetric square laminate with cross-ply layers (0/90) subjected to a sinusoidal load (SSL), a/h=4.

RPIM

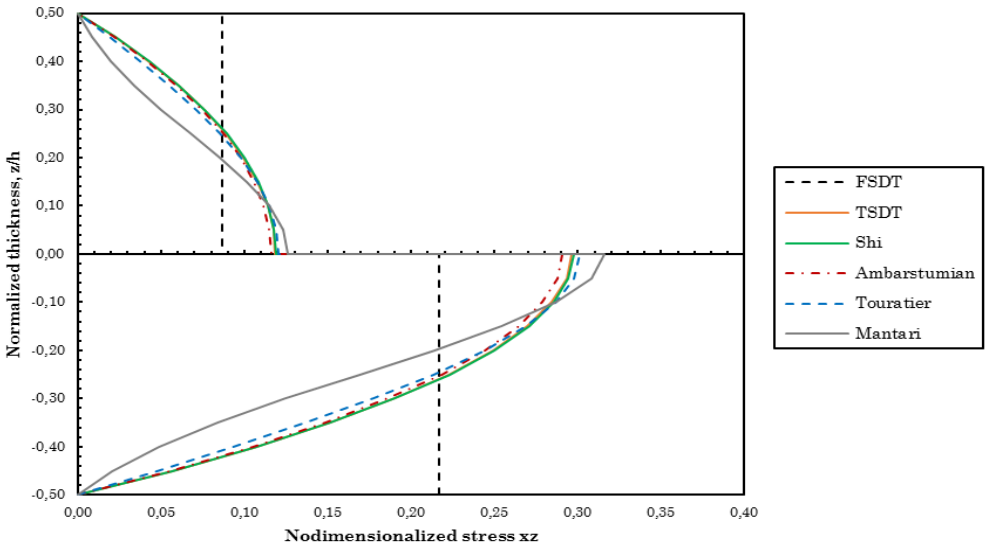

NNRPIM V1

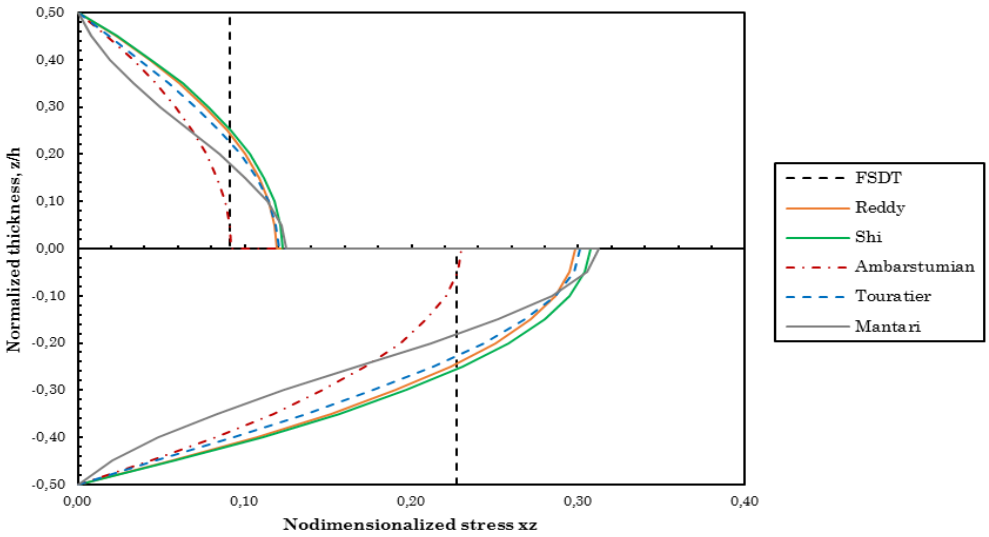

NNRPIM V2

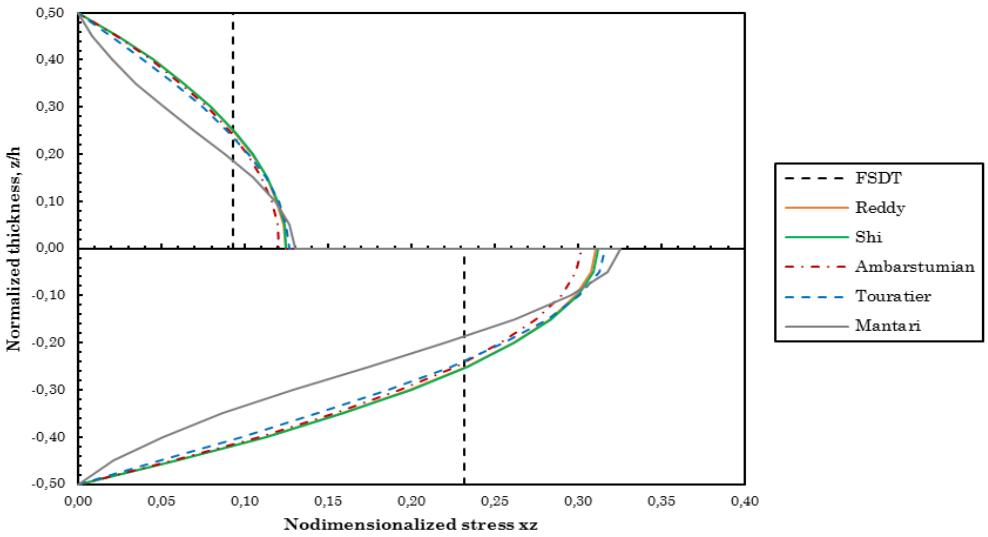

figure 48 – Nondimensionalized stresses τ_{xz} computed with the three numerical methods for a simply supported antisymmetric square laminate with cross-ply layers (0/90) subjected to a sinusoidal load (SSL), a/h=4.

RPIM

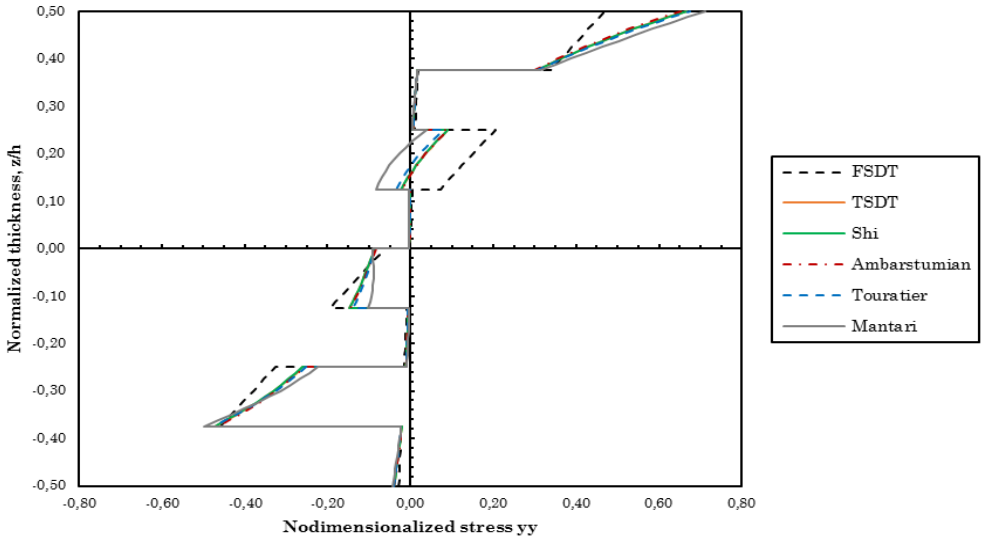

NNRPIM V1

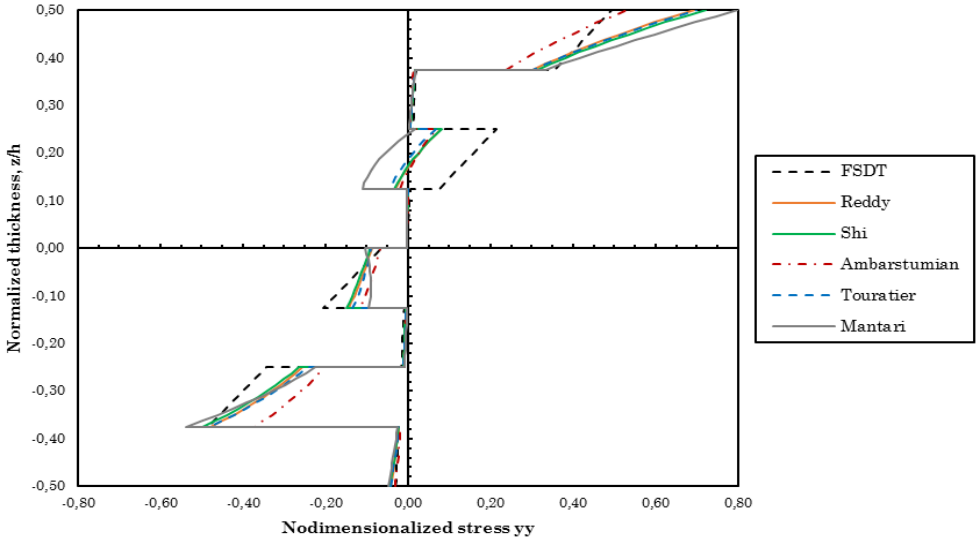

NNRPIM V2

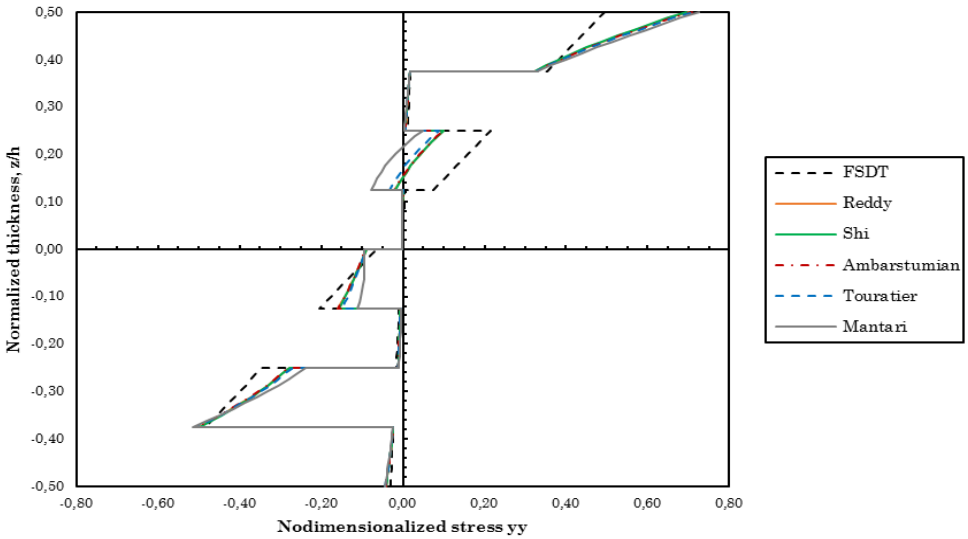

figure 49 – Nondimensionalized stresses σ_{yy} computed with the three numerical methods for a simply supported antisymmetric square laminate with cross-ply layers $(0/90)_4$ subjected to a sinusoidal load (SSL), a/h=4.

RPIM

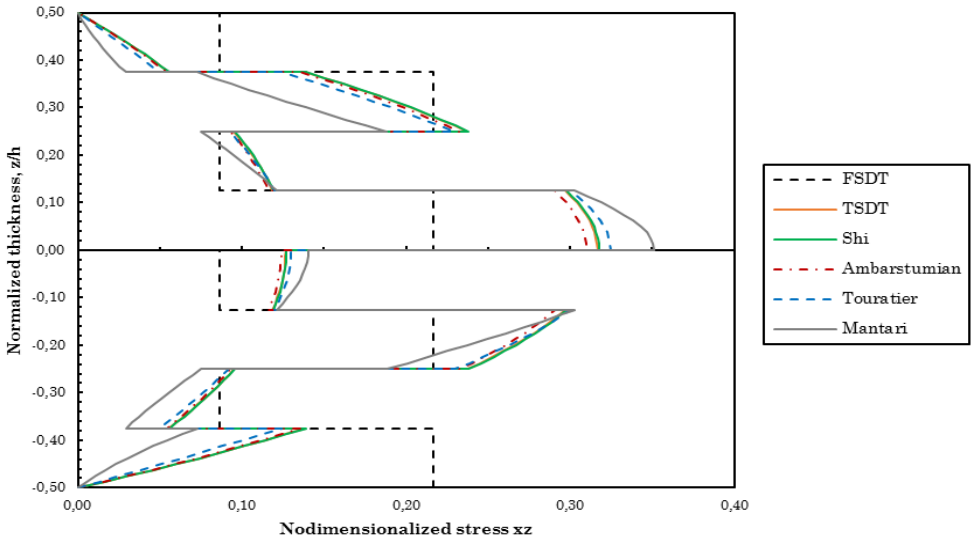

NNRPIM V1

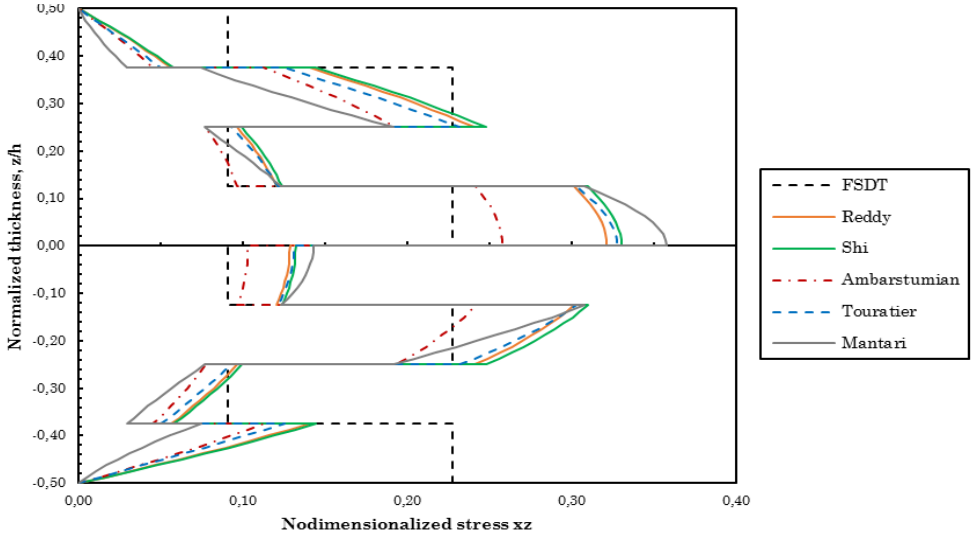

NNRPIM V2

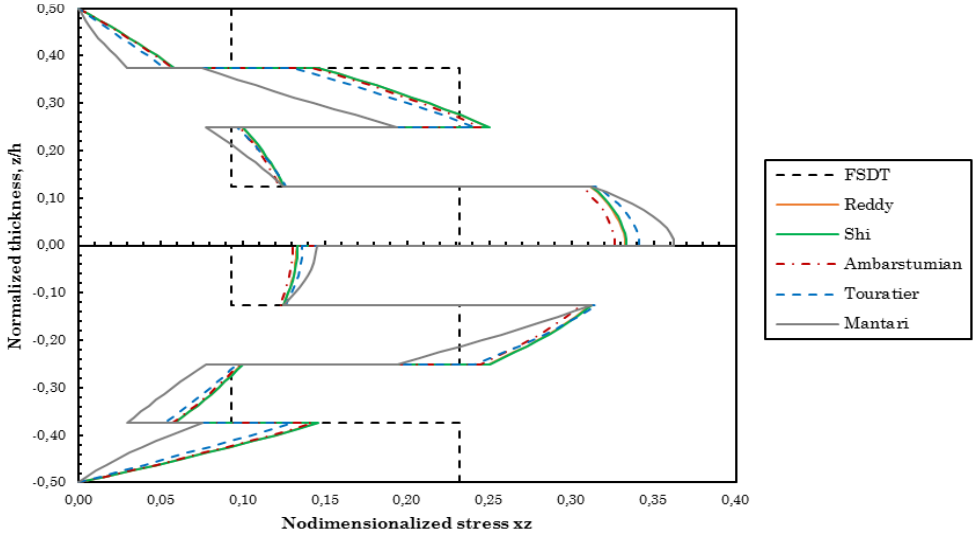

figure 50 – Nondimensionalized stresses τ_{xz} computed with the three numerical methods for a simply supported antisymmetric square laminate with cross-ply layers $(0/90)_4$ subjected to a sinusoidal load (SSL), a/h=4.

5.2.7 Final Remarks

Despite the main conclusions concerning the numerical methods and HSDTs were already stated in 5.1.6. for the symmetric cross-ply laminates, from the analysis of antisymmetric cross-ply laminated plates it can be concluded that not all HSDTs are suitable for every single laminated plate, which are the cases of Karama and Aydogdu theories that showed results completely different from the standard expected solutions.

Also, the way the boundary conditions are imposed is a key step in achieving a better solution for clamped plates using a meshless method.

5.3 Antisymmetric Angle-Ply Laminates

5.3.1 Introduction to the Problem Analysis

The latest static analyses were performed for antisymmetric laminates with angle-ply layers. Firstly, two laminates with stacking sequences of $(-45/45)$ and $(-45/45)_4$ were subjected to sinusoidal and uniformly distributed loads and the transverse displacements and stresses were determined. Then, for six antisymmetric angle-ply laminates with stacking sequences $(5/-5)$, $(5/-5)_3$, $(30/-30)$, $(30/-30)_3$, $(45/-45)$ and $(45/-45)_3$, the transverse transverse displacements were obtained, being the results for the FSDT and TSDT compared to Reddy's analytical solutions, since there are any exact solutions for this kind of laminated plates computed with HSDTs in literature.

In the end, the creation of a new subroutine in the algorithms allowed to represent the maximum normalized central transverse displacement as a function of the ply angle and find which angles maximizes and minimizes its value.

The studies performed with the laminates $(-45/45)$ and $(-45/45)_4$ used the material of table 9. The other solutions were found for the material previously used in the subchapters 5.1. and 5.2..

table 9 – Mechanical properties of the material used for all the static analysis of antisymmetric angle-ply laminates.

E_1	E_2	ν_{12}	$G_{12} = G_{13}$	G_{23}
40 GPa	1 GPa	0.25	0.6 E_2	0.5 E_2

5.3.2 Considerations on the Generic Geometry

All the considerations taken in section 5.1.2. are also valid for the static analysis of composite laminates plates with antisymmetric angle-ply layers, except the z coordinates where the stresses are computed – table 10.

table 10 – z coordinate where the nondimensionalized transverse displacement and stresses are computed.

	w	σ_{xx}	σ_{yy}	τ_{xy}	τ_{yz}	τ_{xz}
$(\theta/-\theta)_n$	0	h/2 (k=n)	h/2 (k=n)	-h/2 (k=1)	0 (k=2)	0 (k=1)

5.3.3 Convergence Studies

Transverse displacements were calculated - using nodal meshes progressively with a higher number of nodes - for antisymmetric angle-ply laminates with different stacking sequences and using the same parameters of the numerical methods adopted before.

By analysing the figures 51-53, it was not observed a dependence on the lamination angle in the way the methods converge. For the configurations $(-5/5)$ and $(-5/5)_3$, the convergence lines have a similar shape to those obtained for the orthotropic plate (figures 21-23), which was expected because the ply angle is small in these cases.

A nodal mesh with 1089 nodes was again selected.

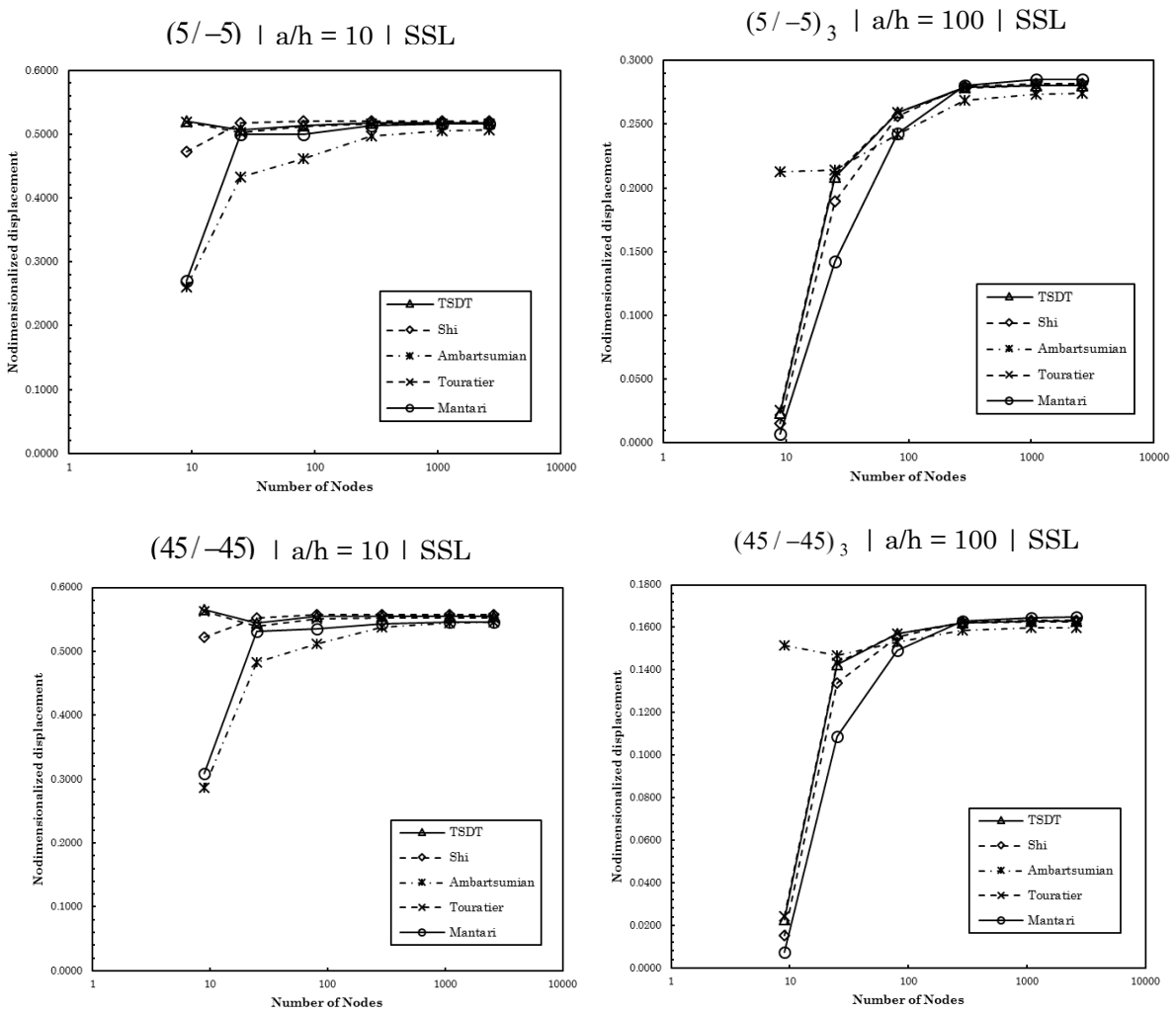

figure 51 – Convergence studies for the RPIM with two antisymmetric angle-ply laminates.

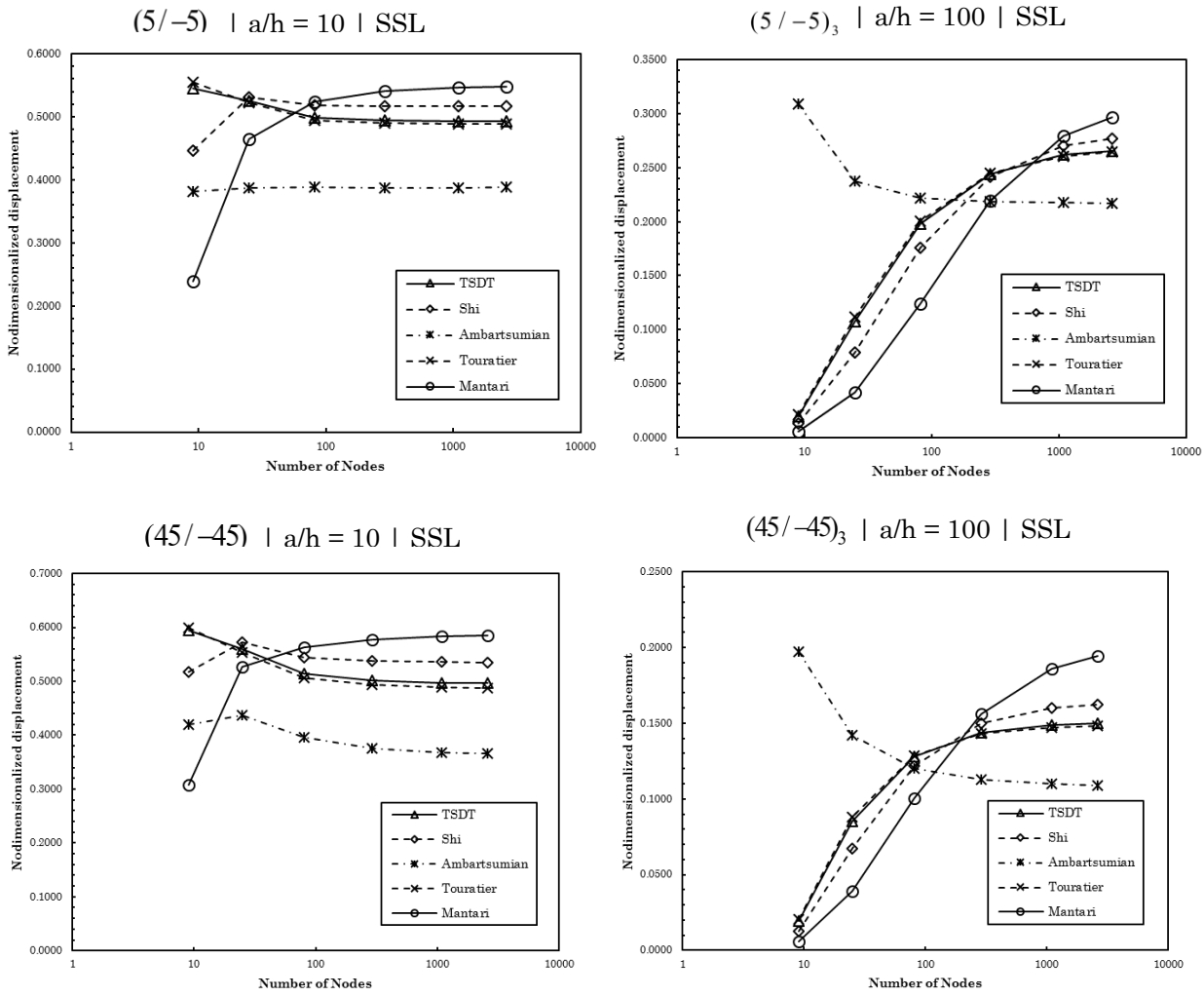

figure 52 – Convergence studies for the NNRPIM V1 with two antisymmetric angle-ply laminates.

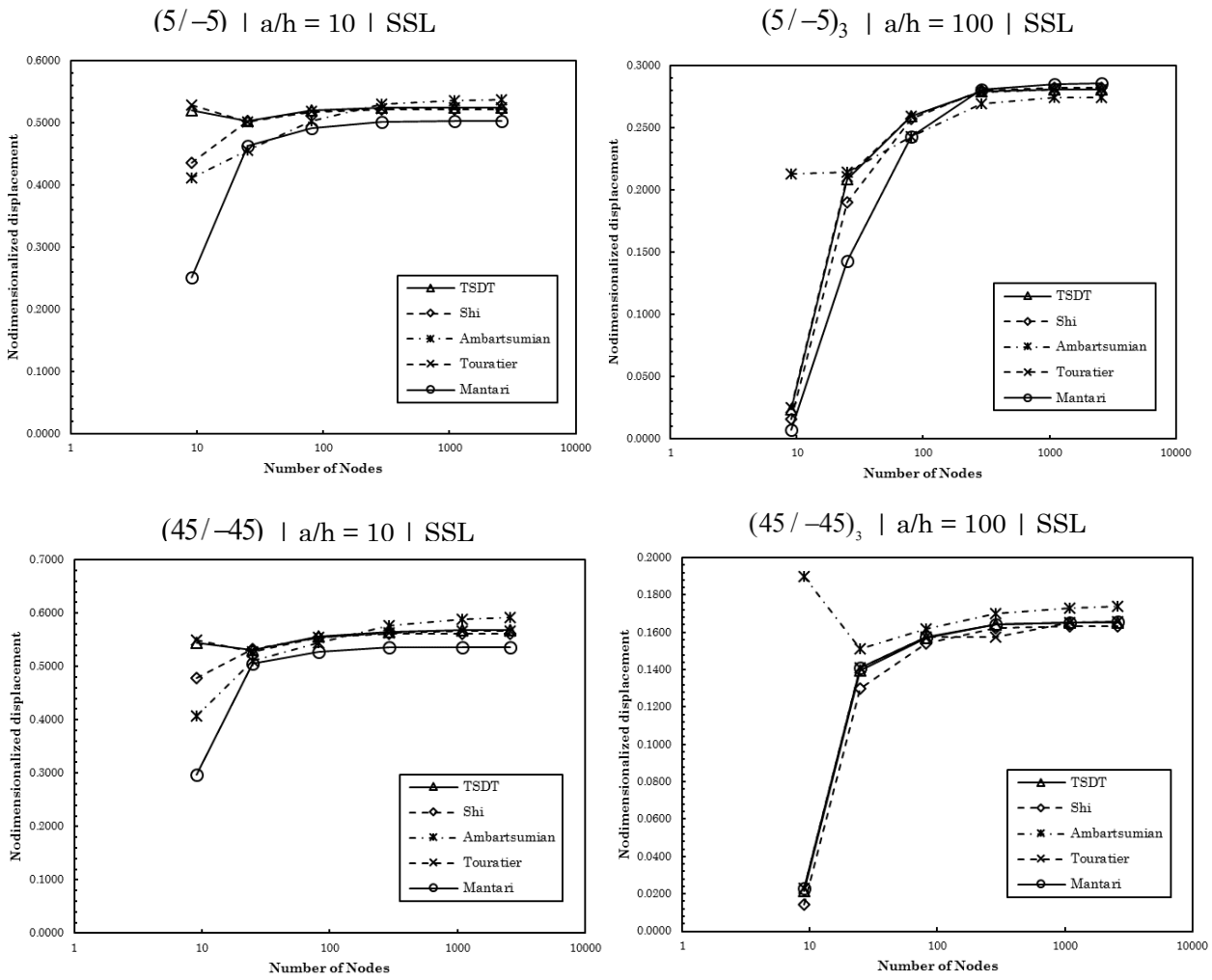

figure 53 – Convergence studies for the NNRPIM V2 with two antisymmetric angle-ply laminates.

5.3.4 Solutions of Nondimensionalized Transverse Displacements and Stresses for Various Laminates

For six different antisymmetric laminates with angle-ply layers ($(5/-5)$, $(5/-5)_3$, $(30/-30)$, $(30/-30)_3$, $(45/-45)$ and $(45/-45)_3$), the maximum transverse displacement from each bending analysis was determined using each HSDTs and, as already done before, computed with the three methods (see tables 71-75 of Appendix A). The solutions obtained for the TSDT were compared with the analytical solutions of J.N. Reddy – figure 54 – because the exact results for the other HSDTs cannot be found in literature.

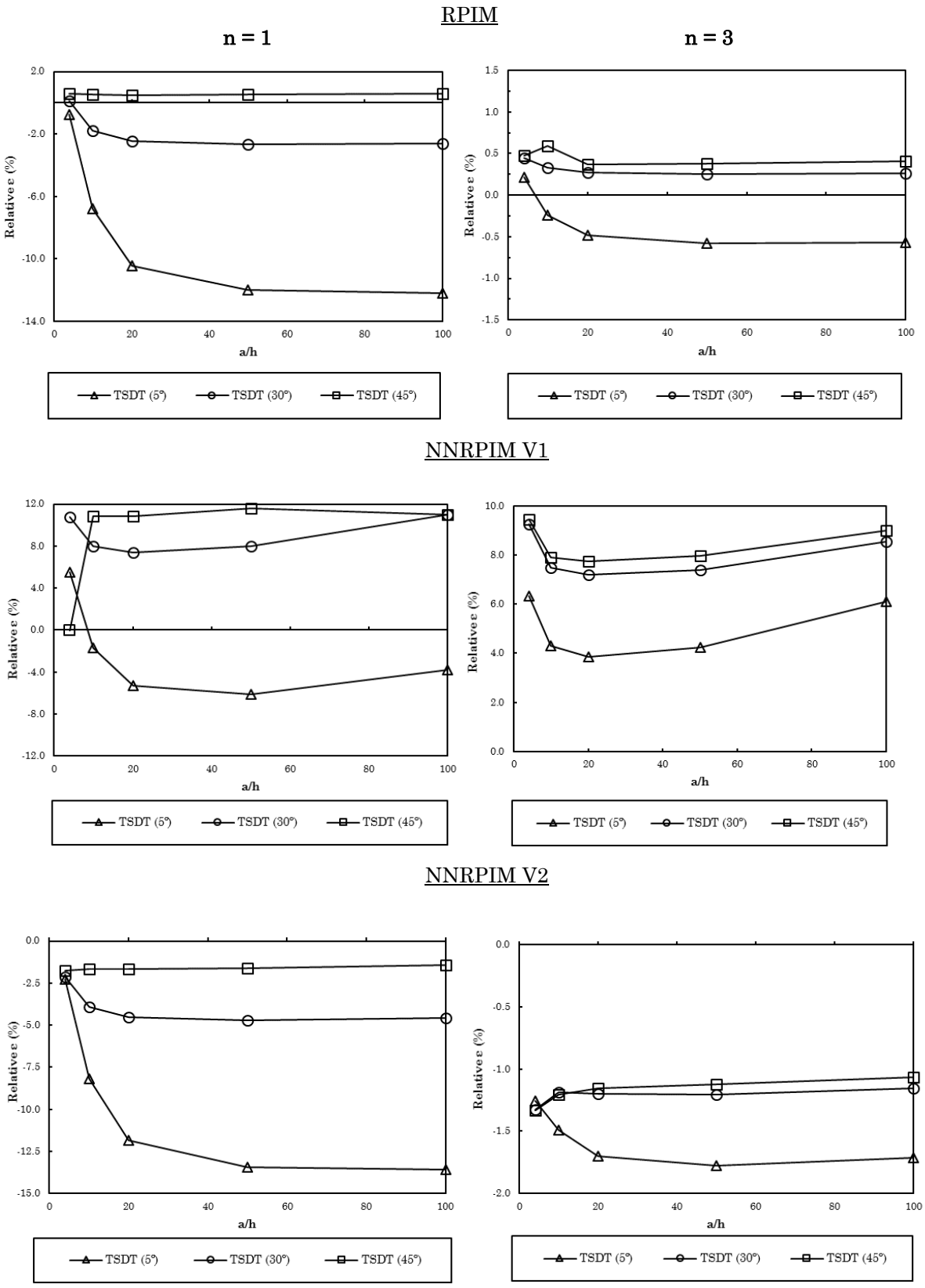

figure 54 – Relative errors ε(%) regarding the respective exact solution for the maximum normalized transverse displacements for two simply supported laminated plates with antisymmetric angle-ply layers $(\theta/-\theta)_n$ subjected to a sinusoidal load (SSL).

The obtained results shown a great agreement with the solutions proposed by Reddy, in particular for the laminates with six layers that can achieve errors lower than 2% for the RPIM and the NNPRIM V2.

5.3.5 Study of the Relation Between the Nondimensionalized Transverse Displacement and the Lamination Angle

The main study performed on antisymmetric angle-ply laminates was the determination of the maximum nondimensionalized transverse displacement as a function of the ply angle for laminates with a general stacking sequence $(\theta/\text{-}\theta)_n$ and using the material of table 4. The graphs of figures 55-57 were obtained from a new developed routine in MATLAB®, which was combined with the previously presented algorithms. With this new computational tool, it is now possible to sweep all the ply angles, θ, between 0^o and 90^o.

From figure 55 it can be determined the ply angles that maximize and minimize the transverse displacements. For the case of a laminate with two layers (n = 1), the maximum deflection occurs for ply angles of 17^o and 73^o, while the minimum deflection occurs for ply angles of 0^o or 90^o, which makes laminate an orthotropic plate. For the latter configuration (equivalent to an orthotropic plate) a laminate with eight layers (n = 4) has its maximum value of deflection, while the minimum is verified for 45^o. In can also be observed that the minimum value of the deflection for laminates with two layers is very close to the maximum value for laminates with eight layers,

Concerning the numerical methods, the RPIM and NNRPIM V2 have similar curves, as was expected since the two methods have shown similar results in other analyses. From the NNRPIM V1 the curves represented are, as expected, more distant.

Notice that in the graphs of figures 55-57, the axis corresponding to the transverse displacement do not start at zero. This graphical representation permits to identify better the difference between the solutions.

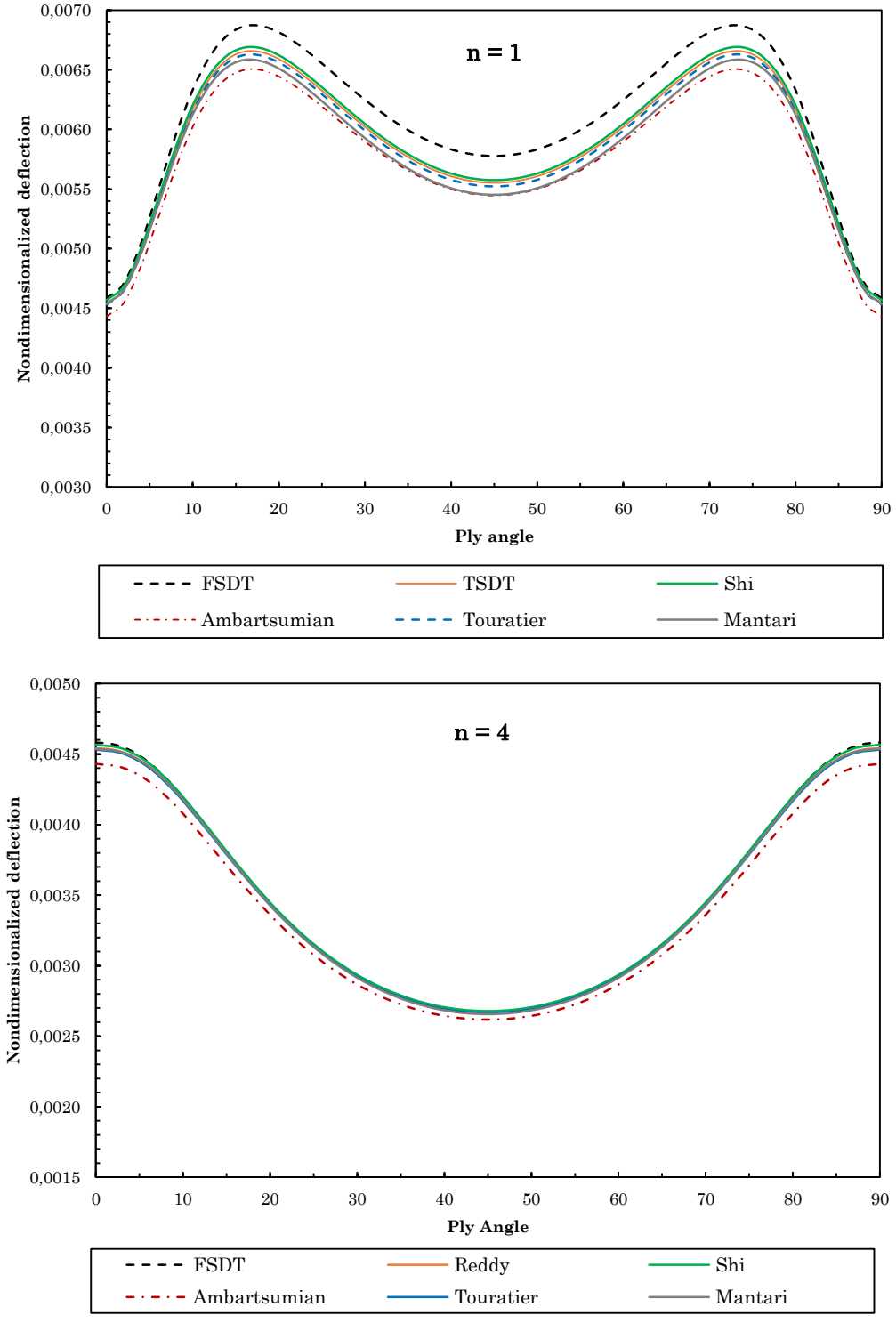

figure 55 - Maximum normalized transverse displacements for two simply supported laminated plates with antisymmetric angle-ply layers $(\theta/-\theta)_n$ subjected to a sinusoidal load (SSL). Displacements as a function of the ply angle computed with the RPIM, a/h=10.

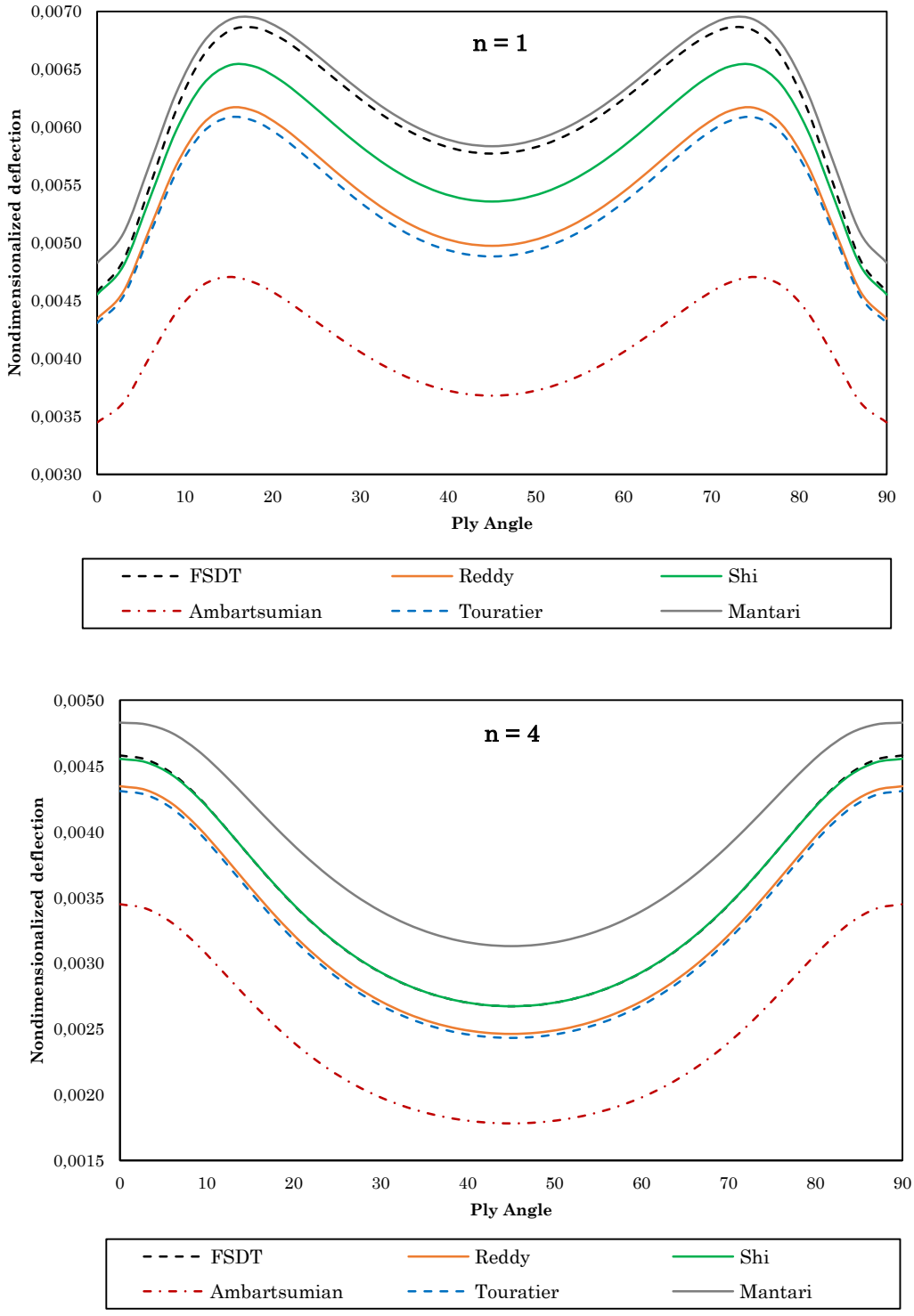

figure 56 - Maximum normalized transverse displacements for two simply supported laminated plates with antisymmetric angle-ply layers $(\theta/-\theta)_n$ subjected to a sinusoidal load (SSL). Displacements as a function of the ply angle computed with the NNRPIM V1, a/h=10.

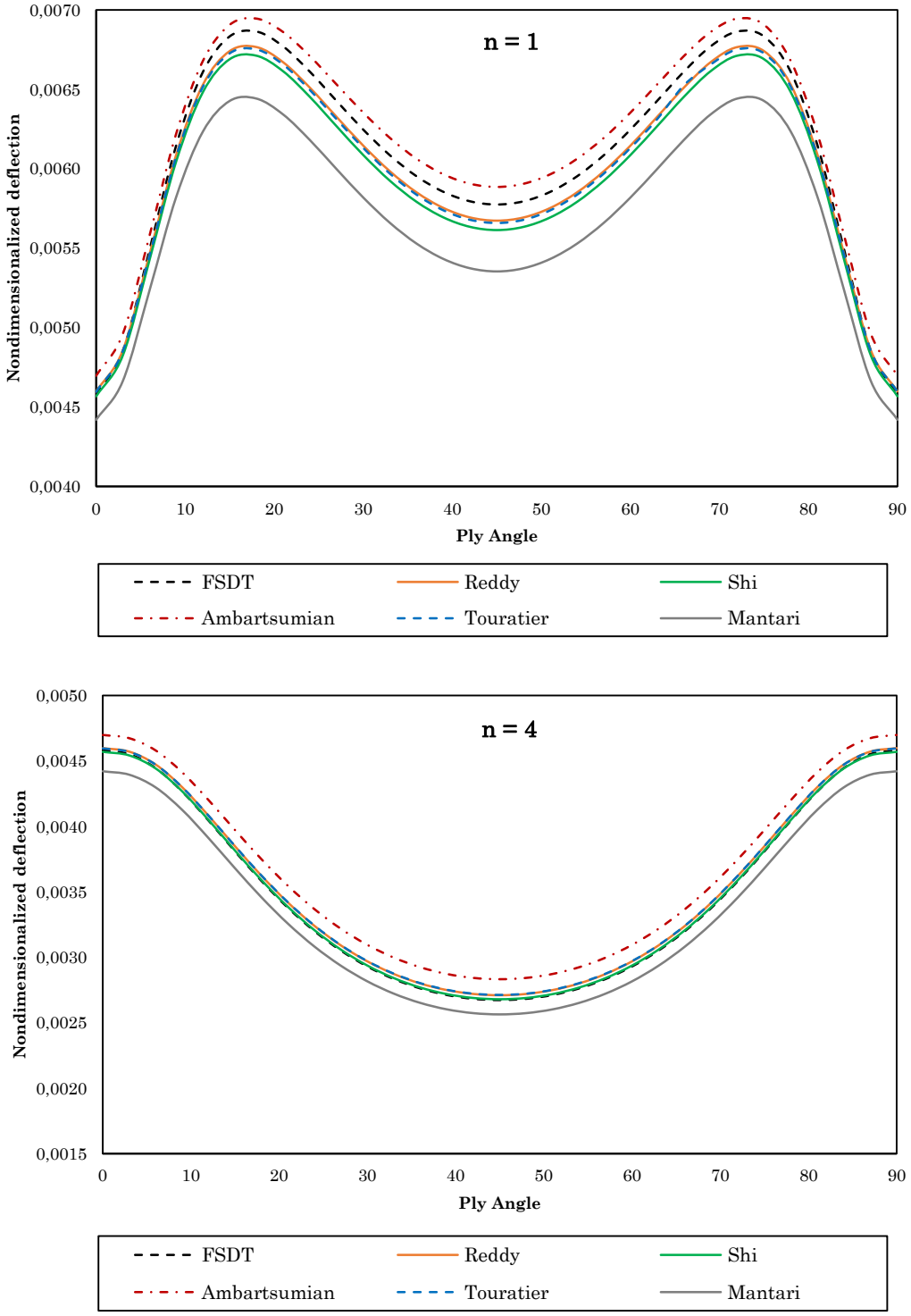

figure 57 - Maximum normalized transverse displacements for two simply supported laminated plates with antisymmetric angle-ply layers $(\theta/-\theta)_n$ subjected to a sinusoidal load (SSL). Displacements as a function of the ply angle computed with the NNRPIM V2, a/h=10.

5.3.6 Final Remarks

As seen for antisymmetric cross-ply laminates, Karama and Aydogdu's theories were not able to provide a similar solution with the analytical Reddy solution for the studied antisymmetric laminates with angle-ply layers.

For Reddy's TSDT, very low errors were achieved with the performed bending analysis, in particular for laminates with plies with 45^{o} orientations of its fibres and with six layers.

From the study of the relation between the ply angle and the transverse displacement, it was found that for a laminate with two layers, an orthotropic configuration of the plate minimizes the transverse displacement. On the other hand, for a laminate with eight layers, a configuration $(45/-45)_4$ minimizes the deflection.

Chapter 6

6 Conclusions

The main objective of this work was to combine, for the first time, the bending analysis of composite laminated plates using equivalent single layer theories that follows high-order shear deformation theories with two recently developed meshless methods. The purpose was successfully accomplished, in the author opinion, since this combination was achieved over the implementation of two algorithms that were properly validated through a wide range of numerical results obtained for distinct problems.

6.1 Conclusions and Remarks

The meshless methods used to perform bending analysis on symmetric and antisymmetric laminates revealed to be robust and accurate numerical tools, constituting as a strong alternative to the traditional FEM, whose use has become widespread in the field of engineering design.

The RPIM is a 'not truly' meshless method since it uses a background nodal independent integration mesh where the Gauss-Legendre quadrature is implemented. With the RPIM, almost all the solutions obtained shown a strong agreement with the analytical results. Linear asymptotic convergences were observed and the method proved to be stable.

The NNRPIM has a similar formulation to the RPIM regarding the interpolation functions. In fact, in the NNRPIM the main differences are intrinsically related to the concept of natural neighbours. Instead of selecting the nodes that belongs to the 'influence-domain' of a certain interest point based on routines that searches the nodes closer to that interest point or the nodes within a fixed shape of the 'influence-domain', the NNRPIM constructs Voronoï cells based on the locations of the nodes that are discretizing the problem domain. In these cells, integration points are collocated and a nodal dependent integration mesh is created. With the full Voronoï diagram, the 'influence-cells' are settled. The results obtained from the NNRPIM are considerably different if the 'influence-cell' is defined considering the first

(V1) or second-degree (V2) neighbours. Despite the lower computational time consumption, the NNRPIM V1 proved to be, at the same time, the less accurate tool, since the percentage errors obtained for certain problems were always higher than those obtained via the NNRPIM V2 or the RPIM. Additionally, the stress distribution curves represented for various laminates proved to be always more widespread in the case of the NNRPIM V1. As regards the NNRPIM V2, this was the numerical method that computed displacements and stresses with the lower errors. Nevertheless, it is more vulnerable than the RPIM to the shear locking phenomenon and consumes more computational time.

Concerning the numerical tools used in this work, it can be concluded that the NNRPIM using second-degree natural neighbours stands as the best meshless method studied. However, it is not applicable to thin plates, unless a reduced integration is implemented in the algorithm.

The mentioned meshless methods were the tool to analyse composite laminated plates using different High-Order Shear Deformation Theories that approximate the in-plane displacements across the plates thickness as nonlinear functions. The theories studied – three third-order shear deformation theories, two exponential theories, one trigonometric theory and one theory that is a combination of trigonometric and exponential functions – were implemented in the algorithms of the RPIM and the NNRPIM. Thus, a wide range of results were obtained. Ambartsumian's theory is the older HSDT studied, proposed in 1960 as an extension of the Classical Plate Theory and applied initially to anisotropic plates and shallow shells. The solutions obtained from the theory of Ambartsumian were far from remarkable in comparison to the 3D Elasticity but the merit of Ambartsumian must be recognized since it was his work and the work developed by Reddy that led the investigation about HSDT. On the other side, Mantari theory showed the best agreement with the 3D Elasticity, in particular in the sensitive aspect of the transverse shear stresses (where the purpose of using HSDT is found). Karama and Aydogdu theories were those that allowed to obtained better results, immediately after Mantari theory, despite they did not work with antisymmetric laminates.

As regards the work itself, and knowing the proposed initial objectives and the fulfilment of all of them (in particular the creation of the two algorithms, the variety of obtained results and the agreement of them with the literature), it is concluded the success of this research.

6.2 Future Work

To produce even more accurate results and continuous stress distributions across the laminates' thicknesses, it could be interesting to implement a layerwise theory in the algorithms of the RPIM and the NNRPIM and established a comparison study between the two models of plate analysis (layerwise and HSDT).

It could be also stimulating to continue this work with the extension of the algorithms to buckling, dynamic and acoustic analysis, and perform analysis not only in composite laminated plates but also in sandwich structures. A multiscale approach could also be performed based on this work.

References

[1] K. H. Huebner, D. L. Dewhirst, D. E. Smith, and T. G. Byrom, *The Finite Element Method for Engineers*, vol. 6: Elastic. Wiley, 2001.

[2] J. N. . R. M. Noronha, J.; Belinha, J., Dinis, L., "The Numerical Analysis of Airplane Windshields due to Bird Strike: A Static Study," *Fac. Eng. Univ. Porto*, 2016.

[3] J. M. Melenk, "On approximation in meshless methods," in *Frontiers of numerical analysis*, Springer, 2005, pp. 65–141.

[4] R. A. Gingold and J. J. Monaghan, "Smoothed particle hydrodynamics: theory and application to non-spherical stars," *Mon. Not. R. Astron. Soc.*, vol. 181, no. 3, pp. 375–389, 1977.

[5] T. Belytschko, Y. Y. Lu, and L. Gu, "Element-free Galerkin methods," *International Journal for Numerical Methods in Engineering*, vol. 37, no. April 1993. pp. 229–256, 1994.

[6] J. Belinha, L. M. J. S. Dinis, and R. M. N. Jorge, "The Natural Neighbour Radial Point Interpolation Method: Solid Mechanics and Mechanobiology Applications," *Fac. Eng. da Univ. do Porto*, 2010.

[7] L. M. J. S. Dinis, R. M. Natal Jorge, and J. Belinha, "Analysis of plates and laminates using the natural neighbour radial point interpolation method," *Eng. Anal. Bound. Elem.*, vol. 32, no. 3, pp. 267–279, Mar. 2008.

[8] S. Viana, D. Rodger, and H. Lai, "Overview of meshless methods," *ICS Newsl.*, vol. 14, no. 2, p. 4, 2007.

[9] J. Belinha, *Meshless Methods in Biomechanics: Bone Tissue Remodelling Analysis*. Springer International Publishing, 2014.

[10] S. N. Atluri and T. Zhu, "A new Meshless Local Petrov-Galerkin (MLPG) approach in computational mechanics," *Comput. Mech.*, vol. 22, no. 2, pp. 117–127, 1998.

[11] W. K. Liu, S. Jun, S. Li, J. Adee, and T. Belytschko, "Reproducing kernel particle methods for structural dynamics," *Int. J. Numer. Methods Eng.*, vol. 38, no. 10, pp. 1655–1679, 1995.

[12] E. Oñate, S. Idelsohn, O. C. Zienkiewicz, and R. L. Taylor, "A finite point method in computational mechanics. Applications to convective transport and fluid flow," *Int. J. Numer. Methods Eng.*, vol. 39, no. December 1995, pp. 3839–3866, 1996.

[13] E. J. Kansa, "Multiquadrics-A scattered data approximation scheme with applications to computational fluid-dynamics-I surface approximations and partial derivative estimates," *Comput. Math. with Appl.*, vol. 19, no. 8–9, pp. 127–145, 1990.

[14] E. J. Kansa, "Multiquadrics-A scattered data approximation scheme with applications to computational fluid-dynamics-II solutions to parabolic, hyperbolic and elliptic partial differential equations," *Comput. Math. with Appl.*, vol. 19, no. 8–9, pp. 147–161, 1990.

[15] G. R. Liu and Y. T. Gu, "A point interpolation method for two-dimensional solids," *Int. J. Numer. Methods Eng.*, vol. 50, no. 4, pp. 937–951, 2001.

[16] G. R. Liu, "A point assembly method for stress analysis for two-dimensional solids," *Int. J. Solids Struct.*, vol. 39, no. 1, pp. 261–276, 2001.

[17] J. G. Wang and G. R. Liu, "A point interpolation meshless method based on radial basis functions," *Int. J. Numer. Methods Eng.*, vol. 54, no. 11, pp. 1623–1648, 2002.

[18] L. M. J. S. Dinis, R. M. N. Jorge, and J. Belinha, "A 3D shell-like approach using a natural neighbour meshless method: Isotropic and orthotropic thin structures," *Compos. Struct.*, vol. 92, no. 5, pp. 1132–1142, 2010.

[19] J. Belinha, L. M. J. S. Dinis, and R. M. N. Jorge, "Composite laminated plate analysis using the natural radial element method," *Compos. Struct.*, vol. 103, pp. 50–67, 2013.

[20] L. M. J. S. Dinis, R. M. Natal Jorge, and J. Belinha, "The Radial Natural Neighbours Interpolators Extended to Elastoplasticity," in *Progress on Meshless Methods - Computational Methods in Applied Sciences*, A. J. M. Ferreira, E. J. Kansa, G. E. Fasshauer, and V. M. A. Leitão, Eds. Springer Netherlands, 2009, pp. 175–198.

[21] J. M. C. Azevedo, J. Belinha, L. M. J. S. Dinis, and R. M. Natal Jorge, "Crack path prediction using the natural neighbour radial point interpolation method," *Eng. Anal. Bound. Elem.*, vol. 59, pp. 144–158, 2015.

[22] N. J. Pagano and H. J. Hatfield, "Elastic Behavior of Multilayered Bidirectional Composites," *AIAA J.*, vol. 10, no. July, pp. 931–933, 1972.

[23] T. N. Nguyen, C. H. Thai, and H. Nguyen-Xuan, "On the general framework of high order shear deformation theories for laminated composite plate structures: A novel unified approach," *Int. J. Mech. Sci.*, vol. 110, pp. 242–255, 2016.

[24] a J. M. Ferreira, "Analysis of Composite Plates Using a Layerwise Theory and Multiquadrics Discretization," *Mech. Adv. Mater. Struct.*, vol. 12, no. 2, pp. 99–112, 2005.

[25] L. Iurlaro, M. Gherlone, M. Di Sciuva, and A. Tessler, "Refined Zigzag Theory for laminated composite and sandwich plates derived from Reissner's Mixed Variational Theorem," *Compos. Struct.*, vol. 133, pp. 809–817, 2015.

[26] J.N. Reddy, "Mechanics of laminated composite plates and shells: theory and analysis." p. 840, 2003.

[27] G. Shi, "A new simple third-order shear deformation theory of plates," *Int. J. Solids Struct.*, vol. 44, no. 13, pp. 4399–4417, 2007.

[28] S. A. Ambartsumian, "On the theory of bending of anisotropic plates and shallow shells," *J. Appl. Math. Mech.*, vol. 24, no. 2, pp. 500–514, Jan. 1960.

[29] M. Touratier, "An efficient standard plate theory," *Int. J. Eng. Sci.*, vol. 29, no. 8, pp. 901–916, 1991.

[30] M. Karama, K. S. Afaq, and S. Mistou, "A new theory for laminated composite plates," *Proc. Inst. Mech. Eng. Part L J. Mater. Des. Appl.*, vol. 223, no. 2, pp. 53–62, 2009.

[31] M. Aydogdu, "A new shear deformation theory for laminated composite

plates," *Compos. Struct. J.*, no. 89, pp. 94–101, 2008.
[32] K. P. Soldatos, "A transverse shear deformation theory for homogeneous monoclinic plates," *Acta Mech.*, 1992.
[33] J. L. Mantari, A. S. Oktem, and C. Guedes Soares, "A new higher order shear deformation theory for sandwich and composite laminated plates," *Compos. Part B Eng.*, vol. 43, no. 3, pp. 1489–1499, 2012.
[34] R. L. Hardy, "Theory and applications of the multiquadric-biharmonic method," *Comput. Math. Applic.*, vol. 19, no. 8/9, pp. 163–208, 1990.
[35] G. M. Kolvik, "Higher Order Shear Deformation Plate Theory," *Fac. Math. Nat. Sci. Univ. Oslo*, no. May, 2012.
[36] R. D. Mindlin, "Influence of Rotatory Inertia and Shear on Flexural Motions of Isotropic, Elastic Plates," *J. Appl. Mech.*, no. 18, pp. 31–38, 1951.
[37] N. Grover, B. N. Singh, and D. K. Maiti, "New Nonpolynomial Shear-Deformation Theories for Structural Behavior of Laminated-Composite and Sandwich Plates," *AIAA J.*, vol. 51, no. 8, pp. 1861–1871, 2013.
[38] H. Nguyen-Xuan, C. H. Thai, and T. Nguyen-Thoi, "Isogeometric finite element analysis of composite sandwich plates using a higher order shear deformation theory," *Compos. Part B Eng.*, vol. 55, pp. 558–574, 2013.
[39] E. Ventsel and T. Krauthammer, *Thin plates and shells*. 2001.
[40] J. N. Reddy and C. M. Wang, "An overview of the relationships between solutions of the classical and shear deformation plate theories," in *Composites Science and Technology*, 2000, vol. 60, no. 12–13, pp. 2327–2335.
[41] M. Levinson, "An accurate simple theory of the statics and dynamics of elastic plates," *Mech. Res. Commun*, no. 7, pp. 343–350, 1980.
[42] M. V. V. Murthy, "An improved transverse shear deformation theory for laminated anisotropic plates," *NASA Tech. Pap. 1903*, no. November, 1981.
[43] Z. Kaczkowski, *Plates. In Statical calculations*. 1968.
[44] V. Panc, *Theories of elastic plates*. 1975.
[45] E. Reissner, "On the theory of transverse bending of elastic plates," *Int. J. Solids Struct.*, vol. 12, no. 8, pp. 545–554, 1976.
[46] A. Idlbi, M. Karama, and M. Touratier, "Comparison of various laminated plate theories," *Compos. Struct.*, vol. 37, no. 2, pp. 173–184, 1997.
[47] M. S. Karama M, Afaq KS, "Mechanical behavior of laminated composite beam by the new multilayered laminated composite structures model with transverse shear stress continuity," *Int. J. Solids Struct.*, vol. 40, no. 6, 2003.
[48] J. N. Reddy, "A refined nonlinear theory of plates with transverse shear deformation," *Int. J. Solids Struct.*, vol. 20, no. 9–10, pp. 881–896, 1984.
[49] X. Wang and G. Shi, "A refined laminated plate theory accounting for the third-order shear deformation and interlaminar transverse stress continuity," *Appl. Math. Model.*, vol. 39, no. 18, pp. 5659–5680, 2015.
[50] C. G. . Mantari, J.L., Oktem, S.A., Soares, "Static and dynamic analysis of laminated composite and sandwich plates and shells by using a new

higher-order shear deformation theory," *Compos. Struct.*, no. 94, pp. 37–49, 2011.

Appendix

A. Solutions of Nondimensionalized Transverse Displacements and Stresses for Various Laminates

Orthotropic Plates and Symmetric Cross-Ply Laminates

table 11 - Maximum normalized transverse displacements and stresses for a simply supported orthotropic plate subjected to a sinusoidal load (SSL), a/h=4.

a/h	Solution	ESL	Load	$\bar{w}$	$\bar{\sigma}_{xx}$	$\bar{\sigma}_{yy}$	$\bar{\tau}_{xy}$	$\bar{\tau}_{yz}$	$\bar{\tau}_{xz}$
4	Exact	TSDT	SSL	-	-	-	-	-	-
		FSDT	SSL	-	-	-	-	-	-
		Elasticity	SSL	-	-	-	-	-	-
	FEM	TSDT	SSL	-	-	-	-	-	-
		FSDT	SSL	-	-	-	-	-	-
	RPIM	Aydogdu	SSL	1.5815	0.7276	0.0608	0.0410	0.0038	0.3872
		Karama	SSL	1.5815	0.7276	0.0608	0.0410	0	0.3872
		Mantari	SSL	1.5431	0.7619	0.0608	0.0406	0	0.4077
		Shi	SSL	1.6192	0.7043	0.0609	0.0413	0	0.3714
		Touratier	SSL	1.5982	0.7152	0.0608	0.0409	0	0.3790
		Ambartsumian	SSL	1.5686	0.6872	0.0603	0.0354	0	0.3645
		TSDT	SSL	1.6104	0.7015	0.0607	0.0408	0	0.3703
		FSDT5	SSL	1.6622	0.4541	0.0549	0.0347	0.0467	0.2567
	NNRPIM V1	Aydogdu	SSL	1.4688	0.7474	0.0609	0.0421	0	0.3843
		Karama	SSL	1.4688	0.7474	0.0609	0.0421	0	0.3843
		Mantari	SSL	1.5884	0.8567	0.0673	0.0430	0	0.4167
		Shi	SSL	1.6049	0.7640	0.0649	0.0430	0	0.3853
		Touratier	SSL	1.4973	0.7394	0.0614	0.0421	0	0.3787
		Ambartsumian	SSL	1.1163	0.5536	0.0458	0.0343	0	0.2907
		TSDT	SSL	1.5214	0.7297	0.0618	0.0421	0	0.3725
		FSDT	SSL	1.6621	0.4777	0.0578	0.0356	0.0492	0.2690
	NNRPIM V2	Aydogdu	SSL	1.6598	0.7471	0.0655	0.0266	0	0.3845
		Karama	SSL	1.6598	0.7471	0.0655	0.0266	0	0.3845
		Mantari	SSL	1.5081	0.7758	0.0622	0.0454	0	0.4209
		Shi	SSL	1.6222	0.7330	0.0637	0.0429	0	0.3899
		Touratier	SSL	1.6237	0.7524	0.0643	0.0403	0	0.3990
		Ambartsumian	SSL	1.6598	0.7471	0.0655	0.0266	0	0.3845
		TSDT	SSL	1.6330	0.7371	0.0642	0.0404	0	0.3895
		FSDT	SSL	1.6620	0.4782	0.0579	0.0372	0.0500	0.2751

table 12 - Maximum normalized transverse displacements and stresses for a simply supported orthotropic plate subjected to a sinusoidal load (SSL), a/h=10.

a/h	Solution	ESL	Load	$\bar{w}$	$\bar{\sigma}_{xx}$	$\bar{\sigma}_{yy}$	$\bar{\tau}_{xy}$	$\bar{\tau}_{yz}$	$\bar{\tau}_{xz}$
	Exact	TSDT	SSL	-	-	-	-	-	-
		FSDT	SSL	0.6383	0.5248	0.0338	0.0246	0.0367	0.3452
								0.0459[1]	0.4315
		Elasticity	SSL	-	-	-	-	-	-
	FEM	TSDT	SSL	-	-	-	-	-	-
		FSDT	SSL	-	-	-	-	-	-
	RPIM	Aydogdu	SSL	0.6309	0.5458	0.0330	0.0248	0.0025	0.4319
		Karama	SSL	0.6309	0.5458	0.0330	0.0248	0	0.4319
		Mantari	SSL	0.6354	0.5576	0.0333	0.0249	0	0.4659
		Shi	SSL	0.6372	0.5427	0.0331	0.0250	0	0.4086
		Touratier	SSL	0.6326	0.5434	0.0330	0.0248	0	0.4197
		Ambartsumian	SSL	0.6183	0.5322	0.0328	0.0230	0	0.4025
		TSDT	SSL	0.6337	0.5409	0.0330	0.0248	0	0.4074
		FSDT	SSL	0.6386	0.4981	0.0321	0.0239	0.0292	0.2742
10	NNRPIM V1	Aydogdu	SSL	0.5957	0.5624	0.0338	0.0252	0	0.4374
		Karama	SSL	0.5957	0.5624	0.0338	0.0252	0	0.4374
		Mantari	SSL	0.6801	0.6287	0.0373	0.0268	0	0.4929
		Shi	SSL	0.6355	0.5810	0.0352	0.0258	0	0.4268
		Touratier	SSL	0.6012	0.5622	0.0339	0.0252	0	0.4270
		Ambartsumian	SSL	0.4823	0.4724	0.0285	0.0219	0	0.3521
		TSDT	SSL	0.6059	0.5617	0.0340	0.0252	00	0.4164
		FSDT	SSL	0.6382	0.5239	0.0338	0.0243	0.0309	0.2875
	NNRPIM V2	Aydogdu	SSL	0.6409	0.5765	0.0349	0.0250	0	0.4529
		Karama	SSL	0.6409	0.5765	0.0349	0.0250	0	0.4529
		Mantari	SSL	0.6185	0.5718	0.0342	0.0274	0	0.4760
		Shi	SSL	0.6373	0.5679	0.0346	0.0259	0	0.4294
		Touratier	SSL	0.6416	0.5736	0.0349	0.0251	0	0.4401
		Ambartsumian	SSL	0.6561	0.5787	0.0355	0.0195	0	0.4208
		TSDT	SSL	0.6416	0.5705	0.0348	0.0251	0	0.4274
		FSDT	SSL	0.6385	0.5246	0.0338	0.0255	0.0308	0.2933

[1] From equilibrium equations.

table 13 - Maximum normalized transverse displacements and stresses for a simply supported orthotropic plate subjected to a sinusoidal load (SSL), a/h=20

a/h	Solution	ESL	Load	$\bar{w}$	$\bar{\sigma}_{xx}$	$\bar{\sigma}_{yy}$	$\bar{\tau}_{xy}$	$\bar{\tau}_{yz}$	$\bar{\tau}_{xz}$
20	Exact	TSDT	SSL	-	-	-	-	-	-
		FSDT	SSL	0.4836	0.5350	0.0286	0.0222	0.0319	0.3501
		Elasticity	SSL	-	-	-	-	-	-
	FEM	TSDT	SSL	-	-	-	-	-	-
		FSDT	SSL	-	-	-	-	-	-
	RPIM	Aydogdu	SSL	0.4366	0.5118	0.0256	0.0206	0.0021	0.4434
		Karama	SSL	0.4799	0.5193	0.0273	0.0216	0	0.4409
		Mantari	SSL	0.4871	0.5266	0.0277	0.0218	0	0.4772
		Shi	SSL	0.4836	0.5200	0.0274	0.0218	0	0.4162
		Touratier	SSL	0.4805	0.5188	0.0273	0.0216	0	0.4280
		Ambartsumian	SSL	0.4695	0.5105	0.0272	0.0204	00	0.4102
		TSDT	SSL	0.4810	0.5183	0.0273	0.0216	0	0.4150
		FSDT	SSL	0.4838	0.5078	0.0271	0.0215	0.0253	0.2781
	NNRPIM V1	Aydogdu	SSL	0.4542	0.5348	0.0281	0.0216	0	0.4497
		Karama	SSL	0.4542	0.5348	0.0281	0.0216	0	0.4497
		Mantari	SSL	0.5229	0.5902	0.0309	0.0235	0	0.5028
		Shi	SSL	0.4822	0.5541	0.0292	0.0223	0	0.4353
		Touratier	SSL	0.4574	0.5362	0.0282	0.0217	0	0.4385
		Ambartsumian	SSL	0.3722	0.4613	0.0242	0.0188	0	0.3619
		TSDT	SSL	0.4605	0.5373	0.0283	0.0217	0	0.4271
		FSDT	SSL	0.4829	0.5333	0.0285	0.0217	0.0270	0.2915
	NNRPIM V2	Aydogdu	SSL	0.4873	0.5490	0.0289	0.0217	0	0.4580
		Karama	SSL	0.4873	0.5490	0.0289	0.0217	0	0.4580
		Mantari	SSL	0.4738	0.5410	0.0284	0.0239	0	0.4777
		Shi	SSL	0.4836	0.5447	0.0287	0.0225	0	0.4365
		Touratier	SSL	0.4872	0.5480	0.0289	0.0218	0	0.4454
		Ambartsumian	SSL	0.4983	0.5549	0.0294	0.0178	0	0.4149
		TSDT	SSL	0.4868	0.5471	0.0289	0.0219	0	0.4327
		FSDT	SSL	0.4837	0.5348	0.0286	0.0227	0.0257	0.2948

table 14 - Maximum normalized transverse displacements and stresses for a simply supported orthotropic plate subjected to a sinusoidal load (SSL), a/h=100.

a/h	Solution	ESL	Load	$\bar{w}$	$\bar{\sigma}_{xx}$	$\bar{\sigma}_{yy}$	$\bar{\tau}_{xy}$	$\bar{\tau}_{yz}$	$\bar{\tau}_{xz}$
100	Exact	TSDT	SSL	-	-	-	-	-	-
		FSDT	SSL	0.4333	0.5385	0.0267	0.0213	0.0302	0.3518
		CLPT	SSL	0.4312	0.5487	0.0267	0.0213	0.03077	0.4398
		Elasticity	SSL	-	-	-	-	-	-
	FEM	TSDT	SSL	-	-	-	-	-	-
		FSDT	SSL	-	-	-	-	-	-
	RPIM	Aydogdu	SSL	0.4302	0.5106	0.0254	0.0205	0.0021	0.4443
		Karama	SSL	0.4204	0.5032	0.0253	0.0195	0	0.4073
		Mantari	SSL	0.4378	0.5159	0.0258	0.0206	0	0.4739
		Shi	SSL	0.4332	0.5124	0.0255	0.0206	0	0.4177
		Touratier	SSL	0.4305	0.5107	0.0254	0.0205	0	0.4311
		Ambartsumian	SSL	0.4204	0.5032	0.0253	0.0195	0	0.4073
		TSDT	SSL	0.4309	0.5109	0.0254	0.0205	0	0.4178
		FSDT	SSL	0.4332	0.5108	0.0254	0.0206	0.0238	0.2787
	NNRPIM V1	Aydogdu	SSL	0.3989	0.5146	0.0255	0.0199	0	0.4488
		Karama	SSL	0.3989	0.5146	0.0255	0.0199	0	0.4488
		Mantari	SSL	0.4288	0.5255	0.0260	0.0207	0	0.4829
		Shi	SSL	0.4150	0.5237	0.0259	0.0204	0	0.4294
		Touratier	SSL	0.4009	0.5156	0.0255	0.0200	0	0.4370
		Ambartsumian	SSL	0.3355	0.4579	0.0226	0.0176	0	0.3260
		TSDT	SSL	0.4027	0.5164	0.0256	0.0200	0	0.4249
		FSDT	SSL	0.4153	0.5151	0.0255	0.0201	0.0224	0.2866
	NNRPIM V2	Aydogdu	SSL	0.4366	0.5396	0.0268	0.0205	0	0.3446
		Karama	SSL	0.4366	0.5396	0.0268	0.0205	0	0.3446
		Mantari	SSL	0.4248	0.5294	0.0264	0.0229	0	0.3203
		Shi	SSL	0.4327	0.5365	0.0267	0.0214	0	0.3281
		Touratier	SSL	0.4362	0.5394	0.0268	0.0206	0	0.3369
		Ambartsumian	SSL	0.4465	0.5471	0.0274	0.0181	0	0.1912
		TSDT	SSL	0.4358	0.5391	0.0268	0.0207	0	0.3283
		FSDT	SSL	0.4327	0.5374	0.0267	0.0220	0.0069	0.2189

table 15 - Maximum normalized transverse displacements and stresses for a simply supported orthotropic plate subjected to a uniformly distributed load (UDL), a/h=4.

a/h	Solution	ESL	Load	$\bar{w}$	$\bar{\sigma}_{xx}$	$\bar{\sigma}_{yy}$	$\bar{\tau}_{xy}$	$\bar{\tau}_{yz}$	$\bar{\tau}_{xz}$
4	Exact	TSDT	UDL	-	-	-	-	-	-
		FSDT	UDL	-	-	-	-	-	-
		Elasticity	UDL	-	-	-	-	-	-
	FEM	TSDT	UDL	-	-	-	-	-	-
		FSDT	UDL	-	-	-	-	-	-
	RPIM	Aydogdu	UDL	2.3335	1.0288	0.0712	0.0849	0.0109	0.6347
		Karama	UDL	2.3335	1.0288	0.0712	0.0849	0	0.6347
		Mantari	UDL	2.2813	1.0802	0.0705	0.0831	0	0.6599
		Shi	UDL	2.3861	0.9947	0.0720	0.0859	0	0.6142
		Touratier	UDL	2.3562	1.0104	0.0716	0.0848	0	0.6240
		Ambartsumian	UDL	2.3006	0.9664	0.0716	0.0715	0	0.6013
		TSDT	UDL	2.3722	0.9906	0.0718	0.0846	0	0.6125
		FSDT	UDL	2.4375	0.6761	0.0700	0.0677	0.1362	0.4379
	NNRPIM V1	Aydogdu	UDL	2.1711	1.0561	0.0691	0.0972	0	0.6317
		Karama	UDL	2.1711	1.0561	0.0691	0.0972	0	0.6317
		Mantari	UDL	2.3767	1.2157	0.0785	0.0870	0	0.6620
		Shi	UDL	2.3674	1.0672	0.0747	0.0999	0	0.6401
		Touratier	UDL	2.2107	1.0419	0.0701	0.0978	0	0.6261
		Ambartsumian	UDL	1.6732	0.8144	0.0553	0.0727	0	0.4827
		TSDT	UDL	2.2438	1.0257	0.0708	0.0981	0	0.6196
		FSDT	UDL	2.4364	0.7027	0.0726	0.0739	0.1565	0.4890
	NNRPIM V2	Aydogdu	UDL	2.3782	1.0529	0.0747	0.0885	0	0.6779
		Karama	UDL	2.3782	1.0529	0.0747	0.0885	0	0.6779
		Mantari	UDL	2.2304	1.0740	0.0709	0.1002	0	0.6925
		Shi	UDL	2.3916	1.0090	0.0744	0.0982	0	0.6578
		Touratier	UDL	2.3963	1.0334	0.0749	0.0894	0	0.6673
		Ambartsumian	UDL	2.4474	1.0204	0.0777	0.0495	0	0.6415
		TSDT	UDL	2.4079	1.0129	0.0750	0.0901	0	0.6560
		FSDT	UDL	2.4393	0.7044	0.0727	0.0763	0.1578	0.4987

table 16 - Maximum normalized transverse displacements and stresses for a simply supported orthotropic plate subjected to a uniformly distributed load (UDL), a/h=10.

a/h	Solution	ESL	Load	$\bar{w}$	$\bar{\sigma}_{xx}$	$\bar{\sigma}_{yy}$	$\bar{\tau}_{xy}$	$\bar{\tau}_{yz}$	$\bar{\tau}_{xz}$
	Exact	TSDT	UDL	-	-	-	-	-	-
		FSDT	UDL	0.9519	0.7706	0.0352	0.0539	0.1529	0.6147
								0.1911[2]	0.7684
		Elasticity	UDL	-	-	-	-	-	-
	FEM	TSDT	UDL	-	-	-	-	-	-
		FSDT	UDL	-	-	-	-	-	-
	RPIM	Aydogdu	UDL	0.9410	0.7992	0.0343	0.0515	0.0093	0.7222
		Karama	UDL	0.9410	0.7992	0.0343	0.0515	0	0.7222
		Mantari	UDL	0.9482	0.8147	0.0347	0.0516	0	0.7750
		Shi	UDL	0.9504	0.7957	0.0345	0.0518	0	0.6850
		Touratier	UDL	0.9435	0.7962	0.0344	0.0514	0	0.7029
		Ambartsumian	UDL	0.9201	0.7794	0.0344	0.0474	0	0.6745
		TSDT	UDL	0.9451	0.7931	0.0344	0.0514	0	0.6832
		FSDT	UDL	0.9522	0.7398	0.0343	0.0486	0.1092	0.4626
10	NNRPIM V1	Aydogdu	UDL	0.8878	0.8218	0.0335	0.0577	0	0.7489
		Karama	UDL	0.8878	0.8218	0.0335	0.0577	0	0.7489
		Mantari	UDL	1.0216	0.9076	0.0397	0.0575	0	0.8226
		Shi	UDL	0.9479	0.8442	0.0358	0.0591	0	0.7378
		Touratier	UDL	0.8958	0.8212	0.0338	0.0579	0	0.7339
		Ambartsumian	UDL	0.7218	0.7078	0.0285	0.0478	0	0.6038
		TSDT	UDL	0.9028	0.8202	0.0340	0.0580	0	0.7183
		FSDT	UDL	0.9514	0.7688	0.0353	0.0535	0.1296	0.5138
	NNRPIM V2	Aydogdu	UDL	0.9573	0.8300	0.0358	0.0558	0	0.7835
		Karama	UDL	0.9573	0.8300	0.0358	0.0558	0	0.7835
		Mantari	UDL	0.9229	0.8256	0.0342	0.0609	0	0.8177
		Shi	UDL	0.9513	0.8205	0.0353	0.0585	0	0.7484
		Touratier	UDL	0.9581	0.8266	0.0358	0.0561	0	0.7642
		Ambartsumian	UDL	0.9807	0.8299	0.0376	0.0411	0	0.7302
		TSDT	UDL	0.9580	0.8231	0.0357	0.0563	0	0.7447
		FSDT	UDL	0.9527	0.7712	0.0352	0.0552	0.1288	0.5235

[2] From equilibrium equations.

table 17 - Maximum normalized transverse displacements and stresses for a simply supported orthotropic plate subjected to a uniformly distributed load (UDL), a/h=20.

a/h	Solution	ESL	Load	$\bar{w}$	$\bar{\sigma}_{xx}$	$\bar{\sigma}_{yy}$	$\bar{\tau}_{xy}$	$\bar{\tau}_{yz}$	$\bar{\tau}_{xz}$
20	Exact	TSDT	UDL	-	-	-	-	-	-
		FSDT	UDL	0.7262	0.7828	0.0272	0.0487	0.1466	0.6194
		Elasticity	UDL	-	-	-	-	-	-
	FEM	TSDT	UDL	-	-	-	-	-	-
		FSDT	UDL	-	-	-	-	-	-
	RPIM	Aydogdu	UDL	0.7204	0.7660	0.0267	0.0445	0.0090	0.7386
		Karama	UDL	0.7204	0.7660	0.0267	0.0445	0	0.7386
		Mantari	UDL	0.7315	0.7757	0.0272	0.0448	0	0.7981
		Shi	UDL	0.7261	0.7672	0.0268	0.0448	0	0.6976
		Touratier	UDL	0.7213	0.7654	0.0267	0.0445	0	0.7172
		Ambartsumian	UDL	0.7036	0.7528	0.0267	0.0420	0	0.6874
		TSDT	UDL	0.7220	0.7648	0.0267	0.0446	0	0.6958
		FSDT	UDL	0.7263	0.7516	0.0267	0.0440	0.1038	0.4667
	NNRPIM V1	Aydogdu	UDL	0.6808	0.7876	0.0259	0.0484	0	0.7862
		Karama	UDL	0.6808	0.7876	0.0259	0.0484	0	0.7862
		Mantari	UDL	0.7903	0.8599	0.0315	0.0504	0	0.8664
		Shi	UDL	0.7241	0.8114	0.0277	0.0498	0	0.7646
		Touratier	UDL	0.6858	0.7891	0.0261	0.0486	0	0.7680
		Ambartsumian	UDL	0.5589	0.6940	0.0219	0.0410	0	0.6365
		TSDT	UDL	0.6904	0.7903	0.0262	0.0487	0	0.7494
		FSDT	UDL	0.7250	0.7800	0.0274	0.0478	0.1258	0.5183
	NNRPIM V2	Aydogdu	UDL	0.7326	0.7978	0.0277	0.0478	0	0.8105
		Karama	UDL	0.7326	0.7978	0.0277	0.0478	0	0.8105
		Mantari	UDL	0.7112	0.7891	0.0265	0.0522	0	0.8414
		Shi	UDL	0.7266	0.7935	0.0273	0.0496	0	0.7715
		Touratier	UDL	0.7323	0.7968	0.0277	0.0480	0	0.7891
		Ambartsumian	UDL	0.7503	0.8030	0.0294	0.0383	0	0.7402
		TSDT	UDL	0.7318	0.7959	0.0276	0.0482	0	0.7676
		FSDT	UDL	0.7267	0.7835	0.0272	0.0495	0.1208	0.5251

table 18 - Maximum normalized transverse displacements and stresses for a simply supported orthotropic plate subjected to a uniformly distributed load (UDL), a/h=100.

a/h	Solution	ESL	Load	$\bar{w}$	$\bar{\sigma}_{xx}$	$\bar{\sigma}_{yy}$	$\bar{\tau}_{xy}$	$\bar{\tau}_{yz}$	$\bar{\tau}_{xz}$
100	Exact	TSDT	UDL	-	-	-	-	-	-
		FSDT	UDL	0.6528	0.7865	0.0245	0.0464	0.1449	0.6206
		CLPT	UDL	0.6497	0.7866	0.0244	0.0463	0.1811	0.7758
		Elasticity	UDL	-	-	-	-	-	-
	FEM	TSDT	UDL	-	-	-	-	-	-
		FSDT	UDL	-	-	-	-	-	-
	RPIM	Aydogdu	UDL	0.6478	0.7546	0.0242	0.0418	0.0087	0.7440
		Karama	UDL	0.6478	0.7546	0.0242	0.0418	0	0.7440
		Mantari	UDL	0.6594	0.7618	0.0248	0.0420	0	0.7967
		Shi	UDL	0.6524	0.7572	0.0243	0.0421	0	0.6994
		Touratier	UDL	0.6484	0.7548	0.0242	0.0419	0	0.7218
		Ambartsumian	UDL	0.6324	0.7434	0.0242	0.0398	0	0.6877
		TSDT	UDL	0.6489	0.7550	0.0242	0.0419	0	0.6995
		FSDT	UDL	0.6525	0.7547	0.0242	0.0421	0.1008	0.4665
	NNRPIM V1	Aydogdu	UDL	0.6023	0.7622	0.0237	0.0430	0	0.8337
		Karama	UDL	0.6023	0.7622	0.0237	0.0430	0	0.8337
		Mantari	UDL	0.6575	0.7774	0.0286	0.0422	0	0.8979
		Shi	UDL	0.6295	0.7735	0.0255	0.0433	0	0.7916
		Touratier	UDL	0.6055	0.7632	0.0239	0.0431	0	0.8107
		Ambartsumian	UDL	0.5047	0.6893	0.0195	0.0381	0	0.6515
		TSDT	UDL	0.6085	0.7641	0.0241	0.0431	0	0.7873
		FSDT	UDL	0.6299	0.7573	0.0253	0.0427	0.1001	0.5287
	NNRPIM V2	Aydogdu	UDL	0.6586	0.7864	0.0251	0.0442	0	0.7261
		Karama	UDL	0.6586	0.7864	0.0251	0.0442	0	0.7261
		Mantari	UDL	0.6399	0.7749	0.0241	0.0491	0	0.7019
		Shi	UDL	0.6523	0.7834	0.0246	0.0463	0	0.6768
		Touratier	UDL	0.6580	0.7862	0.0250	0.0445	0	0.7062
		Ambartsumian	UDL	0.6747	0.7937	0.0266	0.0388	0	0.5448
		TSDT	UDL	0.6573	0.7860	0.0250	0.0447	0	0.6854
		FSDT	UDL	0.6524	0.7861	0.0246	0.0474	0.0692	0.4518

table 19 - Maximum normalized transverse displacements and stresses and relative errors in relation to the respective exact solution for a simply supported symmetric square laminate with cross-ply layers (0/90/0) subjected to a sinusoidal load (SSL), a/h=4.

										Absolute elative |ε| (%) regarding the respective exact solution					
a/h	**Solution**	**ESL**	**Load**	$\bar{w}$	$\bar{\sigma}_{xx}$	$\bar{\sigma}_{yy}$	$\bar{\tau}_{xy}$	$\bar{\tau}_{yz}$	$\bar{\tau}_{xz}$	$\bar{w}$	$\bar{\sigma}_{xx}$	$\bar{\sigma}_{yy}$	$\bar{\tau}_{xy}$	$\bar{\tau}_{yz}$	$\bar{\tau}_{xz}$
	Exact	Aydogdu [1]	SSL	1.9856	0.7810	0.5090	0.0524	0.1970	0.2260	-	-	-	-	-	-
		Karama [2]	SSL	1.9440	0.7750	0.5020	0.0516	0.1910	0.2200	-	-	-	-	-	-
		Mantari [2]	SSL	1.9434	0.8230	0.4970	0.0536	0.2010	0.2450	-	-	-	-	-	-
		Shi [3]	SSL	1.9227	0.7337	0.5021	0.0498	0.2085	0.2856	-	-	-	-	-	-
		Touratier	SSL	-	-	-	-	-	-	-	-	-	-	-	-
		Ambartsumian	SSL	-	-	-	-	-	-	-	-	-	-	-	-
		TSDT	SSL	1.9218	0.7345	-	-	0.1832	-	-	-	-	-	-	-
		FSDT	SSL	1.7758	0.437	-	-	0.1561	-	-	-	-	-	-	-
		Elasticity	SSL	2.0060	0.7550	0.5560	0.0505	0.2172	0.2820	-	-	-	-	-	-
	FEM	TSDT	SSL	-	-	-	-	-	-	-	-	-	-	-	-
		FSDT	SSL	-	-	-	-	-	-	-	-	-	-	-	-
	RPIM	Aydogdu	SSL	1.9269	0.7374	0.4734	0.0489	0.1809	0.2089	3.0	5.6	7.0	6.7	8.2	7.6
		Karama	SSL	1.9269	0.7374	0.4734	0.0489	0.1809	0.2089	0.9	4.9	5.7	5.2	5.3	5.1
		Mantari	SSL	1.9519	0.7915	0.4671	0.0500	0.1874	0.2330	0.4	3.8	6.0	6.6	6.8	4.9
		Shi	SSL	1.9206	0.7019	0.4750	0.0481	0.1738	0.1926	0.1	4.3	5.4	3.5	16.6	32.5
		Touratier	SSL	1.9204	0.7184	0.4742	0.0482	0.1772	0.2003	-	-	-	-	-	-
		Ambartsumian	SSL	1.8537	0.6823	0.4686	0.0406	0.1666	0.1881	-	-	-	-	-	-
4		TSDT	SSL	1.9097	0.6988	0.4742	0.0474	0.1733	0.1920	0.6	4.9	-	-	5.4	-
		FSDT	SSL	1.7764	0.4148	0.4532	0.0358	0.1238	0.4581	0.0	5.1	-	-	20.7	-
	NNRPIM V1	Aydogdu	SSL	1.7836	0.7574	0.4548	0.0504	0.1843	0.2067	10.2	3.0	10.6	3.9	6.4	8.5
		Karama	SSL	1.7836	0.7574	0.4548	0.0504	0.1843	0.2067	8.3	2.3	9.4	2.4	3.5	6.0
		Mantari	SSL	2.0013	0.8986	0.4679	0.0531	0.1814	0.2378	2.98	9.19	5.86	0.87	9.75	2.95
		Shi	SSL	1.9059	0.7667	0.4850	0.0503	0.1793	0.2003	0.88	4.50	3.41	-1.09	14.00	29.88
		Touratier	SSL	1.7948	0.7436	0.4605	0.0498	0.1816	0.1998	-	-	-	-	-	-
		Ambartsumian	SSL	1.2846	0.5328	0.3508	0.0390	0.1463	0.1463	-	-	-	-	-	-
		TSDT	SSL	1.8012	0.7283	0.4652	0.0491	0.1784	0.1929	6.3	0.8	-	-	2.6	-
		FSDT	SSL	1.7763	0.4364	0.4768	0.0367	0.1302	0.1201	0	0.2	-	-	16.6	-
	NNRPIM V2	Aydogdu	SSL	1.9610	0.7752	0.5082	0.0482	0.1908	0.2199	1.2	0.7	0.1	7.9	3.2	2.7
		Karama	SSL	1.9610	0.7752	0.5082	0.0482	0.1908	0.2199	0.9	0.0	1.2	6.5	0.1	0.0
		Mantari	SSL	1.9049	0.8013	0.4942	0.0564	0.1951	0.2401	1.98	2.63	0.56	5.15	2.95	1.99
		Shi	SSL	1.9230	0.7285	0.5048	0.0501	0.1827	0.2021	0.02	0.70	0.54	0.52	12.38	29.25
		Touratier	SSL	1.9505	0.7544	0.5081	0.0478	0.1868	0.2107	-	-	-	-	-	-
		Ambartsumian	SSL	1.9630	0.7429	0.5104	0.0301	0.1734	0.1986	-	-	-	-	-	-
		TSDT	SSL	1.9360	0.7330	0.5071	0.0473	0.1826	0.2018	0.7	0.2	-	-	0.3	-
		FSDT	SSL	1.7762	0.4368	0.4773	0.0383	0.1326	0.1228	0	0	-	-	15.1	

table 20 - Maximum normalized transverse displacements and stresses and relative errors in relation to the respective exact solution for a simply supported symmetric square laminate with cross-ply layers (0/90/0) subjected to a sinusoidal load (SSL), a/h=10.

										Absolute elative |ε| (%) regarding the respective exact solution					
a/h	Solution	ESL	Load	$\bar{w}$	$\bar{\sigma}_{xx}$	$\bar{\sigma}_{yy}$	$\bar{\tau}_{xy}$	$\bar{\tau}_{yz}$	$\bar{\tau}_{xz}$	$\bar{w}$	$\bar{\sigma}_{xx}$	$\bar{\sigma}_{yy}$	$\bar{\tau}_{xy}$	$\bar{\tau}_{yz}$	$\bar{\tau}_{xz}$
10	Exact	Aydogdu [1]	SSL	0.7336	0.5780	0.2750	0.0284	0.1110	0.2820	-	-	-	-	-	-
		Karama [2]	SSL	0.7230	0.5760	0.2720	0.0281	0.1080	0.2720	-	-	-	-	-	-
		Mantari [2]	SSL	0.7342	0.5880	0.2760	0.0288	0.1150	0.3140	-	-	-	-	-	-
		Shi [3]	SSL	0.7133	0.5681	0.2687	0.0277	0.1167	0.3693	-	-	-	-	-	-
		Touratier	SSL	-	-	-	-	-	-	-	-	-	-	-	-
		Ambartsumian	SSL	-	-	-	-	-	-	-	-	-	-	-	-
		TSDT	SSL	0.7125	0.5684	-	-	0.1033	-	-	-	-	-	-	-
		FSDT	SSL	0.6693	0.5134	0.2536	0.0252	0.0914	-	-	-	-	-	-	-
		Elasticity	SSL	-	0.5900	0.2880	0.0289	0.1228	0.3570	-	-	-	-	-	-
	FEM	TSDT	SSL							-	-	-	-	-	-
		FSDT	SSL	0.6692	0.5098	0.2518	0.025	0.0908	0.4060	-	-	-	-	-	-
	RPIM	Aydogdu	SSL	0.7180	0.5474	0.2570	0.0270	0.1026	0.2588	2.1	5.3	6.5	5.0	7.6	8.2
		Karama	SSL	0.7180	0.5474	0.2570	0.0270	0.1026	0.2588	0.7	5.0	5.5	3.9	5.0	4.8
		Mantari	SSL	0.7409	0.5643	0.2612	0.0276	0.1077	0.3002	7.91	8.75	2.32	3.79	5.81	1.42
		Shi	SSL	0.7126	0.5414	0.2545	0.0268	0.0982	0.2331	0.33	2.25	2.39	0.44	12.56	33.99
		Touratier	SSL	0.7136	0.5434	0.2556	0.0268	0.1003	0.2452	-	-	-	-	-	-
		Ambartsumian	SSL	0.6904	0.5299	0.2524	0.0247	0.0941	0.2292	-	-	-	-	-	-
		TSDT	SSL	0.7087	0.5395	0.2541	0.0266	0.0979	0.2324	0.5	5.1	-	-	5.2	-
		FSDT	SSL	0.6696	0.4873	0.2407	0.0244	0.0726	0.1299	0	5.1	5.1	3.1	20.6	-
	NNRPIM V1	Aydogdu	SSL	0.6775	0.5644	0.2552	0.0274	0.1078	0.2618	7.7	2.3	7.2	3.5	2.9	7.1
		Karama	SSL	0.6775	0.5644	0.2552	0.0274	0.1078	0.2618	6.3	2.0	6.2	2.4	0.2	3.7
		Mantari	SSL	0.7923	0.6394	0.2696	0.0299	0.1083	0.3185	7.9	8.7	21.1	3.8	5.8	1.4
		Shi	SSL	0.7110	0.5809	0.2623	0.0278	0.1020	0.2438	0.3	2.3	2.4	0.4	12.6	34.0
		Touratier	SSL	0.6777	0.5627	0.2554	0.0273	0.1056	0.2493	-	-	-	-	-	-
		Ambartsumian	SSL	0.5349	0.4665	0.2193	0.0233	0.0929	0.1994	-	-	-	-	-	-
		TSDT	SSL	0.6773	0.5607	0.2554	0.0271	0.1033	0.2374	4.9	1.4	-	-	0	-
		FSDT	SSL	0.6692	0.5125	0.2531	0.0249	0.0766	0.1362	0	0.2	0.2	1.2	16.2	-
	NNRPIM V2	Aydogdu	SSL	0.7294	0.5778	0.2747	0.0273	0.1067	0.2714	0.6	0.0	0.1	4.0	3.9	3.7
		Karama	SSL	0.7294	0.5778	0.2747	0.0273	0.1067	0.2714	0.9	0.3	1.0	3.0	1.2	0.2
		Mantari	SSL	0.7209	0.5774	0.2751	0.0306	0.1074	0.3073	1.82	1.80	0.33	6.29	6.58	2.14
		Shi	SSL	0.7126	0.5659	0.2698	0.0280	0.1021	0.2448	0.09	0.38	0.40	0.91	12.55	33.70
		Touratier	SSL	0.7236	0.5732	0.2728	0.0272	0.1044	0.2571	-	-	-	-		
		Ambartsumian	SSL	0.7330	0.5765	0.2739	0.0207	0.0936	0.2406	-	-	-	-	-	-
		TSDT	SSL	0.7174	0.5686	0.2707	0.0271	0.1022	0.2438	0.7	0.0	-	-	1.1	-
		FSDT	SSL	0.6695	0.5132	0.2535	0.0260	0.0767	0.1390	0	0	-	-	16.1	-

table 21 - Maximum normalized transverse displacements and stresses and relative errors in relation to the respective exact solution for a simply supported symmetric square laminate with cross-ply layers (0/90/0) subjected to a sinusoidal load (SSL), a/h=20.

										Absolute elative |ε| (%) regarding the respective exact solution					
a/h	**Solution**	**ESL**	**Load**	$\bar{w}$	$\bar{\sigma}_{xx}$	$\bar{\sigma}_{yy}$	$\bar{\tau}_{xy}$	$\bar{\tau}_{yz}$	$\bar{\tau}_{xz}$	$\bar{w}$	$\bar{\sigma}_{xx}$	$\bar{\sigma}_{yy}$	$\bar{\tau}_{xy}$	$\bar{\tau}_{yz}$	$\bar{\tau}_{xz}$
20	Exact	Aydogdu [1]	SSL	0.5110	0.5480	0.2060	0.0232	0.0877	0.2950	-	-	-	-	-	-
		Karama [2]	SSL	0.5080	0.5480	0.2050	0.0231	0.0860	0.2850	-	-	-	-	-	-
		Mantari [2]	SSL	0.5113	0.5510	0.2060	0.0233	0.0900	0.3310	-	-	-	-	-	-
		Shi [3]	SSL	0.5050	0.5458	0.2042	0.0230	0.0919	0.3881	-	-	-	-	-	-
		Touratier	SSL	-	-	-	-	-	-	-	-	-	-	-	-
		Ambartsumian	SSL	-	-	-	-	-	-	-	-	-	-	-	-
		TSDT	SSL	-	-	-	-	-	-	-	-	-	-	-	-
		FSDT	SSL	0.4921	0.5318	0.1997	0.0223	0.0759	-	-	-	-	-	-	-
		Elasticity	SSL	-	0.5520	0.2100	0.0234	0.0938	0.3850	-	-	-	-	-	-
	FEM	TSDT	SSL	-	-	-	-	-	-	-	-	-	-	-	-
		FSDT	SSL	0.4921	0.5281	0.1983	0.0222	0.0754	0.4176	-	-	-	-	-	-
	RPIM	Aydogdu	SSL	0.5038	0.5197	0.1939	0.0222	0.0815	0.2709	1.4	5.2	5.9	4.1	7.1	8.2
		Karama	SSL	0.5038	0.5197	0.1939	0.0222	0.0815	0.2709	0.8	5.2	5.4	3.7	5.2	4.9
		Mantari	SSL	0.5161	0.5282	0.1960	0.0226	0.0851	0.3166	0.9	4.1	4.8	3.1	5.5	4.4
		Shi	SSL	0.5043	0.5196	0.1933	0.0223	0.0786	0.2428	0.1	4.8	5.3	3.0	14.4	37.4
		Touratier	SSL	0.5027	0.5188	0.1934	0.0222	0.0799	0.2560	-	-	-	-	-	-
		Ambartsumian	SSL	0.4889	0.5094	0.1923	0.0210	0.0753	0.2392	-	-	-	-	-	-
		TSDT	SSL	0.5015	0.5179	0.1930	0.0222	0.0784	0.2870	-	-	-	-	-	-
		FSDT	SSL	0.4923	0.5048	0.1895	0.0217	0.0603	0.1336	0.0	5.1	5.1	2.9	20.6	-
	NNRPIM V1	Aydogdu	SSL	0.4767	0.5353	0.1934	0.0223	0.0868	0.2761	6.7	2.3	6.1	4.0	1.0	6.4
		Karama	SSL	0.4767	0.5353	0.1934	0.0223	0.0868	0.2761	6.2	2.3	5.6	3.6	-0.9	3.1
		Mantari	SSL	0.5539	0.5930	0.2027	0.0245	0.0863	0.3351	8.33	7.62	1.62	4.96	4.14	1.25
		Shi	SSL	0.5028	0.5540	0.1992	0.0229	0.0823	0.2542	0.43	1.51	2.43	0.37	10.49	34.49
		Touratier	SSL	0.4785	0.5363	0.1941	0.0223	0.0852	0.2621	-	-	-	-	-	-
		Ambartsumian	SSL	0.3873	0.4598	0.1713	0.0192	0.0752	0.2115	-	-	-	-	-	-
		TSDT	SSL	0.4801	0.5370	0.1946	0.0223	0.0835	0.2489	-	-	-	-	-	-
		FSDT	SSL	0.4914	0.5302	0.1990	0.0219	0.0639	0.1400	0.1	0.3	0.4	1.7	15.8	-
	NNRPIM V2	Aydogdu	SSL	0.5116	0.5492	0.2070	0.0224	0.0809	0.2824	0.1	0.2	0.5	3.5	7.7	4.3
		Karama	SSL	0.5116	0.5492	0.2070	0.0224	0.0809	0.2824	0.7	0.2	1.0	3.1	5.9	0.9
		Mantari	SSL	0.5020	0.5425	0.2063	0.0249	0.0775	0.3199	1.82	1.55	0.13	6.76	13.90	3.35
		Shi	SSL	0.5042	0.5441	0.2048	0.0231	0.0780	0.2553	0.16	0.30	0.32	0.23	15.12	34.22
		Touratier	SSL	0.5096	0.5479	0.2063	0.0224	0.0796	0.2672	-	-	-	-	-	-
		Ambartsumian	SSL	0.5192	0.5540	0.2084	0.0182	0.0653	0.2450	-	-	-	-	-	-
		TSDT	SSL	0.5076	0.5465	0.2056	0.0224	0.0783	0.2530	-	-	-	-	-	-
		FSDT	SSL	0.4923	0.5316	0.1996	0.0229	0.0609	0.1419	0	0	0.1	2.5	19.8	-

table 22 - Maximum normalized transverse displacements and stresses and relative errors in relation to the respective exact solution for a simply supported symmetric square laminate with cross-ply layers (0/90/0) subjected to a sinusoidal load (SSL), a/h=100.

										Absolute elative |ε| (%) regarding the respective exact solution					
a/h	**Solution**	**ESL**	**Load**	$\bar{w}$	$\bar{\sigma}_{xx}$	$\bar{\sigma}_{yy}$	$\bar{\tau}_{xy}$	$\bar{\tau}_{yz}$	$\bar{\tau}_{xz}$	$\bar{w}$	$\bar{\sigma}_{xx}$	$\bar{\sigma}_{yy}$	$\bar{\tau}_{xy}$	$\bar{\tau}_{yz}$	$\bar{\tau}_{xz}$
	Exact	Aydogdu [1]	SSL	0.4350	0.5389	0.1810	0.0214	0.0791	0.3003	-	-	-	-	-	-
		Karama [2]	SSL	0.4350	0.5380	0.1800	0.0213	0.0780	0.2890	-	-	-	-	-	-
		Mantari [2]	SSL	0.4353	0.5390	0.1810	0.0214	0.0810	0.3370	-	-	-	-	-	-
		Shi [3]	SSL	0.4351	0.5389	0.1805	0.0214	0.0828	0.3948	-	-	-	-	-	-
		Touratier	SSL	-	-	-	-	-	-	-	-	-	-	-	-
		Ambartsumian	SSL	-	-	-	-	-	-	-	-	-	-	-	-
		TSDT	SSL	0.4342	0.5390	-	-	0.075	-	-	-	-	-	-	-
		FSDT	SSL	0.4337	0.5384	0.1804	0.0213	0.0703	-	-	-	-	-	-	-
		Elasticity	SSL	-	0.5390	0.1810	0.0213	0.0828	0.3950	-	-	-	-	-	-
	FEM	TSDT	SSL	-	-	-	-	-	-	-	-	-	-	-	-
		FSDT	SSL	0.4336	0.5346	0.1791	0.0212	0.0699	0.4215	-	-	-	-	-	-
	RPIM	Aydogdu	SSL	0.4312	0.5105	0.1706	0.0205	0.0734	0.2753	0.9	5.3	5.8	4.2	7.2	8.3
		Karama	SSL	0.4312	0.5105	0.1706	0.0205	0.0734	0.2753	0.9	5.1	5.2	3.7	5.9	4.8
		Mantari	SSL	0.4388	0.5158	0.1717	0.0207	0.0770	0.3191	0.8	4.3	5.2	3.4	4.9	5.3
		Shi	SSL	0.4340	0.5124	0.1710	0.0206	0.0712	0.2459	0.3	4.9	5.3	3.5	14.1	37.7
		Touratier	SSL	0.4314	0.5107	0.1706	0.0205	0.0721	0.2600	-	-	-	-	-	-
		Ambartsumian	SSL	0.4209	0.5027	0.1702	0.0197	0.0755	0.2397	-	-	-	-	-	-
100		TSDT	SSL	0.4317	0.5108	0.1707	0.0205	0.0709	0.2457	0.6	5.2	-	-	5.5	-
		FSDT	SSL	0.4335	0.5106	0.1713	0.0206	0.0557	0.1347	0.0	5.2	5.0	3.2	20.8	-
	NNRPIM V1	Aydogdu	SSL	0.3999	0.5146	0.1666	0.0200	0.0690	0.2790	8.1	4.5	8.0	6.8	12.8	7.1
		Karama	SSL	0.3999	0.5146	0.1666	0.0200	0.0690	0.2790	8.1	4.3	7.5	6.3	11.6	3.4
		Mantari	SSL	0.4300	0.5256	0.1611	0.0207	0.0761	0.3184	1.23	2.48	11.02	3.34	6.08	5.51
		Shi	SSL	0.4158	0.5237	0.1689	0.0204	0.0673	0.2523	4.43	2.82	6.45	4.64	18.74	36.10
		Touratier	SSL	0.4018	0.5156	0.1672	0.0200	0.0678	0.2644	-	-	-	-	-	-
		Ambartsumian	SSL	0.3362	0.4579	0.1528	0.0176	0.0611	0.1971	-	-	-	-	-	-
		TSDT	SSL	0.4035	0.5165	0.1678	0.0200	0.0666	0.2505	7.1	4.2	-	-	11.3	-
		FSDT	SSL	0.4157	0.5151	0.1723	0.0201	0.0528	0.1383	4.1	4.3	4.5	5.7	24.9	-
	NNRPIM V2	Aydogdu	SSL	0.4376	0.5396	0.1820	0.0204	0.0092	0.2369	0.6	0.1	0.6	4.6	88.4	21.1
		Karama	SSL	0.4376	0.5396	0.1820	0.0204	0.0092	0.2369	0.6	0.3	1.1	4.2	88.2	18.0
		Mantari	SSL	0.4259	0.5293	0.1802	0.0230	-0.0047	0.2528	2.15	1.80	0.47	7.37	105.84	24.97
		Shi	SSL	0.4335	0.5365	0.1809	0.0214	0.0059	0.2134	0.36	0.45	0.25	0.02	92.89	45.94
		Touratier	SSL	0.4371	0.5393	0.1818	0.0205	0.0090	0.2242	-	-	-	-	-	-
		Ambartsumian	SSL	0.4471	0.5467	0.1844	0.0179	0.0098	0.1458	-	-	-	-	-	-
		TSDT	SSL	0.4367	0.5390	0.1816	0.0206	0.0088	0.2121	0.6	0.0	-	-	88.2	-
		FSDT	SSL	0.4331	0.5372	0.1802	0.0219	0.0083	0.1118	0.2	0.2	0.1	2.7	88.2	-

table 23 - Maximum normalized transverse displacements and stresses and relative errors in relation to the respective exact solution for a simply supported symmetric rectangular (b=3a) laminate with cross-ply layers (0/90/0) subjected to a sinusoidal load (SSL), a/h=4,10.

										Absolute elative |ε| (%) regarding the respective exact solution					
a/h	Solution	ESL	Load	$\bar{w}$	$\bar{\sigma}_{xx}$	$\bar{\sigma}_{yy}$	$\bar{\tau}_{xy}$	$\bar{\tau}_{yz}$	$\bar{\tau}_{xz}$	$\bar{w}$	$\bar{\sigma}_{xx}$	$\bar{\sigma}_{yy}$	$\bar{\tau}_{xy}$	$\bar{\tau}_{yz}$	$\bar{\tau}_{xz}$
	Exact	Karama	SSL	2.6838	1.0970	0.1040	0.0272	0.0360	0.2980	-	-	-	-	-	-
		Mantari	SSL	2.6841	1.1180	0.1030	0.0274	0.0360	0.3020	-	-	-	-	-	-
		Touratier	SSL	2.6660	1.0340	0.1030	0.0268	0.0355	0.2850	-	-	-	-	-	-
		TSDT	SSL	2.6410	1.0360	0.1030	0.0263	0.0348	0.2720	-	-	-	-	-	-
		Elasticity	SSL	2.8200	1.1000	0.1190	0.0281	0.0334	0.3870	-	-	-	-	-	-
	RPIM	Karama	SSL	2.6575	1.0262	0.0959	0.0259	0.0328	0.2863	1.0	6.4	7.8	4.7	9.0	3.9
		Mantari	SSL	2.7189	1.1085	0.0994	0.0265	0.0326	0.3218	1.3	0.8	3.5	3.2	9.6	6.6
		Touratier	SSL	2.6428	0.9987	0.0957	0.0256	0.0324	0.2740	0.9	3.4	7.1	4.4	8.7	3.9
4		TSDT	SSL	2.6213	0.9700	0.0952	0.0252	0.0320	0.2619	0.7	6.4	7.6	4.0	8.2	3.7
	NNRPIM V1	Karama	SSL	2.4119	1.0933	0.0893	0.0256	0.0352	0.2778	10.1	0.34	14.2	5.8	2.2	6.8
		Mantari	SSL	2.8213	1.3112	0.1663	0.0284	0.0352	0.3211	4.8	12.6	61.5	1.6	4.7	3.6
		Touratier	SSL	2.4119	1.0933	0.0893	0.0256	0.0352	0.2778	9.5	2.5	13.3	4.4	0.8	2.5
		TSDT	SSL	2.4337	1.0488	0.0918	0.0252	0.0344	0.2582	7.9	1.2	10.9	4.1	1.2	5.1
	NNRPIM V2	Karama	SSL	2.7367	1.0919	0.1069	0.0261	0.0352	0.3010	2.0	0.5	2.8	3.9	2.3	1.0
		Mantari	SSL	2.6309	1.1221	0.0819	0.0293	0.0325	0.3298	2.3	3.7	20.5	4.7	12.2	1.0
		Touratier	SSL	2.7121	1.0606	0.1061	0.0259	0.0347	0.2874	1.7	0.6	3.0	3.4	2.3	0.9
		TSDT	SSL	2.6810	1.0283	0.1050	0.0256	0.0341	0.2743	1.5	0.7	2.0	2.7	1.9	0.8
	Exact	Karama	SSL	0.8768	0.7040	0.0400	0.0117	0.0180	0.3190	-	-	-	-	-	-
		Mantari	SSL	0.8800	0.7080	0.0400	0.0118	0.0180	0.3260	-	-	-	-	-	-
		Touratier	SSL	0.8700	0.6980	0.0401	0.0116	0.0172	0.3020	-	-	-	-	-	-
		TSDT	SSL	0.8620	0.6920	0.0398	0.0115	0.0170	0.2860	-	-	-	-	-	-
		Elasticity	SSL	0.9190	0.7250	0.0435	0.0123	0.0152	0.4200	-	-	-	-	-	-
	RPIM	Karama	SSL	0.8695	0.6571	0.0373	0.0113	0.0161	0.3071	0.8	6.7	6.7	3.6	10.4	3.7
		Mantari	SSL	0.9044	0.6817	0.0393	0.0116	0.0163	0.3581	2.8	3.7	1.8	1.4	9.6	9.9
		Touratier	SSL	0.8634	0.6518	0.0371	0.0112	0.0159	0.2906	0.8	6.6	7.4	3.4	7.3	3.8
10		TSDT	SSL	0.8567	0.6465	0.0369	0.0111	0.0157	0.2752	0.6	6.6	7.3	3.3	7.5	3.8
	NNRPIM V1	Karama	SSL	0.8051	0.6942	0.0360	0.0111	0.0175	0.3053	8.2	1.4	9.88	4.9	2.6	4.3
		Mantari	SSL	1.0040	0.8130	0.0661	0.0131	0.0177	0.3815	12.5	13.1	61.3	9.3	1.7	3.4
		Touratier	SSL	0.8064	0.6916	0.0363	0.0111	0.0173	0.2905	7.3	0.9	9.4	4.3	0.6	3.8
		TSDT	SSL	0.8068	0.6887	0.0366	0.0111	0.0170	0.2765	6.4	0.5	8.1	3.8	0.2	3.3
	NNRPIM V2	Karama	SSL	0.8917	0.7044	0.0413	0.0115	0.0161	0.3224	1.7	0.1	3.3	2.1	10.5	1.1
		Mantari	SSL	0.8642	0.6971	0.0332	0.0126	0.0143	0.3619	3.1	3.0	19.0	4.8	20.8	1.9
		Touratier	SSL	0.8827	0.6979	0.0409	0.0114	0.0160	0.3049	1.5	0.0	2.1	1.8	7.1	1.0
		TSDT	SSL	0.8734	0.6914	0.0405	0.0113	0.0158	0.2886	1.3	0.1	1.8	1.5	6.9	0.9

table 24 - Maximum normalized transverse displacements and stresses and relative errors in relation to the respective exact solution for a simply supported symmetric rectangular (b=3a) laminate with cross-ply layers (0/90/0) subjected to a sinusoidal load (SSL), a/h=20,100.

										Absolute elative |ε| (%) regarding the respective exact solution					
a/h	**Solution**	**ESL**	**Load**	$\bar{w}$	$\bar{\sigma}_{xx}$	$\bar{\sigma}_{yy}$	$\bar{\tau}_{xy}$	$\bar{\tau}_{yz}$	$\bar{\tau}_{xz}$	$\bar{w}$	$\bar{\sigma}_{xx}$	$\bar{\sigma}_{yy}$	$\bar{\tau}_{xy}$	$\bar{\tau}_{yz}$	$\bar{\tau}_{xz}$
	Exact	Karama	SSL	0.5997	0.6440	0.0290	0.0092	0.0140	0.3230	-	-	-	-	-	-
		Mantari	SSL	0.5994	0.6450	0.0290	0.0092	0.0140	0.3290	-	-	-	-	-	-
		Touratier	SSL	0.5960	0.6420	0.0290	0.0091	0.0141	0.3050	-	-	-	-	-	-
		TSDT	SSL	0.5940	0.6410	0.0289	0.0091	0.0139	0.2880	-	-	-	-	-	-
		Elasticity	SSL	0.6100	0.6500	0.0299	0.0093	0.0119	0.4340	-	-	-	-	-	-
	RPIM	Karama	SSL	0.5930	0.6002	0.0269	0.0088	0.0133	0.3104	1.1	6.8	7.3	3.9	5.3	3.9
		Mantari	SSL	0.6114	0.6129	0.0281	0.0090	0.0134	0.3640	2.0	5.0	3.2	1.9	4.5	10.6
		Touratier	SSL	0.5916	0.5990	0.0268	0.0088	0.0131	0.2933	0.7	6.7	7.4	3.0	6.8	3.9
20		TSDT	SSL	0.5901	0.5978	0.0268	0.0088	0.0130	0.2773	0.6	6.7	7.3	3.2	6.5	3.7
	NNRPIM V1	Karama	SSL	0.5508	0.6310	0.0261	0.0086	0.0141	0.3125	8.2	2.0	9.8	6.2	0.5	3.3
		Mantari	SSL	0.6857	0.7252	0.0469	0.0102	0.0139	0.3912	13.7	11.9	61.6	11.1	7.4	4.3
		Touratier	SSL	0.5540	0.6322	0.0264	0.0087	0.0139	0.2967	7.1	1.5	8.9	4.9	1.4	2.7
		TSDT	SSL	0.5569	0.6333	0.0267	0.0087	0.0137	0.2819	6.2	1.2	7.7	4.7	1.2	2.1
	NNRPIM V2	Karama	SSL	0.6074	0.6449	0.0297	0.0089	0.0112	0.3273	1.3	0.1	2.5	3.3	19.8	1.3
		Mantari	SSL	0.5827	0.6295	0.0240	0.0097	0.0090	0.3647	3.4	2.9	17.3	5.4	40.0	2.7
		Touratier	SSL	0.6043	0.6428	0.0295	0.0089	0.0112	0.3093	1.4	0.1	1.9	2.3	20.3	1.4
		TSDT	SSL	0.6011	0.6408	0.0294	0.0089	0.0112	0.2926	1.2	0	1.6	2.4	19.3	1.6
	Exact	Karama	SSL	0.5080	0.6200	0.0250	0.0083	0.0130	0.3230	-	-	-	-	-	-
		Mantari	SSL	0.5083	0.6240	0.0250	0.0083	0.0130	0.3310	-	-	-	-	-	-
		Touratier	SSL	0.5070	0.6240	0.0253	0.0083	0.0131	0.3060	-	-	-	-	-	-
		TSDT	SSL	0.5070	0.6240	0.0253	0.0083	0.0129	0.2890	-	-	-	-	-	-
		Elasticity	SSL	0.5080	0.6240	0.0253	0.0083	0.0108	0.4390	-	-	-	-	-	-
	RPIM	Karama	SSL	0.5032	0.5817	0.0234	0.0080	0.0118	0.3110	0.9	6.2	6.4	3.6	8.9	3.7
		Mantari	SSL	0.5154	0.5903	0.0243	0.0081	0.0118	0.3629	1.4	5.4	2.8	2.4	9.2	9.6
		Touratier	SSL	0.5036	0.5818	0.0234	0.0080	0.0117	0.2936	0.7	6.8	7.4	3.5	10.3	4.0
100		TSDT	SSL	0.5040	0.5820	0.0235	0.0080	0.0116	0.2774	0.6	6.7	7.3	3.4	9.8	4.0
	NNRPIM V1	Karama	SSL	0.4630	0.6040	0.0226	0.0077	0.0068	0.3341	8.9	2.6	9.6	6.9	47.7	3.4
		Mantari	SSL	0.5538	0.6643	0.0386	0.0089	0.0094	0.4136	8.9	6.5	54.2	7.6	33.2	10.0
		Touratier	SSL	0.4666	0.6059	0.0229	0.0078	0.0068	0.3165	8.0	2.9	9.7	6.4	48.3	3.4
		TSDT	SSL	0.4700	0.6076	0.0231	0.0078	0.0067	0.2999	7.3	2.6	8.7	5.9	47.8	3.8
	NNRPIM V2	Karama	SSL	0.5150	0.6253	0.0258	0.0080	0.0157	0.3142	1.4	0.9	3.4	3.1	21.1	2.7
		Mantari	SSL	0.4900	0.6063	0.0208	0.0088	0.0197	0.3319	3.6	2.8	16.7	6.3	40.5	11.7
		Touratier	SSL	0.5139	0.6246	0.0257	0.0081	0.0153	0.2959	1.4	0.1	1.8	2.7	16.8	3.3
		TSDT	SSL	0.5128	0.6240	0.0257	0.0081	0.0149	0.2786	1.1	0	1.4	2.3	15.6	3.6

table 25 - Maximum normalized transverse displacements and stresses for a simply supported symmetric square laminate with cross-ply layers (0/90/0) subjected to a uniformly distributed load (UDL), a/h=4.

a/h	Solution	ESL	Load	$\bar{w}$	$\bar{\sigma}_{xx}$	$\bar{\sigma}_{yy}$	$\bar{\tau}_{xy}$	$\bar{\tau}_{yz}$	$\bar{\tau}_{xz}$
4	Exact	TSDT	UDL	-	-	-	-	-	-
		FSDT	UDL	-	-	-	-	-	-
		Elasticity	UDL	-	-	-	-	-	-
	FEM	TSDT	UDL	-	-	-	-	-	-
		FSDT	UDL	-	-	-	-	-	-
	RPIM	Aydogdu	UDL	2.9242	1.0535	0.6940	0.0959	0.4179	0.3526
		Karama	UDL	2.9242	1.0535	0.6940	0.0959	0.4179	0.3526
		Mantari	UDL	2.9715	1.1385	0.6907	0.0967	0.4242	0.3876
		Shi	UDL	2.9065	0.9993	0.6905	0.0951	0.4069	0.3286
		Touratier	UDL	2.9098	1.0242	0.6922	0.0949	0.4122	0.3399
		Ambartsumian	UDL	2.7917	0.9667	0.6787	0.0784	0.3885	0.3198
		TSDT	UDL	2.8892	0.9948	0.6892	0.0936	0.4058	0.3275
		FSDT	UDL	2.6598	0.6285	0.6320	0.0677	0.3047	0.2020
	NNRPIM V1	Aydogdu	UDL	2.7140	1.0730	0.6657	0.1070	0.4277	0.3498
		Karama	UDL	2.7140	1.0730	0.6657	0.1070	0.4277	0.3498
		Mantari	UDL	3.0690	1.2918	0.6974	0.1024	0.3921	0.3881
		Shi	UDL	2.8870	1.0717	0.7007	0.1082	0.4270	0.3440
		Touratier	UDL	2.7260	1.0487	0.6704	0.1066	0.4257	0.3403
		Ambartsumian	UDL	1.9707	0.7835	0.5174	0.0771	0.3135	0.2460
		TSDT	UDL	2.7306	1.0234	0.6737	0.1059	0.4228	0.3310
		FSDT	UDL	2.6585	0.6534	0.6578	-0.0734	0.3411	0.2279
	NNRPIM V2	Aydogdu	UDL	2.9771	1.0731	0.7386	0.1000	0.4481	0.3779
		Karama	UDL	2.9051	1.1219	0.7270	0.1150	0.4453	0.4074
		Mantari	UDL	2.9115	1.0077	0.7279	0.1068	0.4373	0.3534
		Shi	UDL	2.9566	1.0426	0.7352	0.0997	0.4428	0.3648
		Touratier	UDL	2.9566	1.0426	0.8891	0.0997	0.4428	0.3648
		Ambartsumian	UDL	2.9633	1.0215	0.7322	0.0549	0.4034	0.3416
		TSDT	UDL	2.9301	1.0125	0.7305	0.0993	0.4369	0.3521
		FSDT	UDL	2.6618	0.6548	0.6594	-0.0758	0.3447	0.2323

table 26 - Maximum normalized transverse displacements and stresses for a simply supported symmetric square laminate with cross-ply layers (0/90/0) subjected to a uniformly distributed load (UDL), a/h=10

a/h	Solution	ESL	Load	$\bar{w}$	$\bar{\sigma}_{xx}$	$\bar{\sigma}_{yy}$	$\bar{\tau}_{xy}$	$\bar{\tau}_{yz}$	$\bar{\tau}_{xz}$
10	Exact	TSDT	UDL	-	-	-	-	-	-
		FSDT	UDL	1.0219	0.7719	0.3072	0.0514	0.3107	-
		Elasticity	UDL	-	-	-	-	-	-
	FEM	TSDT	UDL	-	-	-	-	-	-
		FSDT	UDL	-	-	-	-	-	-
	RPIM	Aydogdu	UDL	1.0984	0.8177	0.3257	0.0528	0.3136	0.4461
		Karama	UDL	1.0984	0.8177	0.3257	0.0528	0.3136	0.4461
		Mantari	UDL	1.1335	0.8405	0.3331	0.0539	0.3267	0.5139
		Shi	UDL	1.0898	0.8101	0.3207	0.0525	0.3019	0.4030
		Touratier	UDL	1.0913	0.8125	0.3230	0.0524	0.3075	0.4234
		Ambartsumian	UDL	1.0536	0.7919	0.3182	0.0479	0.2916	0.3960
		TSDT	UDL	1.0836	0.8074	0.3201	0.0520	0.3011	4.0188
		FSDT	UDL	1.0221	0.7404	0.2962	0.0469	0.2272	0.2257
	NNRPIM V1	Aydogdu	UDL	1.0360	0.8372	0.3171	0.0583	0.3480	0.4614
		Karama	UDL	1.0360	0.8372	0.3171	0.0583	0.3480	0.4614
		Mantari	UDL	1.2126	0.9358	0.3436	0.0605	0.3284	0.5441
		Shi	UDL	1.0861	0.8584	0.3253	0.0593	0.3369	0.4351
		Touratier	UDL	1.0361	0.8348	0.3166	0.0581	0.3435	0.4412
		Ambartsumian	UDL	0.8215	0.7058	0.2728	0.0470	0.2675	0.3479
		TSDT	UDL	1.0352	0.8322	0.3158	0.0578	0.3386	0.4221
		FSDT	UDL	1.0212	0.7700	0.3070	-0.0511	0.2628	0.2523
	NNRPIM V2	Aydogdu	UDL	1.1168	0.8498	0.3446	0.0568	0.3488	0.4845
		Karama	UDL	1.1168	0.8498	0.3446	0.0568	0.3488	0.4845
		Mantari	UDL	1.1053	0.8509	0.3470	0.0629	0.3417	0.5438
		Shi	UDL	1.0910	0.8358	0.3361	0.0586	0.3359	0.4414
		Touratier	UDL	1.1077	0.8441	0.3412	0.0567	0.3434	0.4609
		Ambartsumian	UDL	1.1199	0.8447	0.3434	0.0410	0.3044	0.4295
		TSDT	UDL	1.0980	0.8385	0.3376	0.0565	0.3378	0.4386
		FSDT	UDL	1.0228	0.7724	0.3076	-0.0527	0.2618	0.2569

table 27 - Maximum normalized transverse displacements and stresses for a simply supported symmetric square laminate with cross-ply layers (0/90/0) subjected to a uniformly distributed load (UDL), a/h=20

a/h	Solution	ESL	Load	$\bar{w}$	$\bar{\sigma}_{xx}$	$\bar{\sigma}_{yy}$	$\bar{\tau}_{xy}$	$\bar{\tau}_{yz}$	$\bar{\tau}_{xz}$
20	Exact	TSDT	UDL	-	-	-	-	-	-
		FSDT	UDL	0.7572	0.7893	0.2227	0.0453	0.2902	-
		Elasticity	UDL	-	-	-	-	-	-
	FEM	TSDT	UDL	-	-	-	-	-	-
		FSDT	UDL	-	-	-	-	-	-
	RPIM	Aydogdu	UDL	0.7751	0.7849	0.2235	0.0429	0.2862	0.4670
		Karama	UDL	0.7751	0.7849	0.2235	0.0429	0.2862	0.4670
		Mantari	UDL	0.7938	0.7965	0.2270	0.0436	0.3004	0.5445
		Shi	UDL	0.7759	0.7851	0.2224	0.0430	0.2756	0.4189
		Touratier	UDL	0.7734	0.7838	0.2228	0.0428	0.2805	0.4416
		Ambartsumian	UDL	0.7514	0.7694	0.2216	0.0404	0.2685	0.4126
		TSDT	UDL	0.7716	0.7826	0.2220	0.0427	0.2747	0.4177
		FSDT	UDL	0.7574	0.7655	0.2158	0.0415	0.2100	0.2307
	NNRPIM V1	Aydogdu	UDL	0.7327	0.8047	0.2163	0.0461	0.3352	0.4953
		Karama	UDL	0.7327	0.8047	0.2163	0.0461	0.3352	0.4953
		Mantari	UDL	0.8517	0.8797	0.2370	0.0494	0.3222	0.5895
		Shi	UDL	0.7728	0.8291	0.2248	0.0474	0.3204	0.4600
		Touratier	UDL	0.7355	0.8059	0.2170	0.0461	0.3296	0.4715
		Ambartsumian	UDL	0.5970	0.7021	0.1905	0.0385	0.2605	0.3776
		TSDT	UDL	0.7379	0.8069	0.2177	0.0461	0.3238	0.4490
		FSDT	UDL	0.7558	0.7953	0.2229	-0.0445	0.2481	0.2574
	NNRPIM V2	Aydogdu	UDL	0.7880	0.8192	0.2358	0.0457	0.3211	0.5124
		Karama	UDL	0.7880	0.8192	0.2358	0.0457	0.3211	0.5124
		Mantari	UDL	0.7737	0.8120	0.2343	0.0502	0.3053	0.5771
		Shi	UDL	0.7767	0.8136	0.2318	0.0471	0.3058	0.4648
		Touratier	UDL	0.7850	0.8176	0.2345	0.0457	0.3156	0.4858
		Ambartsumian	UDL	0.7990	0.8224	0.2398	0.0364	0.2693	0.4456
		TSDT	UDL	0.7818	0.8161	0.2332	0.0457	0.3100	0.4609
		FSDT	UDL	0.7578	0.7989	0.2230	-0.0461	0.2386	0.2608

table 28 - Maximum normalized transverse displacements and stresses for a simply supported symmetric square laminate with cross-ply layers (0/90/0) subjected to a uniformly distributed load (UDL), a/h=100.

a/h	Solution	ESL	Load	$\bar{w}$	$\bar{\sigma}_{xx}$	$\bar{\sigma}_{yy}$	$\bar{\tau}_{xy}$	$\bar{\tau}_{yz}$	$\bar{\tau}_{xz}$
100	Exact	TSDT	UDL	-	-	-	-	-	-
		FSDT	UDL	0.6697	0.8072	0.1925	0.0426	0.2842	-
		Elasticity	UDL	-	-	-	-	-	-
	FEM	TSDT	UDL	-	-	-	-	-	-
		FSDT	UDL	-	-	-	-	-	-
	RPIM	Aydogdu	UDL	0.6655	0.7732	0.1865	0.0391	0.2747	0.4739
		Karama	UDL	0.6655	0.7732	0.1865	0.0391	0.2747	0.4739
		Mantari	UDL	0.6770	0.7803	0.1883	0.0394	0.2914	0.5498
		Shi	UDL	0.6699	0.7759	0.1871	0.0394	0.2648	4.2310
		Touratier	UDL	0.6659	0.7734	0.1866	0.0392	0.2693	0.4475
		Ambartsumian	UDL	0.6492	0.7612	0.1868	0.0375	0.2765	4.1451
		TSDT	UDL	0.6663	0.7736	0.1867	0.0392	0.2638	0.4228
		FSDT	UDL	0.6693	0.7733	0.1875	0.0393	0.2029	0.2317
	NNRPIM V1	Aydogdu	UDL	0.6182	0.7782	0.1809	0.0397	0.2940	0.5242
		Karama	UDL	0.6182	0.7782	0.1809	0.0397	0.2940	0.5242
		Mantari	UDL	0.6703	0.7915	0.1968	0.0397	0.2617	0.6006
		Shi	UDL	0.6444	0.7897	0.1899	0.0402	0.2707	0.4726
		Touratier	UDL	0.6213	0.7794	0.1822	0.0398	0.2870	0.4966
		Ambartsumian	UDL	0.5195	0.7009	0.1591	0.0349	0.2710	0.3839
		TSDT	UDL	0.6242	0.7803	0.1834	0.0398	0.2800	0.4704
		FSDT	UDL	0.6441	0.7744	0.1923	-0.0396	0.2116	0.2600
	NNRPIM V2	Aydogdu	UDL	0.6763	0.8079	0.1963	0.0406	0.1697	0.4737
		Karama	UDL	0.6763	0.8079	0.1963	0.0406	0.1697	0.4737
		Mantari	UDL	0.6587	0.7961	0.1935	0.0452	0.1329	0.5070
		Shi	UDL	0.6701	0.8046	0.1944	0.0425	0.1504	0.4210
		Touratier	UDL	0.6756	0.8076	0.1960	0.0408	0.1654	0.4477
		Ambartsumian	UDL	0.6907	0.8144	0.2023	0.0356	0.1280	0.3402
		TSDT	UDL	0.6749	0.8073	0.1957	0.0410	0.1610	0.4231
		FSDT	UDL	0.6691	0.8065	0.1932	-0.0434	0.1222	0.2246

table 29 - Maximum normalized transverse displacements and stresses and relative errors in relation to the respective exact solution for a simply supported symmetric square laminate with cross-ply layers (0/90/90/0) subjected to a sinusoidal load (SSL), a/h=4.

										Absolute elative |ε| (%) regarding the respective exact solution					
a/h	Solution	ESL	Load	$\bar{w}$	$\bar{\sigma}_{xx}$	$\bar{\sigma}_{yy}$	$\bar{\tau}_{xy}$	$\bar{\tau}_{yz}$	$\bar{\tau}_{xz}$	$\bar{w}$	$\bar{\sigma}_{xx}$	$\bar{\sigma}_{yy}$	$\bar{\tau}_{xy}$	$\bar{\tau}_{yz}$	$\bar{\tau}_{xz}$
4	Exact	Aydogdu	SSL	1.9590	0.7040	0.6360	0.0465	0.2600	0.2320	-	-	-	-	-	-
		Karama]	SSL	1.9190	0.6690	0.6370	0.0459	0.2530	0.2260	-	-	-	-	-	-
		Mantari	SSL	1.9210	0.7400	0.6350	0.0480	0.2690	0.2540	-	-	-	-	-	-
		Shi [3]	SSL	1.8947	0.6645	0.6316	0.0441	0.2984	0.2306	-	-	-	-	-	-
		Touratier	SSL	1.9098	0.6823	0.6342	0.0450	0.2460	0.2162	-	-	-	-	-	-
		Ambartsumian	SSL	-	-	-	-	-	-	-	-	-	-	-	-
		TSDT	SSL	1.8937	0.6651	0.6322	0.0440	0.2389	0.2064	-	-	-	-	-	-
		FSDT	SSL	1.7100	0.4060	0.5760	0.0308	0.1960	0.1400	-	-	-	-	-	-
		Elasticity	SSL	1.9540	0.7200	0.6630	0.0467	0.2920	0.2190	-	-	-	-	-	-
	FEM	TSDT	SSL	-	-	-	-	-	-	-	-	-	-	-	-
		FSDT	SSL	-	-	-	-	-	-	-	-	-	-	-	-
	RPIM	Aydogdu	SSL	1.9046	0.6662	0.6007	0.0434	0.2392	0.2146	2.8	5.4	5.5	6.6	8.0	7.5
		Karama	SSL	1.9046	0.6662	0.6007	0.0434	0.2392	0.2146	0.8	0.4	5.7	5.4	5.5	5.0
		Mantari	SSL	1.9340	0.7134	0.6017	0.0445	0.2529	0.2414	0.7	3.6	5.2	7.2	6.0	4.9
		Shi	SSL	1.8940	0.6361	0.5987	0.0426	0.2267	0.1966	0.0	4.3	5.2	3.4	24.0	14.7
		Touratier	SSL	1.8961	0.6500	0.5994	0.0428	0.2328	0.2051	0.7	4.7	5.5	5.0	5.4	5.1
		Ambartsumian	SSL	1.8264	0.6186	0.5878	0.0355	0.2195	0.1914	-	-	-	-	-	-
		TSDT	SSL	1.8828	0.6330	0.5972	0.0412	0.2262	0.1959	0.6	4.8	5.5	6.4	5.3	5.1
		FSDT	SSL	1.7101	0.3853	0.5471	0.0299	0.1555	0.1111	0.0	5.1	5.0	3.1	20.6	20.7
	NNRPIM V1	Aydogdu	SSL	1.7752	0.6880	0.5891	0.0454	0.2410	0.2142	9.4	2.3	7.4	2.3	7.3	7.7
		Karama	SSL	1.7752	0.6880	0.5891	0.0454	0.2410	0.2142	7.5	2.8	7.5	1.0	4.8	5.2
		Mantari	SSL	2.0002	0.8171	0.6239	0.0481	0.2486	0.2497	4.1	10.4	1.8	0.1	7.6	1.7
		Shi	SSL	1.8877	0.6979	0.6197	0.0451	0.2336	0.2057	0.4	5.0	1.9	2.2	21.7	10.8
		Touratier	SSL	1.7830	0.6761	0.5926	0.0448	0.2360	0.2061	6.6	0.9	6.6	0.5	4.1	4.7
		Ambartsumian	SSL	1.2781	0.4849	0.4509	0.0351	0.1833	0.1507	-	-	-	-	-	-
		TSDT	SSL	1.7854	0.6629	0.5950	0.0440	0.2307	0.1981	5.7	0.3	5.9	0.1	3.4	4.0
		FSDT	SSL	1.7100	0.4053	0.5756	0.0307	0.1635	0.1164	0.0	0.2	0.1	0.3	16.6	16.8
	NNRPIM V2	Aydogdu	SSL	1.9347	0.6993	0.6412	0.0421	0.2528	0.2252	1.2	0.7	0.8	9.4	2.8	2.9
		Karama	SSL	1.9347	0.6993	0.6412	0.0421	0.2528	0.2252	0.8	4.5	0.7	8.2	0.1	0.3
		Mantari	SSL	1.8799	0.7196	0.6282	0.0497	0.2624	0.2475	2.1	2.8	1.1	3.5	2.5	2.6
		Shi	SSL	1.8934	0.6593	0.6332	0.0441	0.2381	0.2058	0.1	0.8	0.2	0.0	20.2	10.8
		Touratier	SSL	1.9227	0.6816	0.6391	0.0418	0.2460	0.2151	0.7	0.1	0.8	7.2	0.0	0.5
		Ambartsumian	SSL	1.9324	0.6732	0.6395	0.0249	0.2299	0.2017	-	-	-	-	-	-
		TSDT	SSL	1.9060	0.6634	0.6359	0.0413	0.2390	0.2053	0.6	0.2	0.6	6.1	0.1	0.5
		FSDT	SSL	1.7099	0.4058	0.5762	0.0320	0.1668	0.1190	0	0.1	0	3.8	14.9	15.0

table 30 - Maximum normalized transverse displacements and stresses and relative errors in relation to the respective exact solution for a simply supported symmetric square laminate with cross-ply layers (0/90/90/0) subjected to a sinusoidal load (SSL), a/h=10.

										Absolute elative |ε| (%) regarding the respective exact solution					
a/h	**Solution**	**ESL**	**Load**	$\bar{w}$	$\bar{\sigma}_{xx}$	$\bar{\sigma}_{yy}$	$\bar{\tau}_{xy}$	$\bar{\tau}_{yz}$	$\bar{\tau}_{xz}$	$\bar{w}$	$\bar{\sigma}_{xx}$	$\bar{\sigma}_{yy}$	$\bar{\tau}_{xy}$	$\bar{\tau}_{yz}$	$\bar{\tau}_{xz}$
10	Exact	Aydogdu	SSL	0.7340	0.5520	0.3960	0.0273	0.1670	0.3030	-	-	-	-	-	-
		Karama	SSL	0.7240	0.5530	0.3930	0.0272	0.1630	0.2940	-	-	-	-	-	-
		Mantari	SSL	0.7300	0.5610	0.3950	0.0280	0.1770	0.3350	-	-	-	-	-	-
		Shi	SSL	0.7156	0.5454	0.3885	0.0268	0.1923	0.3069	-	-	-	-	-	-
		Touratier	SSL	0.7206	0.5488	0.3906	0.0270	0.1581	0.2787	-	-	-	-	-	-
		Ambartsumian	SSL	-	-	-	-	-	-	-	-	-	-	-	-
		TSDT	SSL	0.7149	0.5456	0.3888	0.0268	0.1530	0.2640	-	-	-	-	-	-
		FSDT	SSL	0.6627	0.4989	0.3614	0.0241	0.1292	0.1670	-	-	-	-	-	-
		Elasticity	SSL	0.7370	0.5590	0.4010	0.0275	0.1960	0.3010	-	-	-	-	-	-
	FEM	TSDT	SSL	-	-	-	-	-	-	-	-	-	-	-	-
		FSDT	SSL	0.6627	0.4954	0.3589	0.0240	0.1280	0.4140	-	-	-	-	-	-
	RPIM	Aydogdu	SSL	0.7190	0.5241	0.3709	0.0261	0.1547	0.2792	2.0	5.1	6.3	4.5	7.4	7.9
		Karama	SSL	0.7190	0.5241	0.3709	0.0261	0.1547	0.2792	0.7	5.2	5.6	4.2	5.1	5.0
		Mantari	SSL	0.7371	0.5385	0.3749	0.0266	0.1664	0.3205	1.0	4.0	5.1	5.0	6.0	4.3
		Shi	SSL	0.7150	0.5198	0.3683	0.0259	0.1454	0.2516	0.1	4.7	5.2	3.2	24.4	18.0
		Touratier	SSL	0.7155	0.5210	0.3693	0.0259	0.1498	0.2648	0.7	5.1	5.4	4.0	5.2	5.0
		Ambartsumian	SSL	0.6921	0.5085	0.3631	0.0240	0.1411	0.2469	-	-	-	-	-	-
		TSDT	SSL	0.7110	0.5179	0.3674	0.0258	0.1451	0.2508	0.5	5.1	5.5	3.9	5.2	5.0
		FSDT	SSL	0.6630	0.4735	0.3430	0.0234	0.1025	0.1323	0.0	5.1	5.1	2.9	20.7	20.8
	NNRPIM V1	Aydogdu	SSL	0.6797	0.5412	0.3717	0.0266	0.1595	0.2833	7.4	2.0	6.1	2.7	4.5	6.5
		Karama	SSL	0.6797	0.5412	0.3717	0.0266	0.1595	0.2833	6.1	2.1	5.4	2.3	2.2	3.6
		Mantari	SSL	0.7909	0.6120	0.3964	0.0288	0.1684	0.3427	8.3	9.1	0.4	2.9	4.9	2.3
		Shi	SSL	0.7144	0.5585	0.3823	0.0270	0.1499	0.2641	0.2	2.4	1.6	0.7	22.0	13.9
		Touratier	SSL	0.6806	0.5402	0.3720	0.0265	0.1550	0.2699	5.5	1.6	4.8	2.0	1.9	3.2
		Ambartsumian	SSL	0.5374	0.4478	0.3184	0.0226	0.1309	0.2158	-	-	-	-	-	-
		TSDT	SSL	0.6805	0.5389	0.3719	0.0263	0.1506	0.2568	4.8	1.1	4.2	1.3	1.3	2.2
		FSDT	SSL	0.6627	0.4980	0.3608	0.0239	0.1079	0.1388	0.0	0.2	0.2	0.7	16.5	16.9
	NNRPIM V2	Aydogdu	SSL	0.7300	0.5530	0.3953	0.0262	0.1627	0.2922	0.5	0.2	0.2	4.0	2.6	3.6
		Karama	SSL	0.7300	0.5530	0.3953	0.0262	0.1627	0.2922	0.8	0	0.6	3.6	0.2	0.6
		Mantari	SSL	0.7164	0.5505	0.3922	0.0293	0.1680	0.3274	1.9	1.9	0.7	4.7	5.1	2.3
		Shi	SSL	0.7147	0.5431	0.3894	0.0270	0.1517	0.2643	0.1	0.4	0.2	0.8	21.1	13.9
		Touratier	SSL	0.7252	0.5493	0.3933	0.0262	0.1578	0.2772	0.6	0.1	0.7	3.1	0.2	0.5
		Ambartsumian	SSL	0.7349	0.5533	0.3947	0.0199	0.1435	0.2593	-	-	-	-	-	-
		TSDT	SSL	0.7195	0.5457	0.3908	0.0261	0.1530	0.2627	0.6	0	0.5	2.6	0	0.5
		FSDT	SSL	0.6629	0.4987	0.3613	0.0249	0.1088	0.1416	0	0	0	3.5	15.8	15.2

table 31 - Maximum normalized transverse displacements and stresses and relative errors in relation to the respective exact solution for a simply supported symmetric square laminate with cross-ply layers (0/90/90/0) subjected to a sinusoidal load (SSL), a/h=20.

										Absolute elative |ε| (%) regarding the respective exact solution					
a/h	**Solution**	**ESL**	**Load**	$\bar{w}$	$\bar{\sigma}_{xx}$	$\bar{\sigma}_{yy}$	$\bar{\tau}_{xy}$	$\bar{\tau}_{yz}$	$\bar{\tau}_{xz}$	$\bar{w}$	$\bar{\sigma}_{xx}$	$\bar{\sigma}_{yy}$	$\bar{\tau}_{xy}$	$\bar{\tau}_{yz}$	$\bar{\tau}_{xz}$
	Exact	Aydogdu	SSL	0.5120	0.5400	0.3060	0.0230	0.1340	0.3260	-	-	-	-	-	-
		Karama	SSL	0.5090	0.5410	0.3060	0.0229	0.1310	0.3160	-	-	-	-	-	-
		Mantari	SSL	0.5110	0.5430	0.3060	0.0230	0.1420	0.3620	-	-	-	-	-	-
		Shi	SSL	0.5069	0.5391	0.3054	0.0228	0.1541	0.3299	-	-	-	-	-	-
		Touratier	SSL	0.5083	0.5400	0.3048	0.0229	0.1272	0.2989	-	-	-	-	-	-
		Ambartsumian	SSL	-	-	-	-	-	-	-	-	-	-	-	-
		TSDT	SSL	0.5060	0.5393	0.3043	0.0228	0.1230	0.2825	-	-	-	-	-	-
		FSDT	SSL	0.4912	0.5273	0.2956	0.0221	0.1087	0.1750	-	-	-	-	-	-
		Elasticity	SSL	0.5128	0.5430	0.3080	0.0230	0.1560	0.3280	-	-	-	-	-	-
	FEM	TSDT	SSL	-	-	-	-	-	-	-	-	-	-	-	-
		FSDT	SSL	0.4912	0.5236	0.2936	0.0219	0.108	0.434	-	-	-	-	-	-
	RPIM	Aydogdu	SSL	0.5053	0.5128	0.2886	0.0220	0.1243	0.3000	1.3	5.0	5.7	4.1	7.3	8.0
		Karama	SSL	0.5053	0.5128	0.2886	0.0220	0.1243	0.3000	0.7	5.2	5.7	3.7	5.1	5.1
		Mantari	SSL	0.5045	0.5122	0.2882	0.0220	0.1206	0.2839	1.3	5.7	5.8	4.3	15.0	21.6
		Shi	SSL	0.5062	0.5132	0.2882	0.0221	0.1175	0.2692	0.1	4.8	5.6	3.0	23.7	18.4
		Touratier	SSL	0.5045	0.5122	0.2882	0.0220	0.1206	0.2839	0.8	5.2	5.5	3.8	5.2	5.0
		Ambartsumian	SSL	0.4904	0.5028	0.2848	0.0209	0.1140	0.2648	-	-	-	-	-	-
20		TSDT	SSL	0.5034	0.5115	0.2876	0.0220	0.1171	0.2684	0.5	5.2	5.5	3.6	4.8	5.0
		FSDT	SSL	0.4914	0.5005	0.2806	0.0214	0.0863	0.1388	0.0	5.1	5.1	3.0	20.6	20.7
	NNRPIM V1	Aydogdu	SSL	0.4784	0.5285	0.2900	0.0221	0.1295	0.3062	6.6	2.1	5.2	3.9	3.3	6.1
		Karama	SSL	0.4784	0.5285	0.2900	0.0221	0.1295	0.3062	6.0	2.3	5.2	3.5	1.1	3.1
		Mantari	SSL	0.5546	0.5850	0.3074	0.0242	0.1344	0.3683	8.5	7.7	0.5	5.3	5.4	1.8
		Shi	SSL	0.5050	0.5475	0.2987	0.0228	0.1212	0.2828	0.4	1.6	2.2	0.2	21.3	14.3
		Touratier	SSL	0.4805	0.5297	0.2909	0.0221	0.1260	0.2911	5.5	1.9	4.6	3.4	0.9	2.6
		Ambartsumian	SSL	0.3889	0.4541	0.2558	0.0190	0.1067	0.2350	-	-	-	-	-	-
		TSDT	SSL	0.4821	0.5307	0.2916	0.0221	0.1226	0.2763	4.7	1.6	4.2	2.9	0.4	2.2
		FSDT	SSL	0.4905	0.5257	0.2947	0.0217	0.0911	0.1455	0.1	0.3	0.3	1.8	16.2	16.8
	NNRPIM V2	Aydogdu	SSL	0.5130	0.5419	0.3076	0.0221	0.1273	0.3123	0.2	0.4	0.5	3.8	5.0	4.2
		Karama	SSL	0.5130	0.5419	0.3076	0.0221	0.1273	0.3123	0.8	0.2	0.5	3.4	2.8	1.2
		Mantari	SSL	0.5019	0.5345	0.3048	0.0246	0.1257	0.3498	1.8	1.6	0.4	6.9	11.4	3.4
		Shi	SSL	0.5061	0.5374	0.3048	0.0229	0.1188	0.2834	0.2	0.3	0.2	0.3	22.9	14.1
		Touratier	SSL	0.5114	0.5408	0.3068	0.0222	0.1238	0.2959	0.6	0.2	0.7	3.2	2.7	1.0
		Ambartsumian	SSL	0.5209	0.5469	0.3093	0.0181	0.1052	0.2720	-	-	-	-	-	-
		TSDT	SSL	0.5094	0.5397	0.3058	0.0222	0.1203	0.2802	0.7	0.1	0.5	2.7	2.2	0.8
		FSDT	SSL	0.4913	0.5271	0.2955	0.0226	0.0888	0.1476	0	0	0	2.2	18.3	15.7

table 32 - Maximum normalized transverse displacements and stresses and relative errors in relation to the respective exact solution for a simply supported symmetric square laminate with cross-ply layers (0/90/90/0) subjected to a sinusoidal load (SSL), a/h=100.

										Absolute elative |ε| (%) regarding the respective exact solution					
a/h	**Solution**	**ESL**	**Load**	$\bar{w}$	$\bar{\sigma}_{xx}$	$\bar{\sigma}_{yy}$	$\bar{\tau}_{xy}$	$\bar{\tau}_{yz}$	$\bar{\tau}_{xz}$	$\bar{w}$	$\bar{\sigma}_{xx}$	$\bar{\sigma}_{yy}$	$\bar{\tau}_{xy}$	$\bar{\tau}_{yz}$	$\bar{\tau}_{xz}$
	Exact	Aydogdu	SSL	0.4350	0.5380	0.2700	0.0213	0.1200	0.3360	-	-	-	-	-	-
		Karama	SSL	0.4350	0.5380	0.2700	0.0213	0.1180	0.3240	-	-	-	-	-	-
		Mantari	SSL	0.4350	0.5390	0.2710	0.0210	0.1280	0.3720	-	-	-	-	-	-
		Shi	SSL	0.4352	0.5386	0.2708	0.0214	0.1389	0.3388	-	-	-	-	-	-
		Touratier	SSL	0.4352	0.5385	0.2707	0.0213	0.1149	0.3068	-	-	-	-	-	-
		Ambartsumian	SSL	-	-	-	-	-	-	-	-	-	-	-	-
		TSDT	SSL	0.4343	0.5387	0.2708	0.0213	0.1120	0.2897	-	-	-	-	-	-
		FSDT	SSL	0.4337	0.5382	0.2704	0.0213	0.1008	0.1780	-	-	-	-	-	-
		Elasticity	SSL	0.4337	0.5390	0.2710	0.0214	0.1390	0.3390	-	-	-	-	-	-
	FEM	TSDT	SSL	-	-	-	-	-	-	-	-	-	-	-	-
		FSDT	SSL	0.4334	0.5382	0.2704	0.0213	0.1010	0.4450	-	-	-	-	-	-
	RPIM	Aydogdu	SSL	0.4312	0.5102	0.2558	0.0205	0.1128	0.3081	0.9	5.2	5.3	3.7	6.0	8.3
		Karama	SSL	0.4312	0.5102	0.2558	0.0205	0.1128	0.3081	0.9	5.2	5.3	3.7	4.4	4.9
		Mantari	SSL	0.4387	0.5152	0.2574	0.0207	0.1232	0.3526	0.8	4.4	5.0	1.3	3.7	5.2
		Shi	SSL	0.4341	0.5120	0.2565	0.0206	0.1071	0.2758	0.3	4.9	5.3	3.5	22.9	18.6
		Touratier	SSL	0.4315	0.5103	0.2559	0.0205	0.1097	0.2914	0.9	5.2	5.5	3.6	4.5	5.0
		Ambartsumian	SSL	0.4206	0.5019	0.2539	0.0198	0.1143	0.2685	-	-	-	-	-	-
100		TSDT	SSL	0.4317	0.5104	0.2559	0.0205	0.1067	0.2753	0.6	5.2	5.5	3.5	4.7	5.0
		FSDT	SSL	0.4335	0.5104	0.2567	0.0206	0.0806	0.1410	0.1	5.2	5.1	3.2	20.1	20.8
	NNRPIM V1	Aydogdu	SSL	0.4000	0.5144	0.2516	0.0199	0.1113	0.3128	8.0	4.4	6.8	6.5	7.3	6.9
		Karama	SSL	0.4000	0.5144	0.2516	0.0199	0.1113	0.3128	8.0	4.4	6.8	6.5	5.7	3.5
		Mantari	SSL	0.4301	0.5254	0.2468	0.0206	0.1302	0.3530	1.1	2.5	8.9	1.8	1.7	5.1
		Shi	SSL	0.4160	0.5235	0.2550	0.0204	0.1078	0.2834	4.4	2.8	5.9	4.8	22.4	16.3
		Touratier	SSL	0.4019	0.5154	0.2524	0.0200	0.1083	0.2968	7.6	4.3	6.8	6.3	5.7	3.2
		Ambartsumian	SSL	0.3364	0.4578	0.2297	0.0176	0.0837	0.2227	-	-	-	-	-	-
		TSDT	SSL	0.4037	0.5163	0.2531	0.0200	0.1055	0.2812	7.0	4.2	6.5	6.1	5.8	2.9
		FSDT	SSL	0.4157	0.5149	0.2585	0.0200	0.0806	0.1450	4.1	4.3	4.4	5.9	20.1	18.6
	NNRPIM V2	Aydogdu	SSL	0.4376	0.5392	0.2724	0.0202	0.0358	0.2681	0.6	0.2	0.9	5.1	70.2	20.2
		Karama	SSL	0.4376	0.5392	0.2724	0.0202	0.0358	0.2681	0.6	0.2	0.9	5.1	69.7	17.2
		Mantari	SSL	0.4258	0.5288	0.2689	0.0228	0.0147	0.2862	2.1	1.9	0.8	8.7	88.5	23.1
		Shi	SSL	0.4336	0.5361	0.2710	0.0212	0.0276	0.2442	0.4	0.5	0.1	0.8	80.2	27.9
		Touratier	SSL	0.4372	0.5389	0.2722	0.0203	0.0340	0.2547	0.5	0.1	0.6	4.6	70.4	17.0
		Ambartsumian	SSL	0.4469	0.5460	0.2756	0.0177	-0.0086	0.1716	-	-	-	-	-	-
		TSDT	SSL	0.4367	0.5386	0.2720	0.0204	0.0322	0.2413	0.6	0	0.4	4.1	71.2	16.7
		FSDT	SSL	0.4330	0.5370	0.2700	0.0217	0.0230	0.1185	0.2	0.2	0.1	1.8	77.1	33.4

table 33 - Maximum normalized transverse displacements and stresses for a simply supported symmetric square laminate with cross-ply layers (0/90/90/0) subjected to a uniformly distributed load (UDL), a/h=4.

a/h	Solution	ESL	Load	$\bar{w}$	$\bar{\sigma}_{xx}$	$\bar{\sigma}_{yy}$	$\bar{\tau}_{xy}$	$\bar{\tau}_{yz}$	$\bar{\tau}_{xz}$
4	Exact	TSDT	UDL	-	-	-	-	-	-
		FSDT	UDL	-	-	-	-	-	-
		Elasticity	UDL	-	-	-	-	-	-
	FEM	TSDT	UDL	-	-	-	-	-	-
		FSDT	UDL	-	-	-	-	-	-
	RPIM	Aydogdu	UDL	2.8897	0.9351	0.8886	0.0865	0.4981	0.3720
		Karama	UDL	2.8897	0.9351	0.8886	0.0865	0.4981	0.3720
		Mantari	UDL	2.9411	1.0075	0.8858	0.0874	0.5188	0.4119
		Shi	UDL	2.8673	0.8909	0.8861	0.0854	0.4763	0.3446
		Touratier	UDL	2.8731	0.9109	0.8871	0.0853	0.4870	0.3575
		Ambartsumian	UDL	2.7516	0.8624	0.8667	0.0692	0.4577	0.3342
		TSDT	UDL	2.8496	0.8868	0.8839	0.0839	0.4753	0.3433
		FSDT	UDL	2.6598	0.6285	0.6320	0.0677	0.3047	0.2020
	NNRPIM V1	Aydogdu	UDL	2.7036	0.9524	0.8669	0.0978	0.5040	0.3722
		Karama	UDL	2.7036	0.9524	0.8669	0.0978	0.5040	0.3722
		Mantari	UDL	3.0719	1.1511	0.9144	0.0932	0.4798	0.4187
		Shi	UDL	2.8621	0.9530	0.9075	0.0983	0.4933	0.3652
		Touratier	UDL	2.7110	0.9319	0.8720	0.0971	0.4971	0.3609
		Ambartsumian	UDL	1.9684	0.7054	0.6794	0.0684	0.3589	0.2569
		TSDT	UDL	2.7103	0.9106	0.8753	0.0962	0.4894	0.3497
		FSDT	UDL	2.5664	0.6067	0.8336	0.0612	0.3746	0.2303
	NNRPIM V2	Aydogdu	UDL	2.9358	0.9461	0.9408	0.0892	0.5313	0.4004
		Karama	UDL	2.9358	0.9461	0.9408	0.0892	0.5313	0.4004
		Mantari	UDL	2.8636	0.9829	0.9241	0.1033	0.5395	0.4338
		Shi	UDL	2.8674	0.8925	0.9306	0.0960	0.5058	0.3732
		Touratier	UDL	2.9139	0.9214	0.9378	0.0889	0.5201	0.3855
		Ambartsumian	UDL	2.9183	0.9083	0.9319	0.0453	0.4773	0.3579
		TSDT	UDL	2.8852	0.8971	0.9331	0.0885	0.5086	0.3711
		FSDT	UDL	2.5696	0.6081	0.8358	0.0631	0.3797	0.2344

table 34 - Maximum normalized transverse displacements and stresses for a simply supported symmetric square laminate with cross-ply layers (0/90/90/0) subjected to a uniformly distributed load (UDL), a/h=10.

a/h	Solution	ESL	Load	$\bar{w}$	$\bar{\sigma}_{xx}$	$\bar{\sigma}_{yy}$	$\bar{\tau}_{xy}$	$\bar{\tau}_{yz}$	$\bar{\tau}_{xz}$
10	Exact	TSDT	UDL	-	-	-	-	-	-
		FSDT	UDL	1.0250	0.7577	0.5006	0.0470	0.3499	-
		Elasticity	UDL	-	-	-	-	-	-
	FEM	TSDT	UDL	-	-	-	-	-	-
		FSDT	UDL	-	-	-	-	-	-
	RPIM	Aydogdu	UDL	1.1116	0.7880	0.5232	0.0495	0.3850	0.4952
		Karama	UDL	1.1116	0.7880	0.5232	0.0495	0.3850	0.4952
		Mantari	UDL	1.1389	0.8069	0.5281	0.0506	0.4120	0.5649
		Shi	UDL	1.1056	0.7832	0.5192	0.0492	0.3637	0.4478
		Touratier	UDL	1.1062	0.7842	0.5209	0.0492	0.3738	0.4705
		Ambartsumian	UDL	1.0682	0.7651	0.5115	0.0451	0.3527	0.4391
		TSDT	UDL	1.0993	0.7805	0.5180	0.0488	0.3627	0.4464
		FSDT	UDL	1.0221	0.7404	0.2962	0.0469	0.2272	0.2257
	NNRPIM V1	Aydogdu	UDL	1.0511	0.8049	0.5180	0.0545	0.4145	0.5163
		Karama	UDL	1.0511	0.8049	0.5180	0.0545	0.4145	0.5163
		Mantari	UDL	1.2214	0.8994	0.5496	0.0567	0.4107	0.6074
		Shi	UDL	1.1037	0.8289	0.5316	0.0555	0.3935	0.4897
		Touratier	UDL	1.0524	0.8039	0.5185	0.0543	0.4051	0.4942
		Ambartsumian	UDL	0.8347	0.6775	0.4488	0.0436	0.3118	0.3848
		TSDT	UDL	1.0522	0.8027	0.5182	0.0541	0.3956	0.4725
		FSDT	UDL	1.0244	0.7561	0.4996	0.0468	0.2947	0.2670
	NNRPIM V2	Aydogdu	UDL	1.1292	0.8181	0.5542	0.0530	0.4228	0.5416
		Karama	UDL	1.1292	0.8181	0.5542	0.0530	0.4228	0.5416
		Mantari	UDL	1.1092	0.8149	0.5516	0.0586	0.4257	0.6016
		Shi	UDL	1.1061	0.8071	0.5458	0.0548	0.3954	0.4950
		Touratier	UDL	1.1218	0.8140	0.5696	0.0529	0.4119	0.5156
		Ambartsumian	UDL	1.1344	0.8168	0.5509	0.0381	0.3700	0.4793
		TSDT	UDL	1.1132	0.8100	0.5473	0.0527	0.4011	0.4905
		FSDT	UDL	1.0258	0.7581	0.5011	0.0483	0.2956	0.2716

table 35 - Maximum normalized transverse displacements and stresses for a simply supported symmetric square laminate with cross-ply layers (0/90/90/0) subjected to a uniformly distributed load (UDL), a/h=20.

a/h	Solution	ESL	Load	$\bar{w}$	$\bar{\sigma}_{xx}$	$\bar{\sigma}_{yy}$	$\bar{\tau}_{xy}$	$\bar{\tau}_{yz}$	$\bar{\tau}_{xz}$
20	Exact	TSDT	UDL	-	-	-	-	-	-
		FSDT	UDL	0.7694	0.8045	0.3968	0.0420	0.3228	-
		Elasticity	UDL	-	-	-	-	-	-
	FEM	TSDT	UDL	-	-	-	-	-	-
		FSDT	UDL	-	-	-	-	-	-
	RPIM	Aydogdu	UDL	0.7908	0.7861	0.3929	0.0405	0.3447	0.5325
		Karama	UDL	0.7908	0.7861	0.3929	0.0405	0.3447	0.5325
		Mantari	UDL	0.8072	0.7967	0.3960	0.0412	0.3721	0.6129
		Shi	UDL	0.7924	0.7872	0.3921	0.0406	0.3259	4.7834
		Touratier	UDL	0.7896	0.7854	0.3922	0.0405	0.3345	0.5042
		Ambartsumian	UDL	0.7669	0.7708	0.3876	0.0383	0.3180	0.4706
		TSDT	UDL	0.7880	0.7847	0.3913	0.0404	0.3247	0.4768
		FSDT	UDL	0.7574	0.7655	0.2158	0.0415	0.2100	0.2307
	NNRPIM V1	Aydogdu	UDL	0.7484	0.8040	0.3888	0.0431	0.3868	0.5685
		Karama	UDL	0.7484	0.8040	0.3888	0.0431	0.3868	0.5685
		Mantari	UDL	0.8655	0.8802	0.4116	0.0465	0.3907	0.6730
		Shi	UDL	0.7896	0.8305	0.4006	0.0444	0.3639	0.5314
		Touratier	UDL	0.7517	0.8058	0.3901	0.0431	0.3768	0.5419
		Ambartsumian	UDL	0.6101	0.6982	0.3454	0.0359	0.2938	0.4297
		TSDT	UDL	0.7543	0.8073	0.3911	0.0431	0.3670	0.5159
		FSDT	UDL	0.7680	0.8015	0.3957	0.0414	0.2738	0.2777
	NNRPIM V2	Aydogdu	UDL	0.8035	0.8210	0.4165	0.0427	0.3822	0.5873
		Karama	UDL	0.8035	0.8210	0.4165	0.0427	0.3822	0.5873
		Mantari	UDL	0.7866	0.8115	0.4138	0.0469	0.3727	0.6539
		Shi	UDL	0.7929	0.8159	0.4124	0.0440	0.3541	0.5355
		Touratier	UDL	0.8009	0.8198	0.4152	0.0427	0.3717	0.5575
		Ambartsumian	UDL	0.8147	0.8256	0.4180	0.0342	0.3226	0.5112
		TSDT	UDL	0.7980	0.8186	0.4137	0.0427	0.3615	0.5288
		FSDT	UDL	0.7699	0.8049	0.3972	0.0428	0.2676	0.2811

table 36 - Maximum normalized transverse displacements and stresses for a simply supported symmetric square laminate with cross-ply layers (0/90/90/0) subjected to a uniformly distributed load (UDL), a/h=100.

a/h	Solution	ESL	Load	$\bar{w}$	$\bar{\sigma}_{xx}$	$\bar{\sigma}_{yy}$	$\bar{\tau}_{xy}$	$\bar{\tau}_{yz}$	$\bar{\tau}_{xz}$
100	Exact	TSDT	UDL	-	-	-	-	-	-
		FSDT	UDL	0.6833	0.8420	0.3558	0.0396	0.3140	-
		Elasticity	UDL	-	-	-	-	-	-
	FEM	TSDT	UDL	-	-	-	-	-	-
		FSDT	UDL	-	-	-	-	-	-
	RPIM	Aydogdu	UDL	0.6791	0.7873	0.3400	0.0369	0.3304	0.5461
		Karama	UDL	0.6791	0.7873	0.3400	0.0369	0.3304	0.5461
		Mantari	UDL	0.6906	0.7944	0.3420	0.0373	0.3626	0.6250
		Shi	UDL	0.6837	0.7901	0.3410	0.0372	0.3127	0.4886
		Touratier	UDL	0.6796	0.7876	0.3402	0.0370	0.3207	0.5165
		Ambartsumian	UDL	0.6622	0.7744	0.3378	0.0355	0.3267	4.7735
		TSDT	UDL	0.6800	0.7878	0.3403	0.0370	0.3115	0.4879
		FSDT	UDL	0.6693	0.7733	0.1875	0.0393	0.2029	0.2317
	NNRPIM V1	Aydogdu	UDL	0.6301	0.7892	0.3309	0.0371	0.3706	0.6033
		Karama	UDL	0.6301	0.7892	0.3309	0.0371	0.3706	0.6033
		Mantari	UDL	0.6781	0.7995	0.3330	0.0381	0.3961	0.6828
		Shi	UDL	0.6555	0.8007	0.3379	0.0379	0.3501	0.5463
		Touratier	UDL	0.6332	0.7905	0.3323	0.0372	0.3595	0.5727
		Ambartsumian	UDL	0.5306	0.7081	0.3015	0.0325	0.2899	0.4366
		TSDT	UDL	0.6361	0.7915	0.3336	0.0372	0.3488	0.5426
		FSDT	UDL	0.6554	0.7869	0.3434	0.0372	0.2591	0.2806
	NNRPIM V2	Aydogdu	UDL	0.6898	0.8236	0.3600	0.0375	0.2220	0.5419
		Karama	UDL	0.6898	0.8236	0.3600	0.0375	0.2220	0.5419
		Mantari	UDL	0.6717	0.8101	0.3563	0.0420	0.1780	0.5766
		Shi	UDL	0.6836	0.8199	0.3580	0.0393	0.1914	0.4874
		Touratier	UDL	0.6891	0.8233	0.3596	0.0377	0.2132	0.5140
		Ambartsumian	UDL	0.7038	0.8307	0.3643	0.0328	0.1338	0.3852
		TSDT	UDL	0.6884	0.8230	0.3593	0.0379	0.2048	0.4863
		FSDT	UDL	0.6825	0.8216	0.3560	0.0401	0.1469	0.2404

table 37 - Maximum normalized transverse displacements and stresses for a simply supported symmetric square laminate with cross-ply layers (0/90/0/90/0) subjected to a sinusoidal load (SSL), a/h=4.

a/h	Solution	ESL	Load	$\bar{w}$	$\bar{\sigma}_{xx}$	$\bar{\sigma}_{yy}$	$\bar{\tau}_{xy}$	$\bar{\tau}_{yz}$	$\bar{\tau}_{xz}$
4	Exact	TSDT	SSL	-	-	-	-	-	-
		FSDT	SSL	-	-	-	-	-	-
		Elasticity	SSL	1.8505	0.685	0.6330	0.0384	0.2290	0.2380
	FEM	TSDT	SSL	-	-	-	-	-	-
		FSDT	SSL	1.562	0.4339	0.4991	0.0233	0.2281	0.3033
	RPIM	Aydogdu	SSL	1.5645	0.6297	0.4864	0.0322	0.2186	0.4123
		Karama	SSL	1.5645	0.6297	0.4864	0.0322	0.2145	0.4123
		Mantari	SSL	1.5324	0.6648	0.4793	0.0324	0.1939	0.4391
		Shi	SSL	1.5951	0.6077	0.4931	0.0321	0.2238	0.3912
		Touratier	SSL	1.5778	0.6178	0.4894	0.0320	0.2196	0.4014
		Ambartsumian	SSL	1.5409	0.5927	0.4840	0.0266	0.2169	0.3817
		TSDT	SSL	1.5858	0.6052	0.4917	0.0316	0.2232	0.3898
		FSDT	SSL	1.5628	0.4147	0.4771	0.0228	0.1905	0.2426
	NNRPIM V1	Aydogdu	SSL	1.4667	0.6483	0.4872	0.0341	0.2158	0.4147
		Karama	SSL	1.4667	0.6483	0.4872	0.0341	0.2158	0.4147
		Mantari	SSL	1.5885	0.7476	0.5182	0.0349	0.1941	0.4576
		Shi	SSL	1.5898	0.6601	0.5180	0.0340	0.2310	0.4104
		Touratier	SSL	1.4910	0.6401	0.4930	0.0338	0.2222	0.4061
		Ambartsumian	SSL	1.1158	0.4788	0.3853	0.0276	0.1823	0.3118
		TSDT	SSL	1.5100	0.6309	0.4979	0.0335	0.2271	0.3965
		FSDT	SSL	1.5628	0.4363	0.5020	0.0235	0.2002	0.2544
	NNRPIM V2	Aydogdu	SSL	1.5891	0.6629	0.5165	0.0303	0.2267	0.4316
		Karama	SSL	1.5891	0.6629	0.5165	0.0303	0.2267	0.4316
		Mantari	SSL	1.4923	0.6766	0.4946	0.0358	0.2013	0.4499
		Shi	SSL	1.5950	0.6323	0.5190	0.0329	0.2352	0.4093
		Touratier	SSL	1.5997	0.6496	0.5193	0.0304	0.2320	0.4200
		Ambartsumian	SSL	1.6293	0.6440	0.5260	0.0175	0.2289	0.4011
		TSDT	SSL	1.6051	0.6358	0.5213	0.0303	0.2358	0.4077
		FSDT	SSL	1.5626	0.4368	0.5024	0.0244	0.2045	0.2600

table 38 - Maximum normalized transverse displacements and stresses for a simply supported symmetric square laminate with cross-ply layers (0/90/0/90/0) subjected to a sinusoidal load (SSL), a/h=10.

a/h	Solution	ESL	Load	$\bar{w}$	$\bar{\sigma}_{xx}$	$\bar{\sigma}_{yy}$	$\bar{\tau}_{xy}$	$\bar{\tau}_{yz}$	$\bar{\tau}_{xz}$
10	Exact	TSDT	SSL	-	-	-	-	-	-
		FSDT	SSL	0.6277	0.5044	0.3852	0.0226	0.1770	0.3535
		Elasticity	SSL	0.6771	0.5450	0.4300	0.0247	0.2230	0.2580
	FEM	TSDT	SSL	-	-	-	-	-	-
		FSDT	SSL	0.6212	0.4986	0.4078	0.0219	0.1984	0.3435
	RPIM	Aydogdu	SSL	0.6186	0.5183	0.3827	0.0227	0.1944	0.4576
		Karama	SSL	0.6186	0.5183	0.3827	0.0227	0.1908	0.4576
		Mantari	SSL	0.6192	0.5328	0.3771	0.0229	0.1815	0.4782
		Shi	SSL	0.6236	0.5121	0.3879	0.0227	0.1927	0.4383
		Touratier	SSL	0.6215	0.5151	0.3855	0.0227	0.1922	0.4486
		Ambartsumian	SSL	0.6073	0.5032	0.3827	0.0213	0.1881	0.4315
		TSDT	SSL	0.6236	0.5121	0.3879	0.0227	0.1927	0.4383
		FSDT	SSL	0.6215	0.4766	0.3898	0.0214	0.1584	0.2748
	NNRPIM V1	Aydogdu	SSL	0.5857	0.5346	0.3875	0.0231	0.1949	0.4668
		Karama	SSL	0.5857	0.5346	0.3875	0.0231	0.1949	0.4668
		Mantari	SSL	0.6644	0.6003	0.4086	0.0247	0.1870	0.5130
		Shi	SSL	0.6265	0.5503	0.4070	0.0237	0.1993	0.4635
		Touratier	SSL	0.5921	0.5334	0.3918	0.0232	0.1972	0.4595
		Ambartsumian	SSL	0.4769	0.4483	0.3400	0.0201	0.1711	0.3824
		TSDT	SSL	0.5975	0.5321	0.3957	0.0232	0.1985	0.4508
		FSDT	SSL	0.6212	0.5013	0.4100	0.0219	0.1666	0.2881
	NNRPIM V2	Aydogdu	SSL	0.6280	0.5474	0.4068	0.0227	0.2015	0.4774
		Karama	SSL	0.6280	0.5474	0.4068	0.0227	0.2015	0.4774
		Mantari	SSL	0.6023	0.5465	0.3919	0.0251	0.1860	0.4869
		Shi	SSL	0.6269	0.5376	0.4101	0.0237	0.2027	4.6237
		Touratier	SSL	0.6300	0.5437	0.4094	0.0228	0.2032	0.4683
		Ambartsumian	SSL	0.6447	0.5473	0.4160	0.0177	0.1956	0.4506
		TSDT	SSL	0.6310	0.5400	0.4116	0.0229	0.2040	0.4579
		FSDT	SSL	0.6214	0.5019	0.4105	0.0228	0.1692	0.2938

table 39 - Maximum normalized transverse displacements and stresses for a simply supported symmetric square laminate with cross-ply layers (0/90/0/90/0) subjected to a sinusoidal load (SSL), a/h=20.

a/h	Solution	ESL	Load	$\bar{w}$	$\bar{\sigma}_{xx}$	$\bar{\sigma}_{yy}$	$\bar{\tau}_{xy}$	$\bar{\tau}_{yz}$	$\bar{\tau}_{xz}$
20	Exact	TSDT	SSL	-	-	-	-	-	-
		FSDT	SSL	0.4814	0.5285	0.3416	0.0217	0.1591	0.3685
		Elasticity	SSL	0.4938	0.5390	0.3800	0.0222	0.2120	0.2680
	FEM	TSDT	SSL	-	-	-	-	-	-
		FSDT	SSL	0.4796	0.5239	0.3722	0.0214	0.1827	0.3592
	RPIM	Aydogdu	SSL	0.4765	0.5112	0.3522	0.0211	0.1833	0.4739
		Karama	SSL	0.4765	0.5112	0.3522	0.0211	0.1799	0.4739
		Mantari	SSL	0.4822	0.5193	0.3521	0.0213	0.1749	0.4903
		Shi	SSL	0.4811	0.5114	0.3551	0.0212	0.1799	0.4582
		Touratier	SSL	0.4776	0.5104	0.3533	0.0211	0.1801	0.4660
		Ambartsumian	SSL	0.4660	0.5011	0.3497	0.0202	0.1753	0.4500
		TSDT	SSL	0.4784	0.5097	0.3541	0.0211	0.1795	0.4565
		FSDT	SSL	0.4798	0.5008	0.3558	0.0209	0.1460	0.2873
	NNRPIM V1	Aydogdu	SSL	0.4514	0.5267	0.3568	0.0211	0.1853	0.4862
		Karama	SSL	0.4514	0.5267	0.3568	0.0211	0.1853	0.4862
		Mantari	SSL	0.5183	0.5821	0.3800	0.0230	0.1784	0.5236
		Shi	SSL	0.4800	0.5450	0.3708	0.0218	0.1853	0.4838
		Touratier	SSL	0.4551	0.5277	0.3592	0.0212	0.1860	0.4801
		Ambartsumian	SSL	0.3709	0.4541	0.3161	0.0183	0.1600	0.4012
		TSDT	SSL	0.4584	0.5286	0.3614	0.0212	0.1860	0.4722
		FSDT	SSL	0.4790	0.5260	0.3737	0.0212	0.1537	0.3013
	NNRPIM V2	Aydogdu	SSL	0.4838	0.5404	0.3745	0.0210	0.1880	0.4893
		Karama	SSL	0.4838	0.5404	0.3745	0.0210	0.1880	0.4893
		Mantari	SSL	0.4691	0.5337	0.3664	0.0233	0.1724	0.4913
		Shi	SSL	0.4810	0.5357	0.3745	0.0219	0.1863	0.4817
		Touratier	SSL	0.4841	0.5391	0.3753	0.0211	0.1885	0.4824
		Ambartsumian	SSL	0.4950	0.5450	0.3800	0.0175	0.1727	0.4558
		TSDT	SSL	0.4842	0.5380	0.3759	0.0212	0.1882	0.4738
		FSDT	SSL	0.4797	0.5273	0.3746	0.0220	0.1531	0.3047

table 40 - Maximum normalized transverse displacements and stresses for a simply supported symmetric square laminate with cross-ply layers (0/90/0/90/0) subjected to a sinusoidal load (SSL), a/h=100.

a/h	Solution	ESL	Load	$\bar{w}$	$\bar{\sigma}_{xx}$	$\bar{\sigma}_{yy}$	$\bar{\tau}_{xy}$	$\bar{\tau}_{yz}$	$\bar{\tau}_{xz}$
100	Exact	TSDT	SSL	-	-	-	-	-	-
		FSDT	SSL	0.4333	0.5383	0.3240	0.0213	0.1519	0.3746
		Elasticity	SSL	0.4338	0.5390	0.3600	0.0213	0.2720	0.2050
	FEM	TSDT	SSL	-	-	-	-	-	-
		FSDT	SSL	0.4331	0.5345	0.3573	0.0211	0.1761	0.3655
	RPIM	Aydogdu	SSL	0.4299	0.5100	0.3398	0.0205	0.1802	0.4810
		Karama	SSL	0.4299	0.5100	0.3398	0.0205	0.1769	0.4810
		Mantari	SSL	0.4371	0.5150	0.3421	0.0207	0.1763	0.4892
		Shi	SSL	0.4330	0.5119	0.3410	0.0206	0.1757	0.4650
		Touratier	SSL	0.4303	0.5102	0.3400	0.0205	0.1764	0.4736
		Ambartsumian	SSL	0.4193	0.5015	0.3359	0.0198	0.1833	0.4519
		TSDT	SSL	0.4306	0.5103	0.3401	0.0205	0.1753	0.4645
		FSDT	SSL	0.4329	0.5103	0.3413	0.0206	0.1420	0.2917
	NNRPIM V1	Aydogdu	SSL	0.3990	0.5144	0.3370	0.0198	0.1779	0.4871
		Karama	SSL	0.3990	0.5144	0.3370	0.0198	0.1779	0.4871
		Mantari	SSL	0.4289	0.5254	0.3357	0.0206	0.1783	0.5051
		Shi	SSL	0.4151	0.5235	0.3417	0.0203	0.1793	0.4811
		Touratier	SSL	0.4009	0.5154	0.3378	0.0199	0.1778	0.4818
		Ambartsumian	SSL	0.3357	0.4578	0.3056	0.0175	0.1355	0.3668
		TSDT	SSL	0.4028	0.5162	0.3386	0.0199	0.1771	0.4743
		FSDT	SSL	0.4153	0.5150	0.3441	0.0200	0.1453	0.3008
	NNRPIM V2	Aydogdu	SSL	0.4363	0.5391	0.3611	0.0200	0.1109	0.3670
		Karama	SSL	0.4363	0.5391	0.3611	0.0200	0.1109	0.3670
		Mantari	SSL	0.4244	0.5286	0.3553	0.0226	0.0815	0.3347
		Shi	SSL	0.4325	0.5360	0.3594	0.0210	0.1007	0.3722
		Touratier	SSL	0.4360	0.5388	0.3610	0.0201	0.1089	0.3680
		Ambartsumian	SSL	0.4457	0.5456	0.3651	0.0174	0.0370	0.2225
		TSDT	SSL	0.4356	0.5385	0.3608	0.0202	0.1063	0.3662
		FSDT	SSL	0.4325	0.5369	0.3591	0.0215	0.0778	0.2325

table 41 - Maximum normalized transverse displacements and stresses for a simply supported symmetric square laminate with cross-ply layers (0/90/0/90/0) subjected to a uniformly distributed load (UDL), a/h=4.

a/h	Solution	ESL	Load	$\bar{w}$	$\bar{\sigma}_{xx}$	$\bar{\sigma}_{yy}$	$\bar{\tau}_{xy}$	$\bar{\tau}_{yz}$	$\bar{\tau}_{xz}$
4	Exact	TSDT	UDL	-	-	-	-	-	-
		FSDT	UDL						
		Elasticity	UDL	-	-	-	-	-	-
	FEM	TSDT	UDL	-	-	-	-	-	-
		FSDT	UDL	-	-	-	-	-	-
	RPIM	Aydogdu	UDL	2.3479	0.8921	0.6915	0.0668	0.4472	0.7283
		Karama	UDL	2.3479	0.8921	0.6915	0.0668	0.4389	0.7283
		Mantari	UDL	2.3015	0.9461	0.6646	0.0664	0.3915	0.7642
		Shi	UDL	2.3923	0.8591	0.7111	0.0668	0.4597	0.6984
		Touratier	UDL	2.3667	0.8740	0.7010	0.0663	0.4503	0.7128
		Ambartsumian	UDL	2.3007	0.8346	0.6961	0.0538	0.4406	0.6794
		TSDT	UDL	2.3776	0.8556	0.7091	0.0656	0.4587	0.6959
		FSDT	UDL	2.3359	0.6255	0.7090	0.0435	0.3964	0.4480
	NNRPIM V1	Aydogdu	UDL	2.2092	0.9074	0.6851	0.0770	0.4401	0.7396
		Karama	UDL	2.2092	0.9074	0.6851	0.0770	0.4401	0.7396
		Mantari	UDL	2.4171	1.0514	0.7186	0.0700	0.3601	0.7955
		Shi	UDL	2.3868	0.9110	0.7353	0.0786	0.4741	0.7528
		Touratier	UDL	2.2436	0.8924	0.6987	0.0771	0.4555	0.7299
		Ambartsumian	UDL	1.7100	0.7005	0.5717	0.0544	0.3414	0.5422
		TSDT	UDL	2.2700	0.8766	0.7106	0.0769	0.4679	0.7187
		FSDT	UDL	2.3348	0.6483	0.7375	0.0475	0.4325	0.5179
	NNRPIM V2	Aydogdu	UDL	2.3856	0.9117	0.7280	0.0673	0.4669	0.7902
		Karama	UDL	2.3856	0.9117	0.7280	0.0673	0.4669	0.7902
		Mantari	UDL	2.2456	0.9412	0.6856	0.0786	0.4085	0.8120
		Shi	UDL	2.3933	0.8694	0.7429	0.0756	0.4878	0.7655
		Touratier	UDL	2.4005	0.8923	0.7373	0.0678	0.4795	0.7752
		Ambartsumian	UDL	2.4387	0.8792	0.7468	0.0319	0.4602	0.7320
		TSDT	UDL	2.4075	0.8729	0.7450	0.0682	0.4890	0.7588
		FSDT	UDL	2.3377	0.6498	0.7393	0.0488	0.4392	0.5269

table 42 - Maximum normalized transverse displacements and stresses for a simply supported symmetric square laminate with cross-ply layers (0/90/0/90/0) subjected to a uniformly distributed load (UDL), a/h=10.

a/h	Solution	ESL	Load	$\bar{w}$	$\bar{\sigma}_{xx}$	$\bar{\sigma}_{yy}$	$\bar{\tau}_{xy}$	$\bar{\tau}_{yz}$	$\bar{\tau}_{xz}$
10	Exact	TSDT	UDL	-	-	-	-	-	-
		FSDT	UDL	0.9727	0.7649	0.5525	0.0436	0.4410	0.6901
		Elasticity	UDL	-	-	-	-	-	-
	FEM	TSDT	UDL	-	-	-	-	-	-
		FSDT	UDL	-	-	-	-	-	-
	RPIM	Aydogdu	UDL	0.9585	0.7828	0.5584	0.0427	0.4344	0.8320
		Karama	UDL	0.9585	0.7828	0.5584	0.0427	0.4264	0.8320
		Mantari	UDL	0.9587	0.8036	0.5459	0.0432	0.4053	0.8635
		Shi	UDL	0.9721	0.7768	0.5696	0.0428	0.4307	0.8027
		Touratier	UDL	0.9632	0.7784	0.5636	0.0426	0.4292	0.8173
		Ambartsumian	UDL	0.9399	0.7597	0.5600	0.0397	0.4176	0.7875
		TSDT	UDL	0.9666	0.7742	0.5681	0.0425	0.4298	0.8000
		FSDT	UDL	0.9646	0.7311	0.5752	0.0391	0.3524	0.5058
	NNRPIM V1	Aydogdu	UDL	0.9079	0.7988	0.5599	0.0469	0.4472	0.8843
		Karama	UDL	0.9079	0.7988	0.5599	0.0469	0.4472	0.8843
		Mantari	UDL	1.0282	0.8891	0.5825	0.0482	0.4037	0.9535
		Shi	UDL	0.9706	0.8194	0.5893	0.0483	0.4592	0.8977
		Touratier	UDL	0.9179	0.7968	0.5675	0.0470	0.4534	0.8747
		Ambartsumian	UDL	0.7425	0.6783	0.5000	0.0381	0.3615	0.7057
		TSDT	UDL	0.9265	0.7948	0.5744	0.0471	0.4573	0.8624
		FSDT	UDL	0.9639	0.7588	0.6003	0.0421	0.3887	0.5796
	NNRPIM V2	Aydogdu	UDL	0.9736	0.8139	0.5902	0.0453	0.4628	0.9224
		Karama	UDL	0.9736	0.8139	0.5902	0.0453	0.4628	0.9224
		Mantari	UDL	0.9343	0.8149	0.5667	0.0496	0.4210	0.9323
		Shi	UDL	0.9726	0.8010	0.5977	0.0475	0.4651	0.9042
		Touratier	UDL	0.9768	0.8087	0.5952	0.0455	0.4672	0.9082
		Ambartsumian	UDL	0.9977	0.8108	0.6034	0.0334	0.4411	0.8678
		TSDT	UDL	0.9787	0.8038	0.5994	0.0457	0.4694	0.8915
		FSDT	UDL	0.9651	0.7608	0.6020	0.0434	0.3924	0.5886

table 43 - Maximum normalized transverse displacements and stresses for a simply supported symmetric square laminate with cross-ply layers (0/90/0/90/0) subjected to a uniformly distributed load (UDL), a/h=20.

a/h	Solution	ESL	Load	$\bar{w}$	$\bar{\sigma}_{xx}$	$\bar{\sigma}_{yy}$	$\bar{\tau}_{xy}$	$\bar{\tau}_{yz}$	$\bar{\tau}_{xz}$
20	Exact	TSDT	UDL	-	-	-	-	-	-
		FSDT	UDL	0.7581	0.8080	0.0484	0.0403	0.4188	0.7166
		Elasticity	UDL	-	-	-	-	-	-
	FEM	TSDT	UDL	-	-	-	-	-	-
		FSDT	UDL	-	-	-	-	-	-
	RPIM	Aydogdu	UDL	0.7518	0.7869	0.5154	0.0377	0.4258	0.8677
		Karama	UDL	0.7518	0.7869	0.5154	0.0377	0.4179	0.8677
		Mantari	UDL	0.7605	0.7986	0.5137	0.0382	0.4074	0.8953
		Shi	UDL	0.7592	0.7874	0.5202	0.0380	0.4170	0.8402
		Touratier	UDL	0.7536	0.7859	0.5173	0.0377	0.4177	0.8539
		Ambartsumian	UDL	0.7348	0.7711	0.5122	0.0361	0.4067	0.8254
		TSDT	UDL	0.7550	0.7849	0.5189	0.0377	0.4159	0.8371
		FSDT	UDL	0.7577	0.7740	0.5225	0.0370	0.3365	0.5285
	NNRPIM V1	Aydogdu	UDL	0.7123	0.8031	0.5179	0.0397	0.4508	0.9455
		Karama	UDL	0.7123	0.8031	0.5179	0.0397	0.4508	0.9455
		Mantari	UDL	0.8160	0.8810	0.5465	0.0428	0.4226	1.0102
		Shi	UDL	0.7570	0.8290	0.5381	0.0411	0.4525	0.9547
		Touratier	UDL	0.7181	0.8045	0.5217	0.0398	0.4531	0.9361
		Ambartsumian	UDL	0.5865	0.6970	0.4629	0.0335	0.3645	0.7648
		TSDT	UDL	0.7234	0.8057	0.5253	0.0399	0.4533	0.9234
		FSDT	UDL	0.7562	0.8031	0.5457	0.0390	0.3738	0.6037
	NNRPIM V2	Aydogdu	UDL	0.7637	0.8212	0.5459	0.0393	0.4577	0.9673
		Karama	UDL	0.7637	0.8212	0.5459	0.0393	0.4577	0.9673
		Mantari	UDL	0.7409	0.8128	0.5343	0.0430	0.4137	0.9650
		Shi	UDL	0.7596	0.8152	0.5470	0.0408	0.4508	0.9557
		Touratier	UDL	0.7642	0.8196	0.5474	0.0394	0.4588	0.9548
		Ambartsumian	UDL	0.7804	0.8257	0.5530	0.0320	0.4201	0.9001
		TSDT	UDL	0.7645	0.8180	0.5486	0.0396	0.4578	0.9392
		FSDT	UDL	0.7580	0.8062	0.5479	0.0403	0.3715	0.6089

table 44 - Maximum normalized transverse displacements and stresses for a simply supported symmetric square laminate with cross-ply layers (0/90/0/90/0) subjected to a uniformly distributed load (UDL), a/h=100.

a/h	Solution	ESL	Load	$\bar{w}$	$\bar{\sigma}_{xx}$	$\bar{\sigma}_{yy}$	$\bar{\tau}_{xy}$	$\bar{\tau}_{yz}$	$\bar{\tau}_{xz}$
100	Exact	TSDT	UDL	-	-	-	-	-	-
		FSDT	UDL	0.6874	0.8264	0.4559	0.0386	0.4108	0.7267
		Elasticity	UDL	-	-	-	-	-	-
	FEM	TSDT	UDL	-	-	-	-	-	-
		FSDT	UDL	-	-	-	-	-	-
	RPIM	Aydogdu	UDL	0.6841	0.7914	0.4971	0.0357	0.4241	0.8822
		Karama	UDL	0.6841	0.7914	0.4971	0.0357	0.4163	0.8822
		Mantari	UDL	0.6953	0.7987	0.5000	0.0361	0.4157	0.8974
		Shi	UDL	0.6890	0.7942	0.4988	0.0360	0.4135	0.8530
		Touratier	UDL	0.6847	0.7917	0.4974	0.0358	0.4149	0.8688
		Ambartsumian	UDL	0.6670	0.7779	0.4915	0.0345	0.4261	0.8314
		TSDT	UDL	0.6853	0.7919	0.4977	0.0358	0.4122	0.8522
		FSDT	UDL	0.6890	0.7919	0.4995	0.0359	0.3321	0.5356
	NNRPIM V1	Aydogdu	UDL	0.6349	0.7908	0.4894	0.0356	0.4582	0.9882
		Karama	UDL	0.6349	0.7908	0.4894	0.0356	0.4582	0.9882
		Mantari	UDL	0.6814	0.8018	0.4852	0.0369	0.4554	1.0246
		Shi	UDL	0.6602	0.8027	0.4961	0.0364	0.4597	0.9741
		Touratier	UDL	0.6380	0.7921	0.4907	0.0357	0.4576	0.9771
		Ambartsumian	UDL	0.5348	0.7072	0.4462	0.0312	0.3564	0.7556
		TSDT	UDL	0.6410	0.7931	0.4920	0.0357	0.4552	0.9617
		FSDT	UDL	0.6609	0.7892	0.5013	0.0358	0.3694	0.6111
	NNRPIM V2	Aydogdu	UDL	0.6947	0.8270	0.5267	0.0357	0.3369	0.8040
		Karama	UDL	0.6947	0.8270	0.5267	0.0357	0.3369	0.8040
		Mantari	UDL	0.6759	0.8124	0.5194	0.0402	0.2686	0.7391
		Shi	UDL	0.6887	0.8229	0.5244	0.0375	0.3118	0.7975
		Touratier	UDL	0.6941	0.8266	0.5265	0.0359	0.3323	0.8014
		Ambartsumian	UDL	0.7089	0.8347	0.5313	0.0312	0.2105	0.5699
		TSDT	UDL	0.6936	0.8263	0.5263	0.0361	0.3264	0.7936
		FSDT	UDL	0.6886	0.8247	0.5236	0.0383	0.2461	0.4987

table 45 - Maximum normalized transverse displacements and stresses for a simply supported symmetric square laminate with cross-ply layers (0/90/90/0/90/90/0) subjected to a sinusoidal load (SSL), a/h=4.

a/h	Solution	ESL	Load	$\bar{w}$	$\bar{\sigma}_{xx}$	$\bar{\sigma}_{yy}$	$\bar{\tau}_{xy}$	$\bar{\tau}_{yz}$	$\bar{\tau}_{xz}$
4	Exact	TSDT	SSL	-	-	-	-	-	-
		FSDT	SSL	-	-	-	-	-	-
		Elasticity	SSL	-	-	-	-	-	-
	FEM	TSDT	SSL	-	-	-	-	-	-
		FSDT	SSL	-	-	-	-	-	-
	RPIM	Aydogdu	SSL	1.5420	0.6195	0.5033	0.0310	0.1214	0.4066
		Karama	SSL	1.5420	0.6195	0.5033	0.0310	0.1110	0.4066
		Mantari	SSL	1.5102	0.6542	0.5038	0.0313	0.0764	0.4330
		Shi	SSL	1.5729	0.5980	0.5049	0.0308	0.1371	0.3860
		Touratier	SSL	1.5554	0.6078	0.5036	0.0307	0.1241	0.3959
		Ambartsumian	SSL	1.5196	0.5837	0.4951	0.0255	0.1331	0.3763
		TSDT	SSL	1.5637	0.5957	0.5033	0.0303	0.1367	0.3846
		FSDT	SSL	1.5476	0.4203	0.4708	0.0218	0.1971	0.2385
	NNRPIM V1	Aydogdu	SSL	1.4464	0.6367	0.5071	0.0327	0.1116	0.4096
		Karama	SSL	1.4464	0.6367	0.5071	0.0327	0.1116	0.4096
		Mantari	SSL	1.5640	0.7334	0.5488	0.0335	0.0767	0.4517
		Shi	SSL	1.5675	0.6484	0.5330	0.0326	0.1417	0.4053
		Touratier	SSL	1.4705	0.6287	0.5102	0.0325	0.1255	0.4012
		Ambartsumian	SSL	1.1042	0.4714	0.3974	0.0265	0.1114	0.3093
		TSDT	SSL	1.4896	0.6199	0.5124	0.0321	0.1390	0.3917
		FSDT	SSL	1.5476	0.4422	0.4953	0.0224	0.2071	0.2501
	NNRPIM V2	Aydogdu	SSL	1.5662	0.6526	0.5335	0.0288	0.1173	0.4252
		Karama	SSL	1.5662	0.6526	0.5335	0.0288	0.1173	0.4252
		Mantari	SSL	1.4712	0.6667	0.5185	0.0345	0.0792	0.4435
		Shi	SSL	1.5728	0.6227	0.5305	0.0314	0.1441	0.4037
		Touratier	SSL	1.5770	0.6396	0.5335	0.0288	0.1311	0.4139
		Ambartsumian	SSL	1.6065	0.6343	0.5377	0.0165	0.1405	0.3952
		TSDT	SSL	1.5828	0.6261	0.5329	0.0288	0.1444	0.4019
		FSDT	SSL	1.5475	0.4427	0.4958	0.0233	0.2116	0.2556

table 46 - Maximum normalized transverse displacements and stresses for a simply supported symmetric square laminate with cross-ply layers (0/90/90/0/90/90/0) subjected to a sinusoidal load (SSL), a/h=10.

a/h	Solution	ESL	Load	$\bar{w}$	$\bar{\sigma}_{xx}$	$\bar{\sigma}_{yy}$	$\bar{\tau}_{xy}$	$\bar{\tau}_{yz}$	$\bar{\tau}_{xz}$
10	Exact	TSDT	SSL	-	-	-	-	-	-
		FSDT	SSL	0.6213	0.5021	0.4107	0.0221	0.1998	0.3459
		Elasticity	SSL	-	-	-	-	-	-
	FEM	TSDT	SSL	-	-	-	-	-	-
		FSDT	SSL	-	-	-	-	-	-
	RPIM	Aydogdu	SSL	0.6123	0.5177	0.3999	0.0223	0.1033	0.4428
		Karama	SSL	0.6123	0.5177	0.3999	0.0223	0.1033	0.4428
		Mantari	SSL	0.6137	0.5331	0.3962	0.0226	0.0746	0.4614
		Shi	SSL	0.6206	0.5127	0.4054	0.0225	0.1238	0.4268
		Touratier	SSL	0.6151	0.5143	0.4023	0.0223	0.1137	0.4347
		Ambartsumian	SSL	0.6010	0.5022	0.3987	0.0210	0.1208	0.4185
		TSDT	SSL	0.6171	0.5110	0.4043	0.0223	0.1235	0.4254
		FSDT	SSL	0.6165	0.4774	0.4046	0.0211	0.1715	0.2675
	NNRPIM V1	Aydogdu	SSL	0.5798	0.5338	0.4060	0.0228	0.1053	0.4523
		Karama	SSL	0.5798	0.5338	0.4060	0.0228	0.1053	0.4523
		Mantari	SSL	0.6582	0.6000	0.4319	0.0243	0.0771	0.4955
		Shi	SSL	0.6199	0.5487	0.4255	0.0233	0.1279	0.4505
		Touratier	SSL	0.5860	0.5323	0.4100	0.0228	0.1164	0.4459
		Ambartsumian	SSL	0.4725	0.4476	0.3550	0.0198	0.1093	0.3721
		TSDT	SSL	0.5914	0.5308	0.4135	0.0228	0.1271	0.4380
		FSDT	SSL	0.6162	0.5021	0.4255	0.0216	0.1804	0.2805
	NNRPIM V2	Aydogdu	SSL	0.6217	0.5470	0.4247	0.0222	0.1090	0.4615
		Karama	SSL	0.6217	0.5470	0.4247	0.0222	0.1090	0.4615
		Mantari	SSL	0.5970	0.5471	0.4109	0.0247	0.0765	0.4696
		Shi	SSL	0.6204	0.5365	0.4271	0.0233	0.1301	0.4487
		Touratier	SSL	0.6235	0.5429	0.4269	0.0223	0.1201	0.4534
		Ambartsumian	SSL	0.6379	0.5462	0.4334	0.0174	0.1258	0.4367
		TSDT	SSL	0.6245	0.5389	0.4287	0.0224	0.1307	0.4441
		FSDT	SSL	0.6164	0.5027	0.4261	0.0224	0.1833	0.2860

table 47 - Maximum normalized transverse displacements and stresses for a simply supported symmetric square laminate with cross-ply layers (0/90/90/0/90/90/0) subjected to a sinusoidal load (SSL), a/h=20.

a/h	Solution	ESL	Load	$\bar{w}$	$\bar{\sigma}_{xx}$	$\bar{\sigma}_{yy}$	$\bar{\tau}_{xy}$	$\bar{\tau}_{yz}$	$\bar{\tau}_{xz}$
20	Exact	TSDT	SSL	-	-	-	-	-	-
		FSDT	SSL	0.4796	0.5276	0.3748	0.0215	0.1840	0.3617
		Elasticity	SSL	-	-	-	-	-	-
	FEM	TSDT	SSL	-	-	-	-	-	-
		FSDT	SSL	-	-	-	-	-	-
	RPIM	Aydogdu	SSL	0.4747	0.5111	0.3743	0.0210	0.1087	0.4560
		Karama	SSL	0.4642	0.5008	0.3709	0.0201	0.1149	0.4348
		Mantari	SSL	0.4807	0.5196	0.3749	0.0213	0.0733	0.4696
		Shi	SSL	0.4792	0.5111	0.3770	0.0211	0.1178	0.4429
		Touratier	SSL	0.4757	0.5102	0.3752	0.0210	0.1087	0.4493
		Ambartsumian	SSL	0.4642	0.5008	0.3709	0.0201	0.1149	0.4348
		TSDT	SSL	0.4765	0.5094	0.3760	0.0210	0.1175	0.4413
		FSDT	SSL	0.4783	0.5008	0.3774	0.0208	0.1611	0.2794
	NNRPIM V1	Aydogdu	SSL	0.4497	0.5266	0.3801	0.0210	0.1021	0.4684
		Karama	SSL	0.4497	0.5266	0.3801	0.0210	0.1021	0.4684
		Mantari	SSL	0.5165	0.5822	0.4069	0.0229	0.0751	0.5023
		Shi	SSL	0.4781	0.5446	0.3947	0.0217	0.1214	0.4686
		Touratier	SSL	0.4533	0.5275	0.3823	0.0211	0.1121	0.4635
		Ambartsumian	SSL	0.3696	0.4540	0.3358	0.0182	0.1043	0.3885
		TSDT	SSL	0.4566	0.5283	0.3845	0.0211	0.1216	0.4570
		FSDT	SSL	0.4775	0.5261	0.3964	0.0211	0.1695	0.2931
	NNRPIM V2	Aydogdu	SSL	0.4820	0.5404	0.3976	0.0209	0.1040	0.4699
		Karama	SSL	0.4820	0.5404	0.3976	0.0209	0.1040	0.4699
		Mantari	SSL	0.4676	0.5341	0.3893	0.0231	0.0725	0.4705
		Shi	SSL	0.4791	0.5354	0.3974	0.0217	0.1223	0.4653
		Touratier	SSL	0.4822	0.5390	0.3983	0.0210	0.1139	0.4644
		Ambartsumian	SSL	0.4930	0.5447	0.4032	0.0173	0.1140	0.4395
		TSDT	SSL	0.4823	0.5377	0.3988	0.0211	0.1233	0.4572
		FSDT	SSL	0.4783	0.5274	0.3974	0.0219	0.1694	0.2962

table 48 - Maximum normalized transverse displacements and stresses for a simply supported symmetric square laminate with cross-ply layers (0/90/90/0/90/90/0) subjected to a sinusoidal load (SSL), a/h=100.

a/h	Solution	ESL	Load	$\bar{w}$	$\bar{\sigma}_{xx}$	$\bar{\sigma}_{yy}$	$\bar{\tau}_{xy}$	$\bar{\tau}_{yz}$	$\bar{\tau}_{xz}$
100	Exact	TSDT	SSL	-	-	-	-	-	-
		FSDT	SSL	0.4332	0.5382	0.3598	0.0213	0.1774	0.3683
		Elasticity	SSL	-	-	-	-	-	-
	FEM	TSDT	SSL	-	-	-	-	-	-
		FSDT	SSL	-	-	-	-	-	-
	RPIM	Aydogdu	SSL	0.4298	0.5100	0.3640	0.0205	0.1079	0.4619
		Karama	SSL	0.4298	0.5100	0.3640	0.0205	0.0987	0.4619
		Mantari	SSL	0.4370	0.5150	0.3666	0.0207	0.0745	0.4672
		Shi	SSL	0.4329	0.5119	0.3653	0.0206	0.1161	0.4489
		Touratier	SSL	0.4302	0.5102	0.3642	0.0205	0.1076	0.4559
		Ambartsumian	SSL	0.4192	0.5015	0.3595	0.0198	0.1208	0.4360
		TSDT	SSL	0.4305	0.5103	0.3643	0.0205	0.1159	0.4484
		FSDT	SSL	0.4329	0.5103	0.3655	0.0206	0.1580	0.2836
	NNRPIM V1	Aydogdu	SSL	0.3989	0.5144	0.3619	0.0198	0.0991	0.4677
		Karama	SSL	0.3989	0.5144	0.3619	0.0198	0.0991	0.4677
		Mantari	SSL	0.4288	0.5254	0.3620	0.0205	0.0747	0.4846
		Shi	SSL	0.4150	0.5234	0.3670	0.0203	0.1183	0.4652
		Touratier	SSL	0.4009	0.5154	0.3627	0.0199	0.1083	0.4639
		Ambartsumian	SSL	0.3356	0.4577	0.3273	0.0175	0.0892	0.3539
		TSDT	SSL	0.4027	0.5162	0.3634	0.0199	0.1170	0.4580
		FSDT	SSL	0.4153	0.5150	0.3686	0.0200	0.1617	0.2928
	NNRPIM V2	Aydogdu	SSL	0.4362	0.5391	0.3866	0.0199	0.0651	0.3448
		Karama	SSL	0.4362	0.5391	0.3866	0.0199	0.0651	0.3448
		Mantari	SSL	0.4243	0.5287	0.3801	0.0226	0.0371	0.3133
		Shi	SSL	0.4324	0.5360	0.3847	0.0210	0.0711	0.3540
		Touratier	SSL	0.4359	0.5388	0.3864	0.0200	0.0701	0.3475
		Ambartsumian	SSL	0.4455	0.5456	0.3908	0.0174	0.0295	0.2067
		TSDT	SSL	0.4355	0.5385	0.3863	0.0201	0.0745	0.3474
		FSDT	SSL	0.4324	0.5369	0.3845	0.0215	0.0933	0.2240

table 49 - Maximum normalized transverse displacements and stresses for a simply supported symmetric square laminate with cross-ply layers (0/90/90/0/90/90/0) subjected to a uniformly distributed load (UDL), a/h=4.

a/h	Solution	ESL	Load	$\bar{w}$	$\bar{\sigma}_{xx}$	$\bar{\sigma}_{yy}$	$\bar{\tau}_{xy}$	$\bar{\tau}_{yz}$	$\bar{\tau}_{xz}$
4	Exact	TSDT	UDL	-	-	-	-	-	-
		FSDT	UDL	-	-	-	-	-	-
		Elasticity	UDL	-	-	-	-	-	-
	FEM	TSDT	UDL	-	-	-	-	-	-
		FSDT	UDL	-	-	-	-	-	-
	RPIM	Aydogdu	UDL	2.3146	0.8787	0.7115	0.0642	0.2421	0.7296
		Karama	UDL	2.3146	0.8787	0.7115	0.0642	0.2214	0.7296
		Mantari	UDL	2.2709	0.9331	0.6959	0.0639	0.1500	0.7658
		Shi	UDL	2.3584	0.8459	0.7244	0.0642	0.2749	0.6998
		Touratier	UDL	2.3330	0.8606	0.7175	0.0638	0.2483	0.7141
		Ambartsumian	UDL	2.2684	0.8224	0.7086	0.0517	0.2640	0.6802
		TSDT	UDL	2.3439	0.8425	0.7223	0.0631	0.2743	0.6972
		FSDT	UDL	2.3116	0.6334	0.7022	0.0416	0.4009	0.4465
	NNRPIM V1	Aydogdu	UDL	2.1801	0.8909	0.7097	0.0735	0.2211	0.7436
		Karama	UDL	2.1801	0.8909	0.7097	0.0735	0.2211	0.7436
		Mantari	UDL	2.3815	1.0309	0.7585	0.0670	0.1394	0.8016
		Shi	UDL	2.3532	0.8940	0.7524	0.0755	0.2833	0.7595
		Touratier	UDL	2.2136	0.8760	0.7193	0.0737	0.2500	0.7340
		Ambartsumian	UDL	1.6931	0.6885	0.5885	-0.0523	0.2050	0.5435
		TSDT	UDL	2.2395	0.8606	0.7276	0.0735	0.2786	0.7229
		FSDT	UDL	2.3105	0.6559	0.7299	-0.0456	0.4356	0.5199
	NNRPIM V2	Aydogdu	UDL	2.3516	0.8988	0.7471	0.0639	0.2349	0.7954
		Karama	UDL	2.3516	0.8988	0.7471	0.0639	0.2349	0.7954
		Mantari	UDL	2.2160	0.9296	0.7153	0.0755	0.1563	0.8179
		Shi	UDL	2.3593	0.8566	0.7550	0.0725	0.2912	0.7718
		Touratier	UDL	2.3661	0.8794	0.7527	0.0644	0.2636	0.7805
		Ambartsumian	UDL	2.4040	0.8666	0.7588	0.0300	0.2757	0.7350
		TSDT	UDL	2.3732	0.8601	0.7571	0.0648	0.2915	0.7642
		FSDT	UDL	2.3134	0.6573	0.7317	-0.0468	0.4427	0.5286

table 50 - Maximum normalized transverse displacements and stresses for a simply supported symmetric square laminate with cross-ply layers (0/90/90/0/90/90/0) subjected to a uniformly distributed load (UDL), a/h=10.

a/h	Solution	ESL	Load	$\bar{w}$	$\bar{\sigma}_{xx}$	$\bar{\sigma}_{yy}$	$\bar{\tau}_{xy}$	$\bar{\tau}_{yz}$	$\bar{\tau}_{xz}$
10	Exact	TSDT	UDL	-	-	-	-	-	-
		FSDT	UDL	0.9643	0.7605	0.6016	0.0422	0.463	0.6927
		Elasticity	UDL	-	-	-	-	-	-
	FEM	TSDT	UDL	-	-	-	-	-	-
		FSDT	UDL	-	-	-	-	-	-
	RPIM	Aydogdu	UDL	0.9500	0.7819	0.5887	0.0418	0.2426	0.8170
		Karama	UDL	0.9500	0.7819	0.5887	0.0418	0.2219	0.8170
		Mantari	UDL	0.9517	0.8045	0.5788	0.0424	0.1599	0.8455
		Shi	UDL	0.9629	0.7747	0.5991	0.0420	0.2657	0.7907
		Touratier	UDL	0.9543	0.7769	0.5934	0.0418	0.2441	0.8037
		Ambartsumian	UDL	0.9309	0.7577	0.5886	0.0389	0.2580	0.7754
		TSDT	UDL	0.9574	0.7721	0.5975	0.0417	0.2652	0.7880
		FSDT	UDL	0.9573	0.7312	0.6033	0.0384	0.3673	0.4999
	NNRPIM V1	Aydogdu	UDL	0.9001	0.7967	0.5926	0.0458	0.2308	0.8735
		Karama	UDL	0.9001	0.7967	0.5926	0.0458	0.2308	0.8735
		Mantari	UDL	1.0205	0.8890	0.6214	0.0472	0.1602	0.9415
		Shi	UDL	0.9615	0.8160	0.6220	0.0473	0.2823	0.8918
		Touratier	UDL	0.9096	0.7940	0.5997	0.0459	0.2559	0.8654
		Ambartsumian	UDL	0.7363	0.6755	0.5273	0.0373	0.2228	0.6977
		TSDT	UDL	0.9649	0.8124	0.6215	0.0442	0.2396	0.9111
		FSDT	UDL	0.9566	0.7581	0.6297	-0.0413	0.4027	0.5772
	NNRPIM V2	Aydogdu	UDL	0.9649	0.8124	0.6215	0.0442	0.2396	0.9111
		Karama	UDL	0.9275	0.8153	0.6600	0.0486	0.1658	0.9191
		Mantari	UDL	0.9275	0.8153	0.5997	0.0486	0.1658	0.9191
		Shi	UDL	0.9633	0.7982	0.6281	0.0465	0.2862	0.8974
		Touratier	UDL	0.9676	0.8066	0.6260	0.0444	0.2643	0.8986
		Ambartsumian	UDL	0.9693	0.8011	0.6298	0.0445	0.2880	0.8835
		TSDT	UDL	0.9649	0.8124	0.6215	0.0442	0.2396	0.9111
		FSDT	UDL	0.9578	0.7600	0.6315	-0.0426	0.4072	0.5858

table 51 - Maximum normalized transverse displacements and stresses for a simply supported symmetric square laminate with cross-ply layers (0/90/90/0/90/90/0) subjected to a uniformly distributed load (UDL), a/h=20.

a/h	Solution	ESL	Load	$\bar{w}$	$\bar{\sigma}_{xx}$	$\bar{\sigma}_{yy}$	$\bar{\tau}_{xy}$	$\bar{\tau}_{yz}$	$\bar{\tau}_{xz}$
20	Exact	TSDT	UDL	-	-	-	-	-	-
		FSDT	UDL	0.7575	0.8059	0.5475	0.0396	0.4438	0.7212
		Elasticity	UDL	-	-	-	-	-	-
	FEM	TSDT	UDL	-	-	-	-	-	-
		FSDT	UDL	-	-	-	-	-	-
	RPIM	Aydogdu	UDL	0.7501	0.7861	0.5556	0.0374	0.2407	0.8474
		Karama	UDL	0.7501	0.7861	0.5556	0.0374	0.2201	0.8474
		Mantari	UDL	0.7594	0.7985	0.5549	0.0379	0.1625	0.8703
		Shi	UDL	0.7573	0.7861	0.5603	0.0376	0.2604	0.8245
		Touratier	UDL	0.7517	0.7847	0.5573	0.0374	0.2405	0.8358
		Ambartsumian	UDL	0.7329	0.7698	0.5511	0.0357	0.2541	0.8095
		TSDT	UDL	0.7531	0.7835	0.5589	0.0374	0.2597	0.8214
		FSDT	UDL	0.7563	0.7730	0.5625	0.0367	0.3546	0.5219
	NNRPIM V1	Aydogdu	UDL	0.7108	0.8011	0.5604	0.0392	0.2350	0.9297
		Karama	UDL	0.7108	0.8011	0.5604	0.0392	0.2350	0.9297
		Mantari	UDL	0.8149	0.8804	0.5944	0.0423	0.1687	0.9911
		Shi	UDL	0.7552	0.8266	0.5817	0.0406	0.2808	0.9452
		Touratier	UDL	0.7164	0.8022	0.5642	0.0393	0.2583	0.9227
		Ambartsumian	UDL	0.5852	0.6944	0.4994	0.0331	0.2265	0.7541
		TSDT	UDL	0.7217	0.8032	0.5677	0.0394	0.2804	0.9123
		FSDT	UDL	0.7548	0.8011	0.5876	-0.0386	0.3909	0.6009
	NNRPIM V2	Aydogdu	UDL	0.7619	0.8195	0.5880	0.0388	0.2396	0.9500
		Karama	UDL	0.7619	0.8195	0.5880	0.0388	0.2396	0.9500
		Mantari	UDL	0.7397	0.8116	0.5762	0.0425	0.1649	0.9449
		Shi	UDL	0.7576	0.8128	0.5888	0.0403	0.2807	0.9445
		Touratier	UDL	0.7623	0.8176	0.5894	0.0389	0.2626	0.9399
		Ambartsumian	UDL	0.7784	0.8237	0.5952	0.0316	0.2624	0.8870
		TSDT	UDL	0.7624	0.8158	0.5906	0.0391	0.2843	0.9268
		FSDT	UDL	0.7565	0.8042	0.5900	-0.0399	0.3897	0.6054

table 52 - Maximum normalized transverse displacements and stresses for a simply supported symmetric square laminate with cross-ply layers (0/90/90/0/90/90/0) subjected to a uniformly distributed load (UDL), a/h=100.

a/h	Solution	ESL	Load	$\bar{w}$	$\bar{\sigma}_{xx}$	$\bar{\sigma}_{yy}$	$\bar{\tau}_{xy}$	$\bar{\tau}_{yz}$	$\bar{\tau}_{xz}$
100	Exact	TSDT	UDL	-	-	-	-	-	-
		FSDT	UDL	0.6896	0.8260	0.5241	0.0381	0.4365	0.7322
		Elasticity	UDL	-	-	-	-	-	-
	FEM	TSDT	UDL	-	-	-	-	-	-
		FSDT	UDL	-	-	-	-	-	-
	RPIM	Aydogdu	UDL	0.6851	0.7903	0.5417	0.0356	0.2411	0.8601
		Karama	UDL	0.6851	0.7903	0.5417	0.0356	0.2205	0.8601
		Mantari	UDL	0.6963	0.7977	0.5451	0.0360	0.1666	0.8700
		Shi	UDL	0.6899	0.7932	0.5435	0.0358	0.2594	0.8359
		Touratier	UDL	0.6857	0.7906	0.5420	0.0356	0.2402	0.8491
		Ambartsumian	UDL	0.6679	0.7768	0.5350	0.0343	0.2670	0.8144
		TSDT	UDL	0.6862	0.7908	0.5422	0.0356	0.2587	0.8351
		FSDT	UDL	0.6900	0.7909	0.5441	-0.0358	0.3515	0.5289
	NNRPIM V1	Aydogdu	UDL	0.6358	0.7886	0.5354	0.0353	0.2398	0.9701
		Karama	UDL	0.6358	0.7886	0.5354	0.0353	0.2398	0.9701
		Mantari	UDL	0.6824	0.8002	0.5322	0.0366	0.1802	1.0046
		Shi	UDL	0.6612	0.8006	0.5424	0.0362	0.2854	0.9631
		Touratier	UDL	0.6390	0.7899	0.5367	0.0354	0.2619	0.9619
		Ambartsumian	UDL	0.5356	0.7046	0.4869	0.0310	0.2202	0.7446
		TSDT	UDL	0.6419	0.7909	0.5378	0.0355	0.2826	0.9494
		FSDT	UDL	0.6618	0.7871	0.5463	-0.0356	0.3875	0.6085
	NNRPIM V2	Aydogdu	UDL	0.6956	0.8249	0.5737	0.0354	0.1801	0.7784
		Karama	UDL	0.6956	0.8249	0.5737	0.0354	0.1801	0.7784
		Mantari	UDL	0.6768	0.8101	0.5653	0.0399	0.1094	0.7127
		Shi	UDL	0.6896	0.8207	0.5713	0.0372	0.1991	0.7798
		Touratier	UDL	0.6950	0.8245	0.5735	0.0356	0.1945	0.7791
		Ambartsumian	UDL	0.7098	0.8329	0.5786	0.0309	0.1334	0.5511
		TSDT	UDL	0.6945	0.8242	0.5733	0.0358	0.2075	0.7746
		FSDT	UDL	0.6896	0.8225	0.5707	-0.0380	0.2655	0.4930

Antisymmetric Cross-Ply Laminates

table 53 - Maximum normalized transverse displacements and stresses for two antisymmetric cross-ply square laminates subjected to a sinusoidal load (SSL), with the boundary conditions of the Case 1, a/h=5.

				Cross-ply laminate (0/90)				Cross-ply laminate $(0/90)_5$			
a/h	**Solution**	**ESL**	**Load**	$\bar{w}$	$\bar{\sigma}_{xx}\times10$	$\bar{\sigma}_{yy}\times10$	$\bar{\tau}_{yz}\times10$	$\bar{w}$	$\bar{\sigma}_{xx}\times10$	$\bar{\sigma}_{yy}\times10$	$\bar{\tau}_{yz}\times10$
5	Exact	TSDT	SSL	1.6670	8.3850	8.3850	3.1550	1.1290	6.3400	6.3400	3.3620
		FSDT	SSL	1.7580	7.1570	7.1570	2.7290	1.1370	5.0090	5.0090	2.7290
	FEM	TSDT	SSL	1.6670	7.6690	7.6690	-	1.1350	5.7620	5.7620	-
		FSDT	SSL	1.7590	6.9480	6.9480	-	1.1370	4.8640	4.8640	-
	RPIM	Mantari	SSL	1.5920	8.1979	8.2018	3.2034	1.1012	6.3645	6.3680	3.5721
		Shi	SSL	1.6635	7.9902	7.9907	2.9957	1.1291	6.0442	6.0445	3.1971
		Touratier	SSL	1.6403	8.0109	8.0121	3.0418	1.1182	6.0930	6.0937	3.2732
		Ambartsumian	SSL	1.6119	7.8120	7.8216	2.9067	1.0920	5.9064	5.9129	3.1095
		TSDT	SSL	1.6550	7.9626	7.9634	2.9855	1.1227	6.0216	6.0222	3.1864
		FSDT	SSL	1.7590	6.7937	6.7938	2.1631	1.1369	4.7545	4.7546	2.1631
	NNRPIM V1	Mantari	SSL	1.6310	9.1658	9.1658	3.2227	1.1522	7.1657	7.1657	3.7068
		Shi	SSL	1.6376	8.5889	8.5889	3.1072	1.1237	6.5188	6.5188	3.3345
		Touratier	SSL	1.5210	8.1811	8.1811	3.0543	1.0589	6.3113	6.3113	3.3232
		Ambartsumian	SSL	1.1248	6.1398	6.1398	2.3703	0.8231	4.9985	4.9985	2.6837
		TSDT	SSL	1.5486	8.1845	8.1845	3.0161	1.0706	6.2669	6.2669	3.2507
		FSDT	SSL	1.7586	7.1465	7.1465	2.2735	1.1369	5.0021	5.0021	2.2730
	NNRPIM V2	Mantari	SSL	1.5619	8.3759	8.3759	3.3028	1.0743	6.5020	6.5020	3.6913
		Shi	SSL	1.6707	8.3432	8.3432	3.1482	1.1299	6.3063	6.3063	3.3592
		Touratier	SSL	1.6707	8.4528	8.4528	3.1901	1.1346	6.4187	6.4187	3.4429
		Ambartsumian	SSL	1.7103	8.5095	8.5095	3.0377	1.1569	6.4216	6.4216	3.2947
		TSDT	SSL	1.6823	8.3925	8.3925	3.1300	1.1371	6.3379	6.3379	3.3499
		FSDT	SSL	1.7588	7.1548	7.1548	2.3189	1.1368	5.0072	5.0072	2.3218

table 54 - Maximum normalized transverse displacements and stresses for two antisymmetric cross-ply square laminates subjected to a sinusoidal load (SSL), with the boundary conditions of the Case 1, a/h=10.

				Cross-ply laminate (0/90)				Cross-ply laminate $(0/90)_5$			
a/h	**Solution**	**ESL**	**Load**	$\bar{w}$	$\bar{\sigma}_{xx}\times10$	$\bar{\sigma}_{yy}\times10$	$\bar{\tau}_{yz}\times10$	$\bar{w}$	$\bar{\sigma}_{xx}\times10$	$\bar{\sigma}_{yy}\times10$	$\bar{\tau}_{yz}\times10$
10	Exact	TSDT	SSL	1.2160	7.4680	7.4680	3.1900	0.6160	5.3460	5.3460	3.4080
		FSDT	SSL	1.2370	7.1570	7.1570	2.7290	0.6150	5.0090	5.0090	2.7290
	FEM	TSDT	SSL	1.2140	6.8290	6.8290	-	0.6190	4.8420	4.8420	-
		FSDT	SSL	1.2380	6.9480	6.9480	-	0.6160	4.8630	4.8630	-
	RPIM	Mantari	SSL	1.2032	7.1949	7.1972	0.5151	0.6159	5.2028	5.2039	3.6912
		Shi	SSL	1.2141	7.1109	7.1112	0.5161	0.6161	5.0899	5.0900	3.2419
		Touratier	SSL	1.2038	7.0985	7.0991	0.5125	0.6119	5.0905	5.0907	3.3323
		Ambartsumian	SSL	1.1769	6.9595	6.9655	0.4870	0.5967	4.9858	4.9882	3.1618
		TSDT	SSL	1.2079	7.0876	7.0881	0.5131	0.6127	5.0725	5.0727	3.2334
		FSDT	SSL	1.2378	6.7936	6.7937	2.1636	1.1369	4.7545	4.7546	2.1631
	NNRPIM V1	Mantari	SSL	1.2559	8.0938	8.0938	3.3376	0.6601	5.8639	5.8639	3.9078
		Shi	SSL	1.1976	7.6125	7.6125	3.1595	0.6151	5.4477	5.4477	3.3947
		Touratier	SSL	1.1204	7.2570	7.2570	3.1193	0.5826	5.2701	5.2701	3.4132
		Ambartsumian	SSL	0.8483	5.7006	5.7006	2.4491	0.4692	4.4481	4.4481	2.8444
		TSDT	SSL	1.1337	7.2862	7.2862	3.0721	0.5869	5.2700	5.2700	3.3250
		FSDT	SSL	1.2365	7.1407	7.1407	2.2749	0.6154	5.0005	5.0005	2.2739
	NNRPIM V2	Mantari	SSL	1.1783	7.3633	7.3633	3.3009	0.5994	5.3373	5.3373	3.7797
		Shi	SSL	1.2185	7.4362	7.4362	3.1740	0.6161	5.3261	5.3261	3.4113
		Touratier	SSL	1.2255	7.4966	7.4966	3.1918	0.6203	5.3729	5.3729	3.4928
		Ambartsumian	SSL	1.2517	7.5871	7.5871	2.9676	0.6335	5.4226	5.4226	3.3137
		TSDT	SSL	1.2273	7.4778	7.4778	3.1298	0.6202	5.3500	5.3500	3.3911
		FSDT	SSL	1.2376	7.1546	7.1546	2.3032	0.6156	5.0071	5.0071	2.3151

table 55 - Maximum normalized transverse displacements and stresses for two antisymmetric cross-ply square laminates subjected to a sinusoidal load (SSL), with the boundary conditions of the Case 2, a/h=5.

				Cross-ply laminate (0/90)				Cross-ply laminate $(0/90)_5$			
a/h	**Solution**	**ESL**	**Load**	$\bar{w}$	$\bar{\sigma}_{xx}\times10$	$\bar{\sigma}_{yy}\times10$	$\bar{\tau}_{yz}\times10$	$\bar{w}$	$\bar{\sigma}_{xx}\times10$	$\bar{\sigma}_{yy}\times10$	$\bar{\tau}_{yz}\times10$
5	Exact	TSDT	SSL	1.3330	6.8160	6.7250	2.5430	1.0010	5.1960	5.6350	2.9740
		FSDT	SSL	1.4770	5.3380	6.0340	2.2970	1.0450	3.7070	4.6280	2.4980
	FEM	TSDT	SSL	1.3170	6.7320	6.2850	-	0.9950	5.0470	5.2090	-
		FSDT	SSL	1.4780	5.4650	5.9140	-	1.0450	3.7550	4.5110	-
	RPIM	Mantari	SSL	1.2304	5.9096	6.0566	2.3478	0.9468	4.7948	5.3003	2.9546
		Shi	SSL	1.3608	5.7776	6.3537	2.3540	1.0167	4.5442	5.3624	2.8101
		Touratier	SSL	1.3511	5.9797	6.4138	2.4128	1.0145	4.8113	5.4413	2.9019
		Ambartsumian	SSL	1.3545	6.0489	6.3899	2.3694	1.0072	4.9370	5.3642	2.8177
		TSDT	SSL	1.3692	5.9076	6.4121	2.3806	1.0219	4.7168	5.4048	2.8379
		FSDT	SSL	1.4777	4.3106	5.6026	1.7558	1.0451	3.1128	4.3546	1.9543
	NNRPIM V1	Mantari	SSL	1.2131	7.6103	6.8109	2.4324	0.9579	6.1038	5.9608	3.0939
		Shi	SSL	1.3251	7.0447	6.9439	2.5232	1.0032	5.3863	5.8228	2.9689
		Touratier	SSL	1.2118	6.7694	6.4946	2.4440	0.9315	5.2835	5.5400	2.9133
		Ambartsumian	SSL	0.8402	5.0256	4.5034	1.7763	0.6738	4.0887	4.0201	2.1682
		TSDT	SSL	1.2433	6.7461	6.5515	2.4307	0.9479	5.2182	5.5413	2.8686
		FSDT	SSL	1.4878	5.3524	6.0663	1.9220	1.0502	3.7157	4.6444	2.0914
	NNRPIM V2	Mantari	SSL	1.1905	6.8570	6.4071	2.5342	0.9137	5.3648	5.5405	3.1246
		Shi	SSL	1.3492	6.7717	6.7632	2.5516	1.0083	5.1424	5.6459	2.9881
		Touratier	SSL	1.3410	6.9520	6.8131	2.5746	1.0087	5.3525	5.7250	3.0534
		Ambartsumian	SSL	1.3527	7.0292	6.7687	2.4238	1.0150	5.4082	5.6598	2.8886
		TSDT	SSL	1.3581	6.8719	6.8024	2.5389	1.0155	5.2540	5.6784	2.9838
		FSDT	SSL	1.4717	5.3188	6.0036	1.9399	1.0421	3.6952	4.6122	2.1197

table 56 - Maximum normalized transverse displacements and stresses for two antisymmetric cross-ply square laminates subjected to a sinusoidal load (SSL), with the boundary conditions of the Case 2, a/h=10.

				Cross-ply laminate (0/90)				Cross-ply laminate $(0/90)_5$			
a/h	**Solution**	**ESL**	**Load**	$\bar{w}$	$\bar{\sigma}_{xx}\times10$	$\bar{\sigma}_{yy}\times10$	$\bar{\tau}_{yz}\times10$	$\bar{w}$	$\bar{\sigma}_{xx}\times10$	$\bar{\sigma}_{yy}\times10$	$\bar{\tau}_{yz}\times10$
10	Exact	TSDT	SSL	0.8480	5.9100	5.2190	2.2900	0.4730	4.0660	4.1100	2.6220
		FSDT	SSL	0.8830	5.4940	5.1090	1.9930	0.4800	3.6420	3.9040	2.1260
	FEM	TSDT	SSL	0.8380	5.9140	4.9320	-	0.4710	4.0300	3.8170	-
		FSDT	SSL	0.8830	5.6680	5.0820	-	0.4800	3.7540	3.8520	-
	RPIM	Mantari	SSL	0.8211	4.7758	4.5706	2.1025	0.4617	3.3943	3.7023	2.6169
		Shi	SSL	0.8592	4.7478	4.7350	2.0253	0.4776	3.2986	3.7885	2.3968
		Touratier	SSL	0.8691	4.8764	4.8445	2.1142	0.4878	3.4642	3.9207	2.5501
		Ambartsumian	SSL	0.8804	5.0094	4.9538	2.1021	0.4985	3.6884	4.0536	2.5628
		TSDT	SSL	0.8723	4.8470	4.8391	2.0705	0.4881	3.4281	3.9045	2.4725
		FSDT	SSL	0.8830	4.3060	4.5678	1.4587	0.4797	2.8813	3.5663	1.6106
	NNRPIM V1	Mantari	SSL	0.8472	6.4679	5.4576	2.3245	0.4932	4.5824	4.3866	2.9413
		Shi	SSL	0.8488	6.0743	5.3797	2.2900	0.4781	4.1762	4.2277	2.6406
		Touratier	SSL	0.7932	5.8295	5.1101	2.2557	0.4535	4.0835	4.0879	2.6543
		Ambartsumian	SSL	0.5770	4.5581	3.8178	1.6979	0.3478	3.3987	3.2549	2.0923
		TSDT	SSL	0.8054	5.8427	5.1514	2.2287	0.4580	4.0718	4.1006	2.5931
		FSDT	SSL	0.8917	5.5067	5.1499	1.6733	0.4836	3.6538	3.9294	1.7867
	NNRPIM V2	Mantari	SSL	0.7947	5.8130	4.9789	2.2809	0.4447	4.0548	3.9577	2.7992
		Shi	SSL	0.8533	5.8700	5.2218	2.2738	0.4739	4.0281	4.0997	2.6232
		Touratier	SSL	0.8632	5.9753	5.3001	2.2985	0.4828	4.1400	4.1866	2.7172
		Ambartsumian	SSL	0.8764	6.0773	5.3469	2.1239	0.4917	4.2335	4.2223	2.5746
		TSDT	SSL	0.8663	5.9472	5.2964	2.2574	0.4832	4.1076	4.1731	2.6409
		FSDT	SSL	0.8774	5.4723	5.0705	1.6654	0.4774	3.6271	3.8818	1.7941

table 57 - Maximum normalized transverse displacements and stresses for two antisymmetric cross-ply square laminates subjected to a sinusoidal load (SSL), with the boundary conditions of the Case 3, a/h=5.

				Cross-ply laminate (0/90)				Cross-ply laminate $(0/90)_5$			
a/h	**Solution**	**ESL**	**Load**	$\bar{w}$	$\bar{\sigma}_{xx}\times10$	$\bar{\sigma}_{yy}\times10$	$\bar{\tau}_{yz}\times10$	$\bar{w}$	$\bar{\sigma}_{xx}\times10$	$\bar{\sigma}_{yy}\times10$	$\bar{\tau}_{yz}\times10$
5	Exact	TSDT	SSL	1.0880	5.6790	5.5050	2.0950	0.8790	4.0250	4.9630	2.6010
		FSDT	SSL	1.2570	3.9110	5.1530	1.9580	0.9450	2.2750	4.2120	2.2480
	FEM	TSDT	SSL	1.0680	5.0600	4.8860	-	0.8690	3.5840	4.4100	-
		FSDT	SSL	1.2570	3.7070	4.9900	-	0.9450	2.1540	4.0860	-
	RPIM	Mantari	SSL	0.9741	5.2648	4.9699	1.9502	0.8073	3.9896	4.6307	2.5700
		Shi	SSL	1.1327	5.1032	5.4266	2.0223	0.9036	3.6414	4.8417	2.5208
		Touratier	SSL	1.1298	5.5779	5.5016	2.0868	0.9119	4.0746	4.9662	2.6345
		Ambartsumian	SSL	1.1424	5.9878	5.5141	2.0663	0.9245	4.4348	4.9876	2.6102
		TSDT	SSL	1.1493	5.4725	5.5166	2.0635	0.9210	3.9501	4.9422	2.5804
		FSDT	SSL	1.2569	3.4406	4.8628	1.5286	0.9446	1.9944	3.9870	1.7732
	NNRPIM V1	Mantari	SSL	0.9264	6.5861	5.1939	1.8876	0.7943	5.1455	4.9473	2.5760
		Shi	SSL	1.0925	5.8889	5.7182	2.0874	0.8858	4.2230	5.1475	2.6118
		Touratier	SSL	0.9852	5.8007	5.2568	2.0004	0.8138	4.2682	4.8304	2.5333
		Ambartsumian	SSL	0.6430	4.2816	3.3638	1.3675	0.5521	3.3086	3.2243	1.7480
		TSDT	SSL	1.0177	5.7476	5.3429	2.0015	0.8327	4.1693	4.8630	2.5086
		FSDT	SSL	1.2732	3.9338	5.2093	1.6422	0.9535	2.2895	4.2437	1.8888
	NNRPIM V2	Mantari	SSL	0.9312	5.7365	5.0299	1.9967	0.7726	4.2909	4.6975	2.6258
		Shi	SSL	1.1105	5.5895	5.5886	2.1079	0.8895	3.9507	5.0020	2.6240
		Touratier	SSL	1.0970	5.9477	5.5997	2.1201	0.8894	4.2879	5.0693	2.6826
		Ambartsumian	SSL	1.0896	6.1363	5.4900	1.9711	0.8862	4.4398	4.9698	2.5182
		TSDT	SSL	1.1167	5.8406	5.6181	2.0995	0.8988	4.1609	5.0470	2.6307
		FSDT	SSL	1.2475	3.8892	5.1046	1.6430	0.9396	2.2609	4.1846	1.9010

table 58 - Maximum normalized transverse displacements and stresses for two antisymmetric cross-ply square laminates subjected to a sinusoidal load (SSL), with the boundary conditions of the Case 3, a/h=10.

				Cross-ply laminate (0/90)				Cross-ply laminate $(0/90)_5$			
a/h	**Solution**	**ESL**	**Load**	$\bar{w}$	$\bar{\sigma}_{xx}\times10$	$\bar{\sigma}_{yy}\times10$	$\bar{\tau}_{yz}\times10$	$\bar{w}$	$\bar{\sigma}_{xx}\times10$	$\bar{\sigma}_{yy}\times10$	$\bar{\tau}_{yz}\times10$
10	Exact	TSDT	SSL	0.6170	4.9520	3.8030	1.7250	0.3750	3.1930	3.2600	2.0830
		FSDT	SSL	0.6560	4.4500	3.7990	1.5230	0.3850	2.6920	3.1350	1.7080
	FEM	TSDT	SSL	0.6050	4.3460	3.3450	-	0.3720	2.7700	2.8710	-
		FSDT	SSL	0.6570	4.2220	3.6610	-	0.3860	2.5500	3.0310	-
	RPIM	Mantari	SSL	0.5842	4.4359	3.4329	1.6514	0.3582	2.9778	2.9804	2.1199
		Shi	SSL	0.6333	4.4011	3.6561	1.6219	0.3816	2.8404	3.1195	1.9814
		Touratier	SSL	0.6505	4.6580	3.7899	1.7124	0.3988	3.0396	3.2902	2.1460
		Ambartsumian	SSL	0.6726	5.0212	3.9387	1.7243	0.4233	3.3420	3.5129	2.2241
		TSDT	SSL	0.6533	4.6142	3.7873	1.6770	0.3989	2.9954	3.2750	2.0798
		FSDT	SSL	0.6563	3.9157	3.5452	1.1719	0.3852	2.3603	2.9458	1.3360
	NNRPIM V1	Mantari	SSL	0.5951	5.4919	3.8315	1.6980	0.3805	3.7346	3.3886	2.2892
		Shi	SSL	0.6263	5.1043	3.9549	1.7354	0.3828	3.3029	3.3788	2.1159
		Touratier	SSL	0.5839	4.9753	3.7377	1.7073	0.3634	3.2759	3.2630	2.1252
		Ambartsumian	SSL	0.4082	3.8817	2.6450	1.2333	0.2669	2.7261	2.4600	1.5924
		TSDT	SSL	0.5950	4.9754	3.7834	1.6914	0.3679	3.2531	3.2828	2.0815
		FSDT	SSL	0.6690	4.4715	3.8638	1.2848	0.3910	2.7079	3.1772	1.4446
	NNRPIM V2	Mantari	SSL	0.5594	4.8369	3.5149	1.6549	0.3421	3.2161	3.0430	2.1498
		Shi	SSL	0.6228	4.8897	3.8239	1.7061	0.3763	3.1503	3.2573	2.0819
		Touratier	SSL	0.6322	5.0883	3.9008	1.7309	0.3867	3.3048	3.3585	2.1758
		Ambartsumian	SSL	0.6358	5.2559	3.9140	1.5836	0.3922	3.4330	3.3806	2.0563
		TSDT	SSL	0.6359	5.0499	3.9056	1.7026	0.3875	3.2642	3.3512	2.1169
		FSDT	SSL	0.6485	4.4248	3.7463	1.2604	0.3818	2.6748	3.1039	1.4339

table 59 - Maximum normalized transverse displacements and stresses for two antisymmetric cross-ply square laminates subjected to a sinusoidal load (SSL), with the boundary conditions of the Case 4, a/h=5.

				Cross-ply laminate (0/90)				Cross-ply laminate $(0/90)_5$			
a/h	**Solution**	**ESL**	**Load**	$\bar{w}$	$\bar{\sigma}_{xx}\times10$	$\bar{\sigma}_{yy}\times10$	$\bar{\tau}_{yz}\times10$	$\bar{w}$	$\bar{\sigma}_{xx}\times10$	$\bar{\sigma}_{yy}\times10$	$\bar{\tau}_{yz}\times10$
	Exact	TSDT	SSL	2.6240	3.1710	13.5510	4.4570	1.6510	2.4820	9.4540	4.7840
		FSDT	SSL	2.7770	2.4690	11.9070	3.9010	1.6630	1.7120	7.5830	3.8830
	FEM	TSDT	SSL	2.6470	2.7220	13.1420	-	1.6700	2.1240	9.1130	-
		FSDT	SSL	2.7760	2.3590	11.6750	-	1.6620	1.6390	7.4290	-
	RPIM	Mantari	SSL	2.5161	2.9749	13.6596	4.6528	1.6171	2.3948	9.7997	5.2582
		Shi	SSL	2.6183	2.8822	13.3610	4.3631	1.6513	2.2543	9.3042	4.6841
		Touratier	SSL	2.5781	2.9059	13.3597	4.4270	1.6336	2.2878	9.3641	4.7979
		Ambartsumian	SSL	2.5391	2.8645	13.0787	4.2851	1.5980	2.2380	9.1013	4.6025
		TSDT	SSL	2.6023	2.8807	13.3035	4.3508	1.6404	2.2521	9.2628	4.6701
		FSDT	SSL	2.7790	2.2628	11.6946	3.1857	1.6639	1.5727	7.4259	3.1686
5	NNRPIM V1	Mantari	SSL	2.5794	2.9136	14.9202	4.5627	1.7485	2.3772	11.0689	5.3699
		Shi	SSL	2.5605	3.0307	14.0513	4.3869	1.6448	2.4158	9.8757	4.7460
		Touratier	SSL	2.3755	2.9351	13.4675	4.3279	1.5330	2.3994	9.5332	4.7246
		Ambartsumian	SSL	1.8118	2.0698	10.7117	3.5424	1.1869	1.8651	7.7255	3.9256
		TSDT	SSL	2.4206	2.9336	13.4826	4.2783	1.5516	2.3753	9.4705	4.6220
		FSDT	SSL	2.7839	2.4618	11.9170	3.2566	1.6666	1.7064	7.5888	3.2392
	NNRPIM V2	Mantari	SSL	2.4543	3.3302	13.3551	4.7007	1.5563	2.6810	9.5566	5.2786
		Shi	SSL	2.6336	3.2312	13.4164	4.4755	1.6506	2.5147	9.3508	4.7913
		Touratier	SSL	2.6449	3.2674	13.5865	4.5536	1.6667	2.5547	9.5350	4.9357
		Ambartsumian	SSL	2.7628	3.2178	13.8269	4.4666	1.7419	2.4781	9.6809	4.8380
		TSDT	SSL	2.6617	3.2344	13.5119	4.4717	1.6694	2.5109	9.4217	4.8003
		FSDT	SSL	2.7732	2.4688	11.8923	3.3238	1.6609	1.7119	7.5726	3.3091

table 60 - Maximum normalized transverse displacements and stresses for two antisymmetric cross-ply square laminates subjected to a sinusoidal load (SSL), with the boundary conditions of the Case 4, a/h=10.

				Cross-ply laminate (0/90)				Cross-ply laminate $(0/90)_5$			
a/h	**Solution**	**ESL**	**Load**	$\bar{w}$	$\bar{\sigma}_{xx}\times10$	$\bar{\sigma}_{yy}\times10$	$\bar{\tau}_{yz}\times10$	$\bar{w}$	$\bar{\sigma}_{xx}\times10$	$\bar{\sigma}_{yy}\times10$	$\bar{\tau}_{yz}\times10$
10	Exact	TSDT	SSL	1.9920	2.6240	12.2950	4.4890	0.9160	1.9240	8.0050	4.8140
		FSDT	SSL	2.0280	2.4420	11.8840	3.8820	0.9150	1.7230	7.5330	3.8530
	FEM	TSDT	SSL	2.0020	2.2120	11.8900	-	0.9260	1.5970	1.7080	-
		FSDT	SSL	2.0270	2.3310	11.6540	-	0.9140	1.6480	7.3840	-
	RPIM	Mantari	SSL	1.9791	2.4337	12.2871	4.7521	0.9195	1.8115	8.0706	5.4005
		Shi	SSL	1.9886	2.3924	12.1326	4.4016	0.9161	1.7590	7.8816	4.7233
		Touratier	SSL	1.9693	2.3988	12.0940	4.4796	0.9088	1.7682	7.8754	4.8567
		Ambartsumian	SSL	1.9278	2.3771	11.8873	4.3184	0.8865	1.7471	7.7258	4.6458
		TSDT	SSL	1.9764	2.3911	12.0832	4.3916	0.9101	1.7574	7.8501	4.7116
		FSDT	SSL	2.0297	2.2318	11.6845	3.1760	0.9155	1.5802	7.3904	3.1499
	NNRPIM V1	Mantari	SSL	2.0607	2.4187	13.4419	4.7413	1.0190	1.8283	9.0571	5.6302
		Shi	SSL	1.9502	2.4971	12.6897	4.4612	0.9167	1.8748	8.2645	4.8056
		Touratier	SSL	1.8219	2.4167	12.1774	4.4257	0.8584	1.8662	7.9756	4.8306
		Ambartsumian	SSL	1.4083	1.8273	9.9996	3.6527	0.6803	1.6174	6.7984	4.0997
		TSDT	SSL	1.8448	2.4265	12.2209	4.3623	0.8656	1.8606	7.9753	4.7055
		FSDT	SSL	2.0327	2.4320	11.8873	3.2482	0.9171	1.7164	7.5377	3.2165
	NNRPIM V2	Mantari	SSL	1.9254	2.7154	12.0203	4.7423	0.8817	2.0126	7.9104	5.3855
		Shi	SSL	1.9979	2.6761	12.1849	4.5211	0.9142	1.9456	7.9395	4.8391
		Touratier	SSL	2.0182	2.6916	12.2888	4.5901	0.9256	1.9534	8.0237	4.9911
		Ambartsumian	SSL	2.1012	2.6729	12.5388	4.4485	0.9672	1.9080	8.1885	4.8505
		TSDT	SSL	2.0196	2.6798	12.2645	4.5019	0.9247	1.9404	7.9908	4.8427
		FSDT	SSL	2.0250	2.4416	11.8698	3.2991	0.9135	1.7230	7.5236	3.2797

table 61 - Maximum normalized transverse displacements and stresses for two antisymmetric cross-ply square laminates subjected to a sinusoidal load (SSL), with the boundary conditions of the Case 5, a/h=5.

				Cross-ply laminate (0/90)				Cross-ply laminate $(0/90)_5$			
a/h	**Solution**	**ESL**	**Load**	$\bar{w}$	$\bar{\sigma}_{xx}\times10$	$\bar{\sigma}_{yy}\times10$	$\bar{\tau}_{yz}\times10$	$\bar{w}$	$\bar{\sigma}_{xx}\times10$	$\bar{\sigma}_{yy}\times10$	$\bar{\tau}_{yz}\times10$
5	Exact	TSDT	SSL	2.2110	5.3490	11.3240	3.8930	1.4500	3.9450	8.2520	4.2340
		FSDT	SSL	2.3350	4.4300	9.8480	3.3900	1.4600	2.9570	6.5900	3.4370
	FEM	TSDT	SSL	2.2210	5.2310	10.1820	-	1.4610	3.8550	7.4240	-
		FSDT	SSL	2.3340	4.4790	9.1400	-	1.4600	2.9930	6.1410	-
	RPIM	Mantari	SSL	2.1163	5.6259	10.2823	3.7183	1.4160	4.3019	7.7562	4.2390
		Shi	SSL	2.2057	5.4605	10.0489	3.4879	1.4492	4.0478	7.3742	3.7919
		Touratier	SSL	2.1733	5.4821	10.0606	3.5395	1.4341	4.0924	7.4261	3.8821
		Ambartsumian	SSL	2.1380	5.3383	9.8422	3.4006	1.4015	3.9594	7.2147	3.7023
		TSDT	SSL	2.2057	5.4605	10.0489	3.4879	1.4401	4.0341	7.3442	3.7797
		FSDT	SSL	2.3359	4.4837	8.6896	2.5357	1.4605	2.9963	5.8554	2.5674
	NNRPIM V1	Mantari	SSL	2.1789	5.4920	12.4922	3.9936	1.5163	4.2184	9.5495	4.7219
		Shi	SSL	2.1637	5.3451	11.7064	3.8332	1.4429	3.9788	8.5756	4.1985
		Touratier	SSL	2.0050	5.1347	11.1794	3.7729	1.3482	3.8965	8.2783	4.1779
		Ambartsumian	SSL	1.5020	3.8414	8.6546	3.0127	1.0409	3.0935	6.6332	3.4275
		TSDT	SSL	2.0424	5.1351	11.1890	3.7282	1.3643	3.8628	8.2240	4.0876
		FSDT	SSL	2.3382	4.4221	9.8459	2.8266	1.4620	2.9517	6.5905	2.8657
	NNRPIM V2	Mantari	SSL	2.0685	5.4413	11.2035	4.0935	1.3698	4.1332	8.3751	4.6642
		Shi	SSL	2.2169	5.3717	11.2224	3.8977	1.4493	3.9550	8.1742	4.2372
		Touratier	SSL	2.2229	5.4424	11.3639	3.9596	1.4604	4.0267	8.3275	4.3567
		Ambartsumian	SSL	2.3026	5.4577	11.5028	3.8384	1.5122	3.9954	8.4017	4.2313
		TSDT	SSL	2.2374	5.3976	11.2953	3.8871	1.4632	3.9675	8.2277	4.2381
		FSDT	SSL	2.3329	4.4285	9.8388	2.8850	1.4587	2.9567	6.5837	2.9279

table 62 - Maximum normalized transverse displacements and stresses for two antisymmetric cross-ply square laminates subjected to a sinusoidal load (SSL), with the boundary conditions of the Case 5, a/h=10.

				Cross-ply laminate (0/90)				Cross-ply laminate $(0/90)_5$			
a/h	**Solution**	**ESL**	**Load**	$\bar{w}$	$\bar{\sigma}_{xx}\times10$	$\bar{\sigma}_{yy}\times10$	$\bar{\tau}_{yz}\times10$	$\bar{w}$	$\bar{\sigma}_{xx}\times10$	$\bar{\sigma}_{yy}\times10$	$\bar{\tau}_{yz}\times10$
10	Exact	TSDT	SSL	1.6580	4.6690	10.2180	3.9270	0.8010	3.2210	6.9870	4.2750
		FSDT	SSL	1.6870	4.4350	9.8470	3.3830	0.8000	2.9680	6.5660	3.4210
	FEM	TSDT	SSL	1.6620	4.5370	9.1380	-	0.8080	3.1020	6.2460	-
		FSDT	SSL	1.6870	4.4910	9.1201	-	0.8000	3.0100	6.0970	-
	RPIM	Mantari	SSL	1.6441	4.8294	9.1247	3.7911	0.8025	3.3846	6.3340	4.3432
		Shi	SSL	1.6552	4.7590	9.0174	3.5106	0.8011	3.2936	6.1936	3.8088
		Touratier	SSL	1.6400	4.7537	8.9955	3.5740	0.7950	3.2989	6.1914	3.9156
		Ambartsumian	SSL	1.6044	4.6566	8.8392	3.4181	0.7752	3.2297	6.0718	3.7284
		TSDT	SSL	1.6457	4.7440	8.9851	3.5022	0.7961	3.2833	6.1708	3.7991
		FSDT	SSL	1.6883	4.5013	8.6567	2.5217	0.8006	3.0183	5.7991	2.5410
	NNRPIM V1	Mantari	SSL	1.7198	4.7885	11.1768	4.1436	0.8802	3.3762	7.8221	4.9637
		Shi	SSL	1.6276	4.6499	10.5144	3.8998	0.8009	3.2323	7.1829	4.2631
		Touratier	SSL	1.5194	4.4643	10.0568	3.8594	0.7524	3.1597	6.9359	4.2851
		Ambartsumian	SSL	1.1595	3.5145	8.0910	3.1165	0.5983	2.7010	5.8862	3.6121
		TSDT	SSL	1.5381	4.4822	10.0942	3.8031	0.7585	3.1558	6.9359	4.1744
		FSDT	SSL	1.6890	4.4251	9.8388	2.8256	0.8013	2.9617	6.5644	2.8544
	NNRPIM V2	Mantari	SSL	1.6034	4.6820	10.0124	4.1184	0.7737	3.2699	6.9264	4.7714
		Shi	SSL	1.6619	4.6907	10.1375	3.9373	0.8000	3.2274	6.9380	4.2915
		Touratier	SSL	1.6759	4.7293	10.2189	3.9833	0.8083	3.2533	7.0052	4.4151
		Ambartsumian	SSL	1.7310	4.7749	10.3799	3.8013	0.8375	3.2574	7.1132	4.2534
		TSDT	SSL	1.6775	4.7138	10.1976	3.9067	0.8078	3.2360	6.9766	4.2849
		FSDT	SSL	1.6858	4.4335	9.8388	2.8678	0.7994	2.9670	6.5597	2.9099

table 63 - Maximum normalized transverse displacements and stresses for two antisymmetric cross-ply square laminates subjected to a sinusoidal load (SSL), with the boundary conditions of the Case 6, a/h=5.

				Cross-ply laminate (0/90)				Cross-ply laminate $(0/90)_5$			
a/h	Solution	ESL	Load	$\bar{w}$	$\bar{\sigma}_{xx}\times10$	$\bar{\sigma}_{yy}\times10$	$\bar{\tau}_{yz}\times10$	$\bar{w}$	$\bar{\sigma}_{xx}\times10$	$\bar{\sigma}_{yy}\times10$	$\bar{\tau}_{yz}\times10$
5	Exact	TSDT	SSL	1.7330	3.7270	8.8190	3.0480	1.2140	2.6080	6.9350	3.5350
		FSDT	SSL	1.8970	2.4340	8.0470	2.7480	1.2580	1.3430	5.7060	2.9510
	FEM	TSDT	SSL	1.7280	3.5440	9.1250	-	1.2140	2.4200	6.9940	-
		FSDT	SSL	1.8970	2.5420	8.3670	-	1.2580	1.4270	5.8440	-
	RPIM	Mantari	SSL	1.6179	3.0906	7.4637	2.6241	1.1553	2.3696	6.1221	3.3084
		Shi	SSL	1.7624	2.9477	7.7689	2.6272	1.2293	2.1024	6.1692	3.1315
		Touratier	SSL	1.7548	3.1502	7.8628	2.7016	1.2344	2.3456	6.3055	3.2591
		Ambartsumian	SSL	1.7655	3.2612	7.8804	2.6797	1.2396	2.5171	6.2993	3.2134
		TSDT	SSL	1.7755	3.0783	7.8570	2.6651	1.2420	2.2580	6.2584	3.1836
		FSDT	SSL	1.8986	1.5688	6.9106	1.9612	1.2588	0.7943	5.0336	2.1706
	NNRPIM V1	Mantari	SSL	1.6208	3.9756	9.3211	2.9577	1.2069	3.0386	7.6163	3.7599
		Shi	SSL	1.7144	3.7756	9.2989	3.0205	1.2166	2.6797	7.2359	3.5280
		Touratier	SSL	1.5718	3.6975	8.7757	2.9440	1.1280	2.7010	6.9173	3.4787
		Ambartsumian	SSL	1.1161	2.6954	6.3973	2.2248	0.8213	2.0247	5.1766	2.6695
		TSDT	SSL	1.6102	3.6625	8.8347	2.9256	1.1470	2.6372	6.9088	3.4207
		FSDT	SSL	1.9117	2.4515	8.0908	2.2979	1.2651	1.3536	5.7291	2.4703
	NNRPIM V2	Mantari	SSL	1.5624	3.9045	8.5029	3.0742	1.1081	2.8609	6.7947	3.7498
		Shi	SSL	1.7514	3.7347	8.9100	3.0631	1.2199	2.5920	6.9065	3.5518
		Touratier	SSL	1.7518	3.8759	9.0008	3.1056	1.2304	2.7449	7.0437	3.6568
		Ambartsumian	SSL	1.7943	3.8953	9.0160	2.9816	1.2623	2.7335	7.0517	3.5231
		TSDT	SSL	1.7703	3.8035	8.9822	3.0609	1.2368	2.6613	6.9819	3.5687
		FSDT	SSL	1.8890	2.4167	8.0067	2.3228	1.2537	1.3321	5.6838	2.5056

table 64 - Maximum normalized transverse displacements and stresses for two antisymmetric cross-ply square laminates subjected to a sinusoidal load (SSL), with the boundary conditions of the Case 6, a/h=10.

				Cross-ply laminate (0/90)				Cross-ply laminate $(0/90)_5$			
a/h	**Solution**	**ESL**	**Load**	$\bar{w}$	$\bar{\sigma}_{xx}\times10$	$\bar{\sigma}_{yy}\times10$	$\bar{\tau}_{yz}\times10$	$\bar{w}$	$\bar{\sigma}_{xx}\times10$	$\bar{\sigma}_{yy}\times10$	$\bar{\tau}_{yz}\times10$
10	Exact	TSDT	SSL	1.1840	3.1580	7.3140	2.8050	0.6070	1.9540	5.2990	3.2250
		FSDT	SSL	1.2230	2.7900	7.1500	2.4490	0.6120	1.5940	5.0290	2.6050
	FEM	TSDT	SSL	1.1800	3.0540	7.7250	-	0.6090	1.8390	5.4830	-
		FSDT	SSL	1.2230	2.8950	7.6100	-	0.6120	1.6740	5.2790	-
	RPIM	Mantari	SSL	1.1568	2.2801	5.8961	2.3785	0.5976	1.4605	4.4276	2.9973
		Shi	SSL	1.1953	2.2603	6.0540	2.2904	0.6231	1.4987	4.6276	2.8114
		Touratier	SSL	1.2067	2.3935	6.1856	2.3925	0.6230	1.5328	4.6485	2.9015
		Ambartsumian	SSL	1.2203	2.5639	6.3295	2.4022	0.6383	1.7864	4.8350	2.9452
		TSDT	SSL	1.2104	2.3636	6.1769	2.3439	0.6231	1.4987	4.6276	2.8114
		FSDT	SSL	1.2231	1.8463	5.8479	1.6573	0.6125	0.9923	4.2314	1.8257
	NNRPIM V1	Mantari	SSL	1.2028	3.2565	7.8319	2.8939	0.6545	2.1299	5.8226	3.6820
		Shi	SSL	1.1773	3.1753	7.6144	2.8115	0.6124	1.9864	5.4933	3.2452
		Touratier	SSL	1.0987	3.0958	7.2768	2.7830	0.5774	1.9909	5.3209	3.2724
		Ambartsumian	SSL	0.8108	2.4240	5.6435	2.1743	0.4424	1.6614	4.3365	2.6505
		TSDT	SSL	1.1150	3.0954	7.3222	2.7489	0.5832	1.9743	5.3315	3.1939
		FSDT	SSL	1.2344	2.8084	7.2025	2.0585	0.6173	1.6083	5.0618	2.1887
	NNRPIM V2	Mantari	SSL	1.1165	3.1826	6.9842	2.8578	0.5705	2.0121	5.1102	3.4976
		Shi	SSL	1.1899	3.1642	7.2727	2.8091	0.6061	1.9426	5.2616	3.2345
		Touratier	SSL	1.2075	3.2457	7.3785	2.8610	0.6199	2.0235	5.3786	3.3694
		Ambartsumian	SSL	1.2428	3.2984	7.4716	2.7270	0.6429	2.0573	5.4696	3.2525
		TSDT	SSL	1.2101	3.2193	7.3716	2.8091	0.6198	1.9963	5.3596	3.2718
		FSDT	SSL	1.2151	2.7710	7.1040	2.0596	0.6091	1.5808	5.0028	2.2055

table 65 - Maximum normalized transverse displacements and stresses for two simply supported antisymmetric cross-ply square laminates subjected to a sinusoidal load (SSL) and a uniformly distributed load (UDL), a/h=10.

				Cross-ply laminate (0/90)				Cross-ply laminate $(0/90)_4$			
a/h	**Solution**	**ESL**	**Load**	$\bar{w}$	$\bar{\sigma}_{yy}$	$\bar{\tau}_{xy}$	$\bar{\tau}_{xz}$	$\bar{w}$	$\bar{\sigma}_{yy}$	$\bar{\tau}_{xy}$	$\bar{\tau}_{xz}$
10	Exact	TSDT	SSL	1.2160	-	-	-	-	-	-	-
			UDL	-	-	-	-	-	-	-	-
		FSDT	SSL	1.2373	0.7157	0.0525	0.2728	0.6216	0.4950	0.0221	0.2728
			UDL	1.9468	1.0715	0.0960	0.5772	0.9660	0.7415	0.0420	0.5787
	RPIM	Mantari	SSL	1.2032	0.7197	0.0515	0.3302	0.6232	0.5144	0.0232	0.3719
			UDL	1.8987	1.0684	0.0911	0.6216	0.9700	0.7566	0.0430	0.7002
		Shi	SSL	1.2141	0.7111	0.0516	0.3035	0.6231	0.5032	0.0229	0.3253
			UDL	1.9137	1.0574	0.0917	0.5754	0.9688	0.7434	0.0424	0.6179
		Touratier	SSL	1.2038	0.7099	0.0513	0.3090	0.6188	0.5032	0.0228	0.3344
			UDL	1.8979	1.0552	0.0910	0.5852	0.9623	0.7428	0.0422	0.6341
		Ambartsumian	SSL	1.1769	0.6965	0.0487	0.2977	0.6034	0.4931	0.0214	0.3191
			UDL	1.8524	1.0347	0.0862	0.5647	0.9366	0.7278	0.0395	0.6059
		TSDT	SSL	1.2079	0.7088	0.0513	0.3025	0.6196	0.5015	0.0227	0.3243
			UDL	1.9039	1.0540	0.0911	0.5736	0.9633	0.7409	0.0421	0.6160
		FSDT	SSL	1.2378	0.6794	0.6794	0.2164	0.6218	0.4698	0.4698	0.2163
			UDL	1.9474	1.0352	1.0229	0.4444	0.9663	0.7153	0.7088	0.4450
	NNRPIM V1	Mantari	SSL	1.2559	0.8094	0.0534	0.3338	0.6684	0.5802	0.0250	0.3921
			UDL	1.9838	1.1966	0.0963	0.6557	1.0412	0.8445	0.0476	0.7617
		Shi	SSL	1.1976	0.7613	0.0526	0.3160	0.6222	0.5388	0.0238	0.3402
			UDL	1.8882	1.1259	0.0973	0.6479	0.9676	0.7893	0.0473	0.6966
		Touratier	SSL	1.1204	0.7257	0.0508	0.3119	0.5893	0.5211	0.0233	0.3421
			UDL	1.7677	1.0744	0.0933	0.6303	0.9173	0.7649	0.0458	0.6903
		Ambartsumian	SSL	0.8483	0.5701	0.0417	0.2449	0.4740	0.4393	0.0202	0.2848
			UDL	1.3396	0.8489	0.0745	0.4767	0.7401	0.6531	0.0377	0.5519
		TSDT	SSL	1.1337	0.7286	0.0511	0.3072	0.5936	0.5211	0.0233	0.3332
			UDL	1.7880	1.0789	0.0940	0.6240	0.9236	0.7654	0.0459	0.6762
		FSDT	SSL	1.2365	0.7141	0.7141	0.2275	0.6216	0.4941	0.4941	0.2274
			UDL	1.9449	1.0687	1.0687	0.4844	0.9656	0.7399	0.7399	0.4848
	NNRPIM V2	Mantari	SSL	1.1783	0.7363	0.0564	0.3301	0.6064	0.5275	0.0255	0.3791
			UDL	1.8610	1.0895	0.1022	0.6680	0.9448	0.7733	0.0492	0.7619
		Shi	SSL	1.2185	0.7436	0.0533	0.3174	0.6229	0.5264	0.0236	0.3418
			UDL	1.9215	1.1006	0.0981	0.6558	0.9691	0.7734	0.0465	0.7047
		Touratier	SSL	1.2255	0.7497	0.0514	0.3192	0.6273	0.5311	0.0228	0.3501
			UDL	1.9325	1.1083	0.0941	0.6561	0.9757	0.7785	0.0445	0.7165
		Ambartsumian	SSL	1.2517	0.7587	0.0418	0.2968	0.6406	0.5360	0.0179	0.3320
			UDL	1.9702	1.1189	0.0749	0.6094	0.9942	0.7834	0.0334	0.6748
		TSDT	SSL	1.2273	0.7478	0.0517	0.3130	0.6271	0.5288	0.0228	0.3398
			UDL	1.9348	1.1061	0.0948	0.6458	0.9752	0.7761	0.0446	0.6986
		FSDT	SSL	1.2376	0.7155	0.7155	0.2303	0.6218	0.4948	0.4948	0.2315
			UDL	1.9482	1.0722	1.0722	0.4884	0.9668	0.7419	0.7419	0.4912

table 66 - Maximum normalized transverse displacements and stresses of two simply supported antisymmetric cross-ply square laminates subjected to a sinusoidal load (SSL) and a uniformly distributed load (UDL), a/h=20.

				Cross-ply laminate (0/90)				Cross-ply laminate $(0/90)_4$			
a/h	**Solution**	**ESL**	**Load**	$\bar{w}$	$\bar{\sigma}_{yy}$	$\bar{\tau}_{xy}$	$\bar{\tau}_{xz}$	$\bar{w}$	$\bar{\sigma}_{yy}$	$\bar{\tau}_{xy}$	$\bar{\tau}_{xz}$
20	Exact	TSDT	SSL	1.1018	-	-	-	-	-	-	-
			UDL	-	-	-	-	-	-	-	-
		FSDT	SSL	1.1070	0.7157	0.0525	0.2728	0.4913	0.4950	0.0221	0.2728
			UDL	1.7582	1.0747	0.0943	0.5802	0.7776	0.7468	0.0402	0.5839
	RPIM	Mantari	SSL	1.1025	0.6937	0.0510	0.3316	0.4959	0.4843	0.0220	0.3748
			UDL	1.7519	1.0420	0.0891	0.6318	0.7847	0.7286	0.0390	0.7202
		Shi	SSL	1.1000	0.6888	0.0510	0.3043	0.4920	0.4790	0.0218	0.3264
			UDL	1.7478	1.0355	0.0892	0.5817	0.7786	0.7220	0.0386	0.6288
		Touratier	SSL	1.0927	0.6866	0.0507	0.3098	0.4888	0.4778	0.0217	0.3357
			UDL	1.7362	1.0322	0.0886	0.5920	0.7736	0.7199	0.0384	0.6464
		Ambartsumian	SSL	1.0660	0.6746	0.0484	0.2983	0.4765	0.4696	0.0208	0.3203
			UDL	1.6922	1.0135	0.0846	0.5706	0.7534	0.7074	0.0368	0.6170
		TSDT	SSL	1.0944	0.6865	0.0507	0.3032	0.4892	0.4774	0.0217	0.3254
			UDL	1.7389	1.0322	0.0887	0.5796	0.7742	0.7196	0.0384	0.6268
		FSDT	SSL	1.1074	0.6793	0.6793	0.2165	0.4915	0.4698	0.4698	0.2164
			UDL	1.7586	1.0383	1.0246	0.4467	0.7779	0.7203	0.7121	0.4488
	NNRPIM V1	Mantari	SSL	1.1487	0.7756	0.0531	0.3321	0.5336	0.5438	0.0238	0.3935
			UDL	1.8256	1.1598	0.0948	0.6850	0.8439	0.8111	0.0434	0.8113
		Shi	SSL	1.0824	0.7342	0.0515	0.3180	0.4911	0.5109	0.0224	0.3420
			UDL	1.7201	1.0991	0.0930	0.6714	0.7771	0.7658	0.0416	0.7256
		Touratier	SSL	1.0163	0.7009	0.0495	0.3142	0.4659	0.4941	0.0218	0.3460
			UDL	1.6155	1.0500	0.0891	0.6571	0.7376	0.7417	0.0402	0.7263
		Ambartsumian	SSL	0.7752	0.5585	0.0403	0.2388	0.3786	0.4246	0.0188	0.2866
			UDL	1.2326	0.8386	0.0715	0.4868	0.6003	0.6413	0.0339	0.5819
		TSDT	SSL	1.0262	0.7045	0.0498	0.3094	0.4689	0.4953	0.0218	0.3367
			UDL	1.6310	1.0553	0.0897	0.6492	0.7423	0.7437	0.0404	0.7091
		FSDT	SSL	1.1027	0.7118	0.7118	0.2277	0.4906	0.4934	0.4934	0.2275
			UDL	1.7509	1.0683	1.0683	0.4881	0.7763	0.7442	0.7442	0.4899
	NNRPIM V2	Mantari	SSL	1.0791	0.7100	0.0555	0.3077	0.4821	0.4974	0.0240	0.3724
			UDL	1.7161	1.0639	0.0990	0.6523	0.7638	0.7470	0.0437	0.7816
		Shi	SSL	1.1037	0.7205	0.0523	0.3106	0.4918	0.5017	0.0224	0.3413
			UDL	1.7544	1.0793	0.0940	0.6608	0.7787	0.7534	0.0412	0.7260
		Touratier	SSL	1.1122	0.7253	0.0506	0.3068	0.4954	0.5045	0.0217	0.3478
			UDL	1.7676	1.0856	0.0908	0.6550	0.7843	0.7569	0.0399	0.7392
		Ambartsumian	SSL	1.1345	0.7350	0.0418	0.2635	0.5061	0.5105	0.0180	0.3198
			UDL	1.8009	1.0976	0.0745	0.5719	0.8002	0.7639	0.0326	0.6796
		TSDT	SSL	1.1118	0.7245	0.0509	0.3019	0.4951	0.5038	0.0217	0.3379
			UDL	1.7669	1.0847	0.0913	0.6453	0.7837	0.7562	0.0400	0.7195
		FSDT	SSL	1.1071	0.7153	0.7153	0.2240	0.4914	0.4947	0.4947	0.2288
			UDL	1.7591	1.0751	1.0751	0.4806	0.7782	0.7471	0.7471	0.4912

table 67 - Maximum normalized transverse displacements and stresses for two simply supported antisymmetric cross-ply square laminates subjected to a sinusoidal load (SSL) and a uniformly distributed load (UDL), a/h=100.

				Cross-ply laminate (0/90)				Cross-ply laminate $(0/90)_4$			
a/h	**Solution**	**ESL**	**Load**	$\bar{w}$	$\bar{\sigma}_{yy}$	$\bar{\tau}_{xy}$	$\bar{\tau}_{xz}$	$\bar{w}$	$\bar{\sigma}_{yy}$	$\bar{\tau}_{xy}$	$\bar{\tau}_{xz}$
100	Exact	TSDT	SSL	1.0651	-	-	-	-	-	-	-
			UDL	-	-	-	-	-	-	-	-
		FSDT	SSL	1.0653	0.7157	0.0525	0.2728	0.4496	0.4950	0.0221	0.2728
			UDL	1.6980	1.0761	0.0933	0.5813	0.7175	0.7494	0.0391	0.5857
	RPIM	Mantari	SSL	1.0655	0.6829	0.0503	0.3188	0.4538	0.4738	0.0215	0.3687
			UDL	1.6970	1.0297	0.0873	0.6114	0.7238	0.7191	0.0372	0.7149
		Shi	SSL	1.0608	0.6803	0.0505	0.2990	0.4494	0.4708	0.0214	0.3252
			UDL	1.6904	1.0265	0.0877	0.5732	0.7170	0.7151	0.0371	0.6294
		Touratier	SSL	1.0550	0.6781	0.0502	0.3077	0.4466	0.4693	0.0213	0.3362
			UDL	1.6811	1.0233	0.0873	0.5893	0.7126	0.7127	0.0368	0.6506
		Ambartsumian	SSL	1.0282	0.6664	0.0482	0.2918	0.4351	0.4616	0.0205	0.3167
			UDL	1.6371	1.0051	0.0836	0.5614	0.6939	0.7008	0.0355	0.6148
		TSDT	SSL	1.0560	0.6784	0.0503	0.3008	0.4469	0.4694	0.0213	0.3256
			UDL	1.6827	1.0237	0.0874	0.5762	0.7131	0.7129	0.0369	0.6302
		FSDT	SSL	1.0632	0.6779	0.6780	0.2182	0.4493	0.4693	0.4694	0.2182
			UDL	1.6941	1.0372	1.0232	0.4495	0.7169	0.7221	0.7130	0.4527
	NNRPIM V1	Mantari	SSL	0.9045	0.6193	0.0437	0.2839	0.4446	0.4823	0.0213	0.3843
			UDL	1.4403	0.9264	0.0777	0.6275	0.7085	0.7258	0.0378	0.8462
		Shi	SSL	0.9506	0.6589	0.0467	0.2845	0.4306	0.4812	0.0211	0.3367
			UDL	1.5146	0.9888	0.0833	0.6321	0.6868	0.7272	0.0374	0.7413
		Touratier	SSL	0.9304	0.6555	0.0464	0.2832	0.4160	0.4738	0.0206	0.3417
			UDL	1.4830	0.9852	0.0827	0.6325	0.6638	0.7173	0.0366	0.7534
		Ambartsumian	SSL	0.7514	0.5547	0.0397	0.1775	0.3475	0.4199	0.0181	0.2525
			UDL	1.1981	0.8354	0.0701	0.4206	0.5551	0.6383	0.0320	0.5672
		TSDT	SSL	0.9350	0.6564	0.0465	0.2792	0.4179	0.4745	0.0207	0.3321
			UDL	1.4901	0.9863	0.0829	0.6232	0.6668	0.7183	0.0367	0.7321
		FSDT	SSL	0.9626	0.6449	0.6449	0.2070	0.4304	0.4728	0.4728	0.2232
			UDL	1.5334	0.9673	0.9673	0.4606	0.6866	0.7149	0.7149	0.4919
	NNRPIM V2	Mantari	SSL	1.0377	0.6954	0.0561	0.0144	0.4402	0.4858	0.0235	0.2183
			UDL	1.6541	1.0465	0.0992	0.1892	0.7029	0.7367	0.0413	0.5515
		Shi	SSL	1.0620	0.7100	0.0525	0.0845	0.4487	0.4928	0.0218	0.2292
			UDL	1.6930	1.0680	0.0932	0.3008	0.7163	0.7466	0.0385	0.5555
		Touratier	SSL	1.0725	0.7154	0.0505	0.0819	0.4524	0.4954	0.0208	0.2369
			UDL	1.7095	1.0755	0.0896	0.3049	0.7221	0.7501	0.0368	0.5801
		Ambartsumian	SSL	1.0953	0.7265	0.0443	-0.0986	0.4625	0.5019	0.0180	0.1115
			UDL	1.7442	1.0897	0.0785	0.0025	0.7375	0.7582	0.0320	0.3703
		TSDT	SSL	1.0713	0.7149	0.0507	0.0845	0.4520	0.4951	0.0209	0.2306
			UDL	1.7076	1.0749	0.0900	0.3050	0.7215	0.7498	0.0370	0.5633
		FSDT	SSL	1.0606	0.7122	0.7122	0.0716	0.4488	0.4938	0.4938	0.1513
			UDL	1.6908	1.0716	1.0716	0.2336	0.7165	0.7483	0.7483	0.3675

Antisymmetric Angle-Ply Laminates

table 68 - Maximum normalized transverse displacements and stresses for two simply supported antisymmetric angle-ply $(-45/45)_n$square laminates subjected to a sinusoidal load (SSL) and a uniformly distributed load (UDL), a/h=10.

				Angle-ply laminate (-45/45)				Angle-ply laminate $(-45/45)_4$			
a/h	**Solution**	**ESL**	**Load**	$\bar{w}$	$\bar{\sigma}_{xx}$	$\bar{\tau}_{xy}$	$\bar{\tau}_{xz}$	$\bar{w}$	$\bar{\sigma}_{xx}$	$\bar{\tau}_{xy}$	$\bar{\tau}_{xz}$
	Exact	TSDT	SSL	-	-	-	-	-	-	-	-
			UDL	-	-	-	-	-	-	-	-
		FSDT	SSL	0.8284	0.2498	0.2336-	0.2728	0.4198	0.1445	0.1384	0.2728
			UDL	1.2792	0.3476	0.4274	0.5072	0.6366	0.1957	0.2463	0.5070
	RPIM	Mantari	SSL	0.7851	0.2442	0.2504	0.2276	0.4170	0.1538	0.1557	0.2617
			UDL	1.2162	0.3427	0.4767	0.4077	0.6333	0.2081	0.3031	0.4679
		Shi	SSL	0.8021	0.2417	0.2506	0.2119	0.4208	0.1492	0.1549	0.2302
			UDL	1.2409	0.3394	0.4791	0.3804	0.6384	0.2027	0.3033	0.4133
		Touratier	SSL	0.7949	0.2417	0.2500	0.2155	0.4184	0.1500	0.1556	0.2368
			UDL	1.2301	0.3394	0.4771	0.3868	0.6350	0.2036	0.3042	0.4248
		Ambartsumian	SSL	0.7837	0.2390	0.2346	0.2093	0.4112	0.1480	0.1456	0.2275
			UDL	1.2111	0.3358	0.4408	3.7000	0.6231	0.2013	0.2775	0.4084
		TSDT	SSL	0.7990	0.2412	0.2496	0.2115	0.4191	0.1490	0.1546	0.2298
			UDL	1.2361	0.3389	0.4759	0.3796	0.6358	0.2025	0.3017	0.4125
		FSDT	SSL	0.8292	0.2272	0.2327	0.1537	0.4200	0.1324	0.1363	0.1538
			UDL	1.2802	0.3234	0.4227	0.2764	0.6368	0.1843	0.2440	0.2768
	NNRPIM V1	Mantari	SSL	0.8518	0.2953	0.2843	0.2314	0.4909	0.2032	0.1688	0.2797
			UDL	1.3222	0.4055	0.5531	0.4416	0.7496	0.2716	0.3344	0.5297
		Shi	SSL	0.7753	0.2606	0.2728	0.2163	0.4199	0.1657	0.1679	0.2372
			UDL	1.1990	0.3551	0.5506	0.4257	0.6371	0.2181	0.3529	0.4648
10		Touratier	SSL	0.7066	0.2413	0.2719	0.2133	0.3821	0.1523	0.1714	0.2367
			UDL	1.0925	0.3275	0.5475	0.4137	0.5790	0.1987	0.3616	0.4566
		Ambartsumian	SSL	0.5309	0.1845	0.2547	0.1784	0.2803	0.1111	0.1679	0.1965
			UDL	0.8202	0.2494	0.4984	0.3280	0.4234	0.1425	0.3448	0.3602
		TSDT	SSL	0.7193	0.2434	0.2712	0.2107	0.3867	0.1527	0.1697	0.2309
			UDL	1.1118	0.3306	0.5458	0.4101	0.5860	0.1997	0.3575	0.4476
		FSDT	SSL	0.8286	0.2461	0.2325	0.1591	0.4199	0.1440	0.1362	0.1591
			UDL	1.2791	0.3414	0.4278	0.3192	0.6364	0.1950	0.2439	0.3193
	NNRPIM V2	Mantari	SSL	0.7692	0.2575	0.2757	0.2294	0.4027	0.1609	0.1506	0.2656
			UDL	1.1926	0.3517	0.5349	0.4432	0.6121	0.2109	0.2936	0.5087
		Shi	SSL	0.8071	0.2612	0.3197	0.2210	0.4208	0.1612	0.1889	0.2403
			UDL	1.2493	0.3572	0.6387	0.4353	0.6388	0.2125	0.3949	0.4714
		Touratier	SSL	0.8137	0.2648	0.3588	0.2230	0.4261	0.1645	0.2166	0.2465
			UDL	1.2598	0.3621	0.7190	0.4370	0.6469	0.2167	0.4608	0.4806
		Ambartsumian	SSL	0.8471	0.2738	0.4332	0.2116	0.4450	0.1709	0.2605	0.2365
			UDL	1.3099	0.3751	0.8665	0.4108	0.6750	0.2264	0.5580	0.4563
		TSDT	SSL	0.8518	0.2953	0.4949	0.2314	0.4258	0.1631	0.2115	0.2394
			UDL	1.2627	0.3609	0.7040	0.4304	0.6464	0.2152	0.4487	0.4683
		FSDT	SSL	0.8291	0.2465	0.2459	0.1617	0.4200	0.1441	0.1441	0.1624
			UDL	1.2809	0.3420	0.4495	0.3229	0.6372	0.1952	0.2568	0.3243

table 69 - Maximum normalized transverse displacements and stresses for two simply supported antisymmetric angle-ply $(-45/45)_n$square laminates subjected to a sinusoidal load (SSL) and a uniformly distributed load (UDL), a/h=20.

				Angle-ply laminate (-45/45)				Angle-ply laminate $(-45/45)_4$			
a/h	**Solution**	**ESL**	**Load**	$\bar{w}$	$\bar{\sigma}_{xx}$	$\bar{\tau}_{xy}$	$\bar{\tau}_{xz}$	$\bar{w}$	$\bar{\sigma}_{xx}$	$\bar{\tau}_{xy}$	$\bar{\tau}_{xz}$
20	Exact	TSDT	SSL	-	-	-	-	-	-	-	-
			UDL	-	-	-	-	-	-	-	-
		FSDT	SSL	0.6981	0.2498	0.2336-	0.2728	0.2896	0.1445	0.1384	0.2728
			UDL	1.0907	0.3496	0.4357	0.5065	0.4483	0.1988	0.2550	0.5050
	RPIM	Mantari	SSL	0.6901	0.2327	0.2397	0.2296	0.2911	0.1385	0.1417	0.2655
			UDL	1.0788	0.3321	0.4470	0.4102	0.4506	0.1941	0.2675	0.4702
		Shi	SSL	0.6915	0.2314	0.2397	0.2128	0.2902	0.1369	0.1418	0.2316
			UDL	1.0809	0.3303	0.4476	0.3801	0.4491	0.1921	0.2677	0.4107
		Touratier	SSL	0.6875	0.2310	0.2393	0.2166	0.2888	0.1369	0.1421	0.2385
			UDL	1.0747	0.3298	0.4466	0.3870	0.4470	0.1921	0.2681	0.4230
		Ambartsumian	SSL	0.6757	0.2287	0.2287	0.2101	0.2837	0.1356	0.1372	0.2291
			UDL	1.0554	0.3265	0.4240	0.3753	0.4388	0.1904	0.2566	0.4062
		TSDT	SSL	0.6888	0.2309	0.2391	0.2123	0.2890	0.1366	0.1418	0.2312
			UDL	1.0767	0.3297	0.4461	0.3793	0.4473	0.1918	0.2673	0.4100
		FSDT	SSL	0.6989	0.2272	0.2329	0.1536	0.2897	0.1324	0.1363	0.1538
			UDL	1.0917	0.3255	0.4286	0.2741	0.1871	0.1867	0.2503	0.2729
	NNRPIM V1	Mantari	SSL	0.7510	0.2802	0.2706	0.2325	0.3468	0.1801	0.1553	0.2838
			UDL	1.1752	0.3911	0.5140	0.4565	0.5381	0.2480	0.2968	0.5457
		Shi	SSL	0.6685	0.2490	0.2576	0.2184	0.2901	0.1513	0.1507	0.2393
			UDL	1.0445	0.3456	0.4978	0.4347	0.4490	0.2065	0.2952	0.4699
		Touratier	SSL	0.6117	0.2311	0.2545	0.2170	0.2644	0.1399	0.1506	0.2409
			UDL	0.9557	0.3199	0.4931	0.4281	0.4089	0.1900	0.2973	0.4687
		Ambartsumian	SSL	0.4598	0.1796	0.2345	0.1798	0.1949	0.1071	0.1429	0.2017
			UDL	0.7179	0.2473	0.4500	0.3377	0.3010	0.1439	0.2817	0.3757
		TSDT	SSL	0.6205	0.2333	0.2543	0.2139	0.2673	0.1408	0.1500	0.2344
			UDL	0.9694	0.3231	0.4922	0.4228	0.4134	0.1915	0.2955	0.4574
		FSDT	SSL	0.6970	0.2456	0.2313	0.1592	0.2894	0.1438	0.1357	0.1592
			UDL	1.0887	0.3430	0.4330	0.3177	0.4479	0.1980	0.2515	0.3151
	NNRPIM V2	Mantari	SSL	0.6753	0.2454	0.2616	0.2246	0.2807	0.1455	0.1389	0.2676
			UDL	1.0567	0.3414	0.4952	0.4409	0.4348	0.1981	0.2642	0.5151
		Shi	SSL	0.6955	0.2501	0.3003	0.2196	0.2900	0.1481	0.1671	0.2420
			UDL	1.0877	0.3481	0.5740	0.4356	0.4492	0.2023	0.3249	0.4734
		Touratier	SSL	0.7035	0.2531	0.3358	0.2206	0.2939	0.1501	0.1872	0.2484
			UDL	1.1002	0.3523	0.6427	0.4380	0.4552	0.2051	0.3672	0.4856
		Ambartsumian	SSL	0.7307	0.2618	0.4197	0.2008	0.3071	0.1560	0.2348	0.2348
			UDL	1.1417	0.3648	0.8021	0.3963	0.4753	0.2136	0.4643	0.4542
		TSDT	SSL	0.7031	0.2525	0.3291	0.2169	0.2935	0.1497	0.1838	0.2411
			UDL	1.0995	0.3516	0.6297	0.4308	0.4545	0.2045	0.3598	0.4719
		FSDT	SSL	0.6987	0.2464	0.2455	0.1592	0.2897	0.1441	0.1440	0.1614
			UDL	1.0921	0.3443	0.4566	0.3158	0.4486	0.1984	0.2651	0.3177

table 70 - Maximum normalized transverse displacements and stresses for two simply supported antisymmetric angle-ply $(-45/45)_n$square laminates subjected to a sinusoidal load (SSL) and a uniformly distributed load (UDL), a/h=100.

				Angle-ply laminate (-45/45)				Angle-ply laminate $(-45/45)_4$			
a/h	**Solution**	**ESL**	**Load**	$\bar{w}$	$\bar{\sigma}_{xx}$	$\bar{\tau}_{xy}$	$\bar{\tau}_{xz}$	$\bar{w}$	$\bar{\sigma}_{xx}$	$\bar{\tau}_{xy}$	$\bar{\tau}_{xz}$
	Exact	TSDT	SSL	-	-	-	-	-	-	-	-
			UDL	-	-	-	-	-	-	-	-
		FSDT	SSL	0.6564	0.2498	0.2336	0.2728	0.2479	0.1445	0.1384	0.2728
			UDL	1.0305	0.3504	0.4417	0.5068	0.3883	0.2005	0.2630	0.5054
	RPIM	Mantari	SSL	0.6577	0.2287	0.2352	0.2211	0.2498	0.1334	0.1372	0.2626
			UDL	1.0318	0.3283	0.4345	0.3944	0.3910	0.1901	0.2562	0.4620
		Shi	SSL	0.6550	0.2279	0.2365	0.2078	0.2479	0.1328	0.1381	0.2302
			UDL	1.0280	0.3273	0.4375	0.3700	0.3882	0.1893	0.2580	0.4050
		Touratier	SSL	0.6522	0.2274	0.2362	0.2134	0.2468	0.1326	0.1381	0.2380
			UDL	1.0237	0.3267	0.4369	0.3801	0.3865	0.1890	0.2582	0.4190
		Ambartsumian	SSL	0.6404	0.2253	0.2289	0.2083	0.2424	0.1315	0.1356	0.2284
			UDL	1.0046	0.3236	0.4218	0.3715	0.3795	0.1875	0.2528	0.4025
		TSDT	SSL	0.6527	0.2275	0.2362	0.2089	0.2469	0.1326	0.1381	0.2305
			UDL	1.0244	0.3267	0.4369	0.3721	0.3867	0.1890	0.2581	0.4057
		FSDT	SSL	0.6563	0.2270	0.2338	0.1500	0.2479	0.1323	0.1369	0.1525
			UDL	1.0300	0.3261	0.4327	0.2665	0.3882	0.1886	0.2557	0.2684
	NNRPIM V1	Mantari	SSL	0.6246	0.2388	0.2354	0.2032	0.2815	0.1621	0.1457	0.2759
			UDL	0.9825	0.3376	0.4394	0.4043	0.4417	0.2274	0.2736	0.5498
100		Shi	SSL	0.5977	0.2309	0.2387	0.1982	0.2424	0.1432	0.1413	0.2355
			UDL	0.9388	0.3239	0.4513	0.3996	0.3798	0.1990	0.2694	0.4701
		Touratier	SSL	0.5623	0.2203	0.2390	0.2011	0.2233	0.1342	0.1400	0.2397
			UDL	0.8826	0.3078	0.4544	0.4068	0.3497	0.1857	0.2686	0.4781
		Ambartsumian	SSL	0.4366	0.1780	0.2219	0.1663	0.1671	0.1058	0.1295	0.2021
			UDL	0.6847	0.2467	0.4232	0.3333	0.2613	0.1448	0.2512	0.3961
		TSDT	SSL	0.5682	0.2219	0.2385	0.1977	0.2255	0.1351	0.1398	0.2326
			UDL	0.8919	0.3102	0.4531	0.3997	0.3530	0.1870	0.2681	0.4642
		FSDT	SSL	0.6164	0.2307	0.2178	0.1459	0.2420	0.1404	0.1317	0.1562
			UDL	0.9682	0.3242	0.4107	0.2933	0.3791	0.1953	0.2506	0.3118
	NNRPIM V2	Mantari	SSL	0.6414	0.2403	0.2599	0.1287	0.2405	0.1402	0.1352	0.2238
			UDL	1.0073	0.3368	0.4858	0.2807	0.3768	0.1944	0.2557	0.4422
		Shi	SSL	0.6577	0.2459	0.2983	0.1391	0.2476	0.1438	0.1605	0.2059
			UDL	1.0329	0.3447	0.5595	0.2983	0.3880	0.1995	0.3041	0.4101
		Touratier	SSL	0.6667	0.2489	0.3312	0.1438	0.2510	0.1454	0.1778	0.2150
			UDL	1.0469	0.3489	0.6214	0.3108	0.3933	0.2020	0.3370	0.4308
		Ambartsumian	SSL	0.6927	0.2578	0.4288	0.0932	0.2625	0.1511	0.2322	0.1784
			UDL	1.0870	0.3616	0.8013	0.2239	0.4110	0.2102	0.4386	0.3682
		TSDT	SSL	0.6655	0.2485	0.3251	0.1417	0.2507	0.1453	0.1751	0.2081
			UDL	1.0450	0.3483	0.6098	0.3052	0.3927	0.2017	0.3318	0.4168
		FSDT	SSL	0.6552	0.2459	0.2515	0.1044	0.2477	0.1440	0.1447	0.1361
			UDL	1.0289	0.3445	0.4721	0.2205	0.3881	0.1999	0.2738	0.2713

table 71 - Maximum normalized transverse displacements for simply supported antisymmetric angle-ply $(\theta/-\theta)_n$ square laminates subjected to a sinusoidal load (SSL), a/h=4

				θ = 5°		θ = 30		θ = 45°	
a/h	Solution	ESL	Load	n = 1	n = 3	n = 1	n = 3	n = 1	n = 3
4	Exact	TSDT	SSL	1.2625	1.2282	1.0838	0.8851	1.0203	0.8375
		FSDT	SSL	1.3165	1.2647	1.2155	0.8994	1.1576	0.8531
	RPIM	Mantari	SSL	1.1971	1.1647	0.9850	0.8352	0.9159	0.7864
		Shi	SSL	1.2789	1.2323	1.0870	0.8849	1.0181	0.8371
		Touratier	SSL	1.2580	1.2150	1.0629	0.8617	0.9945	0.8265
		Ambartsumian	SSL	1.2369	1.1920	1.0592	0.8617	0.9930	0.8149
		TSDT	SSL	1.2719	1.2256	1.0825	0.8812	1.0142	0.8336
	NNRPIM V1	Mantari	SSL	1.2177	1.1979	1.0116	0.9194	0.9401	0.8592
		Shi	SSL	1.2617	1.2204	1.0380	0.8726	0.9668	0.8228
		Touratier	SSL	1.1688	1.1301	0.9364	0.7867	0.8685	0.7421
		Ambartsumian	SSL	0.8531	0.8154	0.7020	0.5546	0.6544	0.5289
		TSDT	SSL	1.1928	1.1506	0.9670	0.8032	0.8988	0.7584
	NNRPIM V2	Mantari	SSL	1.1727	1.1380	0.9718	0.8121	0.9047	0.7657
		Shi	SSL	1.2827	1.2348	1.0965	0.8868	1.0279	0.8392
		Touratier	SSL	1.2798	1.2353	1.0900	0.8921	1.0211	0.8436
		Ambartsumian	SSL	1.3094	1.2635	1.1386	0.9293	1.0707	0.8792
		TSDT	SSL	1.2914	1.2436	1.1070	0.8968	1.0383	0.8487

table 72 - Maximum normalized transverse displacements for simply supported antisymmetric angle-ply $(\theta/-\theta)_n$ square laminates subjected to a sinusoidal load (SSL), a/h=10

				θ = 5°		θ = 30		θ = 45°	
a/h	Solution	ESL	Load	n = 1	n = 3	n = 1	n = 3	n = 1	n = 3
10	Exact	TSDT	SSL	0.4848	0.4485	0.5916	0.3007	0.5581	0.2745
		FSDT	SSL	0.4883	0.4491	0.6099	0.2989	0.5773	0.2728
	RPIM	Mantari	SSL	0.5157	0.4499	0.5927	0.2995	0.5451	0.2730
		Shi	SSL	0.5204	0.4520	0.6046	0.3010	0.5574	0.2746
		Touratier	SSL	0.5161	0.4488	0.5991	0.2994	0.5523	0.2733
		Ambartsumian	SSL	0.5050	0.4387	0.5899	0.2938	0.5446	0.2683
		TSDT	SSL	0.5176	0.4496	0.6021	0.2997	0.5552	0.2729
	NNRPIM V1	Mantari	SSL	0.5465	0.4825	0.6314	0.3505	0.5835	0.3234
		Shi	SSL	0.5174	0.4510	0.5836	0.3011	0.5357	0.2747
		Touratier	SSL	0.4882	0.4257	0.5349	0.2752	0.4884	0.2499
		Ambartsumian	SSL	0.3875	0.3379	0.4058	0.2029	0.3681	0.1827
		TSDT	SSL	0.4928	0.4292	0.5442	0.2782	0.4975	0.2528
	NNRPIM V2	Mantari	SSL	0.5029	0.4377	0.5819	0.2892	0.5354	0.2633
		Shi	SSL	0.5210	0.4521	0.6086	0.3009	0.5615	0.2745
		Touratier	SSL	0.5239	0.4552	0.6131	0.3046	0.5659	0.2781
		Ambartsumian	SSL	0.5357	0.4657	0.6355	0.3173	0.5887	0.2905
		TSDT	SSL	0.5245	0.4552	0.6147	0.3043	0.5674	0.2778

table 73 - Maximum normalized transverse displacements for simply supported antisymmetric angle-ply $(\theta/-\theta)_n$ square laminates subjected to a sinusoidal load (SSL), a/h=20.

				θ = 5°		θ = 30		θ = 45°	
a/h	**Solution**	**ESL**	**Load**	**n = 1**	**n = 3**	**n = 1**	**n = 3**	**n = 1**	**n = 3**
	Exact	TSDT	SSL	0.3579	0.3209	0.5180	0.2127	0.4897	0.1905
		FSDT	SSL	0.3586	0.3208	0.5224	0.2121	0.4944	0.1899
	RPIM	Mantari	SSL	0.3993	0.3264	0.5320	0.2141	0.4878	0.1914
		Shi	SSL	0.3974	0.3242	0.5328	0.2130	0.4891	0.1906
		Touratier	SSL	0.3947	0.3222	0.5296	0.2120	0.4862	0.1897
		Ambartsumian	SSL	0.3858	0.3149	0.5199	0.2080	0.4779	0.1863
		TSDT	SSL	0.3952	0.3224	0.5307	0.2121	0.4872	0.1898
	NNRPIM V1	Mantari	SSL	0.4245	0.3513	0.5670	0.2524	0.5231	0.2294
20		Shi	SSL	0.3949	0.3235	0.5141	0.2134	0.4700	0.1910
		Touratier	SSL	0.3742	0.3064	0.4734	0.1955	0.4303	0.1739
		Ambartsumian	SSL	0.3019	0.2479	0.3598	0.1456	0.3243	0.1279
		TSDT	SSL	0.3770	0.3085	0.4799	0.1974	0.4367	0.1758
	NNRPIM V2	Mantari	SSL	0.3891	0.3173	0.5219	0.2065	0.4787	0.1844
		Shi	SSL	0.3977	0.3241	0.5362	0.2128	0.4925	0.1904
		Touratier	SSL	0.4005	0.3266	0.5418	0.2156	0.4981	0.1930
		Ambartsumian	SSL	0.4094	0.3343	0.5602	0.2246	0.5168	0.2017
		TSDT	SSL	0.4004	0.3264	0.5416	0.2152	0.4978	0.1927

table 74 - Maximum normalized transverse displacements for simply supported antisymmetric angle-ply $(\theta/-\theta)_n$ square laminates subjected to a sinusoidal load (SSL), a/h=50.

				θ = 5°		θ = 30		θ = 45°	
a/h	**Solution**	**ESL**	**Load**	**n = 1**	**n = 3**	**n = 1**	**n = 3**	**n = 1**	**n = 3**
	Exact	TSDT	SSL	0.3215	0.2842	0.4972	0.1878	0.4704	0.1668
		FSDT	SSL	0.3216	0.2841	0.4979	0.1877	0.4712	0.1667
	RPIM	Mantari	SSL	0.3655	0.2904	0.5144	0.1896	0.4713	0.1681
		Shi	SSL	0.3620	0.2874	0.5124	0.1881	0.4697	0.1668
		Touratier	SSL	0.3598	0.2856	0.5099	0.1872	0.4675	0.1661
		Ambartsumian	SSL	0.3515	0.2791	0.4999	0.1837	0.4590	0.1631
		TSDT	SSL	0.3601	0.2858	0.5104	0.1873	0.4679	0.1662
	NNRPIM V1	Mantari	SSL	0.3788	0.3065	0.5286	0.1723	0.4889	0.1994
50		Shi	SSL	0.3557	0.2842	0.4869	0.1874	0.4451	0.1664
		Touratier	SSL	0.3391	0.2706	0.4520	0.1806	0.4107	0.1520
		Ambartsumian	SSL	0.2767	0.2213	0.3467	0.1291	0.3119	0.1122
		TSDT	SSL	0.3413	0.2722	0.4575	0.1739	0.4161	0.1535
	NNRPIM V2	Mantari	SSL	0.3558	0.2821	0.5041	0.1828	0.4620	0.1618
		Shi	SSL	0.3622	0.2872	0.5154	0.1879	0.4727	0.1666
		Touratier	SSL	0.3649	0.2895	0.5215	0.1903	0.4787	0.1689
		Ambartsumian	SSL	0.3730	0.2964	0.5388	0.1983	0.4964	0.1766
		TSDT	SSL	0.3646	0.2892	0.5207	0.1901	0.4779	0.1687

table 75 - Maximum normalized transverse displacements for simply supported antisymmetric angle-ply $(\theta/-\theta)_n$ square laminates subjected to a sinusoidal load (SSL), a/h=100.

				θ = 5°		θ = 30		θ = 45°	
a/h	**Solution**	**ESL**	**Load**	**n = 1**	**n = 3**	**n = 1**	**n = 3**	**n = 1**	**n = 3**
	Exact	TSDT	SSL	0.3162	0.2789	0.4942	0.1842	0.4676	0.1634
		FSDT	SSL	0.3162	0.2789	0.4944	0.1842	0.4678	0.1633
	RPIM	Mantari	SSL	0.3602	0.2850	0.5109	0.1860	0.4681	0.1646
		Shi	SSL	0.3567	0.2820	0.5089	0.1845	0.4664	0.1634
		Touratier	SSL	0.3546	0.2803	0.5067	0.1836	0.4645	0.1627
		Ambartsumian	SSL	0.3464	0.2739	0.4968	0.1801	0.4561	0.1597
		TSDT	SSL	0.3549	0.2805	0.5071	0.1837	0.4648	0.1627
	NNRPIM V1	Mantari	SSL	0.3410	0.2793	0.4631	0.2052	0.4889	0.1862
100		Shi	SSL	0.3367	0.2700	0.4578	0.1800	0.4451	0.1600
		Touratier	SSL	0.3266	0.2607	0.4356	0.1670	0.4107	0.1473
		Ambartsumian	SSL	0.2730	0.2174	0.3448	0.1267	0.3119	0.1099
		TSDT	SSL	0.3281	0.2619	0.4397	0.1685	0.4161	0.1487
	NNRPIM V2	Mantari	SSL	0.3499	0.2764	0.4991	0.1791	0.4575	0.1583
		Shi	SSL	0.3565	0.2816	0.5112	0.1842	0.4688	0.1631
		Touratier	SSL	0.3595	0.2839	0.5177	0.1866	0.4753	0.1654
		Ambartsumian	SSL	0.3677	0.2908	0.5356	0.1945	0.4933	0.1730
		TSDT	SSL	0.3591	0.2837	0.5168	0.1863	0.4743	0.1651

B. Nondimensionalized Maximum Stresses Along the Thickness for Various Laminates

Symmetric Cross-Ply Laminates

RPIM

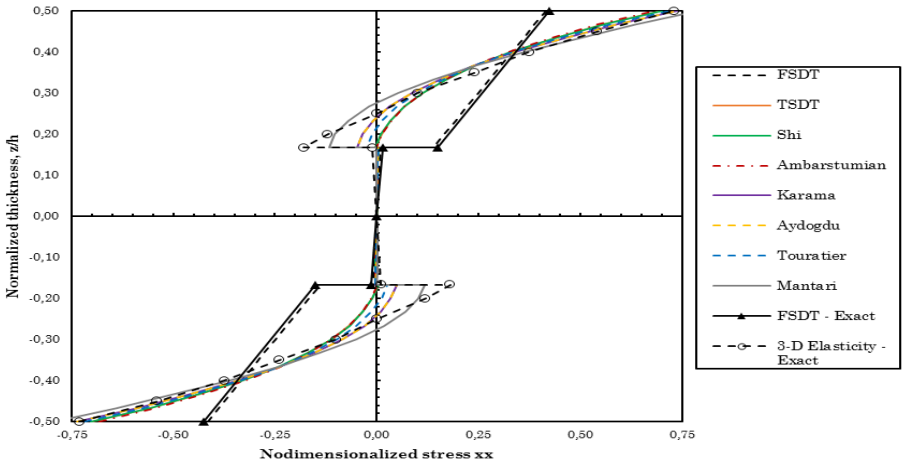

NNRPIM V1

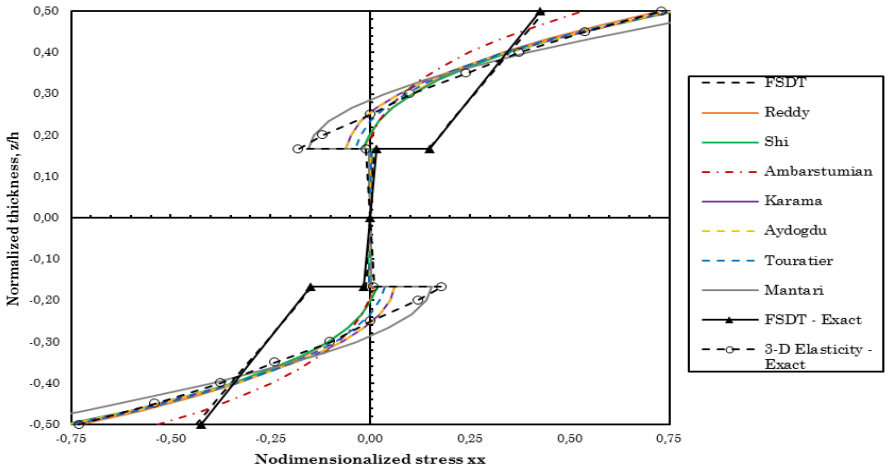

NNRPIM V2

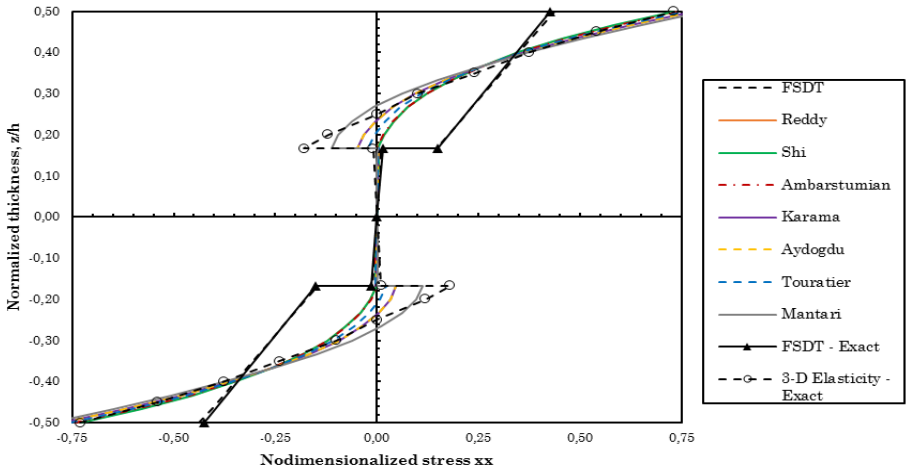

figure 58 – Nondimensionalized stresses σ_{xx} computed with the three numerical methods for a simply supported symmetric square laminate with cross-ply layers (0/90/0) subjected to a sinusoidal load (SSL), a/h=4.

RPIM

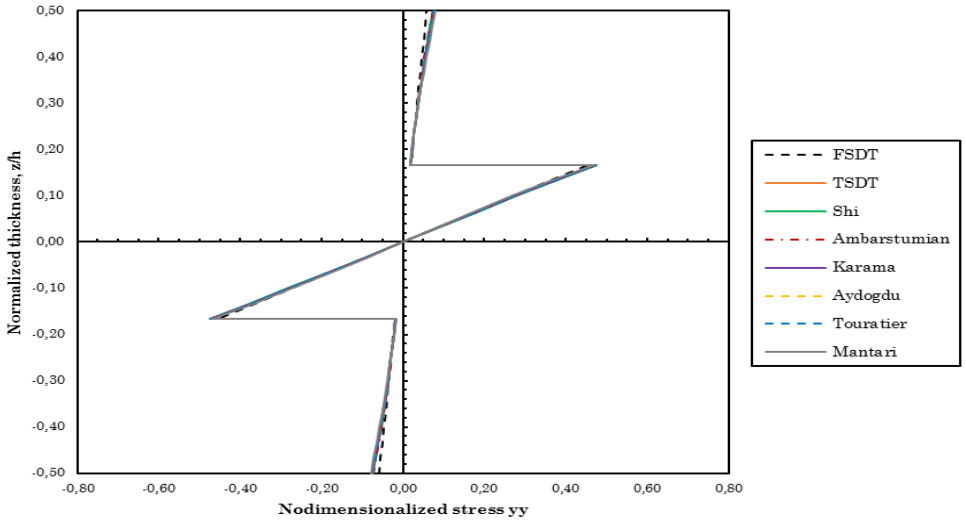

NNRPIM V1

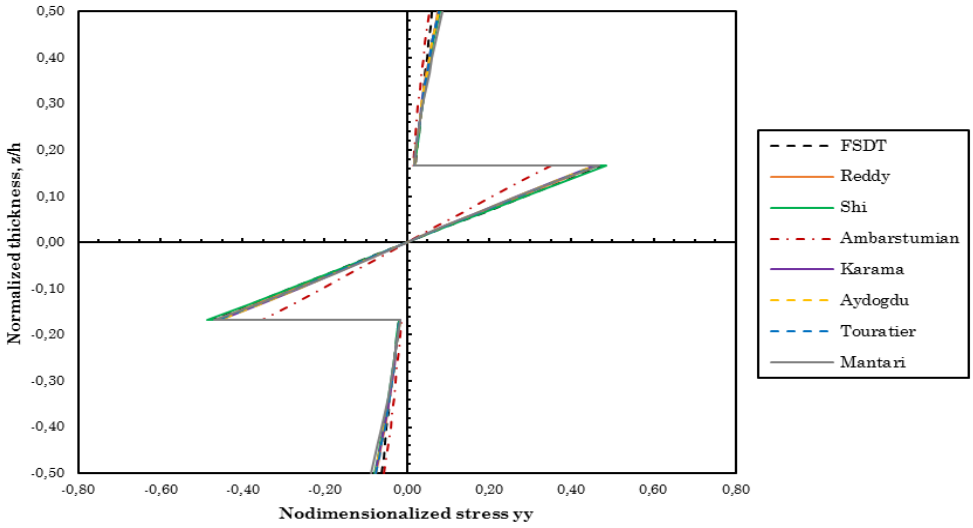

NNRPIM V2

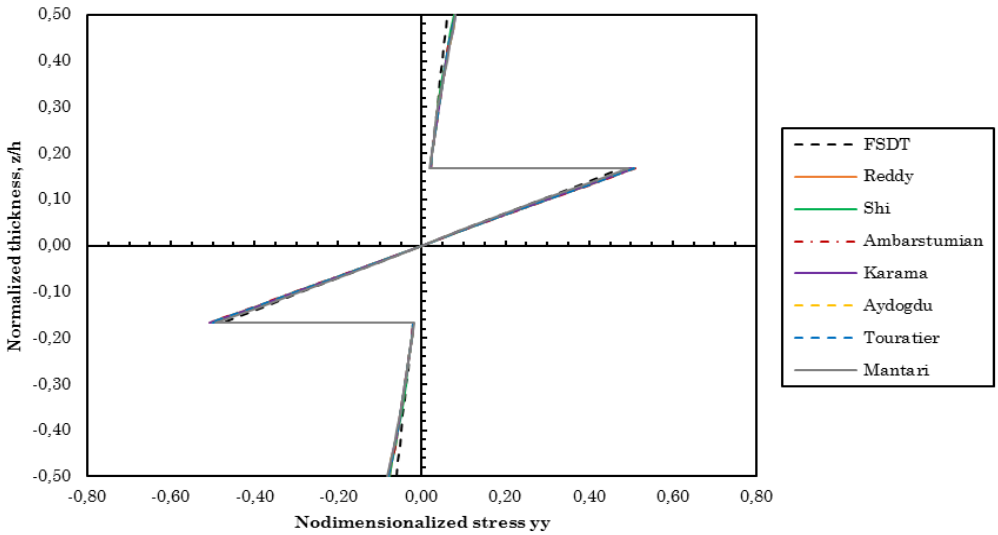

figure 59 – Nondimensionalized stresses σ_{yy} computed with the three numerical methods for a simply supported symmetric square laminate with cross-ply layers (0/90/0) subjected to a sinusoidal load (SSL), a/h=4.

RPIM

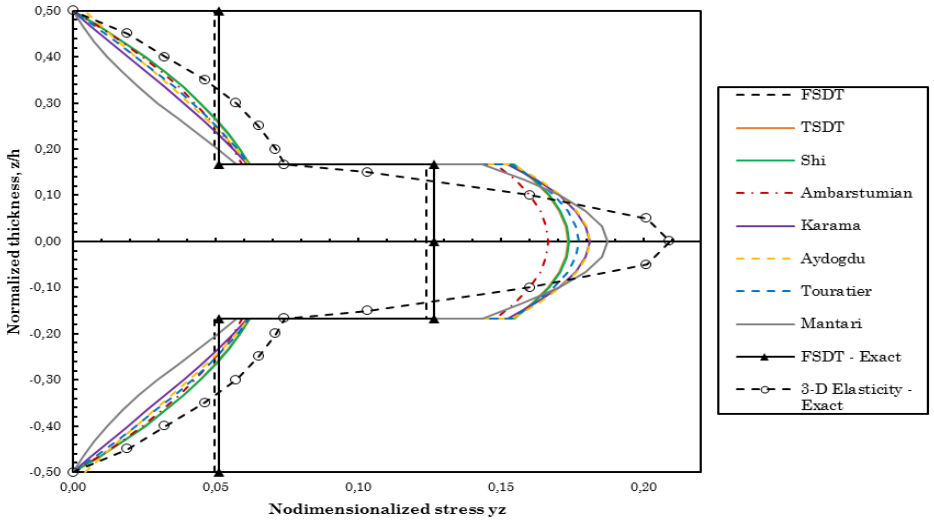

NNRPIM V1

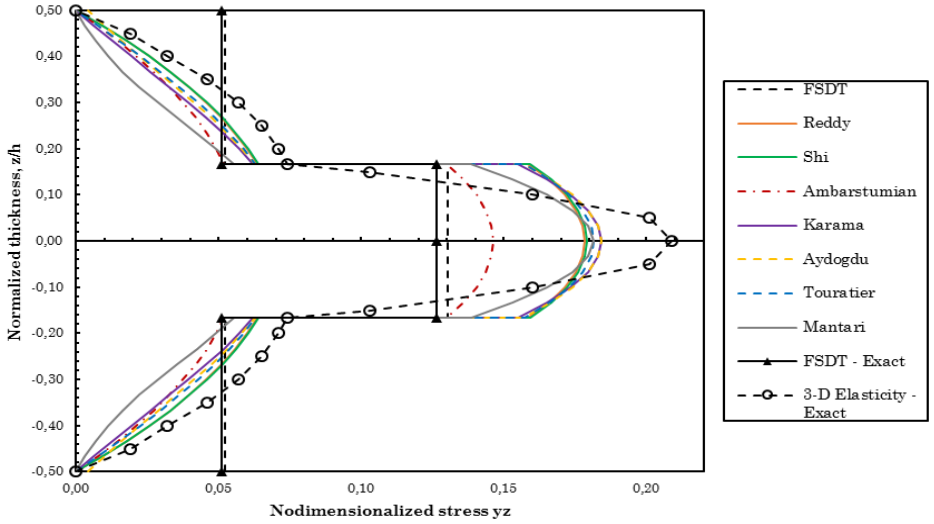

NNRPIM V2

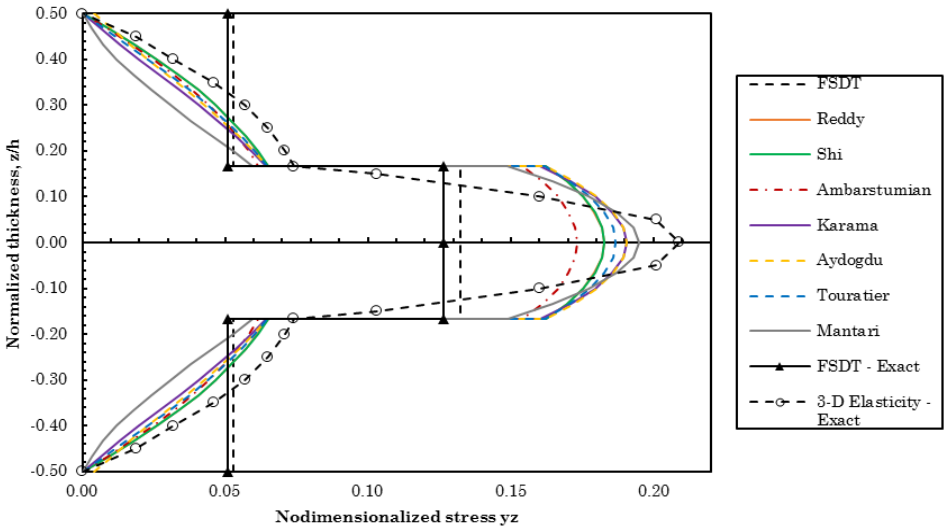

figure 60 – Nondimensionalized stresses τ_{yz} computed with the three numerical methods for a simply supported symmetric square laminate with cross-ply layers (0/90/0) subjected to a sinusoidal load (SSL), a/h=4.

RPIM

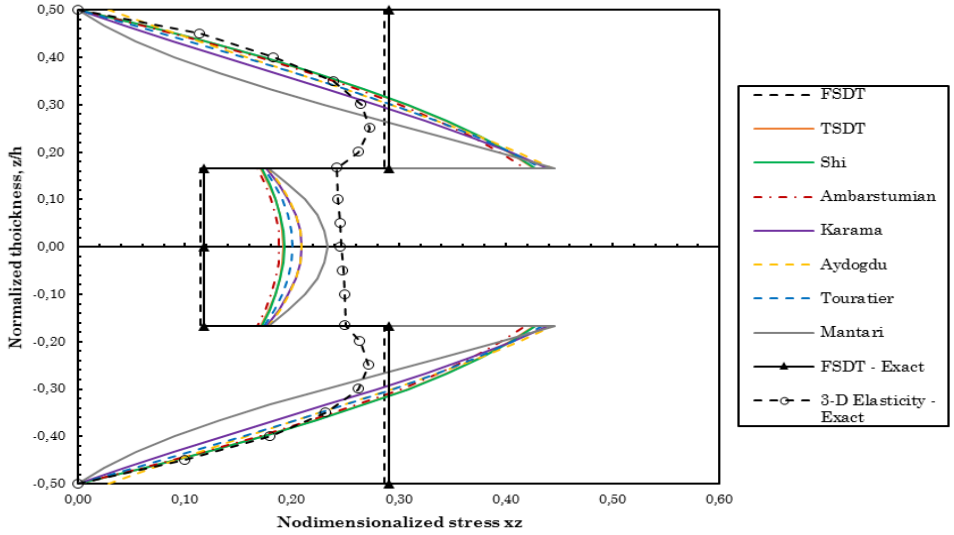

NNRPIM V1

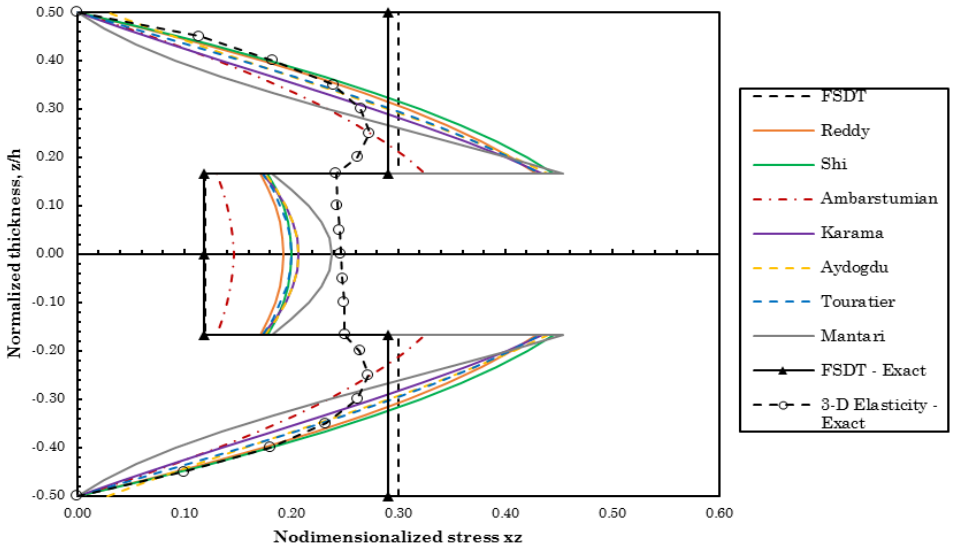

NNRPIM V2

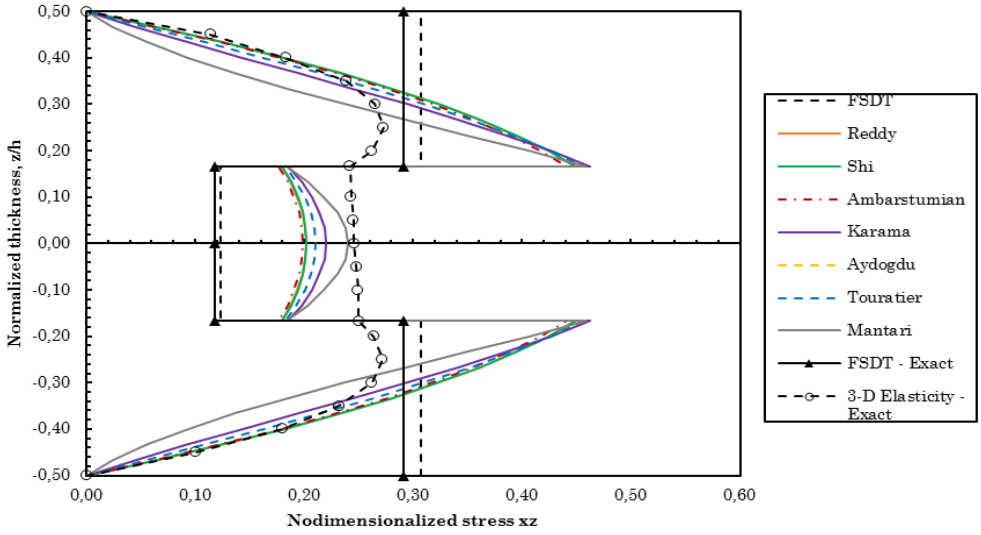

figure 61 – Nondimensionalized stresses τ_{xz} computed with the three numerical methods for a simply supported symmetric square laminate with cross-ply layers (0/90/0) subjected to a sinusoidal load (SSL), a/h=4.

RPIM

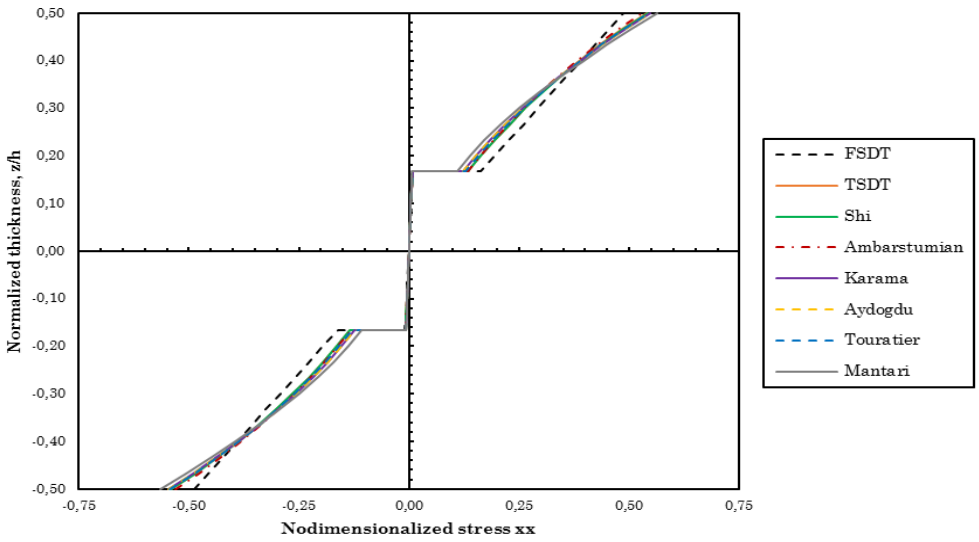

NNRPIM V1

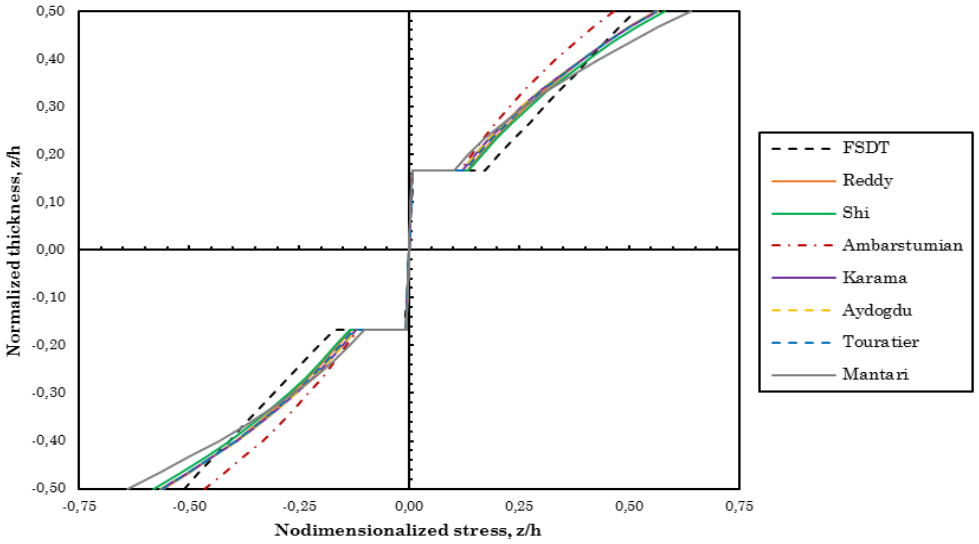

NNRPIM V2

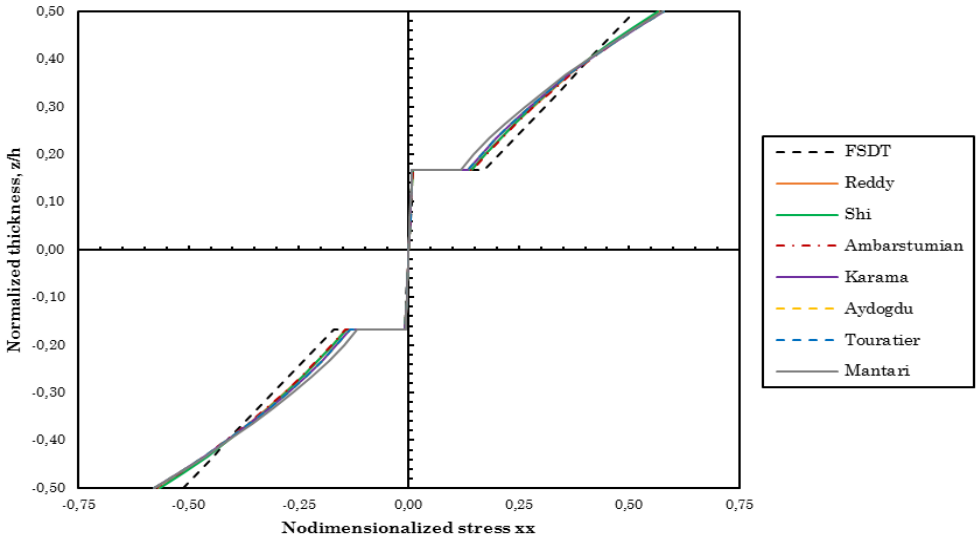

figure 62 – Nondimensionalized stresses σ_{xx} computed with the three numerical methods for a simply supported symmetric square laminate with cross-ply layers (0/90/0) subjected to a sinusoidal load (SSL), a/h=10.

RPIM

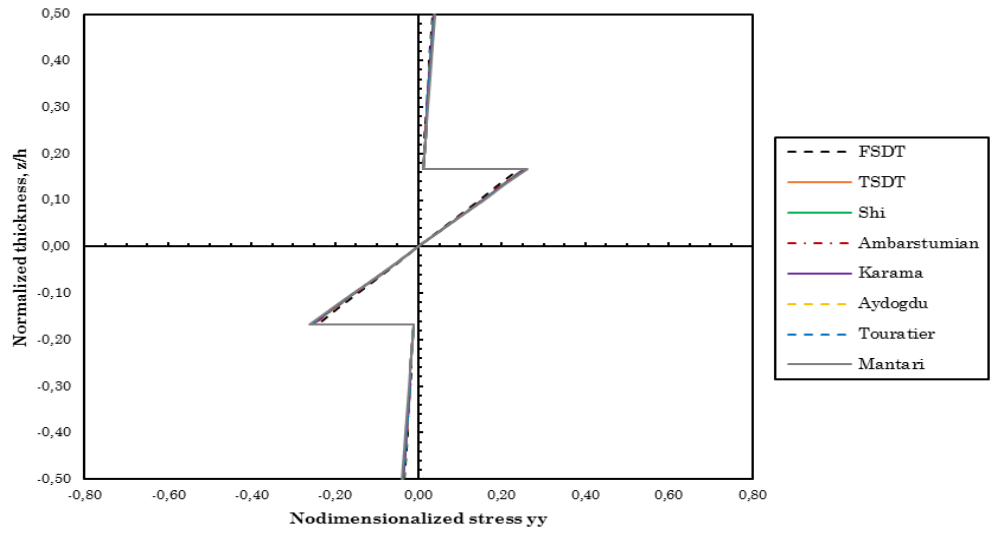

NNRPIM V1

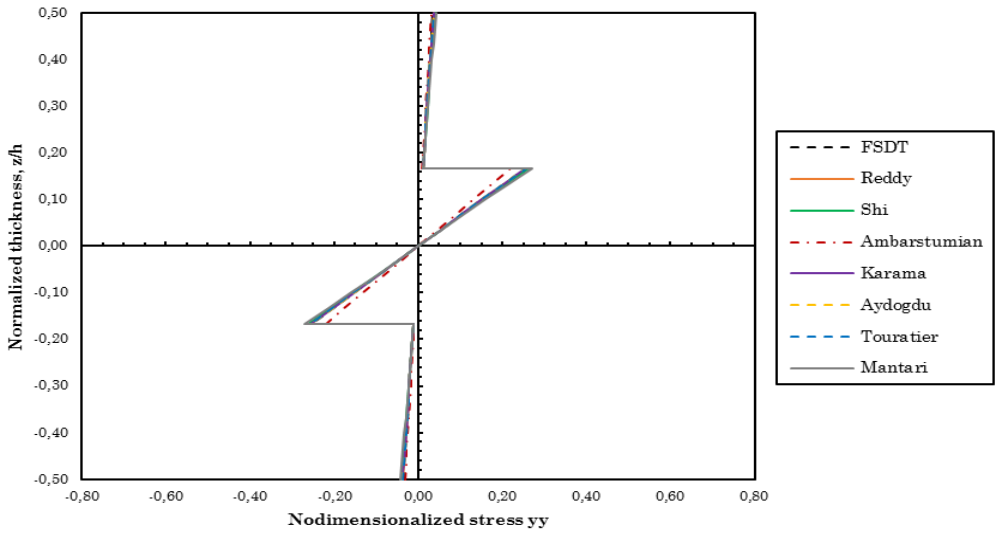

NNRPIM V2

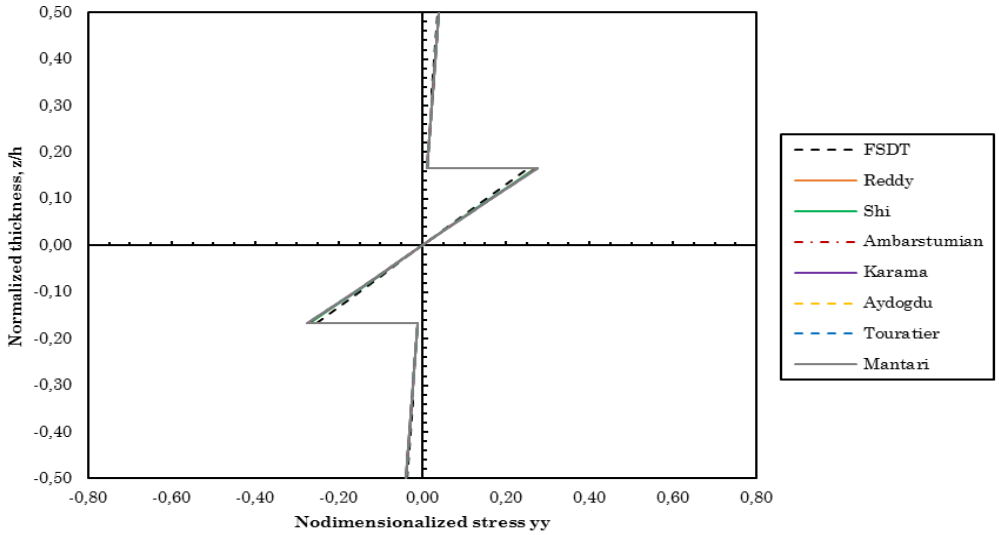

figure 63 – Nondimensionalized stresses σ_{yy} computed with the three numerical methods for a simply supported symmetric square laminate with cross-ply layers (0/90/0) subjected to a sinusoidal load (SSL), a/h=10.

RPIM

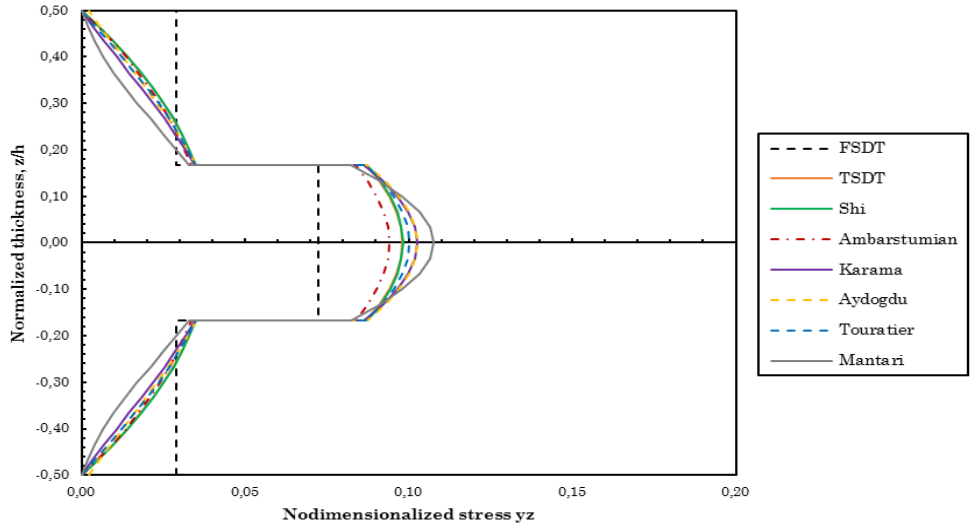

NNRPIM V1

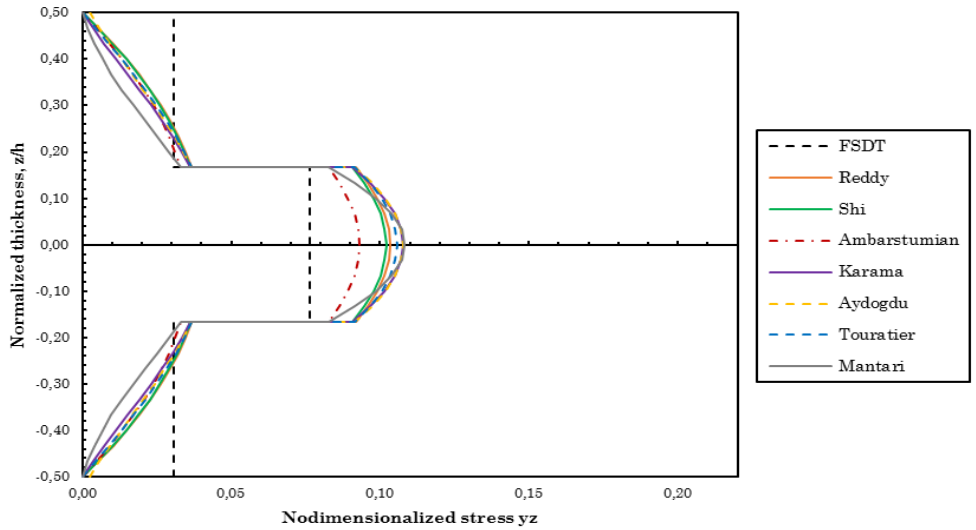

NNRPIM V2

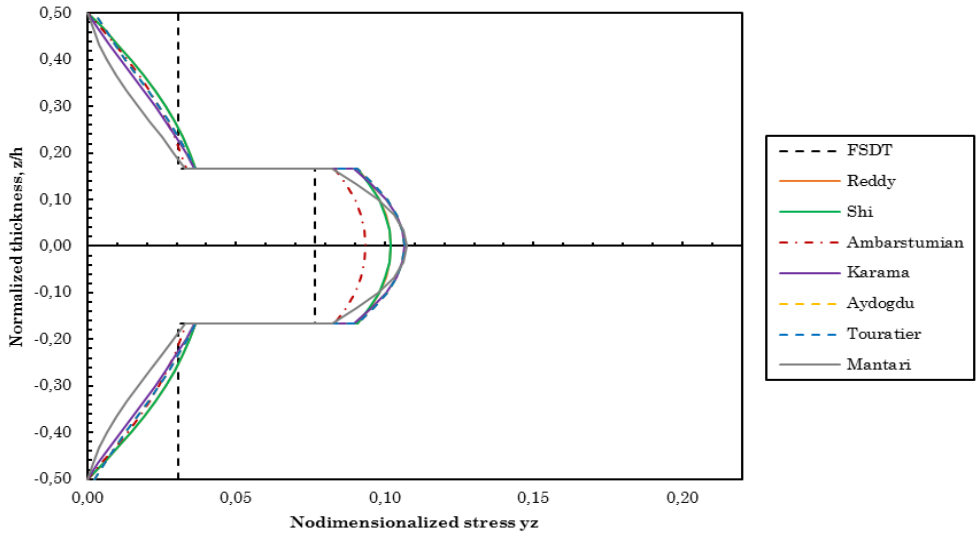

figure 64 – Nondimensionalized stresses τ_{yz} computed with the three numerical methods for a simply supported symmetric square laminate with cross-ply layers (0/90/0) subjected to a sinusoidal load (SSL), a/h=10.

RPIM

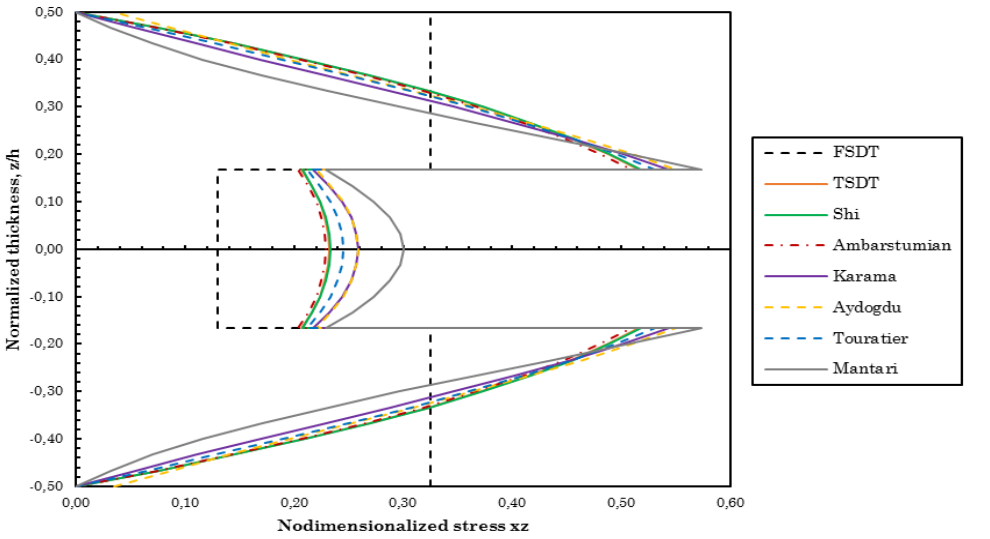

NNRPIM V1

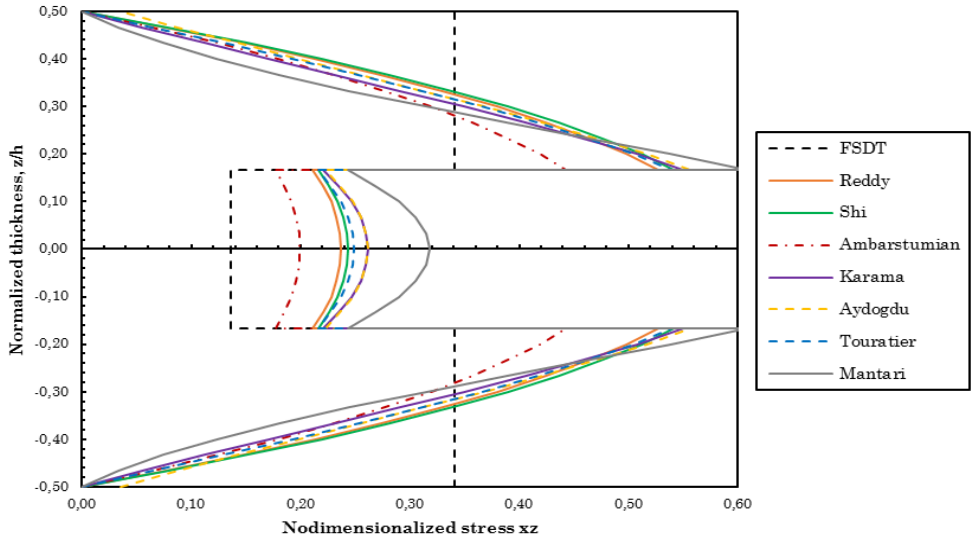

NNRPIM V2

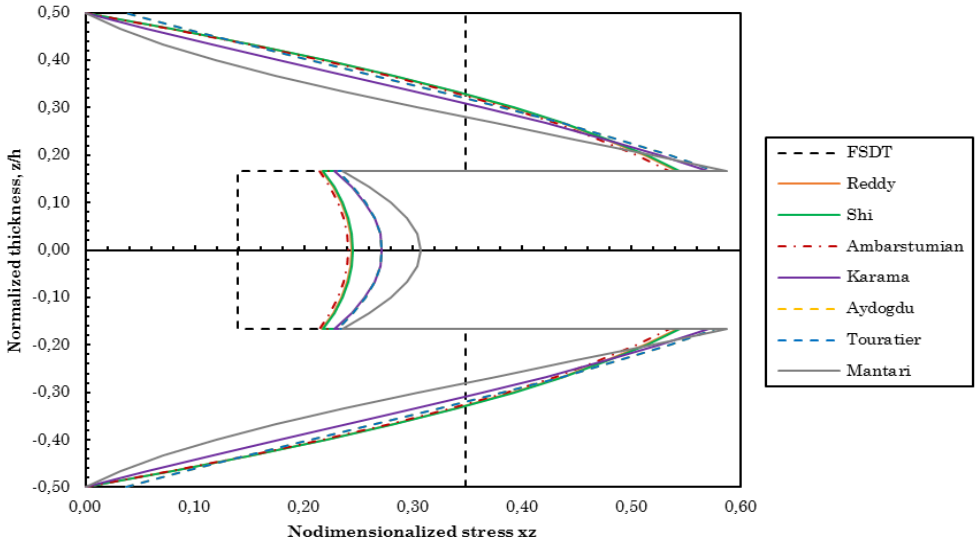

figure 65 – Nondimensionalized stresses τ_{xz} computed with the three numerical methods for a simply supported symmetric square laminate with cross-ply layers (0/90/0) subjected to a sinusoidal load (SSL), a/h=10.

RPIM

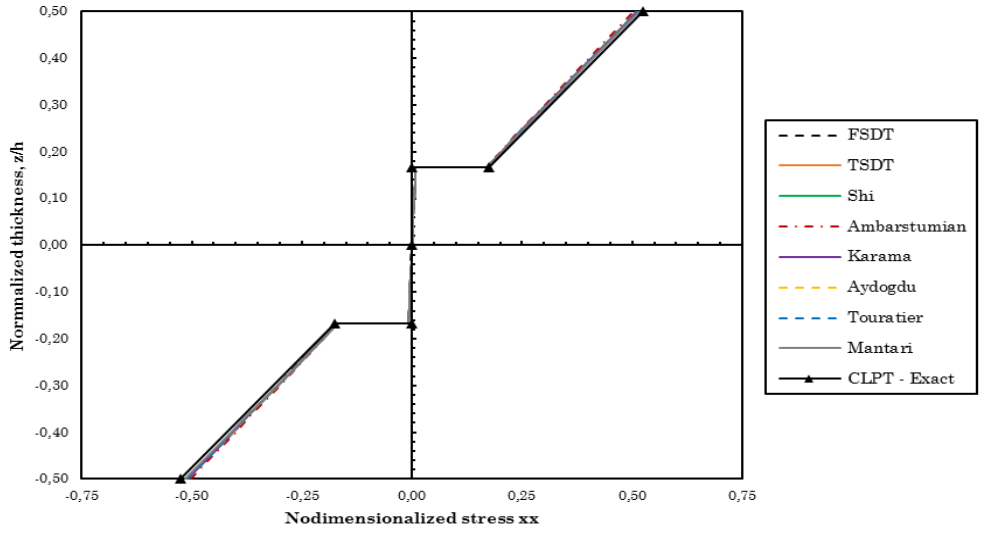

NNRPIM V1

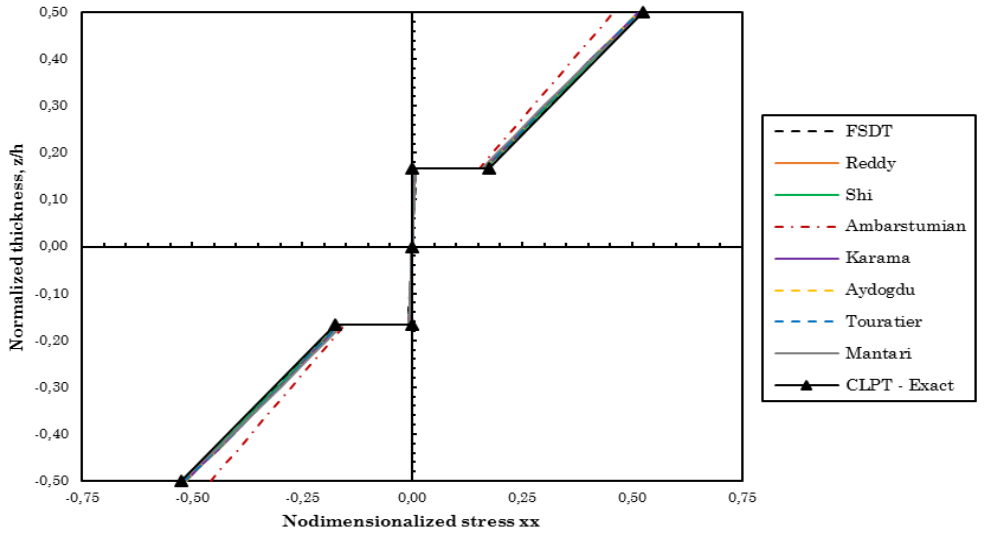

NNRPIM V2

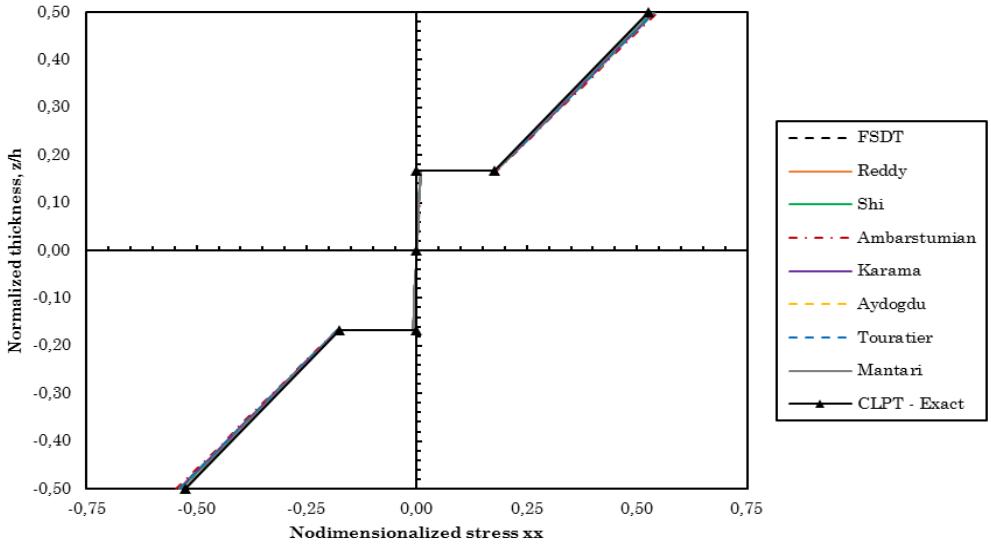

figure 66 – Nondimensionalized stresses σ_{xx} computed with the three numerical methods for a simply supported symmetric square laminate with cross-ply layers (0/90/0) subjected to a sinusoidal load (SSL), a/h=100.

RPIM

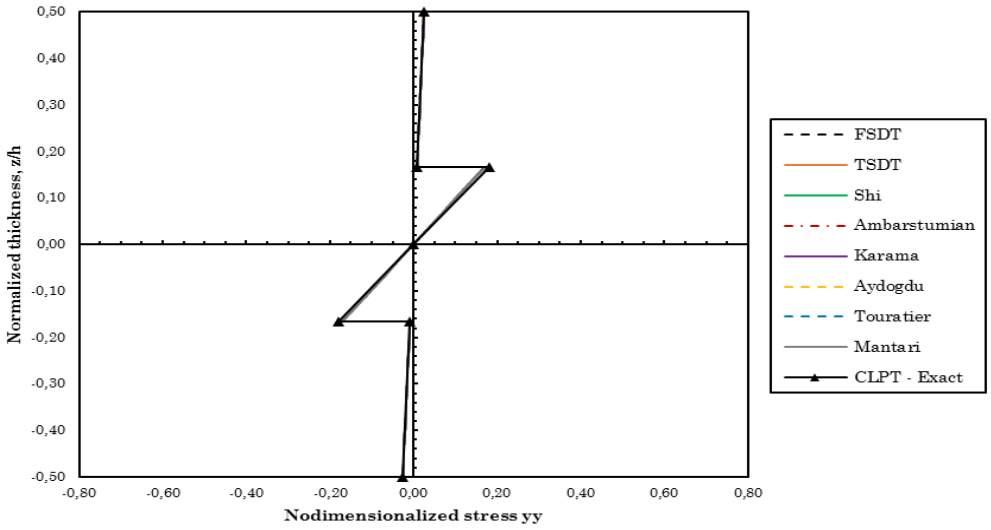

NNRPIM V1

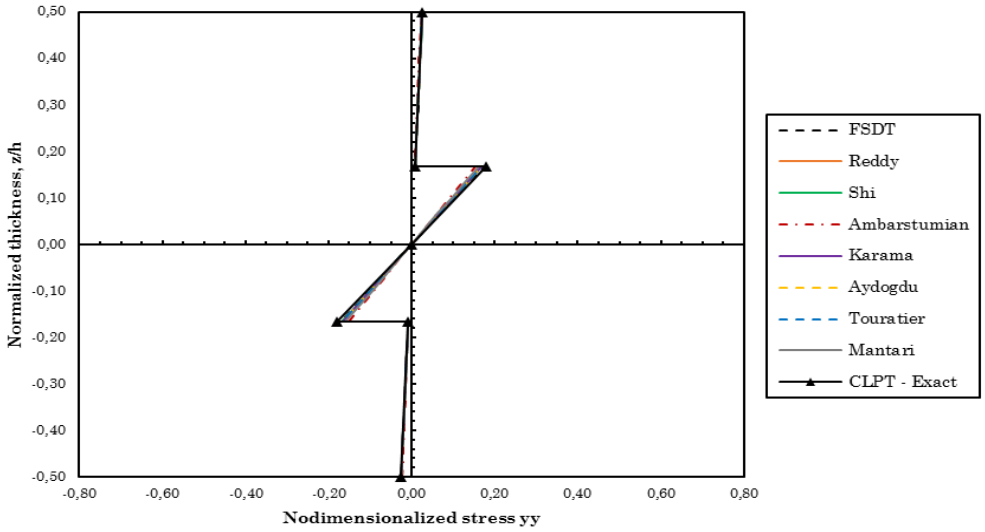

NNRPIM V2

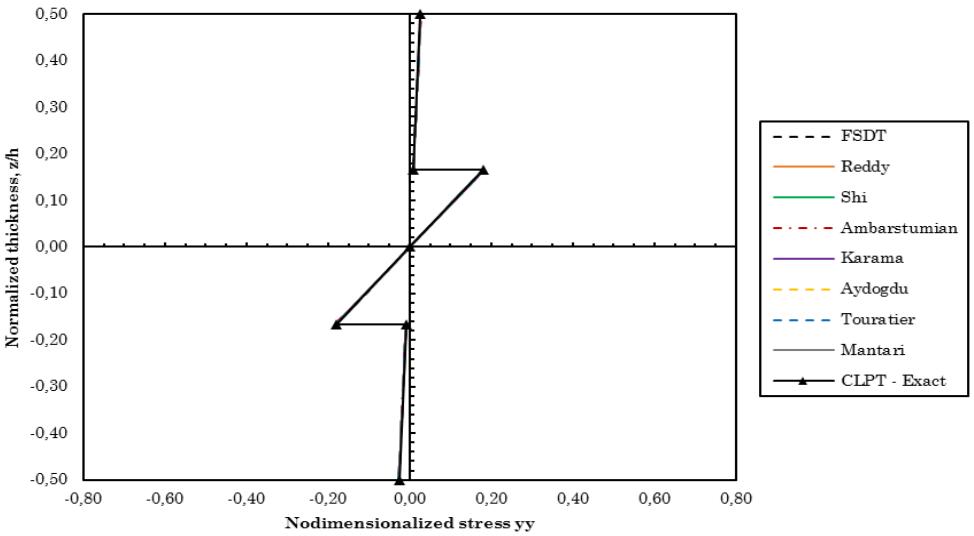

figure 67 – Nondimensionalized stresses σ_{yy} computed with the three numerical methods for a simply supported symmetric square laminate with cross-ply layers (0/90/0) subjected to a sinusoidal load (SSL), a/h=100.

RPIM

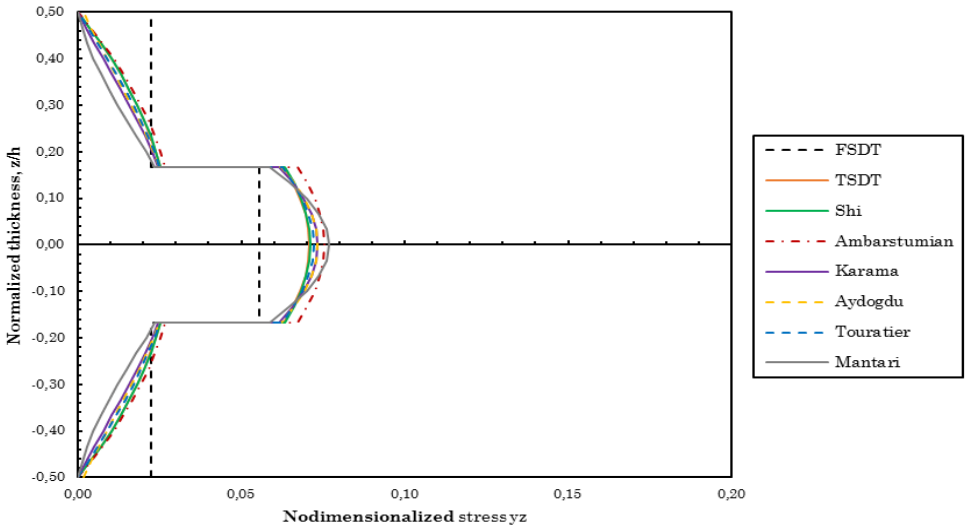

NNRPIM V1

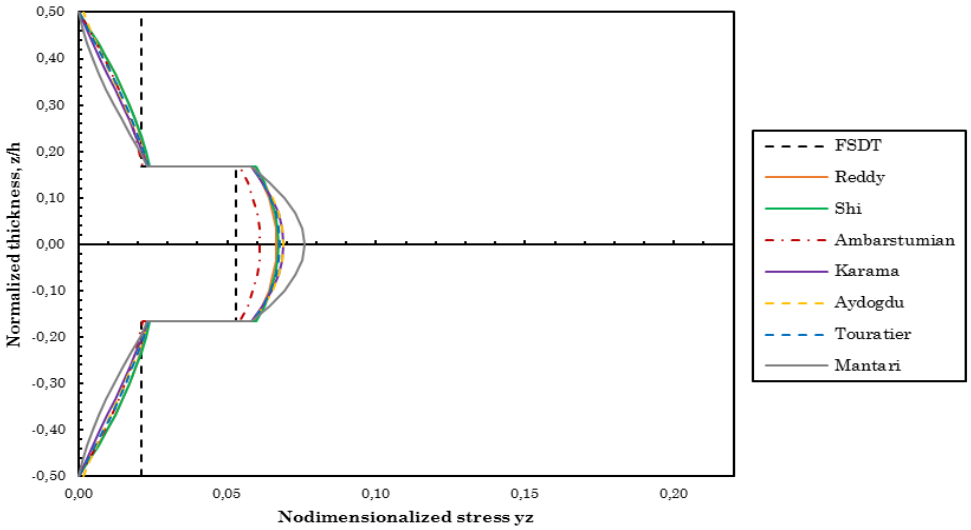

NNRPIM V2

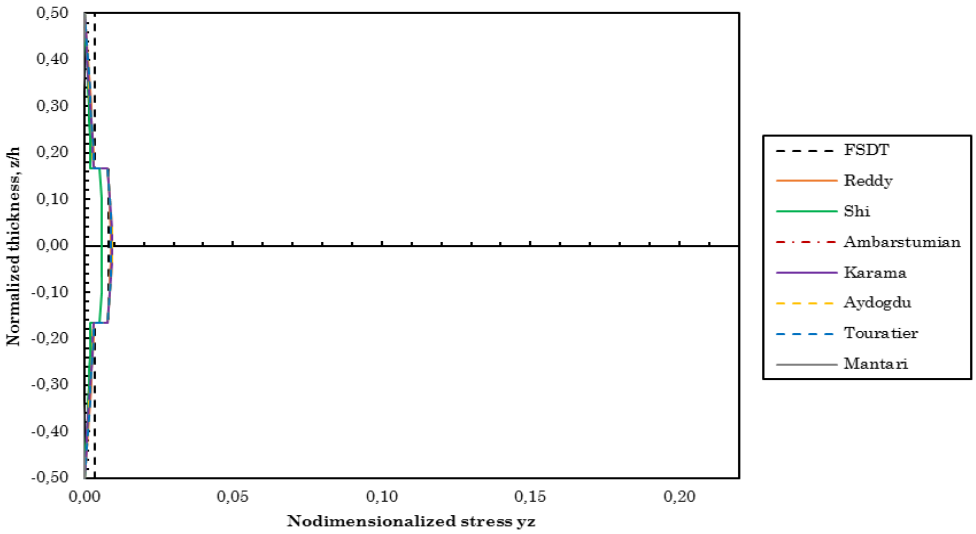

figure 68 – Nondimensionalized stresses τ_{yz} computed with the three numerical methods for a simply supported symmetric square laminate with cross-ply layers (0/90/0) subjected to a sinusoidal load (SSL), a/h=100.

RPIM

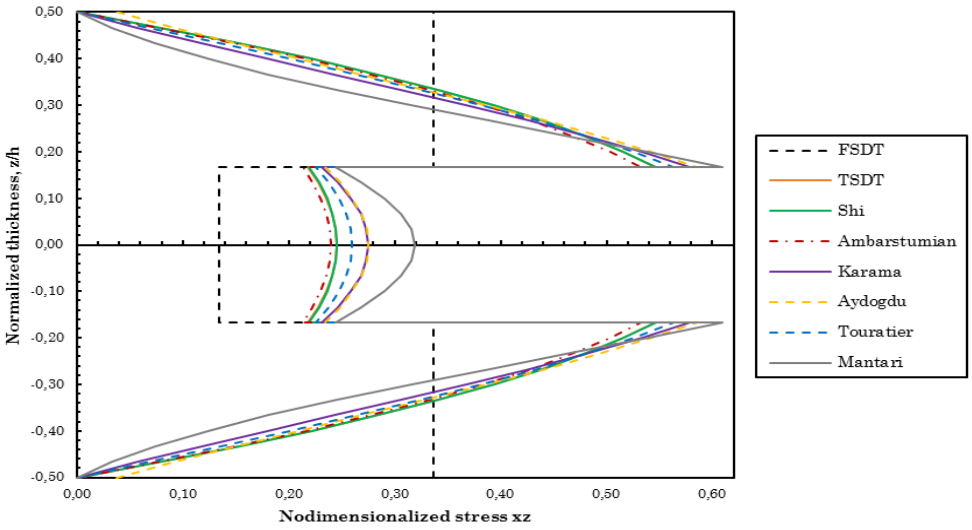

NNRPIM V1

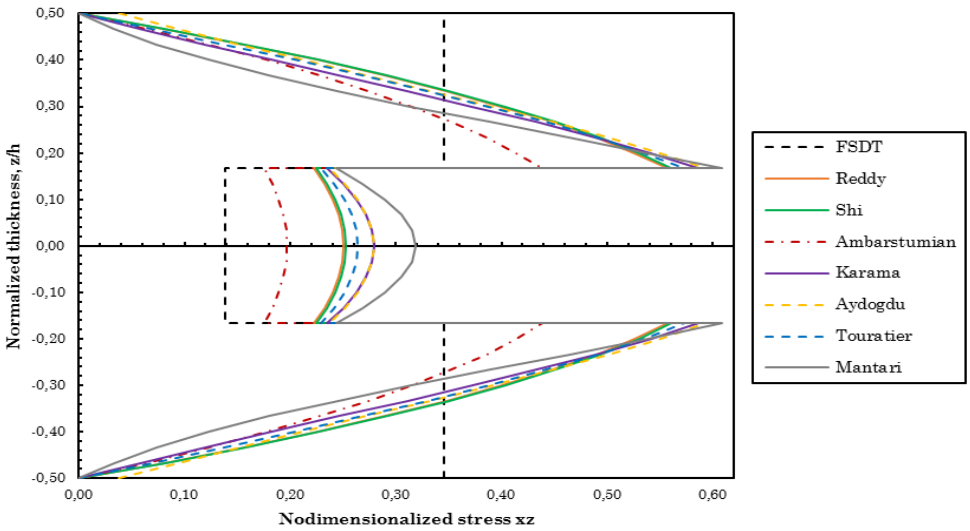

NNRPIM V2

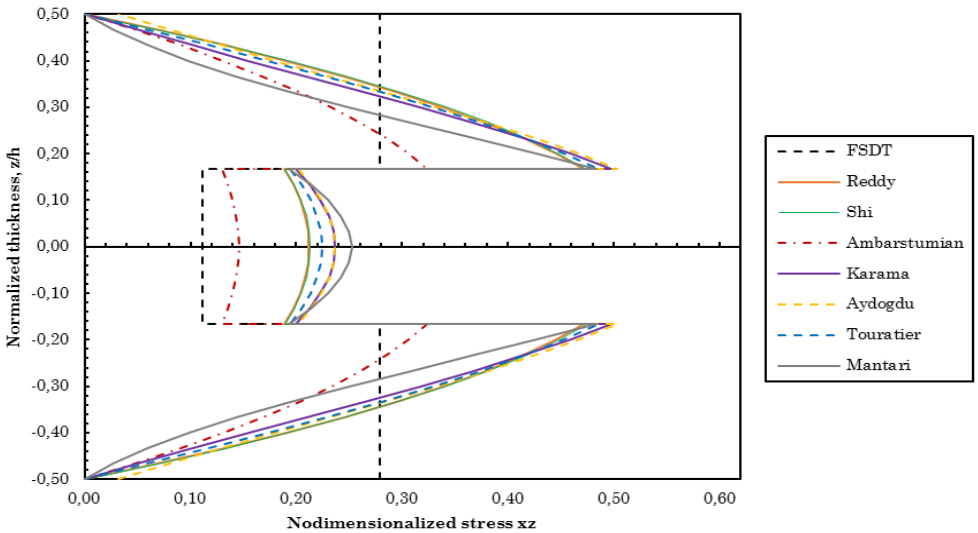

figure 69 – Nondimensionalized stresses τ_{xz} computed with the three numerical methods for a simply supported symmetric square laminate with cross-ply layers (0/90/0) subjected to a sinusoidal load (SSL), a/h=100.

RPIM

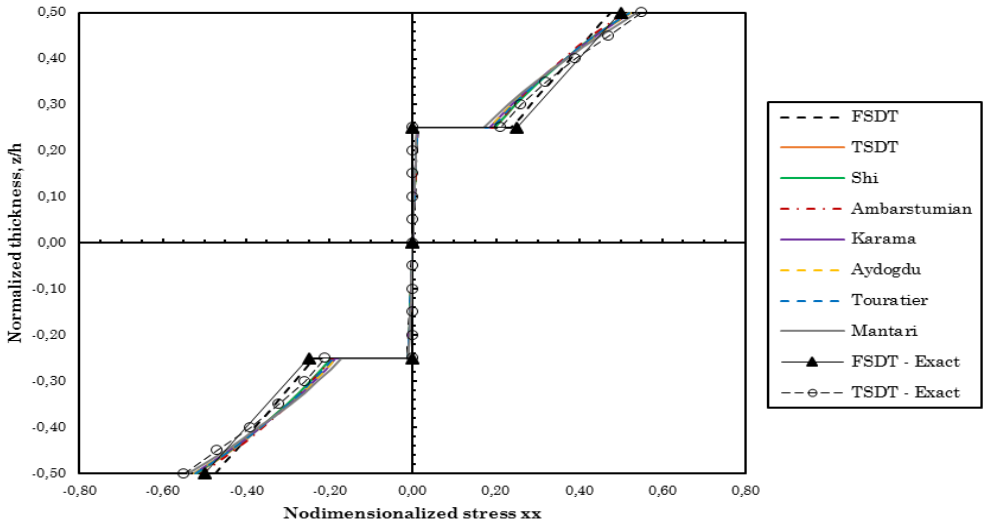

NNRPIM V1

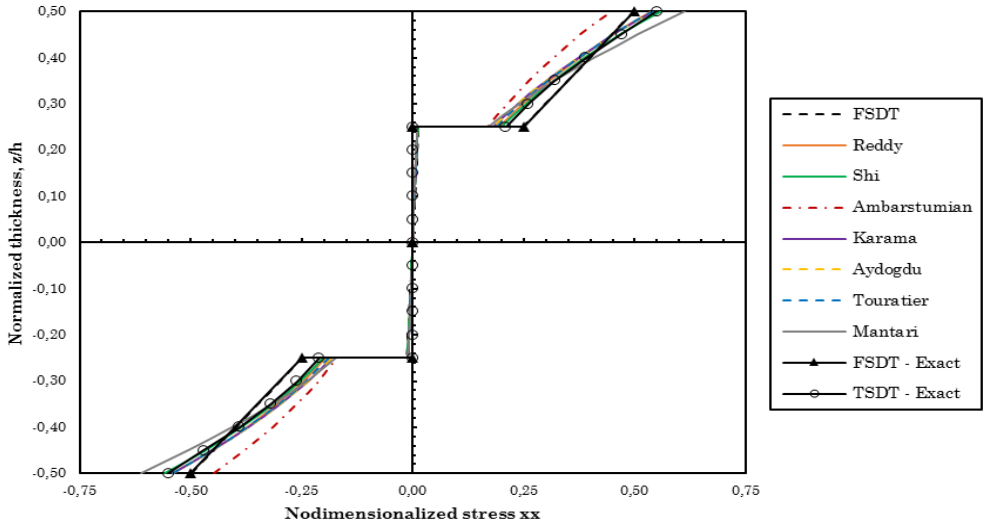

NNRPIM V2

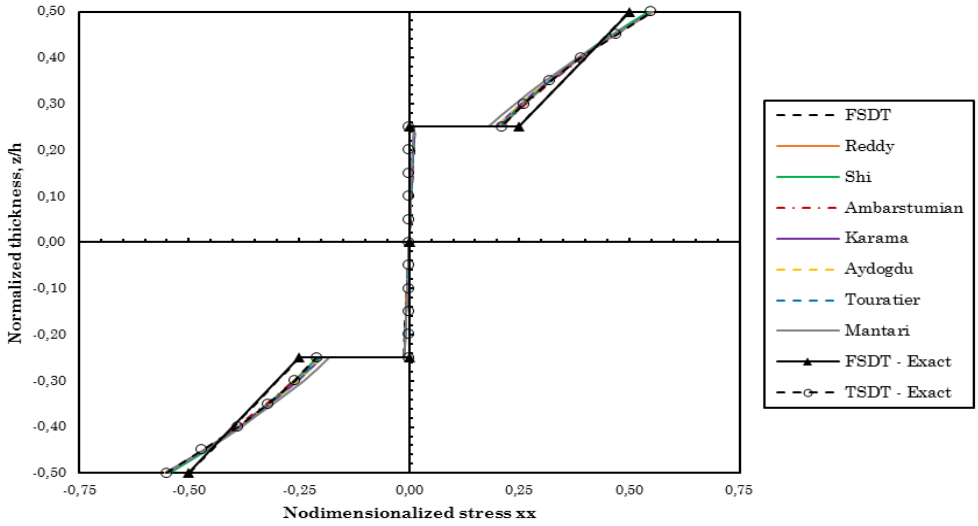

figure 70 – Nondimensionalized stresses σ_{xx} computed with the three numerical methods for a simply supported symmetric square laminate with cross-ply layers (0/90/90/0) subjected to a sinusoidal load (SSL), a/h=10.

RPIM

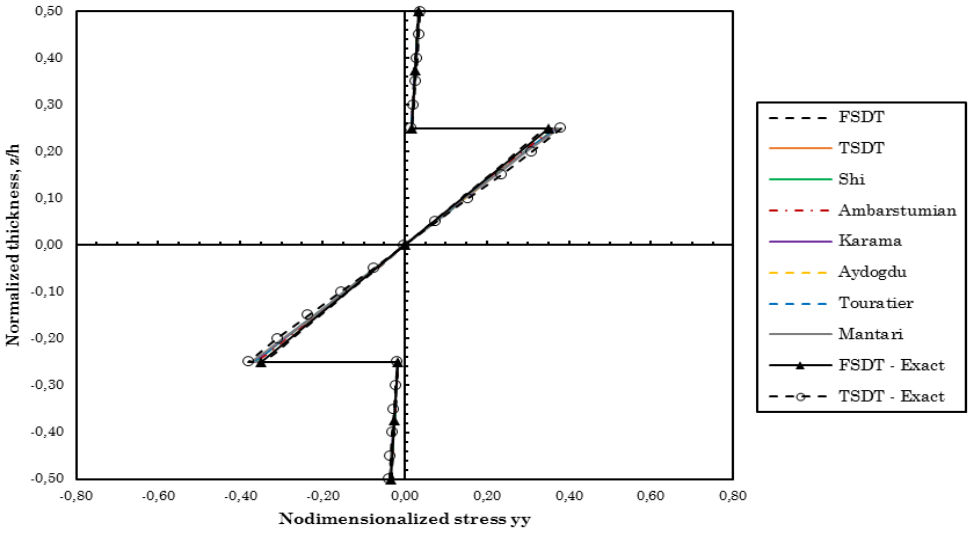

NNRPIM V1

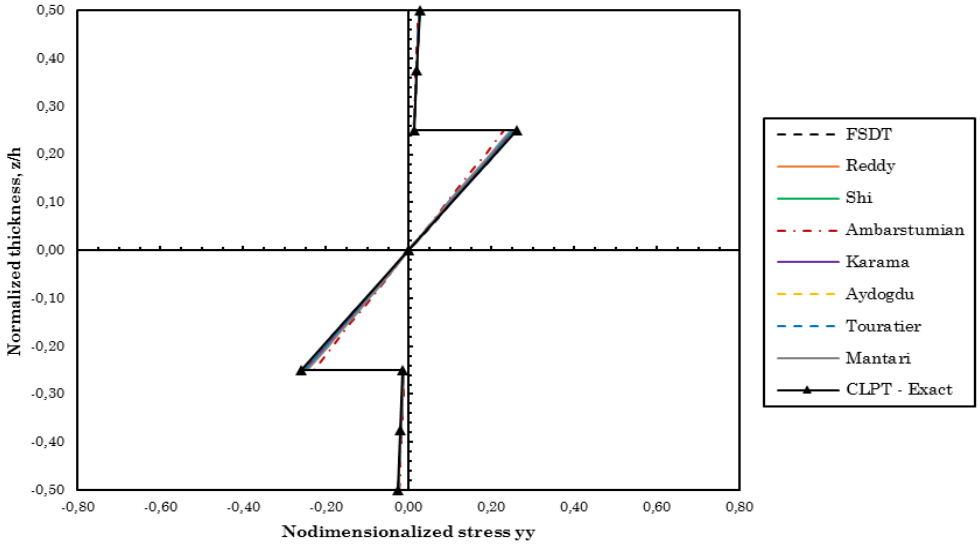

NNRPIM V2

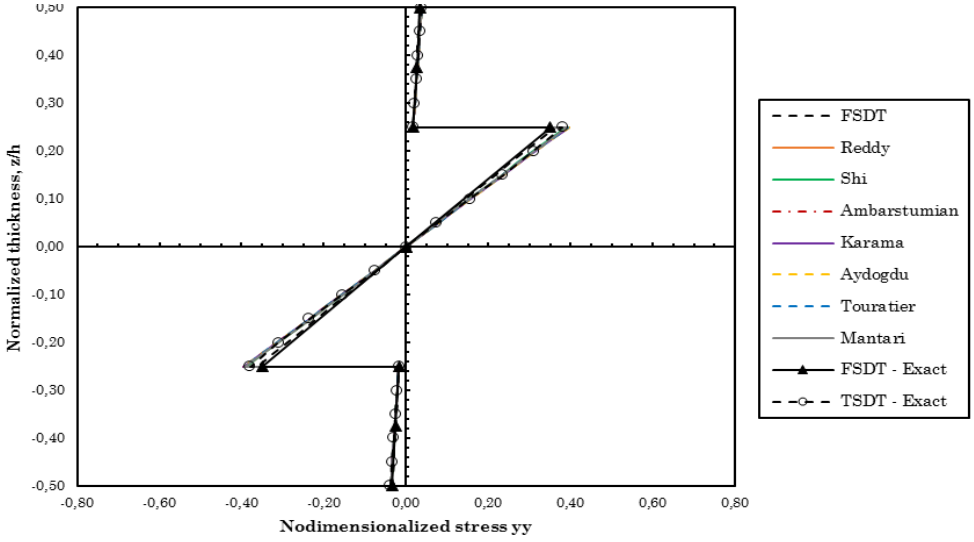

figure 71 – Nondimensionalized stresses σ_{yy} computed with the three numerical methods for a simply supported symmetric square laminate with cross-ply layers (0/90/90/0) subjected to a sinusoidal load (SSL), a/h=10.

RPIM

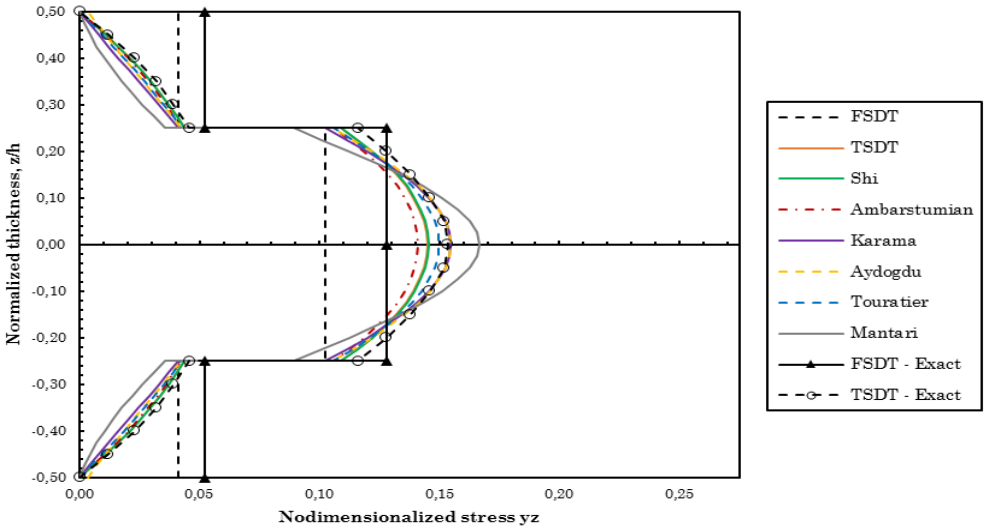

NNRPIM V1

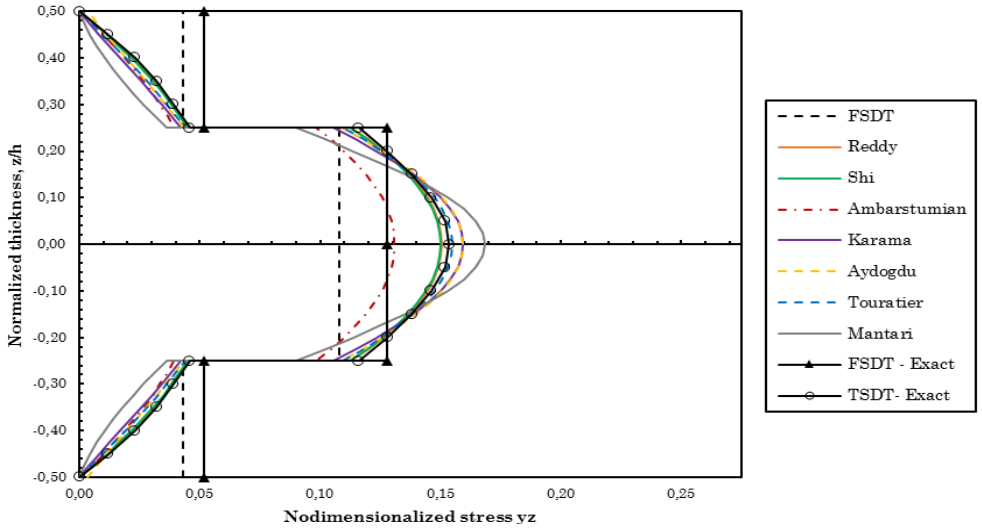

NNRPIM V2

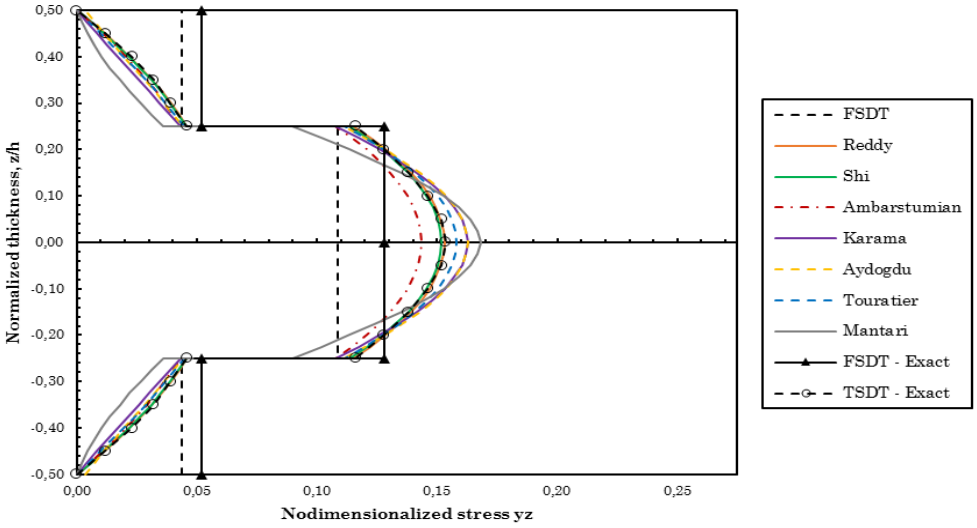

figure 72 – Nondimensionalized stresses τ_{yz} computed with the three numerical methods for a simply supported symmetric square laminate with cross-ply layers (0/90/90/0) subjected to a sinusoidal load (SSL), a/h=10.

RPIM

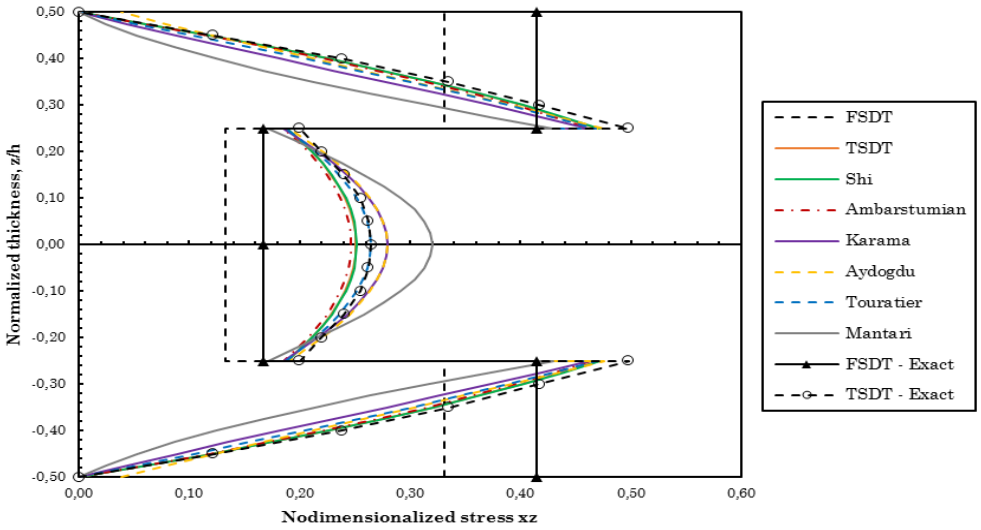

NNRPIM V1

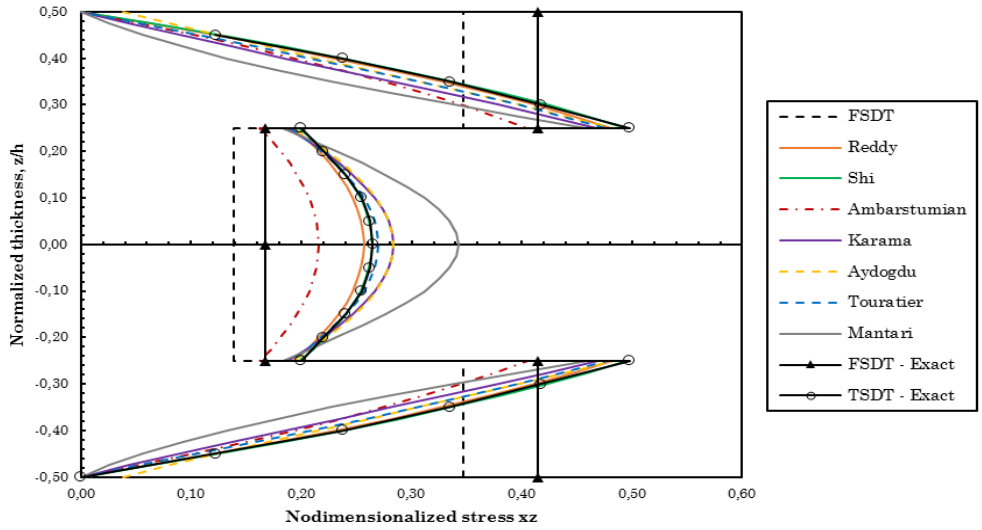

NNRPIM V2

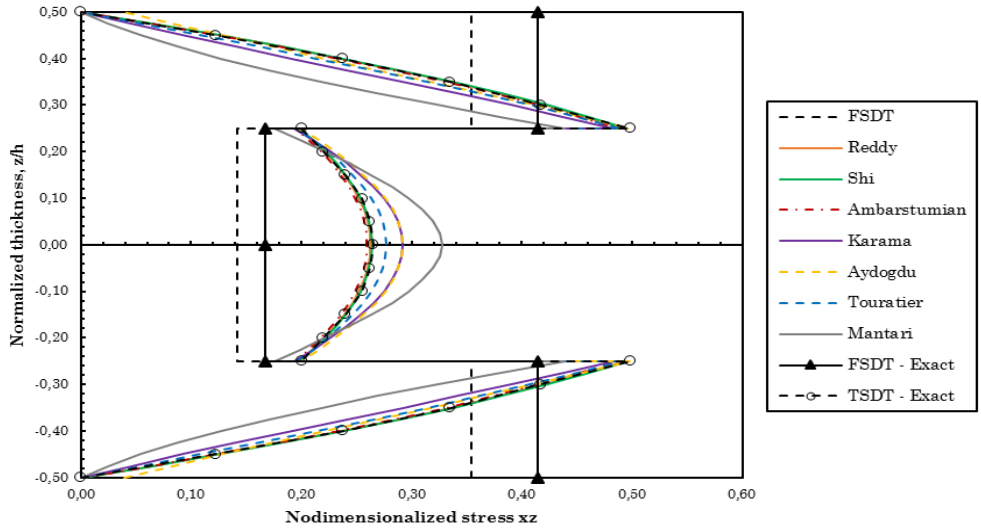

figure 73 – Nondimensionalized stresses τ_{xz} computed with the three numerical methods for a simply supported symmetric square laminate with cross-ply layers (0/90/90/0) subjected to a sinusoidal load (SSL), a/h=10.

RPIM

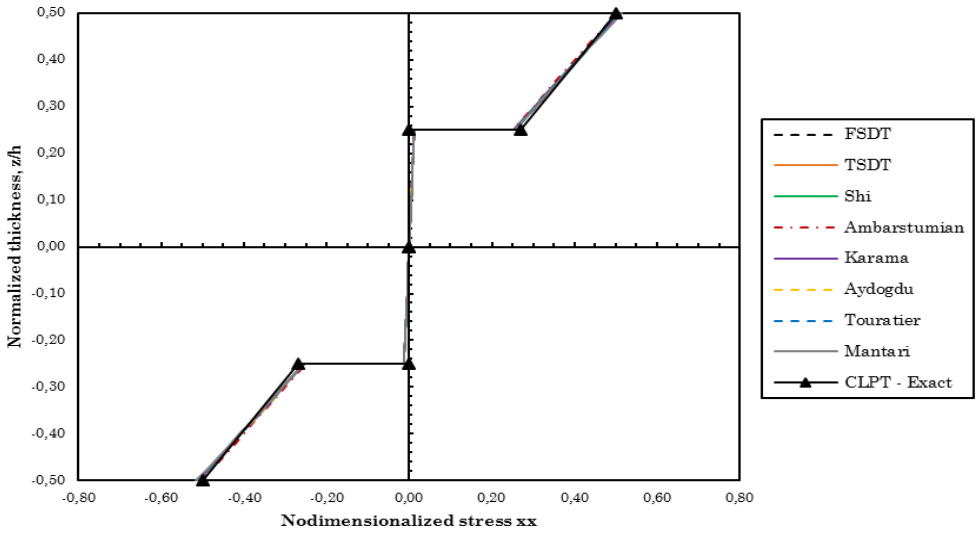

NNRPIM V1

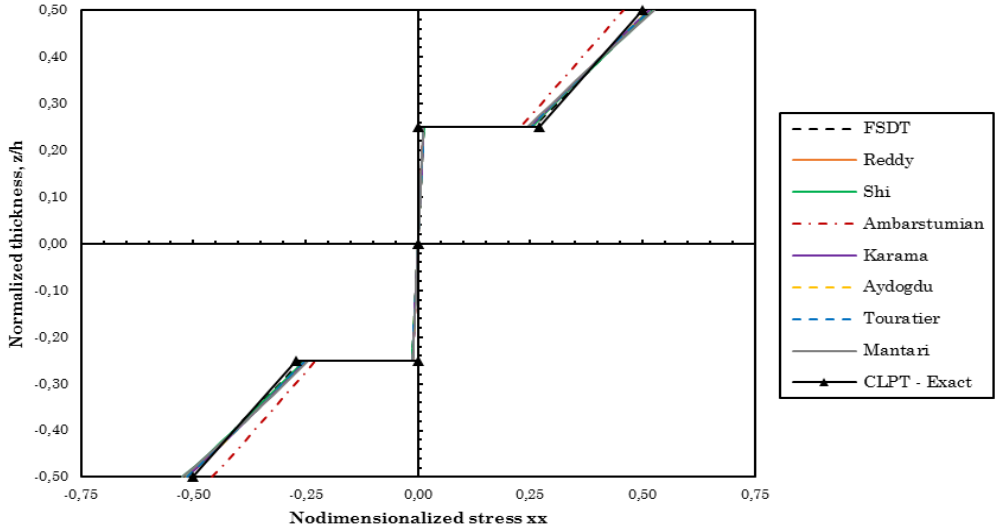

NNRPIM V2

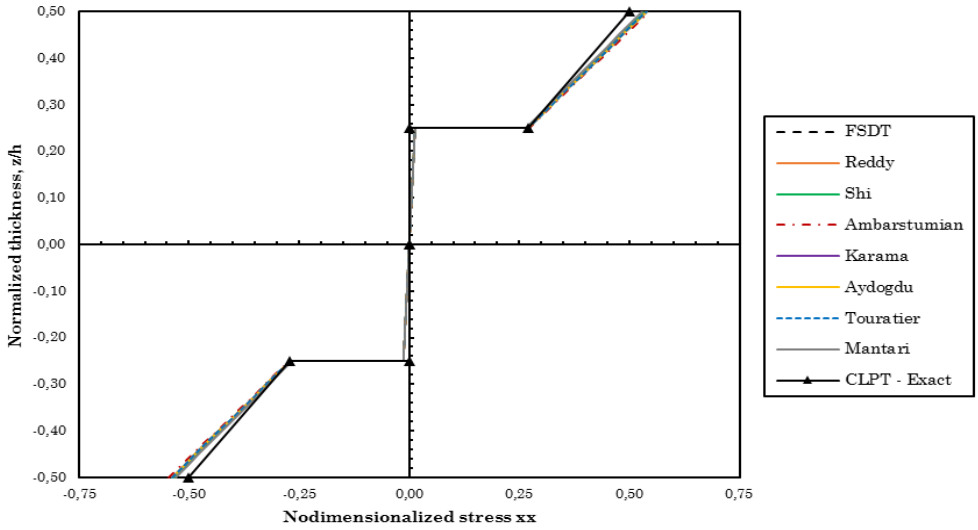

figure 74 – Nondimensionalized stresses σ_{xx} computed with the three numerical methods for a simply supported symmetric square laminate with cross-ply layers (0/90/90/0) subjected to a sinusoidal load (SSL), a/h=100.

RPIM

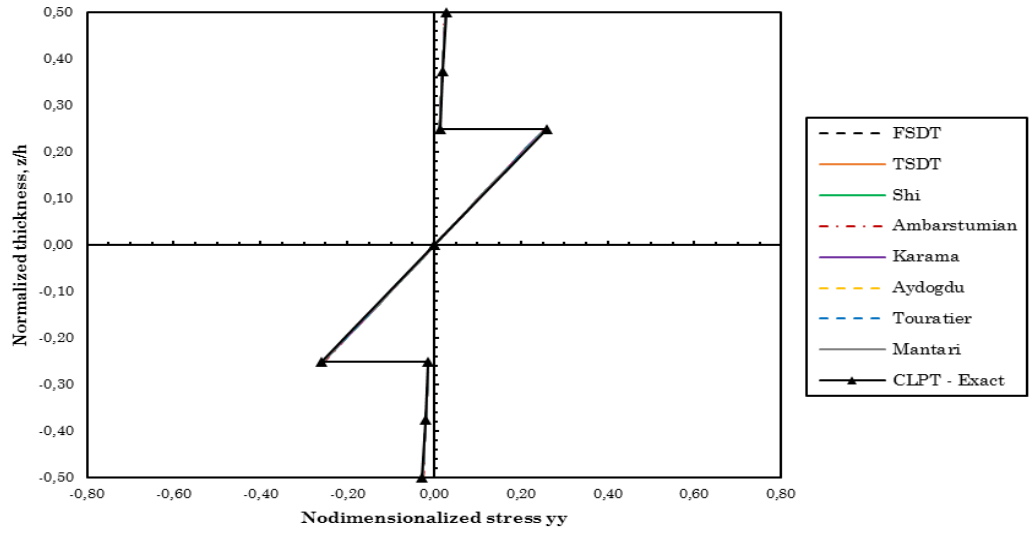

NNRPIM V1

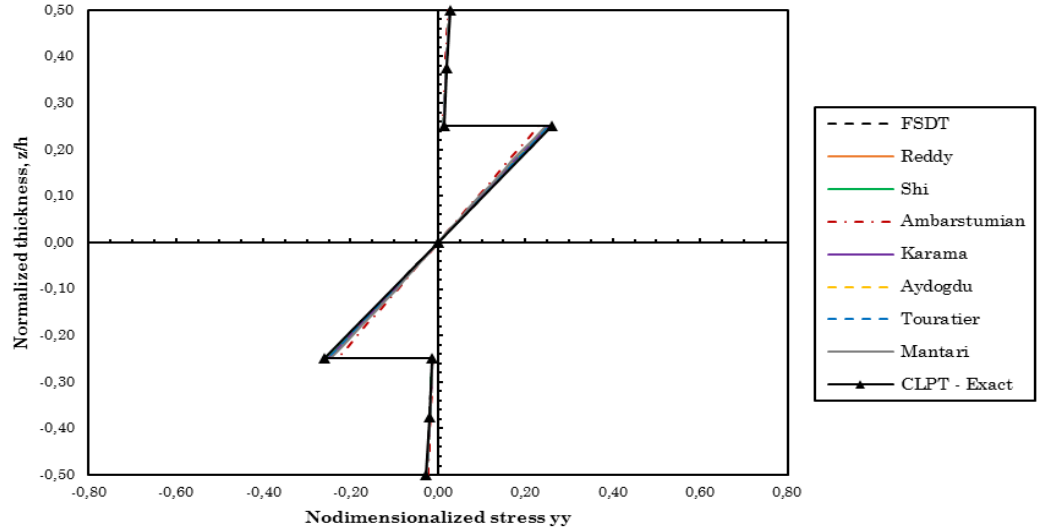

NNRPIM V2

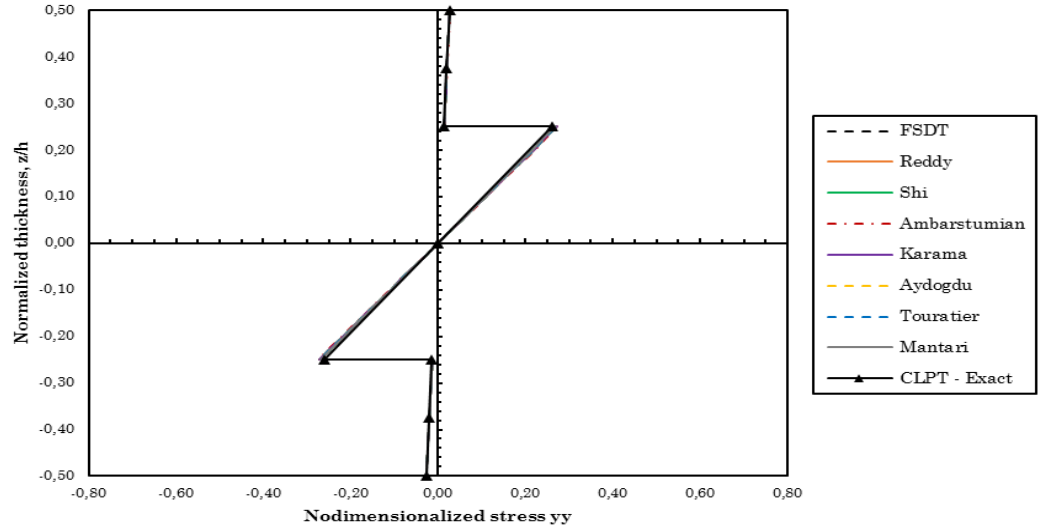

figure 75 – Nondimensionalized stresses σ_{yy} computed with the three numerical methods for a simply supported symmetric square laminate with cross-ply layers (0/90/90/0) subjected to a sinusoidal load (SSL), a/h=100.

RPIM

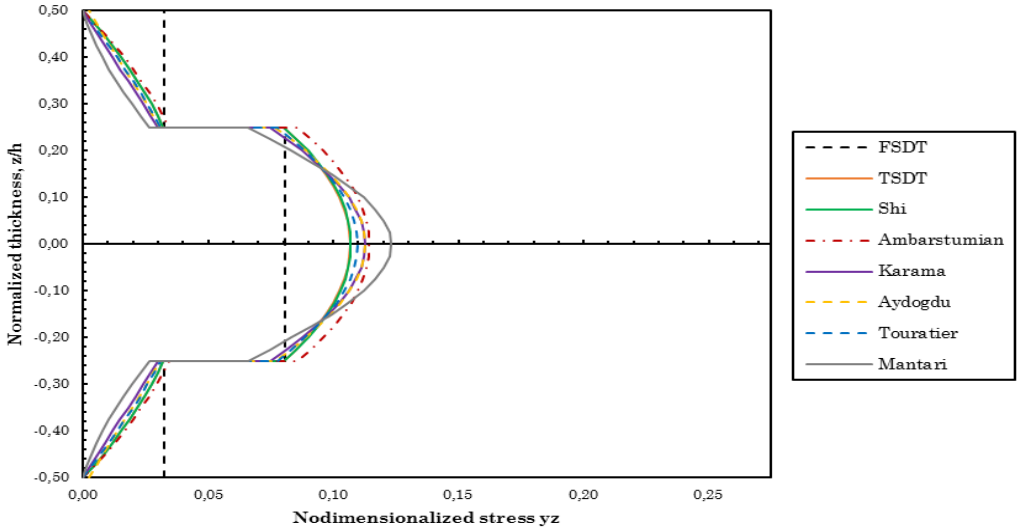

NNRPIM V1

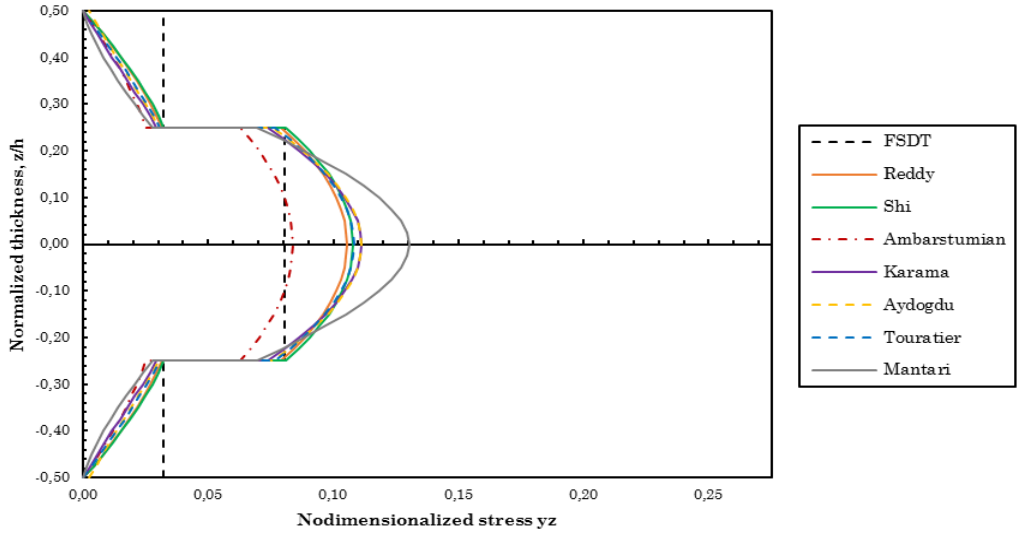

NNRPIM V2

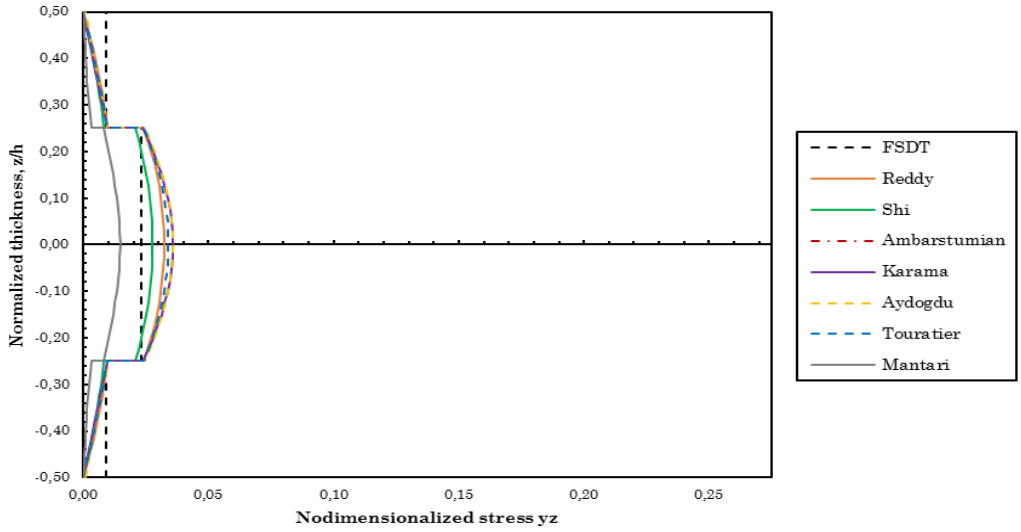

figure 76 – Nondimensionalized stresses τ_{yz} computed with the three numerical methods for a simply supported symmetric square laminate with cross-ply layers (0/90/90/0) subjected to a sinusoidal load (SSL), a/h=100.

RPIM

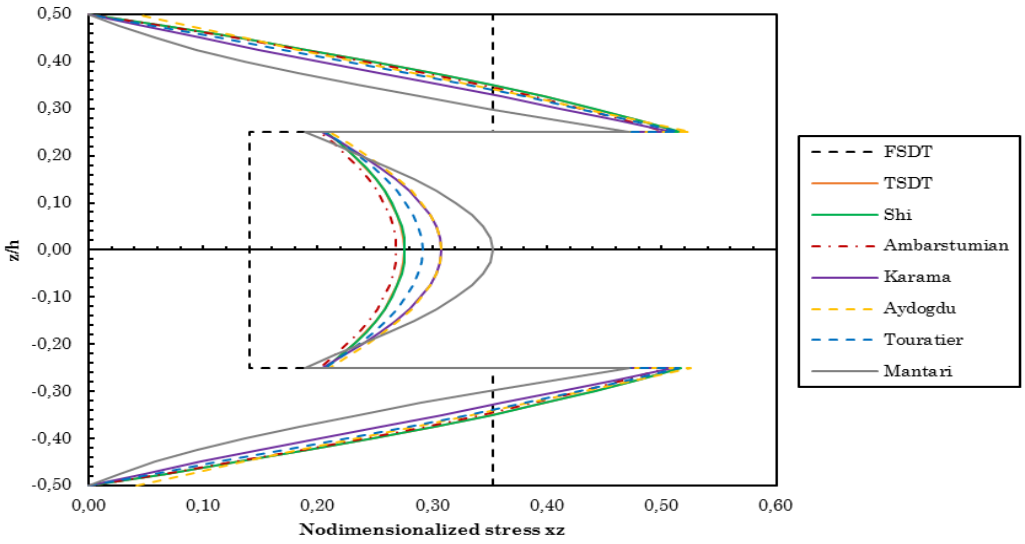

NNRPIM V1

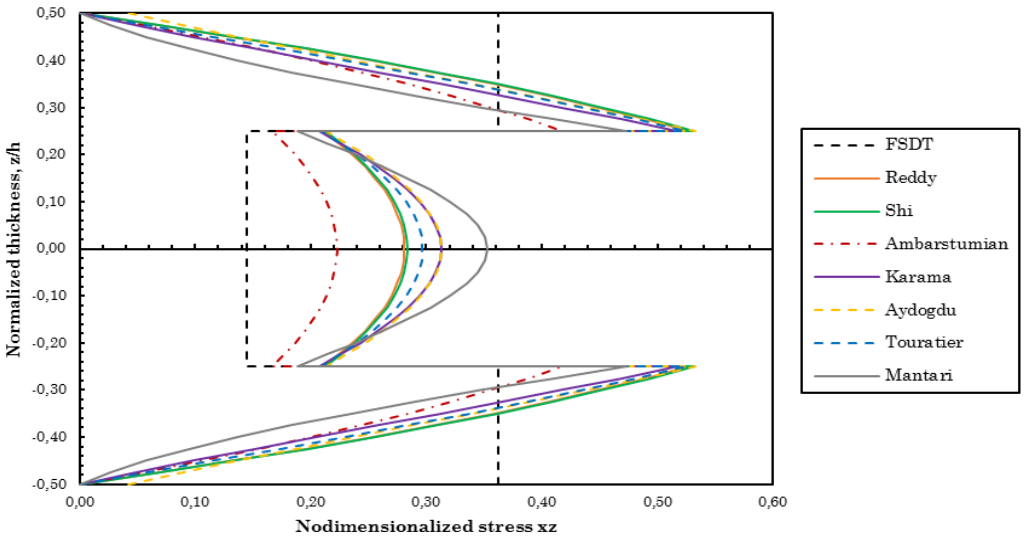

NNRPIM V2

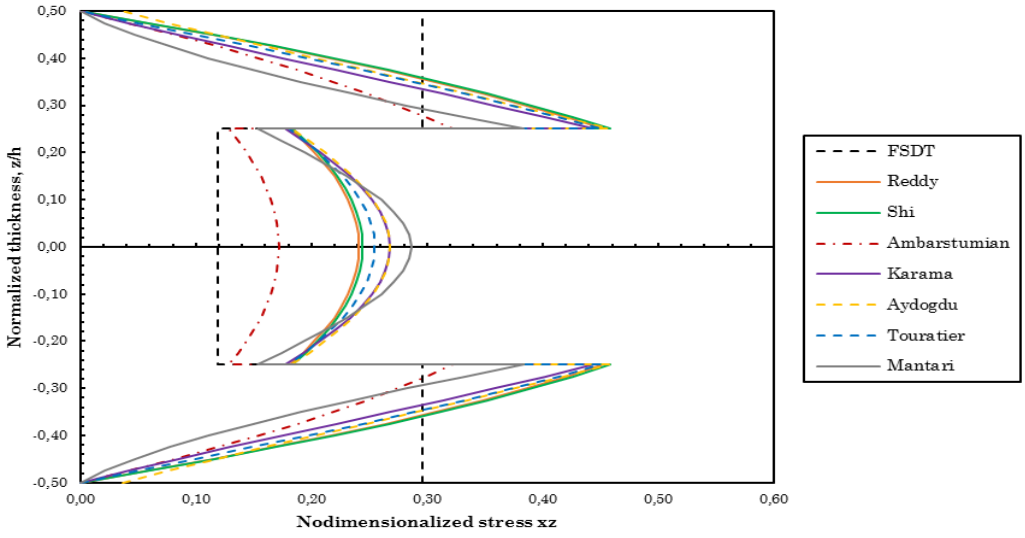

figure 77 – Nondimensionalized stresses τ_{xz} computed with the three numerical methods for a simply supported symmetric square laminate with cross-ply layers (0/90/90/0) subjected to a sinusoidal load (SSL), a/h=100.

RPIM

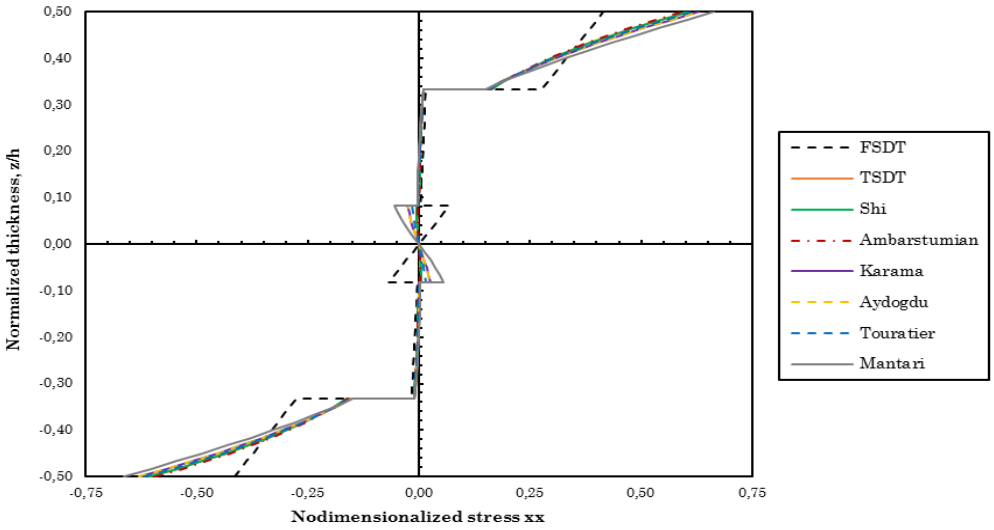

NNRPIM V1

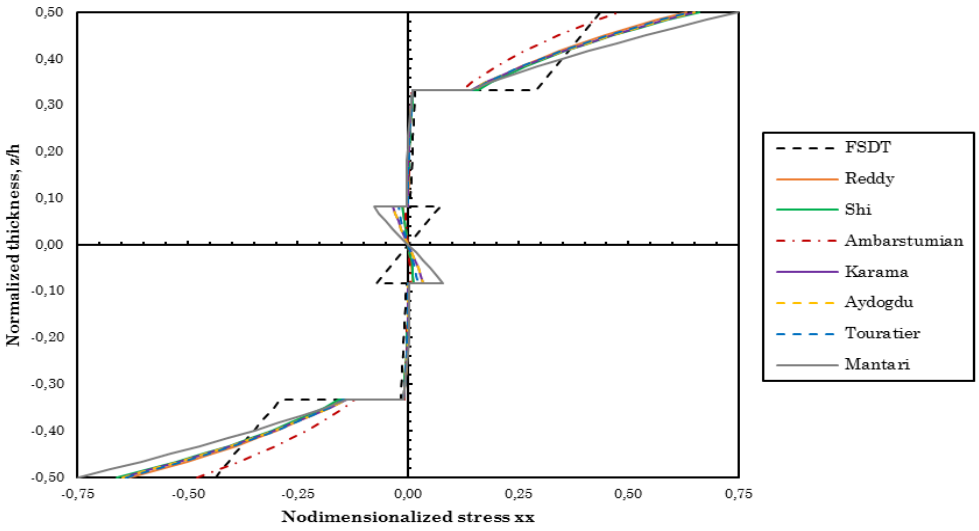

NNRPIM V2

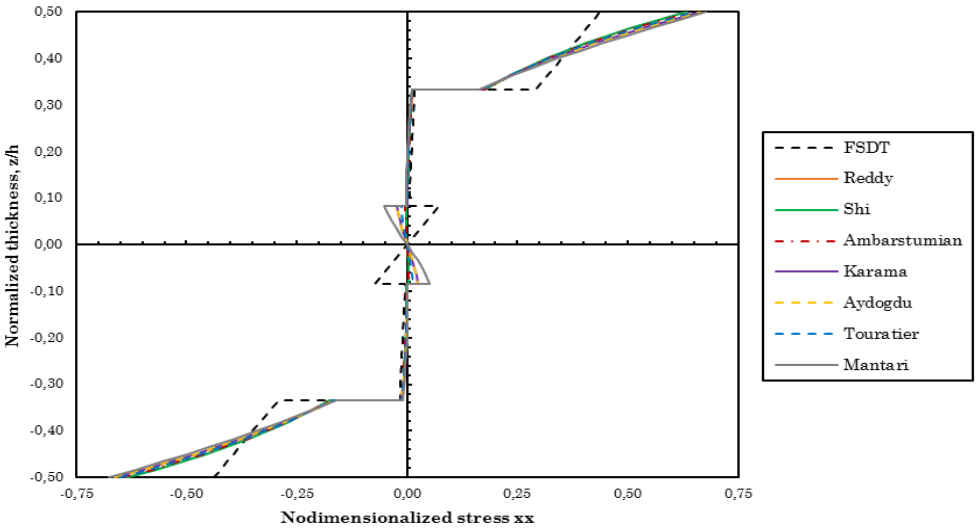

figure 78 – Nondimensionalized stresses σ_{xx} computed with the three numerical methods for a simply supported symmetric square laminate with cross-ply layers (0/90/0/90/0) subjected to a sinusoidal load (SSL), a/h=4.

RPIM

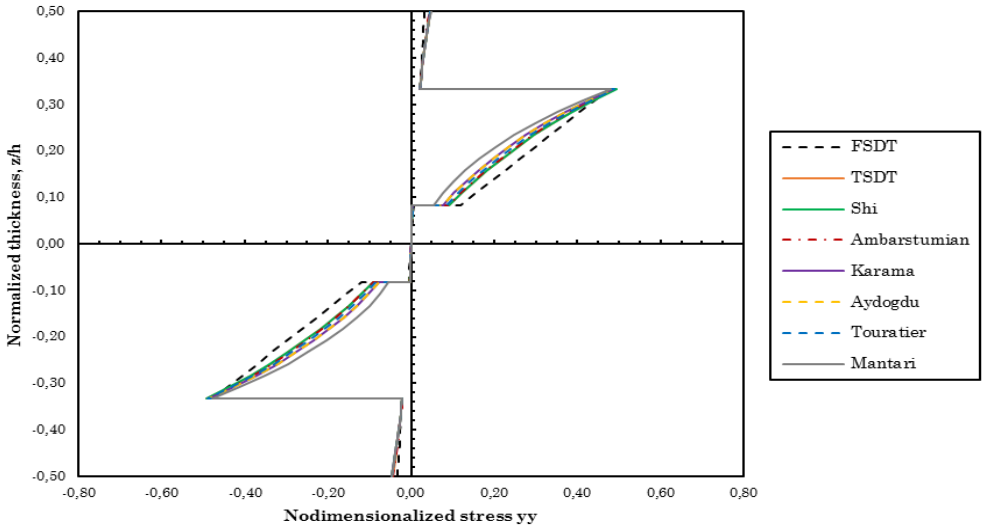

NNRPIM V1

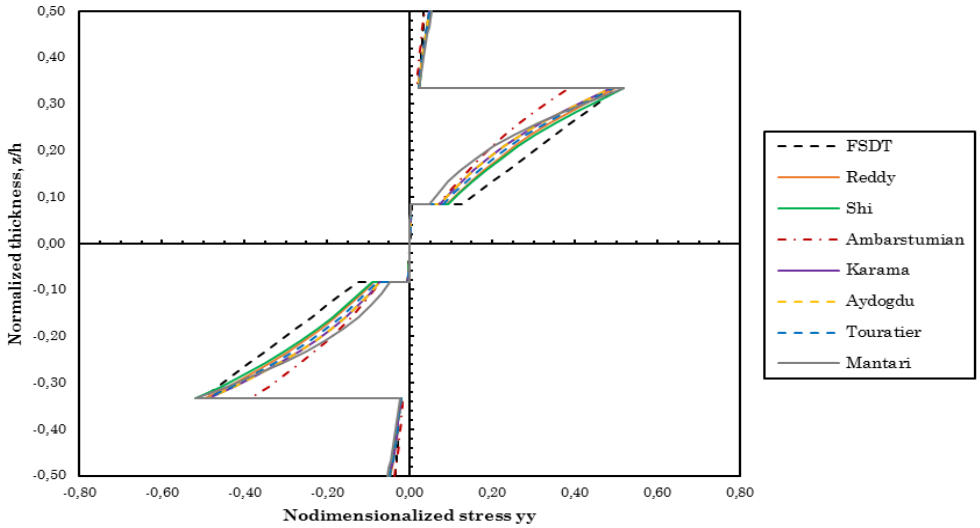

NNRPIM V2

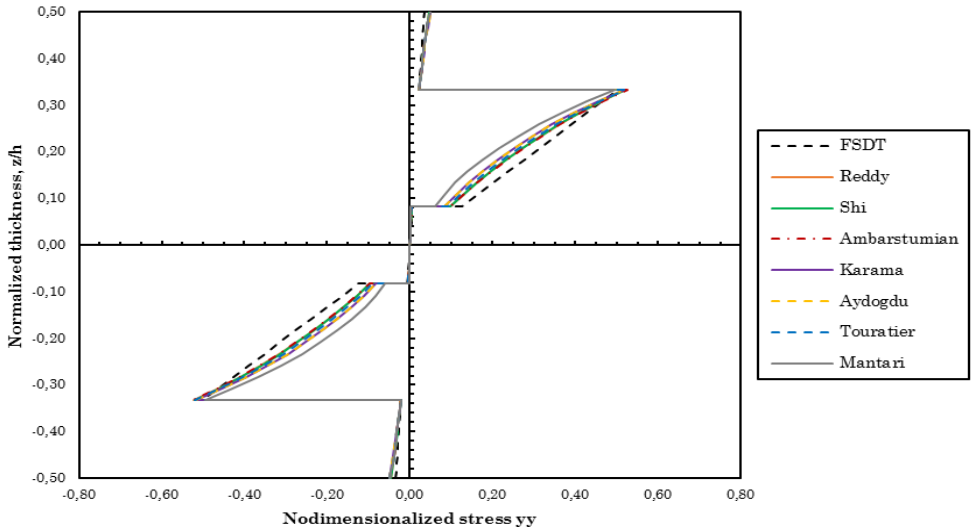

figure 79 – Nondimensionalized stresses σ_{yy} computed with the three numerical methods for a simply supported symmetric square laminate with cross-ply layers (0/90/0/90/0) subjected to a sinusoidal load (SSL), a/h=4.

RPIM

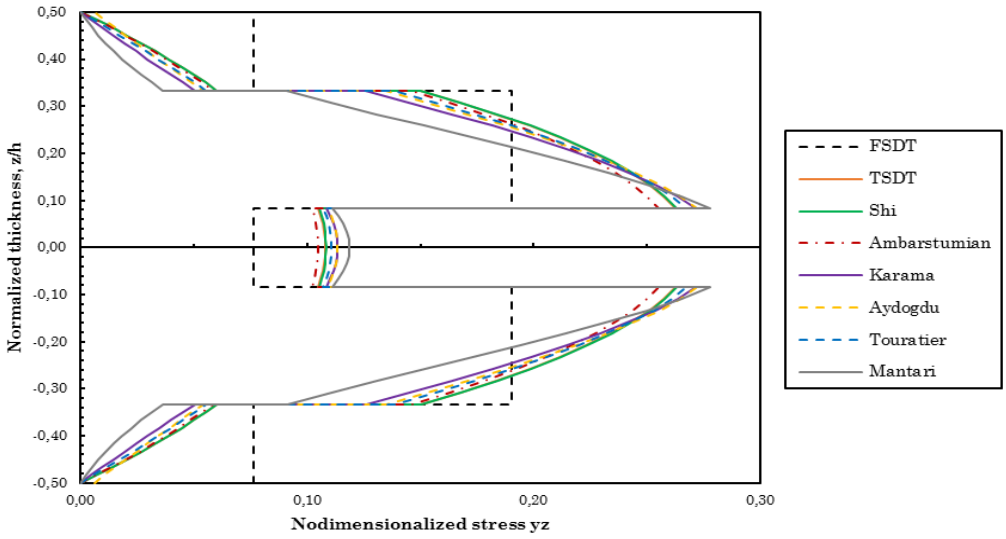

NNRPIM V1

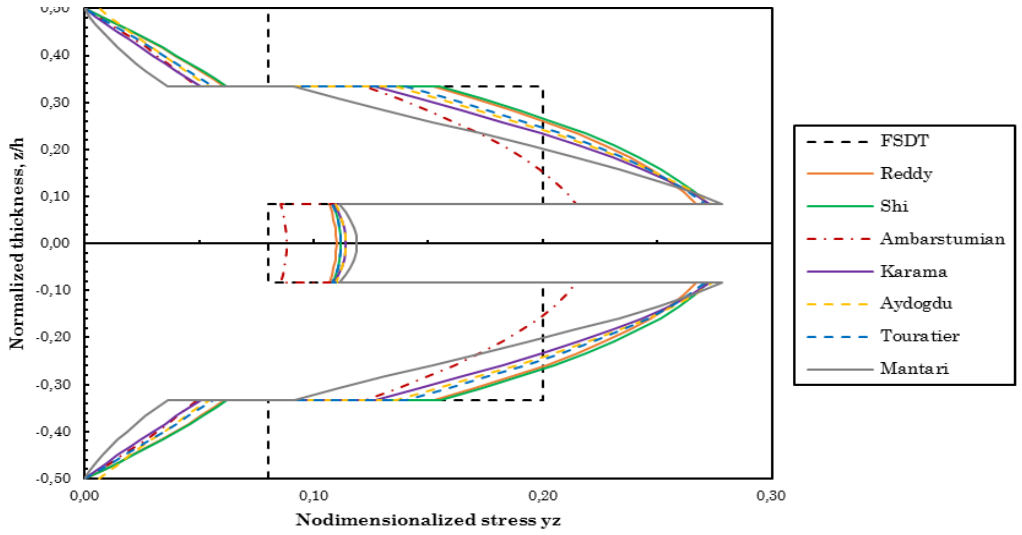

NNRPIM V2

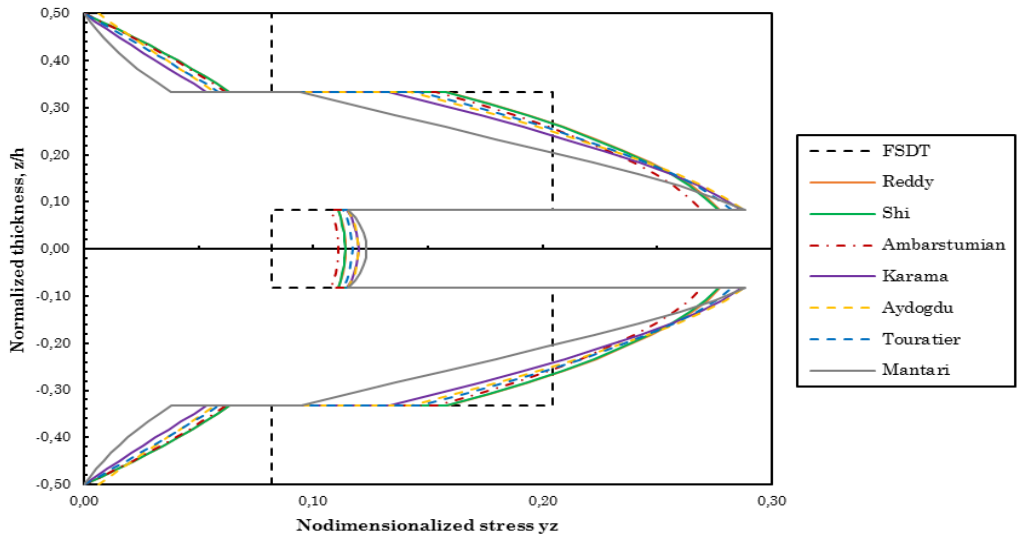

figure 80 – Nondimensionalized stresses τ_{yz} computed with the three numerical methods for a simply supported symmetric square laminate with cross-ply layers (0/90/0/90/0) subjected to a sinusoidal load (SSL), a/h=4.

RPIM

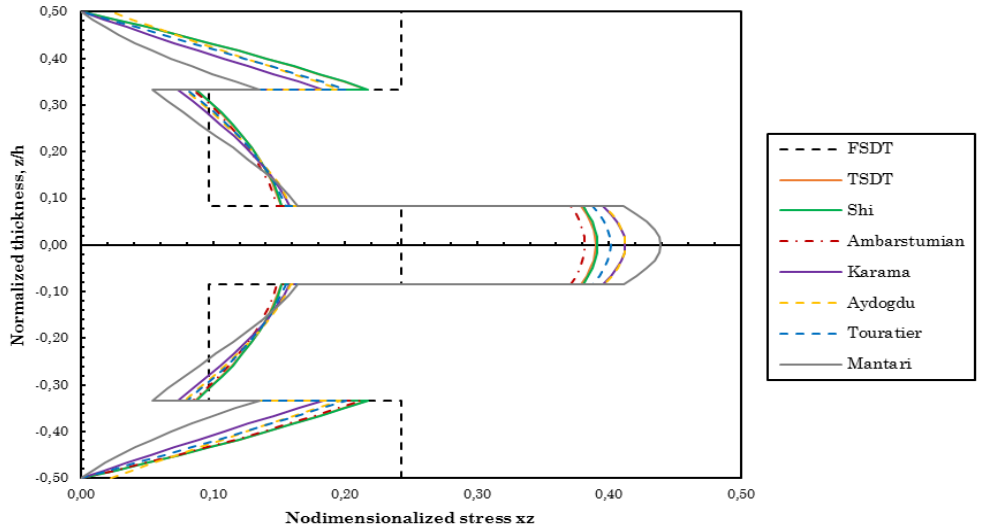

NNRPIM V1

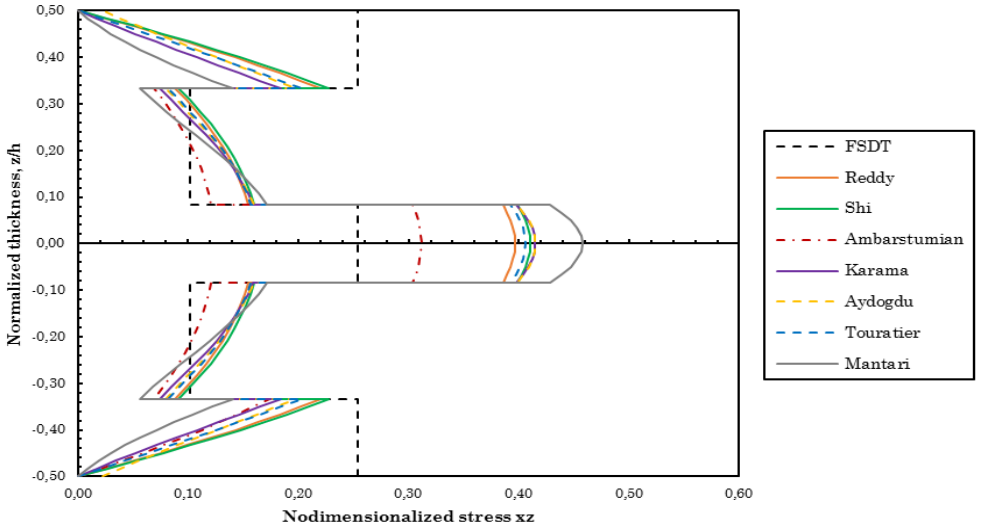

NNRPIM V2

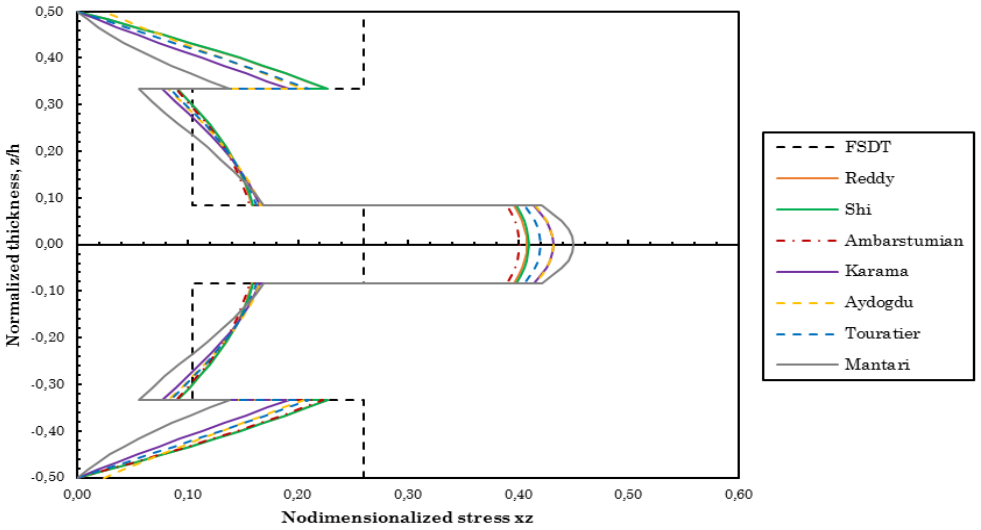

figure 81 – Nondimensionalized stresses τ_{xz} computed with the three numerical methods for a simply supported symmetric square laminate with cross-ply layers (0/90/0/90/0) subjected to a sinusoidal load (SSL), a/h=4.

RPIM

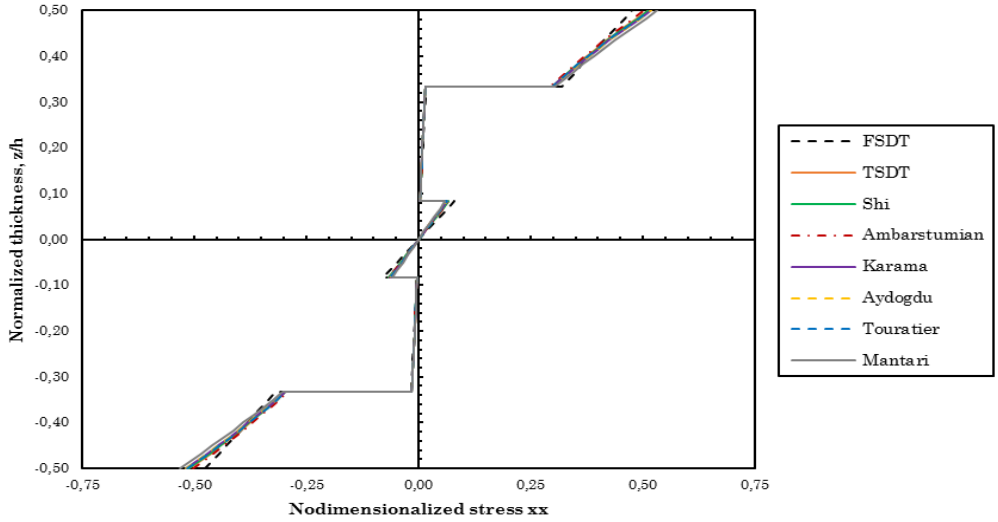

NNRPIM V1

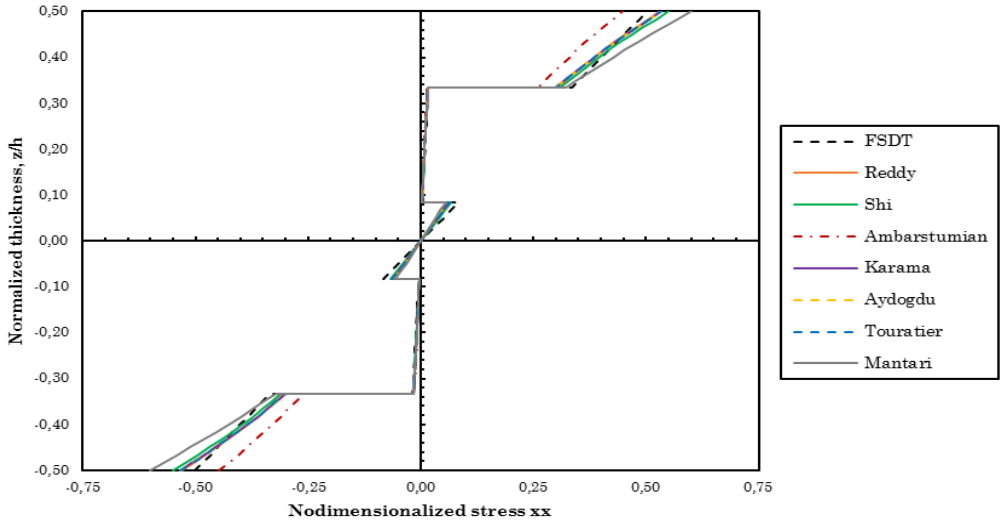

NNRPIM V2

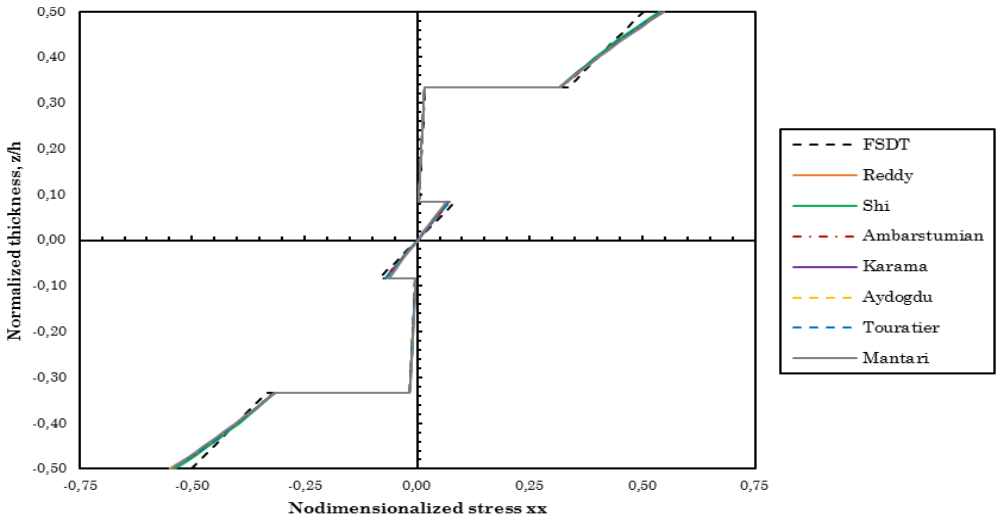

figure 82 – Nondimensionalized stresses σ_{xx} computed with the three numerical methods for a simply supported symmetric square laminate with cross-ply layers (0/90/0/90/0) subjected to a sinusoidal load (SSL), a/h=10.

RPIM

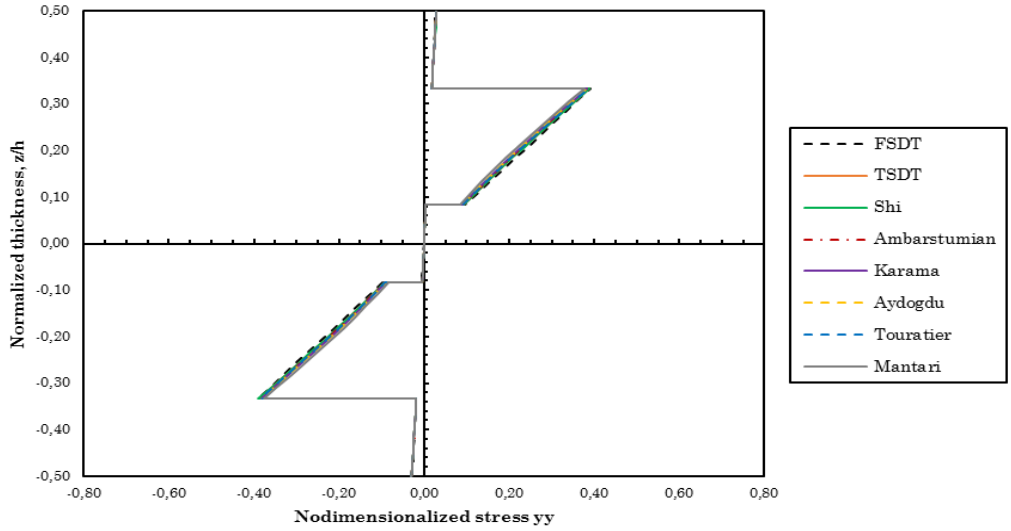

NNRPIM V1

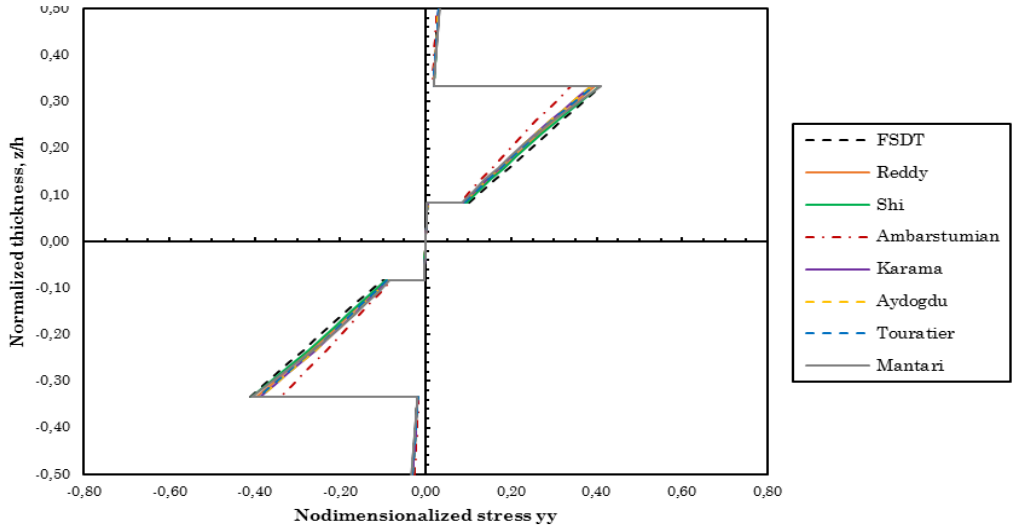

NNRPIM V2

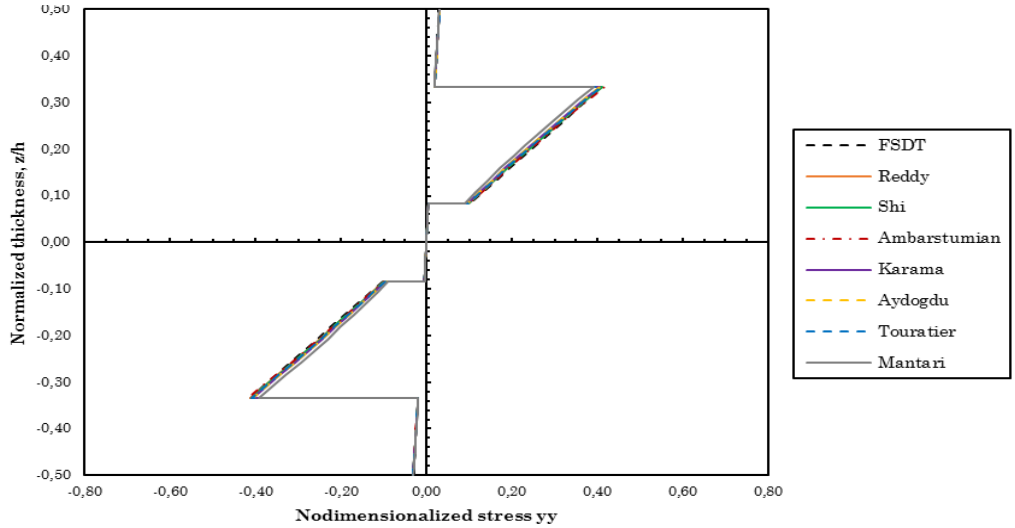

figure 83 – Nondimensionalized stresses σ_{yy} computed with the three numerical methods for a simply supported symmetric square laminate with cross-ply layers (0/90/0/90/0) subjected to a sinusoidal load (SSL), a/h=10.

RPIM

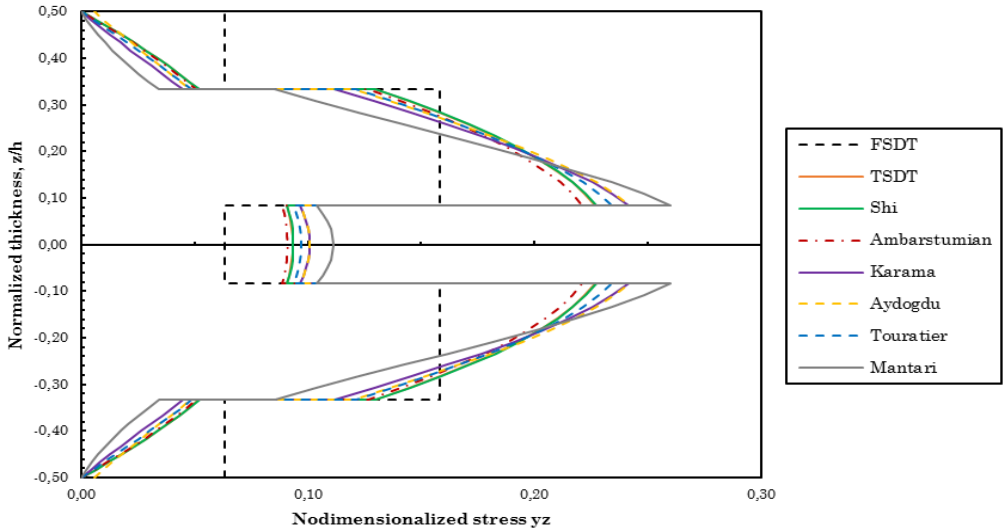

NNRPIM V1

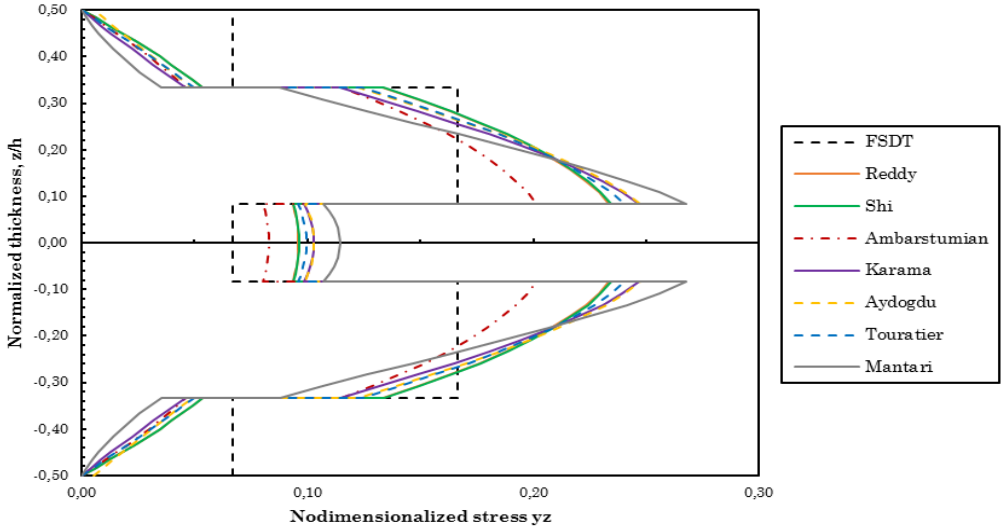

NNRPIM V2

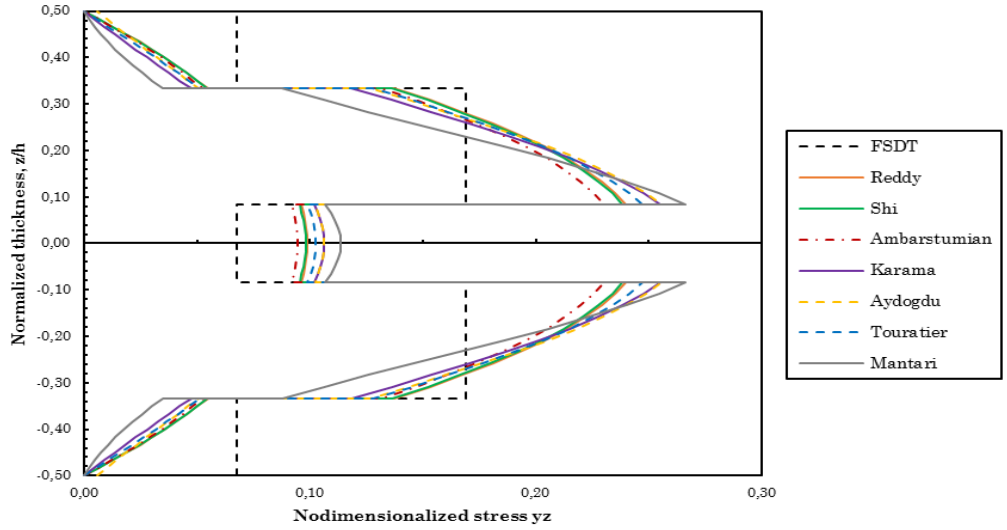

figure 84 – Nondimensionalized stresses τ_{yz} computed with the three numerical methods for a simply supported symmetric square laminate with cross-ply layers (0/90/0/90/0) subjected to a sinusoidal load (SSL), a/h=10.

RPIM

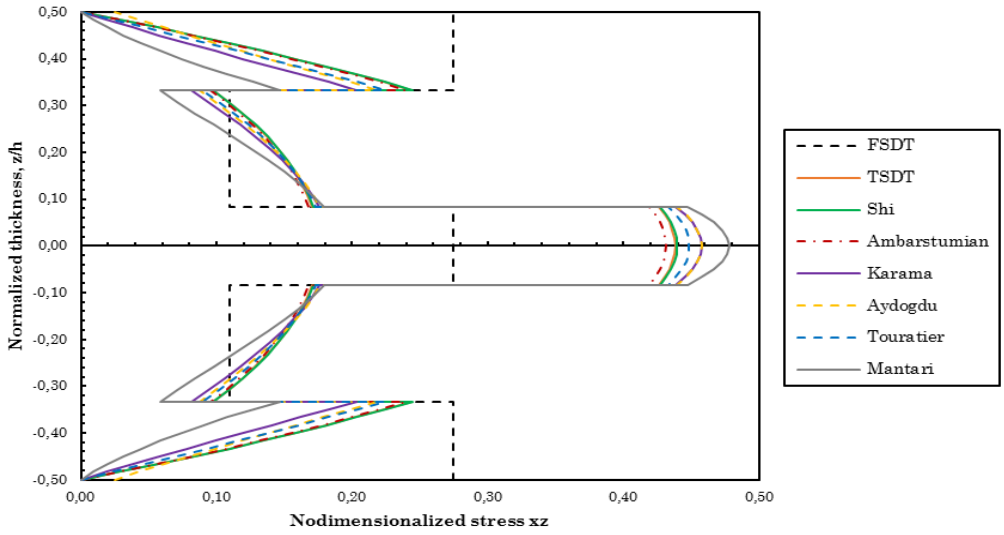

NNRPIM V1

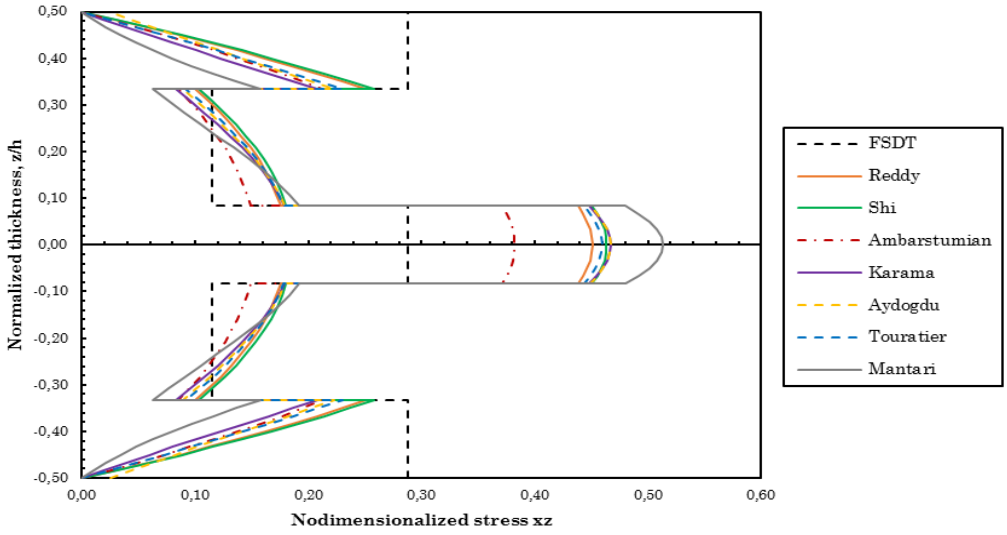

NNRPIM V2

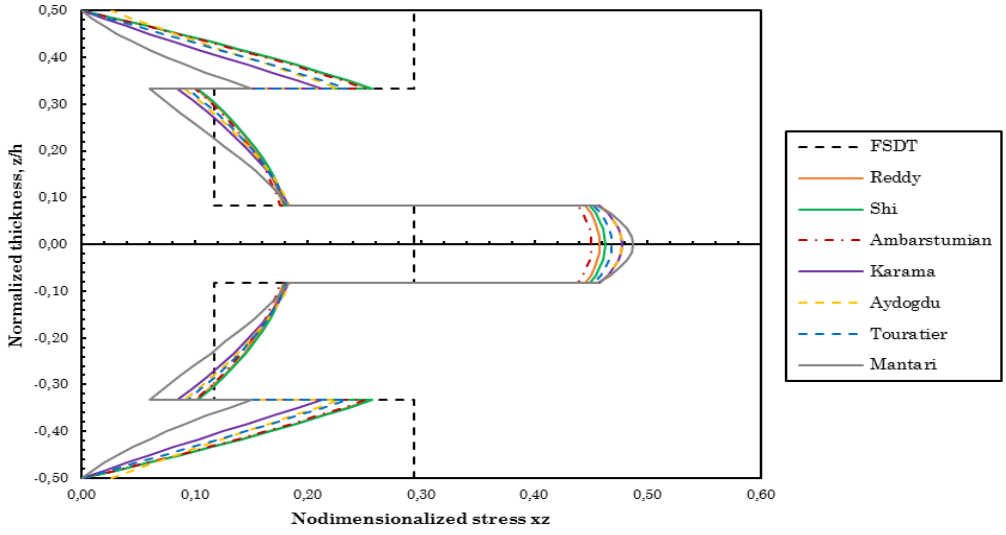

figure 85 – Nondimensionalized stresses τ_{xz} computed with the three numerical methods for a simply supported symmetric square laminate with cross-ply layers (0/90/0/90/0) subjected to a sinusoidal load (SSL), a/h=10.

RPIM

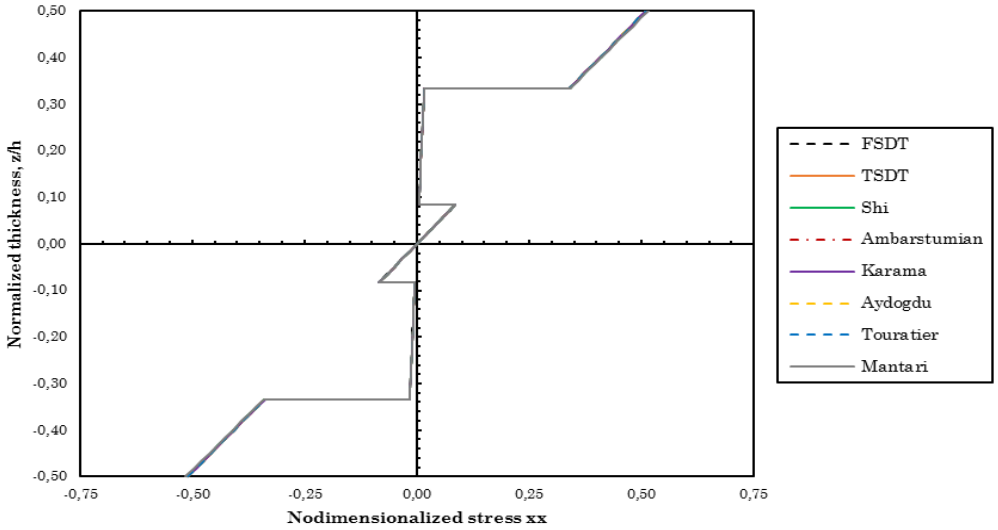

NNRPIM V1

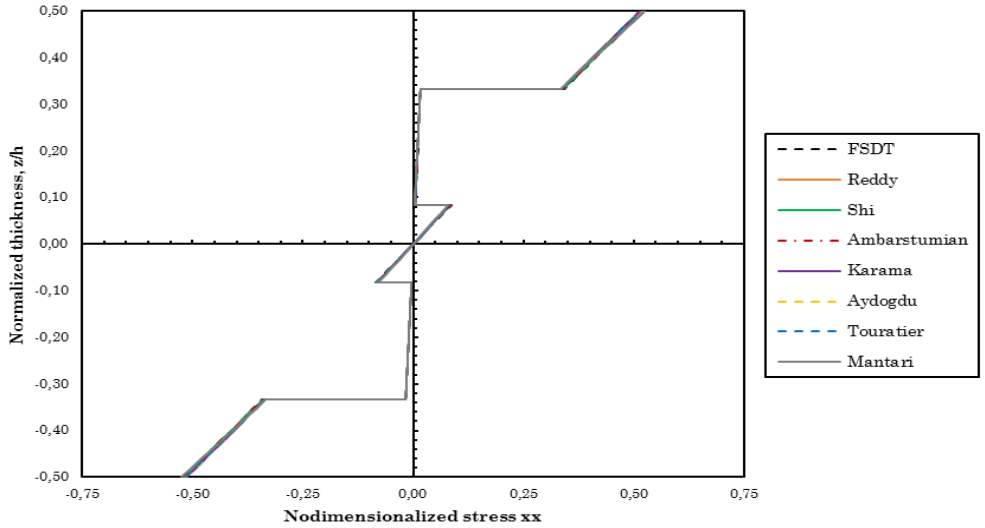

NNRPIM V2

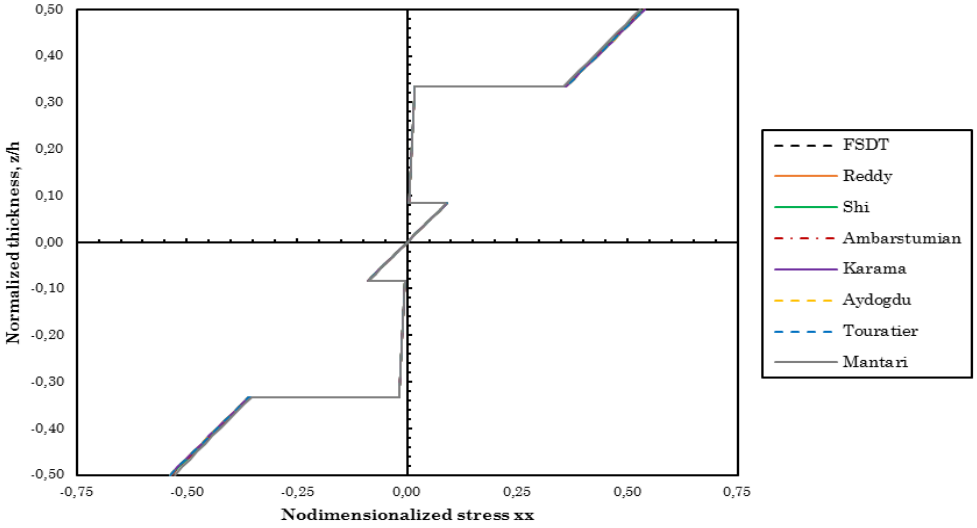

figure 86 – Nondimensionalized stresses σ_{xx} computed with the three numerical methods for a simply supported symmetric square laminate with cross-ply layers (0/90/0/90/0) subjected to a sinusoidal load (SSL), a/h=100.

RPIM

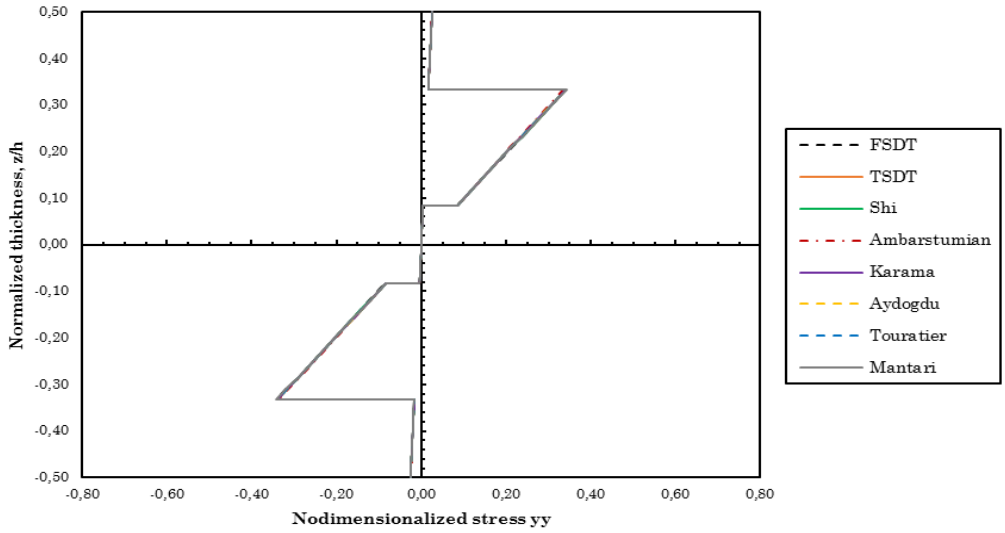

NNRPIM V1

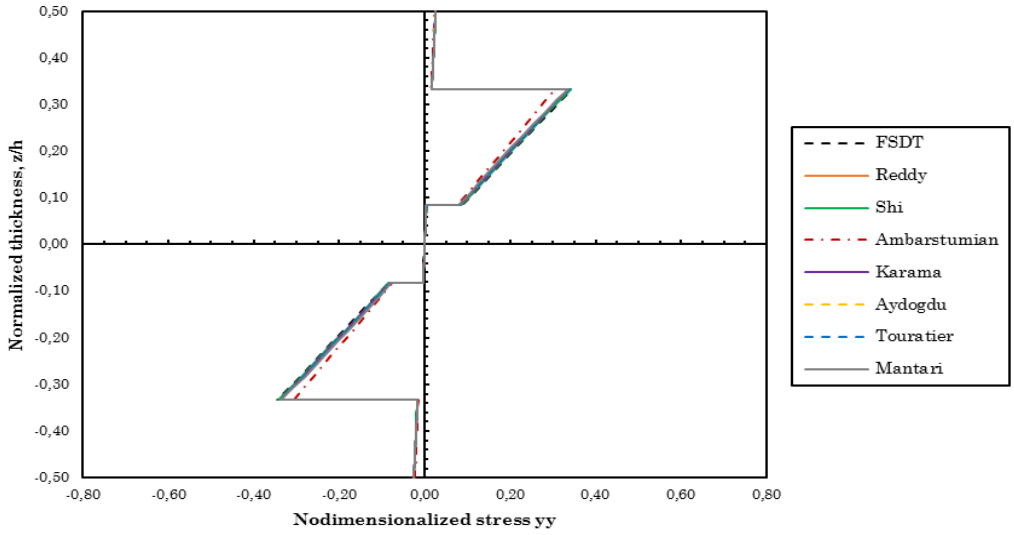

NNRPIM V2

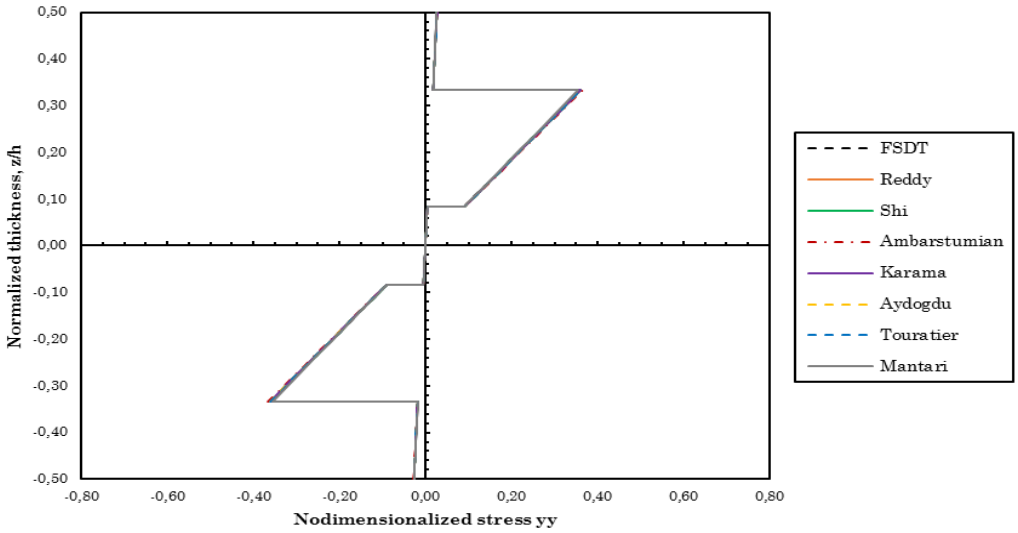

figure 87 – Nondimensionalized stresses σ_{yy} computed with the three numerical methods for a simply supported symmetric square laminate with cross-ply layers (0/90/0/90/0) subjected to a sinusoidal load (SSL), a/h=100.

RPIM

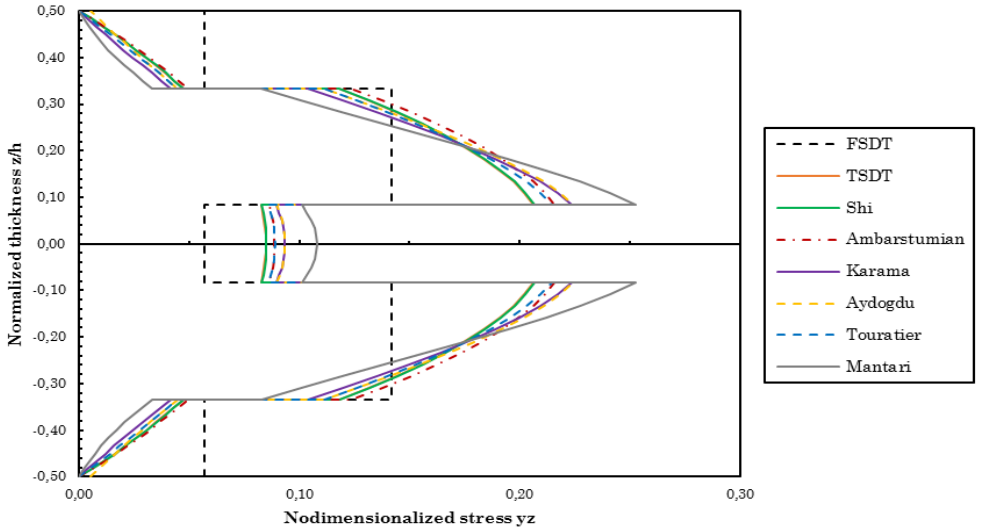

NNRPIM V1

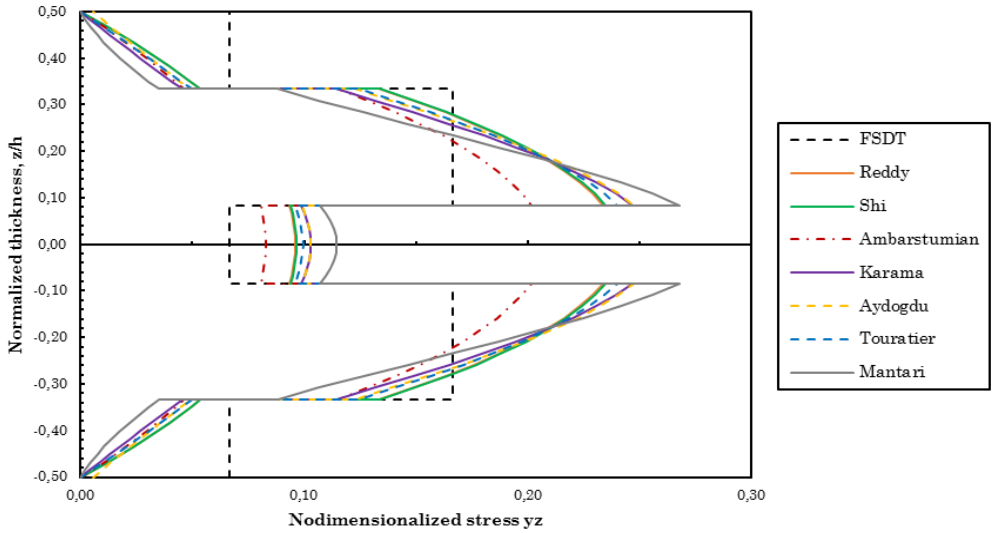

NNRPIM V2

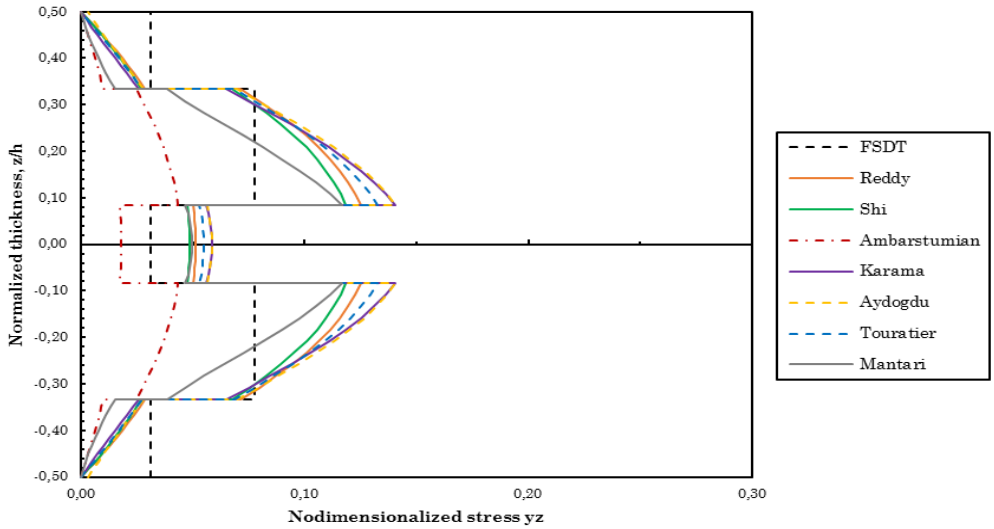

figure 88 – Nondimensionalized stresses τ_{yz} computed with the three numerical methods for a simply supported symmetric square laminate with cross-ply layers (0/90/0/90/0) subjected to a sinusoidal load (SSL), a/h=100.

RPIM

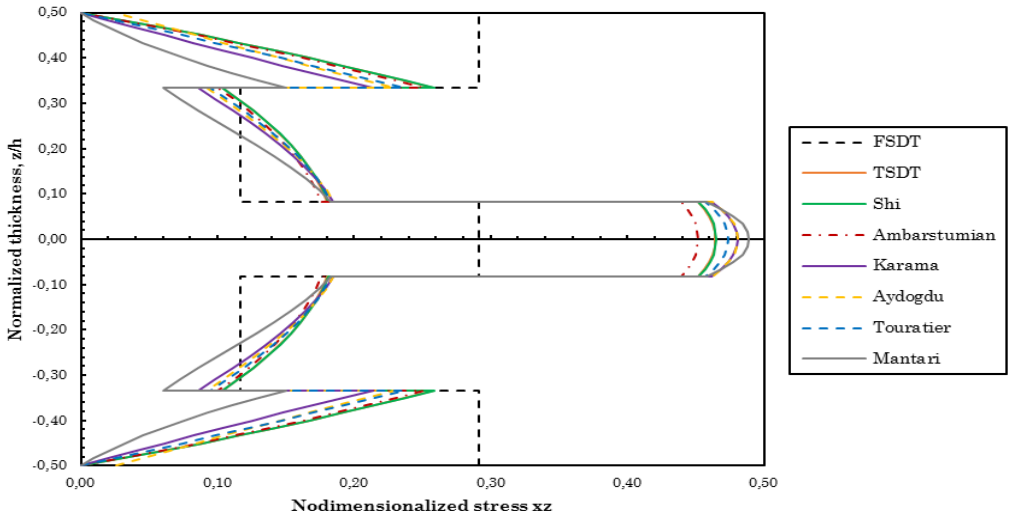

NNRPIM V1

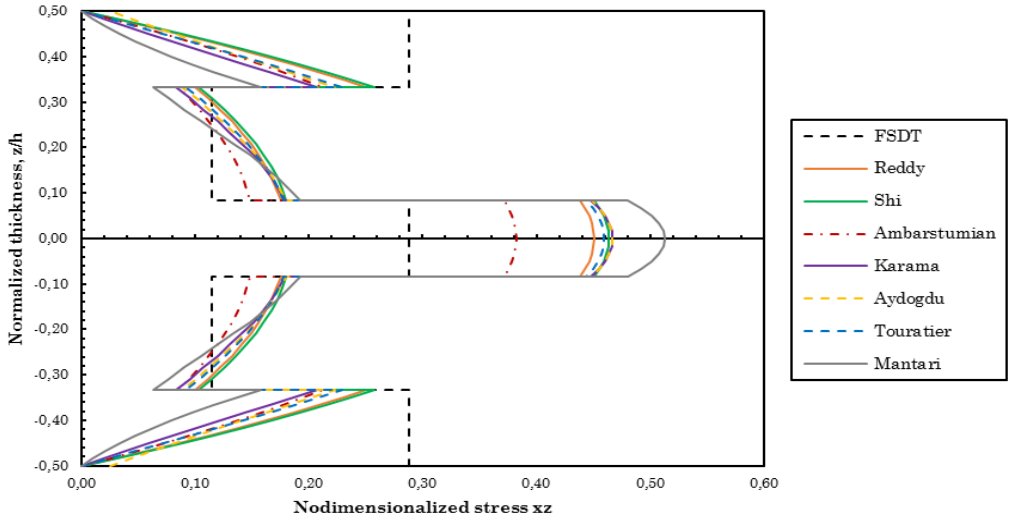

NNRPIM V2

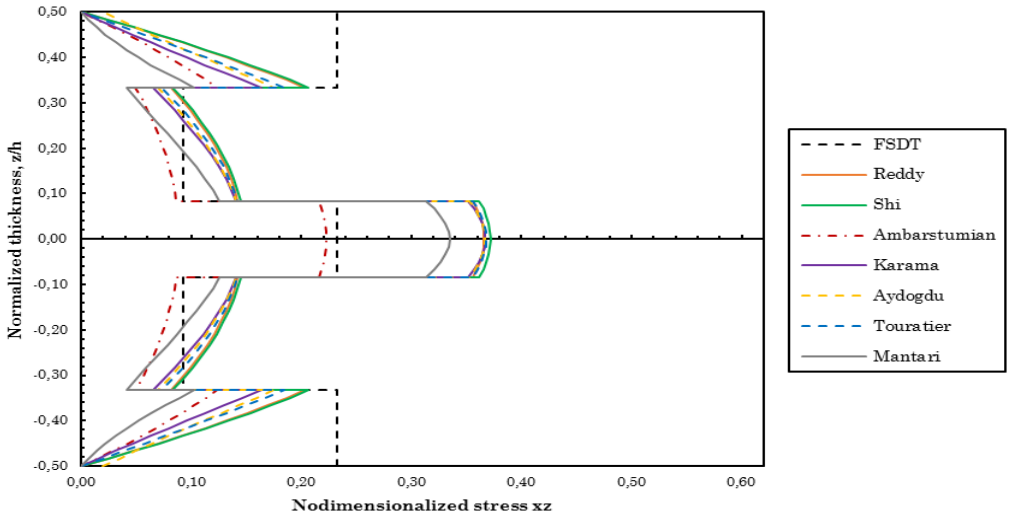

figure 89 – Nondimensionalized stresses τ_{xz} computed with the three numerical methods for a simply supported symmetric square laminate with cross-ply layers (0/90/0/90/0) subjected to a sinusoidal load (SSL), a/h=100.

RPIM

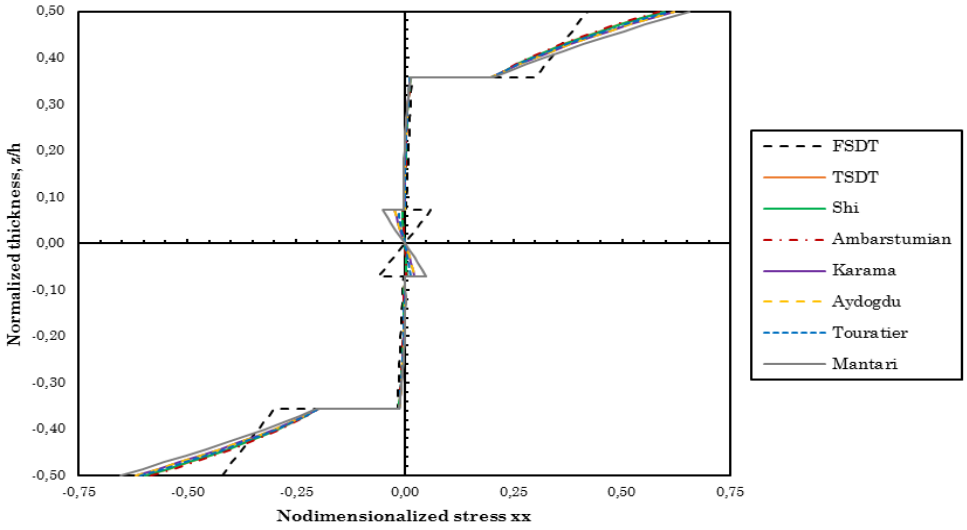

NNRPIM V1

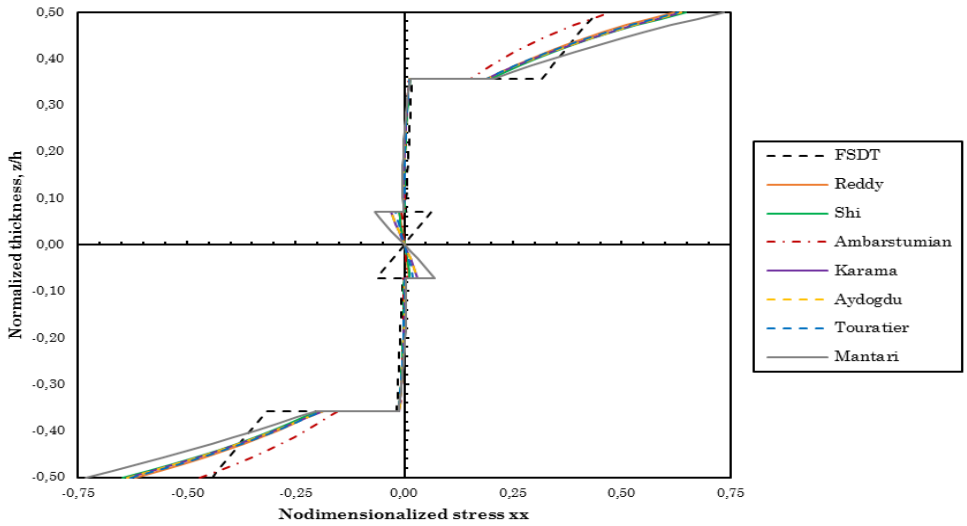

NNRPIM V2

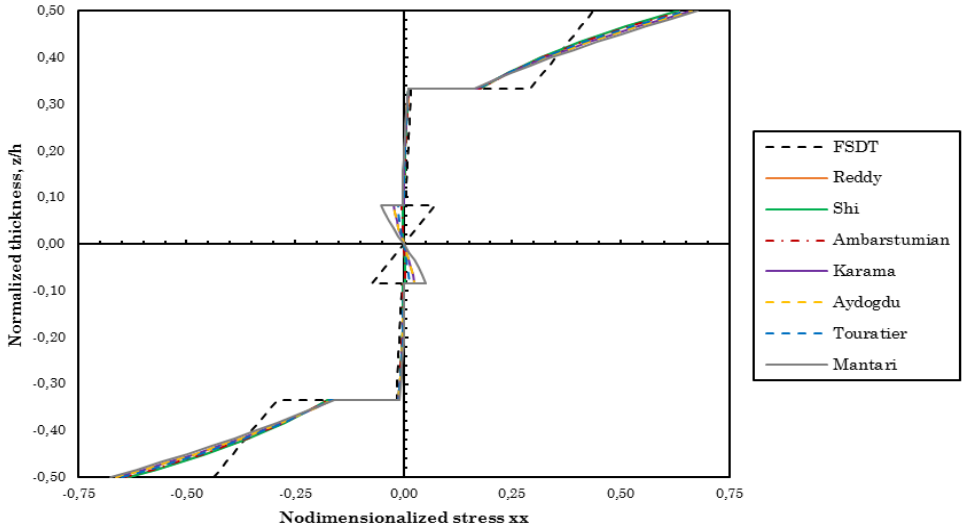

figure 90 – Nondimensionalized stresses σ_{xx} computed with the three numerical methods for a simply supported symmetric square laminate with cross-ply layers (0/90/90/0/90/90/0) subjected to a sinusoidal load (SSL), a/h=4.

RPIM

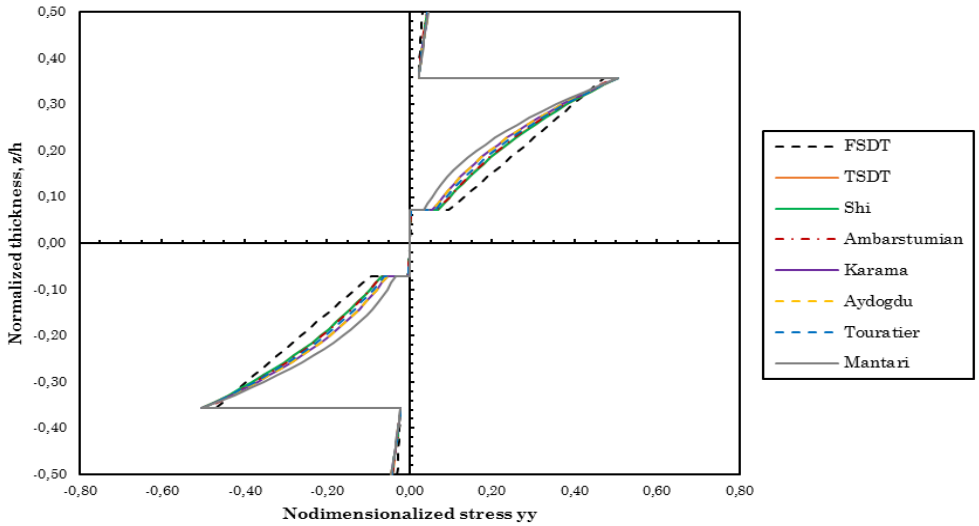

NNRPIM V1

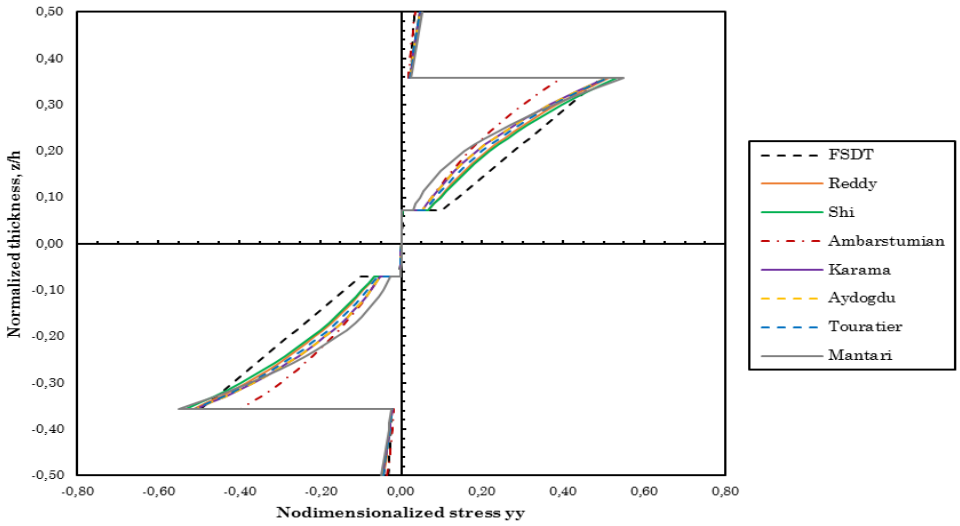

NNRPIM V2

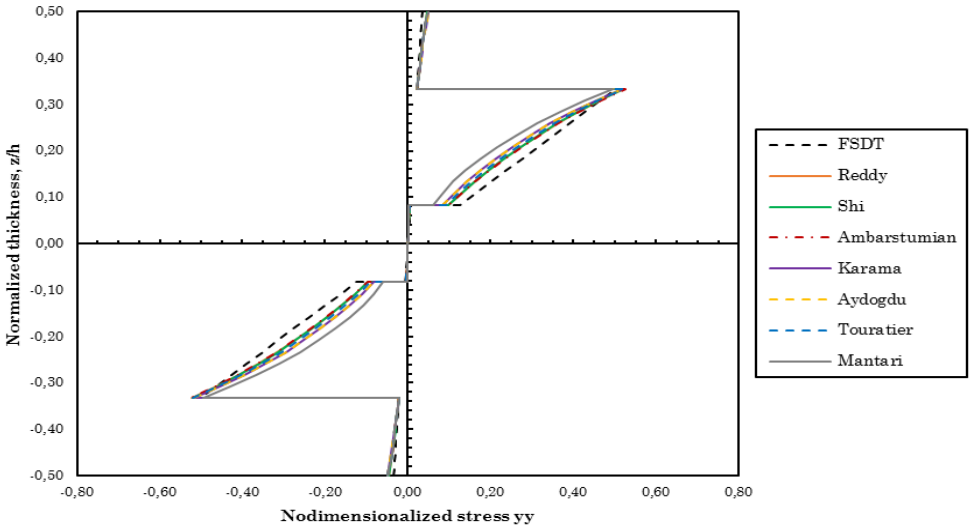

figure 91 – Nondimensionalized stresses σ_{yy} computed with the three numerical methods for a simply supported symmetric square laminate with cross-ply layers (0/90/90/0/90/90//0) subjected to a sinusoidal load (SSL), a/h=4.

RPIM

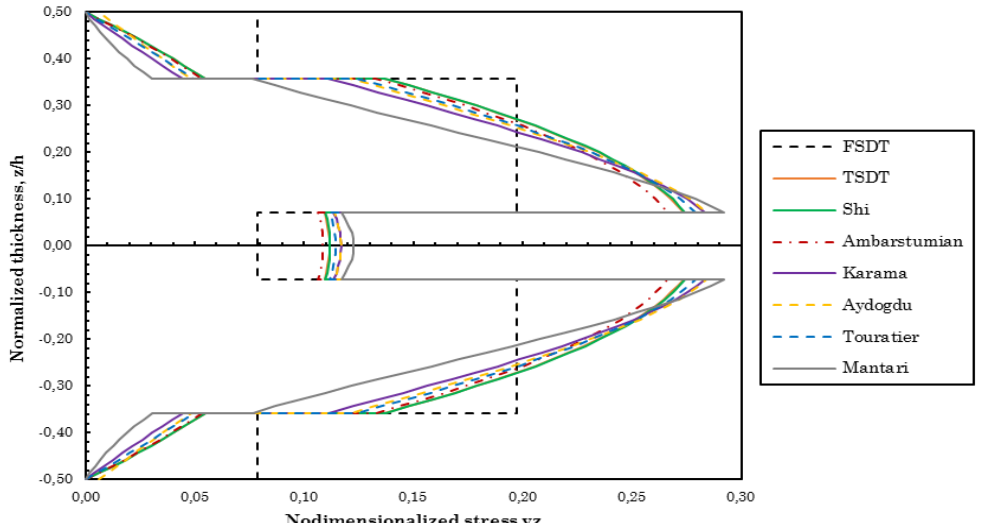

NNRPIM V1

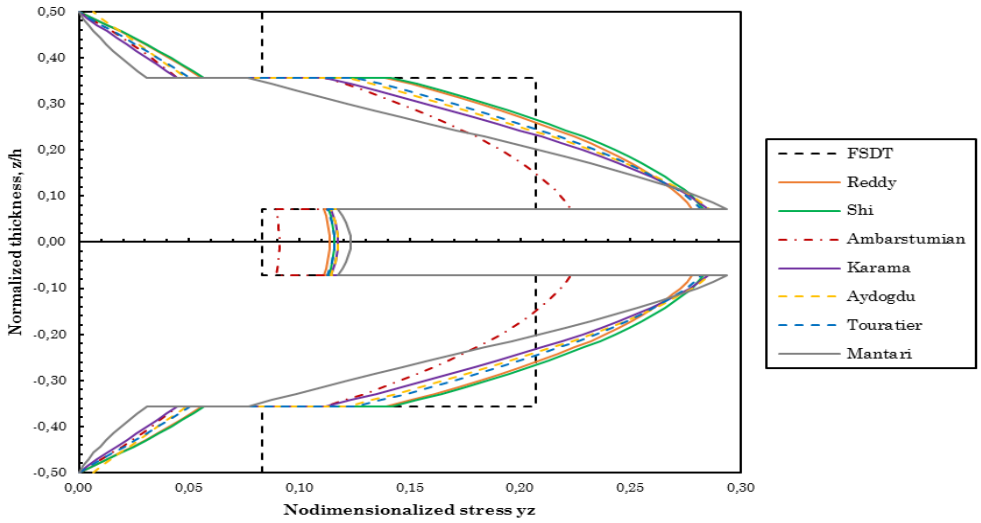

NNRPIM V2

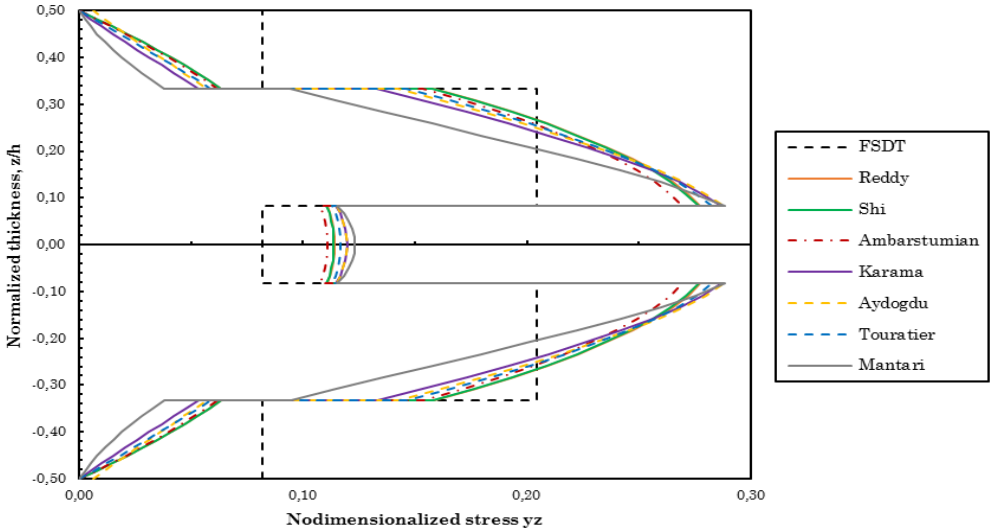

figure 92 – Nondimensionalized stresses τ_{yz} computed with the three numerical methods for a simply supported symmetric square laminate with cross-ply layers (0/90/90/0/90/90/0) subjected to a sinusoidal load (SSL), a/h=4.

RPIM

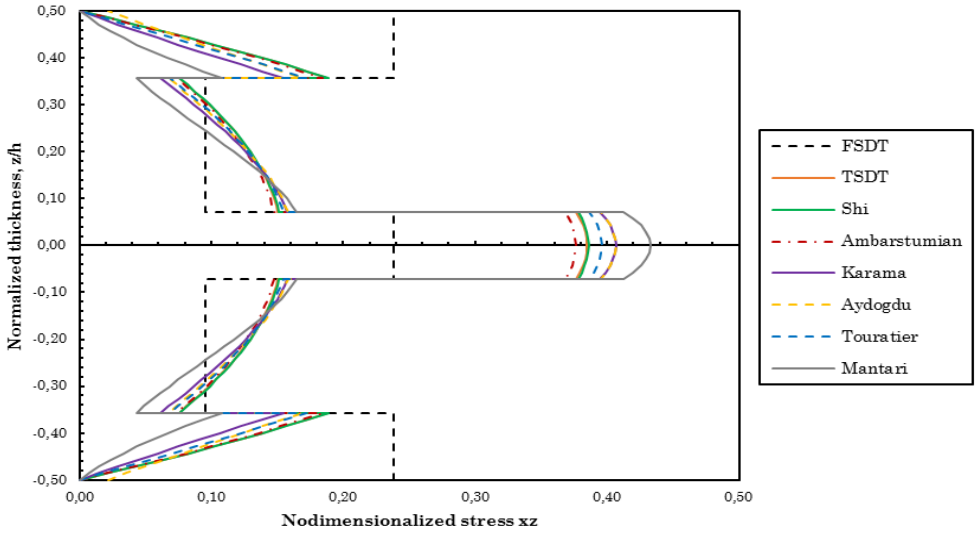

NNRPIM V1

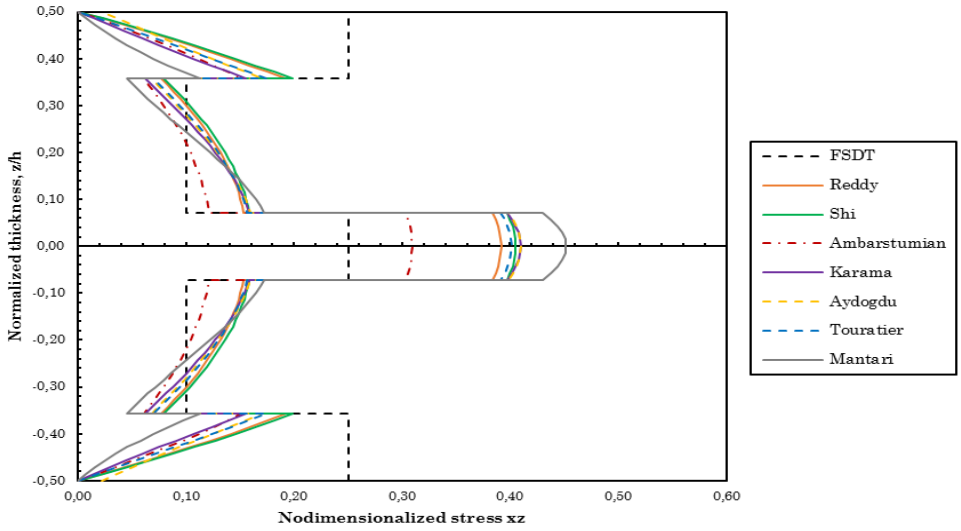

NNRPIM V2

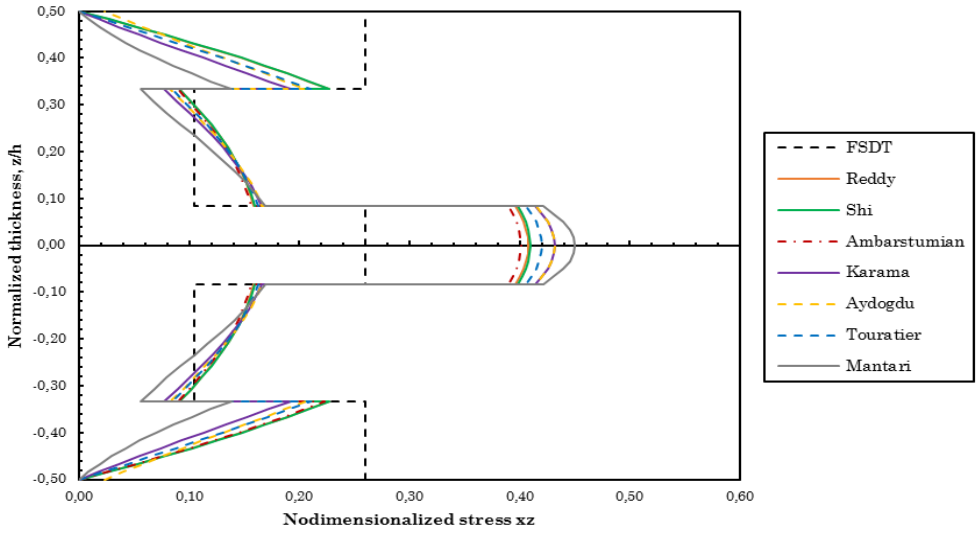

figure 93 – Nondimensionalized stresses τ_{xz} computed with the three numerical methods for a simply supported symmetric square laminate with cross-ply layers (0/90/90/0/90/90/0) subjected to a sinusoidal load (SSL), a/h=4.

RPIM

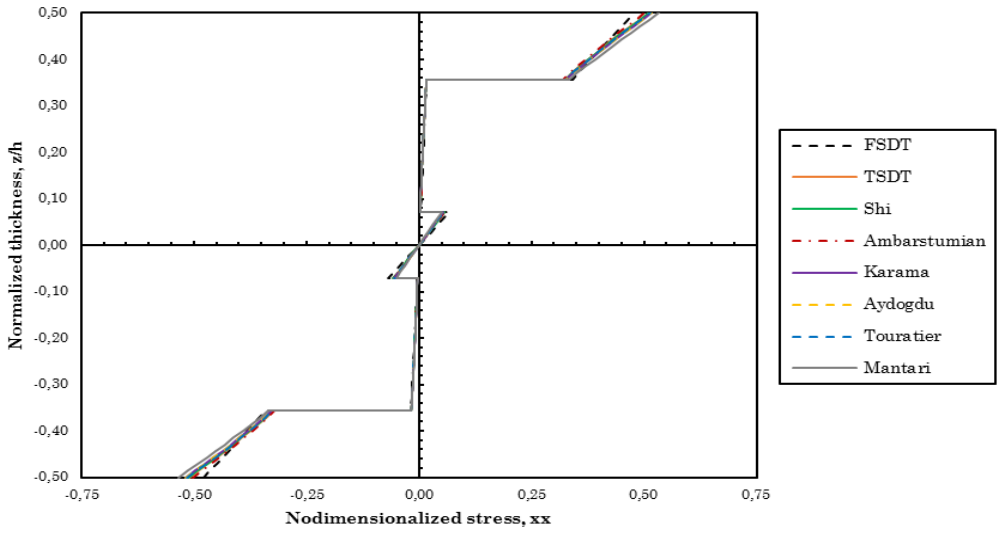

NNRPIM V1

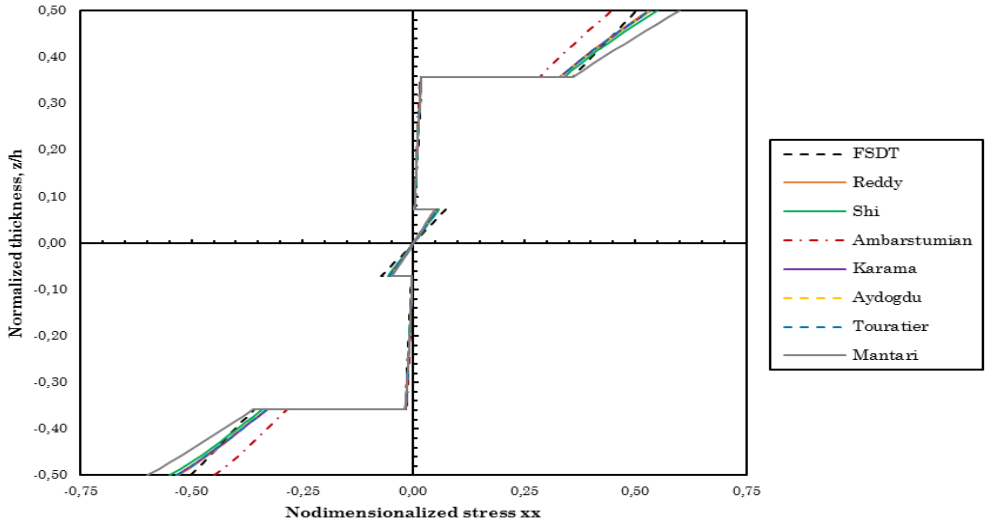

NNRPIM V2

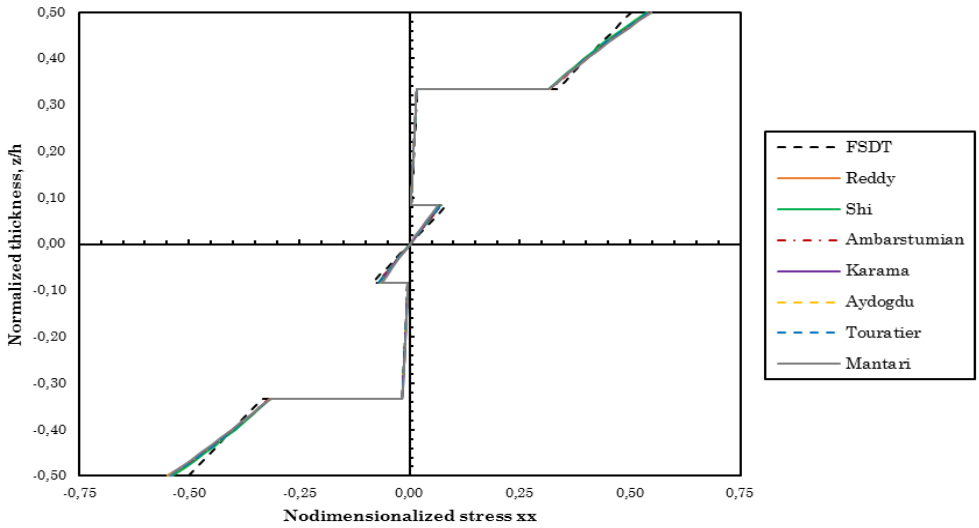

figure 94 – Nondimensionalized stresses σ_{xx} computed with the three numerical methods for a simply supported symmetric square laminate with cross-ply layers (0/90/90/0/90/90/0) subjected to a sinusoidal load (SSL), a/h=10.

RPIM

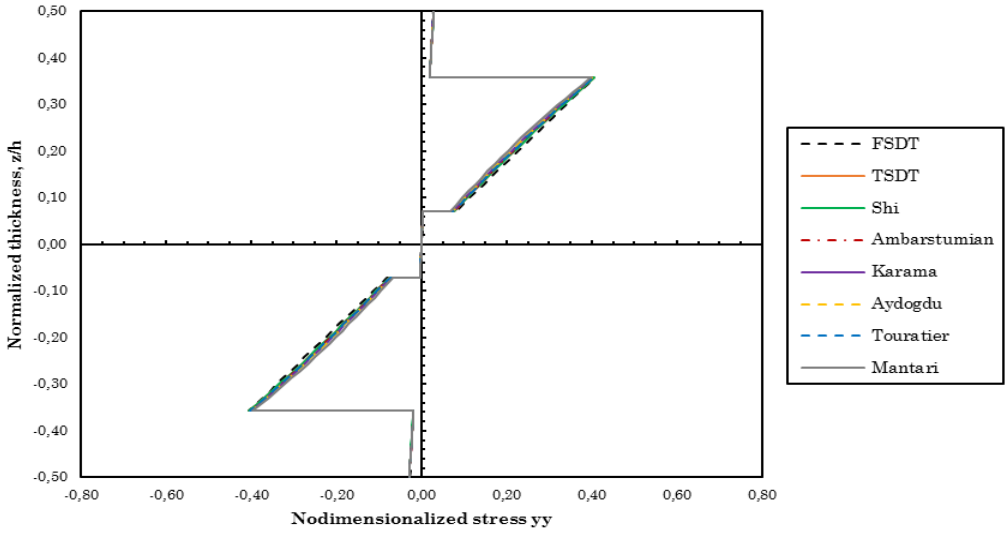

NNRPIM V1

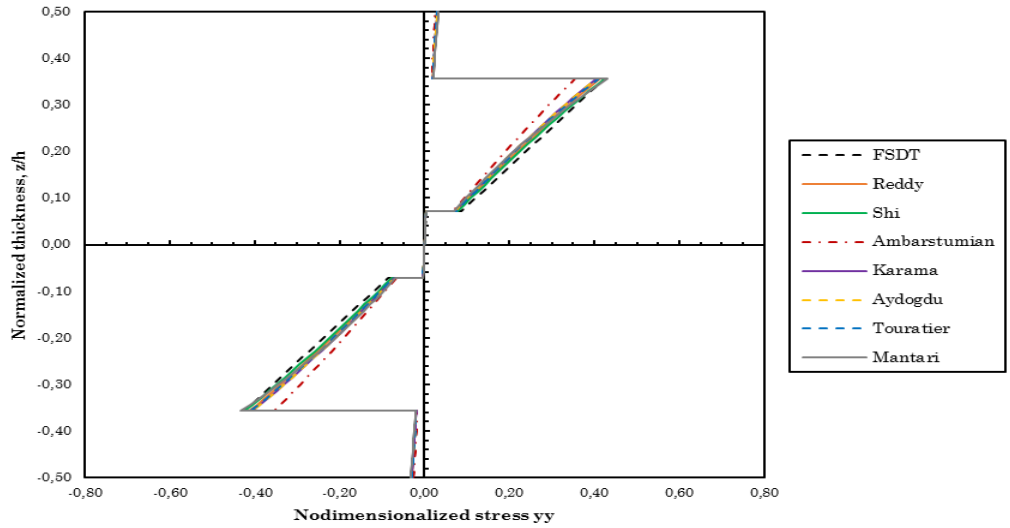

NNRPIM V2

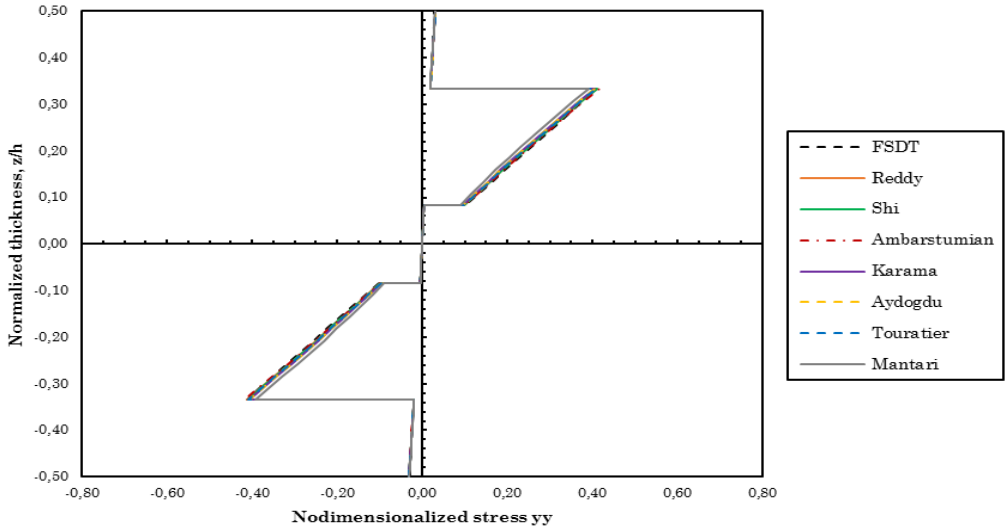

figure 95 – Nondimensionalized stresses σ_{yy} computed with the three numerical methods for a simply supported symmetric square laminate with cross-ply layers (0/90/90/0/90/90/0) subjected to a sinusoidal load (SSL), a/h=10.

RPIM

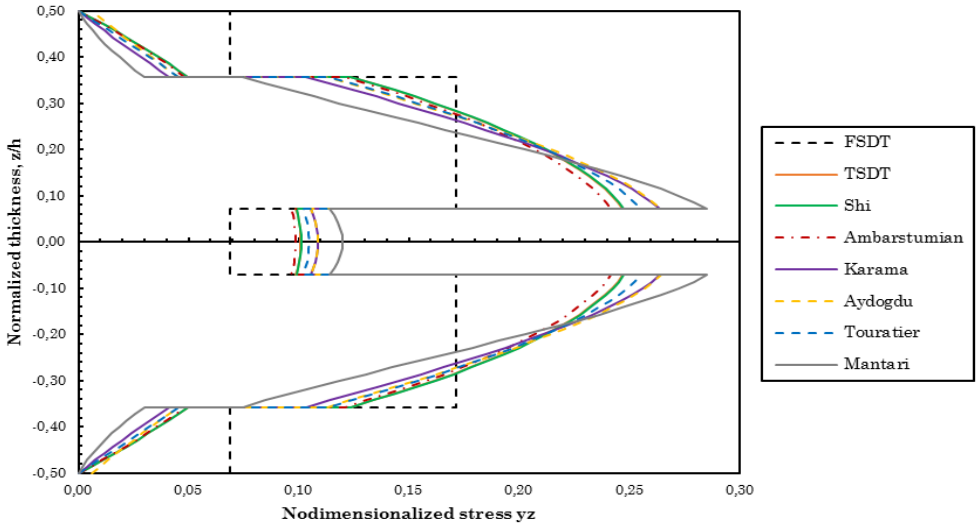

NNRPIM V1

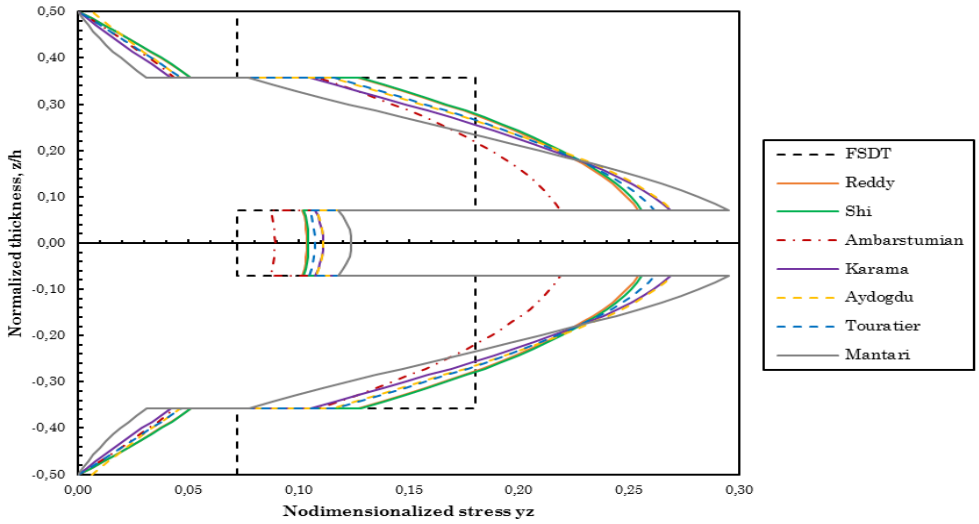

NNRPIM V2

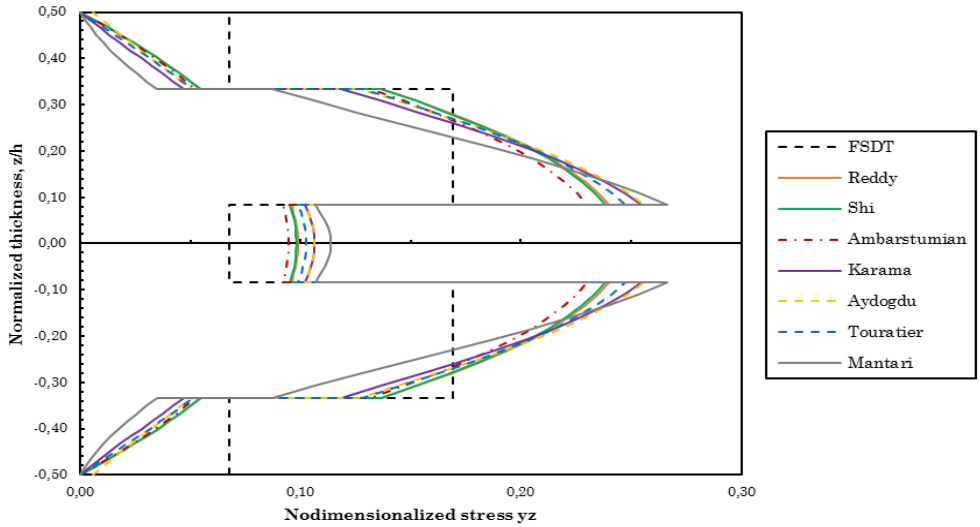

figure 96 – Nondimensionalized stresses τ_{yz} computed with the three numerical methods for a simply supported symmetric square laminate with cross-ply layers (0/90/90/0/90/90/0) subjected to a sinusoidal load (SSL), a/h=10.

RPIM

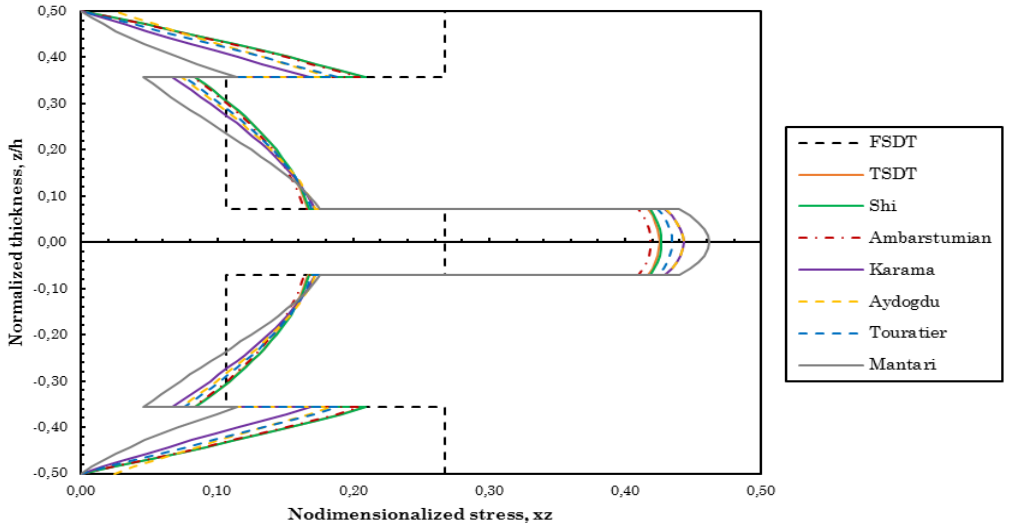

NNRPIM V1

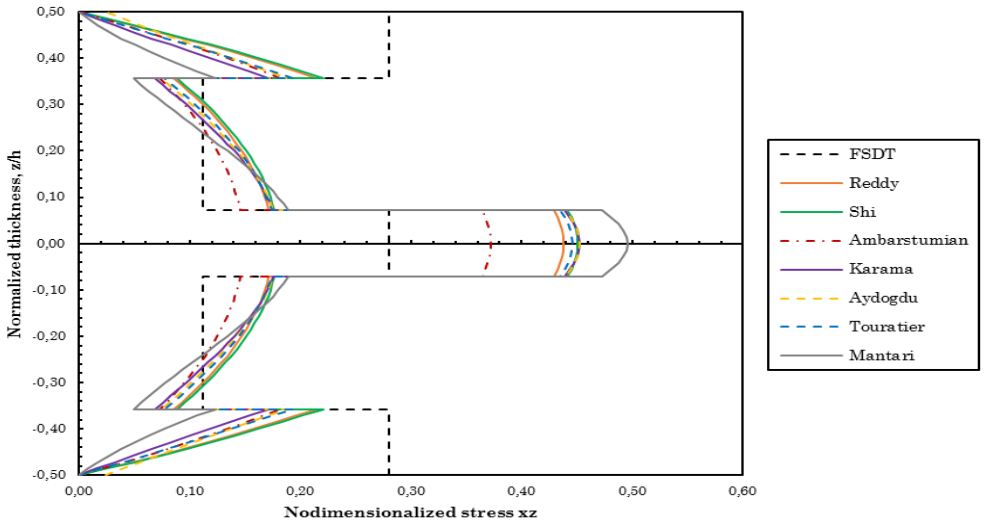

NNRPIM V2

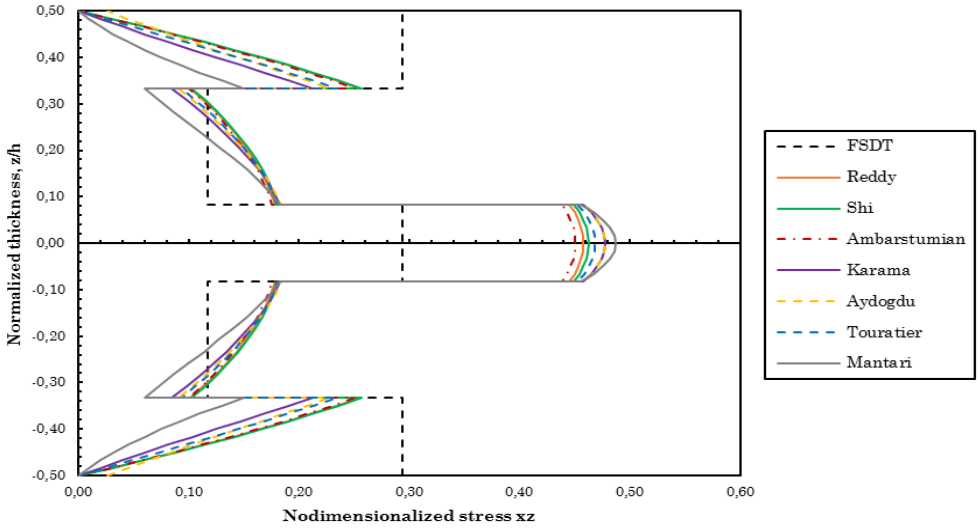

figure 97 – Nondimensionalized stresses τ_{xz} computed with the three numerical methods for a simply supported symmetric square laminate with cross-ply layers (0/90/90/0/90/90/0) subjected to a sinusoidal load (SSL), a/h=10.

RPIM

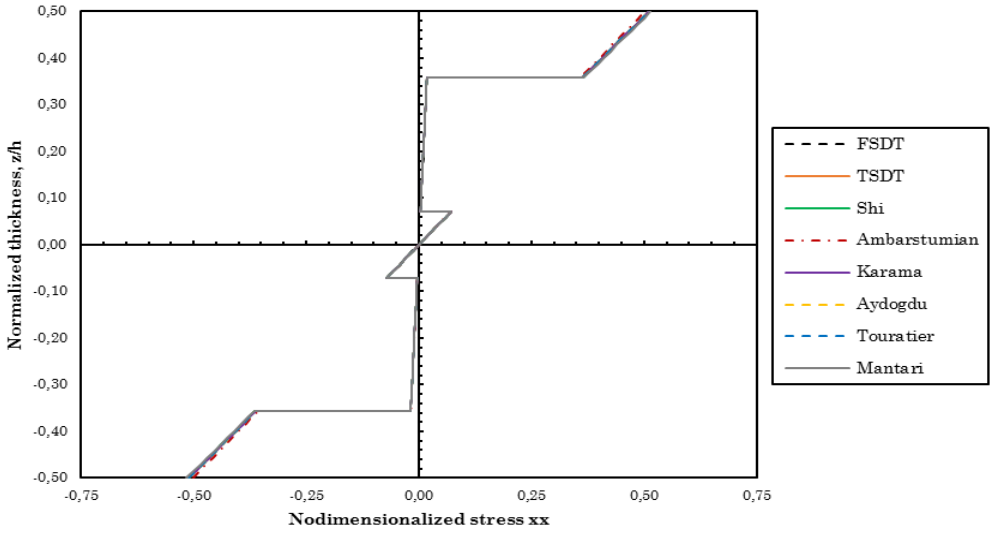

NNRPIM V1

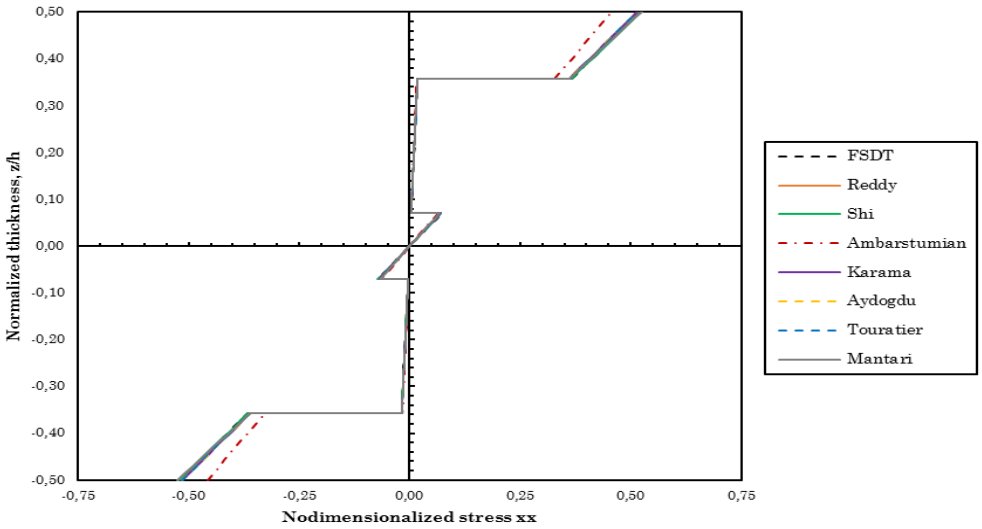

NNRPIM V2

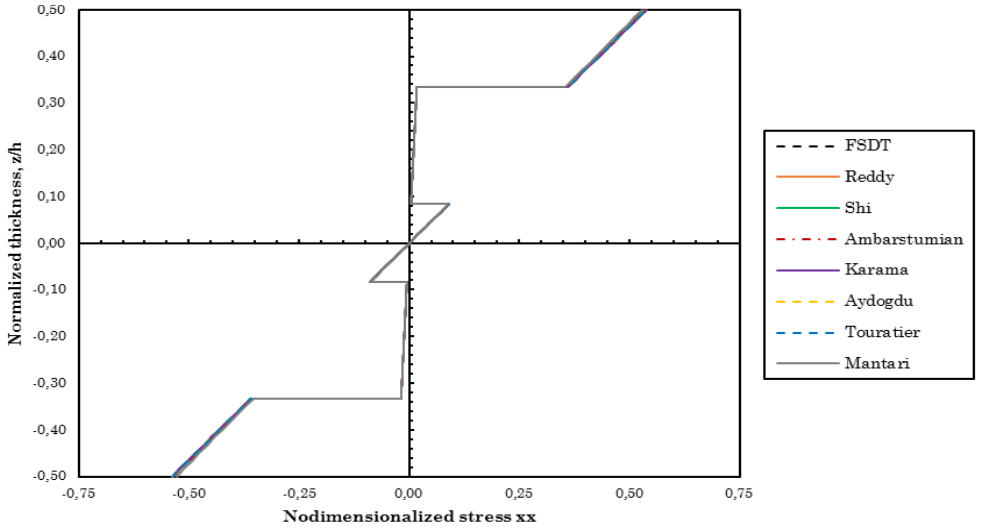

figure 98 – Nondimensionalized stresses σ_{xx} computed with the three numerical methods for a simply supported symmetric square laminate with cross-ply layers (0/90/90/0/90/90/0) subjected to a sinusoidal load (SSL), a/h=100.

RPIM

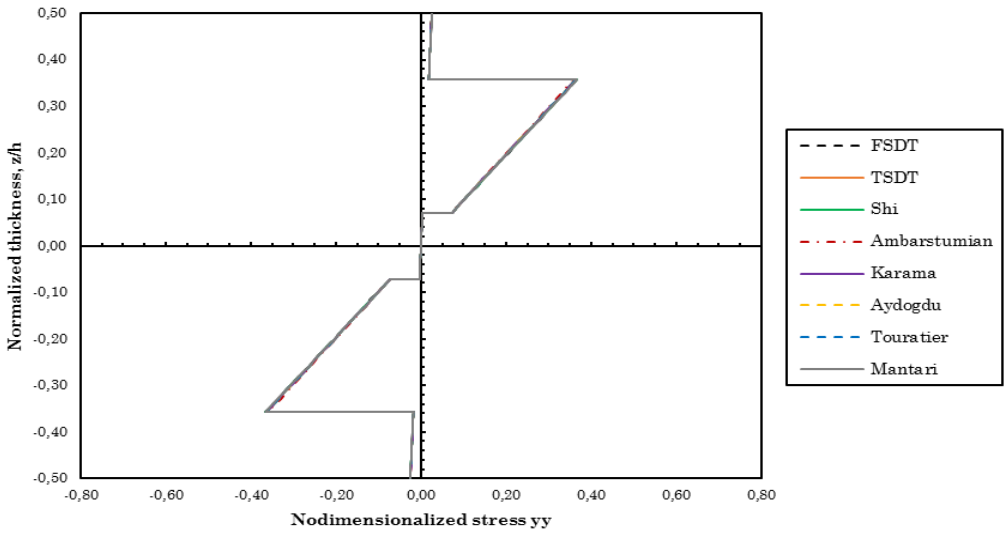

NNRPIM V1

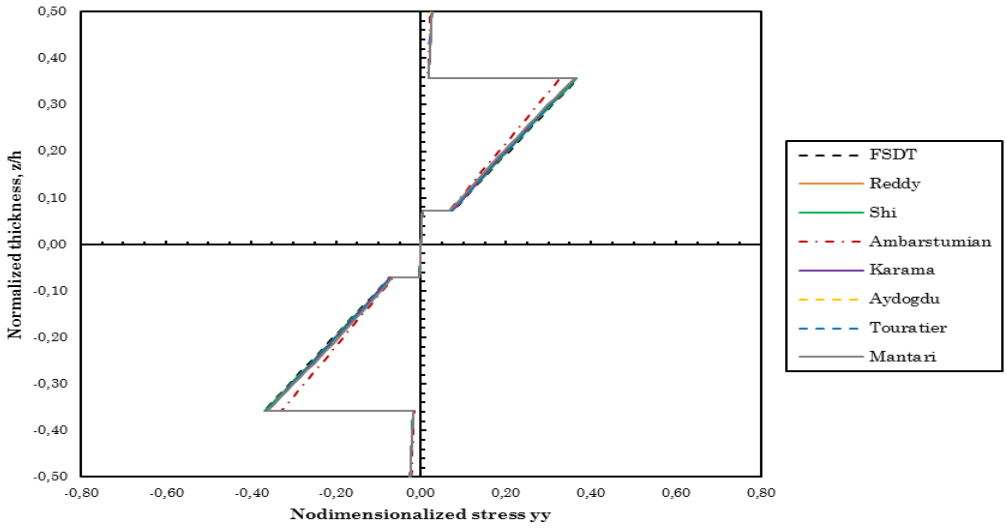

NNRPIM V2

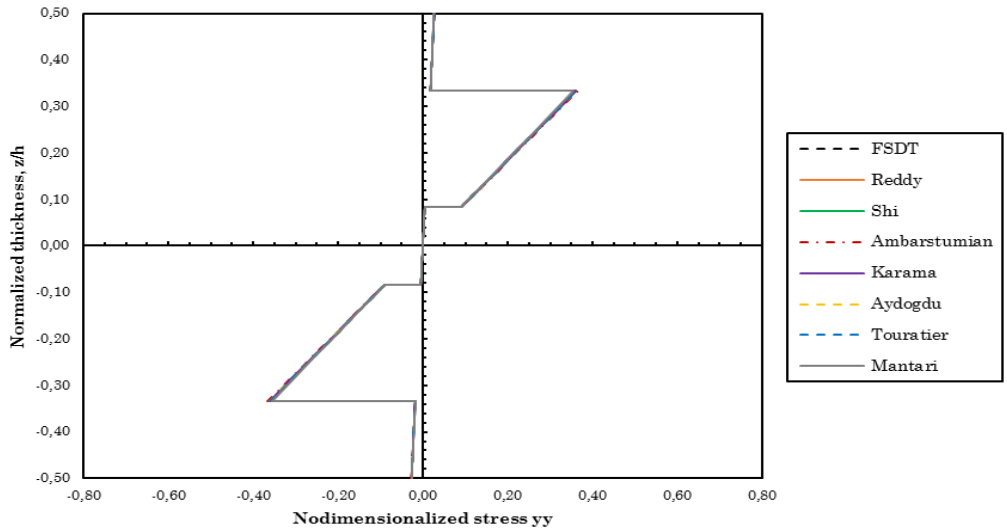

figure 99 – Nondimensionalized stresses σ_{yy} computed with the three numerical methods for a simply supported symmetric square laminate with cross-ply layers (0/90/90/0/90/90/0) subjected to a sinusoidal load (SSL), a/h=100.

RPIM

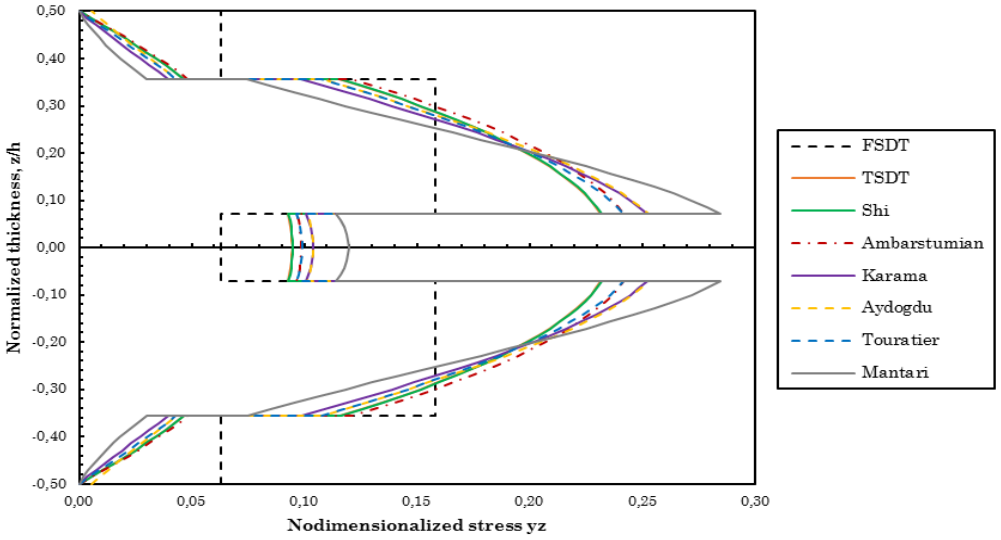

NNRPIM V1

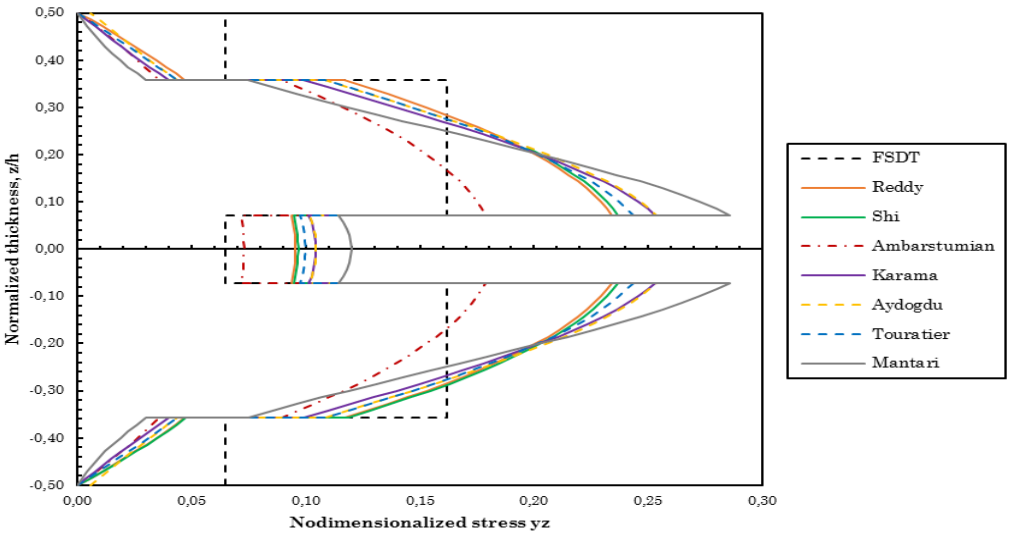

NNRPIM V2

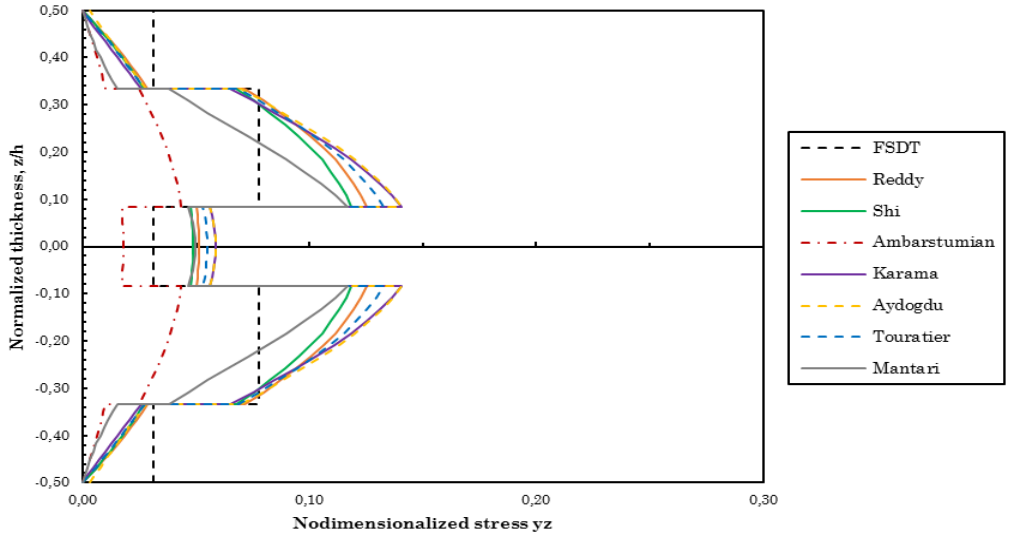

figure 100 – Nondimensionalized stresses τ_{yz} computed with the three numerical methods for a simply supported symmetric square laminate with cross-ply layers (0/90/90/0/90/90/0) subjected to a sinusoidal load (SSL), a/h=100.

RPIM

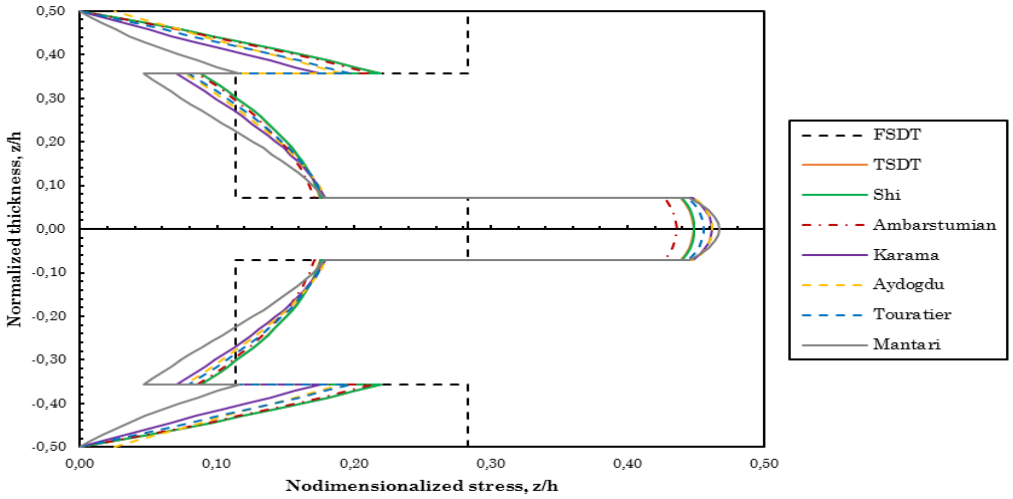

NNRPIM V1

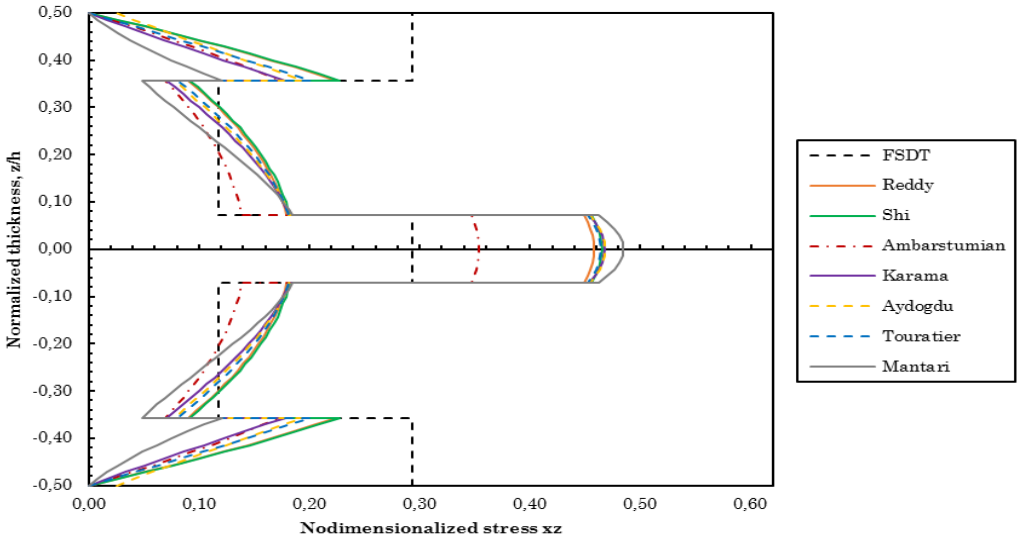

NNRPIM V2

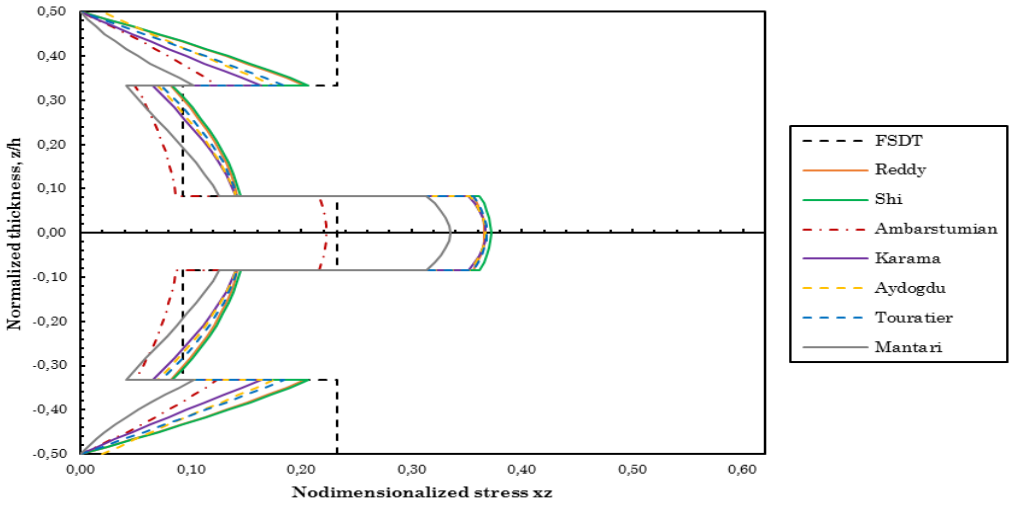

figure 101 – Nondimensionalized stresses τ_{xz} computed with the three numerical methods for a simply supported symmetric square laminate with cross-ply layers (0/90/90/0/90/90/0) subjected to a sinusoidal load (SSL), a/h=100.

Antisymmetric Cross-Ply Laminates

RPIM

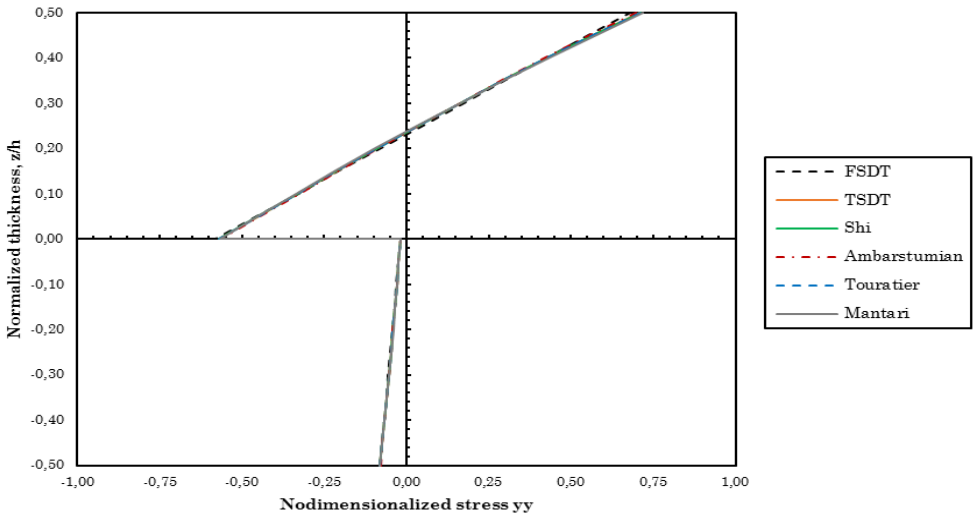

NNRPIM V1

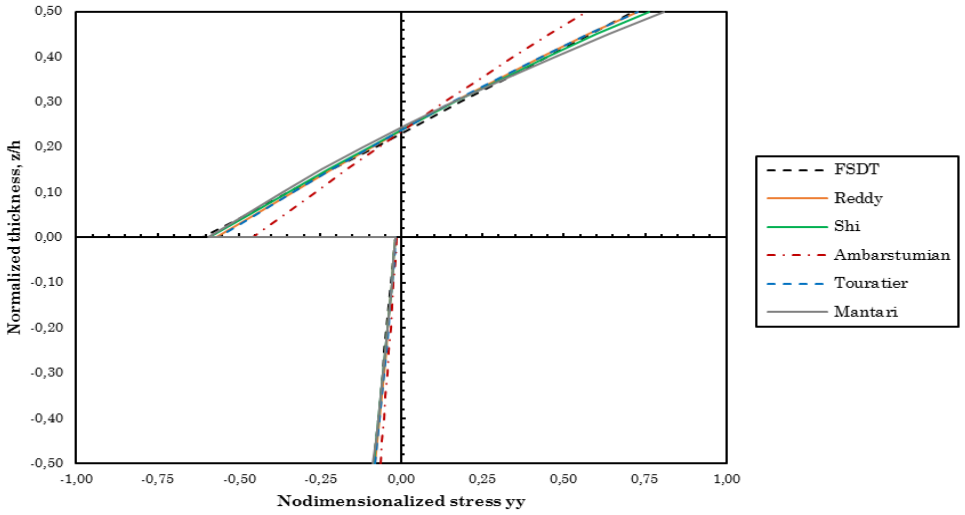

NNRPIM V2

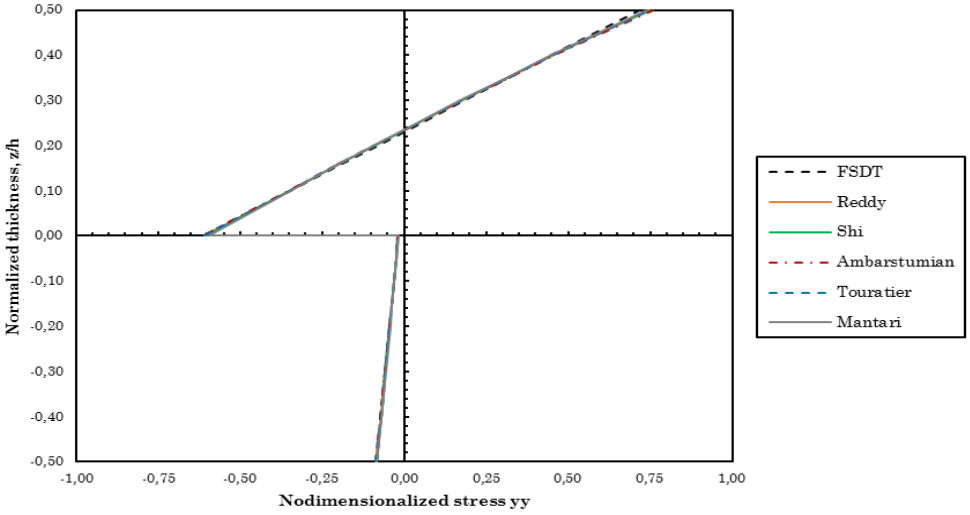

figure 102 – Nondimensionalized stresses σ_{yy} computed with the three numerical methods for a simply supported antisymmetric square laminate with cross-ply layers (0/90) subjected to a sinusoidal load (SSL), a/h=10.

RPIM

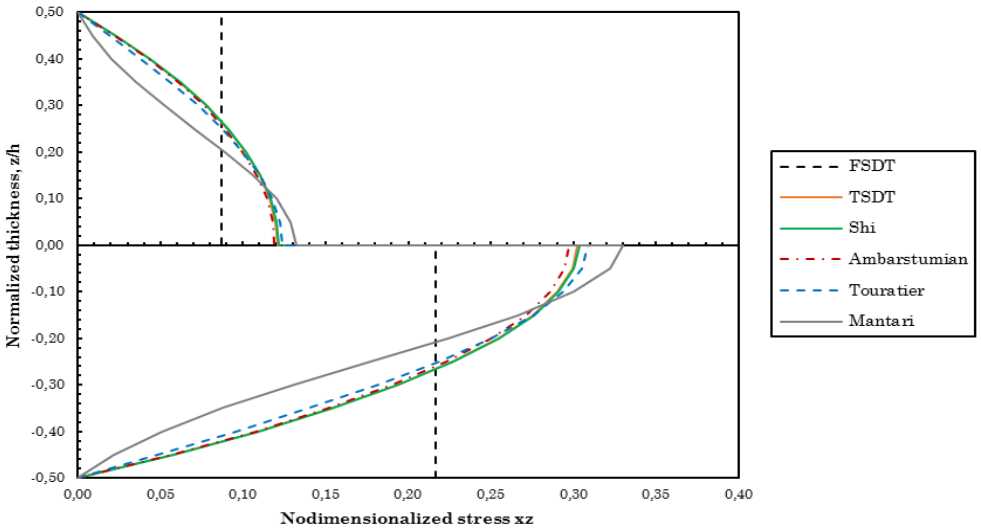

NNRPIM V1

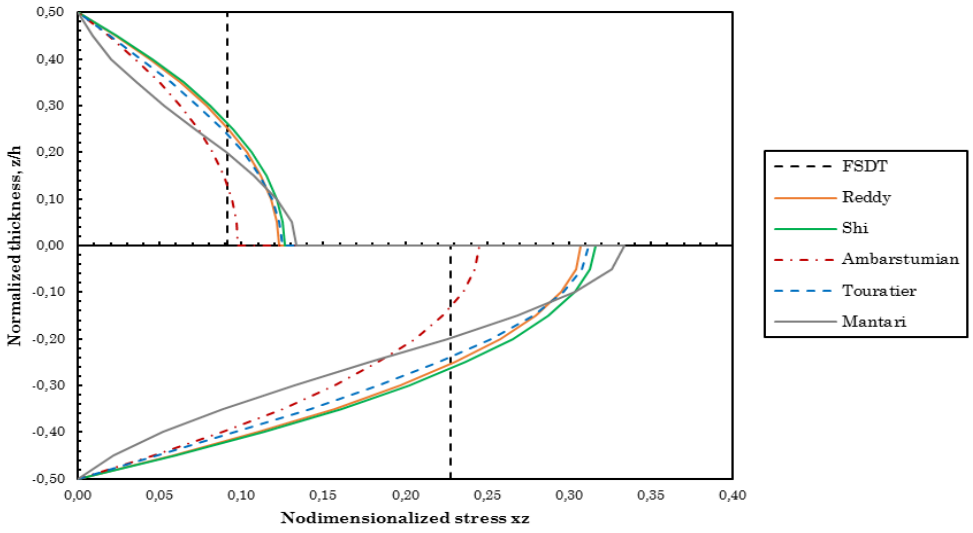

NNRPIM V2

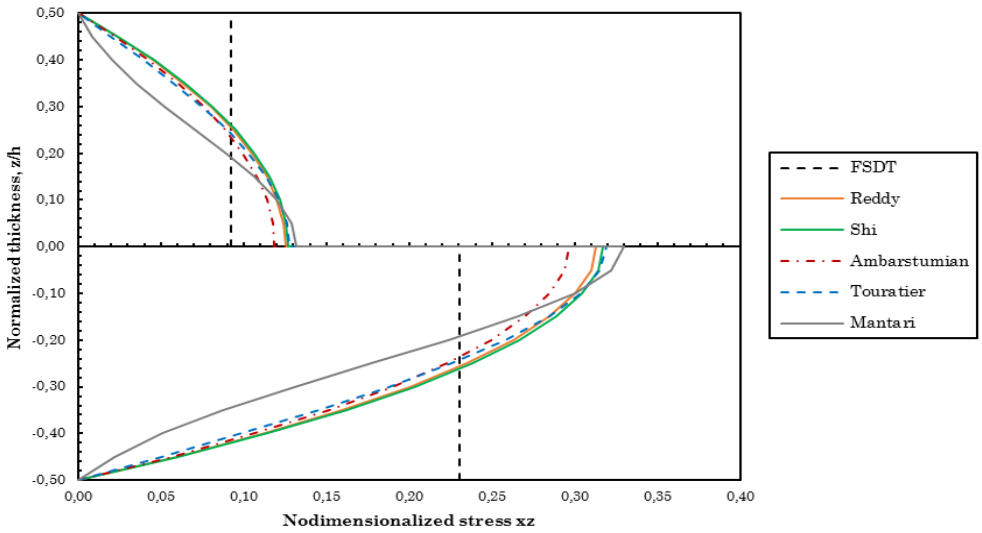

figure 103 – Nondimensionalized stresses τ_{xz} computed with the three numerical methods for a simply supported antisymmetric square laminate with cross-ply layers (0/90) subjected to a sinusoidal load (SSL), a/h=10.

RPIM

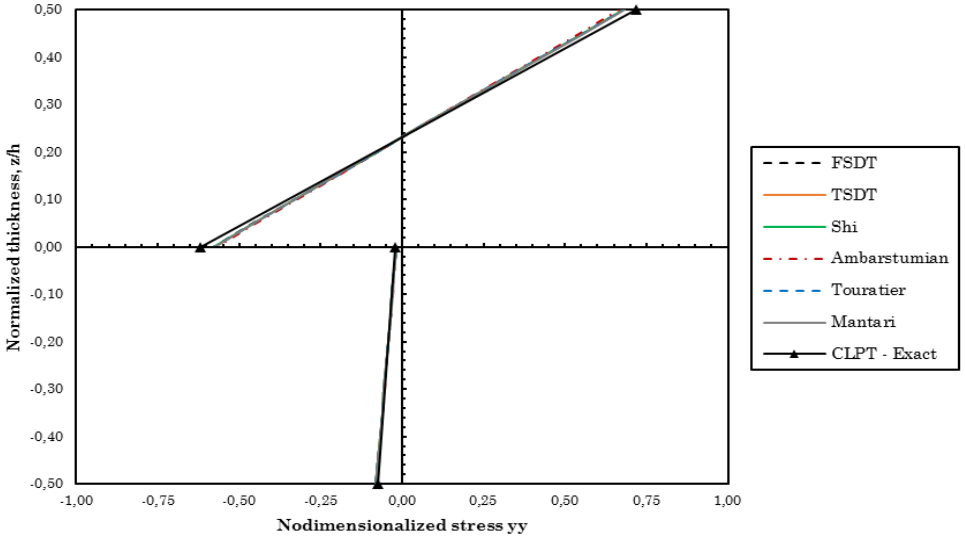

NNRPIM V1

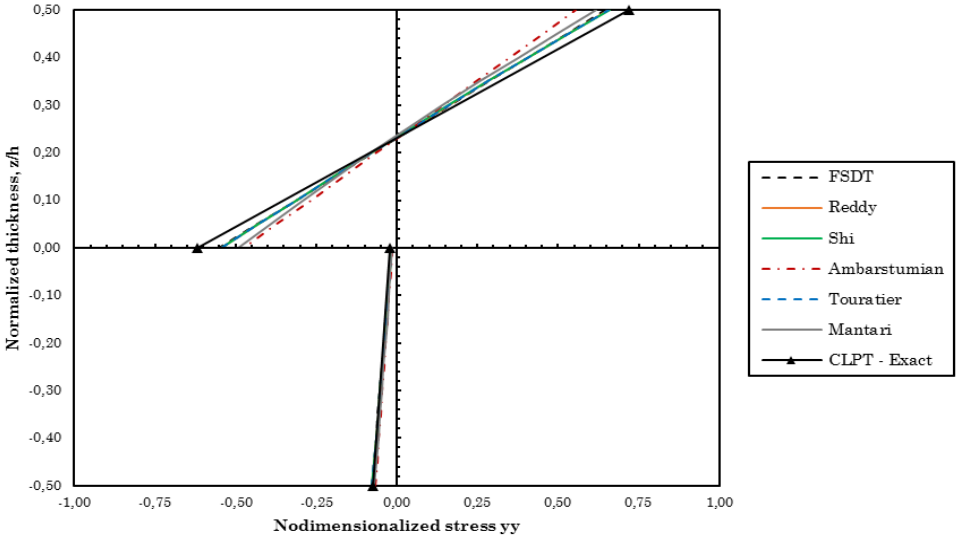

NNRPIM V2

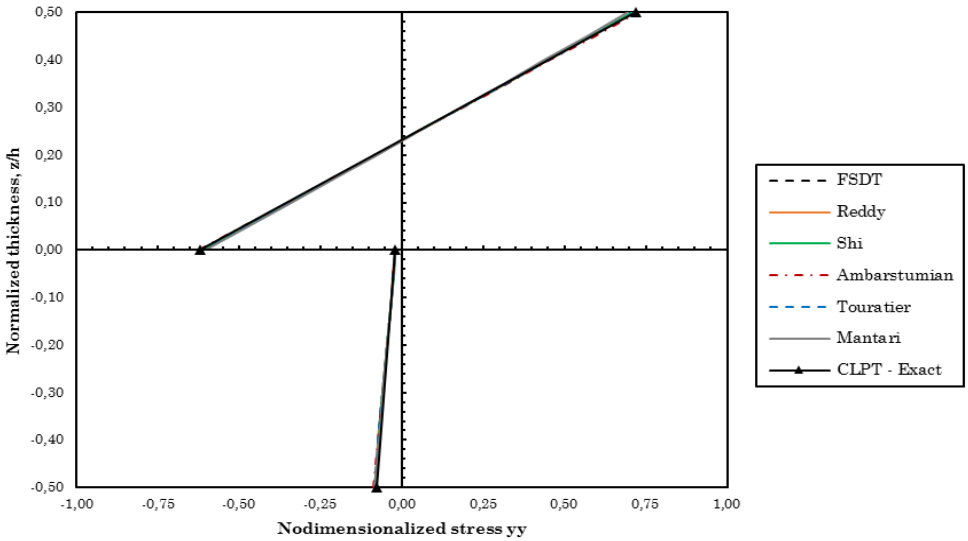

figure 104 – Nondimensionalized stresses σ_{yy} computed with the three numerical methods for a simply supported antisymmetric square laminate with cross-ply layers (0/90) subjected to a sinusoidal load (SSL), a/h=100.

RPIM

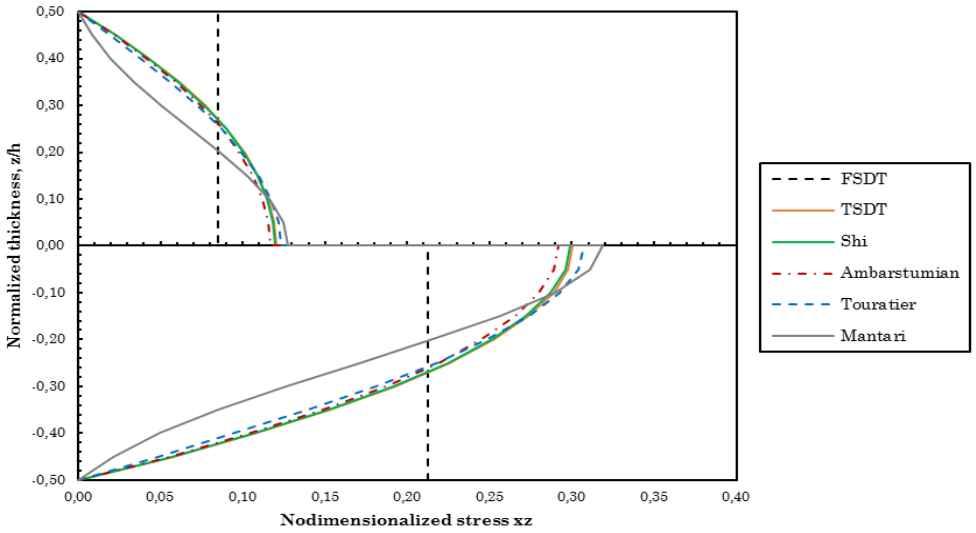

NNRPIM V1

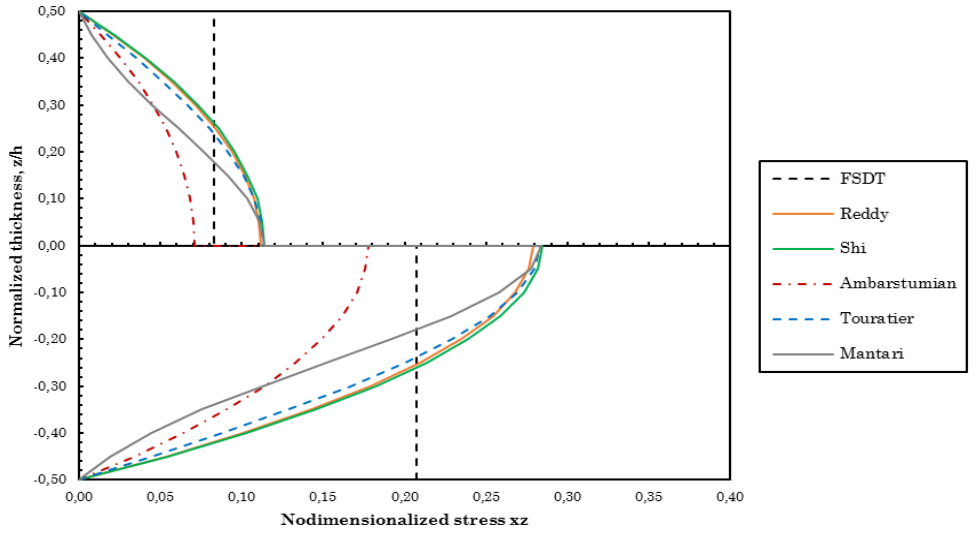

NNRPIM V2

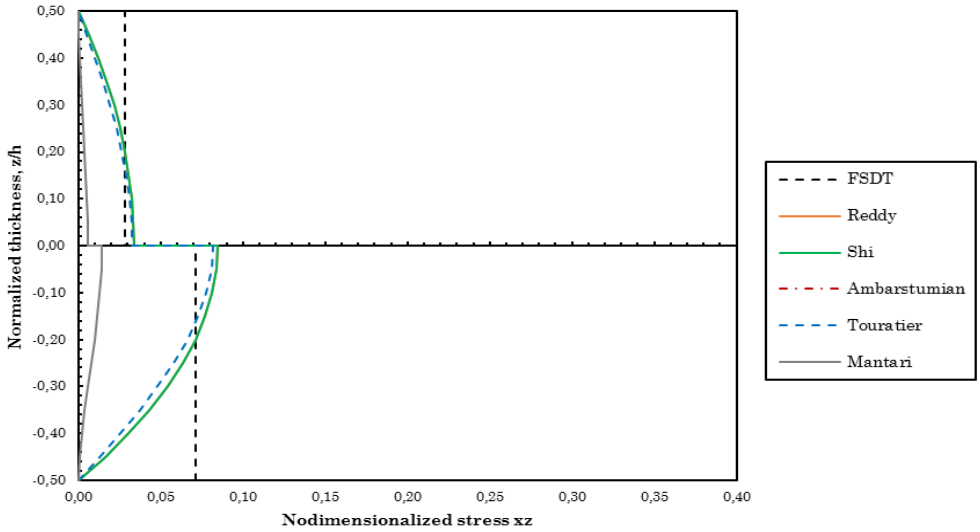

figure 105 – Nondimensionalized stresses τ_{xz} computed with the three numerical methods for a simply supported antisymmetric square laminate with cross-ply layers (0/90) subjected to a sinusoidal load (SSL), a/h=100.

RPIM

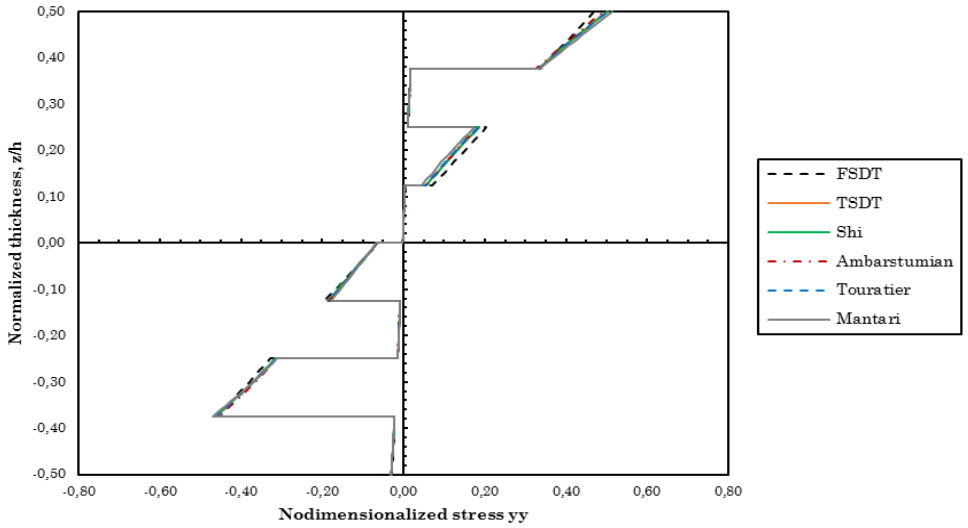

NNRPIM V1

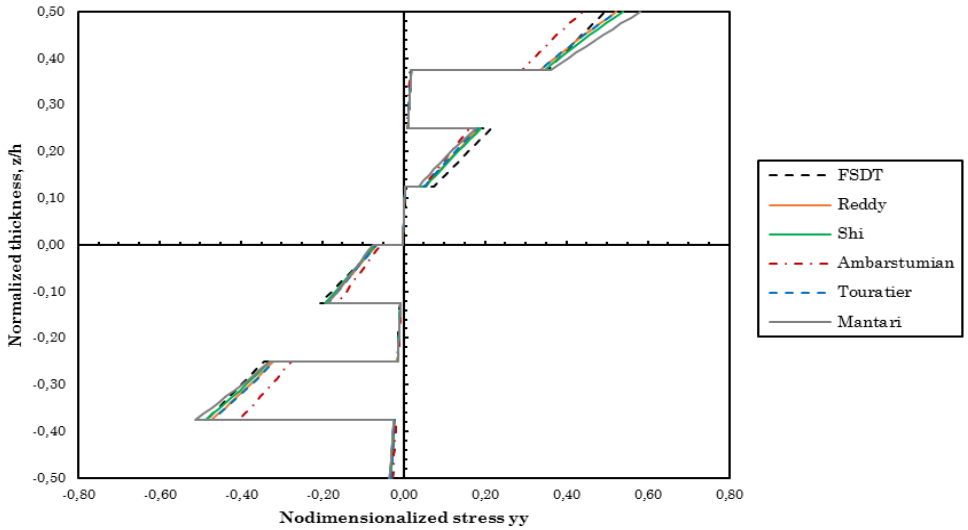

NNRPIM V2

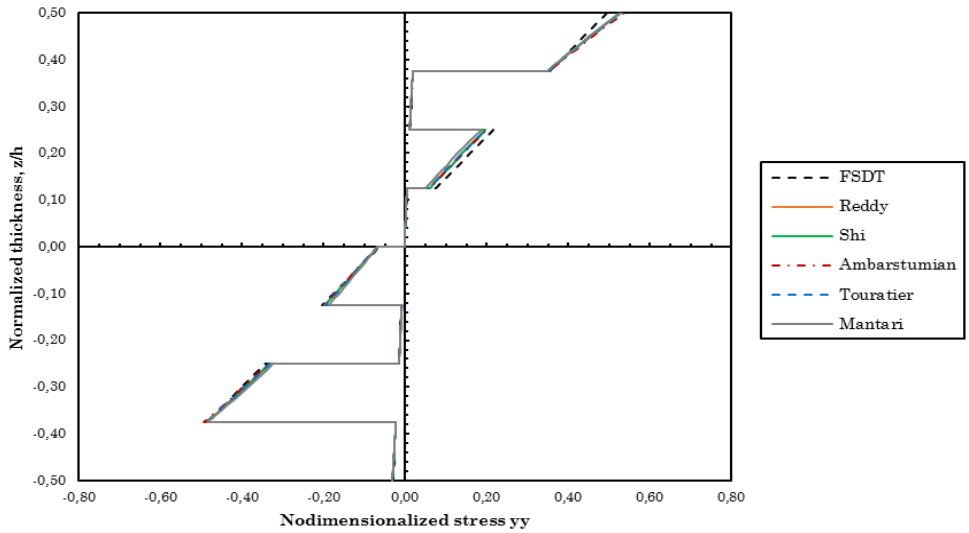

figure 106 – Nondimensionalized stresses σ_{yy} computed with the three numerical methods for a simply supported antisymmetric square laminate with cross-ply layers $(0/90)_4$ subjected to a sinusoidal load (SSL), a/h=10.

RPIM

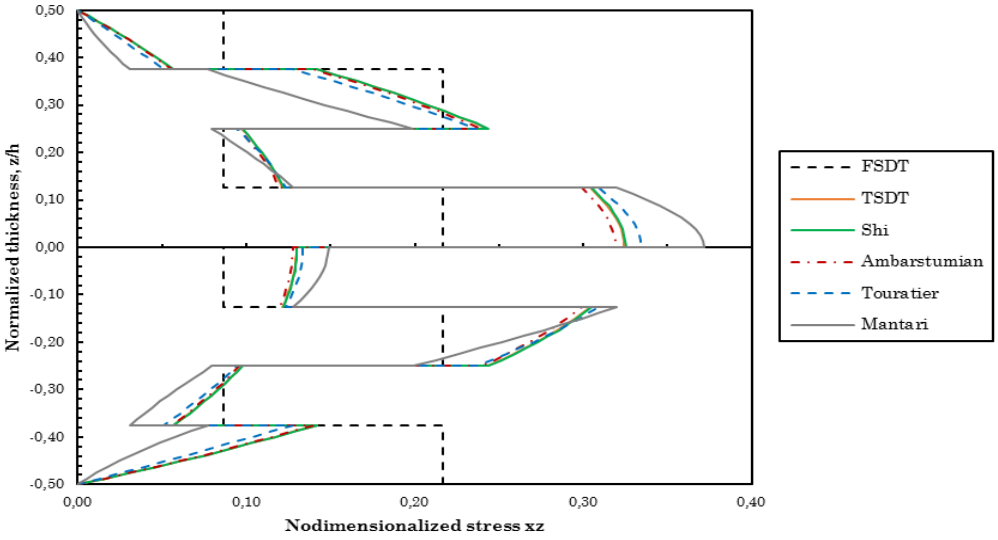

NNRPIM V1

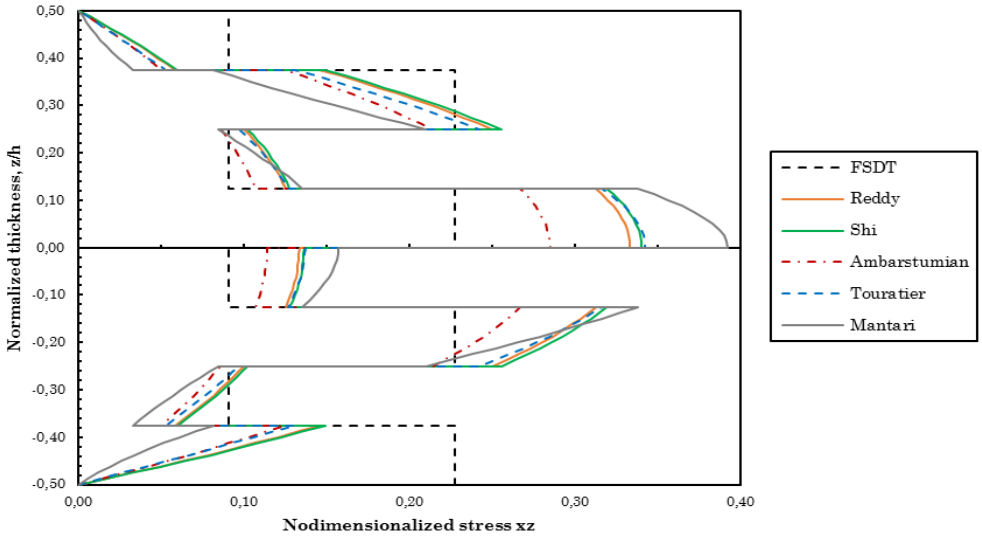

NNRPIM V2

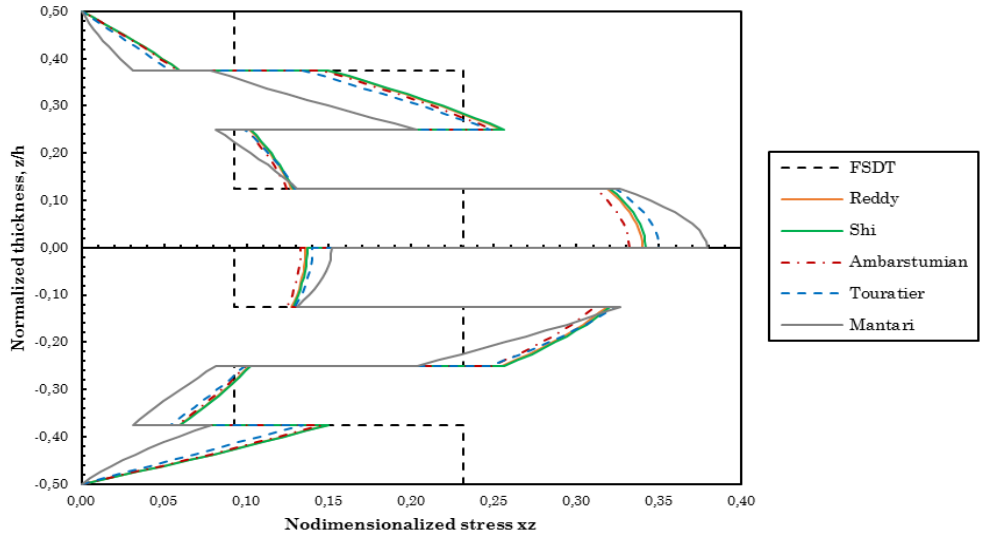

figure 107 – Nondimensionalized stresses τ_{xz} computed with the three numerical methods for a simply supported antisymmetric square laminate with cross-ply layers $(0/90)_4$ subjected to a sinusoidal load (SSL), a/h=10.

RPIM

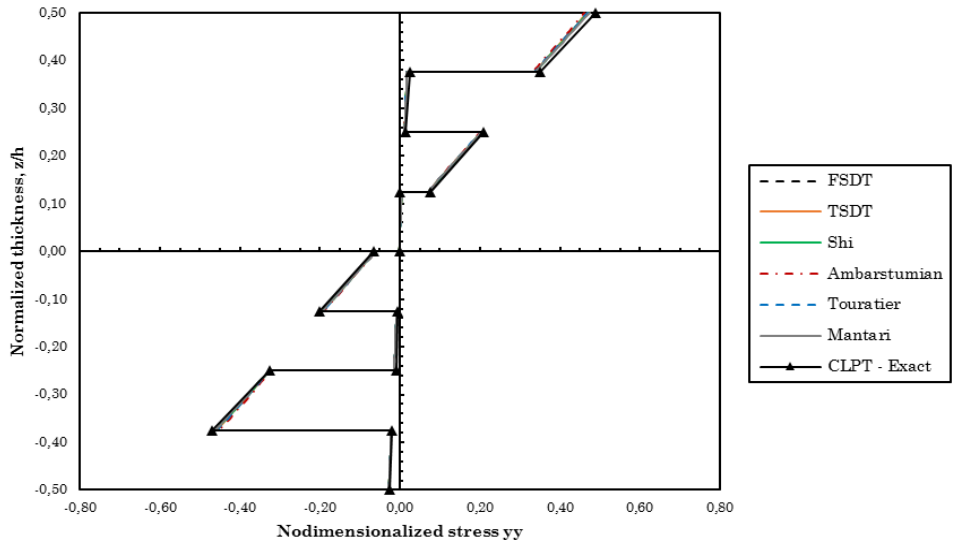

NNRPIM V1

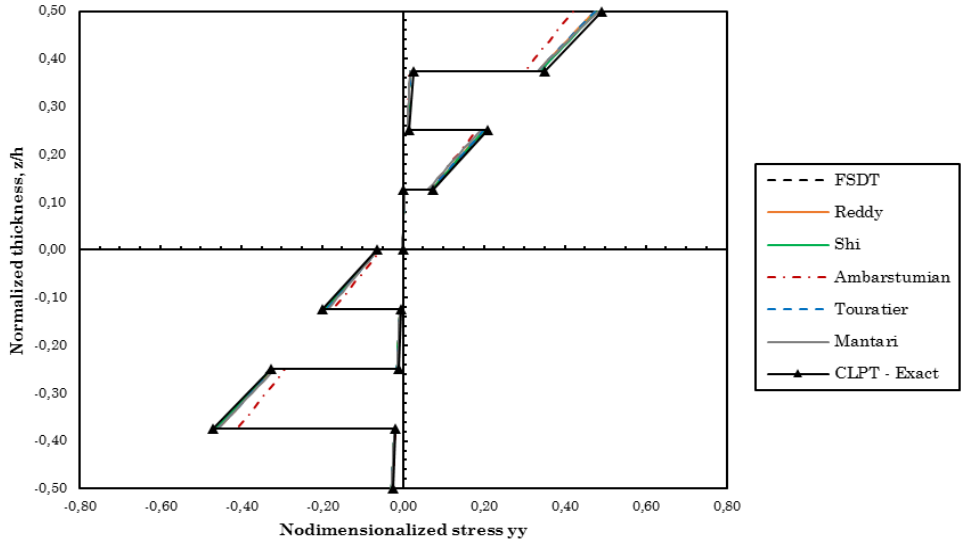

NNRPIM V2

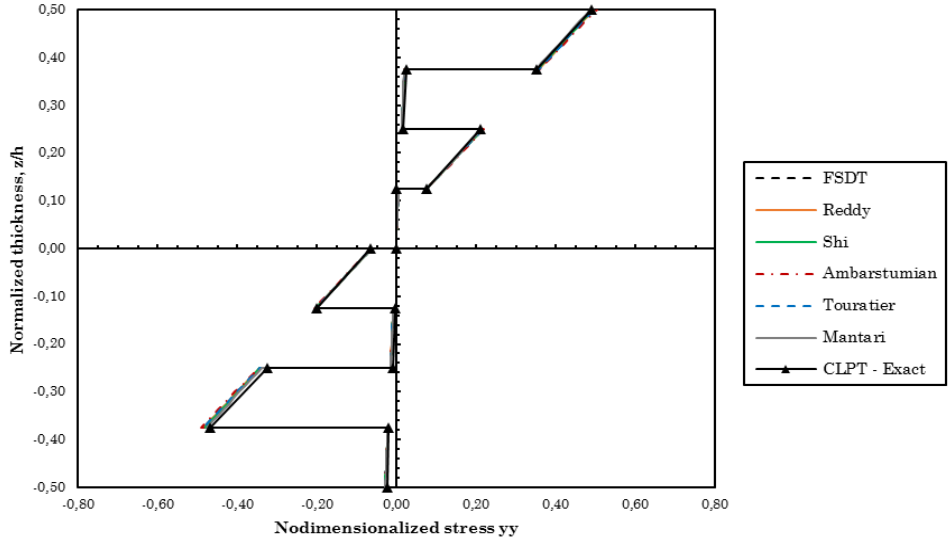

figure 108 – Nondimensionalized stresses σ_{yy} computed with the three numerical methods for a simply supported antisymmetric square laminate with cross-ply layers $(0/90)_4$ subjected to a sinusoidal load (SSL), a/h=100.

RPIM

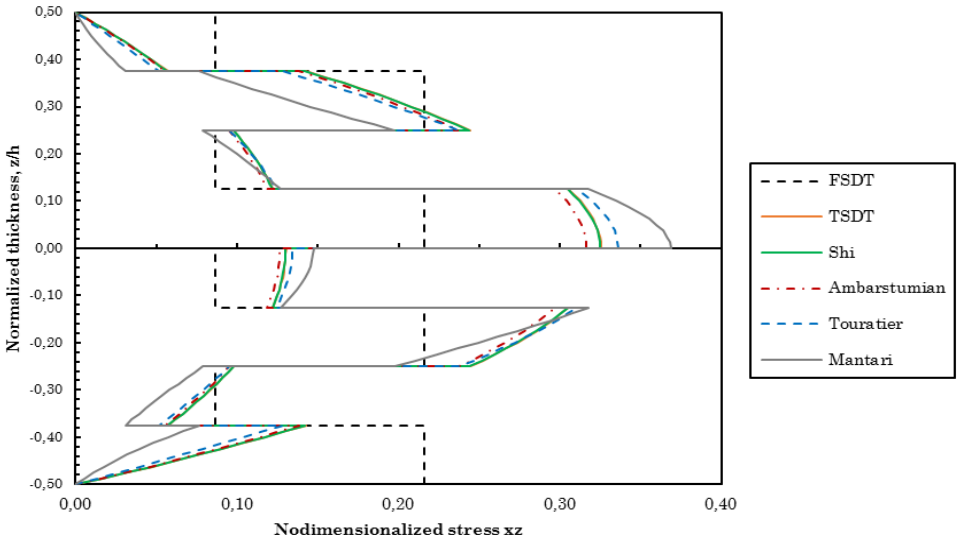

NNRPIM V1

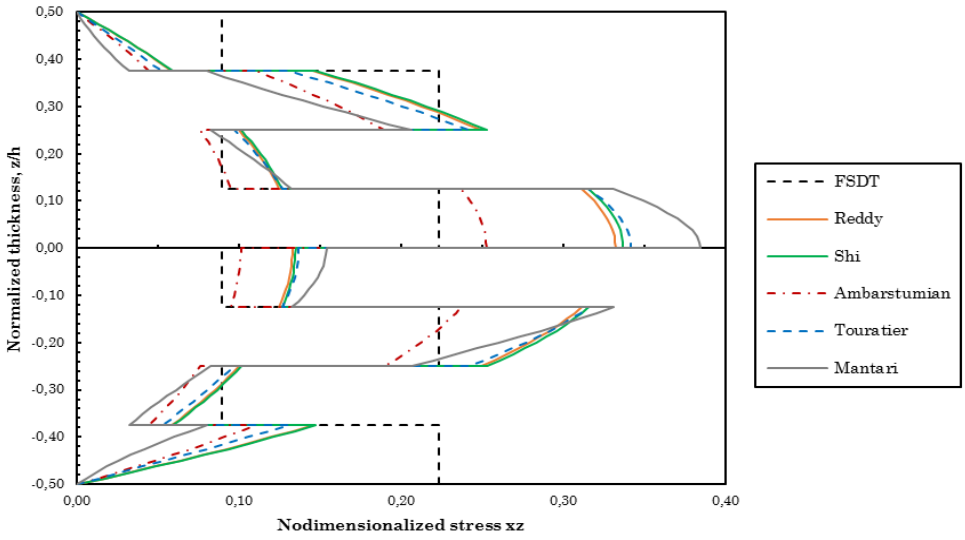

NNRPIM V2

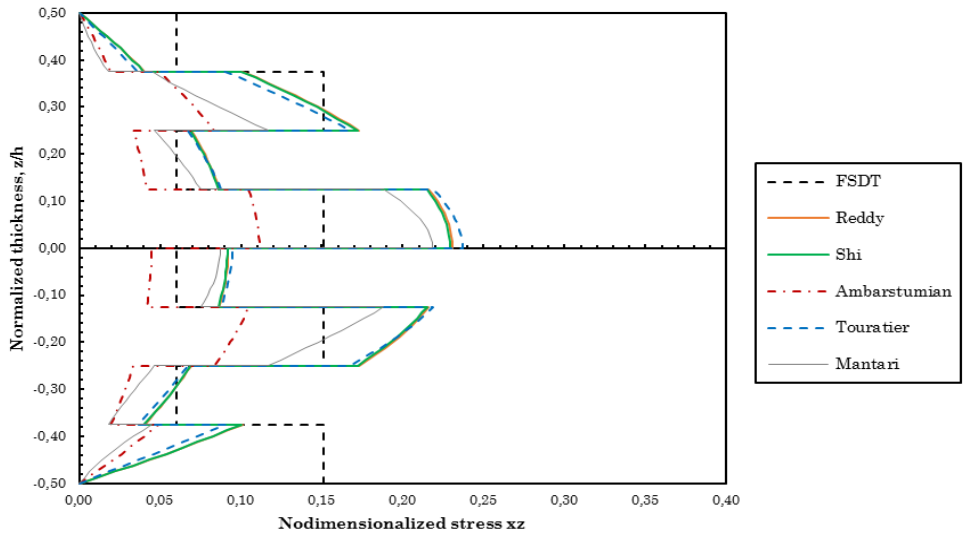

figure 109 – Nondimensionalized stresses τ_{xz} computed with the three numerical methods for a simply supported antisymmetric square laminate with cross-ply layers $(0/90)_4$ subjected to a sinusoidal load (SSL), a/h=100.

C. Computation Time Study

table 76 - Maximum normalized transverse displacements as a function of the number of nodes and the correspondent computation time for a simply supported symmetric square laminate with cross-ply layers (0/90/0), subjected to a sinusoidal load (SSL), a/h=50. (for Aydogdu, Karama and Mantari theories).

		RPIM		NNRPIM V1		NNRPIM V2	
ESL	**Number of nodes**	**Time (s)**	$\bar{w}$	**Time (s)**	$\bar{w}$	**Time (s)**	$\bar{w}$
Aydogdu	9	4.3768	0.1389	4.3293	0.1201	4.4124	0.1341
	25	4.4316	0.4004	4.4860	0.3365	4.6943	0.4051
	81	5.7194	0.4282	4.9887	0.3941	5.9226	0.4353
	289	11.0943	0.4395	7.4421	0.4102	11.7003	0.4461
	1089	37.1507	0.4405	20.0173	0.4153	39.7885	0.4472
	2601	100.9788	0.4405	55.6011	0.4164	115.9798	0.4474
Karama	9	4.2640	0.1389	4.3185	0.1201	4.5125	0.1341
	25	4.5010	0.4004	4.4977	0.3365	4.5793	0.4051
	81	5.6727	0.4282	4.9840	0.3941	6.1789	0.4353
	289	11.1611	0.4395	7.4389	0.4102	11.5007	0.4461
	1089	36.7317	0.4405	19.8597	0.4153	39.6806	0.4472
	2601	97.0398	0.4405	55.3501	0.4164	116.7653	0.4474
Mantari	9	4.2541	0.0422	4.3154	0.0344	4.4241	0.0397
	25	4.4667	0.3529	4.4953	0.1835	4.6748	0.3331
	81	6.0437	0.4212	5.1269	0.3502	6.0990	0.4118
	289	11.8896	0.4457	7.6844	0.4388	12.6355	0.4338
	1089	39.7690	0.4490	20.6549	0.4727	42.5727	0.4365
	2601	104.4135	0.4494	58.5830	0.4806	123.1578	0.4368

table 77 - Maximum normalized transverse displacements as a function of the number of nodes and the correspondent computation time for a simply supported symmetric square laminate with cross-ply layers (0/90/0), subjected to a sinusoidal load (SSL), a/h=50. (for Shi, Touratier, Ambartsumian and TSDT theories).

		RPIM		NNRPIM V1		NNRPIM V2	
ESL	**Number of nodes**	**Time (s)**	$\bar{w}$	**Time (s)**	$\bar{w}$	**Time (s)**	$\bar{w}$
Shi	9	2.5295	0.0869	2.7863	0.0722	2.6890	0.0820
	25	2.7985	0.3912	2.7886	0.2790	2.9339	0.3846
	81	4.1852	0.4301	3.3661	0.3881	4.3560	0.4292
	289	10.0492	0.4423	5.9018	0.4257	10.5748	0.4419
	1089	37.8756	0.4431	18.7315	0.4380	40.3463	0.4429
	2601	98.0788	0.4431	55.1471	0.4407	121.7575	0.4430
Touratier	9	3.1391	0.1322	3.3327	0.1136	3.2169	0.1271
	25	3.2258	0.1322	3.2197	0.3310	3.3647	0.4032
	81	4.5792	0.3998	4.1600	0.3940	4.7638	0.4347
	289	10.5699	0.4397	6.5644	0.4120	10.9501	0.4455
	1089	38.6095	0.4406	19.5708	0.4177	41.2895	0.4466
	2601	103.6270	0.4406	56.6672	0.4189	122.5980	0.4467
Ambartsumian	9	2.5507	0.3348	2.6760	0.4856	2.8601	0.4999
	25	2.8052	0.3472	2.7287	0.3756	2.9386	0.3842
	81	4.2950	0.3918	3.3706	0.3502	4.3069	0.4282
	289	9.9917	0.4233	5.9079	0.3441	10.5655	0.4516
	1089	37.9189	0.4297	18.7781	0.3427	40.5779	0.4563
	2601	99.5964	0.4307	55.5357	0.3425	122.8114	0.4573
TSDT	9	2.5715	0.1259	2.6179	0.1075	2.7594	0.1206
	25	2.8690	0.3990	2.7562	0.3252	2.9818	0.4011
	81	4.3043	0.4288	3.5985	0.3937	4.3431	0.4340
	289	10.3407	0.4398	8.1233	0.4136	10.4712	0.4449
	1089	39.0674	0.4407	18.7487	0.4199	40.3679	0.4460
	2601	99.2710	0.4407	55.2557	0.4212	121.7593	0.4461